Studies on the contribution of the left unique region of the genome to Murine Gammaherpesvirus-68 pathogenesis

Alastair Ian Macrae

PhD

University of Edinburgh

2002

Declaration

I declare that this thesis has been composed by myself and has not been submitted for any other degree. The work described herein is my own except where otherwise indicated and all work of other authors is duly acknowledged.

Alastair Ian Macrae

Laboratory for Clinical and Molecular Virology,
Department of Veterinary Pathology,
Royal (Dick) School of Veterinary Studies,
University of Edinburgh,
Summerhall Square,
Edinburgh,
EH9 1QH

Acknowledgements

I would like to thank my supervisors, Professor James Stewart and Professor Tony Nash for all their assistance and guidance during this project. I am grateful to James for his patient daily supervision and encouragement, and Tony for his support and advice. The substantial involvement and support of Dr. Bernadette Dutia to the work on MHV-76 (Chapter 3) was also greatly appreciated.

A number of people have also assisted with the work described in this thesis. Dr. Jela Mistrikova for the provision of the MHV-76 isolate; Dr. Andrew Davison and Steve Milligan for the sequence analysis of MHV-76 and the provision of the viral cosmids; Dr. Dave Brownstein for assistance in the interpretation of the histopathology; Neil MacIntyre for processing of the histopathology sections; Dr. Ed Usherwood for the *LacZ*-inducible T cell hybridoma assay (Chapter 4); Linda Sharp for technical assistance with the confocal microscopy; Dr. Mazher Husain and Dr. Jeff Sample for the provision of the pSG5 expression constructs (Chapter 4) and Professor John Hopkins for the immunisation of sheep for the generation of anti-M2 antibody. The support, advice and sharing of reagents with all the members of the MHV group (past and present), Dr. Simon Talbot's group and Dr. Bob Dalziel's group, as well as the assistance from the whole department has made this project succeed, and at times become almost enjoyable.

Much of the inspiration for this work was created thanks to the Belhaven Brewery Company Ltd. (Est. 1719), brewers of Belhaven Best; and the financial support to seek this inspiration was gratefully provided by the Wellcome Trust. None of this project would have been possible without the unstinting support of my family, friends and dog Foxy. The commitment and encouragement of my wife Liz throughout all the brief ups and prolonged downs of this PhD has been unwavering, and it goes without saying that all of this work is due to her.

Abstract

Members of the gamma subgroup of the herpesvirus family are characterised by their ability to establish lifelong latent infection in lymphocytes, and their association with lymphoproliferative disease and a range of malignant tumours. Members include the Epstein-Barr virus (EBV) and Kaposi's sarcoma-associated herpesvirus (KSHV), which are linked with clinically important human diseases, as well as alcelaphine herpesvirus 1 (AlHV-1) and ovine herpesvirus 2 (OvHV-2), which are of veterinary importance. Due to the severe limitations on the study of gammaherpesviruses presented by their species specificity and restricted growth *in vitro*, infection of laboratory mice with the naturally occurring virus murine gammaherpesvirus 68 (MHV-68) has become an excellent model system for the study of gammaherpesvirus pathogenesis.

This project involved the characterisation of murine herpesvirus 76 (MHV-76), another of the murine herpesviruses isolated at the same time as MHV-68. Molecular analysis revealed that MHV-76 is a deletion mutant of MHV-68, that lacks four genes unique to MHV-68 (M1, M2, M3 and M4) and eight viral tRNA-like genes that are all present at the left end of the MHV-68 genome. Biological characterisation of MHV-76, including the generation and study of rescue viruses which restored the deleted sequence into MHV-76, showed that loss of these genes leads to enhanced clearance of virus from the lungs due to a vigorous inflammatory response. There was also a significant reduction in splenomegaly and the amount of latent virus detectable in the spleen. These results show that the genes present at the left end of the unique region of the MHV-68 genome play a critical role in the viral immune evasion strategy.

Detailed studies on one of these unique MHV-68 genes, M2, show that it is a 30kDa protein that has localised homology with the Gab2 and semaphorin protein families. Expression of M2 in mammalian cells reveals that it co-localises to the plasma membrane, as well as being present in diffuse areas of the nucleus and cytoplasm. Generation of a recombinant virus with a disruption in the M2 ORF showed that the M2 gene plays a critical role in the establishment of latency and the regulation of the numbers of latently infected cells in the spleen. The M2

gene is not involved in the genesis of splenomegaly. These studies uncover some of the genetic elements involved in gammaherpesvirus pathogenesis.

Contents

List of Figures

List of Tables

Abbreviations

A	Adenosine
a.a.	Amino acid
AIDS	Acquired immunodeficiency syndrome
AlHV-1	Alcelaphine herpesvirus 1
AP	Alkaline phosphatase
APC	Antigen presenting cell
ATP	Adenosine triphosphate
BART	*Bam*HI A rightward transcripts
BCIP	5-bromo-4-chloro-3-indolyl phosphate
bcl-2	B-cell lymphoma/leukaemia 2
BHK	Baby hamster kidney
BHV-4	Bovine herpesvirus 4
BL	Burkitt's lymphoma
bp	Base pair
BSA	Bovine serum albumin
C	Cytidine
CD	Cluster of differentiation
cDNA	Complementary DNA
CMV	Cytomegalovirus
CTL	Cytotoxic T lymphocyte
DAB	3,3' Diaminobenzidine
DMEM	Dulbecco's modified Eagle's medium
DNA	Deoxyribonucleic acid
DTT	Dithiothreitol
dATP	Deoxyadenosine triphosphate
dCTP	Deoxycytidine triphosphate
dGTP	Deoxyguanosine triphosphate
dNTP	Deoxynucleoside triphosphate
dTTP	Deoxythymidine triphosphate
dH_20	Distilled water

diH_20	De-ionised water (18 megohm)
ds	Double stranded
EBER	Epstein-Barr virus-encoded small RNA
EBNA	Epstein-Barr virus nuclear antigen
EBV	Epstein-Barr virus
E. coli	*Escherichia coli*
ECL	Enhanced chemiluminescence
EDTA	Ethylenediaminetetraacetic acid
EGFP	Enhanced green fluorescent protein
EHV-2	Equine herpesvirus 2
ER	Endoplasmic reticulum
FACS	Fluorescent activated cell sorting
FCS	Foetal calf serum
FITC	Fluorescein isothiocyanate
FLICE	FADD homologous ICE/CED-3-like protease
FLIP	FLICE-inhibitory protein
G	Guanosine
g or gp	Prefix for Glycoprotein
g	Gravity
Gab2	Grb2-associated binder 2
GFP	Green fluorescent protein
GPCR	G protein-coupled receptor
GMEM	Glasgow's modified Eagle's medium
GS	Glutathione sepharose
GST	Glutathione S-transferase
HA	Haemagglutinin
HBSS	Hank's buffered salt solution
HCMV	Human cytomegalovirus
HEPES	N'-[2-hydroxyethyl] piperazine-N'-[2-ethanesulphonic acid]
HHV	Human herpesvirus
His_6	Six consecutive histidine residues
HIV	Human immunodeficiency virus

HLA	Human leukocyte antigen
HSUR	Herpesvirus saimiri uRNA
HSV	Herpes simplex virus
HRP	Horseradish peroxidase
HVA	Herpesvirus ateles
HVS	Herpesvirus saimiri
ICAM	Intracellular adhesion molecule
ICP	Infected cell protein
IFN	Interferon
Ig	Immunoglobulin
IL	Interleukin
IM	Infectious mononucleosis
IPTG	Isopropyl-β-D-thiogalactopyranoside
kb	Kilobase
kDa	Kilodalton
KS	Kaposi's sarcoma
KSHV	Kaposi's sarcoma associated herpesvirus
LANA	Latency associated nuclear antigen
LAT	Latency associated transcript
LB	Luria Bertani
LCL	Lymphoblastoid cell line
LCV	Lymphocryptovirus
LGT	Low gelling temperature
LMP	Latent membrane protein
MACS	Magnetic cell separation
MCD	Multicentric Castleman's disease
MCF	Malignant catarrhal fever
MCS	Multiple cloning site
MHC	Major histocompatibility complex
MHV-68	Murine gammaherpesvirus 68
MHV	Murine herpesvirus
MIP	Macrophage inhibitory protein

MOI	Multiplicity of infection
MOPS	3-[N-morpholino] propanesulphonic acid
MoMuLV	Moloney murine leukaemia virus
mRNA	Messenger RNA
NK	Natural killer
NBCS	Newborn calf serum
NBT	Nitro blue tetrazolium
NPC	Nasopharyngeal carcinoma
OAS	2'-5' oligoadenylate synthetase
OD	Optical density
ORF	Open reading frame
Ori	Origin of replication
OvHV-2	Ovine herpesvirus 2
PAGE	Polyacrylamide gel electrophoresis
PBS	Phosphate buffered saline
PCR	Polymerase chain reaction
PEC	Peritoneal exudate cell
PEL	Primary effusion lymphoma
p.i.	Post-infection
PKR	Protein kinase R
PFU	Plaque forming unit
PMSF	Phenylmethylsulphonyl fluoride
POD	Peroxidase
PTLD	Post-transplant lymphoproliferative disease
PVDF	Polyvinylidene fluoride
RIPA	Radioimmunoprecipitation analysis
RNA	Ribonucleic acid
RPMI	Rosewell Park Memorial Institute
RT	Room temperature
RT-PCR	Reverse transcriptase PCR
SDS	Sodium dodecyl sulphate
SSC	Standard saline citrate

STP	Saimiri transformation-associated protein
SV40	Simian vacuolating virus 40
T	Thymidine
TAE	Tris acetate EDTA buffer
TBS	Tris buffered saline
TC	Tissue culture
TE	Tris EDTA buffer
TEMED	N, N, N',N'-tetraethylmethylenediamine
TIP	Tyrosine kinase interacting protein
TK	Thymidine kinase
TNF	Tumour necrosis factor
TPB	Tryptose phosphate broth
TRITC	Tetramethylrhodamine B isothiocyanate
U	Unit
UL or U_l	Unique sequence of the long component of the genome
US or U_s	Unique sequence of the short component of the genome
UV	Ultraviolet light
v/v	Volume per volume
vbcl-2	Viral bcl-2 homologue
vCKBP	Viral chemokine binding protein
vCKR	Viral chemokine receptor
v-cyc	Viral cyclin D homologue
vFLIP	Viral FLICE-inhibitory protein homologue
vGPCR	Viral GPCR homologue
vIL	Viral interleukin homologue
vIRF1	Viral interferon regulatory factor 1 homologue
vMIP	Viral macrophage inhibitory protein homologue
VP	Virion polypeptide
vtRNA	Viral tRNA-like sequence
VZV	Varicella zoster virus
w/v	Weight per volume
X-gal	5-bromo-4-chloro-3-indolyl-β-D-galactoside

Chapter 1: Introduction

1.1. Herpesviruses

1.2. Gammaherpesviruses

1.3. Models of gammaherpesvirus pathogenesis

1.4. Murine gammaherpesvirus 68

1.5. Other murine herpesvirus isolates

1.6. Viruses and immune evasion

1.1. Herpesviruses

The *Herpesviridae* family currently contains over 120 known viruses (Minson *et al.*, 2000), with new members being discovered every year, and they are found in humans, animals and invertebrates (Arzul *et al.*, 2001). They are ubiquitous in their host populations, with over 90% of the human population infected with the Epstein Barr virus (EBV) and over 95% carrying latent varicella-zoster virus (VZV). Their most important biological characteristic is the ability to establish latent infections, which allows herpesviruses to persist for the lifetime of the host. In most instances, this latent virus remains undisturbed in co-existence with the host organism. However, if this balance is disrupted by a variety of external stimuli, for example immunosupression, the latent virus can reactivate leading to the generation of a vast spectrum of diseases. This has made the herpesvirus family the subject of much scientific research.

1.1.1. Characteristics of herpesviruses

Members of the *Herpesviridae* family are distinguished by the architecture of the virus particle (Figure 1.1.1). The virion consists of a core containing a large double-stranded DNA genome enclosed in an icosadeltahedral capsid, approximately 100-110nm in diameter, comprised of 162 capsomeres. An amorphous tegument, predominantly composed of viral proteins present in variable amounts surrounds the nucleocapsid. Surrounding the tegument is the viral envelope, derived from the host cell and containing numerous viral glycoprotein spikes which project from the surface. These structures make up the virus particle, which is 120-300nm in diameter, depending on the amount of tegument present.

All herpesviruses share four major biological properties (Roizman, 1996):

1. They contain open reading frames (ORFs) that specify for enzymes involved in nucleic acid synthesis (e.g. DNA polymerase) and nucleotide metabolism (e.g. thymidine kinase).
2. Viral DNA synthesis and capsid assembly occur in the nucleus.

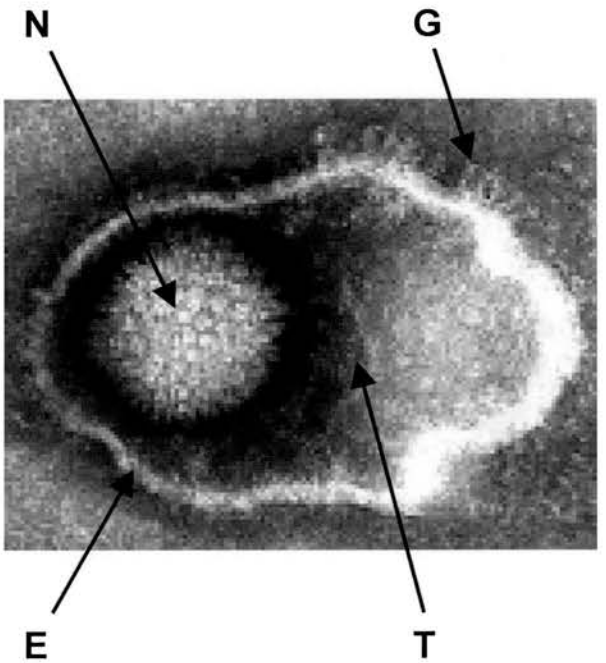

Figure 1.1.1 Electron micrograph of HSV-1 virion. The nucleocapsid (**N**) is approximately 100nm in diameter, and is surrounded by the tegument (**T**). The outer envelope (**E**) containing glycoprotein spikes (**G**) has been permeabilised during the staining process, and therefore appears larger than normal. Photograph taken by Linda Stannard and reproduced from the Big Picture Book of Viruses, available at http://www.virology.net/Big_Virology/BVDNAherpes.html

3. Lytic replication (the production of infectious viral particles) leads to the irreversible destruction of the infected cell.
4. All herpesviruses can remain latent in their natural host. During latent infection, the viral genome forms a closed circular molecule, and expression of a limited subset of viral genes occurs. During latency, no infectious viral particles are produced. However, the latent viral genome can reactivate under certain conditions, leading to lytic viral replication and the production of infectious viral particles.

Despite these similarities in virion structure and general biological properties, there is a massive diversity in pathogenesis and disease associations of the different herpesviruses. This has led to various attempts to divide the herpesvirus family into different subfamilies.

1.1.2. Classification of herpesviruses

Initial attempts to classify herpesviruses into three subfamilies (alpha, beta and gamma) were made on the basis of biological properties (Roizman *et al.*, 1981). Table 1.1 details the main biological properties that were used including host range, duration of reproductive cycle, cytopathology and sites of latency. However there are substantial areas of overlap between the three families, in particular the variable *in vitro* growth characteristics of gammaherpesviruses, that led to the difficulty in the classification of some viruses such as Marek's disease virus that replicates rapidly *in vitro* yet causes lymphoid tumours in chickens.

Another characteristic used to classify herpesviruses was the structure of the genome, and in particular the arrangement of reiterated sequences. The location of repeat sequences positioned at either the end of the viral genome (terminal repeats) or within the genome (internal repeats) means that herpesviruses can be divided into six groups, designated A to F (Figure 1.1.2.1; Roizman *et al.*, 1992). However, this proved to be unsatisfactory for taxonomic purposes.

	Herpesviruses		
	Alpha	**Beta**	**Gamma**
Prototype virus	HSV-1	HCMV	EBV
Host range	Variable	*In vivo* – narrow *In vitro* – usually fibroblasts	*In vivo* – usually narrow Specific for B or T lymphocytes
Duration of reproductive cycle	Short	Long	Variable
Cytopathic effect	Rapid infection of cell culture Destruction of cells	Slow infection Cytomegalia present	Variable
Latent infection	Usually ganglia	Secretory glands, kidneys, lymphoreticular cells	Lymphoid tissue

Table 1.1 Sub-division of herpesviruses according to their biological characteristics (adapted from Roizman *et al.*, 1981).

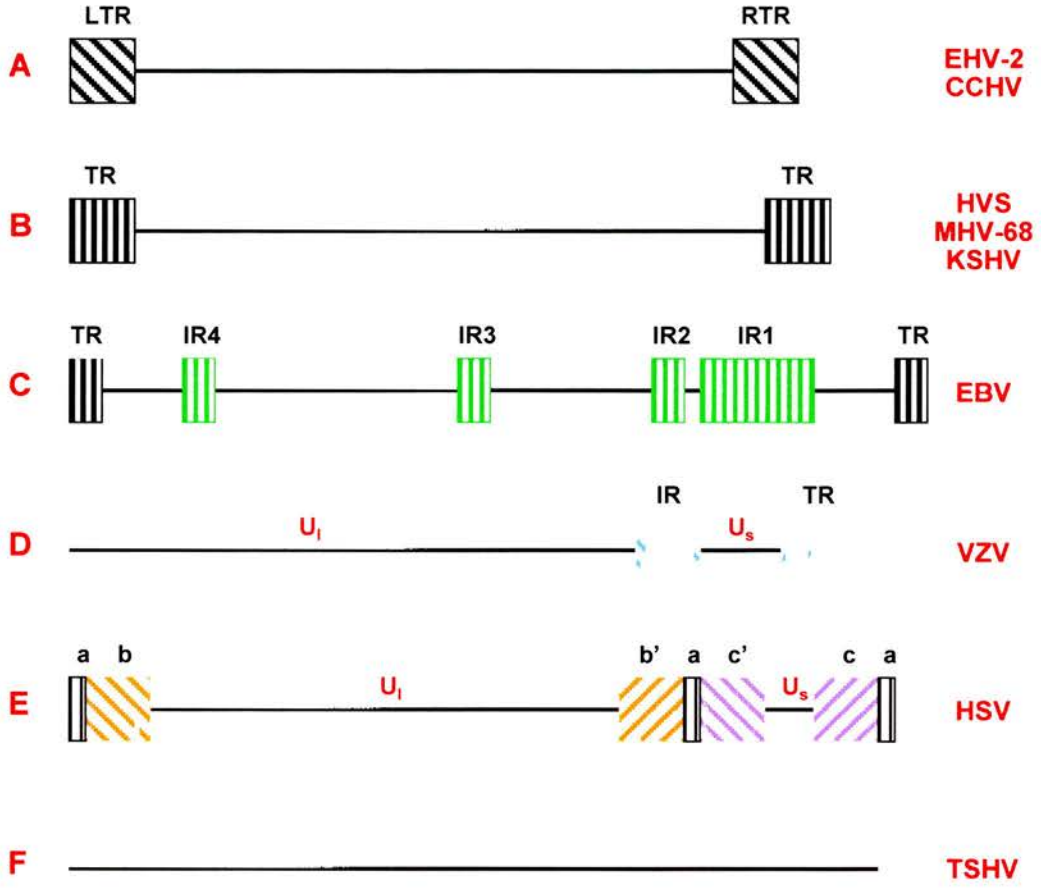

Figure 1.1.2.1 Schematic diagram of the sequence arrangements in the six classes of viral genomes (A-F) in the herpesvirus family, with examples of viruses in each class given in red on the right side. The unique region of the genome is represented by a black horizontal line. Group A viruses (such as channel catfish herpesvirus, CCHV; equine herpesvirus-2, EHV-2) contain a sequence that is directly repeated at both termini (left and right terminal repeats, LTR and RTR). Group B viruses (such as herpesvirus saimiri, HVS; murine gammaherpesvirus-68, MHV-68; Kaposi's sarcoma associated herpesvirus, KSHV) contain numerous copies of a directly repeated sequence at each termini (TR, terminal repeats). Group C viruses (such as Epstein-Barr virus, EBV) contain terminal repeat sequences like Group B viruses, but also contain unrelated internal repeat sequences (IR) greater than 100bp which divide the unique region into several well delineated stretches. In Group D viruses (such as varicella zoster virus, VZV) the sequence at one terminus (TR) is repeated in an inverted orientation internally (IR). This divides up the unique region of the genome into a short component (U_s) and a long component (U_l), and these components can invert relative to each other leading to the formation of two isomers of viral DNA. In Group E viruses (such as herpes simplex virus, HSV), sequences from both termini are repeated in an inverted orientation (b and b', c and c'), and juxtaposed internally, with a further repeat sequence (a) at the end of each termini. This means that the unique region of the genome is also divided into U_s and U_l components, which can invert relative to each other leading to the formation of four isomers of viral DNA. Group F viruses (such as tree shrew herpesvirus, TSHV) do not contain terminal repeat sequences. Adapted from Roizman *et al.*, 1992.

The development of DNA sequencing has led to the determination of the nucleotide sequence of a number of herpesviruses, and this enabled the Herpesvirus Study Group to state "nucleotide sequence data are necessarily the basis of the taxonomy of the family *Herpesviridae*" (Roizman *et al.*, 1992). Sequence analysis of viral genomes means that herpesviruses can be classified according to DNA sequence homology, conservation of genes and gene clusters, and the arrangement of these gene clusters relative to each other. This is assisted by the fact that herpesvirus genomes are compact, with open reading frames that tend to be closely spaced or even overlap. Genes can be transcribed from both strands, and use alternative initiation, polyadenylation or splice sites to give a multitude of different proteins with different functions, such as the six EBNA proteins of EBV. Fortunately, the classification of herpesviruses according to nucleotide sequence of the genome closely matches that based on biological criteria (Roizman *et al.*, 1992), with the notable exceptions of Marek's disease virus, which was reclassified as an alphaherpesvirus on the basis of its genome sequence (Buckmaster *et al.*, 1988; Lee *et al.*, 2000), and human herpesvirus 6, which was reclassified as a betaherpesvirus (Gompels *et al.*, 1995).

The division of the herpesvirus family with examples of members causing disease in humans and animals is illustrated in Figure 1.1.2.2.

1.1.3. Reproductive cycle of herpesviruses

Infection of a cell by herpesviruses can lead to two completely different outcomes. Lytic or productive replication is the replication of the virus with the release of virus progeny and consequent death of the cell. In contrast, latent infection leads to the maintenance of the viral genome as a circular episome and expression of a restricted number of viral genes. The circular episome is amplified to give multiple copies per cell (Sugden *et al.*, 1979), and these viral episomes are partitioned into the two daughter cells at mitosis. No virus progeny is generated during latent infection, although the virus can reactivate leading to production of virus by lytic replication.

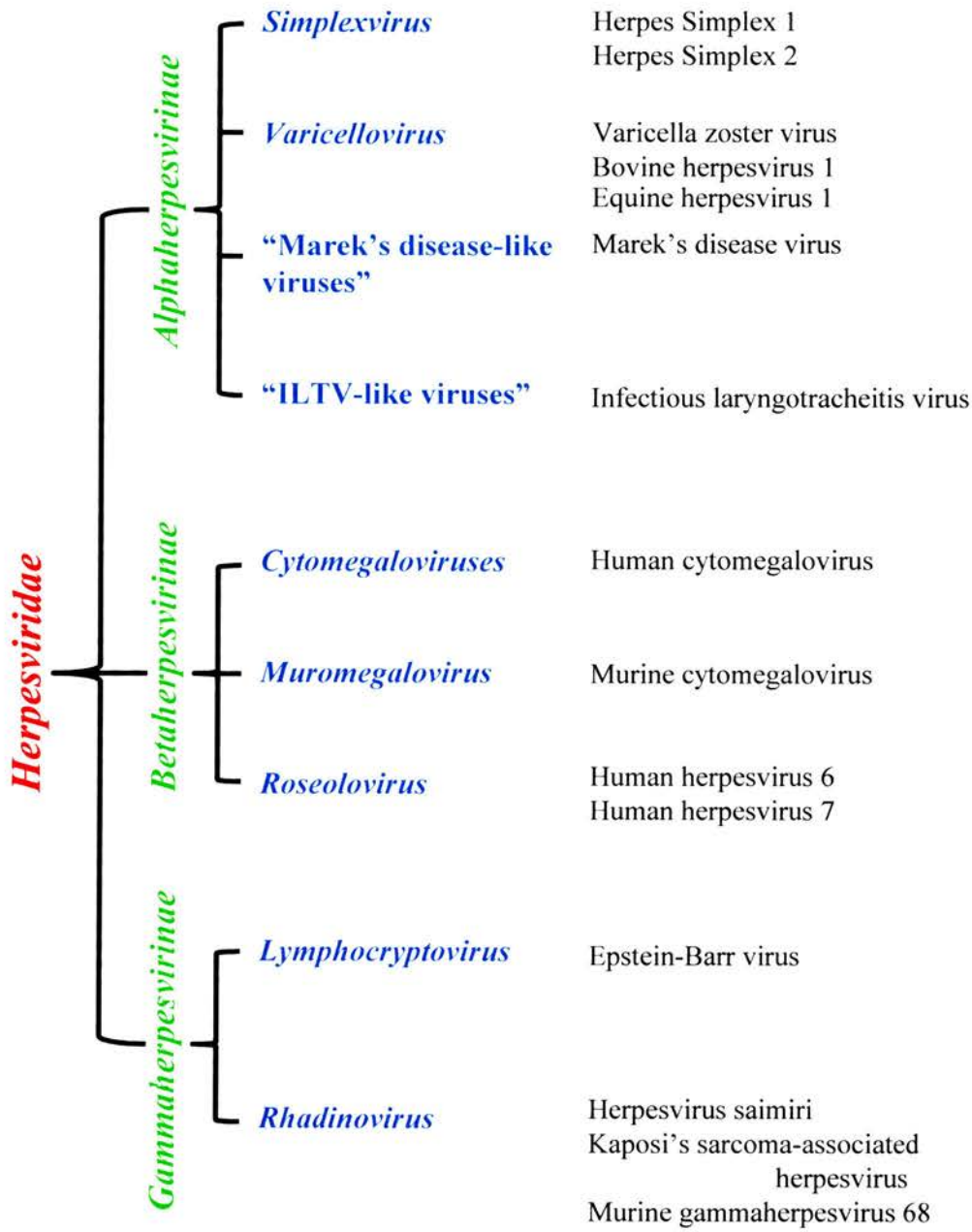

Figure 1.1.2.2 The herpesvirus family. The family *Herpesviridae* is shown in red, with the subfamilies in green and the genera in blue. Examples of each of the genera are shown on the right. Classification is according to the International Committee on Taxonomy of Viruses, available at http://www.ncbi.nlm.nih.gov/ICTV (Minson *et al.*, 2000).

1.1.3.1. Lytic replication

The vast majority of our knowledge of herpesvirus lytic replication has been amassed from the study of HSV-1 (reviewed by Roizman & Sears, 1996). The virus attaches to the cell surface via interactions of the viral glycoproteins with cell surface molecules. In the case of HSV-1, there are multiple attachment pathways including cell surface heparin sulphate and viral gB and gC, and it is thought that these multiple pathways are due to the different cell types that HSV-1 naturally infects (epithelial cells and neurons). In contrast, EBV infection of B lymphocytes is mediated by binding of the viral envelope protein gp350/220 to the cell surface complement receptor CD21 (Fingeroth *et al.*, 1984; Nemerow *et al.*, 1985; Carel *et al.*, 1990), a factor that is thought to result in the restricted host range of EBV *in vitro*. However, recent studies using viruses deleted in gp350/220 (Janz *et al.*, 2000) and demonstration of EBV infection in cells lacking surface CD21 (Yoshiyama *et al.*, 1997) suggests that there may be other mechanisms independent of gp350 that lead to EBV infection, particularly in epithelial cells (Maruo *et al.*, 2001). The attachment process initiates fusion of the viral envelope and cell plasma membrane, a process mediated by the viral glycoproteins gD, gB and gH/gL in HSV-1. Penetration of EBV into the cell is slightly different; the EBV virus particle is internalised into cytoplasmic vesicles, and the viral envelope then fuses with the vesicle membrane (Nemerow & Cooper, 1984). It is also thought that different viral glycoproteins are involved in EBV penetration into the cell as, unlike HSV-1, EBV gB is not localised to the virus envelope or cell surface (Gong *et al.*, 1987; Gong & Kieff, 1990). The glycoprotein complex gH(gp85) / gL(gp25) / gp42 has also been implicated in the penetration of EBV into cells (Wang *et al.*, 1998; Haddad & Hutt-Fletcher, 1989; Oda *et al.*, 2000). After membrane fusion, the virus is uncoated and the nucleocapsids are transported to the cell nucleus where the viral DNA is released and circularises.

Tegument proteins are also liberated during this stage, and serve important functions during HSV-1 infection. The virion host shut-off (VHS) protein causes non-specific degradation of mRNA and closes down host macromolecular synthesis in the cytoplasm (Kwong *et al.*, 1988). Another tegument protein called

VP16 (or αTIF) trans-activates the transcription of the immediate-early (or α) viral genes by host cell RNA polymerase II. HSV-1 contains five immediate-early genes (ICP0, ICP4, ICP22, ICP27 and ICP47) that are transcribed, translated in the cytoplasm and imported into the nucleus where they activate transcription of the early (or β) viral genes. ICP4 also serves to down-regulate transcription of the immediate-early genes (autoregulation). The early genes are translated in the cytoplasm, and the early proteins are involved in viral DNA replication, and include the major DNA binding protein (ICP8), thymidine kinase and DNA polymerase. Viral DNA replication is then initiated, starting from the viral origins of replication, and proceeds by the rolling circle mechanism to produce long concatemeric DNA molecules (Jacob & Roizman, 1977; Jacob *et al.*, 1979). The late (or γ) genes are then transcribed and translated, and these primarily consist of viral structural proteins and proteins needed for virus assembly and egress. The late proteins also function to down-regulate transcription of the immediate-early and early viral genes.

Viral glycoproteins are synthesised and glycosylated in the rough endoplasmic reticulum (ER), and then transported to the Golgi apparatus for further modification and processing. Mature glycoproteins are then transported to the plasma membrane of the cell. Capsids are assembled in the nucleus, and newly replicated viral DNA is cleaved into one genome lengths and packaged into these preformed capsids (Deiss *et al.*, 1986). These DNA-containing capsids bud from the inner nuclear membrane into the lumen of the ER, and therefore acquire an envelope. Two hypotheses then describe the mechanisms whereby the enveloped viral particles in the ER lumen progress to the cell surface in HSV-1 infected cells. In the luminal model, the enveloped virus in the ER is transported via exocytic vesicular transport to the Golgi for modification and processing of the precursor viral glycoproteins, and then to the plasma membrane. The envelope in the mature virions therefore originates from the inner nuclear membrane. In the de-envelopment model, the virions in the ER lumen lose this initial membrane by fusion at the outer nuclear membrane-ER, and the capsids acquire the mature viral envelope by re-envelopment at the Golgi or post-Golgi compartment. In this

model, the envelope in the mature virions therefore originates from the Golgi. Recent studies showing that retention of the viral glycoproteins gH and gD in the ER prevents their incorporation into the viral envelope of secreted virions (Browne *et al.*, 1996; Whiteley *et al.*, 1999; Skepper *et al.*, 2001) and differential ultracentrifugation which showed that enveloped virions are present in the Golgi apparatus and not lysosomes or other cellular compartments (Harley *et al.*, 2001) support the hypothesis that the final virion envelope is acquired in the Golgi and thus the de-envelopment model. Ultrastructural studies suggest that this also occurs in other alphaherpesviruses (Granzow *et al.*, 2001) and also EBV (Gong & Kieff, 1990). Tegument proteins are added during transport to the Golgi apparatus, and the enveloped virus is then transported to the plasma membrane for release by exocytosis.

1.1.3.2. Latent infection

Latent herpesvirus infection is characterised by the lifelong persistence of the viral genome in a circular episomal form, with restricted gene expression and the absence of infectious virus particles (see 1.1.1). The mechanisms that herpesviruses utilise to establish and maintain latency vary greatly between the three sub-families, and the majority of our knowledge of latent infection has emerged from the study of EBV latency *in vitro*. EBV attaches and enters B lymphocytes as previously described (see 1.1.3.1). The viral genome enters the nucleus and immediately circularises to form an episome, and a restricted number of viral genes are then transcribed. The Wp promoter initiates the transcription of messages encoding the six nuclear proteins (EBNA1-6) as a long polycistronic transcript that is spliced to give the individual mRNAs. After the early stages of latent infection (4-6 days post-infection), initiation of transcription of the EBNA proteins is switched in many cells to the nearby Cp promoter (Woisetschlaeger *et al.*, 1990), via an EBNA2-dependant enhancer (Woisetschlaeger *et al.*, 1991). Transactivation of the promoter of the three latent membrane proteins (LMP1, 2A and 2B) by EBNA2 leads to upregulation of LMP transcription (Abbot *et al.*, 1990). Two small non-polyadenylated RNAs (EBER1 and 2) are also transcribed, as are a number of complex transcripts arising from the *Bam*HI A fragment (the

BARTs). The significance of the BARTs is unclear, as no translated protein has yet been identified. The expression of all the EBV latency-associated transcripts is seen during the latency III gene expression programme, but even more highly restricted latent gene expression patterns have been demonstrated (see 1.2.1.2).

The EBNA1 protein binds to the latent viral origin of replication (*ori*P), resulting in the maintenance of the viral episome in latently infected cells (Yates *et al.*, 1985). EBNA1 also associates with metaphase chromosomes, ensuring that viral episomes are equally distributed into the two daughter cells at mitosis (Harris *et al.*, 1985). The viral episome is replicated early in S phase by cellular DNA polymerase, and latently infected cells contain multiple copies of the viral episome (Sugden *et al.*, 1979). As well as the transactivation of the latent viral genes LMP1, 2A and 2B, EBNA2 transactivates a number of cellular genes and plays an important role in the immortalisation of B lymphocytes (Cohen *et al.*, 1989). The LMP1 protein is also a viral oncogene essential for B lymphocyte immortalisation (Kaye *et al.*, 1993), and upregulates cellular activation and adhesion molecules such as ICAM-1 as well as vimentin and bcl-2. EBNA3 and 6 are also required for the immortalisation of B lymphocytes (Tomkinson *et al.*, 1993). These functions of the EBV latent proteins ensure that the infected cell enters into the cell cycle, and continuous cell proliferation occurs. The role of the EBERs is less well understood. They are dispensable for cellular transformation and replication *in vitro* (Swaminathan *et al.*, 1991), and it was thought that they might play a role in RNA splicing or viral mechanisms to counter the interferon response (Sharp *et al.*, 1993) but this has not been fully demonstrated (Swaminathan *et al.*, 1992). Recent studies using the Burkitt's lymphoma cell line Akata showed that the EBERs play a role in cellular transformation and oncogenesis (Komano *et al.*, 1999; Ruf *et al.*, 2000; Takada & Nanbo, 2001). Members of the *Rhadinovirus* genus of the gammaherpesviruses do not contain homologues of the EBV latent genes, but they do contain latent genes with similar functions. The LANA-1 protein (ORF73) of KSHV is hypothesised to tether the viral genome to the host cell chromosomes during mitosis in a similar fashion to EBNA1 (Ballestas *et al.*, 1999).

By comparison, the molecular basis of alpha and betaherpesvirus latency is poorly understood. During latent infection of neurons by HSV-1 the normal lytic cycle transcription cascade is blocked, and transcription is restricted to the production of a single mRNA called the latency-associated transcript (LAT). The LAT mRNA is spliced and a number of small ORFs (ORF-O and ORF-P) have been detected (Lagunoff & Roizman, 1994), but their translation into protein or possible function is unclear (Lock *et al.*, 2001). Changes in the normal physiology of the neuron lead to alterations in the permissiveness of the neuron to HSV-1 lytic replication, and the virus can therefore reactivate from latency. VZV establishes latency in trigeminal and dorsal root ganglia, and at least five ORFs (4, 21, 29, 62, 63) are transcribed during latent infection (Cohrs *et al.*, 1996; Kennedy *et al.*, 1999). These ORFs encode a number of immediate-early proteins involved in the transactivation of viral genes during productive infection, but their detection in the cytoplasm of latently infected cells raises the possibility that VZV maintains latency by restricting these regulatory proteins away from the nucleus (Lungu *et al.*, 1998).

Initial studies on betaherpesvirus latency were complicated by the dilemma of differentiating true latency (which indicates that recurrence would require the reactivation of lytic gene transcription) from low-level persistent productive replication (which signifies that recurrence would require the expansion of existing gene transcription programmes). Extremely sensitive techniques for the detection of infectious virus (sensitive to 1 PFU per organ) and molecular techniques such as PCR and RT-PCR demonstrated the presence of latent murine CMV in multiple organs including the lung, spleen and kidney (Yuhasz *et al.*, 1994; Pollock & Virgin, 1995; Kurz *et al.*, 1997). The presence of latent human CMV in macrophages and granulocyte-macrophage progenitor cells was demonstrated by the presence of circular viral DNA using Gardella gel analysis (Bolovan-Fritts *et al.*, 1999), and the mapping of latency-associated transcripts originating from both strands of the UL122/UL123 (*ie*1/*ie*2) region of the viral genome (Kondo *et al.*, 1996; Hahn *et al.*, 1998). However, the function of ORFs encoded by these transcripts remains unclear as some of these genes are non-essential for latent CMV infection (White *et al.*, 2000). Similar transcripts

from the *ie*1/*ie*2 region have been described during murine CMV latency (Kurz *et al.*, 1999; Grzimek *et al.*, 2001). Reactivation from latency is typically observed in the immunocompromised host, possibly via immune activation of the productive viral replication cycle (Soderberg-Naucler & Nelson, 1999).

The switch from latent infection to lytic replication in EBV is mediated by the immediate-early genes BZLF1 (Z transactivator or Zta) and BRLF-1 (R transactivator or Rta). The Zta promoter is activated by cellular factors (usually via chemical induction for *in vitro* studies) and transactivates the Zta and Rta genes, as well as the early genes. This then leads to the orderly cascade of early and late genes similar to that observed during HSV-1 lytic replication (see 1.1.3.1). Repression of the promoters of these transactivators by cellular factors prevents reactivation from latency. The other gammaherpesviruses also contain homologues of Rta (ORF50), another EBV transactivator Mta (ORF57) and Zta (ORF K8 in KSHV; Lin *et al.*, 1999). However, in contrast to EBV, it appears that the Rta performs the major role in the reactivation of HVS, KSHV and MHV-68 from latency (Sun *et al.*, 1998; Wu *et al.*, 2000; Goodwin *et al.*, 2001).

1.2. Gammaherpesviruses

The gammaherpesvirus sub-family contains a number of important human and animal pathogens and they have been intensively studied due to their association with transformation and oncogenesis. Their genomes contain genes that are shared between all known mammalian herpesviruses (e.g. thymidine kinase) as well as genes unique to the gammaherpesvirus family. Sequence analysis of the viral genomes reveals the wide diversity of the gammaherpesviruses (McGeoch, 2001).

1.2.1. The Epstein Barr Virus

EBV is the prototypic *lymphocryptovirus* (γ_1), and persistently infects over 90% of the adult human population. EBV, like the other gammaherpesviruses, has a restricted host range (see table 1.1) with humans as its natural host. The virus establishes a latent infection of circulating B lymphocytes and this latent infection

does not usually cause disease. However, in certain situations EBV is associated with lymphoproliferative disease and oncogenesis. EBV can infect and immortalise B lymphocytes *in vitro*, resulting in the generation of lymphoblastoid cell lines (LCLs), which are used to study EBV latent infection in detail (see 1.1.3.2). A small percentage of cells (approximately 5%) within the LCL population will also undergo lytic replication.

1.2.1.1. EBV-associated diseases

Asymptomatic primary infection with EBV in developing countries usually occurs in early childhood, and is contracted from persistently infected humans who shed EBV via the saliva. However, in developed countries with high standards of living, primary infection is delayed and occurs in adolescence. This delayed primary infection causes the condition infectious mononucleosis (IM), which varies in severity from a mild fever to a prolonged debilitating illness. The virus enters the body via the oropharynx, and the exact route by which EBV enters the body has been the subject of much debate. EBV can replicate in squamous epithelial cells *in vitro* (Sixbey *et al.*, 1983) and *in vivo* (Niedobitek *et al.*, 1991b), and is also associated with a range of human epithelial tumours (Imai *et al.*, 2001). Thus one hypothesis proposes that EBV initially replicates in the surface epithelial cells before infecting B lymphocytes. However, studies showing that patients with X-linked agammaglobulinaemia who lack mature B cells are not infected with EBV (Faulkner *et al.*, 1999) and sections of tonsils removed from patients with IM demonstrating infection of B cells only (Anagnostopoulos *et al.*, 1995) suggests that EBV enters the body via infection of intraepithelial resting B lymphocytes (Thorley-Lawson & Babcock, 1999; Faulkner *et al.*, 2000). The primary infection induces humoral and cell mediated immune responses, especially a CTL response to viral antigens, which serves to limit the infection. Immunodeficiency syndromes can dramatically alter the course of IM; the genetic defect X-linked lymphoproliferative syndrome is due to a mutated gene encoding the signalling lymphocytic activation molecule-associated protein (SAP; Howie *et al.*, 2000). Upon primary EBV infection, a fatal IM-like syndrome occurs characterised by B lymphocyte proliferation and dysgammaglobulinaemia.

Iatrogenic immunosupression following organ transplantation also results in lymphoproliferative disease during primary EBV infection (Hopwood & Crawford, 2000).

Following primary infection, EBV persists for life with approximately 1 in 10^6 circulating B lymphocytes carrying latent EBV. Bone marrow and lymphoid tissue are thought to be the other major reservoirs of EBV *in vivo* and, as previously mentioned, infectious virus is continuously or intermittently shed in the saliva. However, in certain individuals who become immunocompromised, the equilibrium between viral latency and immune control becomes unbalanced, and this leads to a variety of malignant conditions. The first lymphoid tumour to be associated with EBV was Burkitt's lymphoma (BL), a B lymphocyte tumour of the jaw and occasionally other sites. BL occurs in three recognised forms: endemic BL in equatorial Africa, sporadic (or non-African) BL that occurs at low incidence worldwide, and AIDS-associated BL. The EBV genome is present in 96% of endemic BL tumours (Magrath, 1990), but the association with sporadic BL is not as marked. EBV is considered to be one of the three principal co-factors in the causation of endemic BL, along with malaria (or HIV infection in the case of AIDS-associated BL) and the constitutive expression of the *c-myc* oncogene. It is postulated that EBV viral replication, in conjunction with malaria or HIV, results in polyclonal B-lymphocyte activation. The B lymphocyte proliferation leads to chromosomal translocations, t(8:14, 8:2 or 8:22), that result in the juxtaposition of the *c-myc* oncogene on chromosome 8 and the immunoglobulin heavy (chromosome 14) or light chains (chromosome 2 or 22). This leads to the constitutive expression of *c-myc*, which drives the B lymphocyte into proliferation and inhibits differentiation leading to BL (Klein & Klein, 1985). Recent studies using the Akata BL cell line have demonstrated that EBV plays a direct role in the maintenance of the tumour by upregulation of bcl-2 expression and downregulation of *c-myc* protein levels, thus circumventing cellular apoptotic pathways (Ruf *et al.*, 1999; Takada, 2001). This role of EBV in the maintenance of BL is mediated in part by expression of the EBERs (Komano *et al.*, 1999; Ruf *et al.*, 2000; Takada & Nanbo, 2001).

Nasopharyngeal carcinoma (NPC) is a squamous epithelial tumour of the post-nasal space. It is highly prevalent in southern China, where it is the most common cancer affecting men and the second commonest in women. The commonest form of NPC, termed undifferentiated NPC, is always EBV associated as demonstrated by the presence of EBV DNA in the malignant cells (Niedobitek *et al.*, 1991a) as are a proportion of the differentiated NPC cases (Raab-Traub *et al.*, 1987). Like BL, it is thought that EBV is one component of a complex process resulting in the development of NPC with other co-factors including genetic predisposition (Lu *et al.*, 1990) and environmental factors such as traditional Chinese herbal remedies and salt fish dishes containing carcinogens (Armstrong *et al.*, 1998).

Post-transplant lymphoproliferative disease (PTLD, also called B-lymphoproliferative disease) is observed in transplant patients undergoing immunosuppressive drug therapy or as an AIDS-related condition, and can occur during primary or latent EBV infection (Haque *et al.*, 1996). Over 90% of the lymphomas are EBV positive as demonstrated by the presence of viral DNA or antigens (Thomas *et al.*, 1990). It is proposed that the lymphoproliferative disease is driven by either the expression of viral oncogenes (such as EBNA2 and LMP1) or the high levels of cytokines produced by infiltrating CD4+ T lymphocytes in the lymphomas (Hopwood & Crawford, 2000). Oral hairy leukoplakia (OHL) is a benign lesion caused by lytic EBV replication in the superficial layers of the tongue epithelium (Greenspan *et al.*, 1985; Niedobitek *et al.*, 1991b). It is almost exclusively observed during HIV infection. Another condition that has been associated with EBV is Hodgkin's lymphoma (HL). EBV is associated with approximately 50% of cases of HL, due to the presence of EBV DNA in the lymphoma cells (Weiss *et al.*, 1987; Brocksmith *et al.*, 1991). It is thought that the latent EBV genes LMP1 and LMP2A are central to the pathogenesis of EBV-related HL by providing the growth and survival signals necessary for the initiation of oncogenesis (Kuppers & Rajewsky, 1998; Thorley-Lawson & Babcock, 1999). EBV has also been associated with a number of other diseases, including various T cell lymphomas (Ott *et al.*, 1992) and gastric carcinomas

(Tokunaga *et al.*, 1993) but the contribution of EBV to their causation remains unclear.

1.2.1.2. Molecular biology of EBV

The EBV genome was the first herpesvirus to be fully sequenced (Baer *et al.*, 1984), although the B95-8 strain sequenced was subsequently found to contain a 12kb deletion and this region of EBV DNA was sequenced later from the Raji strain (Parker *et al.*, 1990). It is 172kb in length, and contains a unique region flanked by reiterated 0.5kb terminal repeat sequences that covalently link to form the viral episome during latency. The unique region is divided by four reiterated 3kb internal repeat sequences. There are two subtypes of EBV, EBV-1 and 2, which share extensive homology but differ mainly in the regions of the viral genome encoding the EBNA2-6 proteins and the EBERs (Sample *et al.*, 1990). The two subtypes differ in their geographical distribution and their ability to immortalise B lymphocytes *in vitro* (Rickinson *et al.*, 1987), but these differences are not thought to reflect different disease associations.

During the latent infection of B lymphocytes *in vitro*, EBV expresses a highly restricted subset of viral genes that contribute to the maintenance of the viral genome in infected cells and B lymphocyte immortalisation (see 1.1.3.2). Several different patterns of gene expression have been observed *in vitro* and *in vivo*, and have been classified into three groups. Latency III is observed during latent infection of *in vitro* transformed LCL cells, and is characterised by the expression of all the major latent gene transcripts; namely EBNA1-6, LMP1, 2A and 2B, EBER1 and 2 and the BARTs. This latency program utilises the Wp and Cp promoters (see 1.1.3.2), and is also observed during infectious mononucleosis and PTLD *in vivo*. It is thought that Latency III gene expression is utilised by the virus to ensure growth transformation of the host cells and therefore amplify the number of latently infected cells to ensure viral persistence. In contrast, Latency I involves the silencing of the Cp/Wp promoter, and expression of only EBNA1 from the downstream Qp promoter. The only other detectable gene transcripts are the EBERs and the BARTs, and this highly restricted form of latency is seen in BL cells. Latency II also exhibits restricted expression of EBV latent genes, with

expression of EBNA1 (from the Qp promoter), LMP1, 2A and 2B, the EBERs and BARTs. Latency II gene expression is observed in NPC and HL cells *in vivo*. The significance of these different latency programmes is still the subject of much debate, but one hypothesis is that EBV is taking advantage of normal B cell biology and maturation pathways to establish lifelong persistence in the memory B cell. The viral gene expression programmes mimic the B cell activation and differentiation signals to enable EBV infected cells to survive and mature into memory B cells (Thorley-Lawson & Babcock, 1999). Another hypothesis is that EBV severely restricts latent gene expression to only express EBNA1 during the maintenance of latency to avoid detection by the immune system, as the internal repeat region in EBNA1 interferes with antigen processing and thus prevents CTL recognition of infected cells (Levitskaya *et al.*, 1995).

EBV is the most intensively studied of the gammaherpesviruses, and as more knowledge is amassed concerning its biology, the complexity of the mechanisms that EBV uses to ensure persistence and cause malignant tumours becomes apparent. However, relatively little is known about the initial events during primary infection as is demonstrated by the continuing debate concerning the role of squamous epithelium during primary EBV infection.

1.2.2. Kaposi's sarcoma associated herpesvirus

KSHV (also called human herpesvirus 8 or HHV8) is the most recently discovered human herpesvirus. A viral aetiology had long been suspected for Kaposi's sarcoma (Beral *et al.*, 1990), and the presence of unique herpesvirus DNA in over 90% of Kaposi's sarcoma lesions was confirmed by the technique of representational difference analysis (Chang *et al.*, 1994). Subsequent cloning and sequence analysis of the KSHV genome demonstrated that it was a gammaherpesvirus of the genus *Rhadinovirus* (Moore *et al.*, 1996; Russo *et al.*, 1996).

1.2.2.1. KSHV-associated diseases

Kaposi's sarcoma (KS) occurs in four distinct epidemiological forms. Classic KS is predominantly seen in elderly men in the Mediterranean, and

consists of benign indolent tumours of the extremities. Endemic KS is more aggressive, and occurs in equatorial Africa. The two most recent forms of KS recognised are AIDS-KS, a very aggressive disseminated disease with a high mortality rate, and post-transplant (or iatrogenic) KS. The involvement of an infectious agent in the pathogenesis of AIDS-KS was postulated before the isolation of KSHV due to the fact that KS is 300 times more common in AIDS patients than other immunosupressed patient groups, and 10 times more common in HIV-positive homosexual men than patients who contracted HIV through non-sexual routes (Beral *et al.*, 1990). KSHV is linked to the aetiopathogenesis of KS by the detection of KSHV sequences and gene expression in all forms of KS and KS lesions (Schalling *et al.*, 1995; Dupin *et al.*, 1999), the detection of KSHV sequences in the blood of HIV-positive individuals that predicts those who will subsequently develop KS (Whitby *et al.*, 1995) and serological studies.

KSHV is also associated with primary effusion lymphoma (PEL, also called body-cavity based lymphoma), a B cell lymphoma observed in AIDS patients (Cesarman *et al.*, 1995). Cell lines latently infected with KSHV have been established from cases of PEL, and some are also co-infected with EBV. Studies of these cell lines have greatly assisted the study of KSHV. KSHV is also associated with multicentric Castleman's disease (MCD), a lymphoproliferative disease frequently associated with HIV infection (Soulier *et al.*, 1995). Therefore, like EBV, immunosupression of the host plays a critical role in the pathogenesis of KSHV-associated diseases. The prevalence of KSHV in the general population is the subject of much current debate, but it is currently thought that unlike most other human herpesviruses, KSHV is not ubiquitous in the general population. KSHV seroprevalence in the general population is less than 5%, with a higher prevalence in Mediterranean and African countries and homosexual men (up to 50%) reflecting the higher incidence of KS in these groups (reviewed by Schulz, 2000; Boshoff & Weiss, 2001). Transmission is thought to be by sexual contact, with childhood transmission occurring in developing countries (Schulz, 2000).

1.2.2.2. Molecular biology of KSHV

The genomic sequence of KSHV has been determined from a PEL cell line and a KS biopsy specimen, and contains a 140.5kb unique region containing at least 81 ORFs flanked by reiterated 0.8kb terminal repeat sequences (Russo *et al.*, 1996; Neipel *et al.*, 1997). In common with the other rhadinovirus members, the genome contains ORFs conserved between other members of the herpesvirus family, gammaherpesvirus specific ORFs and KSHV specific ORFs (designated K1-K15). The left unique region of the KSHV genome contains the highly variable K1 ORF, which is used to subdivide KSHV strains (Zong *et al.*, 1999). K1 transforms fibroblasts *in vitro* (Lee *et al.*, 1998b), and interferes with intracellular signal transduction pathways (Lee *et al.*, 1998a; Lagunoff *et al.*, 1999). The most striking feature of the KSHV genome is the number of genes with significant homology to cellular genes, thought to have been captured from host cells ("molecular piracy", Figure 1.4.3.2). It contains cellular homologues of cell-cycle regulators (v-cyc and vGPCR), apoptosis inhibitors (vbcl-2 and vFLIP), interferon signalling pathway regulators (vIRF1) and a wide variety of cytokines, chemokines and chemokine receptors (vGPCR, vIL6, vMIP-I, II and III). The role of these genes in the pathogenesis of KSHV is the subject of much investigation (see 1.6), and is reflected in the hypotheses concerning the role of KSHV in the genesis of KS. One theory states that KSHV directly causes KS by the malignant transformation of epithelial cells, which is supported by evidence showing that most of the tumour cells are clonal in origin (Rabkin *et al.*, 1997; Judde *et al.*, 2000). However, others argue that KS is indirectly caused by the release of numerous secreted viral and cellular growth factors during viral replication (Mesri, 1999), and this is supported by evidence showing that transformation of endothelial cells *in vitro* by KSHV is dependant on paracrine mechanisms (Flore *et al.*, 1998). This is also suggested by the fact that although KSHV latently infects B lymphocytes (Cesarman *et al.*, 1995), the KS lesion is a spindle cell tumour whose cells express endothelial, smooth muscle, macrophage or dendritic cell markers and thus may be due to cellular proliferation.

Studies of latent gene expression have been carried out on PEL cell lines, which harbour episomal latent KSHV (Cesarman *et al.*, 1995). Although a small

proportion (under 1%) of these cells will undergo lytic replication, lytic replication can be induced in the majority of cells by chemical agents such as phorbol esters in a manner similar to EBV-infected cell lines. KSHV transcripts have therefore been classed as either unaffected by chemical treatment (Class I or latent transcripts), normally transcribed in PEL cells but induced to higher transcription levels by chemical treatment (Class II or latent/lytic) or only transcribed after chemical induction of lytic replication (Class III or lytic transcripts; Sarid *et al.*, 1998). These results have shown that LANA-1, v-cyc and vFLIP are transcribed from the same promoter on a polycistronic transcript as Class I (latent) transcripts (Talbot *et al.*, 1999), and another newly discovered gene (K10.5) is also expressed during latency in PEL cells (Rivas *et al.*, 2001). A variety of genes are classified as Class II, including two small polyadenylated RNA species (T0.7 and T1.1) and possibly K10 (Jenner *et al.*, 2001). Rta (ORF 50) induces the switch from latent infection to lytic replication, and leads to the orderly cascade of early and late genes (Class III) similar to that observed during HSV-1 lytic replication (see 1.1.3.1). Most of the cellular homologues encoded by the virus are expressed during lytic replication in both *in vitro* and *in vivo* biopsy specimens, suggesting that expression of these viral growth factors contributes to the pathogenesis of KS (Sun *et al.*, 1999; Jenner *et al.*, 2001).

A large amount of knowledge has therefore been amassed in a short time concerning the molecular biology of KSHV *in vitro* and in biopsy samples. However, little is known about the pathogenesis of KSHV including primary infection in humans, sites of latency *in vivo* and the contribution of the viral-encoded cellular homologues to the pathogenesis of disease.

1.2.3. Herpesvirus saimiri

HVS is the prototypic *rhadinovirus* (γ_2), and naturally infects squirrel monkeys (*Saimiri sciureus*) where it is non-pathogenic. However, in other New World primates, it causes rapidly progressing T-cell lymphomas (Fleckenstein & Desrosiers, 1982). Therefore, unlike EBV and KSHV, it is associated with the T lymphocyte population. A similar virus, herpesvirus ateles (HVA), naturally infects spider monkeys (*Ateles* spp.) and causes T-cell lymphomas in other New

World primates. HVS replicates productively *in vitro* and immortalises monkey and human T lymphocytes (Biesinger *et al.*, 1992). As such, it has been studied extensively for the investigation of virus-mediated oncogenicity and also as a vector for gene therapy, where the non-integrated viral episome can be used to express foreign DNA in a variety of human cell types (Stevenson *et al.*, 2000a; Fickenscher & Fleckenstein, 2001).

The HVS genome contains a 112.9kb unique region containing at least 83 potential genes flanked by reiterated 1.4kb terminal repeat sequences (Albrecht *et al.*, 1992). Similarly to KSHV, it contains ORFs with homology to other herpesviruses, and also a number of genes with cellular homologues including a complement control protein homologue (ORF4), vFLIP, v-cyc, vGPCR and vbcl-2. HVA has also been sequenced, and is closely related to HVS (Albrecht, 2000). Neither HVS nor HVA contain any homologues of the EBV latency-associated genes, and little is known about latent gene expression. Recent studies using a human lung carcinoma cell line containing episomal HVS DNA which can reactivate to give lytic virus upon chemical induction, showed expression of ORF71, 72 and 73 during the latent state (Hall *et al.*, 2000). These genes, corresponding to the vFLIP, v-cyc and LANA-1 homologue in HVS respectively, are also transcribed during latency in KSHV (see 1.2.2).

Of particular interest is the region at the left unique region of the HVS genome (Figure 1.4.3.2), which contains genes essential for transformation and pathogenicity (Koomey *et al.*, 1984; Desrosiers *et al.*, 1985; Murthy *et al.*, 1989). This region contains a unique gene, STP (saimiri transformation-associated protein, ORF1b) and two genes with homology to cellular enzymes (ORF2 and 3), as well as seven small RNA molecules, termed HSURs (herpesvirus saimiri U-RNAs). Based on the heterogeneity at the left unique region of the genome, HVS can be divided into three subgroups A, B and C (Medveczky *et al.*, 1984; Medveczky *et al.*, 1989). Subgroup A contains a functional STP gene, whereas subgroup B contains a non-transforming STP gene (Choi *et al.*, 2000). However, subgroup C viruses contain a functional STP gene and another unique gene TIP (tyrosine kinase interacting protein, ORF1a; Biesinger *et al.*, 1990). STP is a membrane-associated oncoprotein (Jung & Desrosiers, 1991), with subtype C

STP possessing more potent transformation and oncogenic abilities than subtype A STP (Jung *et al.*, 1991). Both STP and TIP are not required for replication and persistence *in vivo*, but are necessary for transformation and oncogenicity (Duboise *et al.*, 1998; Murthy *et al.*, 1989). It is of note that HVA contains a gene in this region of the genome that is homologous to both STP and TIP, termed TIO (two-in-one) that may have similar functions (Albrecht *et al.*, 1999). Thus the left unique region of the genome plays an important role in HVS pathogenesis.

1.2.4. Alcelaphine herpesvirus 1 and Ovine herpesvirus 2

Malignant catarrhal fever (MCF) is a generally fatal sporadic lymphoproliferative disease of domestic cattle, deer and other farm animal species characterised by hyperplasia of lymphoid tissues, T lymphocyte infiltration, vasculitis and necrosis (Reid *et al.*, 1984). It occurs in two forms; either wildebeest-associated MCF in Africa, caused by alcelaphine herpesvirus-1 (AlHV-1) or sheep-associated MCF that occurs world-wide, caused by ovine herpesvirus-2 (OvHV-2). Similarly to HVS, both viruses are non-pathogenic in their natural hosts (wildebeest for AlHV-1 and domestic sheep for OvHV-2) but cause disease when transmitted to other farm animal species or rabbits. In the natural host, the virus is thought to be transmitted at a young age but the basis of transmission from the host species to cause MCF is currently unknown.

AlHV-1 can be grown in tissue culture, and the genomic sequence has been determined (Ensser *et al.*, 1997). It contains a 130.6kb unique region containing at least 70 ORFs flanked by reiterated 1.1kb terminal repeat sequences. In common with the other rhadinovirus members, it contains ORFs with homologues in other herpesviruses and genes with cellular homologues such as vGPCR and vbcl-2. The left unique region of the AlHV-1 genome also contains a block of four unique genes (designated A1-A4, Figure 1.4.3.2), one of which is a semaphorin homologue (ORFA3; Ensser & Fleckenstein, 1995). However, little is known about the functional role of any of these genes in AlHV-1 pathogenesis. In contrast to AlHV-1, relatively little is known about the genomic structure of OvHV-2 as this virus can only be propagated in LCLs generated from animals affected by MCF, in a similar manner to EBV. Limited sequence available from

the OvHV-2 genome shows that OvHV-2 is a separate virus closely related to AlHV-1 (Bridgen & Reid, 1991; Dunowska *et al.*, 2001; J. Rosbottom, M. Ackermann, H. Reid, R. Dalziel and J. Stewart; personal communication). However, little is known about latent gene transcription or pathogenesis in either AlHV-1 or OvHV-2.

1.2.5. Other gammaherpesviruses

A number of other gammaherpesviruses have been isolated and partially characterised. Much research has concentrated on characterisation of the various lymphocryptoviruses and rhadinoviruses that infect primates as models for EBV and KSHV infection in man respectively (see 1.3). Equine herpesvirus 2 and 5 (EHV-2 and EHV-5) were also classified as gammaherpesviruses on the basis of genomic sequence (Telford *et al.*, 1993). The significance of EHV-2 as a pathogen of horses is currently uncertain, although it has been implicated in respiratory disease and immunosupression in foals (Mair, 1999). The complete genomic sequence of EHV-2 has been determined, and led to its classification as a member of the *Rhadinovirus* genera (Telford *et al.*, 1995). It contains a 149.3kb unique region containing at least 77 ORFs flanked by a 17.5kb direct repeat sequence. In common with the other rhadinovirus members, it contains ORFs with homologues in other herpesviruses and genes with cellular homologues such as three vGPCRs, vFLIP and vIL-10. Of particular interest are the large regions of non-coding DNA and the lack of a LANA-1 homologue (ORF73), which is presumed to have a similar function to EBNA-1 in the rhadinoviruses and therefore be essential for maintenance of latent infection (Ballestas *et al.*, 1999). The region at the left unique region of the genome also contains a functional CC chemokine receptor homologue (E1) with a possible role in viral immune evasion (Camarda *et al.*, 1999).

Partial sequence analysis and genomic organisation of bovine herpesvirus-4 (BHV-4) has also shown it to be a gammaherpesvirus (Lomonte *et al.*, 1996). It has been isolated from both healthy and diseased cattle, but no association with disease has been proven (Fenner, 1993). The region at the left unique region of the BHV-4 genome contains two ORFs, one unique and one with homology to

HVS ORF3 (N-formylglycinamide ribotide amidotransferase, FGARAT). A new member, porcine gammaherpesvirus, has also recently been isolated as the cause of PTLD in immunosupressed swine undergoing experimental transplantation (Huang *et al.*, 2001). This final member of the gammaherpesvirus subfamily serves to emphasise the major relationships between this varied collection of viruses: the tropism of gammaherpesviruses for lymphocytes and their association with lymphoproliferative disease and oncogenesis.

1.3. Models of gammaherpesvirus pathogenesis

A number of problems have arisen with the study of gammaherpesvirus pathogenesis. The most important viruses in the field of human medicine are EBV and KSHV, but they have an extremely restricted host range *in vivo*. Studies of natural EBV infection have been limited to the clinical presentation of infectious mononucleosis, but primary infection with these human gammaherpesviruses is frequently asymptomatic, with a substantial delay between infection and the presentation of clinical disease. Initial studies attempted to infect various primate species with EBV, but Old World primates were found to have cross-reacting antibodies due to natural infections with closely related lymphocryptoviruses (Frank *et al.*, 1976). However, New World primates such as the common marmoset (*Callithrix jacchus*) and the cottontop tamarin (*Saguinus Oedipus Oedipus*) are susceptible to EBV infection, but as these animals are not natural hosts for EBV, the disease observed does not mirror human EBV infection. Infection of the common marmoset leads to an infectious mononucleosis-like syndrome (Wedderburn *et al.*, 1984), but without the lymphadenopathy and B cell proliferation normally observed in man (Emini *et al.*, 1986). Infection of the commontop tamarin leads to the rapid development of malignant lymphomas and has therefore been used as a model of EBV tumourogenesis (Shope *et al.*, 1973), and to study candidate EBV vaccination programmes against tumourogenesis (Epstein *et al.*, 1985). Studies of viral gene expression in these lymphomas *in vivo* suggests that they do not show the characteristic latency gene programmes observed in human EBV tumours (Young *et al.*, 1989).

Due to these problems, infection of primates with simian homologues of gammaherpesviruses has been developed as models for EBV and KSHV disease. Lymphocryptoviruses (LCV) such as rhesus monkey LCV and baboon LCV are closely related to EBV genetically (Moghaddam *et al.*, 1998; Rivailler *et al.*, 2002), and cause clinical disease similar to that seen during human primary EBV infection (Moghaddam *et al.*, 1997). The recent discovery of a New World LCV with more distant homology to EBV may also provide insights into the host adaptation of these viruses (Cho *et al.*, 2001). Rhadinoviruses closely related to KSHV have also been isolated from Old World primates (Searles *et al.*, 1999; Alexander *et al.*, 2000). However, experimental infection of primates with these viruses suggests that they may develop an arteriopathy in the context of concurrent immunosupression, but not KS-like lesions (Mansfield *et al.*, 1999). However, a number of problems arise with the use of primate *in vivo* models of gammaherpesvirus pathogenesis, including expense, biosecurity and strict governmental regulation of their use. Our understanding of primate biology and their immune response, including the development of transgenic animals, is also at an early stage of development.

A number of non-primate models have therefore been developed for the study of gammaherpesvirus pathogenesis. The infection of rabbits with primate lymphocryptoviruses leads to the induction of malignant lymphomas (Hayashi & Akagi, 2000) and also hemophagocytic syndrome, a condition seen after EBV infection of humans with X-linked lymphoproliferative syndrome (see 1.2.1.1; Hayashi *et al.*, 2001). Another small animal model that has been developed is the use of the C.B-17 *scid/scid* mice (severe combined immunodeficient, SCID), which lack mature B and T lymphocytes due to a defect in lymphocyte maturation. Reconstitution of these mice with human EBV-positive lymphocytes leads to the development of B cell lymphomas that are latently infected with EBV and show Latency III gene expression (Rowe *et al.*, 1991). They thus resemble PTLD tumour in humans, and have been developed as a model for the study and treatment of PTLD in man (Johannessen & Crawford, 1999). However, due to the species differences between the primate viruses and the laboratory animal hosts,

these models are not natural infections and the murine host influences the pathology observed.

A natural gammaherpesvirus infection in laboratory animals would therefore greatly assist our understanding of gammaherpesvirus pathogenesis, by enabling the manipulation of the host immune system by the use of transgenic mice disabled for various components of the immune system, and evaluation of individual viral genes in viral pathogenesis. It would also permit the investigation of novel antiviral drugs and immunomodulatory therapies *in vivo*.

1.4. Murine gammaherpesvirus 68

MHV-68 is one of five viruses originally isolated from two species of murid rodents in Slovakia (Blaskovic *et al.*, 1980). Initial characterisation of the ultrastructural changes in infected cell cultures revealed typical features of herpesvirus infection (Ciampor *et al.*, 1981), and growth characteristics of these five isolates and their cytopathic effect *in vitro* led to their classification on biological characteristics as members of the alphaherpesvirus subfamily (see 1.1.2; Svobodova *et al.*, 1982a). However, initial studies on the pathogenesis of MHV-68 showed that laboratory mice developed a severe pneumonia with widespread haematogenous dissemination of the virus (Blaskovic *et al.*, 1984; Rajcani *et al.*, 1985), features not normally associated with alphaherpesvirus infection. Subsequent molecular characterisation and partial sequence analysis revealed close homology with the gammaherpesvirus family, and in particular HVS (Efstathiou *et al.*, 1990a; Efstathiou *et al.*, 1990b). This led to the reclassification of MHV-68 as a member of the *rhadinovirus* genera of the gammaherpesvirus subfamily, and this was confirmed by later sequence analysis of the genome (Virgin *et al.*, 1997; Nash *et al.*, 2001).

Infection of laboratory mice with MHV-68 resembles EBV infection in humans in that the primary infection leads to an infectious mononucleosis-like syndrome, and latent infection is associated with lymphoproliferative disease (see 1.4.1). MHV-68 replicates productively in tissue culture, so that virus can be grown to high titres and the viral genome can be manipulated using molecular

techniques *in vitro*. MHV-68 has therefore been used as a laboratory model for the study of gammaherpesvirus infection in a natural host, and has enabled the evaluation of potential antiviral drugs (Barnes *et al.*, 1999) and vaccination strategies (Stewart *et al.*, 1999).

1.4.1. Pathogenesis of MHV-68

The natural route of MHV-68 infection is unknown, but is likely to involve close contact and entry of the virus via the respiratory or gastrointestinal tracts, as the virus can productively replicate in the lung and intestinal epithelium (Sunil-Chandra *et al.*, 1992a; Peacock & Bost, 2000). Recent evidence from a related strain of murine herpesvirus, MHV-72 (see 1.5), suggests that neonatal transmission may occur via the mammary gland (Raslova *et al.*, 2001). Experimental transmission has also been demonstrated via the intravenous and intraperitoneal routes. Intranasal inoculation of MHV-68 results in the productive infection of alveolar epithelial cells and mononuclear cells, causing a severe interstitial pneumonia that may be fatal depending on the age of the mice (Blaskovic *et al.*, 1984; Rajcani *et al.*, 1985; Sunil-Chandra *et al.*, 1992a). Viral titres in the lung peak at day 5-7 post-infection, and infectious virus is cleared from the lungs by approximately day 14 although lymphoid accumulations remain in the lung up to 5 months post-infection (Figure 1.4.1). The virus then enters the bloodstream and is detectable in other organs in the body, including lytic replication in the adrenal glands and latent infection of B lymphocytes in the spleen (Sunil-Chandra *et al.*, 1992a; Sunil-Chandra *et al.*, 1992b). The exact method of dissemination in the body is unclear, with the current hypothesis suggesting that B-lymphocytes traffic the virus to the spleen rather than viral spread via viraemia (Stewart *et al.*, 1998b; Weck *et al.*, 1999a).

MHV-68 establishes latency in splenic B lymphocytes (Sunil-Chandra *et al.*, 1992b; Usherwood *et al.*, 1996c), and there is a characteristic expansion in the number of latently infected cells two weeks post-infection to a peak of 1 per 10^4 splenocytes latently infected (Figure 1.4.1). This peak is associated with a marked splenomegaly, as determined by a doubling in the spleen mass and the total number of spleen cells (Sunil-Chandra *et al.*, 1992a; Usherwood *et al.*, 1996a).

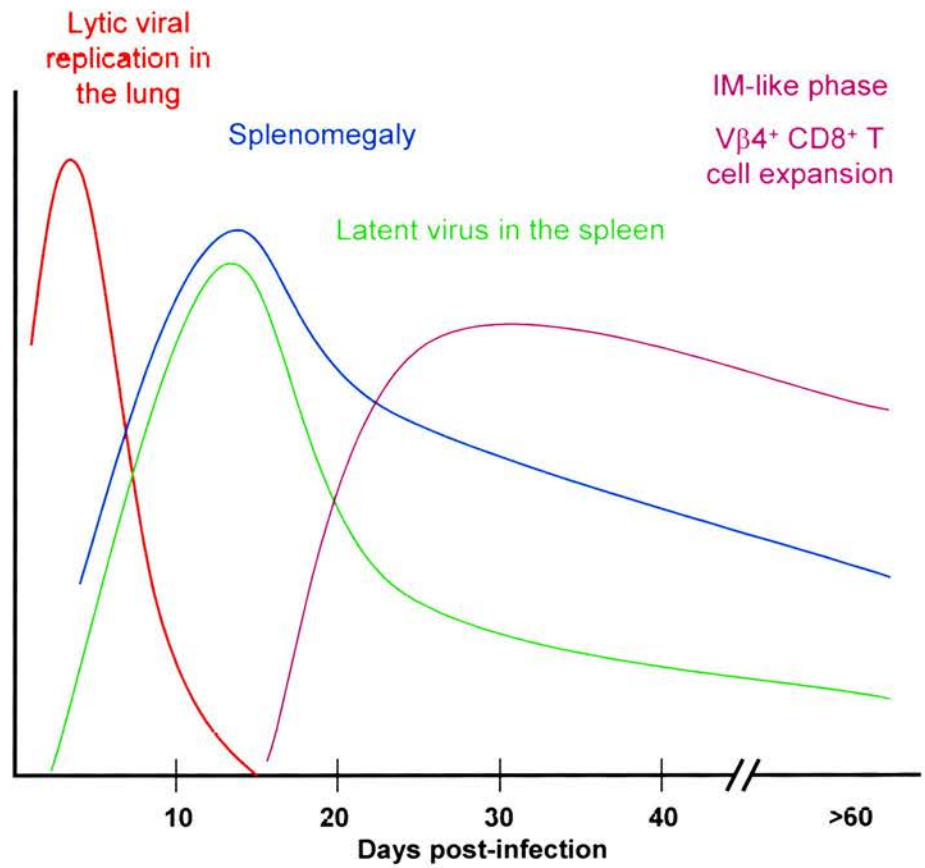

Figure 1.4.1 Schematic representation of the key events during MHV-68 infection *in vivo* after intranasal infection. Initial lytic replication occurs in the lung (red line showing viral titres in the lung) and is cleared by day 14. The virus then establishes latency in B lymphocytes in the spleen (green line showing latent virus levels), characterised by a dramatic splenomegaly (blue line showing total splenocyte numbers) which peaks at two weeks post-infection. A prolonged infectious mononucleosis-like phase then occurs at later stages post-infection (purple line showing Vβ4$^+$ CD8$^+$ T cell numbers in the circulation). Figure adapted from Coppola *et al.*, 1999.

This splenomegaly is driven by CD4+ T cells (Ehtisham *et al.*, 1993; Usherwood *et al.*, 1996a) and is dependant on the presence of MHV-68 infected B lymphocytes in the spleen (Usherwood *et al.*, 1996c; Weck *et al.*, 1996). The splenomegaly observed is similar to that seen during EBV-induced infectious mononucleosis. The levels of latent virus in the spleen then decline to stable lifelong numbers of approximately 1 in 10^6 splenocytes latently infected.

Infection of B cell-deficient mice (μMT mice which lack mature B lymphocytes) with MHV-68 showed that latency was still established in these mice (Usherwood *et al.*, 1996c; Weck *et al.*, 1996), and this led to the discovery of other cell types harbouring latent MHV-68. Linear and episomal DNA was detectable in the lungs of mice at late timepoints post-infection, and *in situ* hybridisation demonstrated the presence of latent vtRNA transcripts in lung epithelial cells in the absence of lytic transcripts, suggesting the presence of latent MHV-68 and confirming the lung as a site of viral persistence (Stewart *et al.*, 1998b). Infection of μMT mice with large doses of MHV-68 intraperitoneally leads to the establishment of latency in peritoneal exudate cells, and macrophages were demonstrated to contain latent MHV-68 in this cell population (Weck *et al.*, 1999b). Another study sorted latently infected splenocytes by FACS into B cells, macrophages and dendritic cells and demonstrated the presence of latent MHV-68 in all of these cell types (Flano *et al.*, 2000). Thus latent virus has been demonstrated in four cell types: B cells, macrophages, dendritic cells and lung epithelial cells.

In common with the other members of the gammaherpesvirus subfamily, long-term latent infection with MHV-68 is associated with lymphoproliferative disease, with approximately 10% of mice developing lymphomas or other forms of lymphoid hyperplasia (Sunil-Chandra *et al.*, 1994). Immunosupression increases this frequency to 60%, and cell lines have been generated from such tumours that harbour latent MHV-68 (Usherwood *et al.*, 1996b). A further disease syndrome was observed in mice deficient in the gamma interferon receptor (IFN-γ R-/-), and thus unresponsive to gamma interferon. Infection of these mice with MHV-68 results in splenic atrophy, characterised by a widespread destruction of

the splenic architecture and fibrosis (Dutia *et al.*, 1997). Further studies revealed that these mice also develop severe large-vessel arteritis and multi-organ fibrosis, with a consequent increase in mortality following high dose intraperitoneal infection (Weck *et al.*, 1997; Ebrahimi *et al.*, 2001). These findings have led to novel insights into the role of viruses in the development of fibrotic disorders and arteritis.

1.4.2. Immune response to MHV-68 infection

Acute productive viral replication in the lung leads to a large inflammatory response consisting mainly of mononuclear phagocytes and lymphocytes (Sunil-Chandra *et al.*, 1992a). The clearance of infectious virus from the lungs is mediated by CD8+ T cells, as demonstrated by results showing that MHV-68 infected mice depleted for CD8+ T cells using monoclonal antibodies cannot control productive viral replication (Ehtisham *et al.*, 1993), although this is dependant on other factors such as viral dose and mouse strain (Stevenson *et al.*, 1999c). Further evidence for the role of CD8+ T cells in the control of acute viral replication is shown by intraperitoneal infection of mice lacking CD8+ T cells (β_2-microglobulin gene deficient; β_2 -/-), which cannot clear infectious virus from the spleen (Weck *et al.*, 1996). A number of MHV-68 lytic cycle CD8+ T cell epitopes have been identified, with the two dominant epitopes being p56/D^b (from ORF6) and p79/K^b (from ORF61), and T cells specific for the p56 epitope dominate during the acute viral infection in the lung (Stevenson *et al.*, 1998; Stevenson *et al.*, 1999a; Liu *et al.*, 1999b). Vaccination programmes using the p56 dominant epitope significantly reduced the acute viral titres in the lung, demonstrating the role of the CD8+ T cell response in the clearance of virus from the lung (Liu *et al.*, 1999c; Stevenson *et al.*, 1999b).

CD4+ T cells appear to play a minor role in the lung during initial infection, but depletion of these cells dramatically reduces the splenomegaly and peak of latently infected splenocytes seen 2-3 weeks after infection with MHV-68 (Ehtisham *et al.*, 1993; Usherwood *et al.*, 1996a), and similar results were obtained by infection of mice with a non-functional CD4+ population due to MHC Class II disruption (Cardin *et al.*, 1996). The splenomegaly is also

dependant on the presence of MHV-68 infected B lymphocytes in the spleen (Usherwood *et al.*, 1996c; Weck *et al.*, 1996), and it is currently thought that they activate CD4+ T cells, leading to the production of elevated levels of cytokines such as IL-6, IL-10 and IFN-γ (Sarawar *et al.*, 1996), which drive the proliferation of infected B cells. Although infection of mice that lack IFN-γ or IL-6 shows no difference in splenomegaly and latently infected cell numbers as compared to wild-type controls (Sarawar *et al.*, 1997; Sarawar *et al.*, 1998), lack of responsiveness to IFN-γ leads to dramatic splenic pathology (see 1.4.1; Dutia *et al.*, 1997) and infection of mice which lack IL-10 results in enhanced splenomegaly and a reduction in the amount of latent virus (Peacock & Bost, 2001). Innate immune mechanisms also play a critical role in the immune response to MHV-68, as mice deficient in the Type I interferon response rapidly succumb to fatal MHV-68 infection (Dutia *et al.*, 1999a).

The splenomegaly and peak of latently infected cells is controlled by CD8+ T cells, as evidenced by the inability to control the viral infection in the spleen at late timepoints after either CD8+ depletion or infection of mice lacking functional CD8+ T cells (Cardin *et al.*, 1996; Weck *et al.*, 1996; Kulkarni *et al.*, 1997). Depletion of CD8+ T cells in latently infected mice lacking B cells (μMT mice) also leads to the recrudescence of infectious virus (Stewart *et al.*, 1998b), confirming a role for the CD8+ T cell subset in the control of long-term latent infection. CD4+ T cells also play a vital role in the control of latent MHV-68 infection, as demonstrated by the infection of mice with disruptions in the MHC Class II gene (Cardin *et al.*, 1996). These mice control the initial infection, but productive viral replication in the lung recurs 3 weeks post-infection leading to death of these mice by 4 months post-infection. The CD8+ T cell epitope dominating at this time post-infection switches to the p79 epitope, suggesting that there is an increase in productive viral replication leading to increased presentation of lytic cycle antigens (Liu *et al.*, 1999b; Stevenson *et al.*, 1999a). In contrast, currently only one CD8+ T cell latent epitope has been discovered, derived from the M2 gene (Husain *et al.*, 1999). The M2 gene and thus the $M2_{91-99}$ CTL epitope is only expressed transiently during the establishment of latency

up to 21 days post-infection, and the immune response against this epitope has been implicated in the control of the initial peak in latently infected splenocytes (Usherwood *et al.*, 2000; Usherwood *et al.*, 2001). High levels of anti-MHV-68 antibody are also produced by approximately 3 weeks post-infection (Usherwood *et al.*, 1996c; Stevenson & Doherty, 1998), but the fact that B cell deficient mice, which cannot produce antibodies, control MHV-68 infection suggests that antibody plays a minor role in controlling MHV-68 infection (Usherwood *et al.*, 1996c; Weck *et al.*, 1996).

Approximately three weeks after infection, a dramatic increase in the circulating activated CD8+ T cell population is observed, similar to that seen during infectious mononucleosis in humans after primary EBV infection. This increase persists for over a month (Figure 1.4.1), and the majority of these cells express the Vβ4 T-cell receptor (Tripp *et al.*, 1997). It was initially proposed that the Vβ4 T-cell receptor might bind to an MHV-68 encoded superantigen, an antigen that binds to a site on the MHC Class II outside the peptide-binding groove (thus presented by many MHC Class II alleles) resulting in the stimulation and expansion of a high frequency of CD8+ T cells (Scherer *et al.*, 1993). However, subsequent studies have shown this $V\beta4^+$ CD8+ expansion to be MHC independent and oligoclonal, arguing against the role of a superantigen (Coppola *et al.*, 1999; Hardy *et al.*, 2000). The precise nature of the ligand and the biological function of this $V\beta4^+$ CD8+ expansion remains to be determined, but appears to be dependant on CD4+ T cell assistance (Flano *et al.*, 1999).

The knowledge of the immune response to MHV-68 has been utilised to determine optimal vaccination strategies against gammaherpesviruses. Vaccination using a vaccinia virus expressing the major virion glycoprotein, gp150, dramatically reduced the splenomegaly and peak of latent virus in the spleen at two weeks post-infection (Stewart *et al.*, 1999). Vaccination using lytic cycle epitopes (the immunodominant p56 and p79 epitopes, subdominant gB epitope and CD4+ gp150 epitope) also led to a reduction in lytic viral titres and peak of latent splenic virus (Liu *et al.*, 1999c; Stevenson *et al.*, 1999b), and DNA vaccination against M2 results in a reduction in the load of latently infected

splenocytes in the initial stages of the latent infection (Usherwood *et al.*, 2001). One interesting result from these studies was that the latent and lytic viral amplification processes appear to be separate, in that high levels of acute viral replication are not necessary for the efficient establishment and amplification of latent virus (Stevenson *et al.*, 1999b). However, none of these vaccination strategies managed to prevent the establishment and maintenance of latency suggesting that multiple approaches may be necessary, and that it may not be possible to protect against the establishment of latent gammaherpesvirus infection.

1.4.3. Molecular biology of MHV-68

The MHV-68 genome contains a 118.2kb unique region containing at least 73 potential genes flanked by reiterated 1.2kb terminal repeat sequences (Virgin *et al.*, 1997; Nash *et al.*, 2001). Like the other members of the rhadinovirus genera, the genome is largely colinear with other members of the gammaherpesvirus family, containing gammaherpesvirus specific ORFs that are most closely related to homologous genes in HVS and KSHV, as well as MHV-68 specific ORFs (designated M1-14). Figure 1.4.3.1. shows a detailed schematic representation of the MHV-68 genome. Conserved herpesvirus family genes include most of the structural proteins (such as capsid proteins and virion glycoproteins) and proteins involved in DNA replication (such as DNA polymerase), and Figure 1.4.3.2 shows that the gammaherpesviruses have large blocks of collinear genes (depicted as orange, green, pink and blue blocks), interspersed with virus-specific ORFs. These virus-specific ORFs are thought to encode genes associated with latency, transformation and pathogenicity, reflecting species and cell type-specific constraints. Thus MHV-68, like the other rhadinoviruses, does not contain any of the EBV latency-associated genes, such as the EBNA or LMP genes.

MHV-68 contains a number of genes with homology to cellular genes. Two ORFs have been shown to be important in the induction of cellular proliferation. The v-cyclin gene (ORF72) has been shown to promote cell cycle progression and is oncogenic when expressed in transgenic mice (van Dyk *et al.*,

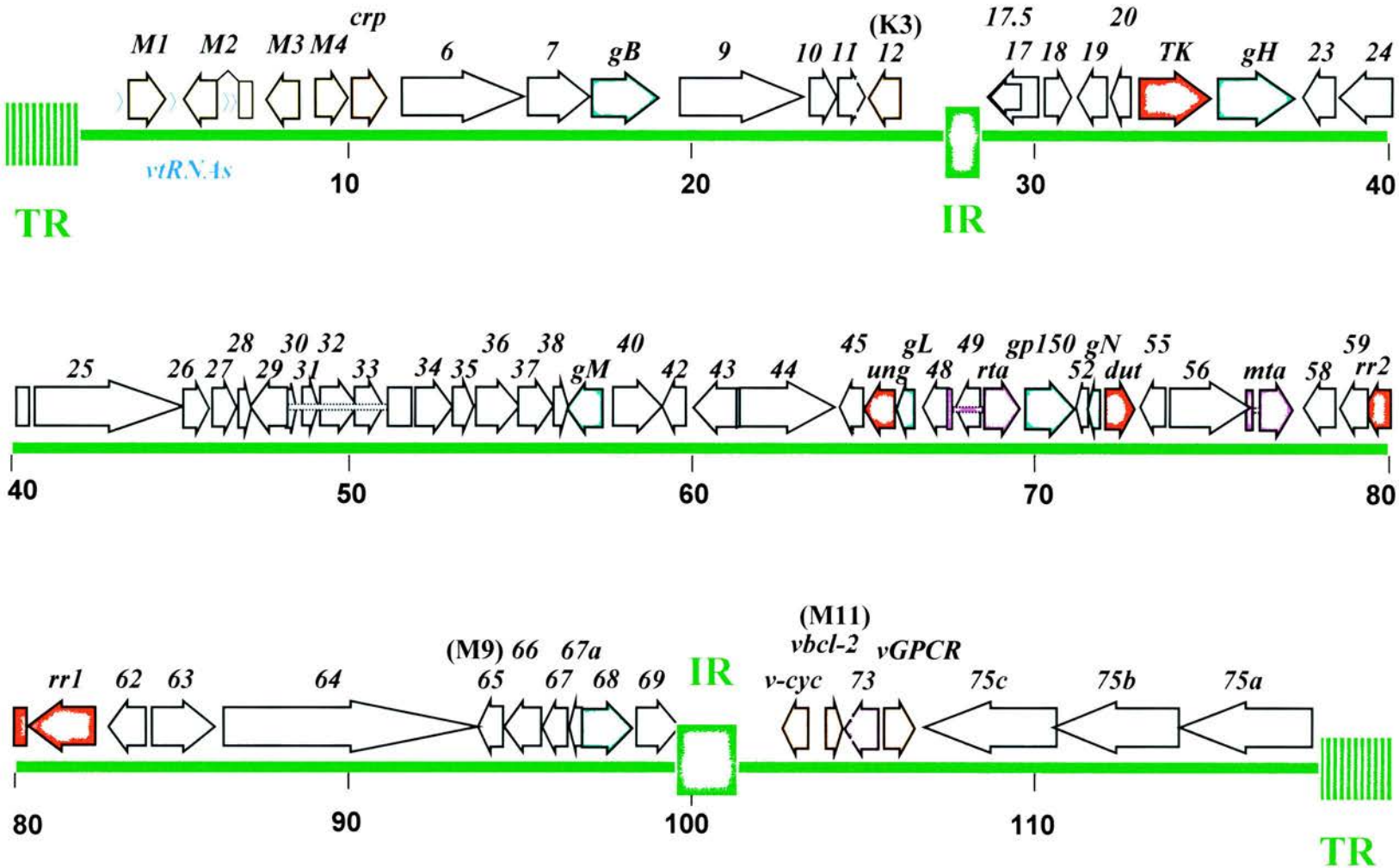

Figure 1.4.3.1 The MHV-68 genome

Figure 1.4.3.1 The MHV-68 genome. A single green line represents the unique region of the MHV-68 viral genome, with the genomic co-ordinates marked at 10kb intervals. The positions of the terminal repeats (TR) and internal repeats (IR) are indicated by the green boxes. The open reading frames (ORFs) are drawn as arrows pointing in the direction of transcription, and are labelled according to either function or designation according to Virgin *et al.*, 1997 and Nash *et al.*, 2001. Blue arrows indicate genes conserved amongst other members of the herpesvirus family, purple arrows indicate genes involved in the control of virus transcription, dark green arrows indicate MHV-68 glycoproteins, red arrows indicate genes involved in nucleotide metabolism, yellow arrows indicate genes that are unique to the MHV-68 genome and orange arrows indicate genes involved in viral pathogenesis and cellular homologues. The eight vtRNAs are represented by blue arrows. Abbreviations used: crp, complement regulatory protein; gB, glycoprotein B; K3, homologue of the KSHV K3 gene; TK, thymidine kinase; gH, glycoprotein H; gM, glycoprotein M; ung, uracil DNA glycosylase; gL, glycoprotein L; rta, R transactivator; gp150, glycoprotein 150; dut, dUTPase; mta, M transactivator; rr2, small subunit ribonucleotide reductase; rr1, large subunit ribonucleotide reductase; v-cyc, viral cyclin D homologue; vbcl-2, viral bcl-2 homologue; vGPCR, viral G-protein coupled receptor homologue. Adapted from Stewart *et al.*, 1998.

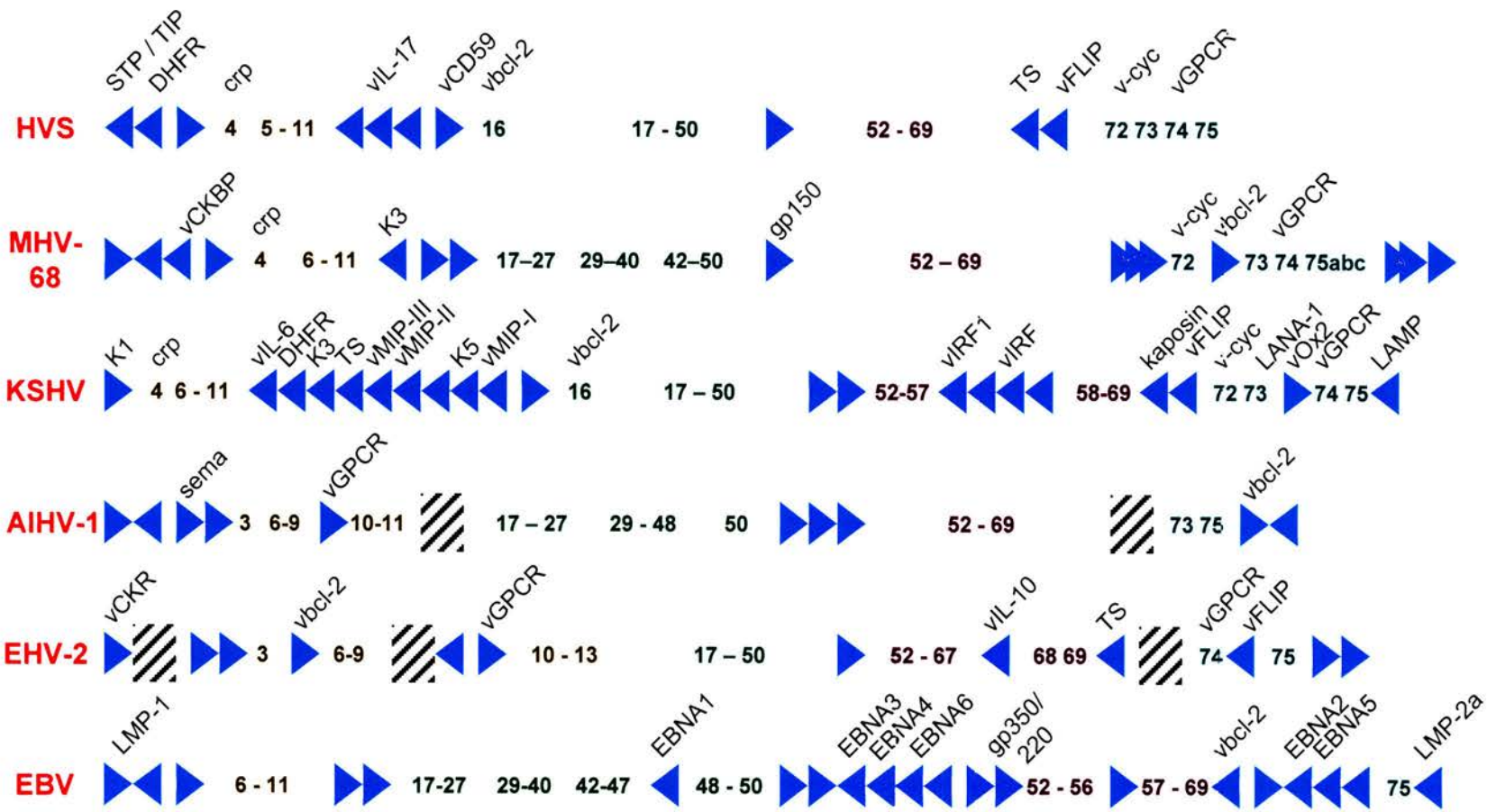

Figure 1.4.3.2 Comparison of the genomic organisation among the members of the gammaherpesvirus subfamily

Figure 1.4.3.2 Comparison of the genomic organisation among the members of the gammaherpesvirus family. The genomes of herpesvirus saimiri (HVS), murine gammaherpesvirus 68 (MHV-68), Kaposi's sarcoma-associated herpesvirus (KSHV), alcelaphine herpesvirus 1 (AlHV-1), equine herpesvirus 2 (EHV-2) and Epstein-Barr virus (EBV) are depicted schematically (not to scale). The EBV genome has been inverted relative to its conventional orientation. The four blocks of genes conserved among the members of the gammaherpesvirus family are shown (block I in orange, block II in green, block III in red and block IV in blue), with open reading frame (ORF) designations referring to the HVS numbering system. Interspersed between these conserved gene blocks are ORFs that are either virus specific or have homology to cellular genes (blue triangles pointing in the direction of transcription). These genes are involved in cell transformation, latency or pathogenesis. Large non-coding regions in the AlHV-1 and EHV-2 genomes are denoted by black diagonal lines. Abbreviations used: STP, saimiri transformation-associated protein; TIP, tyrosine kinase interacting protein; DHFR, dihydrofolate reductase; crp, complement regulatory protein; vIL, viral interleukin homologue; vCD59, viral CD59 homologue; vbcl-2, viral bcl-2 homologue; TS, thymidylate synthetase; vFLIP, viral FLICE inhibitory protein; v-cyc, viral cyclinD homologue; vGPCR, viral G-protein coupled receptor homologue; vCKBP, viral chemokine binding protein; K3 and K5, KSHV specific ORFs (also found in MHV-68) involved in downregulation of surface MHC Class I; gp, glycoprotein; vMIP, viral macrophage inflammatory protein; vIRF, viral interferon regulatory factor; LANA-1, latency-associated nuclear antigen 1; vOx2, viral Ox2 cellular adhesion molecule homologue; LAMP, latency-associated membrane protein; sema, semaphorin homologue; vCKR, viral chemokine receptor homologue; LMP, latent membrane protein; EBNA, EBV nuclear antigen. Adapted from Simas & Efstathiou, 1998.

1999), and the vGPCR (ORF74) can transform rodent fibroblast cells *in vitro* (Wakeling *et al.*, 2001). The functional significance of these genes in MHV-68 pathogenesis is uncertain, as v-cyclin is expressed only during the lytic cycle (van Dyk *et al.*, 1999) and MHV-68 cannot transform lymphocytes *in vitro* (Dutia *et al.*, 1999b), but studies using recombinant viruses deleted for v-cyclin show that it is required for efficient reactivation from latency (Hoge *et al.*, 2000; van Dyk *et al.*, 2000). MHV-68 also contains a gene with homology to the bcl-2 family, which inhibits apoptosis *in vitro* (Wang *et al.*, 1999; Roy *et al.*, 2000), and a homologue of the complement regulatory protein family, which inhibits complement activation (Kapadia *et al.*, 1999). Thus these genes with cellular homologues appear to play an important role in immune evasion during viral pathogenesis (see 1.6).

Several genes are expressed during MHV-68 latency *in vitro* and *in vivo*, including the vtRNAs, M2, M3, v-bcl2, vGPCR and LANA-1 homologue (ORF73). *In vitro* studies have utilised the S11 cell line, which contains episomal MHV-68 and is therefore analogous to the latently infected cell lines of EBV and KSHV (Usherwood *et al.*, 1996b). Northern analysis of RNA extracted from S11 cells coupled with *in situ* hybridisation studies of latently infected mouse tissues have demonstrated the expression of the M2 gene during latency, and the vtRNA-like sequences and M3 during latent and lytic infection *in vitro* and *in vivo* (Bowden *et al.*, 1997; Husain *et al.*, 1999; Simas *et al.*, 1999). These results were confirmed by further studies using RT-PCR, which showed expression of M2, M3, M9, v-bcl2, vGPCR and LANA-1 homologue (ORF73) in latently infected spleen and peritoneal exudate cells derived from B cell deficient mice (Virgin *et al.*, 1999) and M2, M3, vGPCR and v-bcl2 in the lungs and spleens of latently infected BALB/c mice (Roy *et al.*, 2000; Usherwood *et al.*, 2000; Wakeling *et al.*, 2001). The v-bcl2 and vGPCR genes are expressed from a bicistronic transcript (Wakeling *et al.*, 2001). Recent analysis of MHV-68 gene expression using an RNase protection assay suggested that K3, M8 and M9 may also be latent transcripts (Rochford *et al.*, 2001), but caution is required in the interpretation of these results as this study used mouse spleens up to day 16 post-infection when lytic replication is still occurring in the spleen (Usherwood *et al.*, 2000) and M8

and M9 are homologues of known herpesvirus lytic cycle genes (Mta and HVS ORF65 capsid protein respectively; Nash *et al.*, 2001). All these studies on MHV-68 latent gene expression suggest that MHV-68 may have multiple latent gene expression programmes similar to those observed in EBV latency, which vary depending on the cell type (B lymphocyte, dendritic cell, macrophage or epithelial cell) or organ (lung, mediastinal lymph node or spleen) latently infected, the immune response to the particular latent antigens expressed and the degree of permissiveness for lytic replication.

1.4.4. Left end of the unique region of the MHV-68 genome

The region at the left end of the MHV-68 genome is of interest as it contains four genes unique to MHV-68 (M1, M2, M3 and M4) as well as eight vtRNAs. This position of the genome in other gammaherpesviruses contains a block of virus-specific genes involved in cellular transformation (K1 of KSHV), oncogenesis (LMP1 of EBV and STP/TIP of HVS) and immune evasion (A3 in AlHV-1 and E1/vCKR in EHV-2; Figure 1.4.3.2). This region of the MHV-68 genome is hypothesised to encode a viral origin of replication (Bowden *et al.*, 1997), and readily accommodates the insertion of foreign DNA via non-homologous recombination (Simas *et al.*, 1998; D. Roy, I. Atkin, M. Wakeling, unpublished observations). However, insertion of foreign DNA into this region with no apparent disruption of known ORFs leads to alterations in viral phenotype (Clambey *et al.*, 2000; Adler *et al.*, 2001). The current data on the function of the genes in this region is summarised below.

- **M1**. This is predicted to encode a 420 a.a. protein expressed during lytic replication (Virgin *et al.*, 1999), with significant homology to the poxvirus serpins (serine protease inhibitors), which are thought to modulate apoptosis, and the MHV-68 M3 protein (see 1.6; Bowden *et al.*, 1997; Virgin *et al.*, 1997). Two studies have generated recombinant viruses deleted for the M1 gene with little effect on viral replication *in vitro* and *in vivo* (Simas *et al.*, 1998), with one study implicating M1 in the suppression of viral reactivation from latency (Clambey *et al.*, 2000).

- **M2**. Northern analysis on RNA isolated from S11 cells and *in vivo* studies using RT-PCR and *in situ* hybridisation have demonstrated that M2 is a latency-associated gene (Husain *et al.*, 1999; Virgin *et al.*, 1999), and is also expressed at low levels during lytic replication *in vitro* (Virgin *et al.*, 1999; Rochford *et al.*, 2001). It is transiently expressed during the establishment of latency, with no expression detectable in the spleen or lung after one month post-infection (Usherwood *et al.*, 2000). It is expressed as a complex spliced transcript, predicted to encode a 192 a.a. protein (Figure 5.2.1), and utilises an alternative polyadenylation signal (AGUAAA, nucleotide positions 3398-3). A recent survey of polyadenylated expressed sequence tags (ESTs) showed that this variant polyadenylation signal occurs in approximately 3% of human genes (Beaudoing *et al.*, 2000), but is polyadenylated and cleaved with an efficiency of only 30% compared to the normal AAUAAA signal (Sheets *et al.*, 1990). The M2 protein also contains an epitope recognised by the CD8+ T cell response (Husain *et al.*, 1999). Modulation of the immune response to M2 prior to MHV-68 infection, either by the adoptive transfer of M2-specific CD8+ T cells or DNA vaccination using M2 leads to a reduction in the initial load of latently infected splenocytes but not the establishment and maintenance of latency (Usherwood *et al.*, 2000; Usherwood *et al.*, 2001). It is therefore hypothesised that the recognition of the M2 protein by the immune system is important in the control of the initial peak of latently infected cells seen two weeks post-infection.

- **M3**. Northern analysis, RT-PCR and *in situ* hybridisation studies have all shown that M3 is expressed during lytic and latent infection *in vivo* and *in vitro* (Husain *et al.*, 1999; Simas *et al.*, 1999; Virgin *et al.*, 1999; Rochford *et al.*, 2001), with the detection of M3 transcripts by RT-PCR up to 10 months post-infection in the lung and spleen (Usherwood *et al.*, 2000). It is transcribed as a single early-late lytic transcript, and encodes an abundant secreted protein of 44kDa (van Berkel *et al.*, 1999). The M3 protein binds a broad spectrum of chemokines with high-affinity (including CC, CXC, C and CX_3C classes of chemokine), and blocks the interactions of chemokines with their cellular receptors thus preventing their function (Parry *et al.*, 2000; van Berkel *et al.*,

2000). Generation of an M3-deficient recombinant virus lacking chemokine-binding activity (Parry *et al.*, 2000) showed that although the lack of a functional M3 had no effect on lytic viral replication in the lung and spread of virus to the draining lymph nodes, there was a dramatic reduction in the peak of latently infected splenocytes at 2 weeks post-infection (Bridgeman *et al.*, 2001). This reduction could be reversed by CD8+ T cell depletion, suggesting that M3 is necessary to block recruitment of CD8+ T cells into the spleen.

- **M4**. Northern analysis and RT-PCR has shown that this ORF is transcribed solely during lytic replication (Simas *et al.*, 1999; Virgin *et al.*, 1999; Wan, 2002). It is predicted to encode a 459 a.a. protein, containing an N-terminal signal sequence and a heparin sulphate binding domain, and is therefore postulated to have cytokine-like properties (Wan, 2002).

- **vtRNAs**. MHV-68 encodes eight tRNA-like sequences interspersed with the ORFs in this region of the genome (Figure 1.4.3.1 and 3.2C; Bowden *et al.*, 1997; Virgin *et al.*, 1997). They are abundantly expressed during lytic replication and latent infection (Bowden *et al.*, 1997), and have therefore been used as a molecular marker of latency when their transcription is detectable by *in situ* hybridisation in the absence of detectable lytic gene transcription such as TK or gB (Stewart *et al.*, 1998b). Only three of the vtRNAs specify for amino acids, and although they are processed into mature tRNA species, they are not aminoacylated indicating that they are non-functional during normal translation (Bowden *et al.*, 1997). Four of the vtRNAs can be deleted with no effect on viral replication or pathogenesis (Simas *et al.*, 1998). As previously mentioned (see 1.2), other gammaherpesviruses encode small RNA species, including the EBERs in EBV (see 1.1.3.2) and the HSURs of HVS (see 1.2.3), which may play important roles in oncogenesis (Takada & Nanbo, 2001).

1.5. Other murine herpesvirus isolates

MHV-68 was one of five murine herpesviruses originally isolated (Blaskovic *et al.*, 1980). Strains 60, 68 and 72 were isolated from the bank vole (*Clethrionomys glariolus*) and strains 76 and 78 were isolated from the yellow-necked wood mouse (*Apodemus flavicollis*). The isolates were passaged numerous times *in vivo* and *in vitro* prior to isolation, and following ultrastructural analysis of infected cells and growth characteristics of these five isolates *in vitro*, the isolates were subsequently classified as herpesviruses (Ciampor *et al.*, 1981; Svobodova *et al.*, 1982a). However, only the pathogenesis of MHV-68 was studied in mice (Blaskovic *et al.*, 1984) and characterised further, leading to our current knowledge of MHV-68 as a model of gammaherpesvirus pathogenesis (see 1.4).

Of the other murine herpesviruses originally isolated, only MHV-72 has been characterised in detail. This strain has similar biological properties to MHV-68 in that it infects lymphocytes and peritoneal cells *in vitro* and *in vivo* (Mistrikova *et al.*, 1994), immunosupression leads to the recrudescence of latent virus (Mistrikova *et al.*, 1996a) and latent infection is associated with tumourogenesis (Mistrikova *et al.*, 1996b). Recent studies using MHV-72 showing evidence of viral replication in mammary tissue and transmission to neonatal animals via milk suggests that natural infection may occur by this route (Raslova *et al.*, 2001). Limited sequence analysis of MHV-72 has been performed, showing that the gp150 (GenBank Accession No. AF294428) and TK genes are over 99% identical at the nucleotide level to MHV-68 (Raslova *et al.*, 2000), suggesting that they are nearly identical viruses.

Apart from MHV-68 and MHV-72, few studies have been performed on the other murine herpesvirus isolates. Initial serological characterisation showed that all the isolates appeared to be very closely related antigenically (Svobodova *et al.*, 1982b), and polypeptide profiles from lytically infected fibroblasts were also very similar (Reichel *et al.*, 1991). It is of interest that MHV-68 and MHV-78 appear to lack a 46kDa protein compared to the other isolates, although this may be a cellular protein rather than a viral protein. A comparison of DNA from

MHV-76, murine CMV and rat CMV infected cells using restriction endonuclease analysis and cross-hybridisation appeared to show close homology between MHV-76 and rat CMV, leading to the conclusion that MHV-76 was a strain of rat CMV that had infected mice (Hamelin & Lussier, 1992). However none of these studies have determined the sequence of any of these isolates, and thus their relationship to MHV-68 remains unknown. One argument suggests that all the isolates are extremely similar or identical to MHV-68 as they were all isolated in the same geographical region, whereas another hypothesis suggests that the strains may have diverged reflecting the two different species that they were isolated from.

1.6. Evasion of the host response to viral infection

As gammaherpesviruses are the subject of this thesis, this review will concentrate on the immune evasion mechanisms utilised by these viruses, but examples of other viral mechanisms are also detailed where appropriate to illustrate the broad diversity of viral immune evasion strategies.

1.6.1. Immune response to viral infection

The immune response to viral infection is an extremely complex process, and is summarised in Figure 1.6.1. The first line of defence against viruses involves a series of physical barriers such as the skin, mucous membranes and stomach acid. However, once these defences are breached, the initial immune response following infection is antigen non-specific (innate response). This involves a number of effector mechanisms including type I interferons (IFN-α/β), apoptosis of infected cells, activation of complement and destruction of cells by natural killer (NK) cells, macrophages and neutrophils. Viral infection of cells upregulates IRF3 expression, leading to the activation of IFN-β. This IFN-β results in the upregulation of IRF3 and IRF7, leading to the production of IFN-α/β (Taniguchi *et al.*, 2001). IFN-α/β then bind to their cognate receptors on the cell surface, activating the Jak/STAT intracellular signalling pathway which results in the induction of a variety of anti-viral responses, including dsRNA-

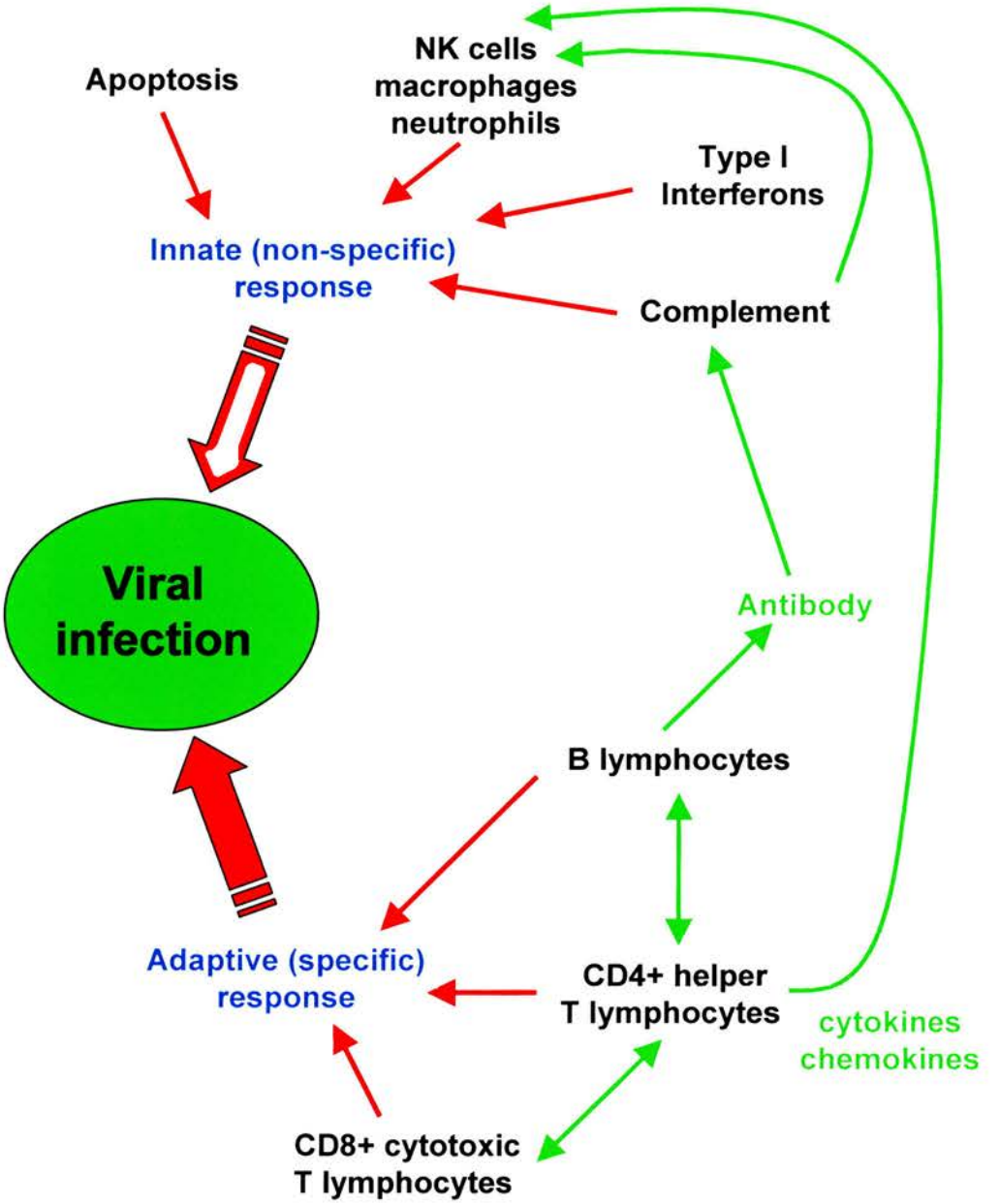

Figure 1.6.1 Overview of the immune response to viral infections. For clarity, the immune response has been divided into innate and adaptive responses. Green arrows indicate some of the many complex interactions between the two types of response that help in the co-ordination of the immune response.

dependant protein kinase R (PKR) that stops protein translation, 2'-5' oligoadenylate synthetase (OAS) that non-specifically degrades mRNA via activation of RNase L, Mx proteins that interfere with virus replication and induction of the caspase pathway leading to apoptosis of the infected cell (Goodbourn *et al.*, 2000). The vital role of type I interferons in the response to viral infections is demonstrated by studies showing that MHV-68 infection is rapidly fatal in mice with disabled type I interferon pathways (Dutia *et al.*, 1999a). Viral infection can also lead to the induction of apoptosis (programmed cell death) via the tumour necrosis factor (TNF) cytokine family or Fas receptor activation, the caspase pathway or a number of other pathways (Barry & McFadden, 1998; Everett & McFadden, 1999). Apoptosis is regulated by the bcl-2 family of proteins that includes both pro and anti-apoptotic family members, and it is postulated that in some instances apoptosis may help viruses disseminate more widely (Everett & McFadden, 1999).

Viral infection of cells also leads to the production of pro-inflammatory cytokines such as IL-1, IL-8 and MIP-1α that recruit and activate inflammatory cells such as macrophages, phagocytes and NK cells. Phagocytosis is enhanced by coating of the infected cell with antibody and complement, a process called opsonisation. During viral infection, the complement pathway is activated by antibody-antigen complexes (classical pathway) resulting in a regulated enzyme cascade that leads to either lysis of the infected cell via the membrane attack complex (MAC) or opsonisation of the infected cell and subsequent phagocytosis. The complement cascade during viral infection is therefore dependant on antibody, and thus the adaptive immune response. NK cells are cytotoxic cells that are the major effector cells of the innate immune response against virally infected cells, and are activated and recruited by type II interferon (IFN-γ). They recognise infected cells via Fc receptors (antibody mediated), and it is also thought that downregulation of MHC Class I in infected cells leads to enhanced NK cell lysis.

Viral proteins are degraded and processed into antigenic peptides by antigen-presenting cells (APC) such as dendritic cells, which then migrate to the

local lymph nodes to initiate the adaptive (specific) immune response. APCs present antigens as a complex with MHC Class II on the cell surface, and this complex is recognised by CD4+ T lymphocytes (helper T cells). This leads to activation of the CD4+ T cells via IL-1 and IL-2, resulting in clonal expansion of the antigen-specific T cell population. The CD4+ T cells secrete a number of cytokines that act to enhance the innate immune response (via IFN-γ), expand the number of T lymphocytes (via IL-2) and regulate antibody production by B lymphocytes (via IL-4 and IFN-γ). The antiviral response is held to be a predominantly Th1 response, although there are substantial areas of overlap between the two types of CD4+ T cell response. Pro-inflammatory cytokines such as IL-1, TNF-α and IFN-γ also lead to the production of chemokines, which result in migration of leukocytes to the site of viral infection (Luster, 1998). Presentation of antigen in association with MHC Class I is recognised by CD8+ T cells (cytotoxic T cells) and this leads to the lysis of the infected cells by secretion of perforin or granzymes, or the induction of apoptosis via Fas receptor binding. These CD8+ T cells also secrete IFN-γ and IL-2, leading to enhancement of the immune response to the virus.

Recognition of antigen by B lymphocytes via the B cell receptor (BCR) results in the activation and clonal expansion of the antigen-specific B lymphocyte population. These then differentiate and produce antibodies (humoral immunity), which can neutralise and precipitate viruses directly, or enhance various innate responses such as complement and phagocytosis. There are substantial interactions between B cells and CD4+ T cells; activated B cells express MHC Class II and can thus present antigen to CD4+ T cells, and IL-4, IL-5 and IFN-γ released by CD4+ T cells assists in the activation of B lymphocytes. A subset of the B and T cell populations activated during the immune response called memory cells persist for many years afterwards, and enable the immune response to respond quickly to repeated infections. Thus there are a number of complex interacting pathways involved in the immune response to viral infections, and viruses have evolved a number of different mechanisms to bypass these responses. Evidence of this is demonstrated by the vast number of genes

encoded by DNA viruses such as poxviruses and herpesviruses that are involved in immune evasion, but even the limited size of the RNA viral genomes can contain multi-functional immunomodulatory genes. Some of these genes have sequence homology to cellular genes and represent genes acquired by "molecular piracy" whereas others have no cellular homologues, representing viral genes that that have either co-evolved with the host or have cellular homologues yet to be identified.

1.6.2. Inhibition of the innate immune response

The innate immune response acts rapidly and non-specifically, and viruses must therefore overcome this response in order to replicate and produce infective progeny virions. Apoptosis can occur as a response to a variety of virally-induced stimuli (Everett & McFadden, 1999), and thus viruses have adopted a number of approaches to counteract this. One approach is to produce homologues of the cellular anti-apoptotic protein bcl-2, and this is demonstrated by the herpesvirus family. MHV-68 encodes a functional bcl-2 homologue that protects cells from Fas and TNFα mediated apoptosis (Wang *et al.*, 1999; Roy *et al.*, 2000). It is also expressed during viral latency suggesting that this protein may protect latently infected cells from apoptosis. Other herpesvirus bcl-2 homologues appear to be expressed during lytic infection only, suggesting a role during initial infection (Barry & McFadden, 1998). Another anti-apoptotic cellular homologue encoded by KSHV, HVS and EHV-2 is the vFLIP (viral FLICE-dependant apoptosis inhibitor) that interferes with apoptosis signalled through the CD95 death receptor (Thome *et al.*, 1997), and these molecules are also involved in tumourogenesis (Djerbi *et al.*, 1999). Other mechanisms by which viruses can inhibit apoptosis include the expression of proteins such as poxvirus serpins that inhibit the caspase pathway (Brooks *et al.*, 1995; Dobbelstein & Shenk, 1996), and inactivation of p53, which is also involved in the apoptotic pathway (Evan & Littlewood, 1998; Friborg *et al.*, 1999). Thus viruses can interfere at multiple stages of the apoptotic pathway.

The anti-viral effects of interferons also present a major barrier to initial viral replication in the cell. The sequestration of dsRNA is one mechanism by

which to avoid the production of IFN (Goodbourn *et al.*, 2000). However, once IFN is produced viruses can target the Jak/STAT signalling pathway to block the actions of IFN as shown by the adenovirus E1A protein (Leonard & Sen, 1996) and EBNA2 of EBV (Kanda *et al.*, 1992). Viruses can target several steps of the interferon pathway at once to ensure complete inhibition of the pathway; adenoviruses and EBV produce small RNA molecules that bind to PKR, but fail to activate it and thus act as competitive inhibitors (Sharp *et al.*, 1993; Mahr & Gooding, 1999). However, other studies suggest that the EBERs can deliberately activate the OAS pathway, possibly to prevent the production of cellular antiviral proteins (Sharp *et al.*, 1999). Inhibition of the IFN-inducible antiviral pathways (PKR and OAS/RNaseL) is achieved by a number of mechanisms such as binding dsRNA (necessary for activation of PKR) or PKR itself (Haig *et al.*, 1998; Sharp *et al.*, 1998), and the expression of cellular RNaseL inhibitors by viruses such as HIV-1 (Martinand *et al.*, 1999). The importance of this inhibition of the IFN pathway in viral pathogenesis is demonstrated by HSV mutants deleted in ICP34.5, an ORF that interferes with PKR function. This mutant virus is attenuated in normal mice, but exhibits wild-type virulence in PKR null mice demonstrating the importance of disruption of the IFN pathway in HSV pathogenesis (Leib *et al.*, 2000).

Disruption of the complement cascade is critical for the virus, both as a means of escaping the antibody response and also phagocytosis via opsonisation. Many herpesviruses and poxviruses encode complement control proteins (Kotwal, 2000), including ORF4 of MHV-68. This protein inactivates C3 convertase, reducing C3 deposition in a similar manner to HVS ORF4 (Fodor *et al.*, 1995; Kapadia *et al.*, 1999). HVS also targets another step in the complement cascade by containing a CD59 homologue that inhibits the terminal C9 polymerisation step (Rother *et al.*, 1994). Other viruses encode IgG Fc receptors, such as gE/gI of HSV-1 and the FcR of murine CMV, which bind IgG and thus prevent Fc-dependant activation of complement (Johnson *et al.*, 1988; Thale *et al.*, 1994). NK cells are another significant effector mechanism of the innate immune response, and it is hypothesised that NK cells destroy cells that do not express MHC Class I molecules (the "missing-self" hypothesis; Lanier, 1997). Thus

viruses that downregulate MHC Class I to escape CD8+ T cell cytotoxicity (see 1.6.3) may be more susceptible to NK-mediated cytotoxicity. It is of interest in this respect that the cytomegaloviruses encode MHC Class I homologues and upregulate HLA-E to inhibit NK cell activity (Farrell *et al.*, 1997; Reyburn *et al.*, 1997; Tomasec *et al.*, 2000; Tortorella *et al.*, 2000).

Co-ordination, recruitment and regulation of the innate and adaptive immune responses is performed by cytokines and chemokines, so therefore viruses have assembled a vast assortment of proteins to inhibit or modulate their activity (Alcami & Koszinowski, 2000; Lalani *et al.*, 2000; Murphy, 2001). Poxviruses contain soluble cytokine receptors that bind IFNα/β, IFN-γ, TNF and IL-1β and therefore prevent binding to their cellular receptors (Alcami & Smith, 1995), and other poxvirus proteins stop the maturation and secretion of cytokines by inhibiting the IL-1β-converting enzyme necessary to convert proIL-1β into the active form (Messud-Petit *et al.*, 1998). Due to the multiple cytokine pathways involved, secretion of a soluble IL-18 binding protein also inhibits IL-18 induced IFN-γ production (Smith *et al.*, 2000). However, viruses not only act to inhibit cytokine pathways but also use them for their advantage. The LMP-1 protein of EBV activates the TNF receptor/CD40 signalling pathway, leading to immortalisation of B cells (Farrell, 1998) and the viral IL-6 homologue encoded by the KSHV K2 gene is a B cell growth factor as well as stimulating angiogenesis, and therefore contributing to KSHV pathology (Aoki *et al.*, 1999).

Chemokines are also important effector molecules during the initial stages of the anti-viral response, trafficking leukocytes to sites of viral infection and activating them (Luster, 1998). KSHV encodes a group of chemokine homologues (vMIP-I, vMIP-II and vMIP-III), some of which are agonists that act to redirect the adaptive immune response and stimulate angiogenesis (vMIP-I; Stine *et al.*, 2000) and others that encode chemokine antagonists that act to decrease inflammation (vMIP-II; Chen *et al.*, 1998). Many poxviruses also contain chemokine homologues (Murphy, 2001), and the affinity of HIV-1 gp120 for CCR5 and CXCR4 receptors enables the virus to bind and infect cells (Littman, 1998). Several poxviruses and herpesviruses encode soluble chemokine-binding

proteins (vCKBP), which act to bind chemokines and therefore inhibit binding to their receptors (Lalani *et al.*, 2000). There are divided into three structural classes, and the broad-spectrum chemokine scavenger of MHV-68 (M3, see 1.4.4) is a member of the vCKBP-III class. These vCKBP have no known cellular homologues. The final mechanism by which viruses can subvert the chemokine pathways is by encoding chemokine receptor homologues. Some of these receptors like the E1 protein of EHV-2 are thought to enable infected cells to respond to chemokines and therefore act in subversion of the immune response (Camarda *et al.*, 1999), but other receptors such as the GPCRs encoded by KSHV and MHV-68 are constitutively active (agonist-independent), and therefore may have a role in cellular transformation (Bais *et al.*, 1998; Wakeling *et al.*, 2001). Thus viruses have adopted numerous mechanisms to not only evade the immune response, but also to utilise it for their advantage.

1.6.3. Inhibition of the adaptive immune response

Viruses such as herpesviruses that establish life-long infections also need to ensure their survival in the face of a vigorous adaptive immune response. The adaptive response requires the recognition of antigen in order to function, and therefore viruses such as HIV and influenza virus can modify their antigenic properties via random mutations (antigenic drift/shift). This variation in antigenic proteins can not only affect immune recognition but also alter proteolysis and MHC association. In order for the CD8+ cytotoxic T cell response to recognise viral antigens, the viral proteins must be degraded and then presented in association with MHC Class I (see 1.6.1). The presence of the Gly-Ala repeat sequence in EBNA-1 inhibits degradation by the proteasomes, and thus processing of EBNA-1 antigens (Levitskaya *et al.*, 1995). As EBNA-1 is thought to play an essential role in the EBV latent life cycle and be permanently expressed during latency (see 1.1.3.2 and 1.2.1), this feature is thought to prevent recognition of infected cells during latency. However, functional cytotoxic T lymphocytes specific for EBNA-1 are still found during EBV infection, and thus there appears to be another mechanism to enable the immune response to process EBNA-1 antigens. Recent research has also postulated that there may be a type of

EBV latency without expression of EBNA-1. After processing, the antigenic peptides are associated with MHC Class I and transported from the ER to the cell surface as a complex with transporter-associated with antigen processing (TAP), and HSV-1 ICP47 prevents peptide binding to the complex by interactions with TAP (Hill *et al.*, 1995). Another way in which viruses can stop surface expression of the MHC Class I-antigen complex is to retain the complex in the ER. HCMV encodes three gene products that interfere with this pathway; US3 that retains MHC Class I in the ER (Jones *et al.*, 1996), and US2 and US11 that relocate MHC Class I into the cytosol for degradation by the proteasome via recruitment of the normal cellular machinery that degrades abnormal proteins (Schust *et al.*, 1998). Proteins encoded by MHV-68 (K3) and KSHV (K3 and K5) serve to downregulate surface expression of MHC Class I via rapid endocytosis (Ishido *et al.*, 2000b; Stevenson *et al.*, 2000b). Another virus that needs to establish long-term persistence is HIV, and it encodes two proteins, Nef and Vpu, that downregulate MHC Class I expression (Kerkau *et al.*, 1997; Cohen *et al.*, 1999). To circumvent the problem of enhanced NK cell lysis due to reduced MHC Class I expression (see 1.6.2), Nef specifically targets certain HLA locus products leaving HLA-C and HLA-E locus products that inhibit NK cell activity, and KSHV also downregulates surface ICAM-1 and B7-2 receptors, which are the ligands for NK cell-mediated cytotoxicity receptors (Ishido *et al.*, 2000a). Thus all these different mechanisms to prevent antigen presentation ensure viral survival from CD8+ T cell cytotoxicity (Brodsky *et al.*, 1999; Haig, 2001).

Prevention of MHC Class II antigen presentation interferes with CD4+ T cell recognition, and thus the numerous effector mechanisms and co-ordination of the antiviral response by these T lymphocytes. Expression of surface MHC Class II is driven by IFN-γ, and thus mechanisms that disrupt interferon pathways also disrupt MHC Class II expression (see 1.6.2). The HCMV protein US2 targets MHC Class II as well as Class I molecules for degradation (Tomazin *et al.*, 1999), whereas the human papillomavirus E5 protein targets the endocytic pathway, which is necessary for transport of proteins and complexes to the cell surface (Straight *et al.*, 1993). The multifunctional Nef and Vpu proteins of HIV also target the CD4+ T cell response but by an alternative mode. Nef interacts with

CD4 at the cell surface, resulting in CD4 endocytosis and transport to the lysosomes. Vpu induces the proteasomal degradation of CD4 in the cytosol via the ubiquitin pathway (Piguet *et al.*, 1999). These two proteins therefore efficiently hijack the host cell machinery to downregulate surface CD4 molecules.

Humoral immunity (antibody) also contributes significantly to the antiviral response. The viral mechanisms of avoiding the complement pathway have already been discussed (see 1.6.2), but the viral Fc receptors also bind to antibodies, thus preventing neutralisation of the virus particles and Fc-dependant immune activation. Viral Fc receptors are particularly common in herpesviruses, and it is postulated that these receptors are especially required as latency and reactivation of herpesviruses requires replication in a previously exposed host where high-affinity antiviral antibody is present as a result of prior infection (Tortorella *et al.*, 2000). Measles virus can also bind to CD32, resulting in antagonism of signals from the B cell receptor and attenuation of antibody production (Ravanel *et al.*, 1997). A model for the establishment of latency by EBV in B lymphocytes suggests that EBV uses the normal B cell differentiation pathway to establish latency in resting memory B cells, using LMP2A to substitute for the B cell receptor and LMP1 to substitute for CD40 to provide the necessary growth and survival signals (Thorley-Lawson & Babcock, 1999). Thus the immune response is used by EBV to provide a suitable host for life-long infection.

The immune response is a highly complicated system to protect the host from infection, but viruses have evolved to evade and also utilise the immune system for their own purposes. Herpesviruses have to subvert the immune response in order to establish life-long latent infection, and the gammaherpesvirus subfamily in particular have evolved to establish latency in lymphocytes, so it is probably not surprising that they have evolved so many complex strategies with a high degree of functional redundancy to achieve this.

Chapter 2: Materials and Methods

The composition of general solutions (Appendix 1), the sequence of PCR primers (Appendix 2), plasmid vectors (Appendix 3) and commercial suppliers (Appendix 4) are detailed in the appendices at the end of Chapter 2.

2.1 Tissue culture

2.1.1. Cell lines

CELL LINE	DESCRIPTION	ECACC No.	REFERENCE
BHK-21	Baby Hamster Kidney cells Fibroblast, adherent	85011433	(Macpherson & Stoker, 1962)
COS-7	African Green monkey kidney cells. SV40 transformed Fibroblast, adherent	87021302	(Gluzman, 1981)
HeLa	Human cervical carcinoma Epithelial, adherent	85060701	(Scherer *et al.*, 1953)
293	Human embryo kidney Epithelial, adherent	85120602	(Graham *et al.*, 1977)
S11	Mouse B-lymphocyte cell line. Suspension. Contains latent MHV-68	-	(Usherwood *et al.*, 1996b)
A20	Mouse B-cell lymphoma line derived from BALB/c mice. Suspension	-	(Kim *et al.*, 1979)

Table 2.1.1 Cell lines used.

All cells were obtained from in-house stocks (Table 2.1.1). They were cultured in sterile plasticware (Nunc) and incubated at 37°C in a humidified atmosphere containing 5% CO_2. Baby Hamster Kidney (BHK) cells were grown in Glasgow's modified Eagle's medium (GMEM, Invitrogen Life Technologies) supplemented with 10% v/v new born calf serum (NBCS, Invitrogen Life Technologies), 10% v/v tryptose phosphate broth (TPB, Invitrogen Life Technologies), 70μg/ml penicillin (Merck), 10μg/ml streptomycin (Sigma) and 2mM L-glutamine (Merck). COS-7, HeLa and 293 cells were grown in Dulbecco's modified Eagle's medium (DMEM, Invitrogen Life Technologies) supplemented with 10% v/v foetal calf serum (FCS, Sigma), 70μg/ml penicillin, 10μg/ml streptomycin and 2mM L-glutamine. S11 cells were grown in Roswell Park Memorial Institute 1640 (RPMI 1640, Invitrogen Life Technologies) supplemented with 10% v/v FCS, 70μg/ml penicillin, 10μg/ml streptomycin, 50μM β-mercaptoethanol (Sigma) and 2mM L-glutamine. A20 cells were grown in RPMI 1640 supplemented with 5% v/v FCS, 70μg/ml penicillin, 10μg/ml streptomycin, 50μM β-mercaptoethanol and 2mM L-glutamine.

2.1.2. Harvesting of adherent cells

Cells were harvested by trypsinisation. The medium was decanted from the flask, and the cell monolayer washed with 0.02% w/v versene. The monolayer was then incubated with a 0.05% w/v trypsin, 0.02% w/v versene solution for approximately 3 mins, until the cells became detached from the surface of the flask. The cells were resuspended in fresh medium, transferred to a sterile universal and pelleted by centrifugation at 500 x *g* for 5 mins. The cell pellet was resuspended in 10ml fresh medium, counted and 1-5 x 10^6 cells used to reseed a new 175cm^2 tissue culture flask (Nunc) containing fresh medium.

2.1.3. Counting cells

Cells were counted by adding 50μl of cell suspension to 50μl of 0.4% Trypan Blue (Sigma), and then placing the mixture in a haemocytometer. The number of unstained viable cells was counted per 1mm square.

2.1.4. Transfection of mammalian cells by electroporation

Cells were subcultured 24 hours before transfection, so that they had achieved approximately 50% confluency on the day of transfection. The cells were harvested, counted and resuspended at 2.5 x 10^6 cells/ml. An 800µl sample of the cell suspension (2 x 10^6 cells) was added to a chilled 4mm electroporation cuvette (EquiBio), 5 - 20µg of DNA added and the suspension mixed thoroughly. The cells were then electroporated using an Easyject electroporator (EquiBio). COS-7 cells were transfected using the single pulse program (260V, 1050µF, 99mΩ). BHK-21, HeLa, 293, A20 and S11 cells were transfected using the double pulse program (600V, 25µF, 99mΩ followed by 0.1s delay then 250V, 1050µF, 99mΩ). Immediately after electroporation, the cell suspension was removed from the cuvette and resuspended in 10ml fresh medium. The cell suspension was then subcultured into 2 wells of a 6 well plate. Transiently transfected cells were harvested 24 or 48 hours post-transfection. The efficiency of transfection was estimated using a control plasmid expressing GFP (such as pEGFP-C1). The cells were examined either under ultraviolet light or by FACS analysis to determine the percentage of cells expressing GFP.

2.2 Molecular biology analysis

All molecular cloning methods were based on methods described in Sambrook *et al.*, 1989. * indicates proprietary formulations contained within kits, for which the manufacturer has not disclosed the chemical composition.

2.2.1. Polymerase Chain Reaction (PCR)

Polymerase chain reaction (PCR) reactions contained 20mM Tris [pH 8.4], 50mM KCl, 1.5mM $MgCl_2$, 0.25mM each of dATP, dGTP, dCTP and dTTP (Ultrapure dNTP set, Amersham Pharmacia), 0.2pmol of each primer, 100-500ng DNA template and 1U *Taq* DNA Polymerase (Invitrogen Life Technologies) in a final volume of 100µl. PCR primers were obtained from MWG-Biotech. Oligonucleotide sequences and pairs were as described in Appendix 2. Negative control reactions were performed using diH_20 instead of template DNA. All

reactions were set up in a contamination-free environment using barrier tips to minimise the risk of false positive reactions. PCR was carried out in thin-walled 0.5ml tubes (Hybaid) on an Omnigene thermal cycler (Hybaid). A modified "hot-start" protocol was used to ensure high product specificity. Reactions were heated to 95°C for 1 min, and then held at the annealing temperature while the *Taq* DNA Polymerase was added. 25 – 40 cycles of PCR amplification were then performed, consisting of 1 min annealing (at primer specific temperatures), extending at 72°C for 1 min/kb of product and 30 s denaturing at 95°C. The reactions were then finally incubated at 72°C for 5 mins.

DNA for cloning or sequencing was amplified using *PfuTurbo*™ DNA Polymerase (Stratagene). PCR reactions contained *PfuTurbo* DNA Polymerase reaction buffer (20mM Tris [pH8.8], 2mM $MgSO_4$, 10mM KCl, 10mM $(NH_4)_2SO_4$, 0.1% TritonX-100, 0.1mg/ml BSA), 0.25mM each of dATP, dGTP, dCTP and dTTP (Ultrapure dNTP set, Amersham Pharmacia), 0.2pmol of each primer, 100-500ng DNA template and 2.5 U of *PfuTurbo* DNA Polymerase in a final volume of 100µl. Reaction conditions were similar to those used for PCR with *Taq* DNA polymerase.

2.2.2. Purification of PCR products

Amplified DNA was purified using CONCERT™ Rapid PCR Purification System (Invitrogen Life Technologies). The PCR reaction was mixed thoroughly with 400µl of Binding Solution (H1*). The mixture was then loaded into the spin cartridge, and the DNA attached to the membrane by centrifugation at 12,000 x *g* for 1 min. The cartridge was washed with 700µl of Wash Buffer (H2*), and then dried by centrifugation twice at 12,000 x *g* for 1 min to ensure that all residual wash buffer was removed. The DNA was recovered by the addition of 50µl TE at 65°C, followed by a 1 min incubation and centrifugation at 12,000 x *g* for 2 mins.

2.2.3. Agarose gel electrophoresis

DNA was analysed by electrophoresis on an agarose gel containing 0.8-3% agarose (SeaKem®, Flowgen) and 0.5µg/ml ethidium bromide (Sigma) in

TAE buffer. The DNA samples were made up to 10-15µl volume with TE, and mixed with 2µl gel loading buffer (15% w/v Ficoll type 400, 0.25% w/v bromophenol blue and 0.25% w/v xylene cyanol or 0.25% w/v Orange G in diH_20). Samples were loaded into the wells, and electrophoresis was carried out in a horizontal tank (BIO-RAD) containing TAE buffer at 70V. DNA molecular weight markers (1µg of 1kb DNA ladder or 1kb Plus DNA ladder, Invitrogen Life Technologies) were used as molecular size standards to estimate the size of DNA bands. DNA bands were visualised under ultraviolet light using an ultraviolet transilluminator (UVP). Images were photographed and stored onto a Personal Computer disk.

2.2.4. Extraction of DNA

DNA was purified by phenol : chloroform extraction. A mixture of phenol (equilibrated to pH 7.8): chloroform: iso-amyl alcohol (25:24:1 v/v) was added to an equal volume of DNA in a 1.5ml Eppendorf tube, and mixed by vortex for 2 mins. After centrifugation at 10,000 x *g* for 3 mins, the aqueous phase was removed to a clean Eppendorf and the process was repeated until no protein debris was observed at the interface between the aqueous and non-aqueous phases. Remaining phenol was then removed by adding a mixture of chloroform : iso-amyl alcohol (24:1 v/v) to an equal volume of the DNA, mixed by vortex for 2 mins and then centrifugation at 10,000 x *g* for 3 mins. The aqueous phase was then removed to a clean Eppendorf, and the DNA concentrated by ethanol precipitation.

2.2.5. Ethanol precipitation

DNA was precipitated by the addition of 0.3 volumes 7.5M ammonium acetate or 0.1 volumes 3M sodium acetate [pH5.2], and then 3 volumes of 96% ethanol (at -20°C). The mixture was mixed thoroughly, and incubated at -20°C for at least 1 hour. The precipitated DNA was recovered by centrifugation at 12,000 x *g* for 5 mins, washed with 70% ethanol, air-dried for 2-5 mins and resuspended in an appropriate volume of TE or diH_20.

2.2.6. Quantification of DNA

DNA concentration was quantified using two methods. Approximate concentrations were obtained by agarose gel electrophoresis of an appropriate volume of DNA, and then comparing the intensity of the DNA to a sample with a known DNA concentration (1kb DNA ladder, Invitrogen Life Technologies). Accurate DNA concentration was measured using a fluorometer (DyNA Quant 200, Hoefer, Amersham Pharmacia). DNA was diluted 1:1000 into 0.2M NaCl, 10mM Tris [pH7.4], 1mM EDTA containing 0.1μg/ml bisbenzimide (Hoechst H33258, Amersham Pharmacia). Binding of the Hoechst dye to DNA results in a shift in the emission spectrum of the dye that can be measured using a photodetector. The DNA concentration was calculated by comparing this shift to that obtained with a 100ng/ml DNA standard.

2.2.7. Restriction enzyme digestion

DNA restriction enzymes were obtained from either Invitrogen Life Technologies or New England Biolabs. They were used according to manufacturer's instructions with recommended buffers (supplied as 10 times working concentration). DNA restriction digests were typically carried out for 2 hours at 37°C, in a suitable volume containing 10 units of enzyme per 1-10μg of DNA.

2.2.8. Generation of deletions using Exonuclease III and Mung Bean Nuclease

A series of deletions in the M2 gene of MHV-68 were generated using Exonuclease III. Cosmid clone A8 (cA8) contains MHV-68 DNA (nucleotide sequence 115,165-26,842 (see Appendix 3)). A 10μg sample of cA8 was digested for 3 hours at 37°C with *Sal*I (Invitrogen Life Technologies). *Sal*I cuts cosmid A8 once at position 4336-4341 (MHV-68 co-ordinates), which is within the M2 ORF. The digestion was extracted twice with phenol : chloroform : iso-amyl alcohol and once with chloroform : iso-amyl alcohol (see 2.2.4). All extractions were performed gently on a rotating wheel with wide bore tips to avoid shearing of the

linearised DNA. The extracted DNA was precipitated with 96% ethanol, washed once with 70% ethanol and resuspended in 20µl 10mM Tris [pH8.5]. Examination of 1µl of the digest by agarose gel electrophoresis showed that the cosmid was completely linearised.

The DNA was resuspended in 50mM Tris [pH8], 5mM $MgCl_2$, 10µg/ml yeast tRNA (Invitrogen Life Technologies) and 10mM β-mercaptoethanol in a final volume of 150µl. The reaction mixture was equilibrated to 23°C for 5 mins, and then 200U of Exonuclease III (Invitrogen Life Technologies) was added and the mixture gently mixed by inverting. The reaction was kept at 23°C and 25µl aliquots (containing approximately 1.5µg of cosmid A8 DNA) of the reaction mixture were removed at 0 s (before the addition of the Exonuclease III), 20, 40, 60, 80 and 100 second intervals after the addition of the enzyme. The aliquots were added to 175µl Mung Bean Nuclease buffer (10mM sodium acetate [pH5], 0.1mM zinc acetate, 1mM L-cysteine, 50mM NaCl, 5% v/v glycerol) and kept at -80°C until all the aliquots were taken. The samples were heated to 68°C for 15 mins, and then placed on ice.

Each sample was then mixed gently by inversion with 7.5U of Mung Bean Nuclease (Invitrogen Life Technologies) and incubated at 30°C for 30 mins. The samples were then made up to 250µl total volume containing 0.4% w/v SDS, 50mM Tris [pH 9.5] and 0.8M LiCl, gently extracted once with phenol : chloroform : iso-amyl alcohol, once with chloroform : iso-amyl alcohol and precipitated with 96% ethanol. The pellet was washed in 70% ethanol, air-dried and resuspended in diH_20. A ligation mixture containing the cosmid DNA was incubated overnight at 4°C (see 2.2.10) and used to transform ElectroMAX DH10B™ bacteria (Invitrogen Life Technologies) by electroporation.

2.2.9. De-phosphorylation of linearised plasmid DNA

To stop self re-ligation of plasmid vectors, the 5'-phosphate group on each end of linearised plasmid DNA was removed using calf intestinal alkaline phosphatase (Roche). Following restriction enzyme digestion, 20U of alkaline phosphatase was added to the reaction mixture and incubated at 37°C for 20 mins.

The reaction was stopped by extraction with phenol : chloroform, and the DNA was recovered by ethanol precipitation.

2.2.10. Ligation of DNA fragments

Ligation reactions were set up using approximately 50-100ng of linearised plasmid DNA and 250-500ng of DNA fragments (1 : 5-10 ratio of plasmid : fragments). The reaction mixture contained T4 DNA ligase buffer (50mM Tris [pH7.6], 10mM $MgCl_2$, 1mM ATP, 1mM DTT, 5% w/v polyethylene glycol-8000, Invitrogen Life Technologies) and 1U T4 DNA ligase (Invitrogen Life Technologies) in a final volume of 20µl. All ligation reactions included negative controls, containing diH_20 instead of DNA fragments to check for self-ligation of the plasmid. Ligation was performed overnight at 4°C.

2.2.11. Transformation of competent bacteria by heat pulse

Escherichia coli bacteria (Epicurian Coli® XL1-Blue competent cells, Stratagene) were transformed according to the manufacturer's protocol. Competent cells were thawed on ice, and a 50µl aliquot was placed into prechilled 15ml Falcon polypropylene tubes. β-mercaptoethanol was then added to a final concentration of 25mM, and the tubes gently mixed on ice for 10 mins. 1µl of the ligation mixture or 50ng of DNA was then added, and the mixture incubated on ice for 30 mins. The tubes were placed at 42°C for 45 s, and then chilled on ice for a further 2 mins. SOC medium (900µl) was then added, and the tubes incubated at 37°C for 1 hour with shaking. A 100µl sample of this mixture was spread onto LB agar plates containing the appropriate antibiotic selection agent (either 100µg/ml ampicillin or 30µg/ml kanamycin, Sigma). The remaining transformation mixture was pelleted by centrifugation at 4,000 x *g* for 2 mins, and the bacterial pellet resuspended in 100µl medium and spread onto another LB agar plate. Plates were incubated overnight at 37°C, and examined for the number of colonies. Plates were stored wrapped in parafilm at 4°C for up to 2 weeks, and bacterial stocks in 15% glycerol were stored at -80°C.

2.2.12. Transformation of competent bacteria by electroporation

Escherichia coli bacteria (ElectroMAX DH10B™ Cells, Invitrogen Life Technologies) were transformed according to the manufacturer's protocol. The DNA was purified and concentrated using a Microcon® YM-30 (Millipore) centrifugal filter device. The DNA was added to the filter device and dried by centrifugation at 12,000 x *g* for 7 mins. The filter device was then washed twice with 200µl di$H_2$0, followed by centrifugation at 12,000 x *g* for 7 mins. The DNA was recovered by adding 50µl of di$H_2$0 to the device, and the sample reservoir was then inverted into a clean Eppendorf and the DNA solution recovered by centrifugation at 12,000 x *g* for 30 s.

A 4µl sample of the purified DNA was then added to a chilled 0.75ml Eppendorf tube. ElectroMAX DH10B™ Cells were thawed on ice, and a 40µl aliquot of the cells was added to the DNA in the tube. The mixture was transferred to a chilled 2mm electroporation cuvette (EquiBio), and electroporated using a single pulse (2500V, 25µF, 156mΩ, 0.004 s). SOC medium (1ml) was then immediately added, and the cell mixture incubated at 37°C for 1 hour with shaking. The bacteria were then spread onto LB agar plates containing the appropriate antibiotic selection agent (see 2.2.11) and incubated overnight at 37°C.

2.2.13. Isolation of DNA from agarose gels

DNA bands were excised from agarose gels using a scalpel blade under ultraviolet light. The agarose gel slice was inserted into clean sterile dialysis tubing (Visking size 2-18/32″, Medicell) and 300µl TAE added. All air bubbles were removed and the tubing sealed at both ends. The dialysis tubing was placed in a mini-gel tank and subjected to electrophoresis at 80V for 1 hour. The current was briefly reversed for 30 s to remove DNA from the side of the tubing. The TAE solution containing the DNA was transferred to a clean Eppendorf tube, and the DNA extracted using phenol : chloroform and recovered by ethanol precipitation.

2.2.14. Small scale preparation of plasmid DNA (mini-prep)

Mini-preps were usually performed using the alkaline lysis method. A single bacterial colony was grown overnight at 37°C with shaking in 10ml LB medium containing either 100μg/ml ampicillin or 30μg/ml kanamycin. A sterile flamed loop was used to streak out a sample of the overnight culture onto LB agar plates containing the appropriate selective antibiotic. The bacterial suspension was pelleted by centrifugation at 4,000 x *g* for 5 mins, and the bacterial pellet resuspended in 200μl of Solution I (50mM glucose, 25mM Tris [pH8], 10mM EDTA, 100μg/ml RNase A (QIAGEN), 1mg/ml lysozyme (Sigma)) and incubated at RT for 15 mins. The solution was then gently mixed by inversion with 400μl of Solution II (0.2N NaOH, 1% w/v SDS), and incubated on ice for 5 mins. Solution III (300μl of 5M potassium acetate, 12% v/v glacial acetic acid [pH4.8]) was added, gently mixed by inversion and incubated on ice for 10 mins. After centrifugation at 10,000 x *g* for 5 mins, the supernatant was removed to a new Eppendorf tube. The nucleic acids were precipitated by the addition of 500μl isopropanol and the solution was incubated on ice for 15 mins. After centrifugation at 10,000 x *g* for 5 mins, the supernatant was removed and the pellet air dried. The pellet was resuspended in 200μl TE, then 100μl of 7.5M ammonium acetate was added and the mixture incubated on ice for 15 mins. Precipitated debris was pelleted by centrifugation at 10,000 x *g*, the supernatant was transferred to a fresh tube and the DNA precipitated using 600μl of 96% ethanol at -20°C for 1 hour. The DNA was pelleted by centrifugation at 10,000 x *g* for 5 mins, washed with 70% ethanol, the pellet was air-dried and resuspended in 20μl TE.

High quality plasmid DNA for sequencing and small scale cosmid DNA preparations were prepared using a QIAprep® Spin Miniprep Kit (QIAGEN) according to the manufacturer's instructions. A single bacterial colony was grown overnight at 37°C with shaking in 10ml LB medium containing the appropriate selective agent. The bacterial suspension was pelleted by centrifugation at 4,000 x *g* for 5 mins, and the bacterial pellet resuspended in 250μl of Buffer P1*. Buffer P2* (250μl) was added, the Eppendorf tube mixed by gentle inversion and

incubated for 5 mins. Buffer N3* (350µl) was added, the solutions mixed gently by inversion and the insoluble fraction pelleted by centrifugation for 10 mins at 10,000 x *g*. The supernatant was placed in a QIAprep spin column and the DNA attached to the membrane by centrifugation at 10,000 x *g* for 1 min. The QIAprep spin column was washed by centrifugation (10,000 x *g*, 1 min) firstly with 500µl Buffer PB* and then 750µl Buffer PE*, and then dried by centrifugation at 10,000 x *g* for 1 min to remove residual wash buffer. The DNA was eluted from the column using 50µl Tris [pH8.5]. Cosmids were eluted with 50µl Tris [pH8.5] heated to 70°C.

2.2.15. Large scale preparation of plasmid DNA (maxi-prep)

Large scale plasmid purification was performed using anion exchange columns (EndoFree Plasmid Maxi Kit, QIAGEN) according to manufacturer's instructions. An overnight bacterial culture (250ml) was pelleted by centrifugation at 6,000 x *g* for 15 mins at 4°C, and the bacterial pellet resuspended in 10ml of Buffer P1 (50mM Tris [pH8], 10mM EDTA, 100µg/ml RNase A). Buffer P2 (10ml of 200mM NaOH, 1% SDS) was then added, the solutions mixed by gentle inversion and incubated at RT for 5 mins. Buffer P3 (10ml of 3M potassium acetate [pH5.5]) was then added, mixed gently by inverting and after 10 mins incubation, the mixture was filtered using a QIAfilter cartridge. Buffer ER* (2.5ml) was added to the filtrate, mixed by inversion and incubated on ice for 30 mins to remove endotoxins. A QIAGEN-tip 500 anion exchange column was equilibrated using 10ml of Buffer QBT (750mM NaCl, 50mM MOPS [pH7], 15% isopropanol, 0.15% TritonX-100), and the filtered lysate applied to the equilibrated column. The column was then washed twice with 30ml Buffer QC (1M NaCl, 50mM MOPS [pH7], 15% isopropanol), and the DNA eluted with 15ml Buffer QN (1.6M NaCl, 50mM MOPS [pH7], 15% isopropanol). The DNA was precipitated with 0.7 volumes isopropanol, pelleted by centrifugation at 15,000 x *g* for 30 mins at 4°C, and the DNA pellet washed twice with 5ml of 70% ethanol. The DNA pellet was air dried, and resuspended in 200µl TE.

2.2.16. Large scale preparation of cosmid DNA (maxi-prep)

Large scale cosmid purification was performed using anion exchange columns (QIAGEN Large-Construct Kit, QIAGEN) according to manufacturer's instructions. Composition of buffers was identical to EndoFree Plasmid Maxi Kit unless otherwise stated (see 2.2.15). An overnight bacterial culture (500ml) was pelleted by centrifugation at 6,000 x *g* for 15 mins at 4°C, and the bacterial pellet resuspended in 20ml of Buffer P1. Buffer P2 (20ml) was then added, the solutions mixed by gentle inversion and incubated at RT for 5 mins. Buffer P3 (20ml) was then added, mixed gently by inversion and incubated on ice for 10 mins. The cell debris was pelleted by centrifugation at 20,000 x *g* for 30 mins at 4°C, and the supernatant filtered to remove all particulate matter. The DNA was precipitated by the addition of 0.6 volumes isopropanol, and pelleted by centrifugation at 15,000 x *g* for 30 mins at 4°C. The DNA pellet was washed with 5ml of 70% ethanol, the pellet air dried and redissolved in 9.5ml Buffer EX (50mM Tris [pH8.5], 10mM $MgCl_2$). ATP-dependant Exonuclease (200µl) and 100mM ATP (300µl) were added to the DNA solution, and incubated for 60 mins at 37°C. This exonuclease digestion step removed contaminating genomic DNA and damaged cosmid DNA, but did not digest supercoiled cosmid DNA. Conditions to allow DNA binding to the column were adjusted by the addition of 10ml of Buffer QS (1.5M NaCl, 100mM MOPS [pH7], 15% isopropanol) to the DNA solution. A QIAGEN-tip 500 anion exchange column was equilibrated using 10ml of Buffer QBT, and the adjusted DNA solution applied to the equilibrated column. The column was then washed twice with 30ml Buffer QC and the DNA eluted with 15ml Buffer QF (1.25M NaCl, 50mM Tris [pH8.5], 15% isopropanol) at 65°C. The DNA was precipitated with 0.7 volumes isopropanol, pelleted by centrifugation at 15,000 x *g* for 30 mins at 4°C, and the DNA pellet washed twice with 5ml of 70% ethanol. The DNA pellet was air dried, and resuspended in 200µl TE.

2.2.17. Preparation of purified viral DNA for sequencing

Ten 175cm^2 tissue culture flasks of BHK-21 cells were infected with virus in suspension at a Multiplicity of Infection (MOI) of 0.1 (see 2.5.1). When 100% cytopathic effect was observed after 4 days, the cells were scraped off into the medium and pelleted by centrifugation at 500 x *g* for 20 mins at 4°C. The supernatant was transferred to a sterile centrifuge bottle, and the virus particles were pelleted by centrifugation at 22,100 x *g* for 2 hours at 4°C, and the pellet was resuspended in 3ml sterile PBS. The virus particles were layered on top of a sorbitol gradient (20% D-sorbitol in PBS), and pelleted by centrifugation at 141,000 x g for 80 mins at 4°C. The viral pellet was resuspended in 500µl DNase buffer (40mM Tris [pH8], 10mM $MgSO_4$, 1mM $CaCl_2$), and 20U of DNase I (Sigma) was added and incubated at 37°C for 20 mins. High Molecular Weight DNA Extraction buffer (5ml of 0.2M Tris [pH8], 0.1M EDTA, 0.5% SDS) was added to the DNA solution, and Proteinase K (Roche) added to 100µg/ml final concentration. The mixture was incubated overnight at 53°C.

The DNA solution was then very gently extracted four times with phenol : chloroform : iso-amyl alcohol. The extraction was carried out on a tilting platform for 30 mins each time. The phases were separated by centrifugation at 500 x *g* for 5 mins, and all pipetting was carried out using wide-bore tips. The DNA solution was then extracted twice with chloroform : iso-amyl alcohol, and the DNA precipitated with 0.3 volumes 7.5M ammonium acetate and 3 volumes of 96% ethanol. The precipitated DNA was spooled, and transferred into 20ml of 70% ethanol. The DNA was pelleted by centrifugation at 8,000 x *g* for 30 mins at 4°C, and the pellet washed twice with 70% ethanol. After briefly air drying the pellet, the DNA was resuspended in 500µl TE.

2.2.18. Preparation of purified viral DNA for electroporation

Ten 175cm^2 tissue culture flasks of BHK-21 cells were infected with virus in suspension at a Multiplicity of Infection (MOI) of 0.1 (see 2.5.1). When 100% cytopathic effect was observed after 4 days, the cells were scraped off into the medium and pelleted by centrifugation at 500 x *g* for 20 mins at 4°C. The cell

pellet was resuspended in 4ml sterile PBS, and the cells disrupted by homogenisation for 30 strokes using a chilled Wheaton-Dounce homogeniser. The suspension was clarified by centrifugation at 2000 x *g* for 20 mins at 4°C. The supernatant was carefully removed and stored at 4°C. The cell pellet was resuspended in 1ml sterile PBS, subjected to homogenisation for 30 strokes using a chilled Wheaton-Dounce homogeniser and clarified by centrifugation at 2000 x *g* for 20 mins at 4°C. The supernatant was removed and pooled with the previous supernatant.

The virus supernatant was layered on top of a sorbitol gradient (20% D-sorbitol in PBS), and pelleted by centrifugation at 141,000 x g for 80 mins at 4°C. The viral pellet was resuspended in 500µl of 50mM Tris [pH8], and 5ml High Molecular Weight DNA Extraction buffer (0.2M Tris [pH8], 0.1M EDTA, 0.5% SDS) was added. Proteinase K (Roche) was added to final concentration of 100µg/ml, and the mixture was incubated overnight at 53°C. The viral DNA solution was then extracted with phenol : chloroform and the viral DNA precipitated as previously described (see 2.2.17).

2.2.19. Preparation of DNA from virally infected cells

One 175cm^2 tissue culture flask of BHK-21 cells was infected with virus in suspension at a Multiplicity of Infection (MOI) of 0.1 (see 2.5.1). When 100% cytopathic effect was observed after 4 days, the cells were scraped off into the medium and pelleted by centrifugation at 1000 x *g* for 20 mins at 4°C. The cell pellet was washed once with PBS, and then resuspended in 10ml High Molecular Weight DNA Extraction buffer (0.2M Tris [pH8], 0.1M EDTA, 0.5% SDS). RNase A (QIAGEN) was added to 20µg/ml, and the solution incubated at 37°C for 1 hour. Proteinase K (Roche) was then added to 100µg/ml, and incubated at 56°C overnight. The DNA solution was then gently extracted with phenol : chloroform three times and chloroform once using a rotator for 15 mins each time. The high molecular weight DNA was precipitated with 0.3 volumes 7.5M ammonium acetate and 3 volumes 96% ethanol as previously described (see 2.2.17).

2.2.20. Southern blot analysis of DNA

DNA samples (10µg per agarose gel lane) were digested with 50-150 units of restriction enzyme for 6-16 hours (see 2.2.7). The digested DNA was precipitated with 0.1 volume sodium acetate [pH5.2] and 3 volumes 96% ethanol and resuspended in 15µl of TE for loading onto the gel. Alternatively, 15µl of PCR products were loaded per well. The DNA samples were electrophoresed through a 0.8-1.5% TAE agarose gel (see 2.2.3), visualised under ultraviolet light using an ultraviolet transilluminator and photographed. The gel was washed in 0.4N NaOH for 20 mins. The blotting rig was assembled by covering the gel platform of an electrophoresis tank in two layers of 3MM filter paper (Whatman) pre-wetted in 0.4N NaOH, with the ends of the filter paper submerged in 0.4N NaOH. The gel was placed on top of the filter paper, and covered in a piece of Hybond N+ (Amersham Pharmacia) pre-wetted in 0.4N NaOH. The membrane was exactly the same size as the gel, and rolled with a Pasteur pipette to ensure that no air bubbles were present. The gel was surrounded by parafilm to stop short-circuiting of the blotting apparatus. Two pieces of 3MM filter paper were placed on top of the membrane, and a stack of dry paper towels was then placed on the top to ensure capillary transfer of the DNA. A 500g weight was placed on top of the paper towels, and the DNA transferred overnight.

The blotting apparatus was disassembled and the membrane removed, having marked the lanes and bottom right corner of the membrane. The DNA was stabilised on the membrane by UV cross-linking using the "auto crosslink" setting (Stratalinker 1800, Stratagene) and the membrane washed with 2 x SSC for 5 mins. The DNA markers were excised using a scalpel blade, and the membrane stored at -20°C.

2.2.21. Staining of DNA molecular weight markers

The membrane strip containing the DNA markers was incubated in 1M acetic acid for 10 mins at RT, and then incubated in staining solution (0.4M acetic acid, 0.4M sodium acetate, 0.2% methylene blue) for 10 mins at RT. The membrane was then washed in diH_20 until the markers were visualised. The

markers were then used to estimate the molecular weight of DNA bands detected on the Southern blot. If the staining of DNA markers was poor, the molecular weight of DNA bands was estimated from the photograph of the gel and ruler taken prior to Southern transfer.

2.2.22. Radiolabelling of DNA probes

DNA probes for hybridisation were labelled using the Random Primed DNA Labelling Kit (Roche) according to manufacturer's instructions. DNA probe (25ng) in a volume of 9µl was heated to 100°C for 10 mins and then cooled rapidly on ice. The DNA was then added to a solution containing 25µM dATP, dGTP, dTTP, hexanucleotide mixture, 50µCi [α^{32}-P]dCTP (Amersham Pharmacia), 2U Klenow DNA polymerase in 20µl total volume. The mixture was incubated at 37°C for 30 mins.

Unincorporated nucleotides were then removed using NICK Columns (Amersham Pharmacia) according to manufacturer's instructions. These columns contain Sephadex G-50, which removes nick-translated DNA from unincorporated nucleotides. Labelled DNA was eluted in 400µl TE [pH7.5], and denatured with 0.1 volumes 3N NaOH for 5 mins at RT. The mixture was then neutralised with 0.05 volumes 1M Tris [pH7.2] and 0.1 volumes 3N HCl, and added to the hybridisation solution.

2.2.23. Hybridisation of Southern blots with DNA probes

The blot was prehybridised in 10ml hybridisation solution (6 x SSC, 5 x Denhardt's reagent, 0.5% SDS, 100µg/ml denatured salmon sperm DNA (Sigma)) for 2 hours at 55-65°C in a Techne roller bottle in a hybridisation oven (Techne Hybridiser HB-1). The solution was then poured off, and replaced with fresh hybridisation solution containing the denatured radiolabelled DNA probe. Hybridisation was performed overnight at 55-65°C. The blot was then washed twice for 15 mins each in 5 x SSC, 0.5% SDS at RT; twice for 15 mins each in 1 x SSC, 0.5% SDS at 37°C; three times for 15 mins each in 0.1 x SSC, 1% SDS and then finally once briefly in 0.1 x SSC at RT. The blot was then wrapped in saran

wrap and exposed to autoradiographic film (X-OMAT, Kodak) at –70°C. Films were developed using an automatic X-ray film processor (Optimax).

2.2.24. Automated DNA sequencing

DNA sequencing was performed using the di-deoxy chain termination sequencing method by Mr. Ian Bennet (Dept. of Veterinary Pathology, University of Edinburgh). Reactions were performed using a SequiTherm EXCEL II DNA Sequencing kit (cycle sequencing protocol) on a 4000L automated sequencing machine (MWG-Biotech).

2.2.25. Sequence analysis of DNA

Analysis of sequenced DNA such as mapping of restriction sites and comparison to other database sequences was made using the University of Wisconsin Genetics Computer Group Sequence Analysis Software Package (GCG10; Devereux *et al.*, 1984). This service was provided by UK Human Genome Mapping Project computer services, UK HGMP Resource Centre, Hinxton, Cambridge, CB10 1SB (http://www.hgmp.mrc.ac.uk/).

2.3 Protein analysis

Protein techniques were predominantly based on methods described by Harlow & Lane, 1988.

2.3.1. Protein analysis and prediction of protein structure

Comparison of the M2 nucleotide and amino acid sequence against all database entries was regularly made using the BLAST database search program (Altschul *et al.*, 1997) available at www.ncbi.nlm.nih.gov/BLAST/. Comparison of the M2 amino acid sequence against known blocks of homology with protein domains was made using the program "Block Searcher" (Henikoff & Henikoff, 1994), available at www.blocks.fhcrc.org/. Sequence alignment of related sequences was made using the Blosum scoring matrix with the "ClustalW"

program (Thompson *et al.*, 1994), and displayed using the "BOXSHADE" program, both available at www.ch.embnet.org/index.html.

Prediction of M2 protein structure was made using programs at Expert Protein Analysis System (ExPASy) Proteomics tools, available at http://ca.expasy.org/tools/ Prediction of hydropathicity was made using "ProtScale" (Kyte & Doolittle, 1982), prediction of common motifs was made using "ScanProsite" (Hofmann *et al.*, 1999), prediction of O-linked glycosylation sites was made using "NetOGlyc 2.0" (Hansen *et al.*, 1998) and prediction of phosphorylation sites was made using "NetPhos 2.0" (Blom *et al.*, 1999).

2.3.2. Sodium dodecyl sulphate – polyacrylamide gel electrophoresis (SDS-PAGE)

SDS-PAGE analysis was performed using an Atto AE-6400 Dual Mini Slab kit (by the method of Laemmli, 1970). The apparatus was assembled as per manufacturer's instructions, ensuring that the glass plates were clean and dry. Depending on the resolution required, resolving gels contained 7.5%, 10% or 15% w/v acrylamide (Ultra Pure Protogel [30% w/v acrylamide : 0.8% w/v bis-acrylamide], National Diagnostics), 375mM Tris [pH8.8], 0.1% w/v SDS, 0.06% w/v ammonium persulphate and 0.08% v/v TEMED (Sigma). The resolving gel was poured and allowed to set before the stacking gel containing 5% w/v acrylamide, 125mM Tris [pH6.8], 0.1% w/v SDS, 0.08% w/v ammonium persulphate and 0.2% v/v TEMED was poured on top of the resolving gel, and a plastic comb inserted to form the sample wells. Once set, the gels were assembled in the tank and 500ml SDS-PAGE running buffer (25mM Tris, 250mM glycine, 0.1% w/v SDS) added to the reservoirs. Samples for analysis were all diluted 1:1 with 2 x SDS-PAGE sample buffer (100mM Tris [pH6.8], 4% w/v SDS, 4% β-mercaptoethanol, 20% v/v glycerol, 0.1% w/v bromophenol blue) and heated to 95°C for 10 mins prior to loading on the gel. A 10µl sample of Broad Range Prestained SDS-PAGE Standards (BIO-RAD) diluted 1:1 with 2 x SDS-PAGE sample buffer was loaded in one lane to enable estimation of protein relative

molecular masses. Electrophoresis was performed at 20mA per gel, until the dye front had reached the end of the gel.

2.3.3. Coomassie staining of SDS-PAGE gels

SDS-PAGE gels were stained by immersion in Coomassie Blue stain (0.25% Coomassie Blue (Sigma), 10% glacial acetic acid, 45% methanol) for 30 mins with gentle shaking. The gel was then destained using Coomassie destain (20% methanol, 5% glacial acetic acid). The destain was replaced at intervals over a period of 12-24 hours until all excess stain was removed. The gel was then dried onto 3MM paper using a Model 583 Gel Dryer and HydroTech Vacuum Pump (BIO-RAD).

2.3.4. Immunoprecipitation

A20 cells were transfected with 20μg of plasmid DNA (see 2.1.4). After 24 hours the cells were harvested, washed once in sterile PBS and then lysed by the addition of 1ml RIPA buffer (50mM Tris [pH7.6], 150mM NaCl, 0.5% w/v sodium deoxycholate, 1% v/v NP-40, 0.1% w/v SDS) for 30 mins at 4°C. The lysate was pre-cleared by the addition of 35μl of 50% v/v protein A-sepharose beads (Protein A Sepharose™ CL-4B, Amersham Pharmacia) in TBS containing 10% w/v BSA, and gently mixed for 30 mins at 4°C, followed by centrifugation at 10,000 x *g* for 1 min to pellet the beads. The supernatant was then divided into four Eppendorf tubes. Rat monoclonal 3F10 anti-HA antibody (1μg; Roche) was added to an aliquot of cell lysate. As a negative control, 1μg of rat IgG (Sigma) was added to an aliquot of cell lysate. The samples were incubated for 2 – 3 hours at 4°C with gentle rotation. Rabbit anti-rat Ig antibody (7μl; DAKO) was then added to the samples, and incubated for 30 mins at 4°C with gentle rotation. Protein A-sepharose beads (35μl of a 50% suspension of beads in TBS containing 10% w/v BSA) was then added to the samples, and incubated for 1 hour at 4°C with gentle rotation.

The beads were pelleted by centrifugation at 10,000 x *g* for 1 min, and then washed five times with 500μl RIPA buffer. The final pellet was transferred

to a clean Eppendorf tube, and resuspended in 35µl of 2 x SDS-PAGE sample buffer.

2.3.5. Inhibition of N-linked glycosylation using tunicamycin

A20 cells were transfected with 20µg of plasmid DNA (see 2.1.4). Immediately following transfection, the cells were divided into two aliquots. Tunicamycin (Sigma) was added to one aliquot to a final concentration of 10µg/ml, and the other aliquot was left untreated. The cells were harvested after 24 hours, washed once in PBS and resuspended in 100µl of 2 x SDS-PAGE sample buffer for analysis by SDS-PAGE and immunoblot (see 2.3.8).

As a positive control to ensure that the tunicamycin was inhibiting N-linked glycosylation, BHK-21 cells were infected with MHV-68 at an MOI of 5 for 1 hour at 37°C. As a negative control, a duplicate experiment was performed with no viral inoculum (mock infection). After infection, the viral inoculum was removed and replaced with medium containing either 10µg/ml tunicamycin or untreated medium. The cells were harvested after 24 hours, washed once in PBS and resuspended in 100µl of 2 x SDS-PAGE sample buffer. The samples were analysed by SDS-PAGE and immunoblot for glycoprotein B expression (see 2.3.8).

2.3.6. Labelling of cells with [9,10(n)-^{3}H] myristic acid

A20 cells were transfected with 20µg of plasmid DNA (see 2.1.4). After 24 hours, the cells were harvested and resuspended in 1ml fresh medium containing 100µCi [9,10(n)-^{3}H] myristic acid (Amersham Pharmacia). The cells were radiolabelled for 4 hours at 37°C, then harvested and washed once with sterile PBS. A sample (4 x 10^5 cells) was resuspended in 40µl of 2 x SDS-PAGE sample buffer, and the rest of the cells were analysed by immunoprecipitation as described previously (see 2.3.4).

The samples were analysed by electrophoresis on a 12.5% SDS-PAGE gel. The gel was then fixed by immersing in protein fixer solution (10% v/v glacial acetic acid, 30% v/v methanol) for 1 hour with gentle agitation. The gel

was impregnated with EN^{3}HANCE (Perkin Elmer Life Science) for 1 hour, washed in water for 30 mins and dried onto 3M filter paper. The dried gel was then exposed to autoradiographic film (X-OMAT, Kodak) at -70°C.

2.3.7. Western blotting (transfer of proteins to PVDF membrane)

After analysis of protein samples by SDS-PAGE gel as previously described, the proteins were transferred to a PVDF membrane (Immobilon-P, Millipore) by the tank transfer system using a Mini-Trans Blot Cell (BIO-RAD). The transfer apparatus was assembled according to the manufacturer's instructions, the tank filled with prechilled transfer buffer (25mM Tris, 250mM glycine, 20% v/v methanol) and the transfer was performed at 250mA for 1 hour.

2.3.8. Immunoblotting

Membranes were incubated in BLOTTO (5% w/v skimmed dried milk, 0.1% v/v Tween-20 in TBS) containing 1% v/v normal rabbit/sheep/donkey serum (depending on which species had been used to raise the secondary antibody) for 1 hour at RT with gentle agitation to prevent non-specific binding to the membrane. The membrane was then washed five times with an excess volume of TBS containing 0.1% v/v Tween-20. Antibodies and their working dilutions are detailed in Table 2.3.8. All antibodies were sourced from commercial suppliers, with the exception of rabbit polyclonal anti-GST (Dr. J. Stewart, unpublished data), rabbit polyclonal anti-MHV-68 (Sunil-Chandra *et al.*, 1992a) and rabbit polyclonal anti-gB (Stewart *et al.*, 1994).

The membrane was incubated with the primary antibody diluted in BLOTTO for 2 hours at RT with gentle agitation, and then washed five times with an excess volume of TBS containing 0.1% v/v Tween-20. The membrane was then incubated with the secondary antibody diluted in BLOTTO for 1 hour at RT with gentle agitation, and then washed five times with an excess volume of TBS containing 0.1% v/v Tween-20. If required, the membrane was then incubated with the tertiary streptavidin conjugate diluted in BLOTTO for 1 hour at RT with gentle agitation. The membrane was then washed seven times with an excess volume of TBS containing 0.1% v/v Tween-20 and then once in TBS before the

detection step. For the detection of phosphoproteins using phospho-specific antibodies, the blocking and incubation steps were performed in TBS containing 0.1% v/v Tween-20 and 1-5% w/v BSA.

Two methods were used to detect enzyme activity. For the detection of alkaline phosphatase (AP) activity, the membrane was incubated with BCIP/NBT solution (Sigma FAST™ 5-bromo-4-chloro-3-indolyl phosphate / nitro blue tetrazolium). Detection of horseradish peroxidase (HRP or POD) activity was performed using the ECL Western Blotting analysis system (Amersham Pharmacia) according to manufacturer's instructions. An equal volume of detection solution 1 was mixed with detection solution 2, and the membrane incubated with the mixture for 1 min. Excess detection solution was drained from the membrane. The membrane was then wrapped in Saran wrap and exposed to autoradiographic film for 1-60 mins (Hyperfilm ECL, Amersham Pharmacia) at RT.

Antigen Detection	Primary antibody	Secondary antibody	Tertiary conjugate
GST	Rabbit anti-GST Polyclonal 1:500	Swine anti-rabbit Ig linked to AP DAKO 1:1000	N/A
MHV-68	Rabbit anti-MHV68 Polyclonal 1:500		
gB	Rabbit anti-gB Polyclonal 1:1,000	Donkey anti-rabbit Ig linked to POD Amersham Pharmacia 1:3,000	
HA	Rat anti-HA Monoclonal (3F10) Roche 1:2,000	Biotinylated rabbit anti-rat Ig DAKO 1:10,000	Streptavidin – POD Roche 1:5,000
GFP	Mouse anti-GFP Monoclonal (JL-8) Clontech 1:1,000	Sheep anti-mouse Ig linked to POD Amersham Pharmacia 1:2,000	N/A
His_6	Mouse anti-His_6 Monoclonal Roche 1:500	Biotinylated rabbit anti-mouse IgG DAKO 1:40,000	Streptavidin – AP Roche 1:1,000
Phosphotyrosine	Recombinant anti-phosphotyrosine (RC20) - HRP BD Transduction Laboratories 1:5,000	N/A	N/A
Phosphotyrosine	Mouse anti-phosphotyrosine Monoclonal (PY99) Santa Cruz 1,2000-5,000	Biotinylated rabbit anti-mouse Ig DAKO 1:20,000-50,000	Streptavidin – POD Roche 1:5,000-20,000
Phosphothreonine	Mouse anti-phosphothreonine Monoclonal (PTR8) Sigma 1:1,000-5,000		
Phosphoserine	Mouse anti-phosphoserine Monoclonal (PSR45) Sigma 1:1,000-5,000		

Table 2.3.8 Antibodies used in immunoblotting. Suppliers are given in green, and working dilutions given in blue.

2.4. Antibody production

2.4.1. Production of a GST fusion protein

The M2 ORF was amplified by PCR (see 2.2.1) using the primers GEX1 and GEX2 (see Appendix 2). The PCR product was purified and ligated into the bacterial expression vector pGEX-2T (Amersham Pharmacia) in frame with the *Schistosoma japonicum* glutathione-S-transferase gene (GST). A 225bp fragment of M2 (corresponding to a 75 a.a internal region of M2) was also amplified by PCR using the primers GEX3 and GEX4 and ligated into pGEX-2T. Ligation and transformation of bacteria by heat pulse were carried out as previously described (see 2.2.10 and 2.2.11).

Clones positive after mini-prep and restriction enzyme digestion for the inserted DNA were tested for expression of the fusion protein. Individual bacterial colonies were grown up overnight in 10ml LB containing 100μg/ml ampicillin, and then diluted 1:10 into 10ml fresh LB and ampicillin. The culture was incubated in a sterile universal at 37°C in an orbital shaker until $O.D._{595} > 0.6$. Protein expression was then induced by the addition of IPTG (Invitrogen Life Technologies) to a final concentration of 0.5 – 1.5mM, and the culture incubated for a further 3 hours. A negative control sample of the culture was not induced.

A 1.5ml sample of the bacterial culture was pelleted by centrifugation at 2,000 x *g* for 5 mins, and the pellet resuspended in 300μl PBS containing 1% v/v Triton-X, 1% v/v Aprotinin and 1mM PMSF. The bacteria were lysed by sonication on ice, and the suspension clarified by centrifugation at 10,000 x *g* for 5 mins. A sample of the supernatant was removed and diluted 1:1 with 2 x SDS-PAGE sample buffer. The pellet was resuspended in 150μl of 2 x SDS-PAGE sample buffer. The soluble and insoluble fractions were then analysed by SDS-PAGE.

2.4.2. Inclusion body preparation of bacterial fusion proteins

Partial purification of GST fusions protein was achieved using the inclusion body protocol (Harlow & Lane, 1988). Bacterial clone number 2 of the

pGEX-2T vector containing the 225bp fragment of M2 (designated pGEX-2T/$M2_{74-148}$) was grown up overnight and diluted 1:10 into 10ml fresh medium. The culture was induced by the addition of IPTG to a final concentration of 0.5mM and incubated for a further 3 hours. The bacterial culture was pelleted by centrifugation at 4,000 x *g* for 5 mins, and the pellet resuspended in 1ml Inclusion Body Prep Buffer (100mM NaCl, 1mM EDTA, 50mM Tris [pH 8.0]). Lysozyme (Sigma) was added to 1mg/ml, and the suspension incubated at RT for 20 mins. After centrifugation at 5,000 x *g* for 10 mins, the pellet was snap frozen at -80°C.

The pellet was thawed, resuspended in 1ml Inclusion Body Prep Buffer containing 0.1% w/v sodium deoxycholate and incubated on ice for 10 mins with occasional mixing. $MgCl_2$ was added to a final concentration of 8mM, and DNaseI (Roche) added to a final concentration of 10µg/ml. The solution was incubated at 4°C with occasional mixing for 1 hour, and then clarified by centrifugation for 10 mins at 2,000 – 10,000 x *g*. A sample of the supernatant was mixed 1:1 with 2 x SDS-PAGE sample buffer. The pellet was washed once with 1ml Inclusion Body Prep Buffer containing 1% v/v NP-40, once with 1ml Inclusion Body Prep Buffer and then resuspended in 200µl of 2 x SDS-PAGE sample buffer. The fractions were then analysed by SDS-PAGE.

2.4.3. Preparation of purified GST-$M2_{74-148}$ fusion protein

The inclusion body protocol produced soluble GST-$M2_{74-148}$ fusion protein, and therefore a modification of this protocol was used to purify the fusion protein. pGEX-2T/$M2_{74-148}$ was grown up overnight and diluted 1:10 in 500ml fresh medium. The culture was induced by the addition of IPTG to a final concentration of 0.5mM, and incubated for a further 3 hours. The bacterial culture was pelleted by centrifugation at 7,000 x *g* for 5 mins, and the pellet resuspended in 50ml Inclusion Body Prep Buffer. Lysozyme (Sigma) was added to 1mg/ml, and the suspension incubated at RT for 20 mins. After centrifugation at 5,000 x *g* for 10 mins, the pellet was snap frozen at -80°C.

The pellet was thawed, resuspended in 50ml Inclusion Body Prep Buffer containing 0.1% w/v sodium deoxycholate and incubated on ice for 10 mins with

occasional mixing. $MgCl_2$ was added to a final concentration of 8mM, and DNaseI added to a final concentration of 10µg/ml. The solution was incubated at 4°C with occasional mixing for 1 hour, and then clarified by centrifugation at 6,000 x *g* for 10 mins. A 10ml suspension of 50% v/v glutathione-sepharose beads (Glutathione Sepharose™ 4B, Amersham Pharmacia), 1% v/v Triton-X in PBS was added to the supernatant, and incubated for 30 mins with gentle rotation. The beads were pelleted by centrifugation at 2,000 x *g* for 5 mins, and the beads washed twice in PBS containing 1% v/v Triton-X, and twice in PBS. The fusion protein was then eluted from the beads by the addition of 5ml of 5mM glutathione (Sigma). The suspension was mixed thoroughly, the beads pelleted by centrifugation at 2,000 x *g* for 5 mins and the supernatant removed and stored. The elution process was repeated three times. The eluted fraction was dialysed against three changes of PBS over 24 hours at 4°C to remove excess glutathione, and the fusion protein solution concentrated using a Centriplus YM-30 (Millipore) centrifugal filter device into a final volume of 2ml. The fusion protein was divided into aliquots and stored at -20°C, and aliquots were analysed by SDS-PAGE.

2.4.4. Immunisation of sheep

Sheep were immunised by Professor J. Hopkins, Department of Veterinary Pathology, R(D)SVS, University of Edinburgh. Two sheep (Numbers 7/413 and 705D) were immunised with fusion protein. Each sheep received two intra-muscular injections containing 18µg of GST-$M2_{74-148}$ fusion protein in PBS mixed by vortex with adjuvant 1:1 (TiterMax® Gold, CytRx) in a total volume of 600µl per injection (36µg fusion protein per immunisation). Both sheep received three booster injections at 4 week intervals. A blood sample was taken prior to immunisation (pre-bleed), and four weeks after each immunisation.

2.4.5. Preparation and purification of serum

Blood samples were allowed to clot overnight at 4°C, and the samples clarified by centrifugation at 2,000 x *g* for 5 mins. The serum was carefully

removed and aliquots stored at -20°C. Aliquots of antibody (1ml of both pre-bleed and third bleed) were purified using caprylic acid followed by ammonium sulphate precipitation. The serum was acidified by the addition of 2 volumes of 60mM sodium acetate [pH4.0], followed by 0.07 volumes of caprylic acid (Sigma) dropwise while the serum was constantly stirring. After 30 mins stirring at RT, the serum was incubated at 4°C overnight. The precipitated protein impurities were pelleted by centrifugation at 5,000 x *g* for 10 mins at 4°C, and the supernatant removed to a fresh universal. One volume saturated ammonium sulphate was added dropwise whilst the sample was constantly stirring. After 30 mins stirring at RT, the serum was incubated at 4°C overnight. The proteins were pelleted by centrifugation at 3,000 x *g* for 30 mins, and the pellet washed twice with 50% saturated ammonium sulphate. The pellet was resuspended in 0.4 volumes PBS, and dialysed against three changes of PBS over 24 hours at 4°C to remove excess ammonium sulphate. The purified antibody was divided into aliquots and stored at -20°C. A sample of each purified antibody was analysed by SDS-PAGE and immunoblot.

2.4.6. Analysis of anti-M2 reactivity of serum

Purified antibody was assessed for reactivity against M2 by immunoblotting and immunofluorescence. Details of secondary antibodies, tertiary conjugates and dilutions used to assess the reactivity of the purified antibodies are detailed in Table 2.4.6.

Primary antibody	Secondary antibody	Tertiary conjugate
Pre-bleed and third bleed 1:1,000-1:10,000	Biotinylated donkey anti-sheep Ig Sigma 1:20,000 - 80,000	Streptavidin – AP Roche 1:2,000
		Streptavidin – POD Roche 1:5,000
Pre-bleed and third bleed 1:100 – 1: 500	Donkey anti-sheep Ig – FITC Sigma 1:250	N/A

Table 2.4.6 Antibodies used in assessing the reactivity of anti-M2 antibody. Suppliers are given in green, and working dilutions given in blue.

2.5. Virological methods

2.5.1. Preparation of viral stocks

MHV-68 working stocks were produced from sub-master stocks of clone g2.4 (Sunil-Chandra *et al.*, 1992a). MHV-76 was kindly provided by Dr. Mistrikova, Slovakia, and plaque purified on BHK-21 cells three times to obtain pure master stocks. Viral stocks were generated by infection of BHK-21 cells. BHK-21 cells (3 x 10^6 cells per 175cm^2 tissue culture flask) were infected with virus in suspension for 1 hour at 37°C on a shaker at a Multiplicity of Infection (MOI) of 0.01. The infected cells were then seeded into 175cm^2 tissue culture flasks (Nunc) and incubated at 37°C for 5 – 7 days until 100% cytopathic effect was observed.

The cells were scraped off into the medium using a cell scraper, and pelleted by centrifugation at 2000 x *g* for 20 mins at 4°C. The cell pellet was resuspended in 5 – 10ml sterile PBS, and the cells disrupted by homogenisation for 30 strokes using a chilled tight-fitting Wheaton-Dounce homogeniser. After homogenisation, the cell suspension was sonicated in a glass universal using a sonicating ice bath for 15 mins. The suspension was clarified by centrifugation at 2000 x *g* for 20 mins at 4°C and the supernatant carefully removed and stored at 4°C. The cell pellet was resuspended in 1ml sterile PBS, subjected to homogenisation for 30 strokes using a chilled Wheaton-Dounce homogeniser and clarified by centrifugation at 2000 x *g* for 20 mins at 4°C. The supernatant was removed and pooled with the previous supernatant. Aliquots were stored in sterile CryoTube™ vials (Nunc) at -80°C.

2.5.2. Titration of infectious virus

Titration of infectious virus was performed by plaque assay on BHK-21 cells as previously described (Sunil-Chandra *et al.*, 1992a). Samples were serially diluted 10-fold in medium in a sterile plastic bijou, and 10^6 BHK-21 cells per 60mm Petri dish added to each dilution. The cell suspension was incubated on a shaker for 1 hour at 37°C, and then placed into 60mm Petri dishes. Medium was

then added to give a final volume of 5ml per dish. All dilutions were performed in duplicate, and negative control incubations containing uninfected BHK-21 cells were also performed. The plates were incubated for 4 days at 37°C. The monolayers were fixed with 4% neutral buffered formaldehyde (Surgipath) for at least 30 mins, and then stained with 0.1% toluidine blue for 15 mins. The number of plaques per dilution was then counted using a light microscope, and the number of plaque-forming units (PFU) was calculated per ml or per organ.

2.5.3. *In vitro* growth curves

In vitro growth curves were performed by infection of sub-confluent BHK-21 cells at an MOI of 5 (single step growth curve) or 0.01 (multi-step growth curve). BHK-21 cells (70 - 80% confluent) in a 24 well plate were infected with virus, and allowed to absorb for 1 hour at 37°C. The cells were then washed three times with fresh medium to remove unbound virus, then 1ml of fresh medium was added to each well and the plates incubated at 37°C. Samples were taken in duplicate at appropriate timepoints by scraping all the cells into the medium, starting immediately after the post-absorption washes (0 hour timepoint). The samples were transferred to a sterile CryoTube™ vial and freeze-thawed three times to release virus. The samples were clarified by centrifugation at 2,000 x *g* for 5 mins at 4°C to pellet the cell debris, and infectious virus was measured by plaque assay (see 2.5.2). All titrations were performed on the same day using the same BHK-21 cells to ensure accurate comparison between values. All experiments were carried out in duplicate.

2.6. Animal experiments

2.6.1. Infection of mice

All animal experiments were performed under a Home Office personal and project license issued under the Animals (Scientific Procedures) Act 1986. Female 3 – 4 week old BALB/c mice were obtained from Bantin and Kingman, and kept in-house for 2 weeks prior to use. Mice underwent light anaesthesia

with halothane (Merial) using an anaesthetic chamber, and were inoculated with 2 x 10^5 PFU virus in 40µl sterile PBS intranasally. At various times post-infection, mice were euthanased by cervical dislocation and tissues harvested for analysis. Blood samples were collected via the tail vein immediately prior to euthanasia. The spleen was removed and kept in complete RPMI medium on ice. Lungs, heart, kidneys and adrenal glands were snap frozen at -80°C.

2.6.2. Determination of spleen weight

Spleen weights were determined using a Mettler AE 163 balance (to the nearest mg).

2.6.3. Infective centre assay for the detection of latent virus

The spleen was placed in a 60mm Petri dish containing 3mls of complete RPMI medium (RPMI 1640 supplemented with 10% v/v FCS, 70µg/ml penicillin, 10µg/ml streptomycin, 50µM β-mercaptoethanol, 2mM L-glutamine and 25mM HEPES (Invitrogen Life Technologies)). The spleen was teased to a single cell suspension using a scalpel blade, and the cells were transferred to a sterile pre-rinsed universal. The cell suspension was pelleted by centrifugation at 600 x *g* for 5 mins at 4°C, and the supernatant discarded. The red blood cells were lysed by osmosis by the addition of 1ml sterile distilled water to resuspend the cell pellet for 15 s followed by the addition of 9mls sterile PBS to establish equilibrium. The cellular debris was allowed to settle, and then the cell suspension was carefully removed, the cells pelleted by centrifugation at 600 x *g* for 5 mins at 4°C and resuspended in 5ml complete RPMI medium.

The splenocytes were counted (see 2.1.3), and the total number of splenocytes per spleen was calculated. The splenocytes were then placed onto a permissive BHK-21 monolayer. BHK-21 cells (10^6 cells) and 5ml complete RPMI medium were added to each 60mm Petri dish and then 10^7, 10^6 and 10^5 splenocytes were added to each dish. All assays were done in duplicate. The plates were incubated at 37°C for 5 days. The monolayers were fixed with 4% neutral buffered formaldehyde (Surgipath) for at least 30 mins, and then stained

with 0.1% toluidine blue for 15 mins. The number of plaques per 10^7 splenocytes were then counted using a light microscope.

Excess splenocytes were stored at -80°C and used to determine the quantity of preformed infectious virus in the spleen cells. The splenocytes were freeze-thawed to disrupt the cells, and infectious virus was measured by plaque assay (see 2.5.2). The number of latently infected splenocytes per 10^7 cells was calculated by subtracting the number of preformed infectious virus plaques from the number of plaques per 10^7 splenocytes as determined by infective centre assay.

A modification of this protocol was used to detect latent virus in blood. Blood (approximately 500µl) was collected prior to euthanasia, and stored on ice in an EDTA collecting tube. The red blood cells were lysed by osmosis, and the cell pellet resuspended in 500µl complete RPMI medium. The white blood cells were counted by adding 10µl cell suspension to 90µl White Blood Cell Counting Fluid (5% v/v glacial acetic acid, 2% v/v ethanol, 0.0002% w/v methylene blue) and then placing the mixture in a haemocytometer. The number of cells was counted per 1mm square.

The white blood cells were then placed onto BHK-21 cell monolayers to give 10^6, 10^5 and 10^4 cells per 60mm Petri dish, and incubated for 5 days at 37°C as previously described.

2.6.4. Titration of infectious virus in mouse tissues

Lung, adrenal, kidney and heart tissues were stored frozen at -80°C. The samples were thawed, and homogenised in a tissue homogeniser containing 1ml Glasgow's complete medium. Lung tissue was homogenised twice in a total volume of 1.8ml Glasgow's complete medium. The suspension was freeze-thawed to disrupt cell membranes, and clarified by centrifugation at 2,000 x *g* for 5 mins at 4°C. Titration of infectious virus was performed by plaque assay on BHK-21 cells (see 2.5.2).

2.6.5. Analysis of data

Data were analysed using Microsoft Excel 97 SR-2 and GraphPad Prism version 3.02 for Windows. The data were statistically analysed using two-way ANOVA with Bonferroni post-tests, and *P* values are indicated in the text.

2.6.6. MACS of latently infected splenocytes

Six week old female BALB/c mice were inoculated intranasally with 2 x 10^5 PFU MHV-76 and the spleens harvested after 14 days. The splenocytes were isolated as described in infective centre assay for the detection of latent virus (see 2.6.3). Splenocytes (10^8 cells) were washed once in cold PBS containing 1% v/v FCS, and resuspended in 1ml PBS containing 1% v/v FCS. The splenocyte suspension was incubated with 10µl rat anti-mouse CD19 antibody (Pharmingen) for 15 mins at 4°C. The splenocytes were washed by the addition of 15ml PBS containing 1% v/v FCS and pelleted by centrifugation at 600 x *g* for 5 mins at 4°C. The cells were resuspended in 800µl PBS containing 1% v/v FCS, and then 200µl goat anti-rat IgG microbeads (Miltenyi Biotec) were added and incubated for 15 mins at 4°C. The microbeads were washed by the addition of 15ml PBS containing 1% v/v FCS, pelleted by centrifugation at 600 x *g* for 5 mins at 4°C and resuspended in 500µl PBS containing 1% v/v FCS. The microbeads were added to a MACS column (Miltenyi Biotec) loaded in the magnet. The column was washed with PBS containing 1% v/v FCS, the flow through collected and the cells recovered by centrifugation at 600 x *g* for 5 mins. This non-B cell fraction was resuspended in RPMI 1640 complete medium.

The column was washed again with 15ml PBS containing 1% v/v FCS, and then the column was removed from the magnet and the B cell fraction eluted with 15ml PBS containing 1% v/v FCS. The B cell fraction was pelleted by centrifugation at 600 x *g* for 5 mins and resuspended in RPMI 1640 complete medium. The amount of latent virus in the B cell, non-B cell and total splenocyte fractions was determined by infective centre assay as previously described (see 2.6.3). The purity of the B-cell and non-B-cell fractions was determined by FACS analysis of a representative aliquot of separated cells (see 2.6.7).

2.6.7. FACS analysis

A sample of 2 x 10^5 cells in 50µl FACS buffer (1% w/v BSA, 0.1% w/v azide in PBS) was dispensed into each FACS tube. Antibodies used in FACS analysis are detailed in Table 2.6.7. Primary antibody (25µl) was added to the tube, and the tubes incubated at RT for 15 mins. The cells were washed by adding 750µl of FACS buffer to the tube and centrifuging at 600 x *g* for 5 mins. If required, 25µl of secondary antibody was added to the cells and the tubes incubated at RT for 15 mins in the dark. The cells were washed by adding 750µl of FACS buffer to the tube and centrifuging at 600 x *g* for 5 mins. The cells were resuspended in 200µl of 2% neutral buffered formaldehyde in PBS and then analysed using a Becton-Dickinson FACScan. The lymphocyte population was identified on the basis of size (forward scatter) and granularity (side scatter), and the lymphocyte population was then analysed for FITC staining.

For the FACS analysis of EGFP expressing A20 cells, the cells were harvested, washed once in PBS and resuspended at 4 x 10^6 cells per ml in PBS with 1% v/v BSA. Cells were then analysed using a Becton-Dickinson FACScan.

Surface marker	Antibody	Supplier
CD4	Rat anti-CD4 FITC conjugate Monoclonal H129.19	Sigma
CD8	Rat anti-CD8 FITC conjugate Monoclonal 53-6.7	Sigma
CD19	Primary – rat anti-mouse CD19. Monoclonal 1D3 Secondary – goat anti-rat Ig FITC conjugate Polyclonal	Pharmingen Pharmingen

Table 2.6.7 Antibodies used in FACS analysis.

2.6.8. Histopathology

Mice were euthanased by CO_2 asphyxiation and the lungs were perfused *in situ* via the trachea using 10% neutral buffered formaldehyde. Portions of spleen were also fixed in 10% neutral buffered formaldehyde and the tissues were processed routinely into paraffin wax-embedded sections. These were stained with haematoxylin and eosin, and examined by light microscopy.

2.6.9. Immunostaining of histopathological samples

Paraffin wax sections of 4μm thickness were fixed onto microscope slides coated with BIOBOND (British Biocell International). The sections were dewaxed using xylene for 15 mins, and then ethanol for 5 mins. The slides were incubated in 0.3% v/v hydrogen peroxide in methanol for 30 mins, and then hydrated through a series of ethanol solutions (100% - 30%). The slides were then incubated in 1% v/v TritonX-100 for 90s, washed twice with water and then digested for 20 mins at 37°C with 10μg/ml Proteinase K (Roche) in 20mM Tris [pH7.0], 2mM $CaCl_2$. After incubation in PBS containing 25mM glycine, 5mM EDTA for 5 mins and PBS for 3 mins, the slides were incubated overnight in PBS with 2% v/v normal goat serum to prevent non-specific antibody binding.

The sections were incubated for 2 hours at RT with 500μl polyclonal rabbit anti-MHV-68 antibody (Sunil-Chandra *et al.*, 1992a) diluted 1:500 in PBS with 2% v/v normal goat serum. The sections were washed three times with PBS, and incubated with 500μl biotinylated goat anti-rabbit IgG (Sigma) diluted 1:500 in PBS with 2% v/v normal goat serum for 2 hours at RT. After three washes with PBS, the slides were incubated for 1 hour with 500μl streptavidin-POD conjugate (Roche) diluted 1:1500 in PBS for 1 hour at RT. The sections were then exposed to DAB substrate (3,3' Diaminobenzidine, SIGMA FAST™ DAB Tablet, Sigma). The slides were washed in PBS and then water, and then lightly counterstained with haematoxylin for 1 min. The slides were then dehydrated through a series of ethanol solutions (30% - 100%) and mounted.

2.6.10. Detection of viral DNA in mouse tissues

Mice were infected with 2 x 10^5 PFU virus, and euthanased five months post-infection. The liver, lung, kidney, spleen and white blood cells were removed, and stored at -80°C. Viral DNA was extracted using a DNeasy Tissue Kit (QIAGEN) according to the manufacturer's instructions. Approximately 25mg of tissue was cut into small pieces, and 180µl Buffer ATL* added to the tissue pieces. Proteinase K was added to a final concentration of 2mg/ml, and the sample incubated at 55°C overnight with occasional mixing by vortex. Buffer AL* (200µl) was added to the digested sample, mixed by vortex and incubated at 70°C for 10 mins. Ethanol (200µl) was added to the sample, mixed by vortex and placed in a DNeasy mini column. After centrifugation at 6,000 x *g* for 1 min, the column was washed with 500µl Buffer AW1* and then 500µl Buffer AW2*. The column was dried by centrifugation at 12,000 x *g* for 3 mins, and the DNA eluted with 200µl Buffer AE*. The extracted DNA was quantified using a fluorometer (see 2.2.6).

PCR amplification (40 cycles) was performed on 1µg of high molecular weight DNA using primers specific for the gp150 or M3 genes as previously described (see 2.2.1). A 15µl sample of the PCR products was electrophoresed through a 1.5% w/v TAE agarose gel, and analysed by Southern blot hybridisation with probes specific for gp150 and M3 to confirm the specificity of the PCR products as previously described (see 2.2.20).

2.7. Fluorescent microscopy analysis

2.7.1. Fixation of cells

Cells were transfected with 20µg of plasmid DNA (see 2.1.4). The cells were harvested 24 hours post-transfection, washed once with PBS and resuspended at approximately 10^6 cells/ml in PBS. The cells were then either air-dried or attached by centrifugation using a Cytospin 2 (ThermoShandon) onto a glass slide. The cells were fixed by incubating the slides with 4% w/v paraformaldehyde in PBS for 10 mins at RT. The slides were washed twice in

PBS, and the cells were then permeabilised by incubating the slides in PBS containing 0.2% v/v TritonX-100 for six to ten mins. The slides were washed four times in PBS, air-dried and stored at -20°C. In some instances when cells were transfected with EGFP fusion proteins, the cells were fixed first in 4% w/v paraformaldehyde in PBS, washed twice in PBS and then cytospun or air-dried onto glass slides.

2.7.2. Fluorescent microscopy

Samples for fluorescent microscopy were mounted in fluorescent mounting medium (DAKO), and initially examined using a Nikon Diaphot 200 Ultraviolet Microscope. Confocal microscopy, image production and analysis were performed using a Leica TCSNT confocal system at the Confocal Microscope Facility, BioMedical Sciences, University of Edinburgh.

2.7.3. Staining of DNA in cells

Cell samples were fixed and permeabilised (see 2.7.1). To visualise DNA using the BandPass filter 600/30, DNA was stained using propidium iodide. The sample was incubated in PBS containing 10μg/ml RNaseA (QIAGEN) and 1μg/ml propidium iodide (Molecular Probes) for 30 mins at 37°C in the dark. The slide was washed twice in PBS, and mounted. To visualise DNA using the LongPass filter LP665, DNA was stained by incubating the sample in PBS containing 10μg/ml RNaseA and 2μM TO-PRO-3 (Molecular Probes) for 30 mins at 37°C in the dark. The slide was washed twice in PBS, and mounted in fluorescent mounting medium (see 2.7.2).

2.7.4. Staining of the plasma membrane

Cells were transfected with 20μg of plasmid DNA (see 2.1.4). The cells were harvested 24 hours post-transfection, washed once with PBS and the cells resuspended at 4 x 10^6 cells/ml in incubation buffer (PBS with 3% w/v BSA, 1% v/v normal rabbit serum and 0.1% w/v azide). A 50μl sample of the cell suspension was placed into a tube. To stain with anti-CD19 antibody, rat anti-

mouse CD19 antibody (Pharmingen) was added to the cell suspension at a dilution of 1:150. To stain with anti-MHC Class II antibody, the cells were pelleted by centrifugation at 500 x *g* for 5 mins, and resuspended in 50µl rat anti-MHC Class II (Monoclonal SW 73.2; Hopkins *et al.*, 1986) in medium with 1% v/v normal rabbit serum and 0.1% w/v azide. The cells were incubated for 1 hour at 4°C.

The cells were washed three times with 750µl cold wash buffer (PBS with 3% w/v BSA and 0.1% w/v azide). The cells were then incubated with 25µl of rabbit polyclonal anti-rat IgG TRITC conjugate (Sigma) diluted 1:150 in incubation buffer for 45 mins in the dark at 4°C. The cells were washed three times with 750µl cold wash buffer and resuspended in 100µl PBS. The cells were cytospun onto glass slides, fixed and examined (see 2.7.2).

2.7.5. Staining of the Endoplasmic Reticulum

Cells were transfected with 20µg of plasmid DNA (see 2.1.4). The cells were harvested 24 hours post-transfection, and resuspended in medium containing 50µg/ml Concanavalin A TRITC conjugate (Molecular Probes). The cells were incubated for 5 mins at 4°C, and then washed twice with PBS. The cells were fixed, cytospun onto glass slides and mounted in fluorescent mounting medium (see 2.7.2).

2.7.6. Staining of lysosomes

Cells were transfected with 20µg of plasmid DNA (see 2.1.4). The cells were harvested 24 hours post-transfection, and resuspended in medium containing 50nM LysoTracker Red DND-99 (Molecular Probes). The cells were incubated at 37°C for 2 hours. An aliquot of cells was resuspended in fresh medium and examined under ultraviolet light to check the cell staining. The cells were then washed once in PBS, and fixed for 30 mins in 2% w/v paraformaldehyde in PBS. The cells were washed three times in PBS, cytopsun onto glass slides and mounted in fluorescent mounting medium (see 2.7.2).

2.7.7. Staining of Golgi apparatus

BODIPY TR (Molecular Probes) was complexed to BSA as per the manufacturer's instructions. Cells were transfected with 20μg of plasmid DNA (see 2.1.4). The cells were harvested 24 hours post-transfection, washed once with HBSS and incubated in HBSS containing 5μM BODIPY TR complex with BSA for 30 mins at 4°C. The cells were then washed twice in ice-cold HBSS and incubated with fresh HBSS for 30 mins at 37°C. The cells were washed once in PBS, fixed, cytospun onto glass slides and mounted in fluorescent mounting medium (see 2.7.2).

2.7.8. Indirect immunofluorescence

Cells were transfected with 20μg of plasmid DNA (see 2.1.4) and the cells were harvested 24 hours after transfection, then fixed and permeabilised (see 2.7.1). To stain cells expressing His_6 epitope-tagged proteins, the slides were blocked by incubation with PBS containing 5% v/v normal rabbit serum for 30 mins at RT. The slides were then incubated with mouse monoclonal anti-His_6 (Roche) diluted 1:10-1:50 in PBS containing 5% v/v normal rabbit serum for 2 hours at 37°C. As a negative control, duplicate slides were incubated with mouse monoclonal anti-LMP1 diluted 1:20 (DAKO). The slides were then washed four times with PBS containing 0.05% v/v Tween-20, and incubated with biotinylated anti-mouse IgG (Sigma) diluted 1:100-1:500 in PBS containing 5% v/v normal rabbit serum for 45 mins at 37°C. The slides were again washed four times with PBS containing 0.05% v/v Tween-20, and the slides were then incubated with streptavidin-FITC conjugate (Sigma) diluted 1:300 in PBS containing 5% v/v normal rabbit serum for 45 mins at 37°C. The slides were washed four times in PBS containing 0.05% v/v Tween-20 and the slides mounted in fluorescent mounting medium (see 2.7.2).

To stain cells expressing HA epitope-tagged proteins, the slides were blocked by incubation with PBS containing 5% v/v normal goat serum for 30 mins at RT. The slides were then incubated with rat monoclonal anti-HA (Roche) diluted 1:300 in PBS containing 5% v/v normal goat serum for 2 hours at 37°C.

As a negative control, duplicate slides were incubated with rat IgG (Sigma) diluted 1:3000. The slides were then washed four times with PBS containing 0.05% v/v Tween-20. The slides were then incubated with goat polyclonal anti-rat Ig FITC conjugate (Pharmingen) diluted 1:250 in PBS containing 5% v/v normal goat serum for 45 mins at 37°C. The slides were washed four times in PBS containing 0.05% v/v Tween-20, the DNA was counterstained with propidium iodide and the slides mounted in fluorescent mounting medium (see 2.7.2).

2.8. Recombinant virus production

2.8.1. Generation of recombinant viruses

Recombinant viruses were generated by co-transfection of BHK-21 cells with purified viral DNA (see 2.2.18) and a fragment of the viral genome allowing homologous recombination. To generate MHV-76 rescue viruses, cosmid A8 (cA8, see Appendix 3) was used to restore the left end of the genome.

To generate deletions and frame-shift mutations in the M2 ORF, a series of deletions were made in cosmid A8 using Exonuclease III and Mung Bean Nuclease (see 2.2.8). Cosmid clones were analysed by restriction enzyme analysis and sequencing of the M2 ORF, and two clones were chosen containing a 4bp deletion in M2 (cA8-M2$\Delta_{4336\text{-}4339}$) and a 256bp deletion in M2 (cA8-M2$\Delta_{4239\text{-}4494}$). These two cosmid clones were used to generate recombinant viruses identical to MHV-68 with deletions in the M2 ORF.

To generate MHV-76 viruses with the M2 ORF and the tRNA7+8 region restored, a DNA sequence corresponding to the terminal 3kb of the left end of the unique region of the MHV-76 genome was amplified by PCR and inserted into pKS(-) to generate the plasmid pKS/76LHE (see 5.2). A 4kb fragment containing the M2 cDNA and promoter region was amplified by PCR and inserted into pKS/76LHE to give the plasmid pKS/76LHE/M2insert. A 1kb fragment containing tRNA7+8 was amplified by PCR and inserted into pKS/76LHE to give the plasmid pKS/76LHE/tRNAinsert. The cassettes were excised from pKS(-) prior to transfection.

BHK-21 cells were transfected with 5μg virus DNA and 10μg of the homologous plasmid / cosmid DNA (see 2.1.4). Following transfection, the cells were placed into 6-well plates and incubated at 37°C overnight. The cells were washed with fresh medium at 24 hours post-transfection. Fresh medium was added to the MHV-76 rescue virus transfections, and all other recombinant virus transfections were overlaid with medium containing 1% w/v LGT agar (Seaplaque® Agarose, Flowgen). The plates were incubated at 37°C, and examined for the presence of viral plaques daily.

2.8.2. Purification of MHV-76 rescue viruses

After 6 days, the infected cell monolayer was harvested, the cells pelleted by centrifugation at 2,000 x *g* for 20 mins and the cells resuspended in 1ml PBS with 1% v/v FCS. Virus particles were released from the cells by freeze-thawing at -70°C three times. The cellular debris was pelleted by centrifugation at 2,000 x *g* for 5 mins, and 20μl of the mixture of viruses in the supernatant was mixed with 20μl PBS and used to infect two 6 week old BALB/c mice. After 14 days, the spleens were harvested and analysed by infective centre assay (see 2.6.3). After two days of the infective centre assay, the monolayer was overlayed with 1% w/v LGT agararose in medium. The plates were incubated at 37°C, and examined for the presence of viral plaques daily.

2.8.3. Purification of recombinant viruses

The positions of viral plaques were marked on the underside of the plate, and a Pasteur pipette was used to remove an agarose plug containing virus-infected cells. The agarose plug was transferred to a sterile CryoTube™ vial containing 500μl of medium. Virus particles were released from the cells by freeze-thawing at -70°C three times. The cellular debris was pelleted by centrifugation at 2,000 x *g* for 5 mins, and the supernatant used in subsequent purification steps.

Viruses were purified using limiting dilution assay. BHK-21 cells were grown until approximately 60% confluent in a 96 well plate. The wells were then

infected with serial dilutions of virus (10^{-1} to 10^{-4}), with the aim of infecting cells at a concentration of 0.4 PFU/well to give rise to single plaques in 40% of the wells. The assay was incubated at 37°C for 6 days, and wells containing single plaques were harvested by scraping the cells into the medium. A 100µl aliquot of the sample was placed in a CryoTube™ vial, and freeze-thawed at -70°C three times to release virus particles. The remainder of the sample was pelleted by centrifugation at 500 x *g* for 5 mins. The cell pellet was washed with 500µl of modified TE (20mM Tris [pH8.0], 1mM EDTA) and then resuspended in 50µl modified TE. The sample was freeze-thawed once, PCR Grade Proteinase K (Roche) was added to a final concentration of 400µg/ml and the sample incubated at 55°C overnight. The sample was heated to 95°C for 10 mins to inactivate the Proteinase K, and 10µl of the sample was used as template for PCR analysis (see 2.2.1). Plaques positive by PCR for the desired insert (M2 or tRNA) were subsequently used to infect the next limiting dilution assay. PCR for ORF74 was used as a control to check for the presence of viral DNA.

A modification of this protocol was used to directly analyse viral plaque picks for the MHV-76 rescue viruses and viral stocks. A 100µl PCR reaction was set up containing 20mM Tris (pH 7.4), 50mM KCl, 1.5mM $MgCl_2$, 100µM dNTP mixture, 0.2pmol primer mixture (M2 or ORF 74) and 10µl of virus sample in medium (containing approximately 10 PFU of virus). Proteinase K (Roche) was then added to a final concentration of 200µg/ml. The reaction was run at 55°C for 20 mins, and then 95°C for 10 mins. One unit of *Taq* DNA polymerase (Invitrogen Life Technologies) was then added and 40 cycles of PCR performed (see 2.2.1).

Plaques positive by PCR for the desired insert (M2 or tRNA) were subsequently used to infect the next limiting dilution assay. Viruses were purified until homogeneous by PCR screening. Master stocks were made by infecting BHK-21 cells in a $25cm^2$ tissue culture flask at an MOI of 0.01, and incubating for 4-6 days until 100% CPE was observed. The cells were scraped into the medium, pelleted by centrifugation at 2,000 x *g* for 20 mins and resuspended in 1ml medium. Virus particles were released from the cells by freeze-thawing at -

70°C three times. The sample was clarified by centrifugation at 2,000 x *g* for 5 mins, and the supernatant divided into CryoTube™ vials and stored at -70°C.

2.8.4. Analysis of recombinant viruses

DNA was made from virally infected cells (see 2.2.19), and analysed by Southern blotting (see 2.2.20) and PCR for MHV-68 specific ORFs (see 2.2.1).

Appendix 1 General solutions

Unless otherwise stated, all chemicals were obtained from Sigma or Merck BDH

TE buffer	: 10mM Tris-HCl [pH8.0], 1mM EDTA
TAE buffer	: 40mM Tris-acetate, 1mM EDTA
Luria-Bertani (LB) medium	:1% w/v tryptone, 1% w/v NaCl, 0.5% yeast extract, pH7.0
LB Agar	: LB containing 1.5% Bacto-Agar (BD)
SOC medium	: LB containing 20mM glucose, 20mM $MgCl_2$
20 x SSC	: 3M NaCl, 300mM Na citrate, pH7.0
50 x Denhardt's solution	: 1% w/v Ficoll 400, 1% w/v polyvinylpyrrolidone, 1% BSA (FractionV)
Tris-buffered saline (TBS)	: 50mM Tris-HCl, 150mM NaCl, pH 7.6
Phosphate-buffered saline (PBS)	: 150mM NaCl, 2.5mM KCl, 10mM Na_2HPO_4, 1mM KH_2PO_4, pH 7.4
Hank's buffered salt solution (HBSS):	150mM NaCl, 25mM HEPES, 5mM KCl, 5mM glucose, 1mM $CaCl_2$, 1mM KH_2PO_4, 1mM $MgCl_2$, 1mM Na_2HPO_4, 1mM $MgSO_4$, 0.001% w/v phenol red, pH 7.0

Appendix 2 PCR primers

All primers were synthesised by MWG Biotech AG.

Primer	Primer pair sequence	Annealing temperature	Amplified region MHV-68 sequence	Product size
M2GEX1	*Bam*HI 5'-GCGGGATCCATGGCCCCAACACCCCCAC-3'	55°C	4000 – 4606	624bp
M2GEX2	*Eco*RI 5'-GCGGAATTCGTTATGTTCTGCGTTAGCACC-3'			
M2GEX1	*Bam*HI 5'-GCGGGATCCATGGCCCCAACACCCCCAC-3'	45°C	4031 – 4606	614bp
M2-HIS	*Eco*RI 6 x His 5'-CGCGAATTCTTAATGATGATGATGATGATG CTCCTCGCCCCACTCCAC-3'			
M2GEX3	*Bam*HI 5'-GCGGGATCCAGGACTCGCTTTCCTAAAACC-3'	50°C	4163 – 4387	242bp
M2GEX4	*Eco*RI 5'-GCGGAATTCACTGTCAGTCGAGCCAGAG-3'			
M1rev	5'-GTTACCTAGGACATACAGTGG-3'	55°C	2686 – 2964	278bp
M1for	5'-CAGAACCTTACCAGTCATGTG-3'			
M2GEX1	*Bam*HI 5'-GCGGGATCCATGGCCCCAACACCCCCAC-3'	55°C	4031 – 4606	593bp
M2GFP-N	*Eco*RI 5'-CAGAATTCGCTCCTCGCCCCACTCCAC-3'			
M3+	5'-TGGCACTCAAACTTGGTTGTGG-3'	55°C	6566 – 6946	381bp
M3-	5'-TAACAGGCAGATTGCCATTCCC-3'			
M4A	5'-GCGCGGATCCGACACCTGGAGAAGATG ATGATATTCC-3'	55°C	8616 – 9785	1185bp
M4B	5'-CGCGGAATTCGGTTCTAGAAAGTCATAAA TCTCAATACC-3'			

Primer	Primer pair sequence	Annealing temperature	Amplified region MHV-68 sequence	Product size
M11+	5'-TTAGAAGGCACTATGACAGCG-3'	50°C	103560 – 103779	219bp
M11-	5'-AACTTGCTAACGTACTGTGT-3'			
gp150A	5'-GCGCAAGCTTCGCCGCCACCATGT GTGGCGTTAAAT-3'	51°C	69465 – 70917	1481bp
gp150B	5'-CGCGCTCGAGTTATTCATGTAAA CACACACAG-3'			
gp150-1	5'-ACACCTAAACCCTCCTCAC-3'	50°C	69880 – 70109	229bp
gp150-2	5'-GCGTCCGATGAAGAAGTAG-3'			
GCR-5'	5'-GCCACGATGCTTGTCCTGCG-3'	55°C	105057-106067	1010bp
GCR-3'	5'-TTAGGAGCTTAGTCTACAAACTG-3'			
ORF73+	5'-TGTCTGAGACCCTTGTCC-3'	50°C	103927 – 104373	446bp
ORF73-	5'-TTGTCGACTGAATTTTACACA-3'			
76LHE1	*Bam*HI 5'-GCGGATCCTAGAGGGACGGGCAATTT ATATAATTTATCACCAAATTGGAC-3'	47°C	9539 – 12563	3040bp
76LHE2	*Eco*RI 5'-GCGGAATTCCACAAAGATCACACATGG-3'			
M2-insert1	*Not*I 5'-GCGGCCGCGCTACAATACTGCGTGGTC-3'	53°C	3011 – 7032	4035bp
M2-insert2	*Bam*HI 5'-GCGGATCCCTTCATGAGCTTCAAGGGC-3'			
tRNA7+8-insert1	*Not*I 5'-GCGCGGCCGCTCATCAGACTAGTGCCTGT-3'	51°C	4623 – 5806	1200bp
tRNA7+8-insert2	*Bam*HI 5'-GCGGATCCTCTGGGCCTAAGAGGGAATG-3'			

Primer	Primer pair sequence	Annealing temperature	Amplified region MHV-68 sequence	Product size
tRNA7for	5'- GAG CGG CAG ACA CCA-3'	58°C	4967 - 5034	68bp
tRNA7rev	5'-TAG CTG GCC AGG ACT-3'			

Appendix 3 Plasmid Vectors

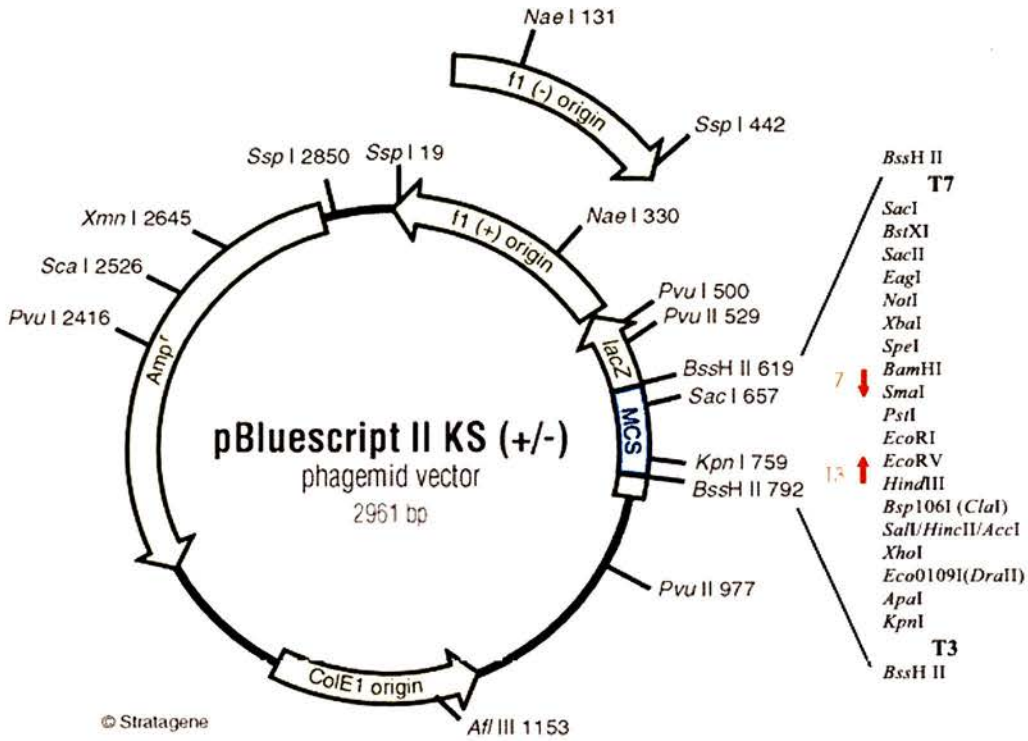

pBluescript II KS (-) was obtained from Stratagene.

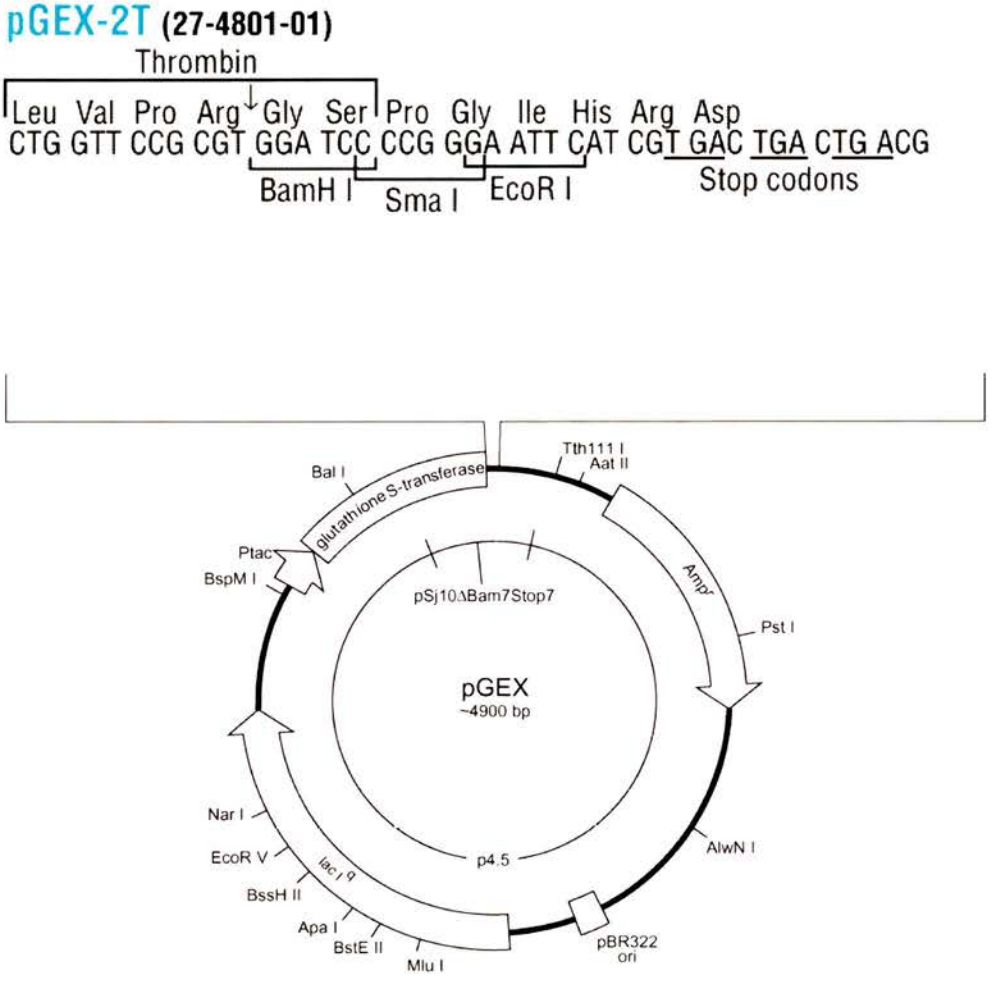

pGEX-2T was obtained from Amersham Pharmacia.

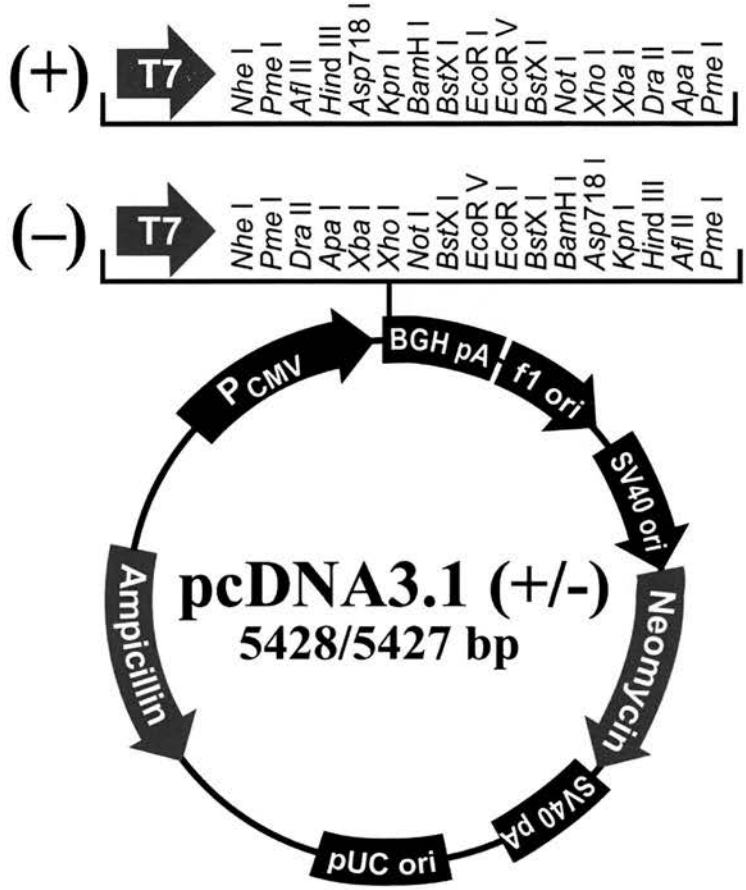

pcDNA3.1 was obtained from Invitrogen

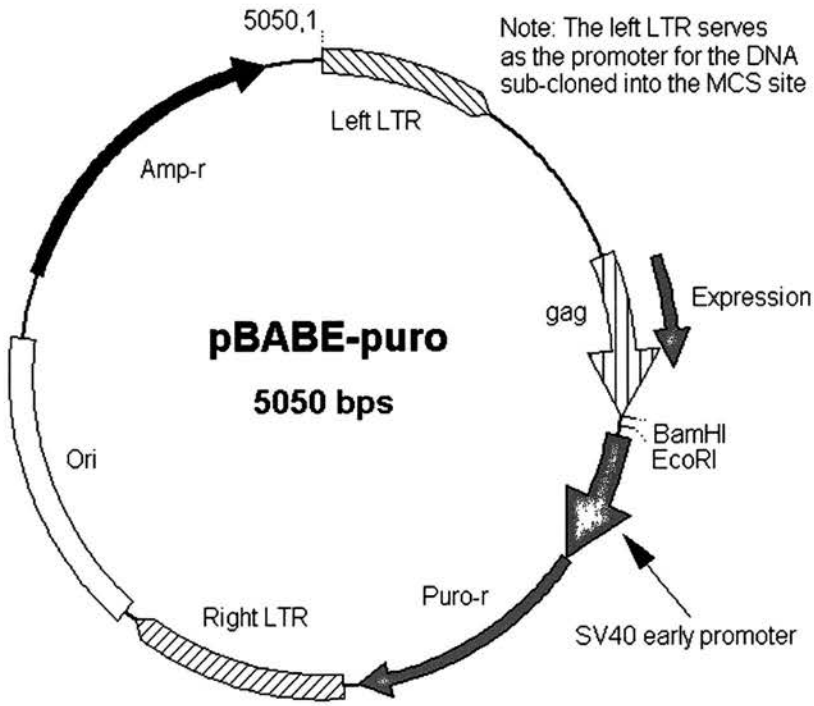

pBABE puro retroviral vector (Morgenstern & Land, 1990). The plasmid map was obtained from www.pharmacy.purdue.edu/~phrm302/molbiol

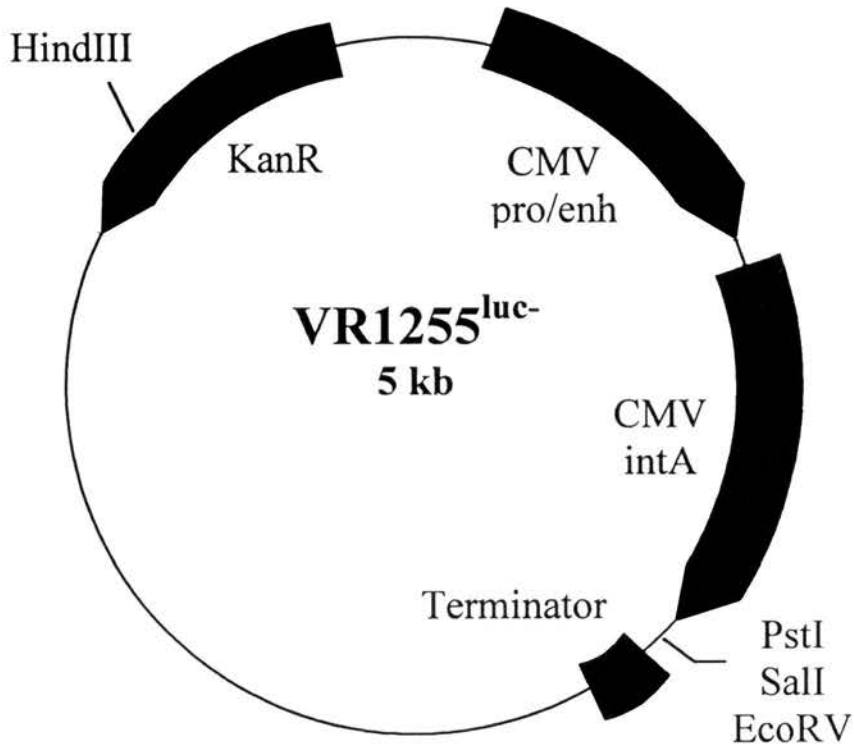

pVR1255 was obtained under license from Vical Incorporated (Hartikka *et al.*, 1996). To obtain pVR1255^{luc-}, pVR1255 was cut with *Not*I and *Bam*HI to excise the luciferase gene. The termini were filled in and the blunt ends ligated to give the multiple cloning site containing *Pst*I, *Sal*I and *Eco*RV.

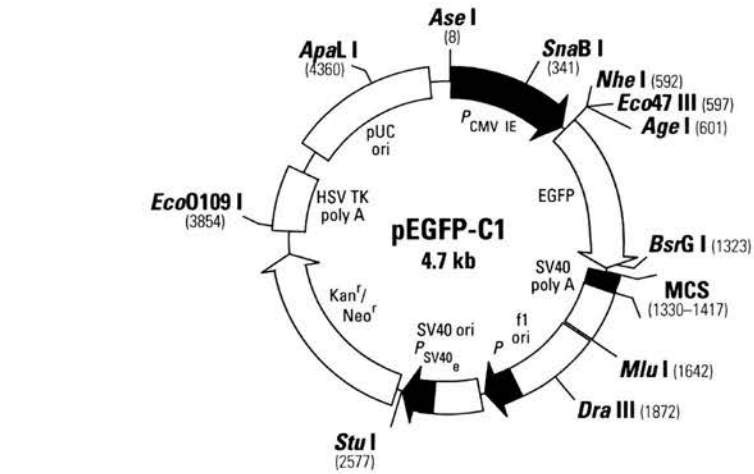

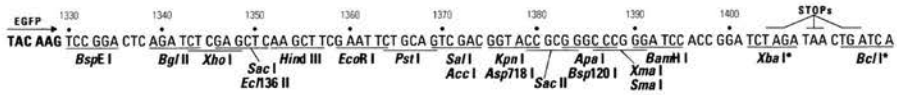

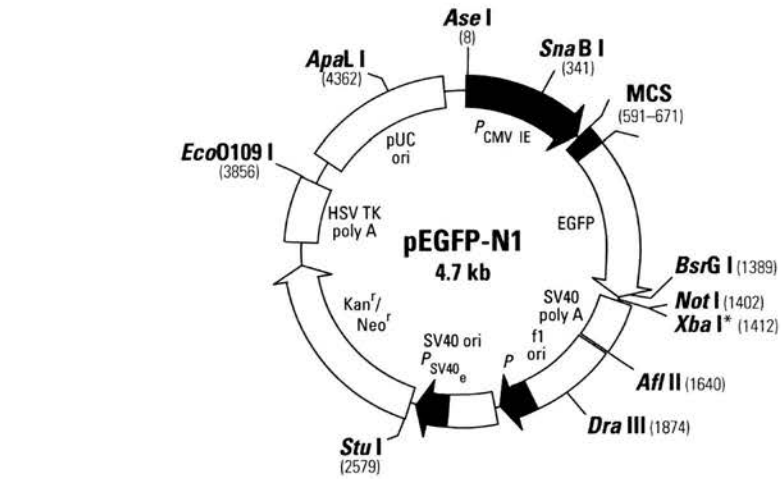

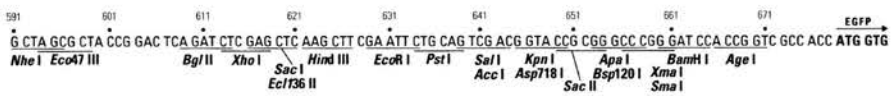

pEGFP-C1 and pEGFP-N1 were obtained from BD Biosciences Clontech.

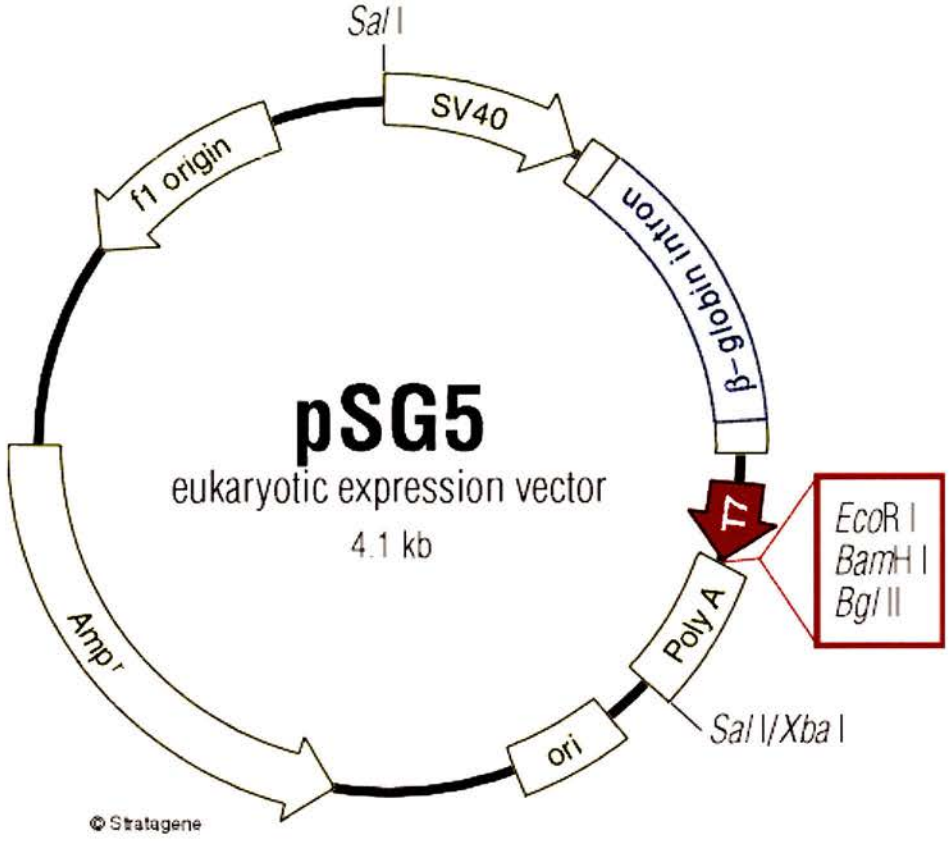

The plasmids pSG5/M2-3'HA and pSG5/M2-5'HA were kindly provided by Dr. Jeff Sample, St. Jude Children's Research Hospital, Memphis. The plasmids contained the M2 gene with three consecutive 27bp DNA sequences corresponding to the influenza haemagglutinin (HA) protein epitope (YPYDVPDYA) inserted in frame either immediately upstream of the M2 ORF (pSG5/M2-5'HA) or immediately upstream of the M2 STOP codon (pSG5/M2-3'HA). As positive controls, pSG5/Jκ-HA (Zhao *et al.*, 1996) and pSG5/IRF7-HA (Zhang & Pagano, 1997) were also kindly provided by Dr. Sample.

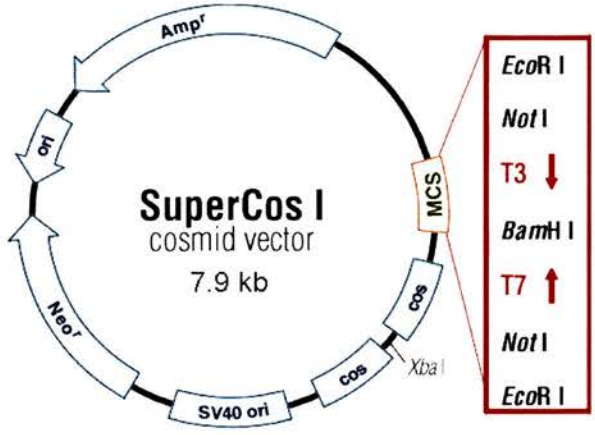

The parent cosmid vector SuperCos 1 was modified by the replacement of the *Not*I fragment of the original cloning site with a cloning region containing the configuration *Eco*RI – *Not*I – *Asc*I – *Pac*I – *Bam*HI – *Asc*I – *Pac*I – *Not*I - *Eco*RI (Cunningham & Davison, 1993).

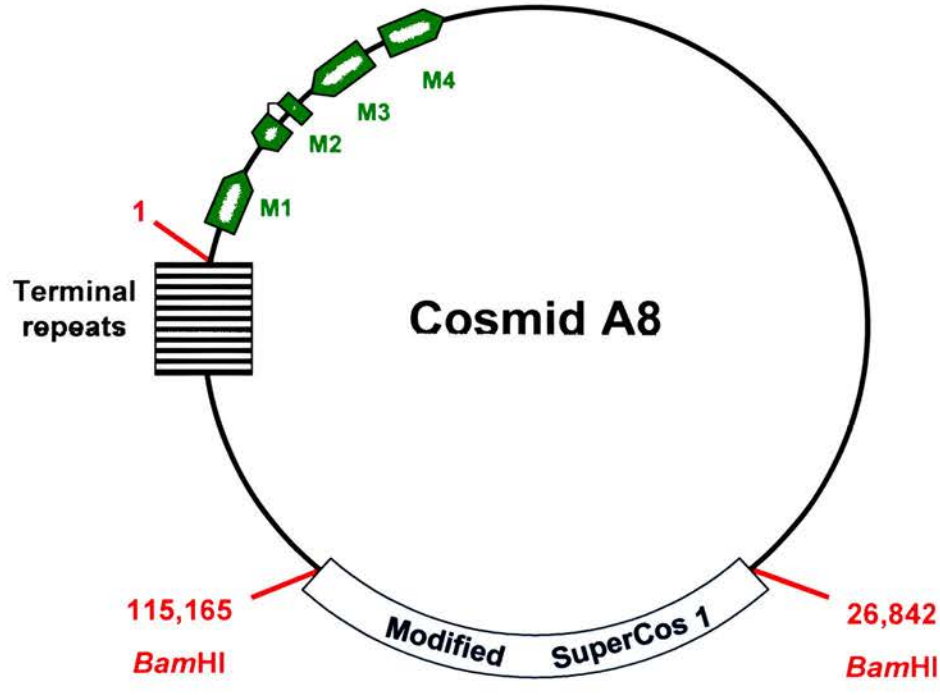

Cosmid A8 was kindly provided by Dr. Andrew Davison, MRC Virology Unit, Glasgow. This cosmid was a modified SuperCos 1 containing nucleotides 115165 to 26842 of MHV-68 DNA inserted into the *Bam*HI site (MHV-68 co-ordinates shown in red). To aid interpretation, the four MHV-68 genes (M1, M2, M3 and M4) present at the left end of the unique region of the MHV-68 viral genome are shown in green.

Appendix 4 Commercial suppliers

Amersham Pharmacia Biotech UK Limited, Amersham Place, Little Chalfont Buckinghamshire HP7 9NA
www.apbiotech.com

BD Biosciences, 21 Between Towns Road, Cowley, Oxford, OX4 3LY
www.bd.com

BD Biosciences Clontech UK, Unit 2, Intec 2, Wade Rd., Basingtoke, Hampshire RG24 8NE
www.clontech.com

BD PharMingen, 10975 Torreyana Road, San Diego, CA 92121
www.pharmingen.com

BD Transduction Laboratories, 133 Venture Court, Lexington, KY 40511
www.translab.com

Bio-Rad Laboratories Ltd., Bio-Rad House, Maylands Avenue, Hemel Hempstead, Hertfordshire HP2 7TD
www.bio-rad.com

British Biocell International, Golden Gate, Ty Glas Avenue, Cardiff, CF14 5DX
www.british-biocell.co.uk

CytRx Corporation, 154 Technology Parkway Suite 200, Norcross, Georgia 30092
www.cytrx.com

DAKO Ltd., Denmark House, Angel Drove, Ely, Cambridgeshire CB7 4ET
www.dako.com

EquiBio, Action Court, Ashford Road, Ashford, Middlesex, TW15 1XB, U.K
www.equibio.com

Flowgen, Novara House, Excelsior Road, Ashby Park, Ashby de-la Zouch, Leicestershire, LE65 1NG
www.flowgen.co.uk

Invitrogen Life Technologies, Invitrogen Ltd, 3 Fountain Drive, Inchinnan Business Park, Paisley, PA4 9RF
www.invitrogen.com

Merck Ltd., Hunter Boulevard, Magna Park, Lutterworth, Leics, LE17 4XN
www.merckeurolab.ltd.uk

Millipore (U.K.) Limited, Units 3&5 The Courtyards, Hatters Lane, Watford, WD18 8YH
www.millipore.com

Miltenyi Biotec Ltd., Almac House, Church Lane, Bisley, Surrey, GU24 9DR
www.miltenyibiotec.com

Molecular Probes Europe, PoortGebouw, Rijnsburgerweg 10, 2333 AA Leiden The Netherlands
www.probes.com

MWG-Biotech AG, Mill Court, Featherstone Road, Wolverton Mill South, Milton Keynes, MK12 5RD
www.mwg-biotech.com

Nalge Nunc International, 75 Panorama Creek Drive, P.O. Box 20365, Rochester, NY 14602-0365
www.nalgenunc.com

National Diagnostics, Unit 4, Fleet Business Park, Itlings Lane, Hessle, Hull, HU13 9LX
www.nationaldiagnostics.com

New England Biolabs (UK) Ltd., 73 Knowl Piece, Wilbury Way, Hitchin, Hertfordshire, SG4 0TY
www.neb.com

Perkin Elmer Life Sciences, Perkin Elmer House, 204 Cambridge Science Park, Cambridge, CB4 0GZ
www.perkinelmer.com

Roche Diagnostics Ltd., Bell Lane, Lewes, East Sussex, BN7 1LG
http://biochem.roche.com

QIAGEN Ltd., Boundary Court, Gatwick Road, Crawley, West Sussex, RH10 2AX
www.qiagen.com

Santa Cruz Biotechnology, 2161 Delaware Avenue, Santa Cruz, CA 95060 USA
www.scbt.com

Sigma-Aldrich Company Ltd., The Old Brickyard, New Road, Gillingham, Dorset, SP8 4XT
www.sigma-aldrich.com

Stratagene Europe, Gebouw California, Hogehilweg 15 ,1101 CB Amsterdam Zuidoost, The Netherlands

www.stratagene.com

Surgipath Europe Ltd., Venture Park, Stirling Way, Bretton, Peterborough PE3 8YD
www.surgipath.com

ThermoHybaid, Action Court, Ashford Road, Ashford, Middlesex, TW15 1XB
www.thermohybaid.com

ThermoShandon, 171 Industry Drive, Pittsburgh, PA 15275, USA
www.thermo.com

Vical Incorporated, 9373 Towne Centre Drive, Suite 100, San Diego, California 92121-3088, USA
www.vical.com

Chapter 3: Characterisation of MHV-76

3.1. Aims

The field studies in Slovakia that resulted in the isolation of MHV-68 recovered five strains of herpesvirus from two species of rodents (Blaskovic *et al.*, 1980). Strains 60, 68 and 72 were isolated from the bank vole (*Clethrionomys glariolus*) and strains 76 and 78 were isolated from the yellow-necked wood mouse (*Apodemus flavicollis*). However, only MHV-68 and MHV-72 have been studied in detail (for recent reviews see Mistrikova *et al.*, 2000; Nash *et al.*, 2001). It was hypothesised that the study of MHV-76, which was isolated from a different species of rodent, might reveal differences between the viral strains that would yield further insights into gammaherpesvirus pathogenesis.

The aim of this project was to characterise MHV-76, and compare the molecular structure and biological features of MHV-76 with MHV-68. By comparing the two viruses, it would be possible to determine which differences in the viral genome were responsible for any alterations in phenotype observed.

3.2. Molecular characterisation of the MHV-76 genome

MHV-76 virus stocks were kindly provided by Dr. Mistrikova, Comenius University, Slovak Republic, and the virus stocks were plaque purified by limiting dilution three times on BHK-21 cells to obtain a pure virus stock (see 2.8.3). All virus stocks were grown by infection of BHK-21 cells at an MOI of 0.01 (see 2.5.1), and purified viral DNA was prepared for molecular analysis (see 2.2.17).

Detailed molecular characterisation of MHV-76 was performed by Dr. Andrew Davison and Steven Milligan at the MRC Virology Institute, Glasgow. Restriction fragment banding patterns with eight different restriction endonucleases and sequencing of the MHV-76 viral genome from co-ordinates 115,587 to 26,842 revealed the following differences between the MHV-68 and MHV-76 viral genomes (Macrae *et al.*, 2001).

1. Copy number variation in the internal repeat sequences (approximately 10 copies fewer of the 40bp element, and 12 copies more of the 100bp element).

2. A deletion of 9,538bp at the left end of the unique region in MHV-76 compared to MHV-68. MHV-76 therefore lacks the unique MHV-68 genes M1, M2, M3 and M4 and all 8 vtRNA-like sequences.
3. A nucleotide substitution at position 12,280, which leads to a substitution of a serine for a glycine residue in ORF 6.

To check that the 9,538bp deletion was a true deletion and not re-arranged elsewhere within the viral genome, MHV-76 genomic DNA was analysed by PCR as previously described (see 2.2.1). MHV-76 and MHV-68 viral DNA was purified from infected BHK-21 cells, and 40 cycles of PCR were performed on 1μg viral DNA template. Primers were used to amplify MHV-68 specific ORFs (see Chapter 2, Appendix 2) including M1 (M1for and M1rev primers), M2 (M2GEX1 and M2GEX2 primers), M3 (M3+ and M3- primers), M4 (M4A and M4B primers), gp150 (gp150A and gp150B primers), M11 (M11+ and M11- primers), ORF73 (ORF73+ and ORF73-) and ORF74 (GCR-5' and GCR-3' primers). Negative control reactions were performed for all primer sets using water instead of template DNA. A 10μl sample of the products was analysed on a 1% TAE agarose gel.

All primer sets were able to amplify correctly sized sequences from MHV-68 DNA (Figure 3.2A and 3.2B). In contrast, no sequences corresponding to M1, M2, M3 and M4 were amplified from MHV-76 DNA showing that these ORFs are absent in MHV-76. However, correctly sized sequences corresponding to gp150, M11, ORF73 and ORF74 were amplified (Figure 3.2A and 3.2B). These results are consistent with the previous molecular characterisation, and show that MHV-76 is a deletion mutant of MHV-68 that lacks M1, M2, M3, most of the 5' portion of M4 and all eight vtRNA-like genes. This result is depicted schematically in Figure 3.2C.

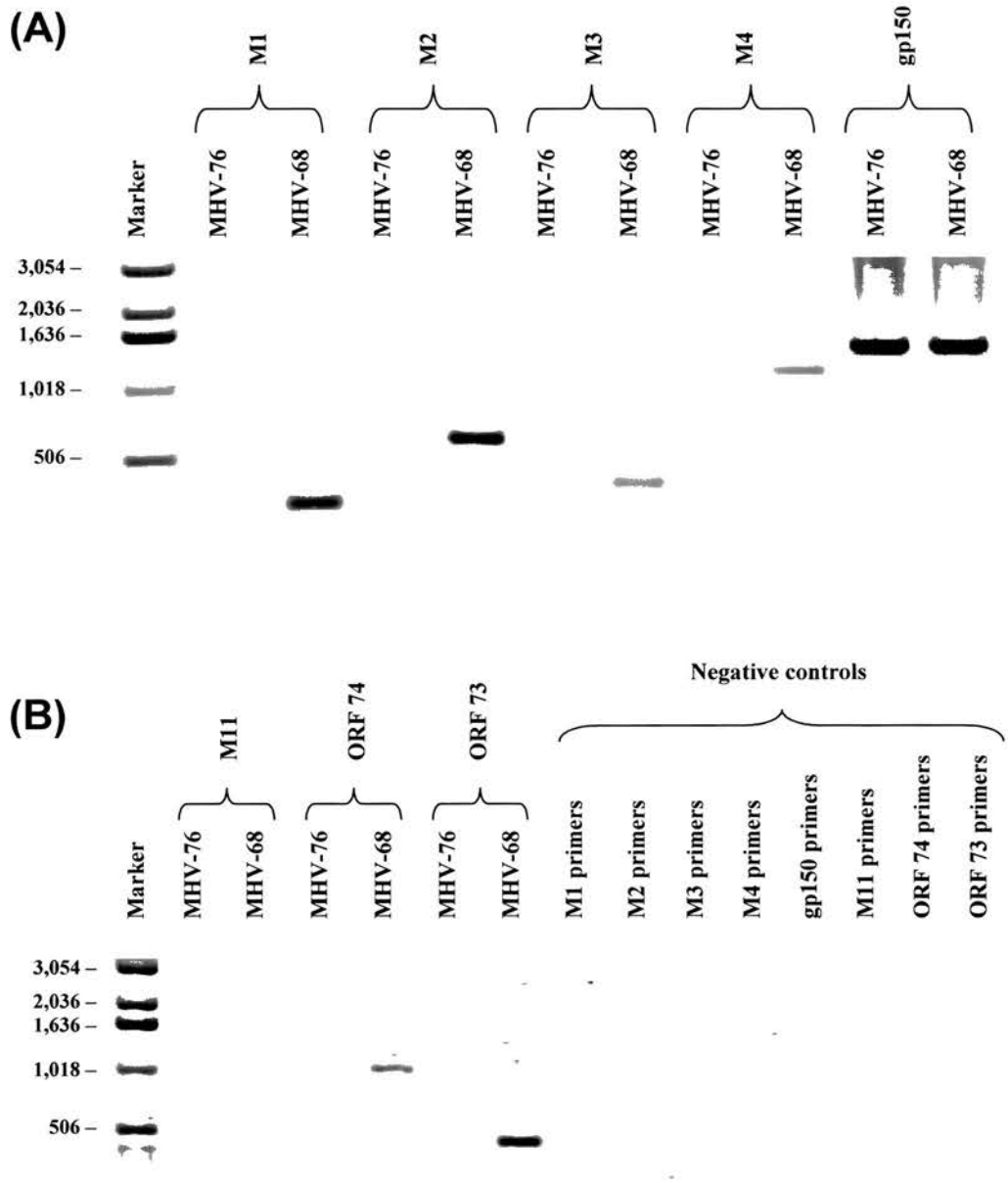

Figure 3.2 PCR analysis of MHV-76 and MHV-68 viral genomes. 40 cycle PCR was performed on 1μg viral DNA, and the products were analysed on a 1% TAE agarose gel. Molecular weights are shown relative to the marker on the left hand side. **(A)** PCR using primers specific for the M1, M2, M3, M4 and gp150 genes. **(B)** PCR using primers specific for M11, ORF 74 and ORF 73, and negative control reactions.

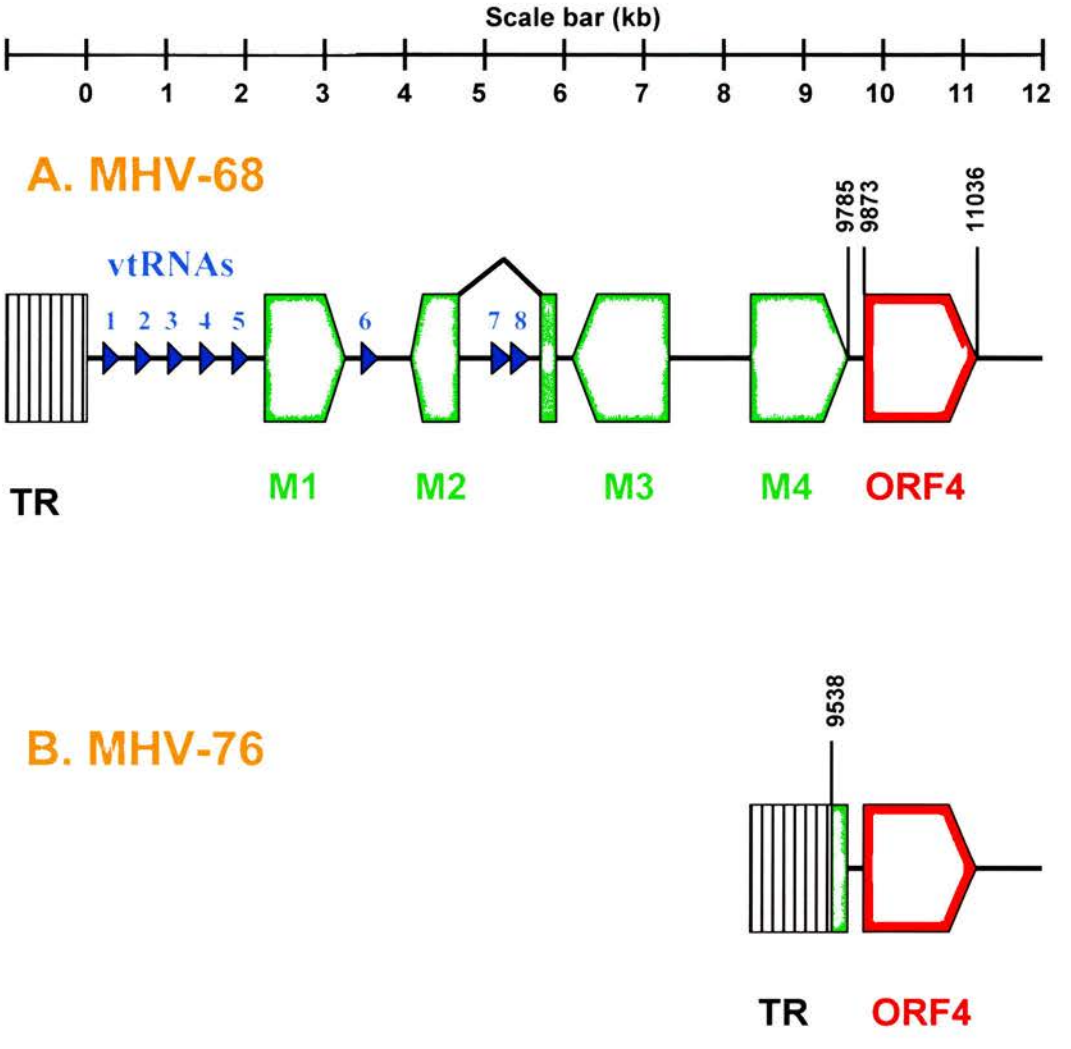

Figure 3.2C Schematic diagram of the structures present at the left end of the unique region of the genome in MHV-68 (A) and MHV-76 (B). The unique region of the genome from the terminal repeats to 12kb is shown as a black line, with green arrows indicating MHV-68 unique ORFs (M1, M2, M3 and M4), blue arrowheads indicating the eight viral tRNA-like sequences (vtRNAs) and the red arrow indicating ORF 4 (complement regulatory protein). The green rectangle in MHV-76 denotes the remaining M4 sequence, joined to the terminal repeats (TR). Scale bar at the top of the diagram represents 1kb divisions. Genomic co-ordinates of relevant positions are given in black above the features, according to Virgin *et al.*, 1997.

3.3. Biological characterisation of MHV-76

3.3.1. Replication *in vitro*

The replication of MHV-76 *in vitro* was assessed by a one-step growth curve. BHK-21 cells were infected with MHV-76 or MHV-68 at an MOI of 5, and harvested at various timepoints post-infection as previously described (see 2.5.3). MHV-76 replicated with the same kinetics and achieved similar titres to MHV-68 (Figure 3.3.1). Thus there was no significant difference between the replication of MHV-68 and MHV-76 *in vitro* as measured by this assay.

3.3.2. Replication in the lung

The ability of MHV-76 to replicate productively *in vivo* was assessed. Mice were infected with 2 x 10^5 PFU MHV-76 or MHV-68 (see 2.6.1) and the virus titre in the lungs determined at various times post-infection by plaque assay (see 2.6.4). Figure 3.3.2 shows the results of a single experiment, and is representative of four separate experiments. When compared to MHV-68, MHV-76 replication in the lungs peaked at day 4 post-infection (compared to day 6 in MHV-68 infection) and was cleared more rapidly from the lungs. At day 6 post-infection, there was approximately a $\log_{10}$ difference in viral titres between MHV-76 and MHV-68 ($P<0.001$), and by day 8, MHV-76 had nearly been cleared from the lung. These results show than MHV-76 can replicate productively *in vivo*, but is cleared more rapidly from the site of primary viral replication.

3.3.3. Lytic replication in other organs

Examination for other sites of lytic viral replication *in vivo* was also undertaken. Mice were infected with 2 x 10^5 PFU MHV-76 or MHV-68 (see 2.6.1) and the virus titre in the adrenal glands, heart and kidneys determined at various times post-infection by plaque assay (see 2.6.4). In the adrenal glands, virus was detectable in MHV-68 infected mice in variable amounts up to 8 days post-infection, achieving maximum titres of 100 PFU per adrenal (Figure 3.3.3). In contrast, no virus was detectable in the adrenals of mice infected with MHV-

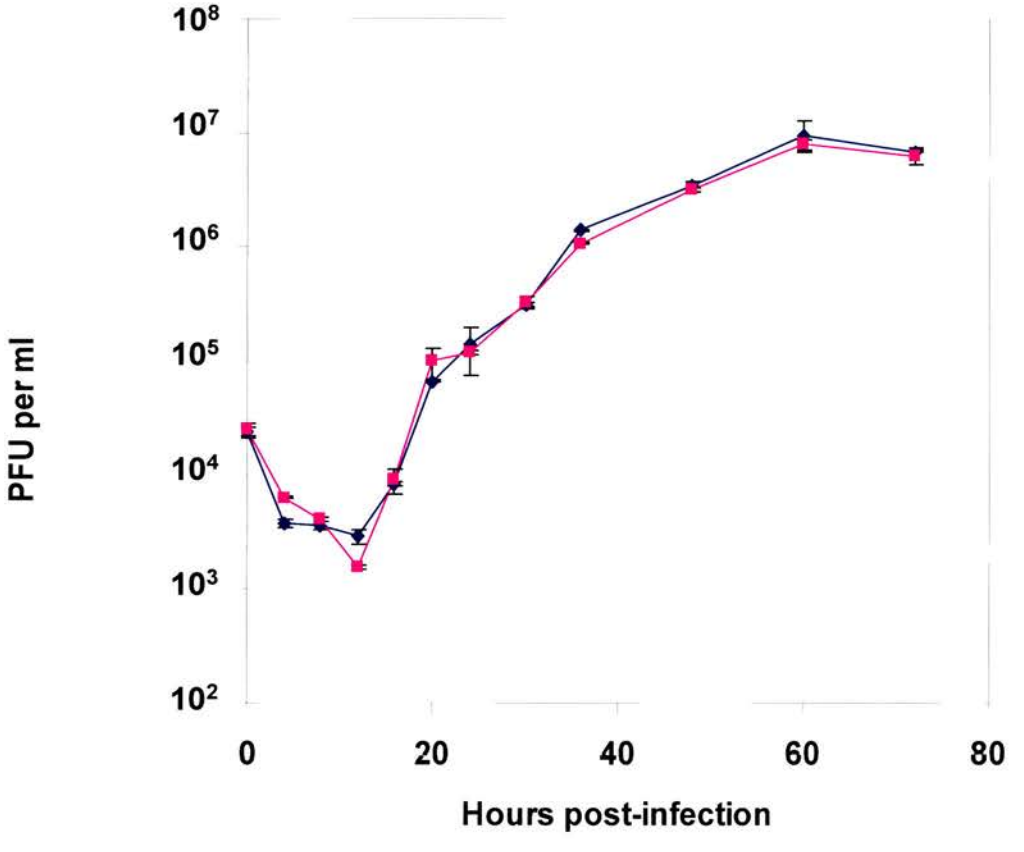

Figure 3.3.1 One step growth curve of MHV-68 (◆) and MHV-76 (■) on BHK-21 cells at an MOI of 5. Data points are shown for virus titre $\log_{10} \pm$ standard error. The results shown are representative of two separate experiments, each carried out in duplicate.

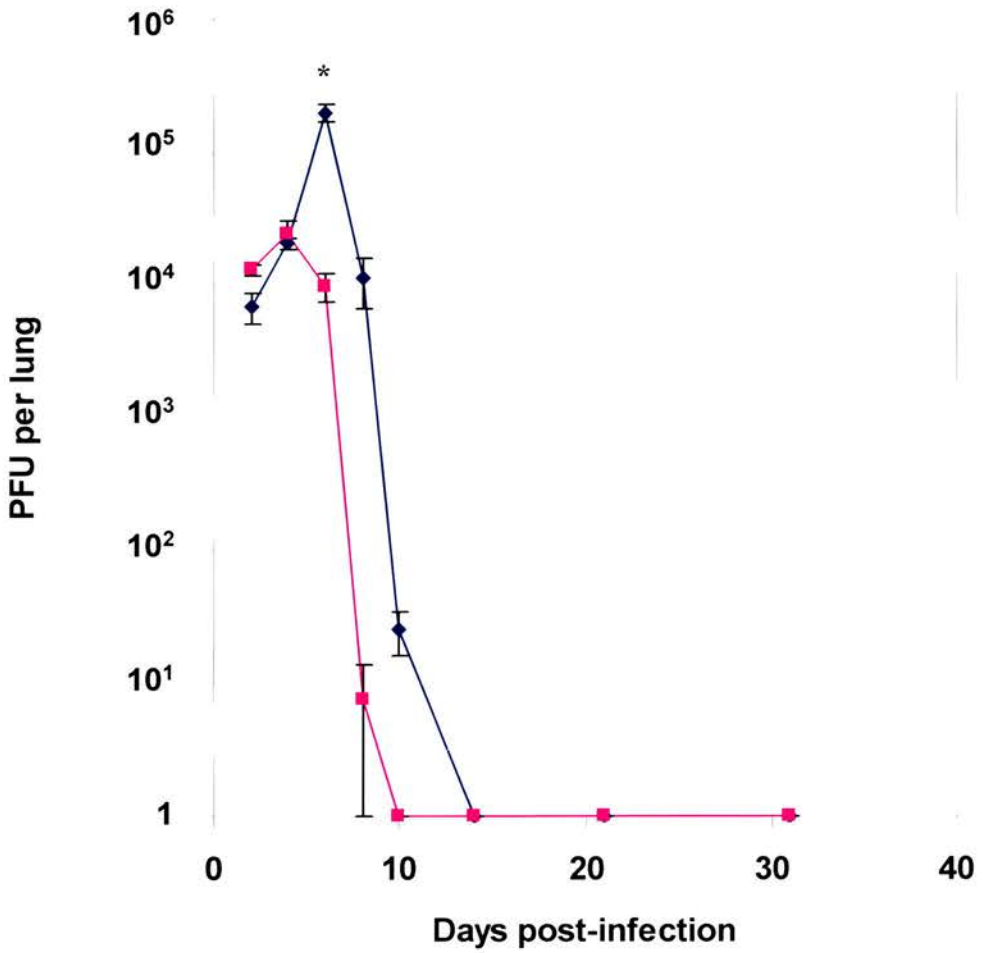

Figure 3.3.2 Viral titres in the lungs of BALB/c mice infected intranasally with 2 x 10^5 PFU of MHV-68 (◆) or MHV-76 (■). Mean virus titre $\log_{10}$ per lung ± standard error for four mice per group is shown for each time point. The results are representative of four separate experiments. * indicates statistically significant difference between MHV-76 and MHV-68 viral titres as determined by two-way ANOVA with Bonferroni post-tests.

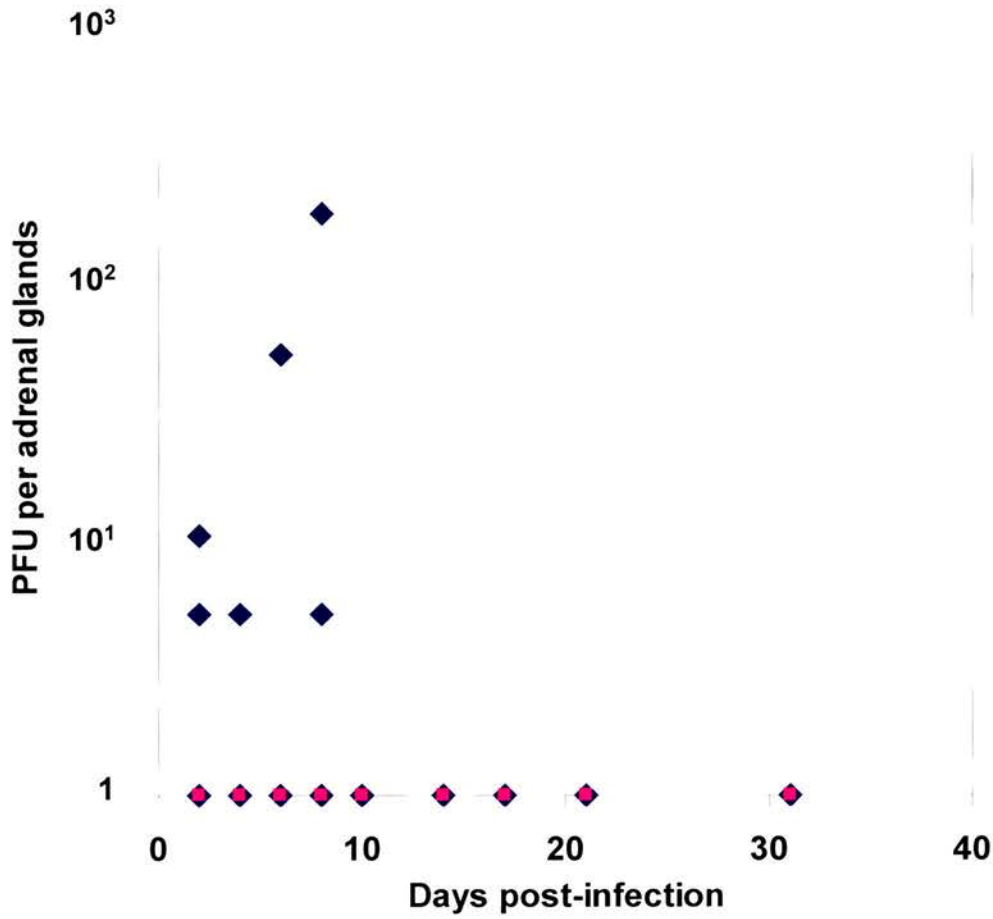

Figure 3.3.3 Infectious virus in the adrenal glands of BALB/c mice infected intranasally with 2 x 10^5 PFU of MHV-68 (◆) or MHV-76 (■). Virus titre $\log_{10}$ per adrenal glands per mouse is shown for four mice per group for each timepoint.

76. No virus was detectable by plaque assay in the heart or kidneys of mice infected with either MHV-76 or MHV-68 (data not shown).

3.3.4. Virus-induced splenomegaly

To determine the extent of splenomegaly during MHV-76 infection, the spleen weight (see 2.6.2) and total number of splenocytes (see 2.6.3) was determined in BALB/c mice infected intranasally with either MHV-76 or MHV-68. As seen in Figure 3.3.4A and B, MHV-68 induced a characteristic increase in spleen weight and total splenocyte numbers that peaked at two weeks post-infection. MHV-76 infection also caused a slight increase in spleen weight and cell numbers, but there was a significant reduction in total spleen weight and total number of splenocytes after infection with MHV-76 compared with MHV-68. This difference in spleen cell numbers was most pronounced at day 14 post-infection ($P<0.001$) and continued during the resolution phase (day 17 and 21: $P<0.01$). Figure 3.3.4 shows the results of a single experiment, and is representative of four separate experiments.

3.3.5. Latent virus in blood leukocytes

The ability to detect latent virus in blood leukocytes was determined for mice infected with MHV-76 and MHV-68 by infective centre assay (see 2.6.3). Latent virus was detectable at 2 – 3 weeks post-infection, with less than 1 in 10^5 blood leukocytes latently infected with MHV-68 (Figure 3.3.5). Only one mouse had detectable latent MHV-76 in blood leukocytes, but the low level of detectable latent virus in all mice meant that these results were not significant.

3.3.6. Latent virus in the spleen

The establishment of latency *in vivo* was determined using an infective centre assay (see 2.6.3) to detect latently infected splenocytes at various timepoints post-infection in BALB/c mice infected intranasally with MHV-76 and MHV-68. Latent MHV-68 was detected at day 6 post-infection and peaked at 2 weeks post-infection (Figure 3.3.6). Latent MHV-76 was also detected in the

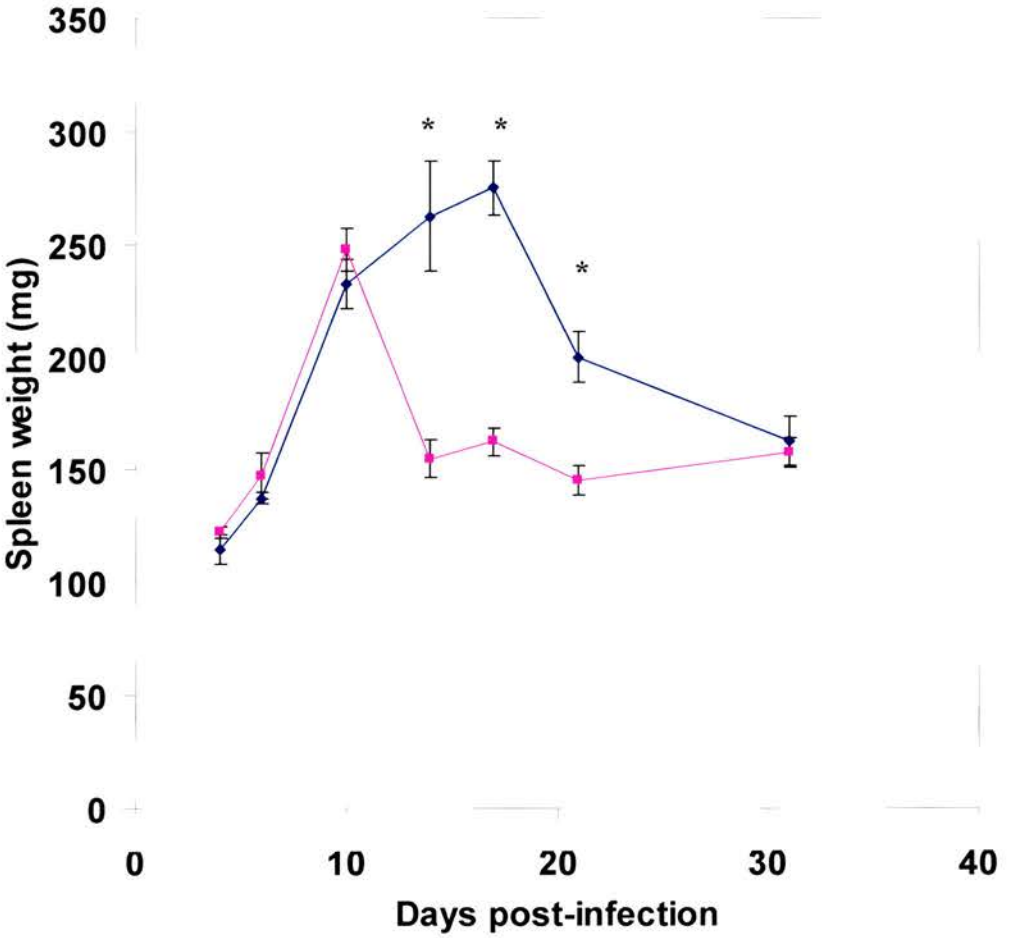

Figure 3.3.4A Spleen weights of BALB/c mice infected intranasally with 2 x 10^5 PFU of MHV-68 (—◆—) or MHV-76 (—■—). Mean spleen weight (mg) ± standard error is shown for four mice per group for each timepoint. The results are representative of four separate experiments. * indicates statistically significant difference between MHV-76 and MHV-68 spleen weights as determined by two-way ANOVA with Bonferroni post-tests.

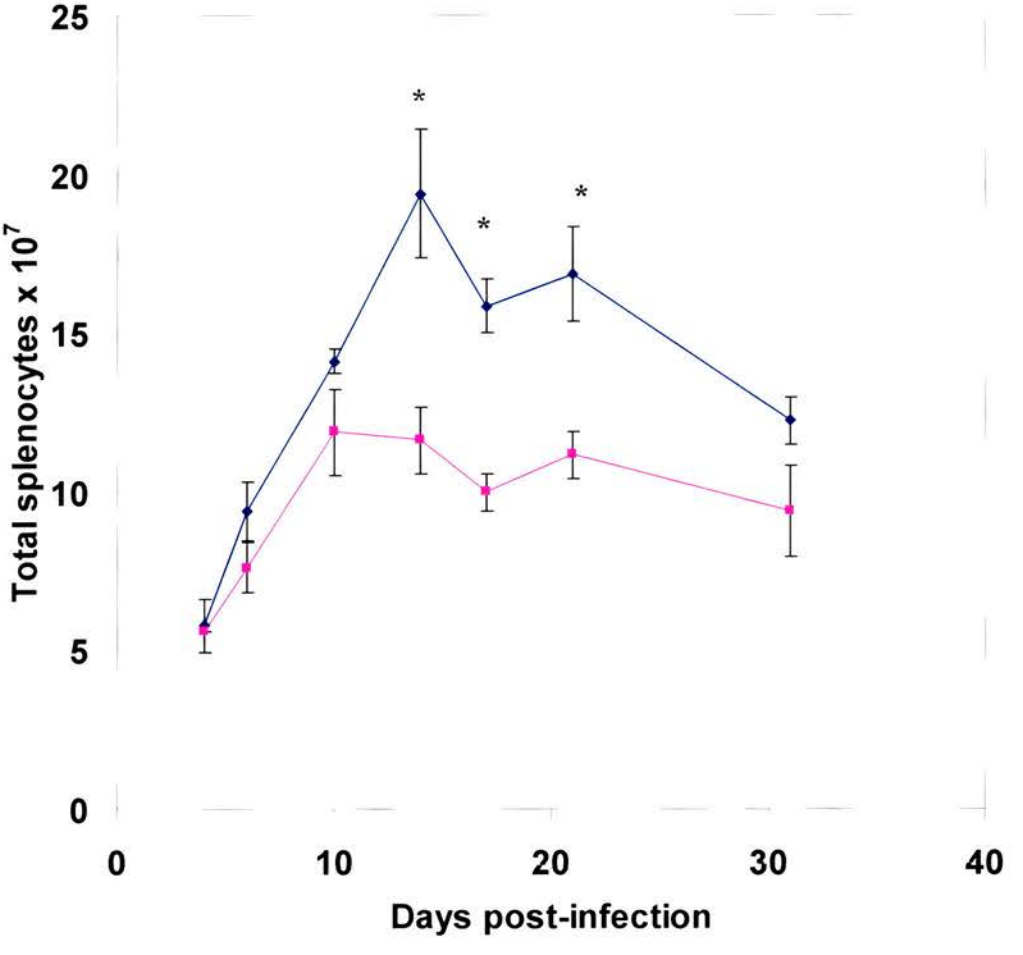

Figure 3.3.4B Total splenocyte numbers of BALB/c mice infected intranasally with 2 x 10^5 PFU of MHV-68 (◆) or MHV-76 (■). Mean total number of splenocytes ± standard error is shown for four mice per group for each timepoint. The results are representative of four separate experiments. * indicates statistically significant difference between MHV-76 and MHV-68 total splenocyte numbers as determined by two-way ANOVA with Bonferroni post-tests.

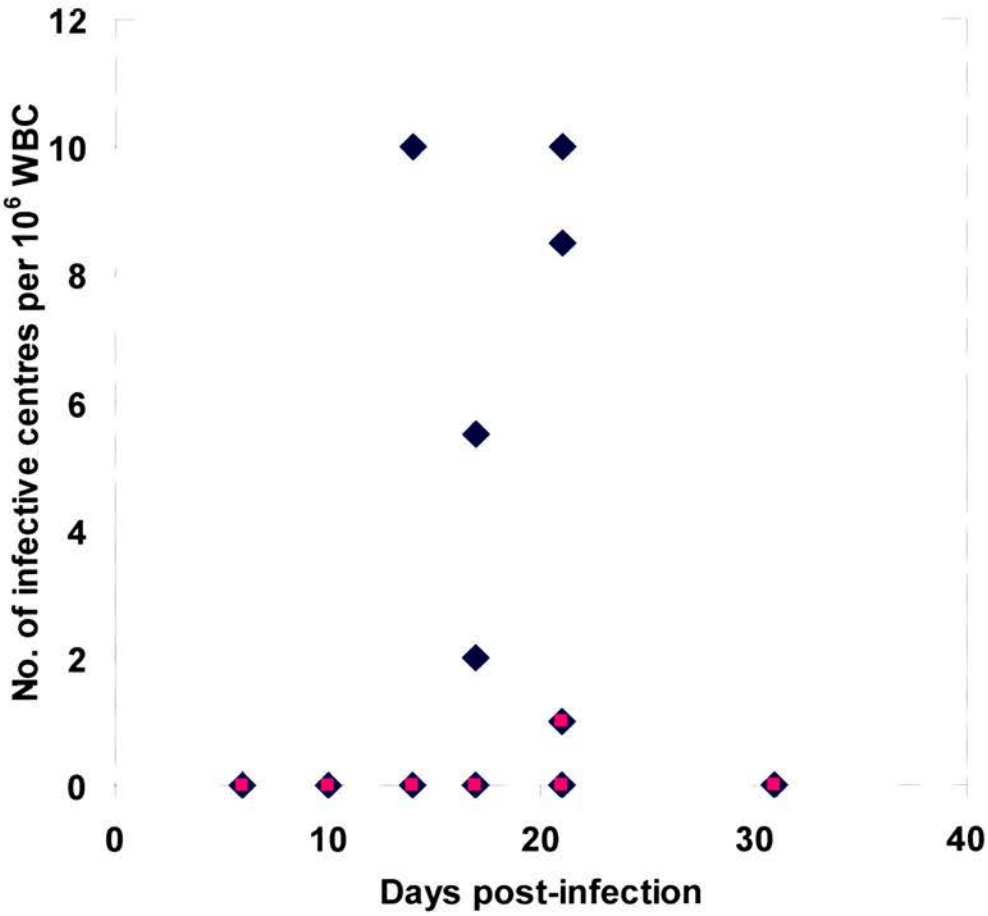

Figure 3.3.5 Latent virus in blood leukocytes of BALB/c mice infected intranasally with 2 x 10^5 PFU of MHV-68 (◆) or MHV-76 (■) as determined by infective centre assay. The number of infective centres per 10^6 blood leukocytes is shown per mouse with four mice per virus per timepoint. No preformed infectious virus was detected.

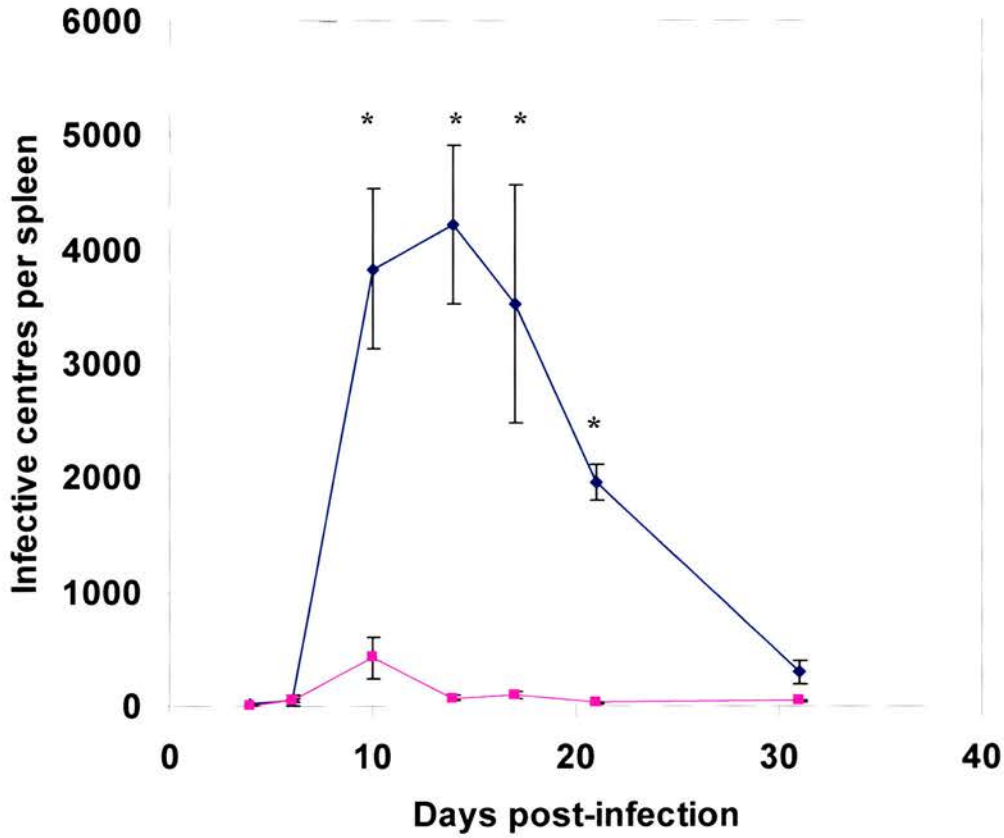

Figure 3.3.6 Latent virus in the spleens of BALB/c mice infected intranasally with 2 x 10^5 PFU of MHV-68 (◆) or MHV-76 (■) as determined by infective centre assay. Infectious virus titres (less than 50 PFU per spleen) were subtracted from the infective centre results. Mean infective centres per spleen ± standard error for four mice per group is shown for each timepoint. The results are representative of four separate experiments. * indicates statistically significant difference between the number of infective centres in mice infected with MHV-76 and MHV-68 as determined by two-way ANOVA with Bonferroni post-tests.

spleen, peaking at day 10 post-infection. However, the amount of latent MHV-76 was dramatically reduced compared to MHV-68. (Day 10, 14 and 17: $P<0.001$; Day 21: $P<0.01$). Figure 3.3.6 shows the results of a single experiment, and is representative of four separate experiments. A small amount of infectious virus (less than 50 PFU per spleen) was detectable in splenocytes up to 14 days post-infection (data not shown). Splenocytes latently infected with MHV-76 were still detectable at 31 days post-infection, at levels of 5 in 10^7 splenocytes. This result showed that MHV-76 can still establish latency in the spleen cell population *in vivo*, but at much lower detectable levels compared to MHV-68. This could be due to lower levels of latently infected splenocytes during MHV-76 infection, or due to defective reactivation from latency in the infective centre assay.

3.4. Determination of the splenocyte population harbouring latent MHV-76

One possible explanation for the marked reduction in latently infected splenocytes following MHV-76 infection was that MHV-76 might have an altered cellular tropism compared to MHV-68. To check which spleen cell populations were infected with latent MHV-76, two mice were infected with MHV-76, the spleens harvested at 14 days post-infection and the splenocytes separated into CD19+ cells (B lymphocytes) and CD19- cells (non-B lymphocytes) using MACS (see 2.6.6). The purity of the separated fractions was assessed by FACS analysis (see 2.6.7). The B lymphocyte population was over 90% pure, and the non-B cell fraction was contaminated with less than 3% CD19+ cells in both mice (Table 3.4).

The amount of latent virus in the B cell, non-B cell and total splenocyte populations was determined by infective centre assay (see 2.6.3). The majority of infective centres were present within the CD19+ B lymphocyte sub-population, with a small amount of latent virus detectable within the CD19- non-B lymphocyte fraction in one mouse (Figure 3.4). Separating the splenocyte populations by MACS did not have a significant effect on the ability of latent virus to reactivate in the infective centre assay, as judged by comparing the

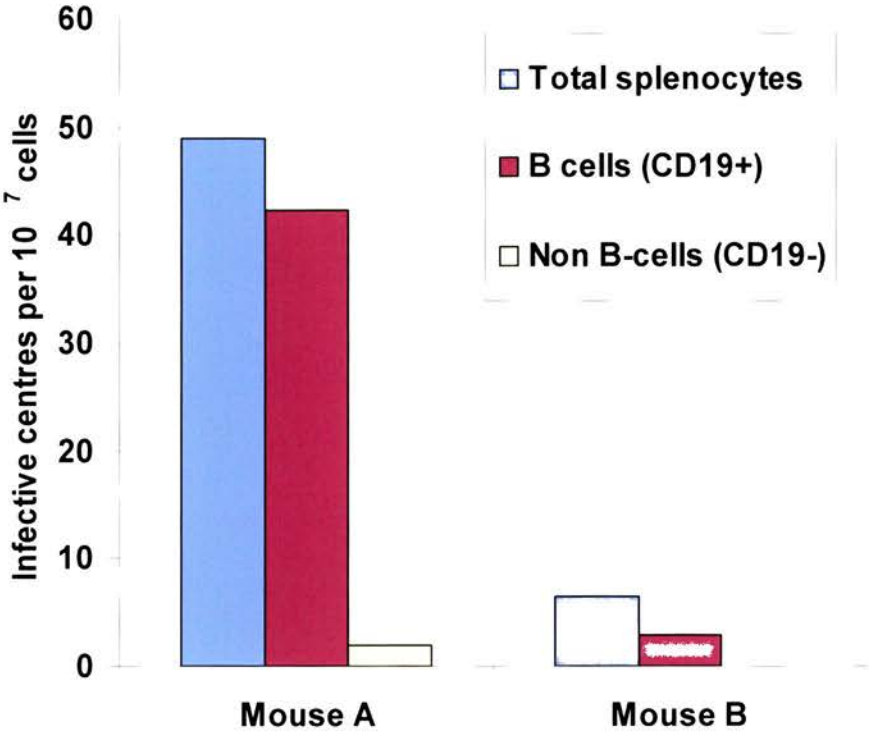

Figure 3.4 Determination of the splenocyte population harbouring latent MHV-76. Two mice were infected with 2 x 10^5 PFU of MHV-76, and the spleens harvested at day 14 post-infection. The splenocytes were sorted by MACS using CD19 antibody, and the amount of latent virus in the B cell (CD19+), non B cell (CD19-) and total splenocyte populations determined by infective centre assay. Results are shown as number of infective centres per 10^7 splenocytes for each fraction, for two mice.

	Mouse A			Mouse B		
	Total cells	B cells	Non B cells	Total cells	B cells	Non B cells
CD19+	68.5	95.1	2.9	58.1	92.0	1.12
CD4+	19.7	3.2	56.3	25.4	6.1	64.7
CD8+	7.2	0.5	24.0	7.6	0.5	28.63

Table 3.4 Purity of separated MHV-76 infected splenocytes sorted by MACS. Aliquots of each sorted fraction (Total cells, B cells, Non B cells) were incubated with fluorescent conjugated antibodies to cell surface markers CD4, CD8 and CD19, and analysed by FACS. Values are given as percentage of the total cells for each fraction.

number of infective centres in the total splenocyte populations with the separated cell fractions. The distribution of latent MHV-76 within the splenocyte population therefore appears to be similar to that of MHV-68, predominantly infecting B lymphocytes (Sunil-Chandra *et al.*, 1992b).

3.5. Long-term persistence of MHV-76 *in vivo*

The results of the infective centre assays showed that MHV-76 was able to establish latency *in vivo*. To determine whether MHV-76 is able to maintain long term persistence or is cleared by the immune system, mice were infected with MHV-76 and MHV-68. At 5 months post-infection, organs from these mice were analysed for the presence of virus. Three of the four mice infected with MHV-76 were positive by infective centre assay for latent virus in the spleen at levels of approximately 1-2 latently infected cells per 10^7 splenocytes. No infectious virus was detected in the splenocyte populations.

To detect virus in other organs, DNA was extracted from the liver, lung, kidney, spleen and white blood cells of four mice infected with MHV-76 at five months post-infection (see 2.6.10). As a positive control, one mouse infected with MHV-68 was harvested at 5 months post-infection. As a negative control, two uninfected mice were also analysed by this method. Extracted DNA was quantified (see 2.2.6), and PCR amplification was performed on 1μg of the extracted high molecular weight DNA using primers specific for the gp150 gene (Chapter 2, Appendix 2: gp150-1 and gp150-2). This was followed by Southern blot hybridisation with a ^{32}P-radiolabelled gp150-specific probe to confirm the identity of the PCR products (see 2.2.20). Positive controls (purified viral DNA template) and negative controls (no DNA template) were included for each set of PCR reactions. To determine the sensitivity of detection of viral DNA, tenfold copy number dilutions of cloned template DNA in a background of 1μg of high molecular weight DNA were analysed by this method. It was determined that this process was sensitive to between 1 and 10 copies of the viral genome in 1μg of high molecular weight DNA (data not shown).

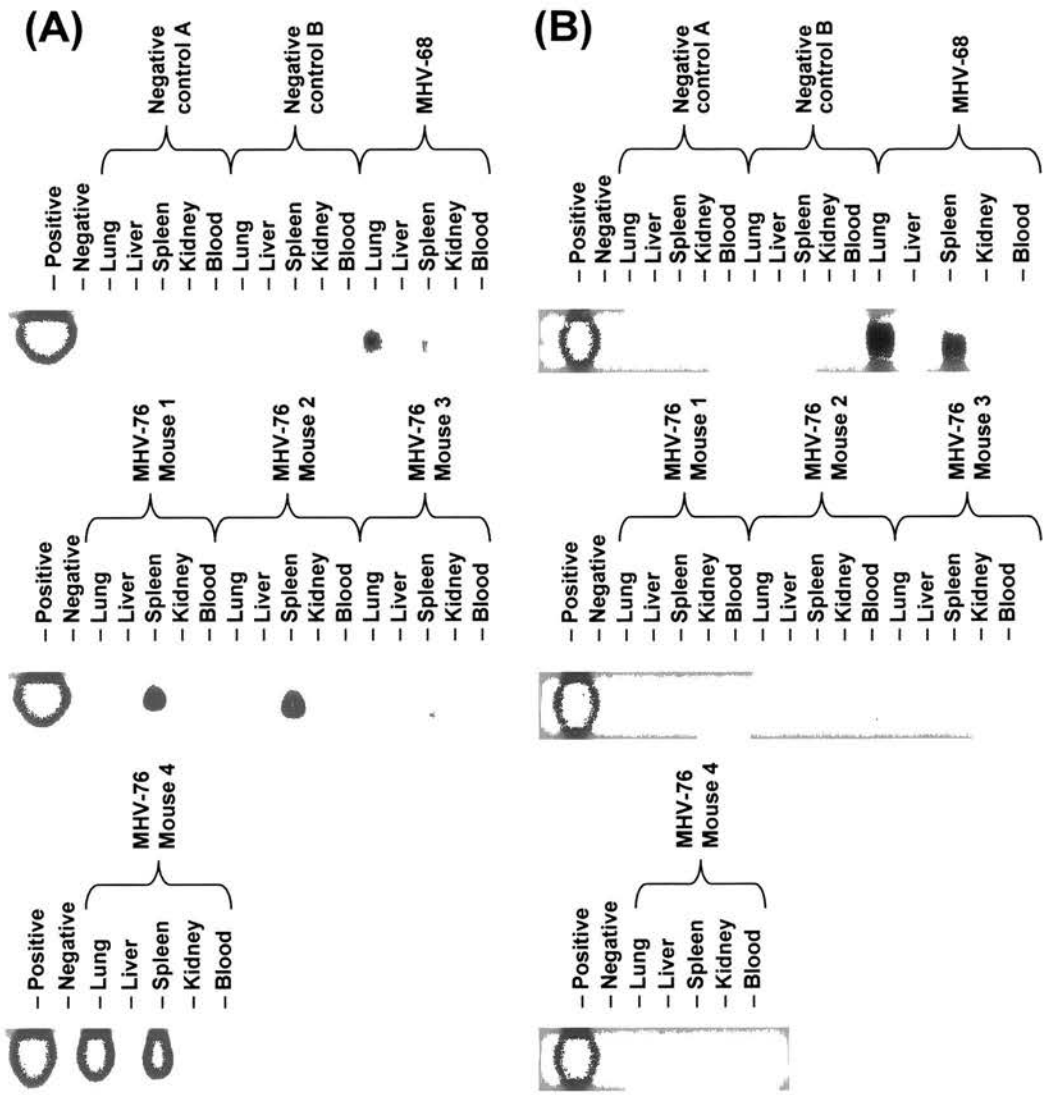

Figure 3.5 Detection of viral DNA in the tissues of mice at 5 months post-infection. Four BALB/c mice were infected with 2 x 10^5 PFU of MHV-76 and the lungs, liver, spleen, kidney and blood was harvested at 5 months post-infection. Two uninfected mice were also harvested as negative controls, and one mouse infected with MHV-68 was harvested as a positive control. Viral DNA was extracted and PCR amplification performed on 1µg of high molecular weight DNA. Positive control reactions containing MHV-68 viral DNA (first lane) and negative control reactions containing no DNA (second lane) were also performed. **(A)** PCR amplification using primers specific for gp150, followed by Southern hybridisation with ^{32}P-labelled gp150 probe to confirm specificity. **(B)** PCR amplification using primers specific for M3 (a gene absent from MHV-76), followed by Southern hybridisation with ^{32}P-labelled M3 probe to confirm specificity.

As shown in Figure 3.5A, viral DNA was not detected in any negative control reactions or uninfected mice. In the MHV-68 infected positive control mouse, viral DNA was detected in the lung and spleen, but not in the liver, kidney or white blood cells. In the MHV-76 infected mice, viral genomes were found in the spleens of all four mice, but only in the lungs of one mouse.

To ensure that the persisting virus detected in mice infected with MHV-76 was not due to contamination with MHV-68, 1μg of the extracted DNA was analysed by PCR using primers specific for the M3 gene (Chapter 2, Appendix 2: M3+ and M3-). The M3 gene is present in MHV-68 but absent from MHV-76. This was followed by Southern blot hybridisation with a ^{32}P-radiolabelled M3-specific probe to confirm the identity of the PCR products (see 2.2.20). As shown in Figure 3.5B, the M3 sequence was detected only in the positive control mouse infected with MHV-68, and not in the negative control uninfected mice or any of the mice infected with MHV-76. This results shows that the MHV-76 viral stocks were free of MHV-68, and the persisting virus in the mice was definitely MHV-76. The ability to detect MHV-76 both by infective centre assay and by the presence of the viral genome by PCR at late timepoints post-infection shows that MHV-76 can persist long-term *in vivo*.

3.6. Histopathological changes during MHV-76 infection

In order to examine any differences in the inflammatory response to MHV-76, mice were infected with either MHV-76 or MHV-68. The lungs and spleens were harvested at various times post-infection and examined by histopathology (see 2.6.8).

3.6.1. Histopathology of lung after viral infection

In the lung at day 4 following intranasal infection with MHV-76, there was a marked inflammatory reaction consisting of perivascular infiltration of lymphoid cells and oedema (Figure 3.6.1A). However, no inflammatory changes were observed at this time following MHV-68 infection (Figure 3.6.1B). By day 6 post-infection, the inflammatory changes seen during MHV-76 infection were

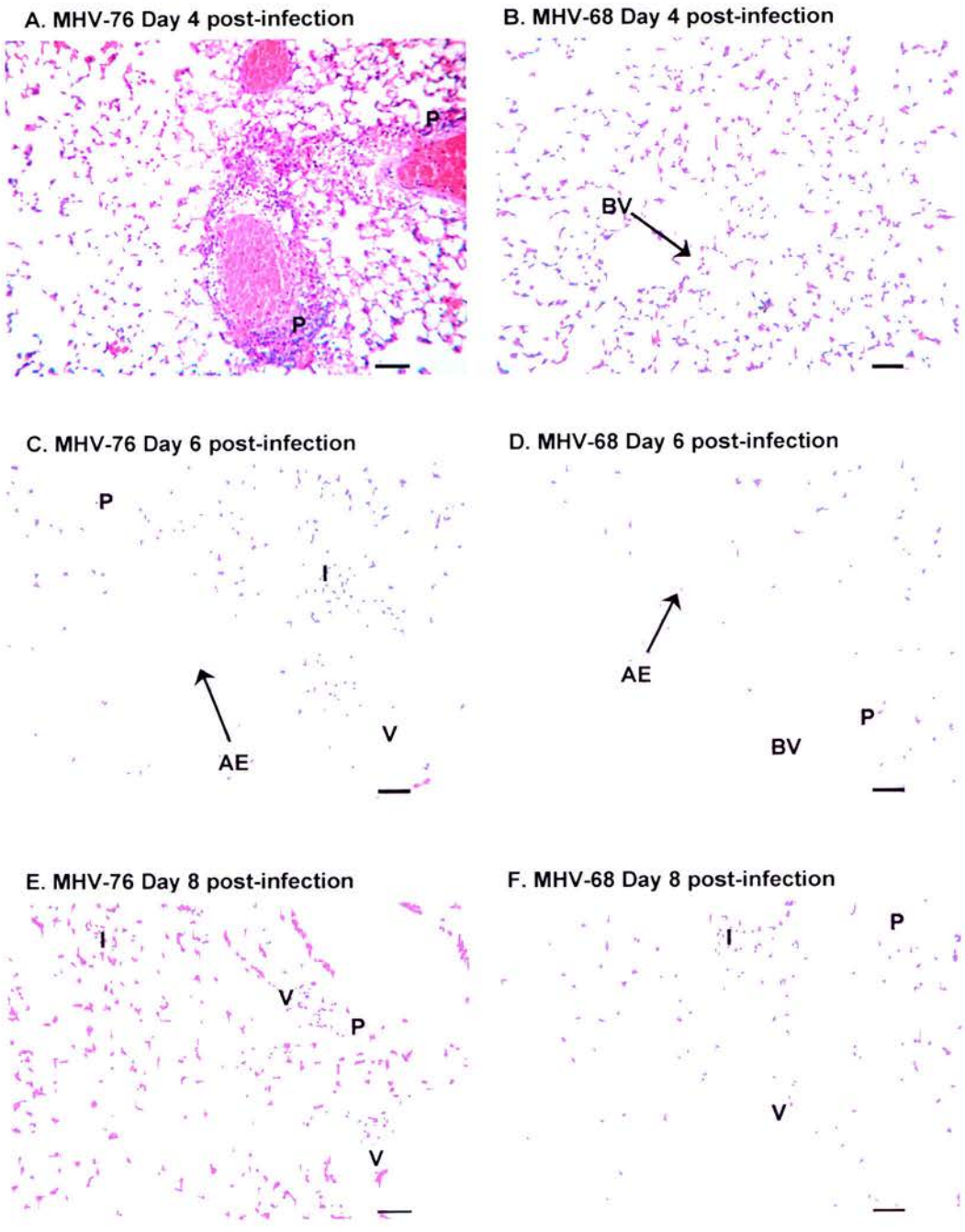

Figure 3.6.1 Histopathological changes in the lungs of mice infected with MHV-76 or MHV-68. Representative sections of lung stained with haematoxylin and eosin are shown for mice infected at the timepoints indicated. Scale bar represents 0.5mm Abbreviations: **P** – perivascular infiltration; **BV** – blood vessel; **AE** – alveolar exudate; **I** – interstitial infiltration; **V** – vasculitis.

marked, consisting of perivascular and interstitial lymphoid infiltration, intra-alveolar exudates and vasculitis (Figure 3.6.1C). Subpleural lymphoid accumulations were also observed (data not shown). In contrast, inflammatory changes were relatively minor in mice infected with MHV-68 at day 6 post-infection, consisting mostly of perivascular lymphoid aggregations and alveolar exudate (Figure 3.6.1D). At days 8 and 10 post-infection in the lung, no significant differences were observed in the inflammatory response between MHV-76 and MHV-68, which consisted of vasculitis and interstitial lymphoid accumulations (Figure 3.6.1E and 3.6.1F). These results demonstrate that the inflammatory changes seen in the lung during MHV-76 infection occur earlier and are more substantial compared to MHV-68.

3.6.2. Detection of viral antigens by immunostaining in the lungs

The enhanced inflammatory response to MHV-76 may have suppressed the expression of viral antigens in the lung, or altered the cell tropism of the virus. To examine for this possibility, lung sections were examined for the presence of viral antigens by immunostaining at days 4 and 6 post-infection using polyclonal anti-MHV-68 serum, and stained by the peroxidase method using DAB substrate (see 2.6.9). Viral antigen was readily detected in the lungs of MHV-76 and MHV-68 infected mice, showing that MHV-76 expresses very similar antigens to MHV-68 (Figure 3.6.2). Numerous positive cells were observed at day 4 and 6 post-infection in MHV-76 infected lungs, but there was no observable difference in either the amount or distribution of antigen-positive cells between MHV-76 and MHV-68 infected lungs (Figure 3.6.2 A and B). Most antigen positive cells were alveolar epithelial cells (Figure 3.6.2 C and D), and strong staining was observed in both the nucleus and cytoplasm. These results are consistent with previous results of immunostaining on MHV-68 infected lungs (Sunil-Chandra *et al.*, 1992a).

3.6.3. Histopathology of spleen after viral infection

The dramatic differences between the splenomegaly and amount of latent virus detectable following MHV-76 infection might lead to alterations in the

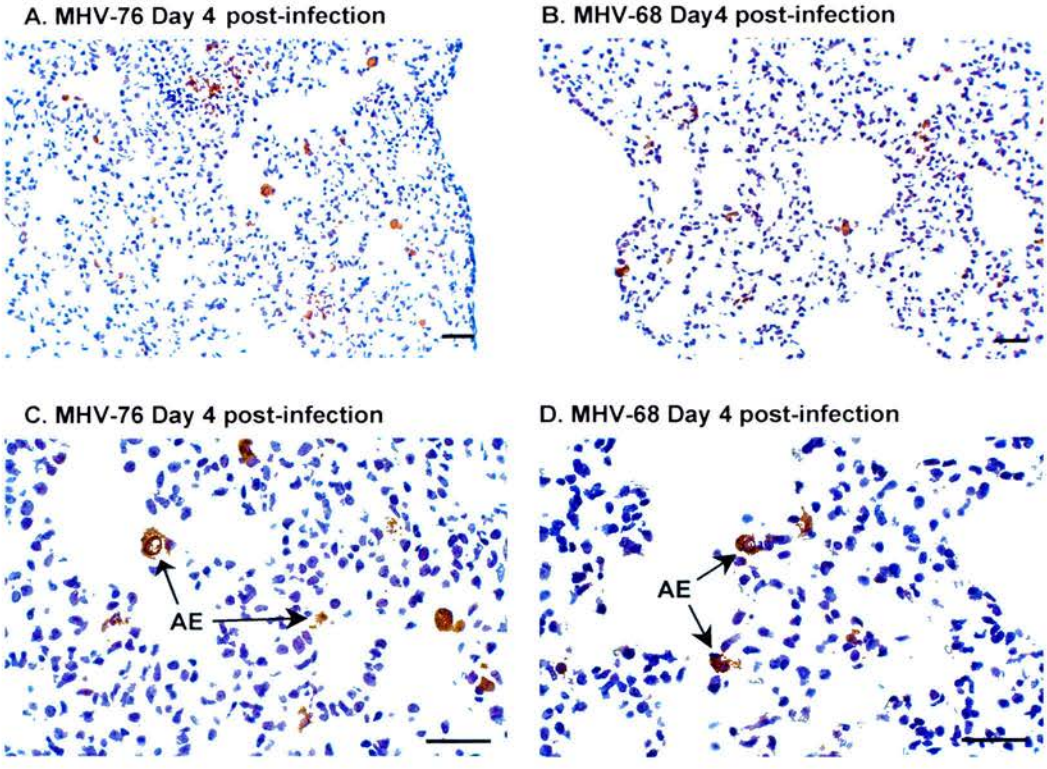

Figure 3.6.2 Detection of viral antigens by immunostaining in the lungs of mice infected with MHV-76 or MHV-68. Representative sections of lung were labelled using polyclonal anti-MHV-68 antiserum, and stained by the peroxidase method using DAB substrate. Sections were then counterstained with haematoxylin. Scale bar represents 0.5mm. Abbreviation: **AE** – alveolar epithelial cell.

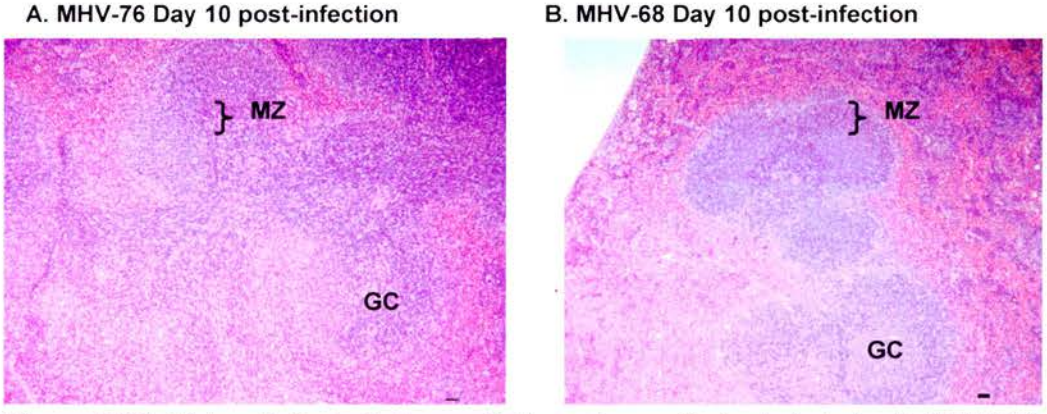

Figure 3.6.3 Histopathological changes in the spleens of mice infected with MHV-76 or MHV-68. Representative sections of spleen stained with haematoxylin and eosin are shown for mice infected at the timepoints indicated. Scale bar represents 0.5mm. Abbreviations: **GC** – germinal centre; **MZ** – marginal zone.

typical inflammatory response seen in the spleen following MHV-68 infection (Sunil-Chandra *et al.*, 1992a). To examine this, spleens of mice infected with MHV-76 and MHV-68 were examined by histopathology (Figure 3.6.3). In the spleen at day 10 and 14 post-infection with MHV-68 and MHV-76, there was evidence of active inflammation as shown by follicular hyperplasia, with germinal centre formation and an increase in the marginal zone of the white pulp (Figure 3.6.3A and 3.6.3B). There were no detectable histopathological differences between MHV-68 and MHV-76.

3.7. Construction and molecular characterisation of rescue viruses

To determine whether the differences in phenotype observed between MHV-68 and MHV-76 were due to deletion of genes at the left end of the unique region of the viral genome or due to unidentified mutations elsewhere in the genome, rescue viruses (rescuants) were constructed by reintroducing the left end of the unique region of the MHV-68 genome into MHV-76.

3.7.1. Construction and purification of rescue viruses

Rescuants were generated using cosmid A8 (Chapter 2, Appendix 3), by the co-transfection of BHK-21 cells with MHV-76 genomic DNA and cosmid A8 (see 2.8.1). Rescuants in which the deletion had been restored were likely to be less attenuated *in vivo* than MHV-76, and thus the resulting mixture of viruses was passaged in BALB/c mice. The spleens were harvested at 14 days post-infection and the latent virus reactivated using an infective centre assay (see 2.8.3). Individual plaques were then picked and purified by limiting dilution assay on BHK-21 cells (see 2.8.3). Virus plaques containing rescuants were identified by the presence or absence of M2 DNA using a PCR amplification screening method (see 2.8.3) with primers M2GEX1 and M2GEX2 (Chapter 2, Appendix 2). PCR amplification of ORF 74 DNA (Primers GCR-5' and GCR-3'; Chapter 2, Appendix 2) was used to check that the viral DNA was suitable for PCR amplification (data not shown). After 3 rounds of plaque purification and

screening, the plaques were judged to represent pure viral clones as evidenced by the fact that all subsequent viral plaque picks were positive for the M2 ORF by the PCR screening method.

After plaque purification, 3 individual viral clones were chosen for further characterisation. MHV-76(cA8+)3 and MHV-76(cA8+)4 were both positive for M2 by PCR, and were therefore rescuants in which the deleted region had been restored to MHV-76. MHV-76(cA8-)5 was negative for M2 by PCR but had been selected in exactly the same way as the rescue viruses, and was therefore chosen to control for any possible effects that the *in vivo* passage and subsequent isolation procedures may have had on the viruses.

3.7.2. Southern analysis of rescue viruses

DNA was made from virally infected cells (see 2.2.19) and Southern analysis was performed using diagnostic *Hin*dIII and *Eco*RI digestions (see 2.2.20). These digests were then probed with a ^{32}P-radiolabelled cosmid A8 probe. The cosmid A8 probe identifies the MHV-68 *Hin*dIII fragments B, C, E, G, I, J, N, S, T_2, U_2, Z_2 (Figure 3.7.2.2). However, in MHV-76 the *Hin*dIII E and U_2 fragments are deleted, and the J fragment is reduced in size (fragment JΔ) but becomes bound to the terminal repeats. Southern analysis showed that the rescue viruses MHV-76(cA8+)3 and MHV-76(cA8+)4 yielded identical profiles to MHV-68, containing the *Hin*dIII E fragment (Figure 3.7.2.1A). The *Hin*dIII E fragment was not present in MHV-76 or MHV-76(cA8-)5. The *Hin*dIII fragments S and Z_2 were too small to be visualised on the blot, and fragments containing the terminal repeats (U_2^+, T_2^+ and $J\Delta^+$) appeared as high molecular weight products.

A ^{32}P-radiolabelled probe consisting of the full length M3 ORF DNA (which crosses the *Hin*dIII E and J fragment junction; Figure 3.7.2.2) was also used to analyse the *Hin*dIII digest. The results showed that the correct sized *Hin*dIII E and J fragments were present in MHV-68, MHV-76(cA8+)3 and MHV-76(cA8+)4 but not in MHV-76 or MHV-76(cA8-)5 (Figure 3.7.2.1B). These results show that the rescue viruses MHV-76(cA8+)3 and MHV-76(cA8+)4 contain all of the sequence deleted in MHV-76.

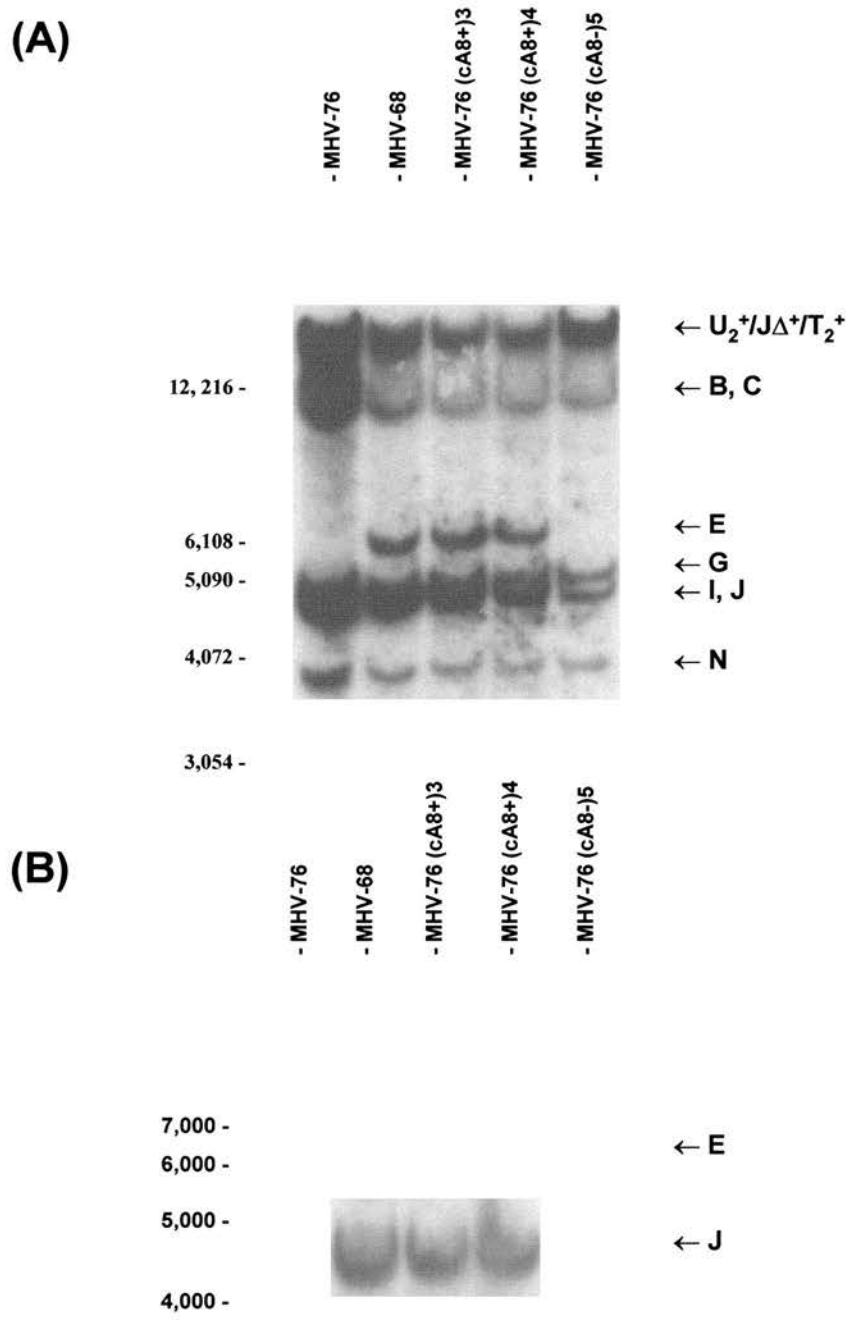

Figure 3.7.2.1 Southern analysis of rescue viruses. DNA was isolated from BHK-21 cells infected with MHV-76, MHV-68, MHV-76(cA8+)3, MHV-76(cA8+)4 and MHV-76(cA8-)5, digested with *Hin*dIII and analysed by Southern blot on a 0.8% agarose gel. The blots were hybridised with ^{32}P-labelled probes of **(A)** cosmid A8 or **(B)** M3 (nucleotides 6060-7277). The sizes of molecular weight markers in bp are shown on the left, and *Hin*dIII fragments on the right side of each autoradiograph.

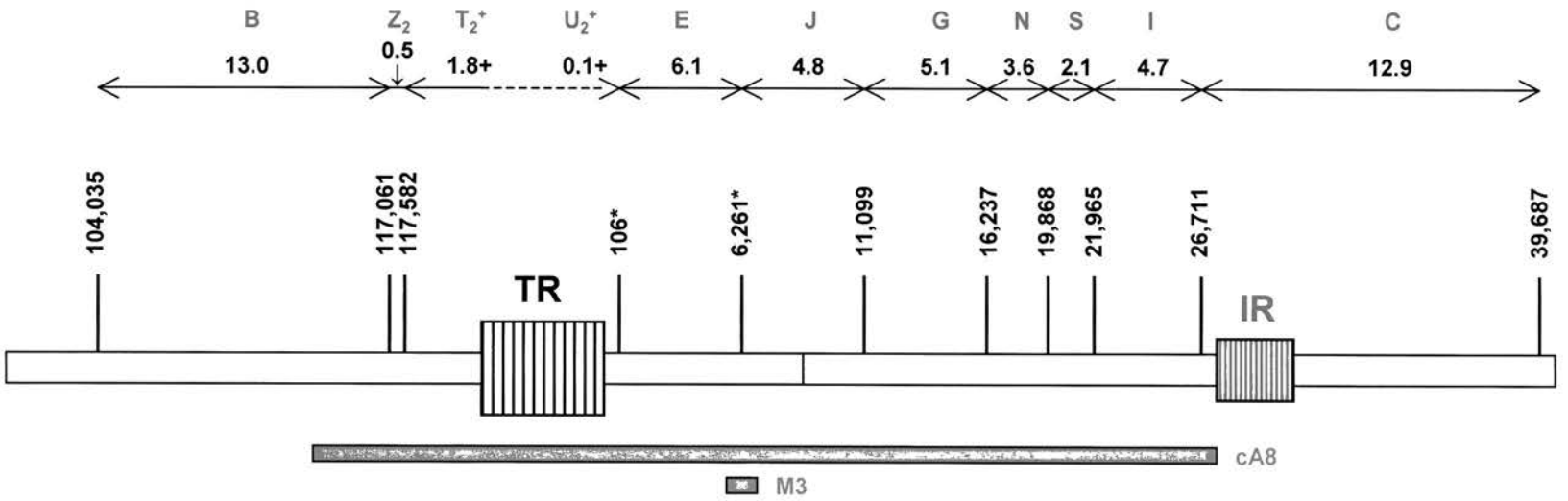

Figure 3.7.2.2 Interpretation of Southern analysis of rescue viruses. The unique region of the MHV-68 genome from nucleotide co-ordinates 100kb to 40kb is shown as a yellow bar, with the terminal repeats (TR) shown in black vertical bars, the 40bp internal repeat sequence (IR) in red vertical bars and the deletion present in MHV-76 represented in blue (MHV-68 co-ordinates: 1-9538). Restriction enzyme sites for *Hin*dIII are shown, with the fragment sizes in kb above and *Hin*dIII fragment designation in red above each fragment size (according to Efstathiou *et al.*, 1990a and Virgin *et al.*,1997). + denotes fragments that are bound to the terminal repeats in MHV-68 and thus appear as a ladder of larger bands on Southern blot. * denotes the *Hin*dIII restriction enzyme sites deleted in MHV-76. The location of probes used in Southern analysis is shown underneath by blue bars; cA8 (115,165-26,842) and M3 (6060-7277). Genomic co-ordinates are given according to Virgin *et al.*,1997.

3.7.3. PCR analysis of rescue viruses

To fully characterise the rescue viruses and check that all the deleted ORFs had been restored (Figure 3.2C), rescue virus DNA was analysed by PCR. Primers were used to amplify MHV-68 specific ORFs (see Chapter 2, Appendix 2) including M1 (M1for and M1rev primers), M2 (M2GEX1 and M2GEX2 primers), M3 (M3+ and M3- primers) and M4 (M4A and M4B primers). The results showed that M1, M2, M3 and M4 were all present in the rescue viruses MHV-76(cA8+)3 and MHV-76(cA8+)4, but were not present in the control virus MHV-76(cA8-)5 (Figure 3.7.3). As a control to check for template DNA integrity and concentration, primers for ORF 74 (GCR-5' and GCR-3' primers) amplified correctly sized DNA fragments from all three viral DNA samples. To check the purity of viral stocks, PCR amplification following proteinase K digestion of viral samples (see 2.8.3) gave the same results (data not shown). This result demonstrated that the rescuants MHV-76(cA8+)3 and MHV-76(cA8+)4 contain the unique MHV-68 genes M1, M2, M3 and M4, whereas the control virus MHV-76(cA8-)5 and MHV-76 do not contain these genes.

Dr. Andrew Davison, MRC Virology Institute, Glasgow, also undertook sequence analysis of the region containing nucleotide 12280. This showed that MHV-68, MHV-76(cA8+)3 and MHV-76(cA8+)4 contained a G residue at this position, and that MHV-76 and MHV-76(cA8-)5 contained an A residue. This showed that sequences adjacent to the deletion in MHV-76 had also been rescued by cosmid A8.

3.7.4. Derivation of rescue viruses

The MHV-76 rescue viruses did not contain any marker genes (e.g. green fluorescent protein or β-galactosidase), and therefore contamination with wild-type MHV-68 was a possibility. In other gammaherpesviruses such as EBV, the copy number of the internal repeat sequences has been shown to vary between viral strains (Bornkamm *et al.*, 1980) and this has recently been shown to also occur in MHV-68 (Adler *et al.*, 2000). Therefore determination of the copy number of the 100bp repeat in the viral genome would help to assess the origin of the rescue viruses. Viral DNA was digested with *Hin*cII (which digests the viral

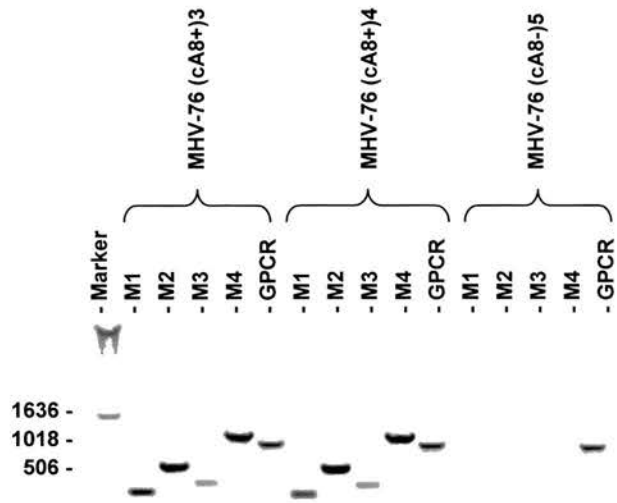

Figure 3.7.3 PCR analysis of viral DNA from MHV-76(cA8+)3, MHV-76(cA8+)4 MHV-76(cA8-)5. 40 cycle PCR analysis was performed using primers specific for the unique MHV-68 genes M1, M2, M3 and M4 and also ORF 74 (GPCR), and the products analysed on a 1% agarose gel. The sizes of molecular weight markers in bp are shown on the left.

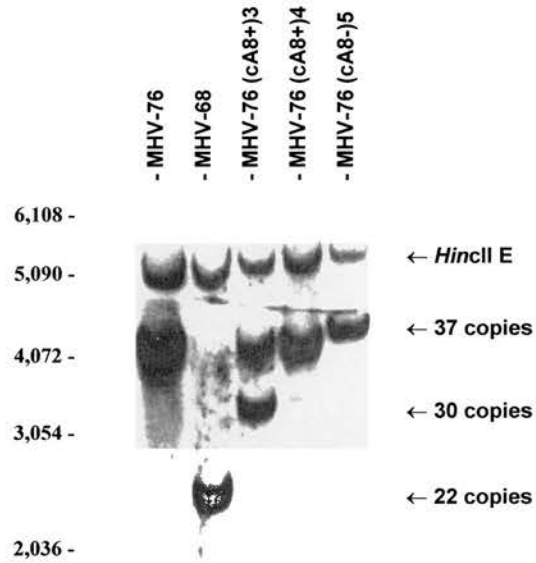

Figure 3.7.4.1 Derivation of rescue viruses. DNA was isolated from BHK-21 cells infected with MHV-76, MHV-68, MHV-76(cA8+)3, MHV-76(cA8+)4 and MHV-76(cA8-)5, digested with *Hin*cII and analysed by Southern blot on a 0.8% agarose gel. The blots were hybridised with ^{32}P-labelled *Bam*M probe (containing the 100bp repeat). The sizes of molecular weight markers in bp are shown on the left, and *Hin*cII E fragment or approximate copy number of the 100bp repeat sequence on the right side of the autoradiograph.

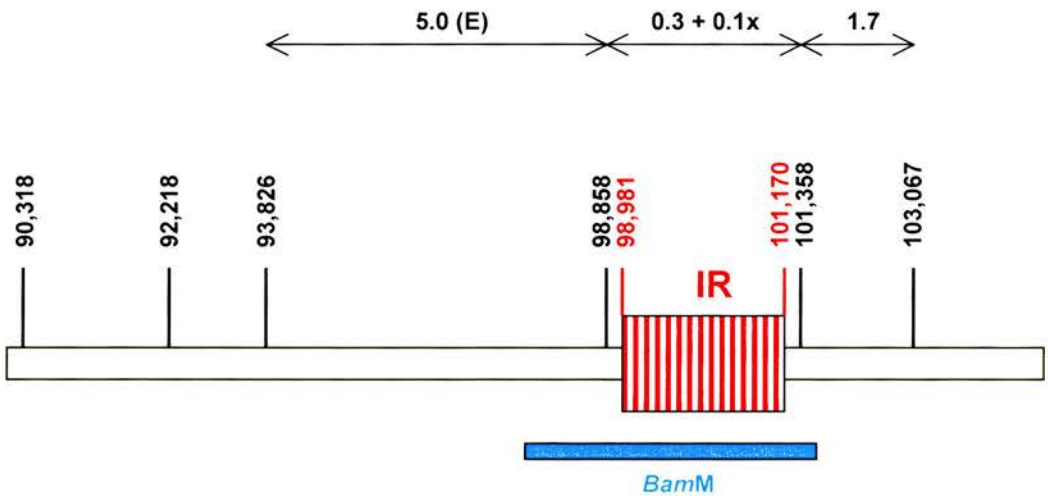

Figure 3.7.4.2 Interpretation of Southern analysis for the determination of the copy number of the 100bp internal repeat sequence. The unique region of the MHV-68 genome from nucleotide co-ordinates 90kb to 105kb is shown as a yellow bar, with the 100bp internal repeat sequence (IR) in red vertical bars (MHV-68 nucleotide co-ordinates 98,981 - 101,170 shown in red above). Restriction enzyme sites for *Hin*cII are shown in black, with the fragment sizes in kb and fragment designation above. The location of the *Bam*M probe used in Southern analysis is shown underneath as a blue bar (nucleotide co-ordinates 97,586 - 101,653). The size of the *Hin*cII fragment containing the 100bp internal repeat sequence is given in kb by the formula 0.3 + 0.1x, where x is the number of copies of the 100bp internal repeat sequence. Genomic co-ordinates are given according to Virgin *et al.*, 1997.

genomic DNA at positions 98858 and 101358 either side of the 100bp repeat), and then analysed by Southern blot using a radiolabelled *Bam*M probe (Efstathiou *et al.*, 1990b), which is predicted to hybridise to the fragment containing the 100bp repeat (Figure 3.7.4.2). This confirmed that the estimated copy number of the MHV-68 100bp internal repeat sequence was 22 (21 complete copies and a 90bp partial repeat; Figure 3.7.4.1; Virgin *et al.*, 1997). However in MHV-76, MHV-76(cA8+)4 and MHV-76(cA8-)5, the fragment containing the 100bp repeat was approximately 4kb in size, corresponding to approximately 37 copies of the 100bp repeat (Figure 3.7.4.1). MHV-76(cA8+)3 appeared to consist of two viral populations with 37 and 30 copies of the 100bp repeat sequence. MHV-76, the two rescue viruses and the control virus contained a larger number of copies of the 100bp repeat compared to MHV-68, and these results prove that the rescue viruses were all derived from MHV-76, and were not produced by contamination with MHV-68. As MHV-76(cA8+)3 appeared to consist of two virus populations, this virus was not studied further.

3.8. Biological characterisation of rescue viruses

3.8.1. Replication *in vitro*

To investigate the effect of the 9.5kb deletion in MHV-76 on viral replication *in vitro*, the replication of MHV-68, MHV-76, MHV-76(cA8+)4 and MHV-76(cA8-)5 was compared in a single round of replication in BHK-21 cells (one-step growth curves at an MOI of 5; see 2.5.3). The one-step growth curves showed that all viruses replicated at a similar rate *in vitro* (Figure 3.8.1), demonstrating that the deleted sequence has no detectable effect on lytic replication in BHK-21 cells.

3.8.2. Replication in the lung

BALB/c mice were infected with 2 x 10^5 PFU of MHV-68, MHV-76, MHV-76(cA8+)4 or MHV-76(cA8-)5 intranasally and the virus titre in the lungs was assessed at various timepoints post-infection by plaque assay (see 2.6.4). The

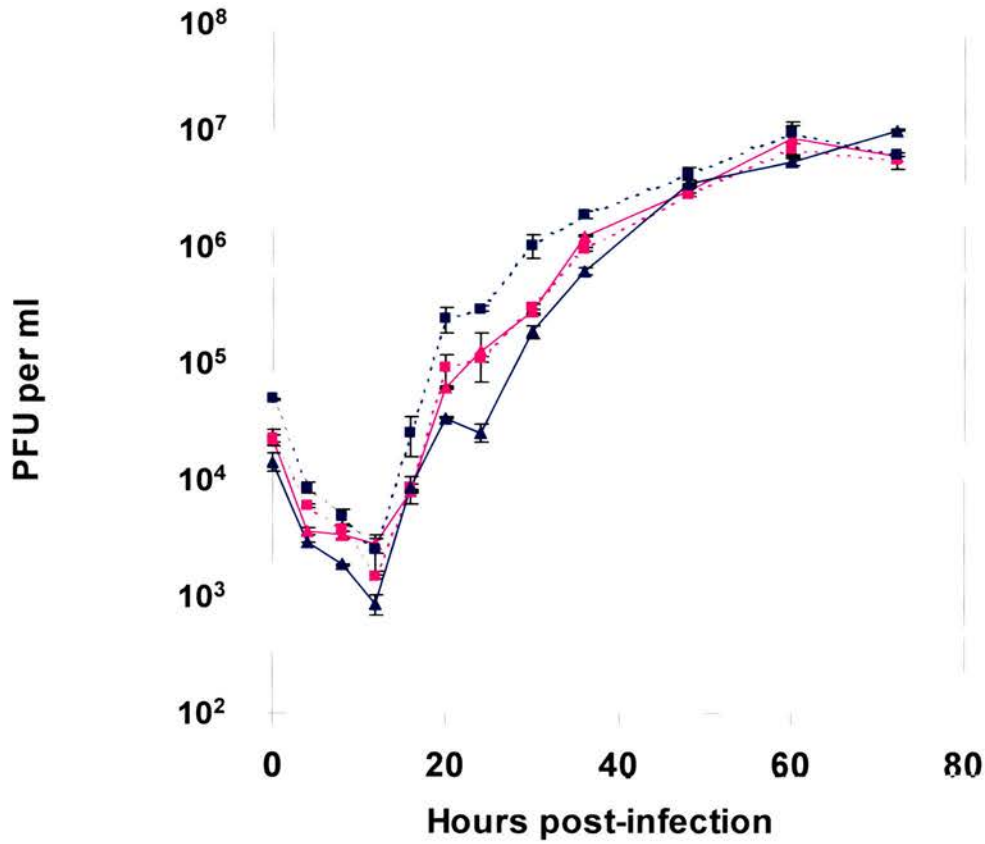

Figure 3.8.1 One step growth curve of MHV-68 ( ), MHV-76 ( ), MHV-76(cA8+)4 ( ) and MHV-76(cA8-)5 ( ) on BHK-21 cells at an MOI of 5. Data points are shown for virus titre $\log_{10} \pm$ standard error.

rescue virus MHV-76(cA8+)4 showed peak lung titres at day 7 comparable to MHV-68 (Figure 3.8.2). However, MHV-76 and MHV-76(cA8-)5 were cleared from the lungs more rapidly than MHV-68 and the rescue virus (Day 7 lung titre MHV-68 vs. MHV-76; $P<0.001$: MHV-76(cA8+)4 vs. MHV-76; $P<0.01$). This data therefore shows that deletion of M1, M2, M3, M4 and the 8 vtRNAs leads to a significant attenuation of infection in the lungs.

3.8.3. Virus-induced splenomegaly

To determine the effect of the 9.5kb deletion on splenomegaly during infection, BALB/c mice were infected with 2 x 10^5 PFU of MHV-68, MHV-76, MHV-76(cA8+)4 or MHV-76(cA8-)5 intranasally. The extent of splenomegaly was determined by spleen weight (see 2.6.2) and counting the total number of splenocytes (see 2.6.3; Figure 3.8.3A and B). There was a significant reduction in spleen weight and total splenocyte numbers after infection with MHV-76 or MHV-76(cA8-)5 compared to MHV-68 (Day 14 splenocyte numbers MHV-68 vs. MHV-76; $P<0.001$). The rescue virus MHV-76(cA8+)4 showed splenomegaly comparable to wild-type MHV-68, peaking at 14 days post-infection (Day 14 splenocyte numbers MHV-76(cA8+)4 vs. MHV-76; $P<0.001$). This data shows that deletion of M1, M2, M3, M4 and the 8 vtRNAs leads to a significant reduction in the degree of splenomegaly observed during MHV-68 infection.

3.8.4. Latent virus in the spleen

BALB/c mice were infected with 2 x 10^5 PFU of MHV-68, MHV-76, MHV-76(cA8+)4 or MHV-76(cA8-)5 intranasally and the amount of latent virus in the spleen quantified by infective centre assay (see 2.6.3). The rescue virus MHV-76(cA8+)4 showed levels of latent virus comparable to MHV-68, peaking at day 14 post-infection (Figure 3.8.4). Latent MHV-76 and MHV-76(cA8-)5 were detectable in the spleen, but at significantly lower levels than MHV-68 (MHV-76(cA8+)4 vs. MHV-76; Day 14 $P<0.001$: MHV-76 vs. MHV-68; Day 14 $P<0.001$). Latently infected splenocytes were still detectable in MHV-76 and MHV-76(cA8-)5 infected mice at day 32 post-infection. This data shows that deletion of M1, M2, M3, M4 and the 8 vtRNAs leads to a significant reduction in

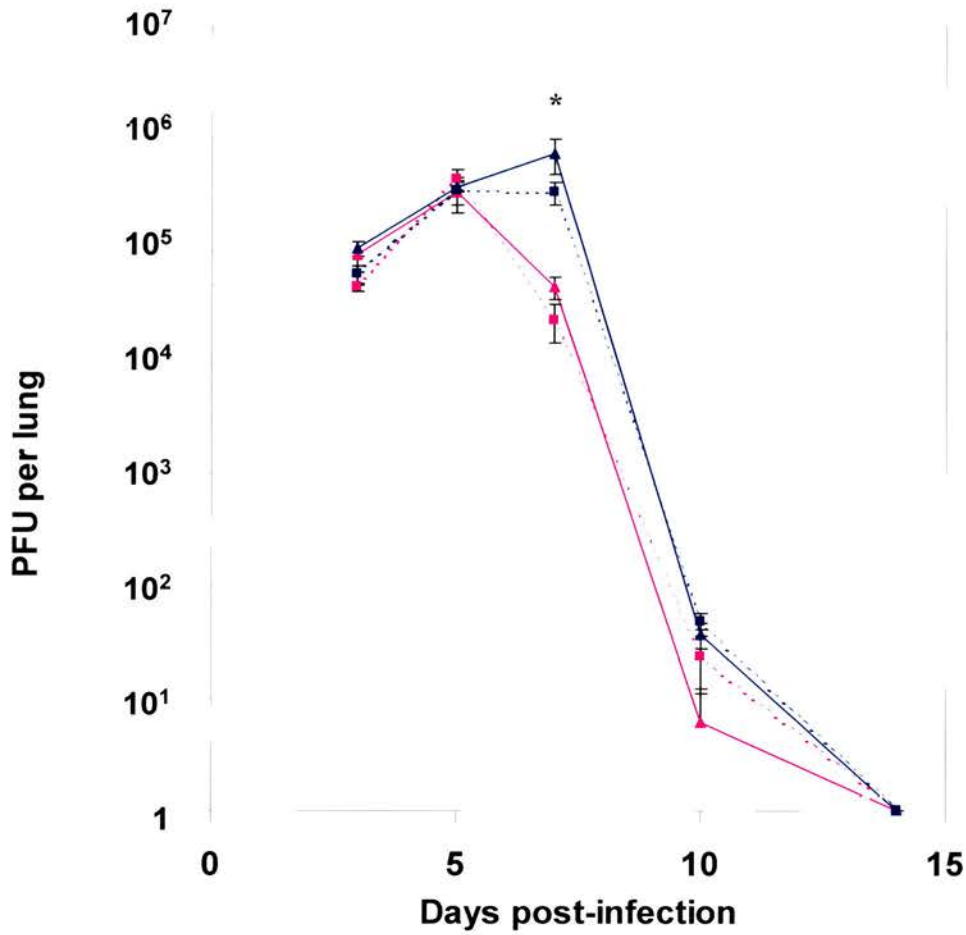

Figure 3.8.2 Viral titres in the lungs of BALB/c mice infected intranasally with 2 x 10^5 PFU of MHV-68 (—▲—), MHV-76 (—▲—), MHV-76(cA8+)4 (---■---) and MHV-76(cA8-)5 (---■---). Mean virus titre $\log_{10}$ per lung ± standard error for four mice per group is shown for each time point. * indicates statistically significant difference between lung viral titres in mice infected with MHV-76 compared with MHV-68 and MHV-76(cA8+)4 as determined by two-way ANOVA with Bonferroni post-tests.

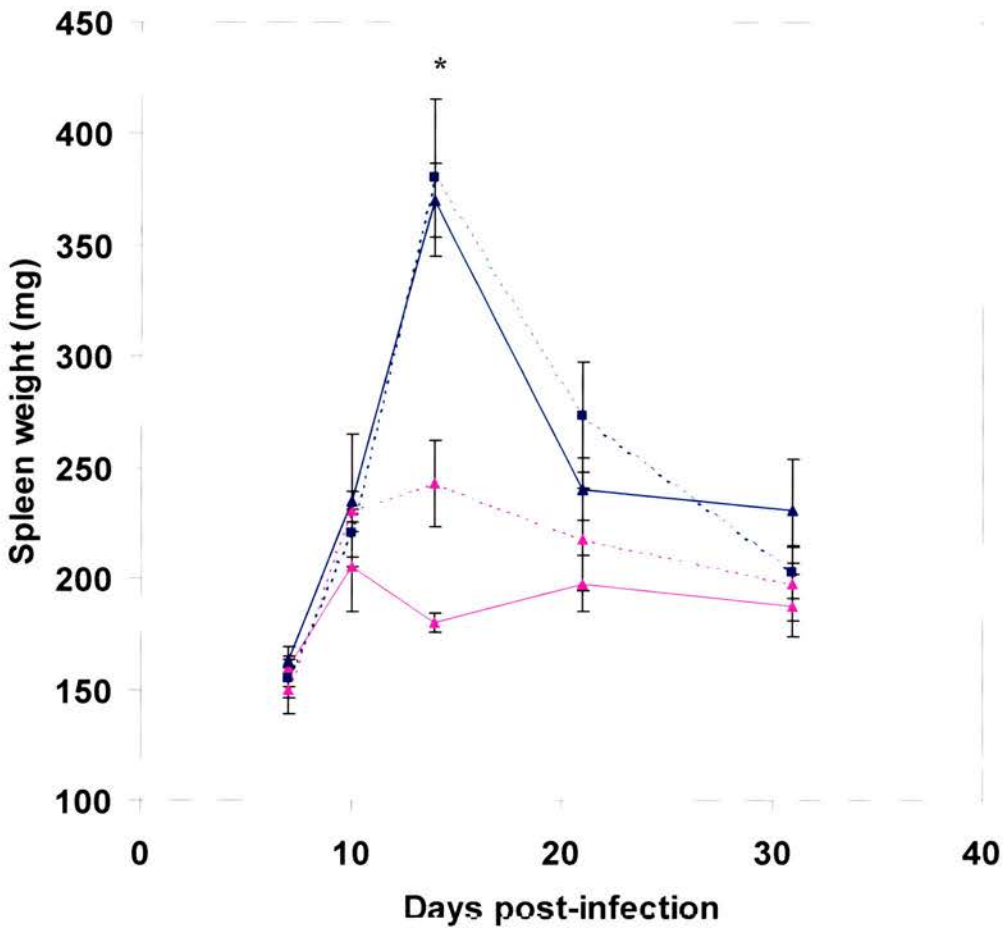

Figure 3.8.3A Spleen weights of BALB/c mice infected intranasally with 2 x 10^5 PFU of MHV-68 (—▲—), MHV-76 (—▲—), MHV-76(cA8+)4 (--■--) and MHV-76(cA8-)5 (--■--). Mean spleen weight (mg) ± standard error is shown for four mice per group for each timepoint. * indicates statistically significant difference between spleen weights in mice infected with MHV-76 compared with MHV-68 and MHV-76(cA8+)4 as determined by two-way ANOVA with Bonferroni post-tests.

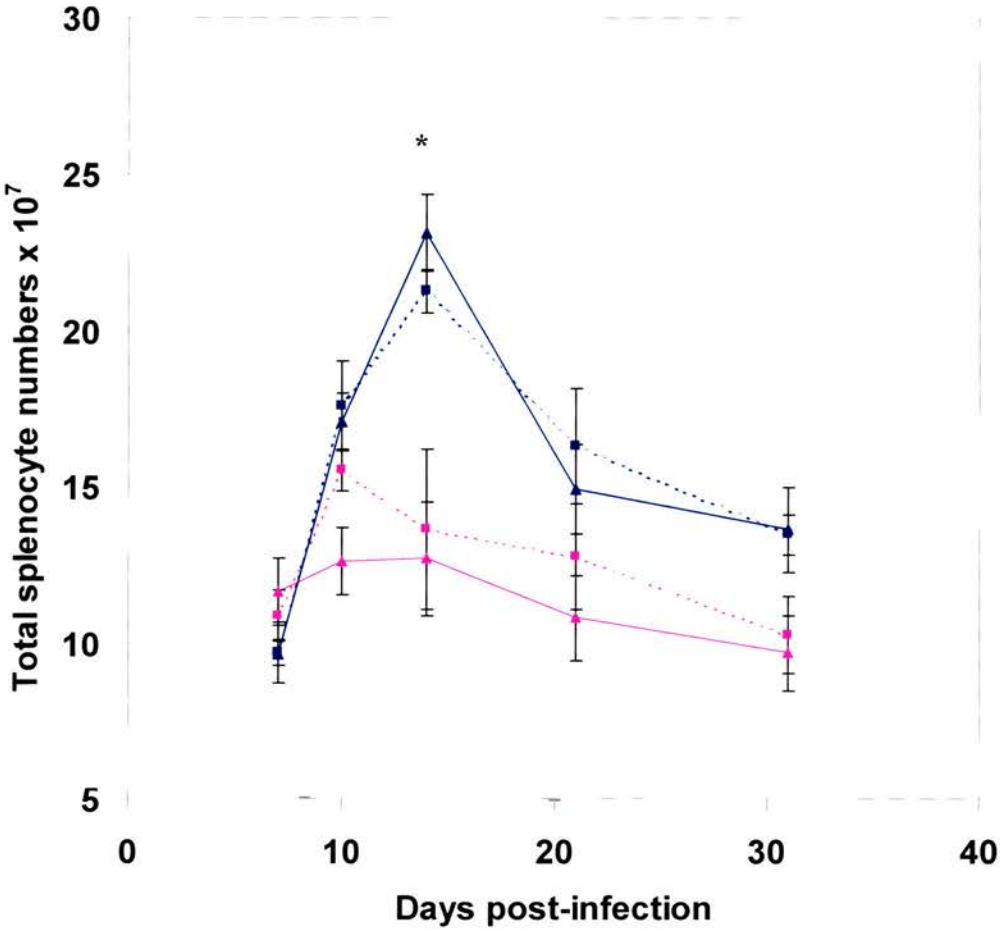

Figure 3.8.3B Total splenocyte numbers of BALB/c mice infected intranasally with 2 x 10^5 PFU of MHV-68 (—▲—), MHV-76 (—▲—), MHV-76(cA8+)4 (- -■- -) and MHV-76(cA8-)5 (- -■- -). Mean total number of splenocytes ± standard error is shown for four mice per group for each timepoint. * indicates statistically significant difference between total splenocyte numbers in mice infected with MHV-76 compared with MHV-68 and MHV-76(cA8+)4 as determined by two-way ANOVA with Bonferroni post-tests.

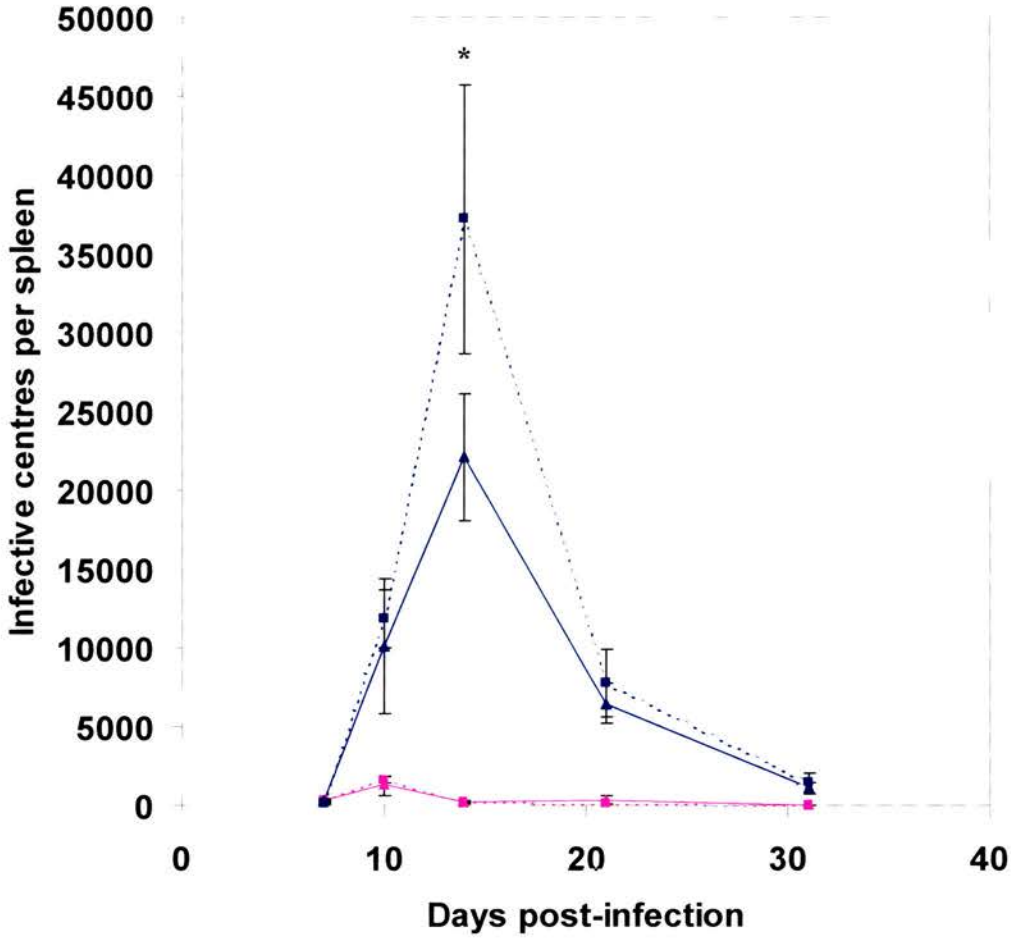

Figure 3.8.4 Latent virus in the spleens of BALB/c mice infected intranasally with 2 x 10^5 PFU of MHV-68 ( ), MHV-76 ( ), MHV-76(cA8+)4 ( ) and MHV-76(cA8-)5 ( ) as determined by infective centre assay. Infectious virus titres (less than 50 PFU per spleen) were subtracted from the infective centre results. Mean infective centres per spleen ± standard error for four mice per group is shown for each timepoint. * indicates statistically significant difference between the number of infective centres in mice infected with MHV-76 compared with MHV-68 and MHV-76(cA8+)4 as determined by two-way ANOVA with Bonferroni post-tests.

the amount of latent virus detectable in the spleen following viral infection, but is not essential for the establishment of latency and persistence.

3.9. Discussion

The detailed molecular characterisation of MHV-76 described here and by Steven Milligan and Andrew Davison (Macrae *et al.*, 2001) has shown that MHV-76 is very similar to MHV-68, except for a 9538bp deletion at the left end of the unique region of the genome. This deletion means that MHV-76 lacks the unique MHV-68 genes M1, M2, M3 and M4 as well as all eight of the vtRNA-like molecules. This deletion had no effect on viral replication *in vitro*, but led to a significant reduction in pathogenesis *in vivo*. The analysis of rescue viruses with the deletion restored to MHV-76 confirmed that this deletion plays a key role in viral pathogenesis.

These results have resolved some of the ambiguity concerning the classification of MHV-76. MHV-76 was originally described as an independent herpesvirus isolate derived from the yellow-necked wood mouse, *Apodemus flavicollis* (Blaskovic *et al.*, 1980), and was initially characterised as an alphaherpesvirus due to its cytopathic effect *in vitro* (Ciampor *et al.*, 1981; Svobodova *et al.*, 1982a). However, another study used restriction enzyme analysis and dot-blotting to conclude that MHV-76 was a betaherpesvirus (Hamelin & Lussier, 1992). The results presented here conclusively show that MHV-76 is a gammaherpesvirus. However, these results show that MHV-76 is probably not a novel herpesvirus isolate but a deletion mutant derived from MHV-68. This deletion more than likely occurred during the *in vivo* and *in vitro* passages subsequent to isolation (Blaskovic *et al.*, 1980). The evidence that MHV-76 is derived from MHV-68 (or an extremely closely related virus) is that apart from the 9538bp deletion, there is only one base difference in the remaining 20kb of MHV-76 DNA that was sequenced. ORF 74 is also 100% identical at the nucleotide level between the two viruses (M.Wakeling, unpublished observations). These results show the extremely close relationship between MHV-68 and MHV-76, and also raises the possibility that the other original herpesvirus

isolates may not be novel isolates but closely related to MHV-68. Indeed, the TK gene of MHV-72 has been shown to be identical in DNA sequence to that of MHV-68 (Raslova *et al.*, 2000).

The spontaneous deletion of sequences in gammaherpesvirus genomes is not uncommon. In EBV, deletions have been described in the Raji, P3HR-1 and Daudi strains (Bornkamm *et al.*, 1980; Cho *et al.*, 1984; Hatfull *et al.*, 1988). In HVS, spontaneous deletions also occur at the left end of the genome (Koomey *et al.*, 1984), and deletions in this region alter the oncogenic potential of HVS but not viral replication (Medveczky *et al.*, 1984; Desrosiers *et al.*, 1985; Medveczky *et al.*, 1989). This is due to deletion of the STP gene (ORF1b; see 1.2.3; Murthy *et al.*, 1989). It is notable that there are similarities between the left end of the genome in HVS and MHV-68, in that the left end of the HVS genome contains few ORFs and also encodes seven small viral RNAs (HSURs; Albrecht *et al.*, 1992). The left end of the MHV-68 genome also appears to have a high capability for undergoing recombination events *in vitro* (Simas *et al.*, 1998; D. Roy, I. Atkin, M. Wakeling, unpublished observations). This may be due to the proximity of the terminal repeats, the presence of the highly transcribed vtRNA genes or a putative origin of replication (Bowden *et al.*, 1997). It is probable that recombination occurred during the *in vivo* and *in vitro* passage steps during viral isolation to delete a portion of the genome from MHV-68.

PCR analysis demonstrated that MHV-76 lacks the unique MHV-68 genes M1, M2, M3 and M4 and all eight vtRNA-like sequences. To confirm that this deletion leads to the dramatic differences observed *in vivo*, rescue viruses were constructed to restore the deleted sequence by recombination with MHV-68 sequences. These rescuants showed the same phenotype as MHV-68, proving that genes within the deleted sequence play a key role in viral pathogenesis. Although the entire overlapping region where homologous recombination occurred has been sequenced in MHV-76 (Macrae *et al.*, 2001), it is possible that the single nucleotide substitution at position 12,280 in ORF 6 may affect the observed phenotype in MHV-76. However, this point mutation leads to a semi-conservative substitution of a serine for a glycine residue, and this residue (position 356) is not near the ORF 6 CD8+ T cell epitope p56 (residues 487-495) (Stevenson *et al.*,

1999a). It is also likely that a harmful point mutation would revert under selection *in vivo*, and this residue is not conserved in another independently isolated murine herpesvirus, MHV-Brest (S. Milligan, C. Chastel, S. Efstathiou and A. Davison, unpublished data).

These results show that the left unique region of the genome plays a critical role in MHV-68 pathogenesis. It contains four unique genes (M1, M2, M3 and M4) and eight vtRNA-like sequences whose importance in viral pathogenesis is only recently becoming understood (see 1.4.4). In particular, the broad-spectrum chemokine-binding protein M3 appears to play a critical role in the establishment of splenic latency *in vivo* (Bridgeman *et al.*, 2001). It is of note that insertion of foreign DNA sequences into this region of MHV-68 without the obvious disruption of known ORFs can have marked effects on viral pathogenesis (Clambey *et al.*, 2000; Adler *et al.*, 2001) It has also been postulated that some MHV-68 ORFs may extend through or within the terminal repeats (Virgin *et al.*, 1997), possibly existing as multiple spliced transcripts like the LMP2 transcripts of EBV, and therefore deletions in this region may affect these undiscovered transcripts.

Virus-specific genes at the left end of the unique region of the genome have also attracted considerable attention in other gammaherpesviruses as well as MHV-68 (see 1.2; Figure 1.4.3.2). In KSHV, this region contains the K1 gene, which shows a high level of variability in different viral isolates (Zong *et al.*, 1999; Hayward, 1999) and is associated with cellular transformation (Lee *et al.*, 1998b). In HVS, this region contains seven small RNAs (HSURs) and the STP gene (Albrecht *et al.*, 1992), which is required for cellular immortalisation and oncogenesis (Desrosiers *et al.*, 1985; Murthy *et al.*, 1989). In EBV, this region encodes LMP-1, a classic oncogene that is essential for B cell immortalisation (Kieff, 1996). This region of the genome has thus been implicated in viral pathogenesis in a range of gammaherpesviruses.

These results show that the unique MHV-68 genes M1, M2, M3 and M4 and all eight vtRNA-like sequences are non-essential for lytic virus replication *in vitro* and *in vivo*, and for the establishment and maintenance of latency *in vivo*, but have important roles in viral pathogenicity. The enhanced clearance of MHV-

76 from the lungs, combined with an increased inflammatory response, shows that this region plays a key role in evasion of the host response to the virus during productive infection. The M1, M3, M4 and vtRNA genes have all been shown to be transcribed during lytic infection (Virgin *et al.*, 1999; Simas *et al.*, 1999), and M2 expression has also been detected in the lungs at 3 – 6 days post-infection (Rochford *et al.*, 2001). Therefore all the genes may be involved in immune evasion in the lung. Although previous studies have examined viruses deleted for the M1 ORF, neither studied viral replication in the lung following intranasal inoculation (Simas *et al.*, 1998; Clambey *et al.*, 2000). However, studies of a virus with a disruption in the M3 gene suggested that a lack of M3 may lead to enhanced viral clearance from the lungs (Bridgeman *et al.*, 2001), and thus the chemokine-binding actions of M3 may play an important role in the lung.

A possible explanation for the lower levels of productive viral replication in the lung and the reduction in latent virus in the spleen is that MHV-76 has an altered cell tropism compared to MHV-68. The results of the infective centre assay using MACS sorted splenocytes shows that MHV-76 establishes a latent infection primarily in B lymphocytes, like MHV-68 (Sunil-Chandra *et al.*, 1992b). The small amount of latent virus detectable in the CD19 negative fraction could either be due to the small amount of contamination by CD19+ cells, or latent virus in other cell types (Weck *et al.*, 1999b; Flano *et al.*, 2000). Similarly, the immunostaining suggests that MHV-76 does not have any alteration in cellular tropism in the lung. Although not significant, the low levels of productive virus detectable in the adrenal glands of mice infected with MHV-76, an organ where productive MHV-68 is detectable post-infection (Sunil-Chandra *et al.*, 1992a), suggests that the levels of MHV-76 during the viraemic phase are lower and this may be a reflection on the enhanced viral clearance from the lungs.

The dramatic reduction in splenomegaly and the amount of latently infected splenocytes seen during MHV-76 infection shows that this region of the genome plays an important role in the splenic pathology and establishment of latency. There are two possible explanations for the low levels of latent MHV-76 observed using the infective centre assay; either there is a low level of latent virus present in splenocytes or latent MHV-76 is unable to fully reactivate from latency

in vitro. The data from the one-step growth curves demonstrates that there is no alteration in viral replication *in vitro*, favouring the first explanation. However, techniques such as quantitative fluorescent (QF)-PCR to determine the viral DNA load would be necessary to prove this (Usherwood *et al.*, 2001).

M2, M3 and the vtRNAs are all transcribed during the establishment of latency 1-3 weeks post-infection (Bowden *et al.*, 1997; Husain *et al.*, 1999; Simas *et al.*, 1999; Usherwood *et al.*, 2000), but there may also be a role for M1 and M4 in splenomegaly as low levels of productive viral replication occur in the spleen during the establishment of latency. Chemokines play an important role due to their ability to direct the migration of leukocytes into sites of inflammation (Luster, 1998), and these results provide evidence that the chemokine-binding actions of M3 may function in the development of splenomegaly. Studies using a virus with a disruption in the M3 ORF have shown that M3 is responsible for the B cell activation and amplification of latently infected B cells observed during the establishment of latency (Bridgeman *et al.*, 2001). The reduction in latent virus observed was reversed by CD8+ T cell depletion, and this suggests that M3 may act to prevent chemokine-mediated recruitment of cells into the lymphoid tissue. Another possible hypothesis for the reduction in splenomegaly and the amount of latent virus observed during MHV-76 infection is that the transient expression of the M2 CD8+ T cell epitope during the establishment of latency (Husain *et al.*, 1999; Usherwood *et al.*, 2000) assists the virus by expanding the numbers of latently infected cells (Usherwood *et al.*, 2001). Although not significant, the low levels of detectable latent virus in circulating blood leukocytes during MHV-76 infection reflects this lack of expansion in the number of latently infected cells in the spleen, which then enter the bloodstream. One report has also implicated M1 in the suppression of viral reactivation, but this effect was observed only at later timepoints in peritoneal exudate cells after intraperitoneal infection (Clambey *et al.*, 2000). No suppressive effect was observed in these experiments.

Despite the dramatic effects on splenomegaly and the establishment of latency, this deletion has no effect on the long-term maintenance of latency and viral persistence. Virus was detectable up to 5 months post-infection by infective centre assay (a biological measure of latency) and detection of viral DNA by PCR

in the spleen and lungs of mice infected with MHV-76. Although these results do not definitively show this persistent MHV-76 to be latent as defined by the presence of episomal forms of the genome or the absence of lytic transcripts, other studies have shown the absence of lytic transcripts (ORF 50) in the spleens of B cell deficient mice 46 days post-infection (Virgin *et al.*, 1999) and BALB/c mice at 10 months post-infection (Usherwood *et al.*, 2000). It is therefore probable that the persisting MHV-76 is in a latent form. This result also shows that MHV-76 can persist in multiple sites, similar to MHV-68 (Sunil-Chandra *et al.*, 1992b; Stewart *et al.*, 1998b).

These results show that the left end of the MHV-68 genome containing the unique genes M1, M2, M3, M4 and the vtRNA genes plays a major role in viral pathogenesis and the development of immunopathology, and it is probable that these genes have a central role in the viral immune evasion strategy during infection.

Chapter 4: Characterisation of the M2 protein

4.1. Aims

Previous work on the M2 ORF of MHV-68 has shown that this gene is latency associated (Husain *et al.*, 1999; Virgin *et al.*, 1999), and is expressed transiently in the first three weeks post-infection (Usherwood *et al.*, 2000). The M2 protein also contains an epitope recognised by CD8+ T lymphocytes (Husain *et al.*, 1999), and the immunological response to M2 has therefore been implicated in the control of viral pathogenesis (Usherwood *et al.*, 2000; Usherwood *et al.*, 2001). However, little is known about the basic biochemical properties of the M2 protein. The aim of this work was to characterise the M2 protein of MHV-68, including the generation of an antibody against the M2 protein, expression of M2 in mammalian cells and determination of the cellular localisation of M2. This would help in the understanding of the function of M2, and its role in viral infection.

4.2. Sequence analysis of the M2 protein

Previous work on the M2 ORF has shown that the M2 transcript is spliced (Husain *et al.*, 1999), and due to the splice acceptor site used, the M2 ORF encoded by the cDNA is 7 amino acids shorter than the genomic M2 ORF (Virgin *et al.*, 1997). It should be highlighted that previous work has designated the CTL epitope as the $M2_{91\text{-}99}$ CD8+ T cell epitope (Husain *et al.*, 1999), but due to the cDNA sequence the epitope is in fact present at residues 84 to 92. The M2 ORF is therefore predicted to encode a 192 amino acid protein, with a predicted molecular mass of 21.2kDa. It is also predicted to be proline-rich, containing 19.8% proline residues.

A database search was regularly performed using the program "BLAST" against all database protein entries. Apart from predicted similarities to other proline-rich proteins due to random alignment of proline residues, the only low but significant sequence similarity was between the M2 protein and the Grb2-associated binder-2 protein (Gab2) of the mouse, rat and human. As shown in Figure 4.2.1A and C, the strongest homology is present at M2 amino acid residues 122 to 150, with another region present at $M2_{30\text{-}38}$. A search was also performed

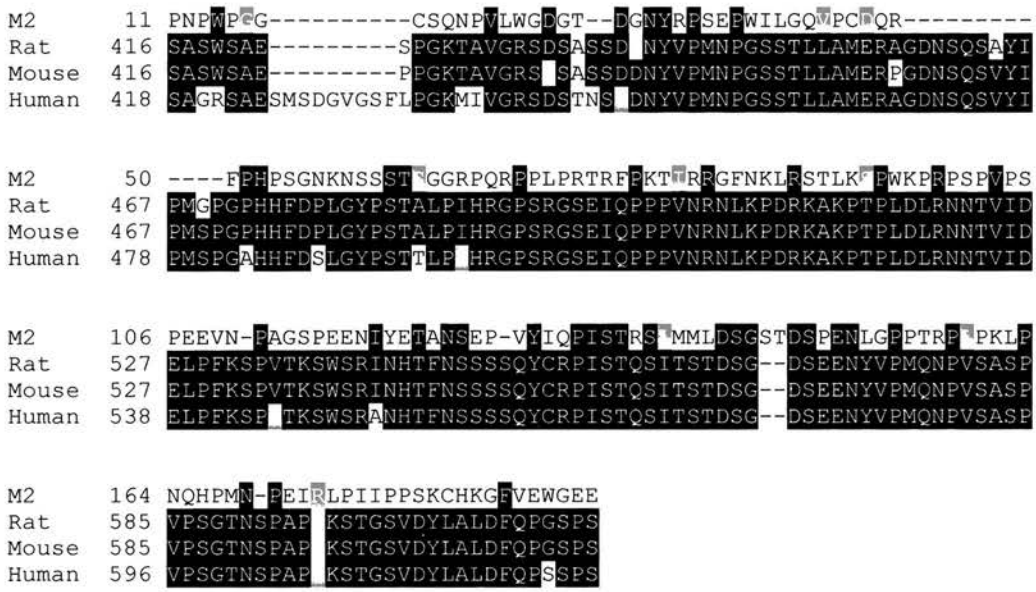

Figure 4.2.1A Sequence alignment of the M2 protein of MHV-68 and the Gab2 protein of the rat, mouse and human. The sequences were aligned using the Blosum scoring matrix with the "ClustalW" program, and displayed using the "BOXSHADE" program. Residues that are identical in two or more sequences are highlighted in black, while synonymous residues are highlighted in grey.

Figure 4.2.1B Sequence alignment of the M2 protein of MHV-68, semaphorin 3 A, B, C and E domains of the mouse, AlHV-1 A3 and vaccinia virus A39R . Sequence homology was detected using the "Block Searcher" program. The sequences were aligned using the Blosum scoring matrix with the "ClustalW" program, and displayed using the "BOXSHADE" program. Residues that are identical in four or more sequences are highlighted in black, while synonymous residues are highlighted in grey.

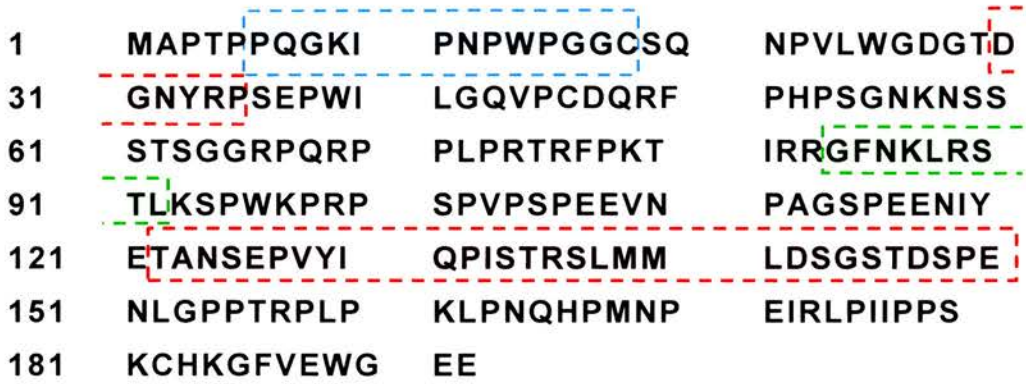

Figure 4.2.1C Location of the areas of sequence homology present in the M2 protein. The amino acid sequence of M2 is shown (according to Virgin *et al*., 1997 and Husain *et al*., 1999). The area of homology to the mouse semaphorin 3 domain is shown highlighted by a blue dashed box, the main areas of homology to the Gab2 family of proteins are shown highlighted by a red dashed box and the CD8+ T cell epitope (Husain *et al*., 1999) is shown surrounded by a green dashed box.

using the "Block Searcher" program against a database of highly conserved protein domains (Henikoff & Henikoff, 1994), which is used to detect short regions of homology with families of proteins that may be missed in searches of sequence databases. This revealed a region of sequence homology at the N-terminus of M2 to the semaphorin domain, with the closest homology to the semaphorin 3 family. Figure 4.2.1B shows the alignment of M2 with the mouse semaphorin 3 A, B, C and E family domains (the human semaphorin 3 A, B, C and E domains are identical to the mouse sequence), and also the AlHV-1 A3 semaphorin homologue (Ensser & Fleckenstein, 1995) and the vaccinia virus A39R semaphorin homologue (Comeau *et al.*, 1998). This region of homology to the semaphorin domain is present at position $M2_{6\text{-}18}$ (Figure 4.2.1C).

A hydropathicity plot of the M2 amino acid sequence was performed (see 2.3.1), to examine whether the M2 protein contained any transmembrane or membrane-anchoring regions. These regions of a protein typically contain a 20 amino acid hydrophobic region (Kyte & Doolittle, 1982). As shown in Figure 4.2.2, the M2 protein is largely hydrophilic, with no predicted regions of membrane affiliation.

A variety of programs were also used to predict potential post-translational modifications in the M2 protein (see 2.3.1). The amino acid consensus sequence for N-linked protein glycosylation [N-any amino acid (not proline)-S/T] was observed at residue 58 (Figure 4.2.3 highlighted blue), and 8 O-linked protein glycosylation sites (Figure 4.2.3 highlighted purple) are also potentially present in M2. Co-translational amide linkage of myristic acid to N-terminal glycine residues (myristylation) has been shown to be important for cellular localisation of proteins to the plasma membrane and protein function (Cross *et al.*, 1984; Resh, 1994). There are three predicted myristylation sites in the N-terminus of the M2 protein (Figure 4.2.3 highlighted green).

The phosphorylation of proteins has been shown to be important in the regulation of protein function and signal transduction pathways (Edelman *et al.*, 1987; Zhou *et al.*, 1997), including the function of a variety of viral proteins (Sylla *et al.*, 1998; Yokoyama *et al.*, 2001). The program "NetPhos 2.0" was used to predict phosphorylated amino acid residues. Figure 4.2.3 shows that there are

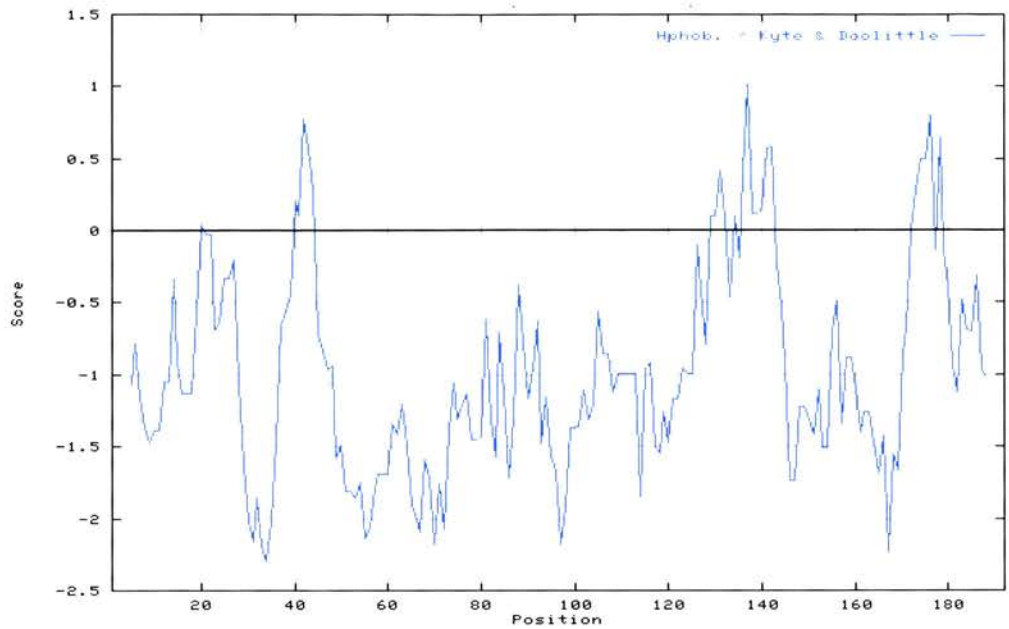

Figure 4.2.2 Hydropathicity plot of the M2 protein (using the method of Kyte and Doolittle, 1982). Hydrophobic regions of the protein have positive values, and hydrophilic regions have negative values.

1	MAPTPPQGKI	PNPWPGGCSQ	NPVLWGDGTD	GNYRPSEPWI	LGQVPCDQRF
51	PHPSGNKNSS	STSGGRPQRP	PLPRTRFPKT	IRRGFNKLRS	TLKSPWKPRP
101	SPVPSPEEVN	PAGSPEENIY	ETANSEPVYI	QPISTRSLMM	LDSGSTDSPE
151	NLGPPTRPLP	KLPNQHPMNP	EIRLPIIPPS	KCHKGFVEWG	EE

Figure 4.2.3 Diagrammatic representation of the potential post-translational modifications present in the M2 protein. The amino acid sequence (according to Virgin *et al.*, 1997 and Husain *et al.*, 1999) is shown with predicted motifs as follows: N-linked glycosylation site (highlighted blue); O-linked glycosylation sites (highlighted purple); myristylation sites (highlighted green); phosphorylation sites (red letter underlined).

predicted to be eleven phosphorylated serine residues, two phosphorylated threonine residues and two phosphorylated tyrosine residues (shown by an underlined red letter).

4.3. Generation of anti-M2 antibody

4.3.1. Expression of M2 as a GST fusion protein

In order to investigate the cellular localisation and function of M2 *in vitro*, it was decided to generate an anti-M2 antibody. The M2 protein was therefore expressed in bacteria to generate sufficient antigen that could be used to raise an immune response *in vivo*. It was decided to express M2 as a GST fusion protein using the pGEX bacterial expression system, as this system provides a convenient method to express proteins in *E. coli* and their subsequent purification. The M2 ORF was amplified using primer pair M2GEX1 and M2GEX2 (Chapter 2, Appendix 2) with *PfuTurbo*™ DNA polymerase (a proof-reading DNA polymerase), and cloned into the pGEX-2T vector (Chapter 2, Appendix 3) using the *Bam*HI and *Eco*RI restriction enzyme sites to give the vector pGEX-2T/M2. The M2 gene was inserted in frame with the glutathione S-transferase gene of *Schistosoma japonicum*, and would be expressed as a GST fusion protein. XL-1 Blue bacterial clones positive for the M2 insert in pGEX-2T by mini-prep were tested for their ability to express the GST-M2 fusion protein. Expression of the fusion protein was induced by the addition of 0.5mM IPTG during exponential growth phase of the culture (see 2.4.1). Upon induction with IPTG, the repression of the P_{tac} promoter by the *lac* repressor is stopped leading to expression of the fusion protein via the P_{tac} promoter. The bacterial culture was harvested 3 hours after induction, the bacterial pellet sonicated and the cell lysate analysed on a 10% SDS-PAGE gel. As shown in figure 4.3.1.1A, all five colonies positive for the M2 insert induced with IPTG produced a small band with an apparent molecular mass of 50kDa. This band was not present in colony number 6 that did not contain any insert and thus produced only GST (visualised as a band at approximately 27.5kDa) or in the uninduced cultures (data not shown). The molecular mass of

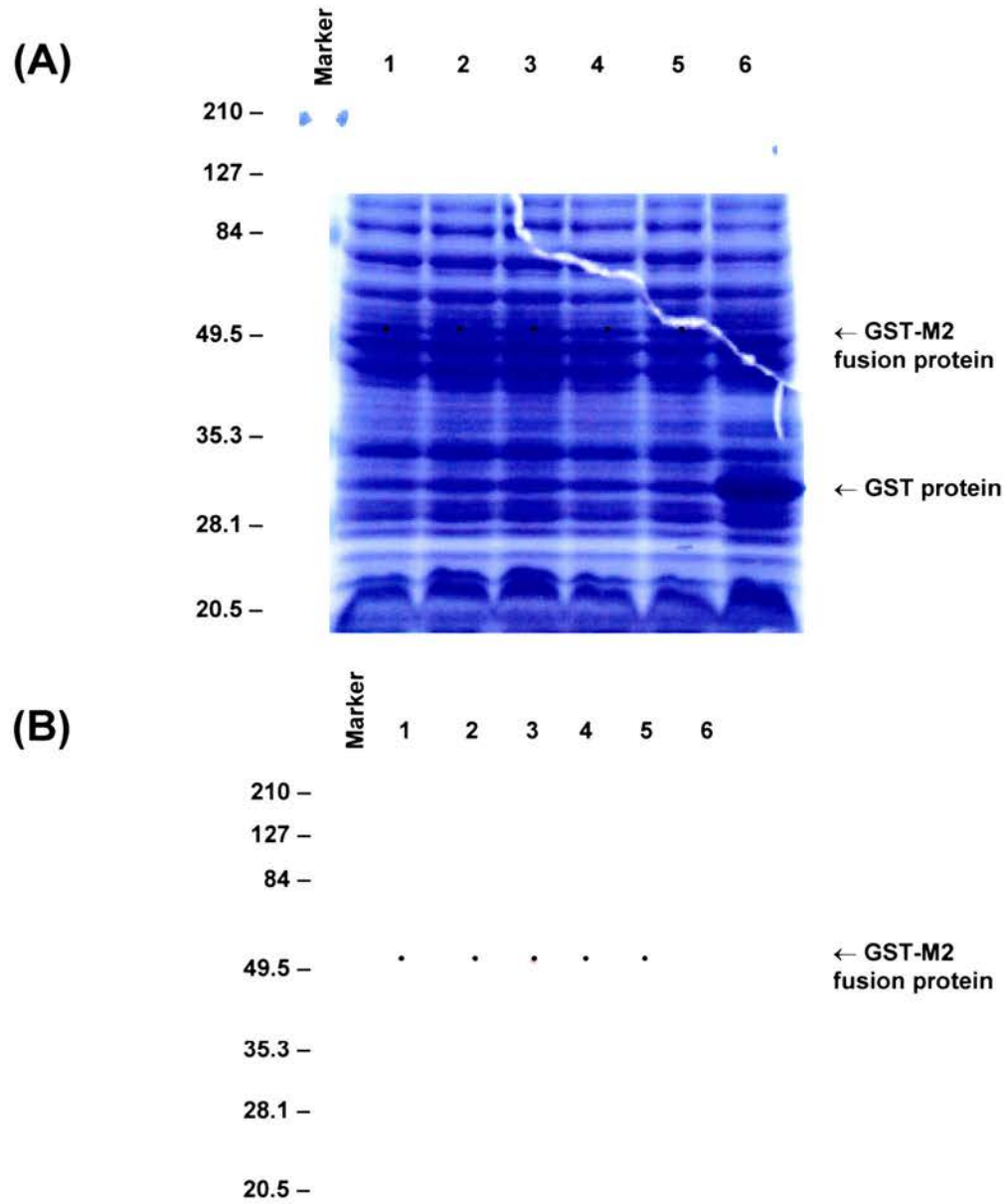

Figure 4.3.1.1 Expression of the M2 protein as a GST-fusion protein. Five separate bacterial colonies (lanes 1-5) with the correct M2 insert and one bacterial colony (lane 6) with no insert were tested for expression of the fusion protein after induction with 0.5mM IPTG. Crude cell lysates were analysed on a 10% SDS-PAGE gel. **(A)** Coomassie blue stained gel **(B)** Immunoblot probed with polyclonal anti-MHV-68, followed by anti-rabbit Ig-AP and visualised using Sigma FAST BCIP/NBT solution. For clarity, a black dot has been placed just above each of the GST-M2 fusion protein bands. Molecular weights are given in kilodaltons relative to the marker in the left lane.

native GST is 27.5kDa, and the predicted molecular mass of M2 is 21.2kDa. Thus the expected size of the GST-M2 fusion protein is 48.7kDa, which is the approximate size of the GST-M2 fusion protein band on the gel. The level of GST-M2 expression was poor in all five clones.

To confirm that this band represented the GST-M2 fusion protein, an identical gel to Figure 4.3.1.1A was analysed by immunoblot. The blot was incubated with polyclonal anti-MHV-68 antibody (diluted 1:500), followed by swine anti-rabbit Ig conjugated to AP (diluted 1:1000) and visualised using Sigma FAST BCIP/NBT solution. As shown in Figure 4.3.1.1B, the polyclonal anti-MHV-68 antibody recognised the 50kDa GST-M2 fusion protein in the five colonies positive for the M2 insert, but not in colony 6 (negative for the M2 insert). Thus the 50kDa band was the GST-M2 fusion protein, and the M2 fusion protein was recognised by polyclonal anti-MHV-68 antibody (raised using antigens from lytically infected cells). However, this confirmed that the expression level of GST-M2 was poor.

To test the solubility of the GST-M2 fusion protein, the five colonies were again induced with 0.5mM IPTG and harvested after three hours. After harvesting and sonication of the bacterial pellet, the samples were separated by centrifugation to give the supernatant (soluble) and cell pellet (insoluble) fractions and the samples analysed on a 10% SDS-PAGE gel. This showed that the GST-M2 fusion protein was only present in the cell pellet fraction (data not shown) and not the supernatant fraction and was therefore insoluble.

It was decided to try and maximise the expression levels of the GST-M2 fusion protein, so that an inclusion body preparation could be used to produce enough antigen for the generation of antiserum. Bacterial clone 1 of pGEX-2T/M2 was induced with 0.5, 1.0 or 1.5mM IPTG and harvested after 3 hours. The bacterial pellet was then analysed on a 10% SDS-PAGE gel for GST-M2 fusion protein production. As can be observed in Figure 4.3.1.2A, there was no difference in the intensity of the GST-M2 band between the three samples with varying concentrations of IPTG. This showed that varying the concentration of IPTG had no effect on the levels of expression of fusion protein.

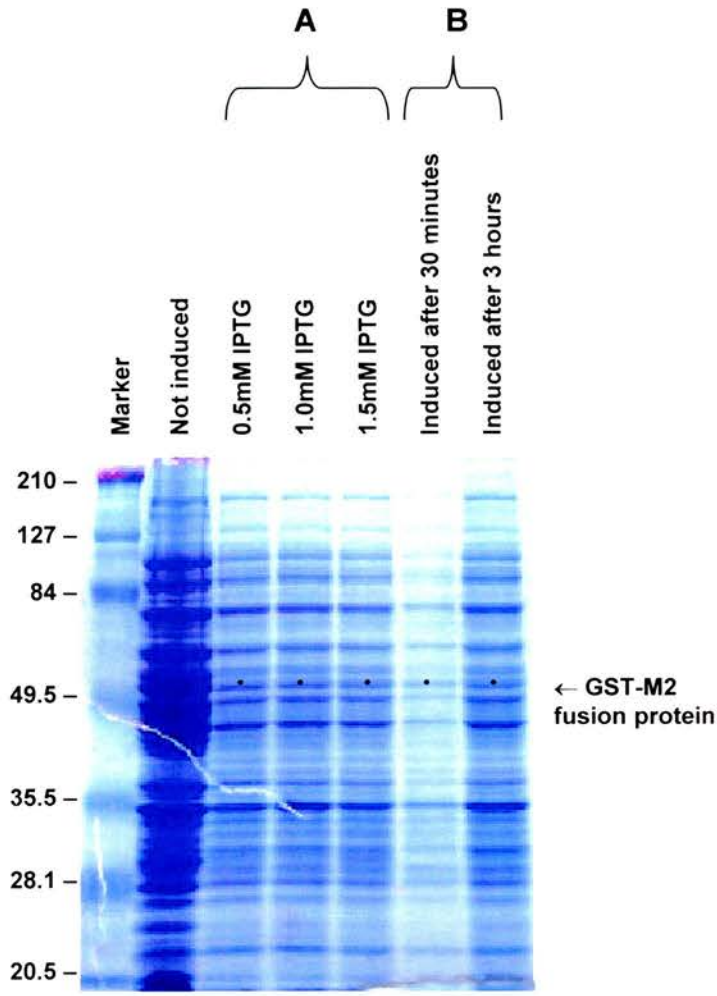

Figure 4.3.1.2 Poor expression of GST-M2 fusion protein in bacteria. **(A)** The bacterial culture was induced with 0.5, 1.0 or 1.5mM IPTG, and left for 3 hours before harvesting. **(B)** The bacterial culture was induced with 0.5mM IPTG after 30 minutes (OD_{595}~0.3) or 3 hours (OD_{595}~1.2), and then left for 3 hours before harvesting. A control sample was not induced. Crude cell lysates were analysed on a 10% SDS-PAGE gel, and the gel was stained with Coomassie blue. For clarity, a black dot has been placed just above each of the GST-M2 fusion protein bands. Molecular weights are given in kilodaltons relative to the marker in the left lane.

Another factor that can lead to poor expression of GST fusion proteins is toxicity of the fusion protein. To analyse if this was the case with GST-M2, one bacterial culture was induced in early exponential growth phase after 30 minutes (the OD_{595} of the bacterial culture was 0.3), and another bacterial culture was induced in late exponential / stationary growth phase after 3 hours (OD_{595} was 1.2). The cultures were harvested after a further 3 hours, and the bacterial pellet analysed on a 10% SDS-PAGE gel for GST-M2 fusion protein production. One culture was not induced, and left to grow for 6 hours (the same length of time as the culture induced after 3 hours of growth). As can be observed in Figure 4.3.1.2B, there was no difference in the intensity of the GST-M2 band between the two samples induced with IPTG. However, there was a dramatic difference between the total protein yields of the cultures as estimated by intensity on the Coomassie blue stained gel. Figure 4.3.1.2B shows that the culture induced in the early exponential growth phase (after 30 minutes) contains much less total protein than the culture induced in late exponential / stationary growth phase (after 3 hours), and these cultures contain much less protein than the uninduced negative control culture. This result showed that induction of GST-M2 fusion protein expression by the addition of IPTG leads to a large reduction in bacterial protein production, and this is suggestive that the GST-M2 fusion protein may be toxic in bacteria. However, the lack of a suitable control expressing only GST means that this reduction in total protein yield may also be due to the induction of foreign protein expression in bacteria, with consequent disruption of normal bacterial protein synthesis.

4.3.2. Expression of a 75 amino acid fragment of M2 ($M2_{74-148}$) as a GST fusion protein

The previous results showed that attempts to produce a GST fusion protein in bacteria containing the full length M2 protein led to the poor expression of an insoluble GST-M2 fusion protein that was toxic in bacteria. This could have been due to a number of factors including the high proline content (Wilkinson & Harrison, 1991) or structure of the M2 protein (Makrides, 1996). It was therefore decided to express a smaller region of the M2 protein in an attempt to circumvent

these problems. A 75 amino acid region from amino acid residues 74 to 148 of the M2 protein (designated $M2_{74-148}$) was chosen as it contained predominantly hydrophilic regions (see Figure 4.2.2). This polypeptide also contained the $M2_{91-99}$ CD8+ T cell epitope (Husain *et al.*, 1999) and contained only 14.6% proline residues.

The $M2_{74-148}$ coding region was amplified using primer pair M2GEX3 and M2GEX4 (Chapter 2, Appendix 2) with *PfuTurbo*™ DNA polymerase and cloned into the pGEX-2T vector (Chapter 2, Appendix 3) using the *Bam*HI and *Eco*RI restriction enzyme sites to give the vector pGEX-2T/$M2_{74-148}$. Six XL-1 Blue bacterial clones positive for the $M2_{74-148}$ insert in pGEX-2T by mini-prep were tested for their ability to express the GST-$M2_{74-148}$ fusion protein. Expression of the fusion protein was induced by the addition of 0.5mM IPTG during exponential growth phase of the culture (see 2.4.1), and one culture of colony number 1 was left uninduced as a negative control. The bacterial culture was harvested 3 hours after induction, the bacterial pellet sonicated and separated into supernatant (soluble) and cell pellet (insoluble) fractions by centrifugation, and the samples analysed on a 10% SDS-PAGE gel. The proteins were transferred to a membrane by Western Blot, and the blot was incubated with polyclonal anti-GST antibody (diluted 1:500), followed by swine anti-rabbit Ig conjugated to AP (diluted 1:1000) and visualised using Sigma FAST BCIP/NBT solution.

As can be seen in Figure 4.3.2.1A, analysis of the insoluble cell pellet fraction by immunoblot showed that colonies 2 and 6 expressed a GST-$M2_{74-148}$ fusion protein as a band at approximately 40kDa, with colony 6 expressing an additional slightly larger band. This band was not present in the uninduced negative control lane. The predicted molecular mass of the $M2_{74-148}$ protein is 8.4kDa, and therefore the predicted mass of the GST-$M2_{74-148}$ fusion protein is 35.9kDa. Thus the observed band is slightly larger than expected. The fusion protein was also degraded, as evidenced by the multiple smaller bands observed in the immunoblot and the major band at approximately 27.5kDa, which is comprised of either native GST or a fusion protein consisting of GST with a few amino acid residues of the $M2_{74-148}$ polypeptide. The actions of proteases were reduced by sonication in a solution containing the protease inhibitors Aprotinin

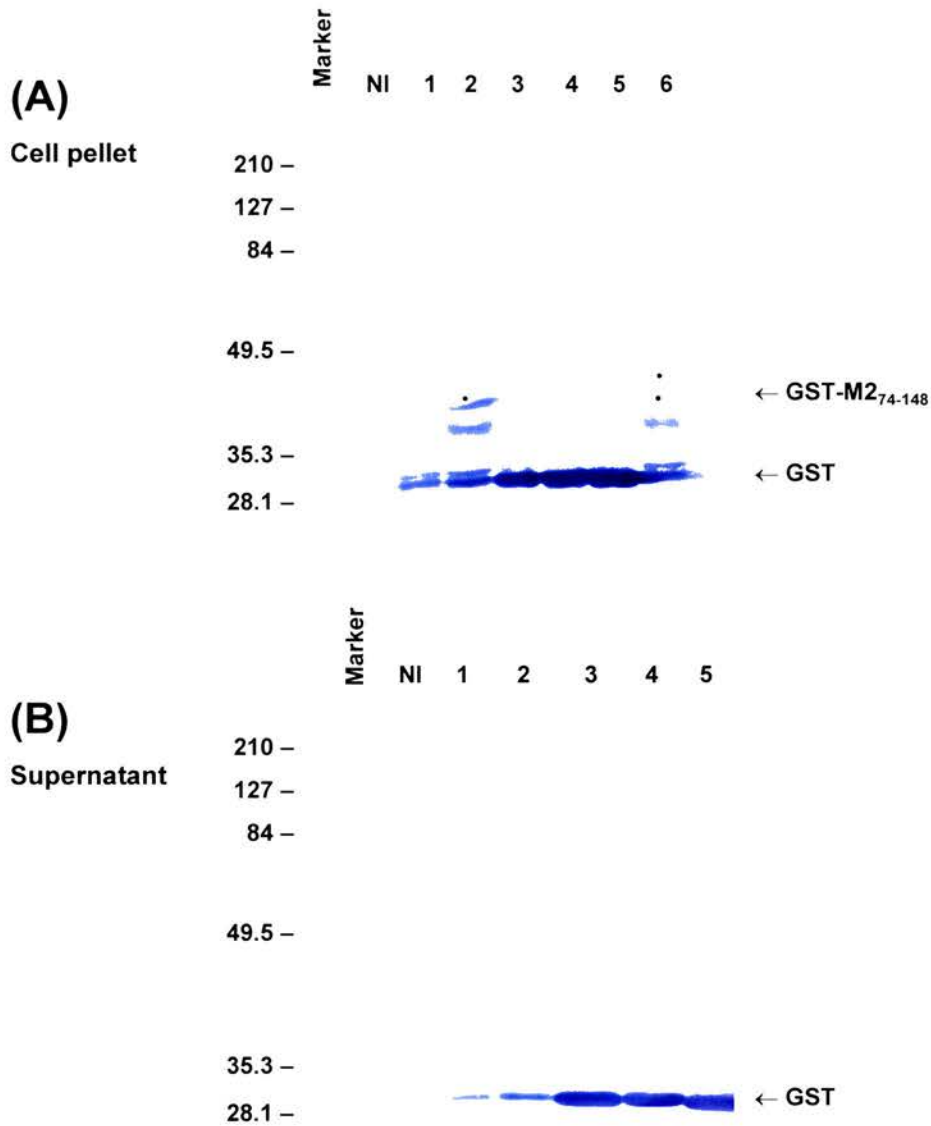

Figure 4.3.2.1 Expression of a 75 a.a. fragment of M2 ($M2_{74-148}$) as a GST fusion protein. 6 separate bacterial colonies (lanes 1-6) with the correct insert were tested for expression of the fusion protein after induction with 0.5mM IPTG. One culture of colony 1 was not induced as a negative control **(NI)**. After harvesting and sonication, the samples were centrifuged and separated into cell pellet **(A)** and supernatant **(B)** fractions. The samples were analysed on a 10% SDS-PAGE gel followed by immunoblotting. The immunoblots were probed with rabbit anti-GST, followed by anti-rabbit Ig-AP and visualised using Sigma FAST BCIP/NBT solution. For clarity, a black dot has been placed just above each of the GST-$M2_{74-148}$ fusion protein bands. Molecular weights are given in kilodaltons relative to the marker in the left lane.

and PMSF, and maintaining all solutions after harvesting of the bacterial culture at 4°C. Poor expression of the GST-$M2_{74-148}$ fusion protein was also observed. Figure 4.3.2.1B shows that the soluble supernatant fraction contained only native GST, and no soluble GST-$M2_{74-148}$ fusion protein was detected.

It was therefore decided to attempt an inclusion body preparation (see 2.4.2) in order to produce enough antigen for the generation of antiserum. Clone number 2 of pGEX-2T/$M2_{74-148}$ was induced with 0.5mM IPTG, and incubated for a further 3 hours before harvesting. One culture was left uninduced as a negative control. A sample of the induced culture was sonicated, and the cell lysate used as a positive control to ensure expression of the GST-$M2_{74-148}$ fusion protein. The bacterial culture was harvested, resuspended in inclusion body preparation buffer and subjected to gentle lysis with lysozyme and DNase I. The samples were divided into equal aliquots and separated by centrifugation over a range of centrifugal forces (from 2,000 to 10,000*g*) to determine the optimum centrifugal force that separated the insoluble GST-$M2_{74-148}$ fusion protein from the contaminating bacterial cell proteins. Samples of the supernatant (soluble) and cell pellet (insoluble) fractions were analysed on a 12.5% SDS-PAGE gel. The proteins were transferred to a membrane by Western Blot, and the blot examined for the presence of GST by immunoblot analysis using the rabbit polyclonal anti-GST antibody as previously described.

Figure 4.3.2.2 shows that GST-$M2_{74-148}$ fusion protein was expressed upon induction with IPTG, and that no fusion protein was observed in the uninduced culture. Surprisingly, the GST-$M2_{74-148}$ fusion protein was observed in the soluble fraction (Figure 4.3.2.2B) as well as the insoluble fraction (Figure 4.3.2.2A), and appeared to be present in higher concentrations in the soluble fraction. There was no observed difference in the amount of GST-$M2_{74-148}$ fusion protein detected upon varying the centrifugal force used to separate the soluble and insoluble fractions. All the smaller breakdown products of the fusion protein were observed in the soluble fraction.

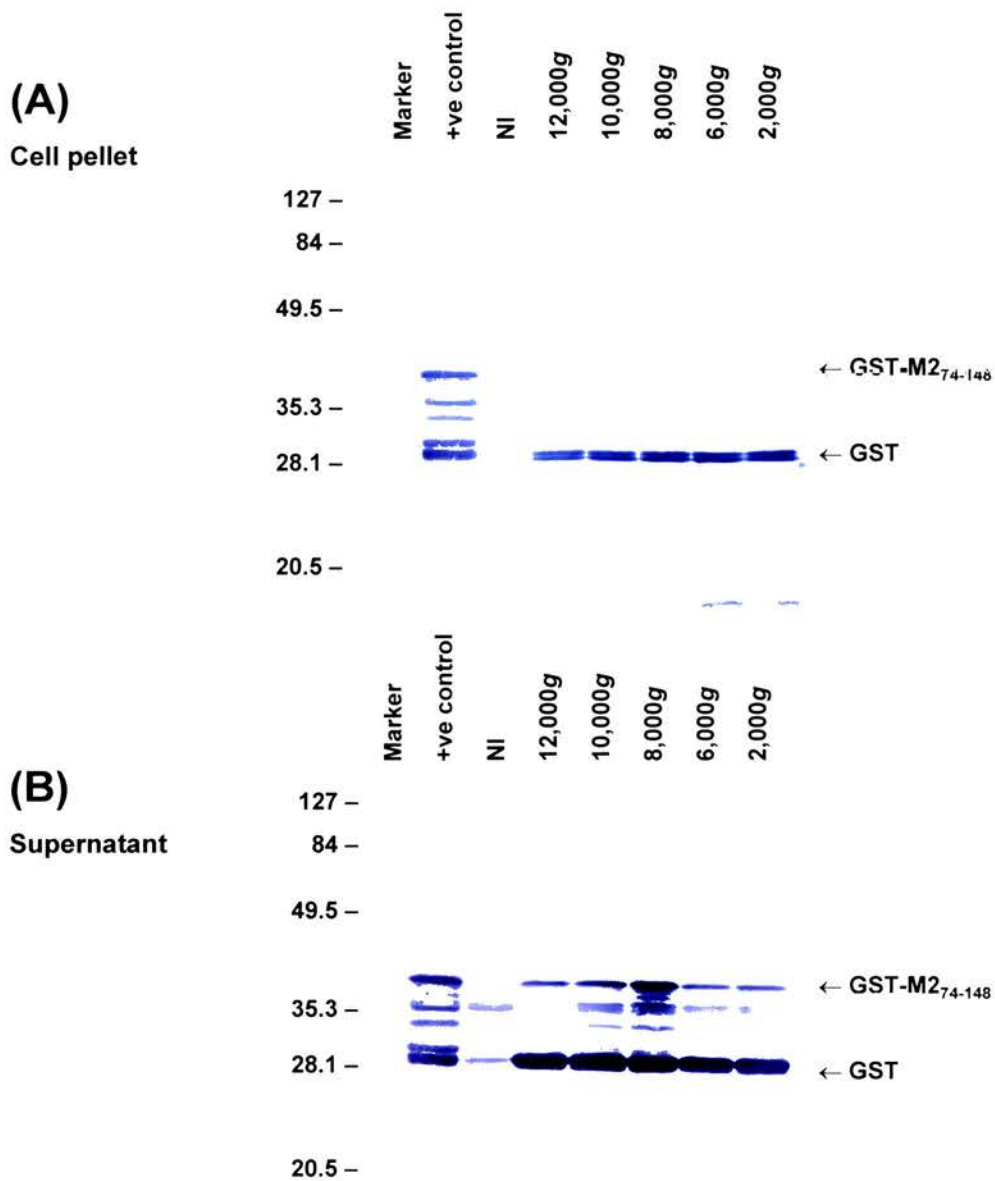

Figure 4.3.2.2 Inclusion body preparation of pGEX-2T/M2$_{74-148}$. Clone 2 was induced with 0.5mM IPTG, and incubated for 3 hours before harvesting. One culture was not induced as a negative control **(NI)**. An aliquot was sonicated and resuspended in SDS-PAGE sample buffer **(+ve control)**. The culture was harvested, subjected to gentle lysis with lysozyme and DNase I and centrifuged (2,000 – 10,000*g*). The cell pellet **(A)** and supernatant **(B)** fractions were analysed on a 12.5% SDS-PAGE gel followed by immunoblotting. The immunoblots were probed with rabbit anti-GST, followed by anti-rabbit Ig-AP and visualised using Sigma FAST BCIP/NBT solution. Molecular weights are given in kilodaltons relative to the marker in the left lane.

4.3.3. Purification of GST-M2$_{74-148}$ fusion protein

The solubility of the GST-M2$_{74-148}$ fusion protein after the inclusion body preparation meant that the fusion protein could be purified using the affinity of the GST fusion protein for glutathione immobilised on sepharose beads, and therefore large quantities of purified fusion protein could be made (see 2.4.3). Clone number 2 of pGEX-2T/M2$_{74-148}$ was induced with 0.5mM IPTG, and incubated for a further 3 hours before harvesting. One culture was left uninduced as a negative control. A sample of the induced culture was sonicated, and the cell lysate used as a positive control to ensure expression of the GST-M2$_{74-148}$ fusion protein. The bacterial culture was harvested, resuspended in inclusion body preparation buffer and subjected to gentle lysis with lysozyme and DNase I. The protein preparation was clarified by centrifugation to remove insoluble debris, and the soluble GST-M2$_{74-148}$ fusion protein in the supernatant incubated with glutathione-sepharose beads. The beads were washed and the fusion protein eluted from the beads using 5mM glutathione three times to ensure as much of the GST-M2$_{74-148}$ fusion protein was recovered as possible. Excess glutathione was removed by dialysis, and the final GST-M2$_{74-148}$ fusion protein preparation concentrated into a final volume of 2ml using a centrifugal filter device. Samples of the positive control, GS beads after elution and final fusion protein preparation were analysed on 12.5% SDS-PAGE gels. The gels were either stained using Coomassie blue to determine protein yields, or analysed by immunoblot using the rabbit polyclonal anti-GST antibody as previously described.

Figure 4.3.3A shows that the GST-M2$_{74-148}$ fusion protein was present in the final preparation, at a low concentration but detectable on the Coomassie blue stained gel. The GST-M2$_{74-148}$ fusion protein had therefore been successfully purified. The breakdown products (down to native GST) were also present in the final protein preparation, as well as a large amount of native GST. A significant amount of GST-M2$_{74-148}$ fusion protein and native GST had remained bound to the GS beads after three separate elutions, suggesting that the fusion protein had a high affinity for the beads. Figure 4.3.3B confirmed that these bands present on the Coomassie gel were GST fusion proteins, and verified that the GST-M2$_{74-148}$ fusion protein was expressed upon induction of the bacterial culture with IPTG. A

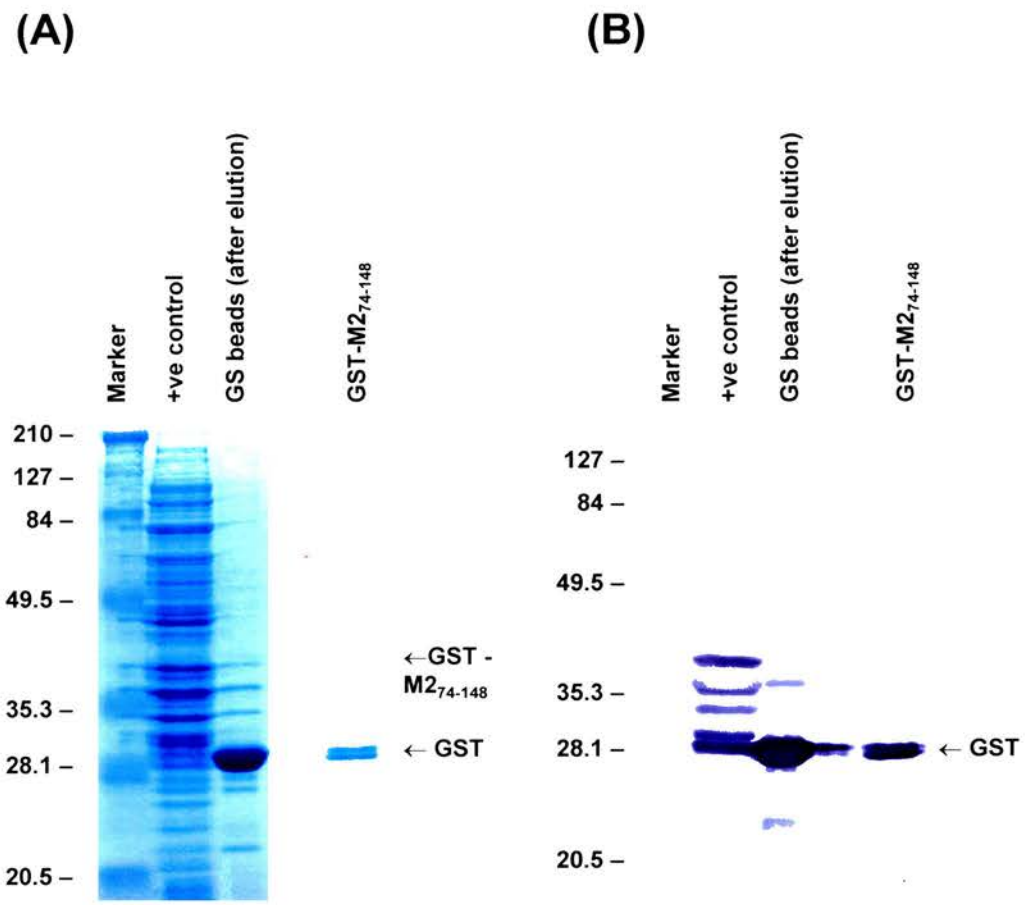

Figure 4.3.3 Purification of GST-$M2_{74-148}$ fusion protein. Clone 2 was induced with 0.5mM IPTG, and incubated for 3 hours before harvesting. An aliquot was sonicated and resuspended in SDS-PAGE sample buffer **(+ve control)**. The fusion protein was partially purified using an inclusion body preparation, and the soluble GST fusion protein was bound to glutathione-sepharose beads. The purified GST-$M2_{74-148}$ fusion protein was eluted from the beads, dialysed to remove excess glutathione and concentrated. Aliquots of the glutathione beads (after elution) and final GST- $M2_{74-148}$ fusion protein preparation were analysed on a 12.5% SDS-PAGE gel. **(A)** Coomassie blue stained gel. **(B)** Immunoblot probed with rabbit anti-GST, followed by anti-rabbit Ig-AP and visualised using Sigma FAST BCIP/NBT solution. Molecular weights are given in kilodaltons relative to the marker in the left lane.

faint band was present at the level of the full-length GST-$M2_{74-148}$ fusion protein on the immunoblot, but was poorly reproducible on the photograph. The immunoblot showed that a substantial amount of the fusion protein preparation remained bound to the beads, and that a large amount of native GST was present in the final GST-$M2_{74-148}$ fusion protein preparation. However, purified GST-$M2_{74-148}$ fusion protein had been made and sufficient antigen was available to be used to raise an immune response *in vivo*.

4.3.4. Purification and reactivity of sheep antisera

Two sheep (numbers 7/413 and 705D) were immunised by Professor J. Hopkins, Department of Veterinary Pathology, Edinburgh. Each sheep received two intramuscular injections, each containing 18μg of GST-$M2_{74-148}$ fusion protein with adjuvant. The sheep received three booster injections at four week intervals, and a blood sample was taken prior to immunisation (pre-bleed) and four weeks after each immunisation. The serum was separated from the blood sample, and samples of the pre-bleed and third bleed were purified and used to assess the anti-M2 reactivity of the sheep serum. The serum was first purified using caprylic acid, a short-chain fatty acid that precipitates most serum proteins under mildly acidic conditions, with the exception of IgG. The IgG molecules were then precipitated and concentrated using ammonium sulphate (see 2.4.5), producing moderately pure IgG antibodies. The pellet was resuspended in PBS, dialysed to remove excess ammonium sulphate and a sample of the purified antibody analysed on a 12.5% SDS-PAGE gel. The proteins were transferred to a membrane by Western Blot, and then incubated with biotinylated donkey anti-sheep Ig antibody (diluted 1:20,000), followed by streptavidin conjugated to AP (diluted 1:2,000) and visualised using Sigma FAST BCIP/NBT solution. Figure 4.3.4.1 shows that all samples contained immunoglobulin heavy (55kDa) and light (25kDa) chains, and therefore sheep antibodies were present after the purification process. The antibodies were present in approximately equal concentrations in all the samples.

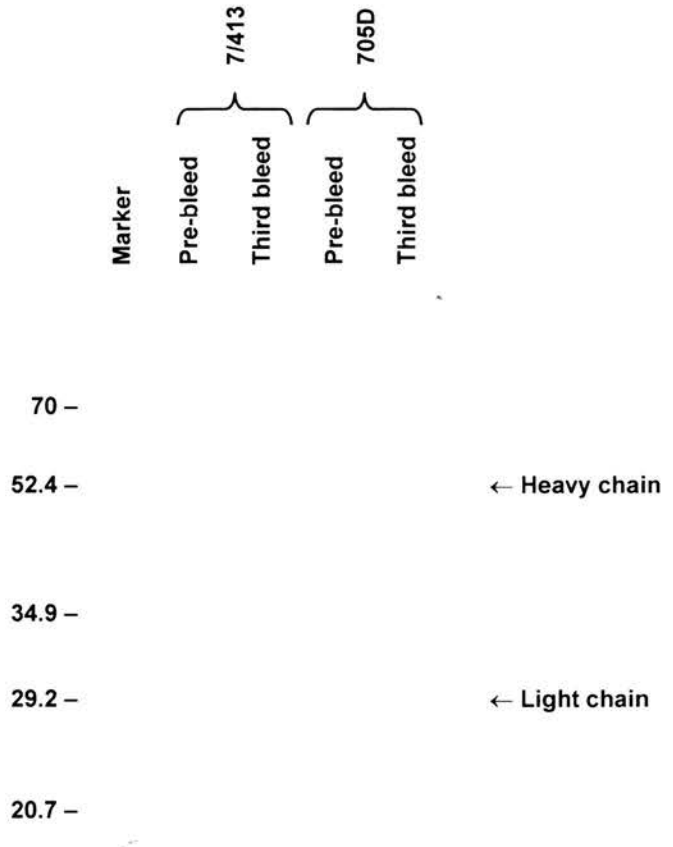

Figure 4.3.4.1 Purification of sheep anti-M2 antibodies. Aliquots of sheep serum taken before immunisation **(pre-bleed)** and four weeks after the third immunisation with GST- $M2_{74-148}$ **(third bleed)** were purified using caprylic acid followed by ammonium sulphate precipitation. Aliquots of purified antibody were analysed on a 12.5% SDS-PAGE gel, followed by immunobloting. The blot was probed with biotinylated anti-sheep Ig, followed by streptavidin-AP and visualised using Sigma FAST BCIP/NBT solution. Results are shown for both sheep (**7/413** and **705D**). Molecular weights are given in kilodaltons relative to the marker in the left lane.

To assess the anti-M2 reactivity of the purified sheep antibodies, four identical 15% SDS-PAGE gels were prepared containing the following samples:

A. GST-$M2_{74-148}$ fusion protein (used as the antigen to raise the immune response in the sheep). Although a sample containing only GST should have been included to confirm that there were no antibodies present in sheep that might cross-react with GST, it was decided that the GST-$M2_{74-148}$ fusion protein preparation contain a large amount of native GST (see Figure 4.3.3) and thus this sample was also used as this control.

B. Cell lysate from 293 cells transfected with the pVR1255/M2-His vector (this mammalian expression vector was thought to express M2 [see 4.4.1 and 4.4.2]).

C. Cell lysate from 293 cells transfected with the control vector pVR1255.

D. S11 cell lysate (S11 cells are known to express the M2 protein; Husain *et al.*, 1999).

The proteins were transferred to a membrane by Western Blot, and incubated with purified pre-bleed or third bleed sheep antibody (diluted 1:1,000-10,000). This was followed by biotinylated donkey anti-sheep Ig antibody (diluted 1:20,000-40,000), and then streptavidin conjugated to AP (diluted 1:2,000) and visualised using Sigma FAST BCIP/NBT solution. Figure 4.3.4.2 shows that the third bleed antibody samples from both sheep (panels B and D) recognised the GST-$M2_{74-148}$ fusion protein, whereas the pre-bleed samples did not (panels A and C). This result shows that both sheep have raised antibodies against the GST-$M2_{74-148}$ fusion protein. When compared with the pre-bleed samples, the third bleed antibodies displayed no specific reactivity with the cell lysate from 293 cells transfected with pVR1255/M2-His. This result agrees with data showing that no M2 expression was detectable from this vector by immunoblot analysis using anti-His_6 antibody to detect the polyhistidine epitope (see 4.4.2). However, the third bleed antibody of sheep 705D (panel D) reacted against a band at approximately 30-35kDa in the S11 cell lysate. This band was not present in the pre-bleed immunoblot (panel C). This suggested that sheep 705D had produced antibodies against a protein in the S11 cells, and this protein could be the M2

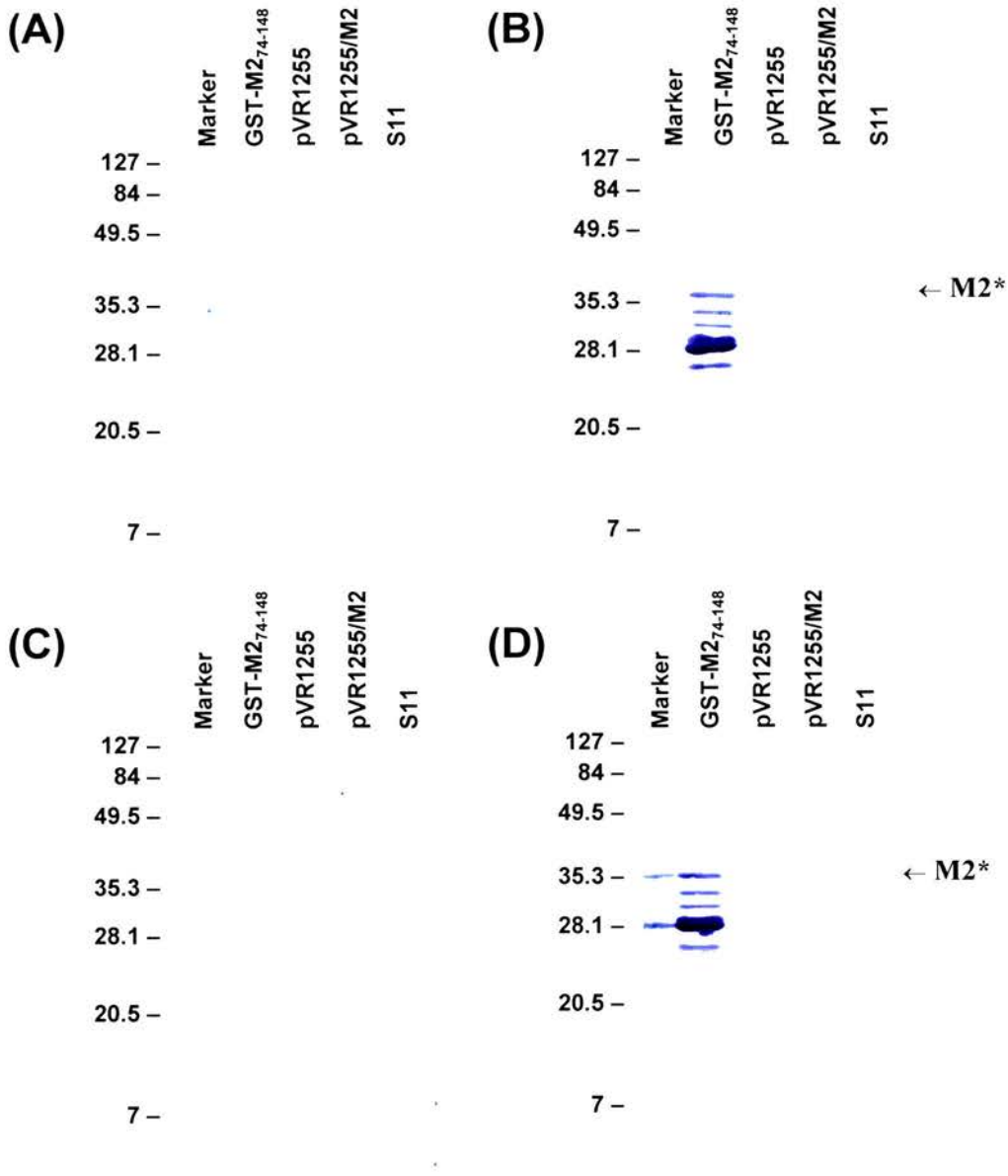

Figure 4.3.4.2 Reactivity of purified sheep anti-M2 antibodies. The ability of the sheep antibodies to detect M2 protein was assessed by immunoblot. Samples of GST- $M2_{74-148}$ protein (lane 2), cell lysates of 293 cells transfected with pVR1255 (lane 3) or pVR1255/M2-His (lane 4) and S11 cells (lane 5) were separated on a 15% SDS-PAGE gel, and transferred onto a membrane by Western blot. The blots were probed with pre-bleed **(A)** and third bleed **(B)** from sheep 7/413, and pre-bleed **(C)** and third bleed **(D)** from sheep 705D. The sheep antibodies were detected using biotinylated anti-sheep Ig, followed by streptavidin-AP and visualised using Sigma FAST BCIP/NBT solution. **M2*** indicates predicted position of M2 protein. Molecular weights are given in kilodaltons relative to the marker in the left lane.

protein. The observed band at 30-35kDa was slightly larger than the expected molecular weight of M2 (21.2kDa).

Antibodies from sheep 705D were therefore used in subsequent experiments to determine the reactivity of the purified sheep anti-M2 antibodies. High levels of background staining were observed in all the immunoblots probed with the sheep antibodies due to non-specific binding of the sheep antibodies to proteins on the Western blot. In order to try and overcome this high background staining, a range of different dilutions of the primary sheep antibody (1:1,000-1:10,000) and secondary biotinylated donkey anti-sheep Ig (1:20,000-1:80,000) were used. It was also decided to use ECL, as the enhanced sensitivity of detection by ECL meant that more dilute concentrations of antibody could be used. Two identical 12.5% SDS-PAGE gels were prepared containing samples of S11 cell lysate, cell lysate from A20 cells transfected with pSG5/M2-3'HA (this mammalian expression vector was known to express M2 [see 4.4.2]) and cell lysate from A20 cells (a negative control for the transfected cell lysate). The proteins were transferred to a membrane by Western Blot, and the blots were incubated with purified pre-bleed or third bleed sheep antibody (diluted 1:10,000). This was followed by biotinylated donkey anti-sheep Ig antibody (diluted 1:80,000), and then streptavidin conjugated to POD (diluted 1:5,000) and visualised using ECL. Figure 4.3.4.3 shows that high background staining was present in the immunoblot, which obscured any possible reactivity of the third bleed antibody of sheep 705D (panel B) against the predicted M2 protein band present at 30kDa. When compared with the pre-bleed samples, the third bleed antibodies displayed no specific reactivity with the cell lysate from A20 cells transfected with pSG5/M2-3'HA. High background levels were again observed in all immunoblots at a range of different antibody concentrations. This suggested that the non-specific binding of the sheep antibodies to proteins on the Western blot was leading to high background levels that prevented definitive recognition of M2 by immunoblot.

The reactivity of the sheep antibodies to the M2 protein was also assessed by immunofluorescence. S11 cells were fixed onto glass slides, and stained by indirect immunofluorescence (see 2.7.8). The slides were incubated with either

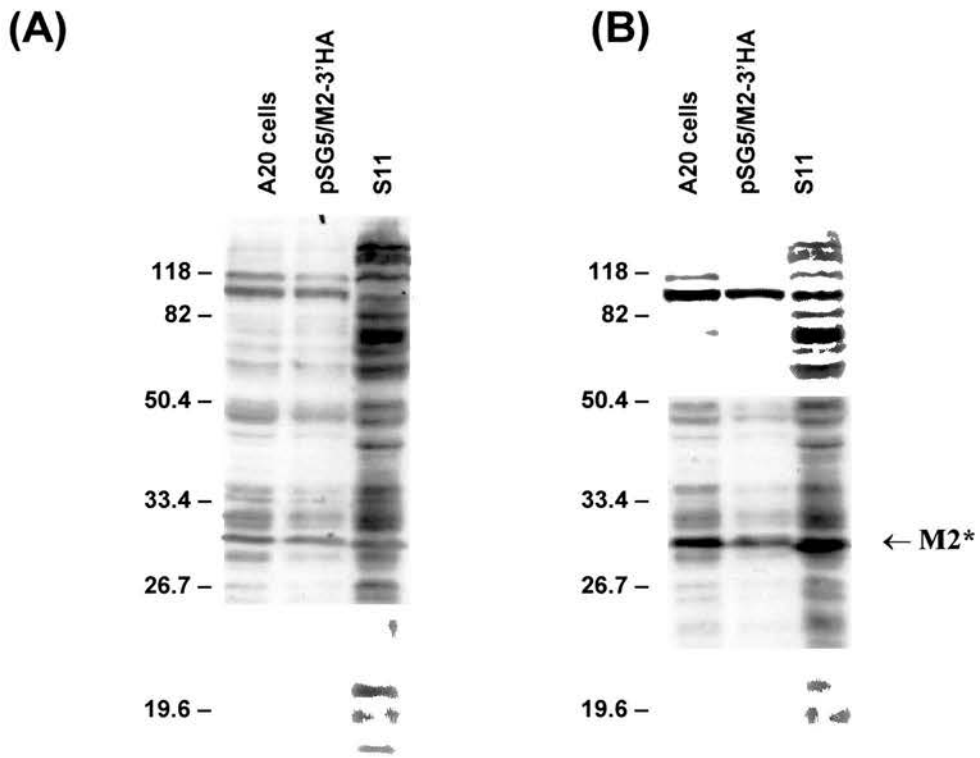

Figure 4.3.4.3 Reactivity of purified sheep anti-M2 antibodies. The ability of the sheep antibodies to detect M2 protein was assessed by immunoblot. Aliquots of cell lysates of A20 cells (lane 1), A20 cells transfected with pSG5/M2-3'HA (lane 2) and S11 cells (lane 3) were separated on a 12.5% SDS-PAGE gel, and transferred onto a membrane by Western blot. The blots were probed with pre-bleed **(A)** and third bleed **(B)** from sheep 705D. The sheep antibodies were detected using biotinylated anti-sheep Ig, followed by streptavidin-POD and visualised using ECL. **M2*** indicates predicted position of M2 protein. Molecular weights are given in kilodaltons on the left side.

pre-bleed or third bleed purified antibodies from sheep 705D diluted 1:100-1:500 in PBS containing 5% v/v normal donkey serum, followed by donkey anti-sheep Ig-FITC conjugate (diluted 1:250). There were no differences in FITC localisation between the pre-bleed and the third bleed samples in the S11 cells. High levels of background FITC staining were observed, even at lower antibody dilutions.

4.4. Expression of M2 in mammalian cells

4.4.1. Expression constructs and epitope tagging of M2

Due to the lack of a reliable antibody to the M2 protein, it was decided to investigate the cellular localisation and function of M2 by expressing the M2 protein with an epitope tag. This epitope tag could then be used to detect protein expression by the use of commercially available antibodies. It was decided to use six histidine residues (His_6) fused to the carboxy terminus as there are commercially available antibodies to this epitope, it has been used successfully to characterise as wide variety of proteins (Kao *et al.*, 1994; Lackner & Condit, 2000) and the His_6 epitope can be used to concentrate and / or purify proteins via affinity chromatography (Hochuli *et al.*, 1988; Bornhorst & Falke, 2000). The M2 cDNA ORF was amplified using primer pair M2GEX1 and M2-HIS (Chapter 2, Appendix 2) with *Taq* DNA polymerase and cloned into the pcDNA3.1(+) vector (Chapter 2, Appendix 3) using the *Bam*HI and *Eco*RI restriction enzyme sites to give the vector pcDNA3.1/M2-His (Figure 4.4.1.1A). The pcDNA3.1 vector contains the HCMV immediate-early promoter for efficient, high-level expression of inserted genes (Foecking & Hofstetter, 1986; Xu *et al.*, 2001). The sequence corresponding to the six histidine residues was inserted immediately upstream of the M2 STOP codon so that it would be translated in frame with the M2 protein. Determination of the sequence of the DNA insert in pcDNA3.1(+) (see 2.2.24) showed that it was 100% identical at the nucleotide level to the M2 cDNA ORF, with the sequence corresponding to the six histidine residue epitope present at the 3' end (data not shown).

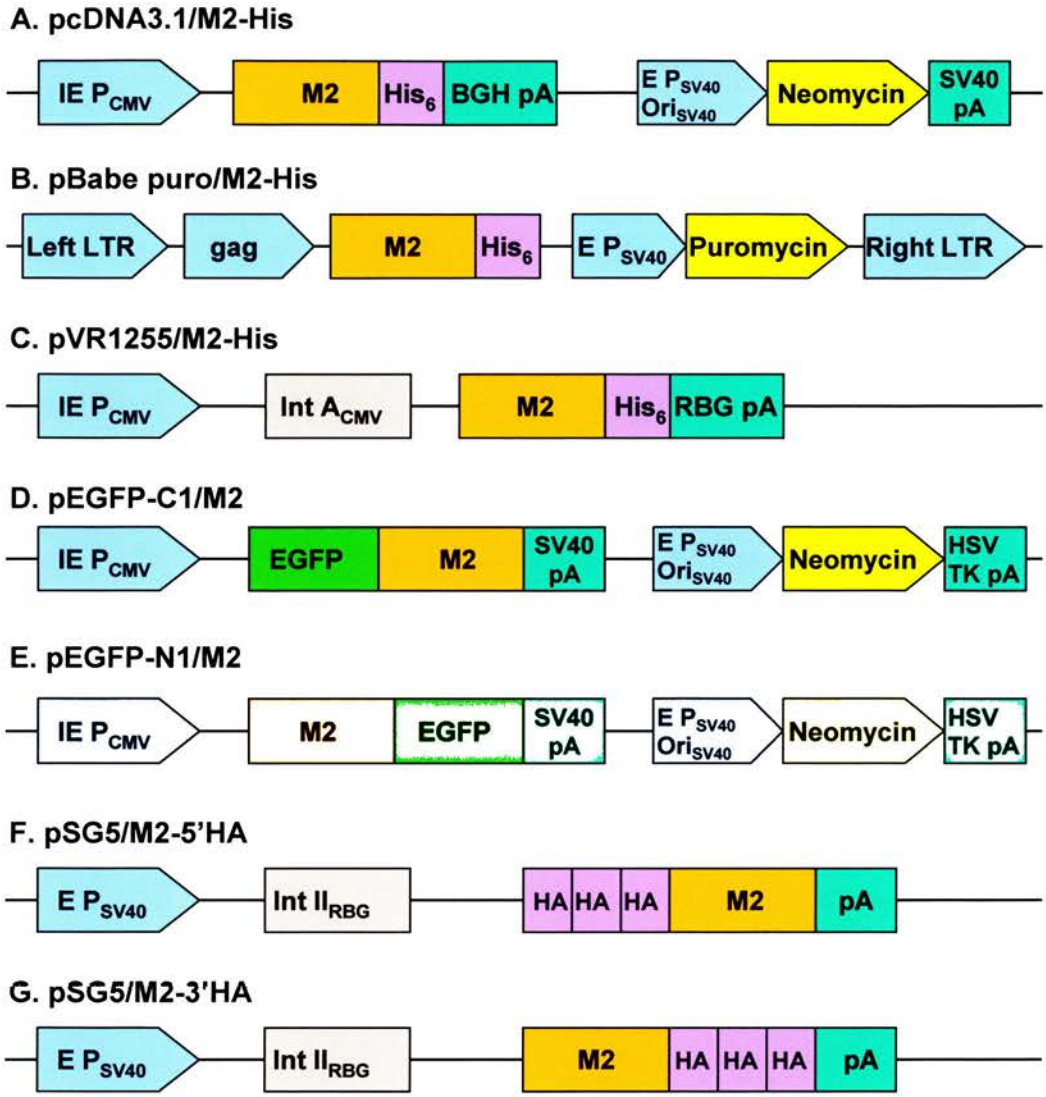

Figure 4.4.1.1 Schematic drawing (not to scale) of constructs for the expression of M2 in mammalian cells, showing relevant features. Abbreviations: **IE P_{CMV}**, human cytomegalovirus immediate-early promoter/enhancer; **His_6**, six consecutive histidine residues; **BGH pA**, bovine growth hormone polyadenylation signal; **E P_{SV40}**, SV40 early promoter; **Ori_{SV40}**, SV40 origin of replication; **SV40 pA**, SV40 polyadenylation signal; **LTR**, Moloney murine leukaemia virus long terminal repeats; **Int A_{CMV}**, Intron A of the CMV immediate early gene; **RBG pA**, rabbit β-globin polyadenylation signal; **EGFP**, enhanced green fluorescent protein; **HSV TK pA**, herpes simplex virus thymidine kinase polyadenylation signal; **Int II_{RBG}**, Intron II of rabbit β-globin gene; **HA**, influenza haemagglutinin epitope; **pA**, polyadenylation signal. For full details of plasmid vectors, see Chapter 2 Appendix 3.

The pcDNA3.1/M2-His or pcDNA3.1 (empty negative control vector) plasmid DNA (20μg) was transfected into BHK-21, COS-7 or HeLa cells by electroporation (see 2.1.4), and the cells harvested after 24 hours. The cell lysates were analysed by immunoblot following separation by SDS-PAGE. The blot was incubated with mouse monoclonal anti-His_6 antibody (diluted 1:500), followed by biotinylated rabbit anti-mouse Ig (diluted 1:40,000) and then streptavidin-AP conjugate (diluted 1:1,000). The reactive proteins were visualised using Sigma FAST BCIP/NBT solution. No specific protein bands corresponding to M2 were seen in the pcDNA3.1/M2-His cell lysate for any of the cell types transfected (data not shown).

Attempts were also made to generate cell lines stably transfected with the pcDNA3.1/M2-His plasmid. COS-7 cells (which express the SV40 large T antigen) were transfected with 20μg of pcDNA3.1 (empty negative control vector) or pcDNA3.1/M2-His by electroporation (see 2.1.4), which both contain the SV40 origin of replication. Stably transfected cells were selected 24 hours after transfection with 400μg/ml G418 antibiotic (Invitrogen Life Technologies). Resistant foci of cells were cloned, and kept under G418 selection for a minimum of 3 weeks. Cell lysates were again tested for M2-His expression by immunoblot analysis using the mouse monoclonal anti-His_6 antibody as previously described. No specific protein bands corresponding to M2 were seen in the pcDNA3.1/M2-His cell lysate for any of the G418 resistant cell clones analysed (data not shown). DNA from G418 resistant cell clones transfected with pcDNA3.1/M2-His was isolated using a DNeasy Tissue Kit (see 2.6.10), quantified (see 2.2.6) and tested for the presence of the M2 DNA insert by 40 cycles of PCR (see 2.2.1) using the primer pair M2GEX1 and M2-HIS (Chapter 2, Appendix 2). No M2 insert DNA was detectable in any of the cell clones analysed (data not shown), suggesting that the M2-His insert had been lost from these cells.

It was postulated that the high level of expression of M2 protein from the HCMV immediate-early promoter might be leading to cytotoxicity, and therefore poor levels of expression. It was therefore decided to use a retroviral expression vector, pBabe puro (Chapter 2, Appendix 3). This vector expresses inserted DNA

under the control of the Moloney murine leukaemia virus (MoMuLV) long terminal repeats (Morgenstern & Land, 1990), which gives lower levels of expression than the HCMV immediate early promoter (Martin-Gallardo *et al.*, 1988). The M2 cDNA ORF was amplified using primer pair M2GEX1 and M2-HIS (Chapter 2, Appendix 2) and cloned into the pBabe puro vector using the *Bam*HI and *Eco*RI restriction enzyme sites to give the vector pBabe puro/M2-His (Figure 4.4.1.1B). The pBabe puro/M2-His or pBabe puro (empty negative control vector) plasmid DNA (20μg) was transfected into BHK-21 or HeLa cells by electroporation (see 2.1.4), and the cells harvested after 24 hours. Cell lysates were again tested for M2-His expression by immunoblot analysis using the mouse monoclonal anti-His_6 antibody as previously described. No specific protein bands corresponding to M2 were seen in the pBabe puro/M2-His cell lysate for any of the cell types transfected (data not shown).

Due to the failure to detect any expression of M2 by transient or stably transfected cell lines with the expression vectors pcDNA3.1/M2-His or pBabe puro/M2-His, it was hypothesised that the levels of M2 expression might be below levels detectable by immunoblot. It was therefore decided to use a *lacZ*-inducible T cell hybridoma line specific for the $M2_{91-99}$ CD8+ T cell epitope to detect expression of the M2 protein. *LacZ*-inducible T cell hybridomas contain a β-galactosidase gene (*lacZ*) under the transcriptional control of the nuclear factor of activated T cells element of the IL-2 enhancer (Karttunen & Shastri, 1991). The recognition of its cognate epitope by the T-cell receptor of the hybridoma results not only in the production of IL-2, but also in the production of β-galactosidase, which can be detected by staining with X-gal. This technique is therefore extremely sensitive for the individual ligand-activated T-cell detection of antigen (Karttunen *et al.*, 1992; Usherwood *et al.*, 1999). A *LacZ*-inducible T cell hybridoma had been developed in the Department of Immunology, St. Jude Children's Research Hospital, Memphis specific for the $M2_{91-99}$ CD8+ T cell epitope, and Dr. E. Usherwood performed analysis of the plasmid vectors for M2 expression.

Cells were transfected with the expression vectors pcDNA3.1/M2-His or pBabe puro/M2-His, and these cells were used as antigen-presenting cells for the *LacZ*-inducible T cell hybridoma. The numbers of cells positive for blue X-gal staining were then counted per well. Negative control cells (either not transfected or transfected with the plasmid pBabe puro/GPCR) showed only 1 – 3 positive cells per well. Positive control S11 cells showed 73 positive cells per well. Cells transfected with the expression vector pcDNA3.1/M2-His showed over 200 positive cells per well, and cells transfected with pBabe puro/M2-His showed 29 positive cells per well. These results showed that cells transfected with the M2 expression vectors presented the $M2_{91-99}$ CD8+ T cell epitope to the *lacZ*-inducible T cell hybridoma, and were therefore expressing M2 protein. This was an extremely sensitive assay, and the results suggested that the expression of M2 by these vectors in BHK-21, COS-7 and HeLa cells was occurring, but was below levels detectable by immunoblot.

Previous work had shown detectable levels of gp150 expression using the mammalian expression vector pVR1255 (Dr. I. Atkin, unpublished observations). This vector has been modified to increase gene expression levels, and uses the HCMV immediate-early promoter to express the reporter luciferase gene (Hartikka *et al.*, 1996). The vector was obtained under license from Vical Inc., and had been modified to remove the luciferase gene giving the plasmid $pVR1255^{luc-}$ (Chapter 2, Appendix 3). The M2 gene was excised from the sequenced plasmid pcDNA3.1/M2-His using the restriction enzymes *Pme*I and *Eco*RV, and the M2-His fragment isolated from a 1% agarose gel (see 2.2.13). The vector $pVR1255^{luc-}$ was digested with the restriction endonuclease *Eco*RV, and the M2-His insert was ligated into the digested vector. The ligation mixture was used to transform XL-1 Blue bacteria (see 2.2.11), and colonies analysed by the mini-prep method (see 2.2.14). Diagnostic restriction enzyme digestion with *Eco*RV only, or *Eco*RV and *Hin*dIII, or *Eco*RV and *Sal*I was used to confirm the presence of the M2-His insert in the correct orientation, giving the vector pVR1255/M2-His (Figure 4.4.1.1C). pVR1255/M2-His or pVR1255 (negative control vector expressing luciferase) plasmid DNA (20μg) was transfected into BHK-21 or 293 cells by electroporation (see 2.1.4), and the cells harvested after

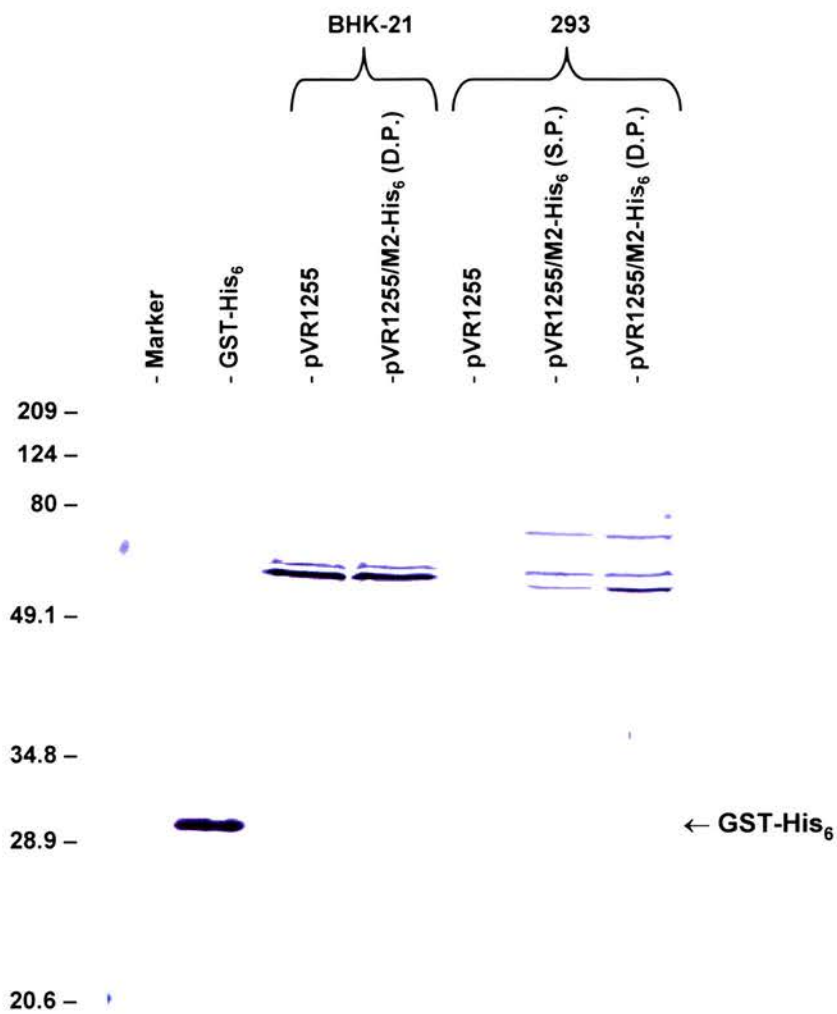

Figure 4.4.1.2 Expression of His_6 tagged M2 protein in mammalian cells. BHK-21 or 293 cells were transfected with 20µg of plasmid DNA and harvested 24 hours after transfection. Cells were transfected using either the single pulse (**S.P.**) or double pulse (**D.P.**) electroporation program with pVR1255 (negative control) or pVR1255/M2-His_6. The cell lysates were analysed on a 12.5% SDS-PAGE gel, and transferred onto a membrane by Western blot. Lane 1 contained GST-His_6 as a positive control. The blots were probed with mouse monoclonal anti-His_6, followed by biotinylated rabbit anti-mouse Ig and then streptavidin-AP. The conjugates were visualised using Sigma FAST BCIP/NBT solution. Molecular weights are given in kilodaltons on the left side.

24 hours. Cell lysates were again tested for M2-His expression by immunoblot analysis using the mouse monoclonal anti-His_6 antibody as previously described. As a positive control, 100ng of GST tagged with the His_6 epitope (GST-His_6; kindly provided by Dr. I. Atkin) was analysed on the same immunoblot. Figure 4.4.1.2 shows that the GST-His_6 protein was visualised at the expected molecular mass of approximately 27.5kDa. However, there were no differences specific for M2 observed between the control plasmid pVR1255 and pVR1255/M2-His in either the BHK-21 or 293 cell lysates by immunoblot analysis. There was therefore no detectable expression of M2 by the plasmid pVR1255/M2-His by immunoblot analysis.

Attempts were also made to detect expression of M2 by immunofluorescence. COS-7, BHK-21, HeLa or 293 cells were transfected with 20μg of plasmid DNA (see 2.1.4), harvested 24 hours later and fixed onto slides (see 2.7.1). The plasmids used were pcDNA3.1 and pcDNA3.1/M2-His; pBabe puro and pBabe puro/M2-His; pVR1255 and pVR1255/M2. The slides were incubated with either mouse monoclonal anti-His_6 (diluted 1:10-1:50) or mouse monoclonal anti-LMP1 (isotype specific negative control for non-specific binding; diluted 1:20), followed by biotinylated rabbit anti-mouse IgG (diluted 1:100-1:500) and then streptavidin-FITC conjugate (diluted 1:300; see 2.7.8). No specific FITC staining was detectable in cells expressing the His_6-tagged M2 protein, and there was therefore no detectable expression of M2 by these plasmids by immunofluorescence analysis.

These results showed that no expression of M2 was detectable from the expression vectors pcDNA3.1/M2-His, pBabe puro/M2-His and pVR1255/M2-His by immunoblot or immunofluorescence. However, expression was detectable from the expression vectors pcDNA3.1/M2-His and pBabe puro/M2-His using very sensitive assays for the $M2_{91-99}$ CD8+ T cell epitope. This result suggested that the levels of M2 expression were below levels detectable by antibody, and a more sensitive assay was required. It was therefore decided to construct GFP fusion proteins, which would enable localisation of M2 in mammalian cells at very low levels (Chalfie *et al.*, 1994). GFP fusion proteins have been made for a wide range of proteins, including viral proteins such as HIV-1 integrase

(Pluymers *et al.*, 1999), EBNA-1 of EBV (Marechal *et al.*, 1999) and LANA-1 of KSHV (Piolot *et al.*, 2001). GFP fusion proteins usually localise and function identically to the native protein (Stauber & Pavlakis, 1998; Lorenzon *et al.*, 2001), and the GFP thus serves as an excellent means of identifying proteins in living and fixed cells.

The M2 cDNA ORF was amplified using primer pair M2GEX1 and M2GEX2 (Chapter 2, Appendix 2) with *PfuTurbo*™ DNA polymerase, and cloned into the pEGFP-C1 vector (Chapter 2, Appendix 3) using the *Bgl*II and *Eco*RI restriction enzyme sites to give the vector pEGFP-C1/M2 (Figure 4.4.1.1D). The pEGFP series of expression vectors expresses cloned DNA inserts as EGFP fusion proteins using the HCMV immediately early promoter. EGFP is a variant of GFP that has been optimised for brighter fluorescence and higher expression in mammalian cells. The M2 gene was therefore inserted in frame with the EGFP protein, and would be expressed as a fusion to the C terminus of the EGFP protein. Diagnostic restriction enzyme digestion of mini-prep DNA samples with *Pst*I only, or *Bsp*EI and *Eco*RI, or *Nco*I and *Pst*I was used to confirm the presence of the M2 insert in the correct orientation.

The M2 cDNA ORF was amplified using primer pair M2GEX1 and M2GFP-N (Chapter 2, Appendix 2) with *PfuTurbo*™ DNA polymerase, and cloned into the pEGFP-N1 vector (Chapter 2, Appendix 3) using the *Bgl*II and *Eco*RI restriction enzyme sites to give the vector pEGFP-N1/M2 (Figure 4.4.1.1E). The M2 gene was therefore inserted in frame with the EGFP protein, and would be expressed as a fusion to the N terminus of the EGFP protein. Diagnostic restriction enzyme digestion of mini-prep DNA samples with *Pst*I only, or *Nhe*I and *Eco*RI, or *Nco*I and *Pst*I was used to confirm the presence of the M2 insert in the correct orientation.

Two M2 expression constructs were kindly provided by Dr. Jeff Sample, St. Jude Children's Research Hospital, Memphis. They contained the eukaryotic expression vector pSG5, which expresses inserted DNA from the SV40 early promoter (Chapter 2, Appendix 3). The plasmid pSG5/M2-5'HA contained the M2 gene with three consecutive 27bp DNA sequences corresponding to the

influenza haemagglutinin (HA) epitope (YPYDVPDYA) inserted immediately upstream of the M2 ORF so that it would be translated in frame with the M2 protein (Figure 4.4.1.1F). The plasmid pSG5/M2-3'HA contained the M2 gene with the three HA epitope sequences inserted immediately upstream of the M2 STOP codon (Figure 4.4.1.1G). Dr. Sample also provided two control plasmids that had been shown to express HA epitope tagged proteins in mammalian cells. The plasmid pSG5/Jκ-HA expresses the cellular DNA-binding protein Jκ (Zhao *et al.*, 1996), and plasmid pSG5/IRF7-HA expresses the interferon regulatory factor-7 (IRF7) (Zhang & Pagano, 1997).

4.4.2. Expression of M2

A20 and 293 cells were transfected with 20μg of the HA epitope-tagged expression constructs pSG5/IRF7-HA, pSG5/Jκ-HA, pSG5/M2-5'HA and pSG5/M2-3'HA. Mock transfected cells were used as a negative control. The cells were harvested 24 hours after transfection, and the cell lysates were analysed on a 12.5% SDS-PAGE gel, and transferred onto a membrane by Western blot. The blot was incubated with mouse monoclonal anti-HA antibody (diluted 1:2000), followed by biotinylated rabbit anti-rat Ig (diluted 1:10,000) and then streptavidin-POD conjugate (diluted 1:5,000). The reactive proteins were visualised using ECL. Figure 4.4.2.1 shows the results of the immunoblot analysis of A20 cells for the expression of HA epitope-tagged proteins. The positive control proteins IRF7-HA (a 70kDa protein) and Jκ-HA (a 60kDa protein) were visualised as bands at their appropriate relative molecular masses. Unique bands were also observed in the A20 cell lysates containing HA epitope-tagged M2 at a relative molecular mass of approximately 30kDa. This is larger than the expected mass of 22.3kDa (consisting of the 21.2kDa predicted molecular mass of M2 with the 1.1kDa HA epitope). There did not appear to be any substantial size differences between the M2-5'HA or M2-3'HA proteins, which are epitope-tagged with HA at the N-terminus and C-terminus respectively. This result suggested that there was no post-translational cleavage of the M2 protein. The HA epitope-tagged M2 proteins also appeared as a doublet, a characteristic that is also

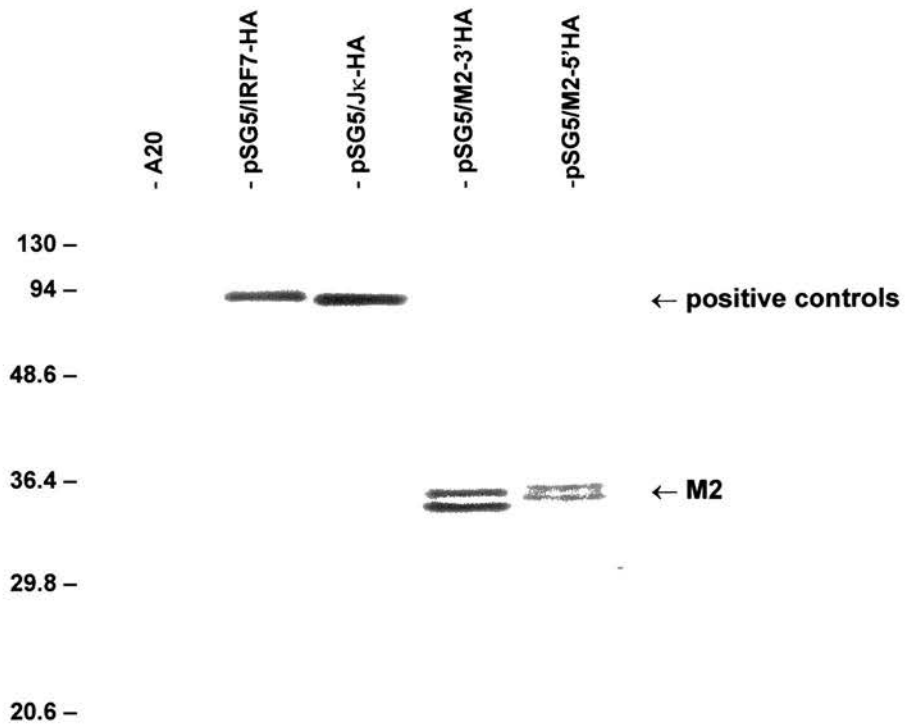

Figure 4.4.2.1 Expression of HA-epitope tagged M2 protein in A20 cells. Cells were transfected with 20μg of plasmid DNA and harvested 24 hours after transfection. Mock transfected A20 cells were used as a negative control, and two positive controls (pSG5/IRF7-HA and pSG5/Jκ-HA) were also included. The cell lysates were analysed on a 12.5% SDS-PAGE gel, and transferred onto a membrane by Western blot. The blots were probed with rat monoclonal anti-HA, followed by biotinylated rabbit anti-rat Ig and then streptavidin-POD. The conjugates were visualised using ECL. Molecular weights are given in kilodaltons on the left side.

observed following SDS-PAGE analysis of many phosphorylated proteins. The bands observed for all the HA epitope-tagged proteins were not observed in the negative control lane, containing mock transfected A20 cells. These results show that the M2 protein is a 30kDa protein that appears as a doublet by Western blot analysis. In contrast, immunoblot analysis of 293 cells transfected with the HA epitope-tagged expression constructs only resulted in the visualisation of the positive control proteins IRF7-HA and Jκ-HA as bands at their appropriate relative molecular masses. No HA epitope-tagged M2 was visualised after transfection of 293 cells.

In a complementary approach, A20 cells were transfected with 20μg of the EGFP expression constructs pEGFP-C1 and pEGFP-N1, and the EGFP-M2 fusion protein expression constructs pEGFP-C1/M2 and pEGFP-N1/M2. Mock transfected cells were used as a negative control. The cells were harvested 24 hours after transfection, and the cell lysates were analysed on a 10% SDS-PAGE gel, and transferred onto a membrane by Western blot. The blot was incubated with mouse monoclonal anti-GFP antibody (diluted 1:1000), followed by sheep anti-mouse Ig conjugated to POD (diluted 1:2,000). The reactive proteins were visualised using ECL. Figure 4.4.2.2 shows the results of immunoblot analysis for the expression of EGFP in A20 cells. The positive control vector pEGFP-N1 shows a large positive band at 27kDa, which is the expected size of native EGFP protein. The positive control vector pEGFP-C1 expresses the EGFP protein with the multiple cloning site (MCS) attached to the C terminus (see Chapter 2, Appendix 3). This attaches an extra 26 amino acids to the C terminus, which adds 2.5kDa to the 27kDa mass of EGFP protein. The EGFP protein expressed by the pEGFP-C1 vector was therefore visualised as a large positive band with an apparent molecular mass of 30kDa (white asterisk in Figure 4.4.2.2), with a breakdown product corresponding to native EGFP at 27kDa (white dot in Figure 4.4.2.2). Due to the exposure time needed to visualise the GFP-M2 fusion protein via ECL, both positive control EGFP protein bands are significantly overexposed and a small background band is also visualised with an apparent molecular mass of 30kDa. A smaller band with an apparent molecular mass of 23kDa was also

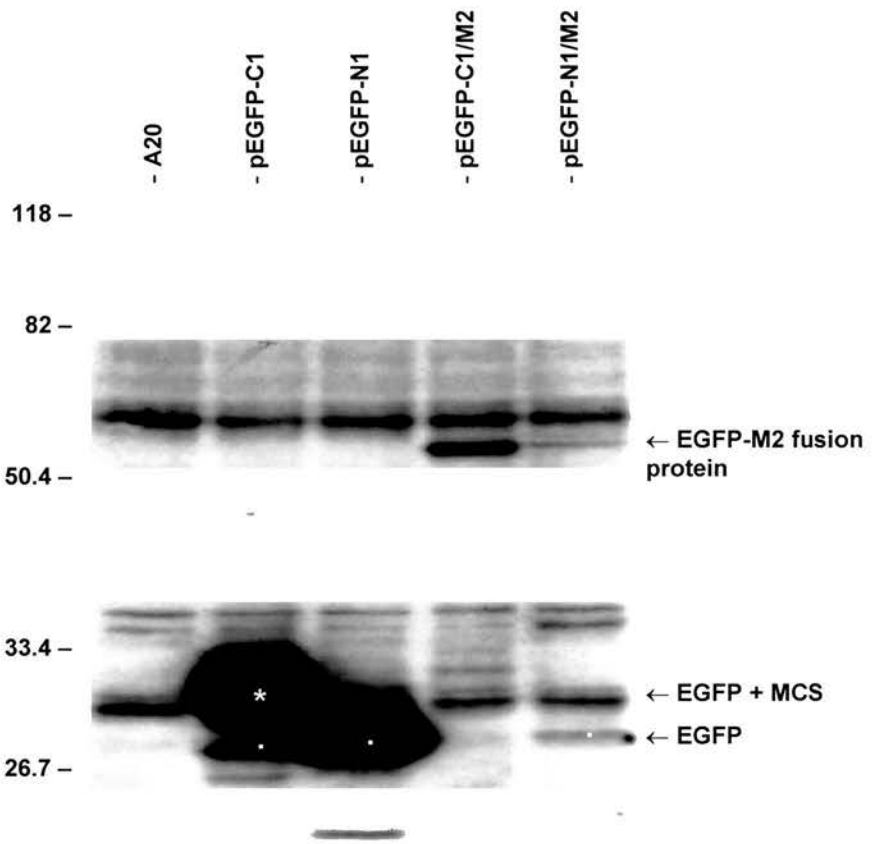

Figure 4.4.2.2 Expression of EGFP fusion proteins in A20 cells. Cells were transfected with 20μg of plasmid DNA and harvested 24 hours after transfection. Mock transfected A20 cells were used as a negative control. The cell lysates were analysed on a 10% SDS-PAGE gel, and transferred onto a membrane by Western blot. The blots were probed with mouse monoclonal anti-EGFP, followed by sheep anti-mouse Ig linked to POD. The conjugates were visualised using ECL. For clarity, a white asterisk has been placed on the EGFP + MCS protein band and a white dot placed on the EGFP protein bands. Molecular weights are given in kilodaltons on the left side. Abbreviations: **MCS**, multiple cloning site present at the C terminus of pEGFP-C1, which adds a 2.5kDa polypeptide to the EGFP protein (see text).

visualised in the positive control vector pEGFP-N1, possibly corresponding to an EGFP breakdown product.

The expression vector pEGFP-C1/M2 produced a single band with an apparent molecular weight of 60kDa. This is larger than the expected 48.2kDa mass of the EGFP-M2 fusion protein (containing the 27kDa EGFP protein with the 21.2kDa M2), but does agree with the observation that the HA epitope-tagged M2 migrates at an apparent molecular mass of 30kDa, giving an expected molecular weight of the EGFP-M2 fusion protein at 57kDa. The expression vector pEGFP-N1/M2 produced a faint single band with an apparent molecular weight of 60kDa. However, there was also a band at 27kDa in the pEGFP-N1/M2 lane, showing that there was also native EGFP present in this sample. This suggests that the M2-EGFP fusion protein is unstable, and is broken down in this sample to give native EGFP. This breakdown to give a band at 27kDa was only observed in cells transfected with pEGFP-N1/M2, and not pEGFP-C1/M2. The bands observed for all the EGFP proteins were not observed in the negative control lane, containing mock transfected A20 cells. These results show that these expression vectors produce a 60kDa EGFP-M2 fusion protein that migrates as a single band on Western blot analysis. However, the M2-EGFP fusion protein produced by the pEGFP-N1/M2 vector appears to be unstable, and is broken down to native EGFP.

A20 cells that were transfected with the EGFP expression constructs were observed to fluoresce green under ultraviolet light (see 4.5.1). However, the number of cells fluorescing following transfection with the pEGFP-C1/M2 and pEGFP-N1/M2 vectors was substantially lower than the number of fluorescent cells after transfection with the control vectors pEGFP-C1 and pEGFP-N1. This observation corresponded with the reduced intensity of the bands seen by immunoblot for the EGFP-M2 fusion proteins as compared to the quantity of EGFP expressed by the control plasmids (Figure 4.4.2.2). This suggested that even though large numbers of cells had been efficiently transfected (as evidenced by the high numbers of cells fluorescing after transfection with the control plasmids), many fewer cells were expressing the EGFP-M2 fusion protein. To quantify this observation, A20 cells were transfected with the EGFP expression

constructs and analysed 24 hours after transfection by FACS analysis for EGFP expression (see 2.6.7). As shown in Figure 4.4.2.3, large numbers of A20 cells transfected with the control vectors pEGFP-C1 and pEGFP-N1 showed green fluorescence (37.4% for pEGFP-C1 [Figure 4.4.2.3B], 36.3% for pEGFP-N1 [Figure 4.4.2.3C]) as compared to the mock transfected negative control cells (Figure 4.4.2.3A). This showed that A20 cells were efficiently transfected with plasmid DNA by electroporation. However, cells transfected with the EGFP-M2 fusion protein expression vectors exhibited an approximate 10-fold decrease in the number of fluorescing cells when compared to the control vectors (4.7% for pEGFP-C1/M2 [Figure 4.4.2.3D], 2.9% for pEGFP-N1/M2 [Figure 4.4.2.3E]). This result suggested that either the intensity of the EGFP fluorescence was being decreased by the addition of M2 in the EGFP-M2 fusion protein, or that the level of EGFP-M2 fusion protein expression was below the limit of detection by FACS analysis in the majority of cells transfected. The results of the immunoblot analysis would suggest the latter explanation, as there is substantially less EGFP protein present in these cells. This finding suggests that the toxicity of the M2 protein in mammalian cells leads to substantially lower levels of expression of EGFP-M2 fusion protein.

4.5. Cellular localisation of M2

4.5.1. Expression of EGFP-M2 fusion protein

The expression of M2 fused to either the C-terminus of EGFP (by the expression vector pEGFP-C1/M2) or N-terminus of EGFP (by the expression vector pEGFP-N1/M2) enabled the visualisation and thus the cellular localisation of the EGFP-M2 fusion protein. 293 cells (a human epithelial cell line, see Table 2.1) were initially used for localisation studies as they showed high transfection efficiencies (50%) by electroporation. 293 cells were transfected with 20μg of plasmid DNA (pEGFP-C1, pEGFP-N1, pEGFP-C1/M2 and pEGFP-N1/M2) and harvested 24 hours after transfection. The cell nuclei were counterstained with propidium iodide, which stains nucleic acids red (specific nuclear staining was

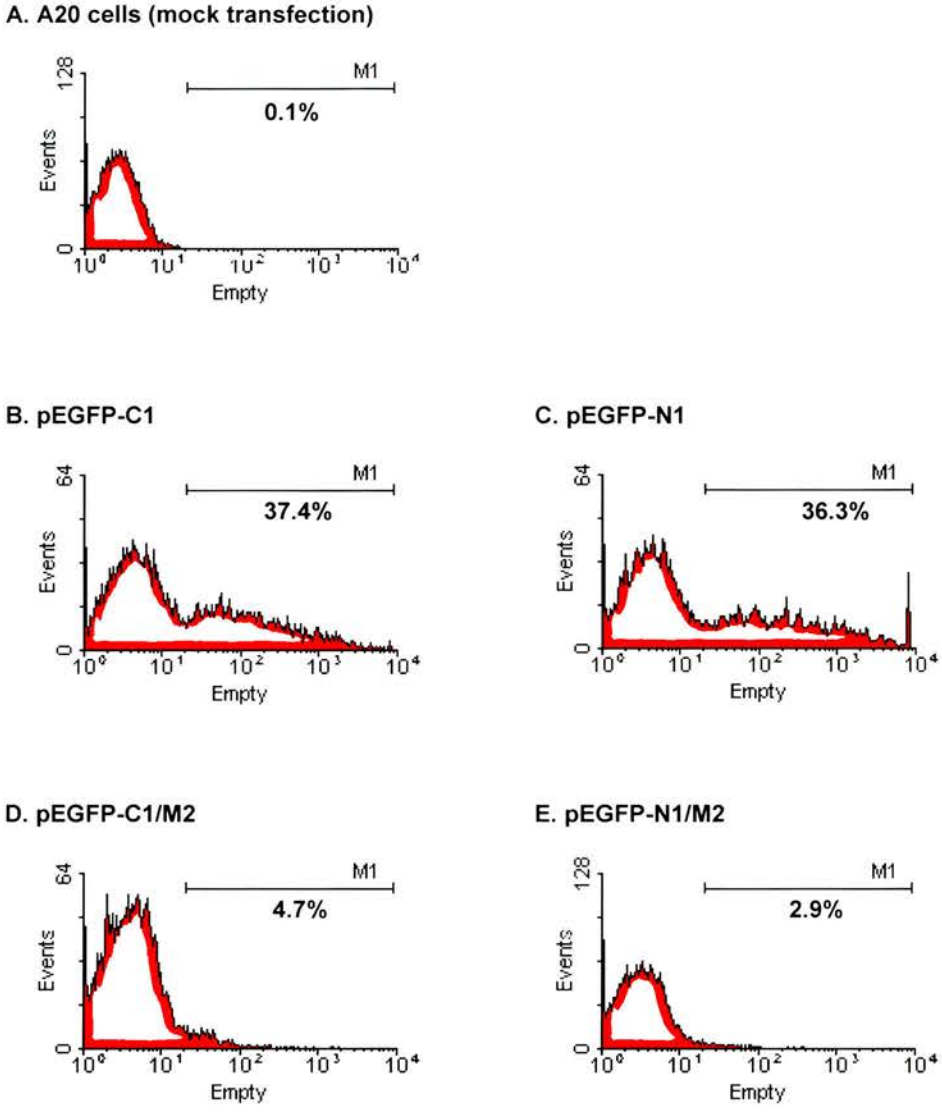

Figure 4.4.2.3 Expression of EGFP fusion proteins in A20 cells. Cells were transfected with 20μg of plasmid DNA, harvested 24 hours after transfection and analysed by FACS. The M1 marker details the number of fluorescent cells (given as a percentage of the total number of cells analysed) for each transfection compared to the negative control. Panel A shows A20 cells mock transfected (negative control); panel B shows A20 cells transfected with pEGFP-C1; panel C shows A20 cells transfected with pEGFP-N1; panel D shows A20 cells transfected with pEGFP-C1/M2; panel E shows A20 cells transfected with pEGFP-N1/M2. The results are representative of three separate experiments.

achieved by treatment of the cells with RNase A at the same time as staining), and the cells analysed by confocal microscopy. Figure 4.5.1.1 shows that 293 cells were efficiently transfected, as evidenced by the numerous cells transfected with pEGFP-C1 and pEGFP-N1 expressing EGFP (panels A and D). Cells transfected with the control vectors and thus expressing EGFP alone show typical localisation of EGFP throughout the nucleus and cytoplasm (panels A-C and D-F). This is illustrated by the image analysis in Figure 4.5.1.2, where the confocal images were examined using the Leica TCSNT confocal analysis software which illustrates the intensity of red or green fluorescence along a line of analysis via a graph. The graph in Figure 4.5.1.2A and B shows that EGFP is expressed throughout the nucleus (red fluorescence present) and cytoplasm (no red fluorescence). There was no difference in EGFP localisation between the two control vectors pEGFP-C1 and pEGFP-N1 (despite the extra 26 amino acid sequence present at the C-terminus of the pEGFP-C1 vector).

In contrast, 293 cells transfected with pEGFP-C1/M2 expressing EGFP-M2 showed localisation of EGFP in the central region and at the periphery of the cell (Figure 4.5.1.1G-I and 4.5.1.2C and D). Only one area of the nucleus showed co-localisation with EGFP-M2 as evidenced by the yellow fluorescence in the overlay image (Panel I), with the other nuclear areas showing no EGFP-M2 present. However, the nucleus in the majority of cells transfected with pEGFP-C1/M2 demonstrated nuclear fragmentation (Figure 4.5.1.1H), a feature characteristic of apoptosis (Bellamy *et al.*, 1995). This was not observed in neighbouring cells or cells transfected with the control plasmids, suggesting that this was not a fixation artefact. 293 cells transfected with pEGFP-N1/M2 also showed localisation of M2-EGFP in the central region, with patches present at the periphery of the cell (Figure 4.5.1.1J-L and 4.5.1.2E and F). There was also diffuse M2-EGFP present in the cytoplasm of cells transfected with pEGFP-N1/M2, and nuclear fragmentation was observed in some cells. There were substantially fewer cells fluorescing after transfection with pEGFP-C1/M2 and pEGFP-N1/M2 compared to cells transfected with the control EGFP expression vectors (pEGFP-C1 and pEGFP-N1), in agreement with Figure 4.4.2.3.

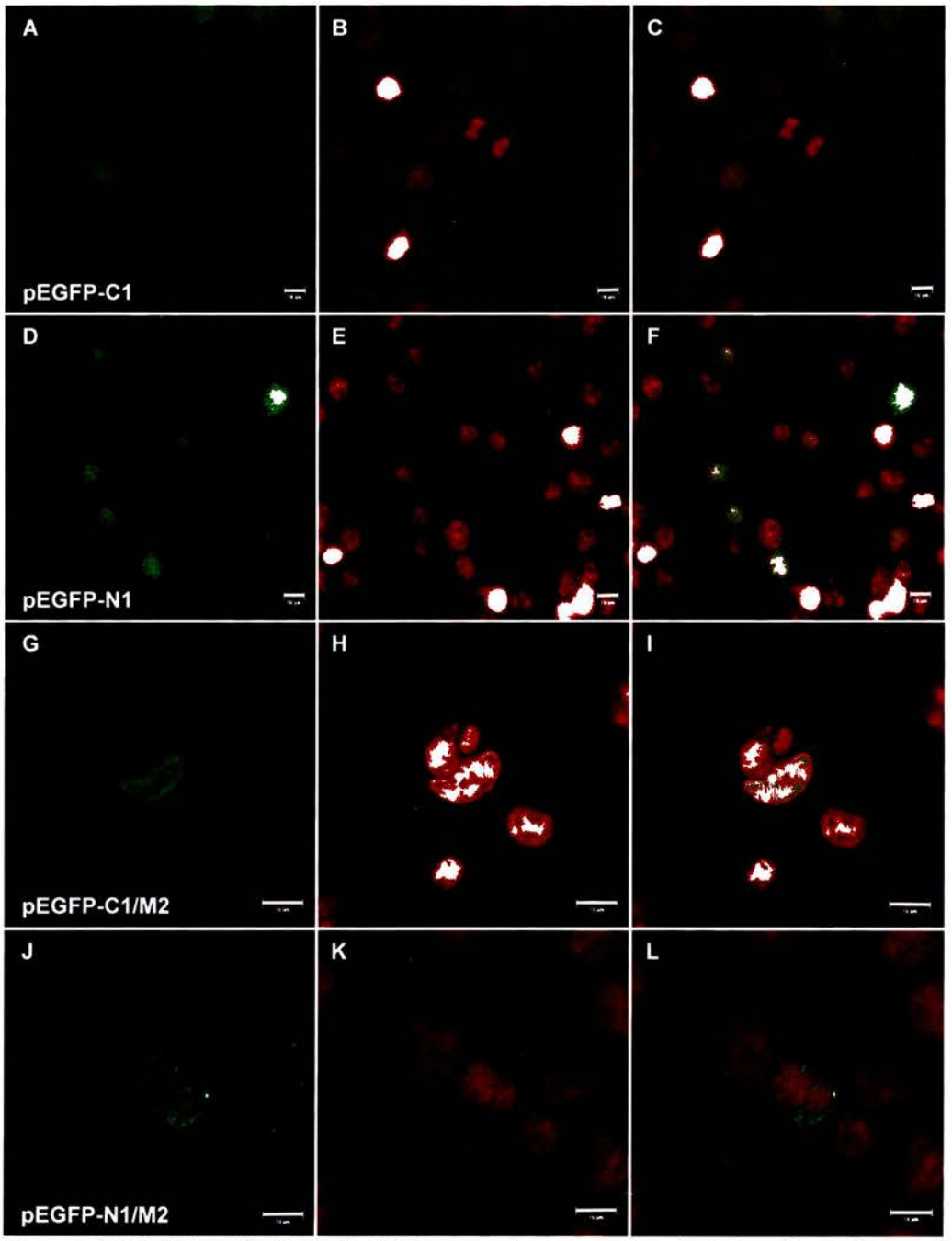

Figure 4.5.1.1 Transfection of EGFP expression constructs in 293 cells. Cells were transfected with 20μg of plasmid DNA and harvested 24 hours after transfection. Panels A, D, G and J show EGFP localisation; panels B, E, H and K show DNA stained with propidium iodide; panels C, F, I and L show overlay images. Panels A, B and C show pEGFP-C1; panels D, E and F show pEGFP-N1; panels G, H and I show pEGFP-C1/M2; panels J, K and L show pEGFP-N1/M2. All images are single confocal slices, with scale bar representing 10μm.

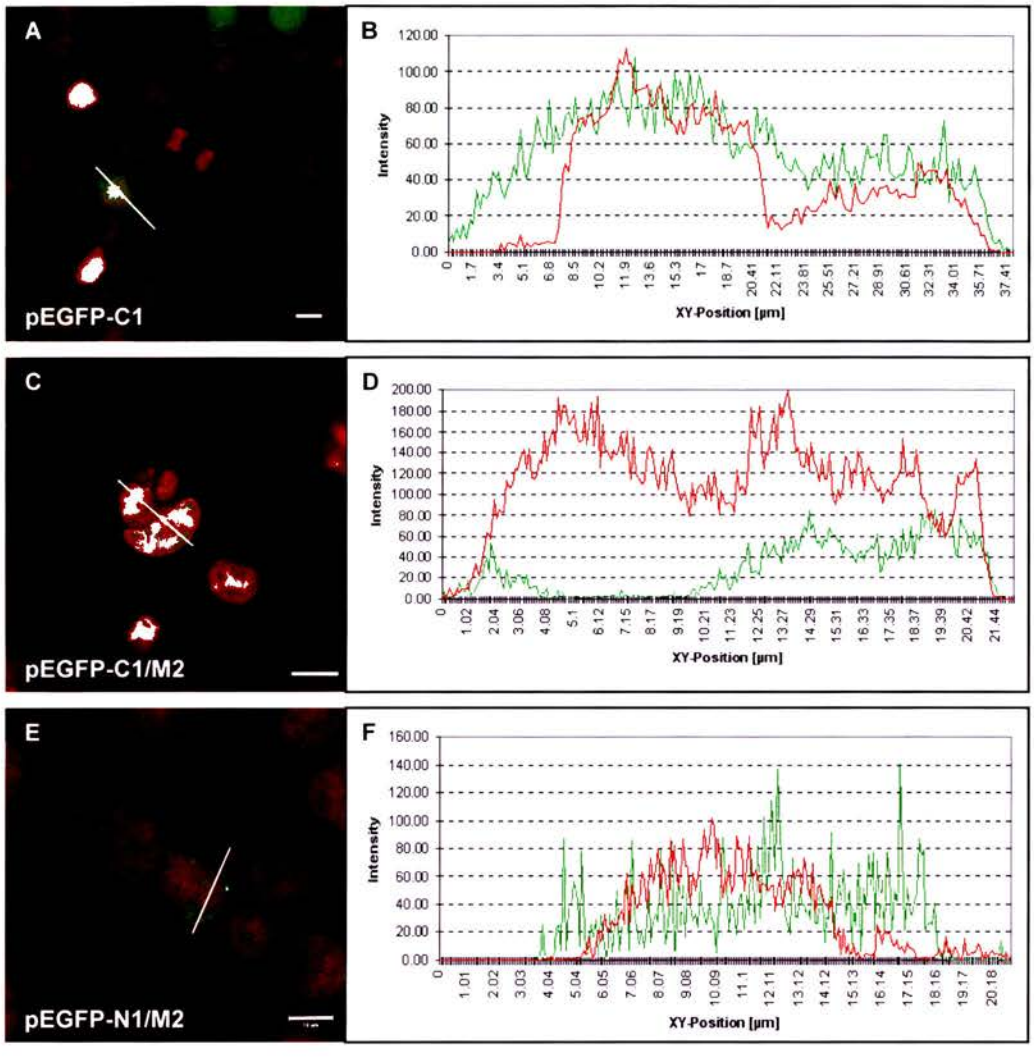

Figure 4.5.1.2 Analysis of confocal images of EGFP expression constructs transfected into 293 cells. The images in Figure 4.5.1.1 were analysed using Leica TCSNT confocal analysis software. Panels on the left show line of analysis (in white) superimposed on the overlay single slice image, and graph on the right shows the intensity of fluorescence of the image along the white line, plotted against XY position on the line. Panel A shows pEGFP-C1; panel B shows image analysis of pEGFP-C1; panel C shows pEGFP-C1/M2; panel D shows image analysis of pEGFP-C1/M2; panel E shows pEGFP-N1/M2; panel F shows image analysis of pEGFP-N1/M2. Scale bar represents 10µm.

The nuclear degeneration observed in 293 cells 24 hours after transfection with the M2-EGFP expression vectors suggested that 293 cells might not be suitable for the expression of M2, either due to species or cell type specificities of the M2 protein. It was therefore decided to use A20 cells (a murine B-lymphocyte line, see Table 2.1) for all further expression studies as these cells could be efficiently transfected by electroporation (see Figure 4.4.2.3) and were as close as possible to the cell type known to express M2 (S11 cells; Usherwood *et al.*, 1996b; Husain *et al.*, 1999). A20 cells were transfected with 20μg of plasmid DNA (pEGFP-C1, pEGFP-N1, pEGFP-C1/M2 and pEGFP-N1/M2) and harvested 24 hours after transfection. The cell nuclei were counterstained with propidium iodide, and the cells analysed by confocal microscopy. In agreement with the previous transfections in 293 cells, A20 cells transfected with pEGFP-C1 and pEGFP-N1 showed typical localisation of EGFP throughout the nucleus and cytoplasm (Figure 4.5.1.3A-C and D-F, Figure 4.5.1.4A and B). A20 cells transfected with pEGFP-C1/M2 showed localisation of EGFP-M2 at the periphery of the cell, with patches of EGFP-M2 present throughout the cell (Figure 4.5.1.3G-I and 4.5.1.4C and D). The EGFP-M2 present in the central region of the cell did not show yellow fluorescence in the overlay image (Panel I) suggesting that the DNA and EGFP-M2 were not closely associated. A similar pattern of M2-EGFP localisation was also observed in cells transfected with pEGFP-N1/M2 (Figure 4.5.1.3J-L and 4.5.1.4E and F), with the only difference being that the intracellular M2-EGFP appeared more diffuse, reflecting the native EGFP produced by the pEGFP-N1/M2 construct (Figure 4.4.2.2). The specific nuclear EGFP-M2 localisation and nuclear degeneration observed in 293 cells transfected with pEGFP-C1/M2 and pEGFP-N1/M2 (Figure 4.5.1.1) was not seen in A20 cells. Again, there were substantially fewer cells fluorescing after transfection with pEGFP-C1/M2 and pEGFP-N1/M2 compared to cells transfected with the control EGFP expression vectors (pEGFP-C1 and pEGFP-N1), in agreement with Figure 4.4.2.3.

S11 cells have been shown to express the M2 protein (Husain *et al.*, 1999), and it was postulated that expression of the EGFP-M2 fusion proteins in these cells might result in the localisation of the EGFP-M2 with the native M2 protein,

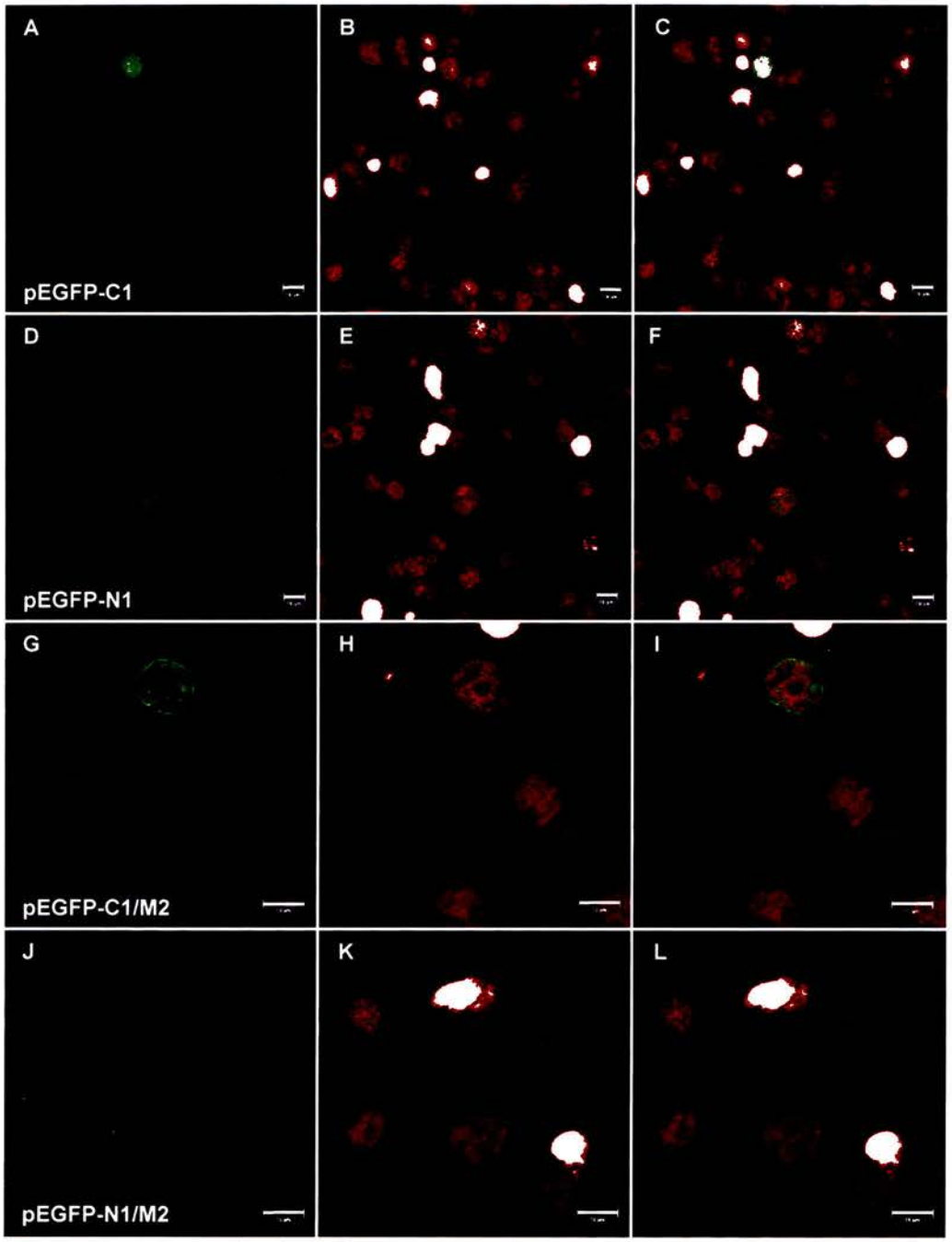

Figure 4.5.1.3 Transfection of EGFP expression constructs in A20 cells. Cells were transfected with 20μg of plasmid DNA and harvested 24 hours after transfection. Panels A, D, G and J show EGFP localisation; panels B, E, H and K show DNA stained with propidium iodide; panels C, F, I and L show overlay images. Panels A, B and C show pEGFP-C1; panels D, E and F show pEGFP-N1; panels G, H and I show pEGFP-C1/M2; panels J, K and L show pEGFP-N1/M2. All images are single confocal slices, with scale bar representing 10μm.

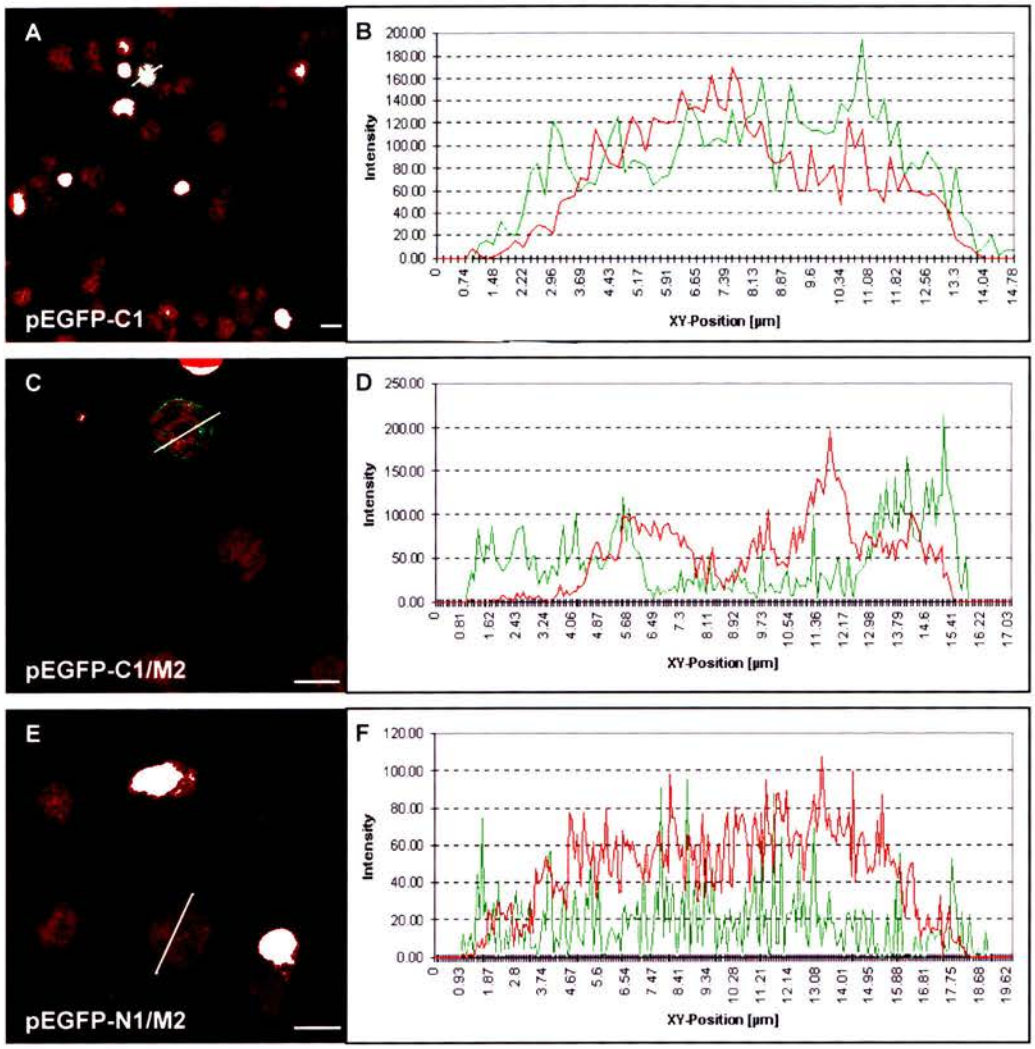

Figure 4.5.1.4 Analysis of confocal images of EGFP expression constructs transfected into A20 cells. The images in Figure 4.5.1.3 were analysed using Leica TCSNT confocal analysis software. Panels on the left show line of analysis (in white) superimposed on the overlay single slice image, and graph on the right shows the intensity of fluorescence of the image along the white line, plotted against XY position on the line. Panel A shows pEGFP-C1; panel B shows image analysis of pEGFP-C1; panel C shows pEGFP-C1/M2; panel D shows image analysis of pEGFP-C1/M2; panel E shows pEGFP-N1/M2; panel F shows image analysis of pEGFP-N1/M2. Scale bar represents 10µm.

leading to a more accurate indication of the cellular localisation of M2. S11 cells were transfected with 20μg of plasmid DNA (pEGFP-C1, pEGFP-N1, pEGFP-C1/M2 and pEGFP-N1/M2), harvested 24 hours after transfection and the cells analysed by confocal microscopy. In agreement with previous results, the S11 cells transfected with pEGFP-C1 and pEGFP-N1 showed typical localisation of EGFP throughout the nucleus and cytoplasm (Figure 4.5.1.5A). S11 cells transfected with pEGFP-C1/M2 showed localisation of EGFP-M2 at the periphery of the cell, as well as EGFP present centrally within the cell (Figure 4.5.1.5B). However, S11 cells were very poorly transfected with plasmid DNA as evidenced by the low numbers of cells fluorescing after transfection with pEGFP-C1 (despite a range of electroporation parameters being used) and thus were not used further in the expression studies.

All the cells had been harvested 24 hours after transfection, and there was a concern that harvesting cells at this stage after electroporation did not give the cells enough time to recover from the procedure. It was also hypothesised that the localisation of the EGFP-M2 might alter at later timepoints after transfection, due to the cellular transportation of EGFP-M2 from the diffuse staining seen in the centre of the cell to the periphery. A20 cells were transfected with 20μg of plasmid DNA (pEGFP-C1 and pEGFP-C1/M2) and harvested 48 hours after transfection. The cell nuclei were counterstained with propidium iodide, and the cells analysed by confocal microscopy. Figure 4.5.1.6 shows that A20 cells transfected with pEGFP-C1/M2 showed strong localisation of EGFP-M2 at the periphery of the cell, with diffuse EGFP-M2 also present throughout the cell (panels A-E). This was very similar to previous results, and due to the rapid growth of the A20 cells (even in reduced FCS supplementation) it was therefore decided to continue harvesting at 24 hours after transfection. There did not appear to be any substantial difference in EGFP-M2 localisation at later timepoints after transfection compared to 24 hours after transfection.

It was decided to determine the exact localisation of the EGFP-M2 fusion proteins observed at the periphery of the cell. A20 cells were transfected with 20μg of plasmid DNA (pEGFP-C1, pEGFP-N1, pEGFP-C1/M2 and pEGFP-

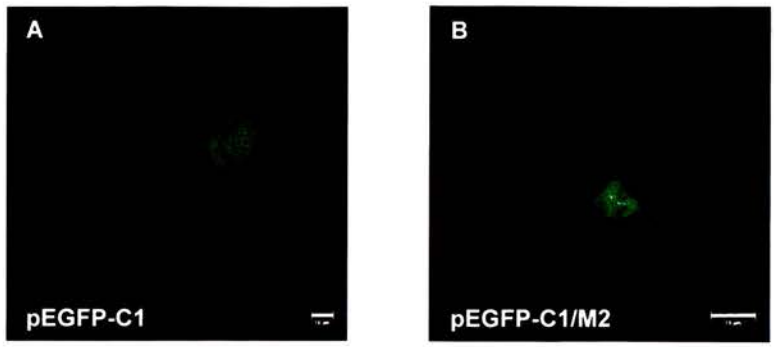

Figure 4.5.1.5 Transfection of EGFP expression constructs in S11 cells. Cells were transfected with 20μg of plasmid DNA and harvested 24 hours after transfection. Panels A shows pEGFP-C1; panels B shows pEGFP-C1/M2. Both images are single confocal slices, with scale bar representing 10μm.

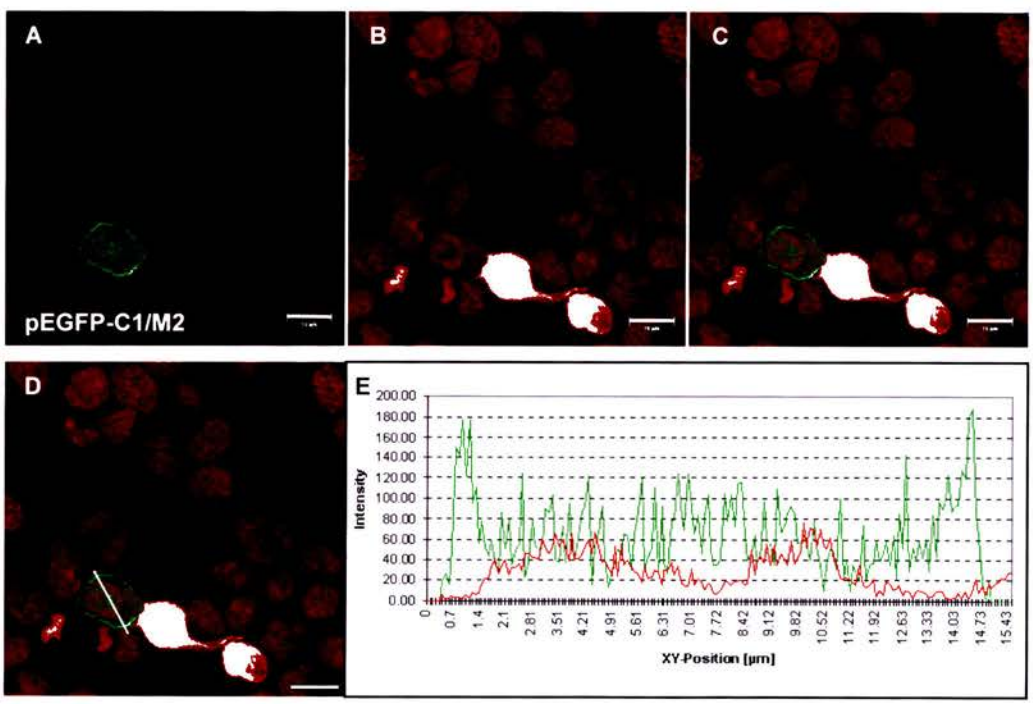

Figure 4.5.1.6 Transfection of pEGFP-C1/M2 expression construct in A20 cells. Cells were transfected with 20μg of plasmid DNA and harvested 48 hours after transfection. Panel A shows EGFP localisation; panel B shows DNA stained with propidium iodide; panel C shows overlay image. The image in panel C was analysed using Leica TCSNT confocal analysis software. Panel D shows line of analysis (in white) superimposed on the overlay single slice image, and the graph in panel E shows the intensity of fluorescence of the image along the white line, plotted against XY position on the line. All images are single confocal slices. Scale bar represents 10μm.

N1/M2) and harvested 24 hours after transfection. The cells were stained for the B-lymphocyte surface marker CD19 (Janeway *et al.*, 1999) using rat anti-mouse CD19 antibody, followed by anti-rat IgG TRITC conjugate (see 2.7.4). All solutions included 0.1% w/v azide and were kept at 4°C to prevent capping and internalisation of the cell surface markers. Control cells incubated with rat IgG or no primary antibody followed by anti-rat IgG TRITC conjugate showed no TRITC staining (data not shown). The cells were then attached by centrifugation onto glass slides, fixed and analysed by confocal microscopy. Cells transfected with the control vector pEGFP-C1 showed typical localisation of EGFP throughout the cell, with no specific cell surface EGFP localisation (Figure 4.5.1.7A-C, Figure 4.5.1.8A and B). However, cells transfected with pEGFP-C1/M2 showed co-localisation of the cell surface marker CD19 (red fluorescence) with M2-EGFP (Figure 4.5.1.7D-I). This was demonstrated by the visualisation of a yellow area of co-localisation in the overlay confocal images (Panels F and I), and quantitated by analysis of the images using Leica TCSNT confocal analysis software. Analysis of Figure 4.5.1.7I showed a sharp peak of co-localisation at the periphery of the cell between the CD19 (red line) and EGFP-M2 (green line), as well as diffuse low-level EGFP-M2 throughout the cell (Figure 4.5.1.8C and D). However, cells transfected with pEGFP-N1/M2 did not show consistent co-localisation between CD19 and M2-EGFP (Figure 4.5.1.7J-L), and this was demonstrated by analysis of the image (Figure 4.5.1.8E-F). This result with the pEGFP-N1/M2 plasmid may have been influenced by the amount of native EGFP produced by this expression construct (Figure 4.4.2.2). These results demonstrated co-localisation of the cell surface marker CD19 and the EGFP-M2 fusion protein in A20 cells.

To confirm this finding, A20 cells were transfected with 20μg of plasmid DNA (pEGFP-C1, pEGFP-N1, pEGFP-C1/M2 and pEGFP-N1/M2) and the cells were stained for the cell surface marker MHC Class II, which is present on activated B-lymphocytes (Janeway *et al.*, 1999). The cells were harvested 24 hours after transfection, and stained using rat monoclonal SW73.2 anti-MHC Class II antibody, followed by anti-rat IgG TRITC conjugate (see 2.7.4).

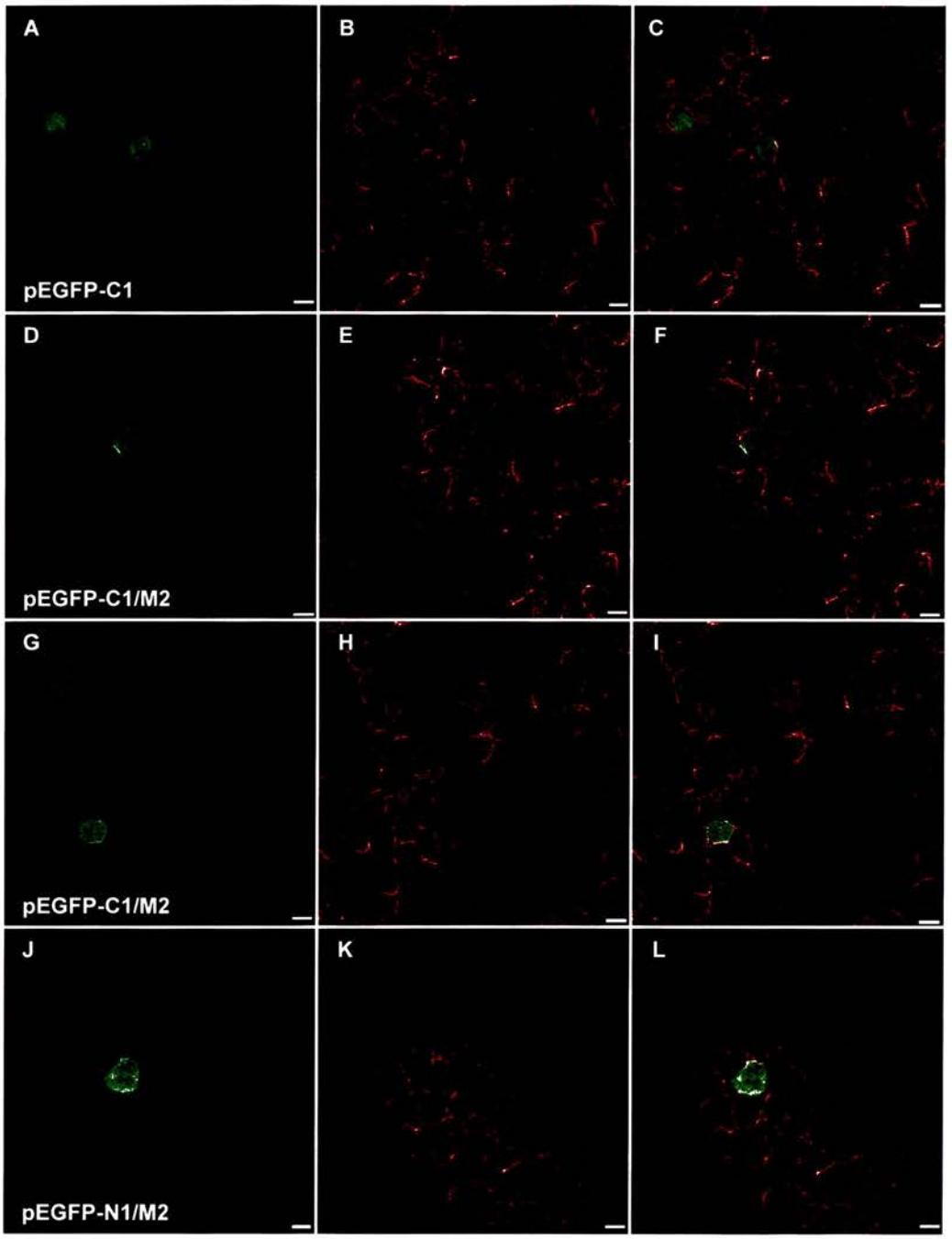

Figure 4.5.1.7 Co-localisation of CD19 and EGFP expression constructs in A20 cells. Cells were transfected with 20μg of plasmid DNA, harvested 24 hours after transfection and stained with rat anti-mouse CD19 antibody, followed by anti-rat IgG TRITC conjugate. Panels A, D, G and J show EGFP localisation; panels B, E, H and K show CD19 localisation; panels C, F, I and L show overlay images. Panels A, B and C show pEGFP-C1; panels D-I show pEGFP-C1/M2; panels J, K and L show pEGFP-N1/M2. All images are single confocal slices, with scale bar representing 10μm.

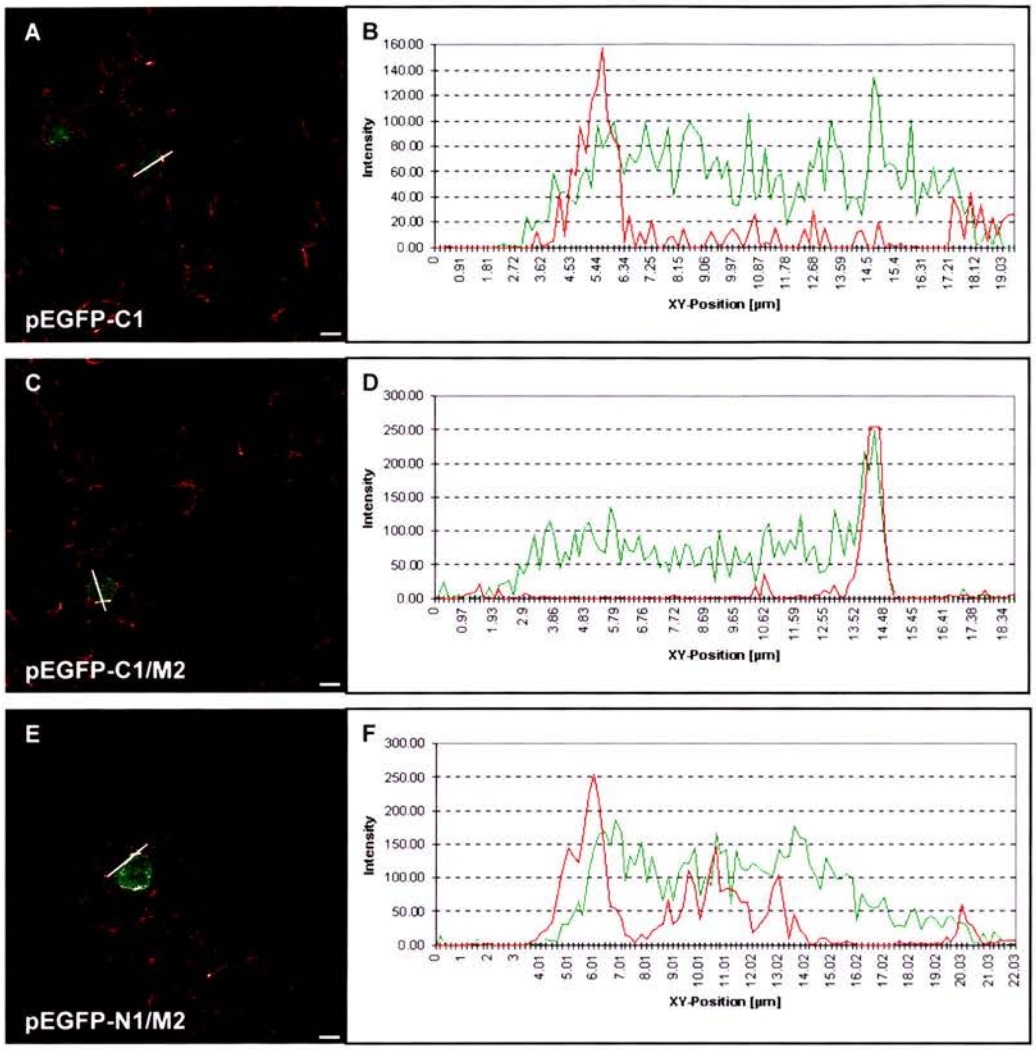

Figure 4.5.1.8 Analysis of confocal images of EGFP expression constructs transfected into A20 cells, and stained with anti-CD19 antibody. The images in Figure 4.5.1.7 were analysed using Leica TCSNT confocal analysis software. Panels on the left show line of analysis (in white) superimposed on the overlay single slice image, and graph on the right shows the intensity of fluorescence of the image along the white line, plotted against XY position on the line. Panel A shows pEGFP-C1; panel B shows image analysis of pEGFP-C1; panel C shows pEGFP-C1/M2; panel D shows image analysis of pEGFP-C1/M2; panel E shows pEGFP-N1/M2; panel F shows image analysis of pEGFP-N1/M2. Scale bar represents 10µm.

Although initially raised against sheep MHC Class II, the rat monoclonal SW73.2 anti-MHC Class II antibody shows cross-reactivity against the BALB/c mouse MHC Class II molecule (Hopkins *et al.*, 1986). All solutions included 0.1% w/v azide and were kept at 4°C to prevent capping and internalisation of the cell surface markers. Control cells incubated with rat IgG or no primary antibody followed by anti-rat IgG TRITC conjugate showed no TRITC staining (data not shown). In agreement with previous results, cells transfected with pEGFP-N1 showed localisation of EGFP throughout the cell, with no specific localisation with the cell surface (Figure 4.5.1.9A-C, Figure 4.5.1.10A and B). However, cells transfected with pEGFP-C1/M2 showed co-localisation of EGFP-M2 with MHC Class II (Figure 4.5.1.9D-I), as demonstrated by the yellow area at the cell margin in the overlay image (Panels F and I) and the overlapping peaks of red and green fluorescence upon analysis of the image (Figure 4.5.1.10C and D). Similar results were obtained in cells transfected with pEGFP-N1/M2, demonstrating co-localisation of M2-EGFP and MHC Class II cell surface marker (Figure 4.5.1.9J-L, Figure 4.5.1.10E and F).

The results of the co-localisation of the EGFP-M2 fusion protein and cell surface markers CD19 and MHC Class II in A20 cells demonstrated that EGFP-M2 was specifically localised to the plasma membrane, as well as diffuse localisation throughout the cell. However, the resolution of the confocal microscope is 180nm but the thickness of the plasma membrane is 6-10nm. It is therefore not possible to demonstrate if the co-localisation of EGFP-M2 with cell surface markers is due to the position of EGFP-M2 at the inner or outer surface of the plasma membrane. These results have therefore shown localisation of the EGFP-M2 fusion protein to the plasma membrane.

It was also decided to investigate the pathways by which EGFP-M2 might be trafficked to the plasma membrane, and the localisation of the EGFP-M2 distributed diffusely in the central region of the cell. The endoplasmic reticulum (ER) is the site of lipid biosynthesis in the cell, and the location of protein production by ribosomes that bind to the ER. The process of N-linked glycosylation of proteins also commences in the ER. Concanavalin A is a plant lectin, which binds the oligosaccharide residues α-mannopyranosyl and α-

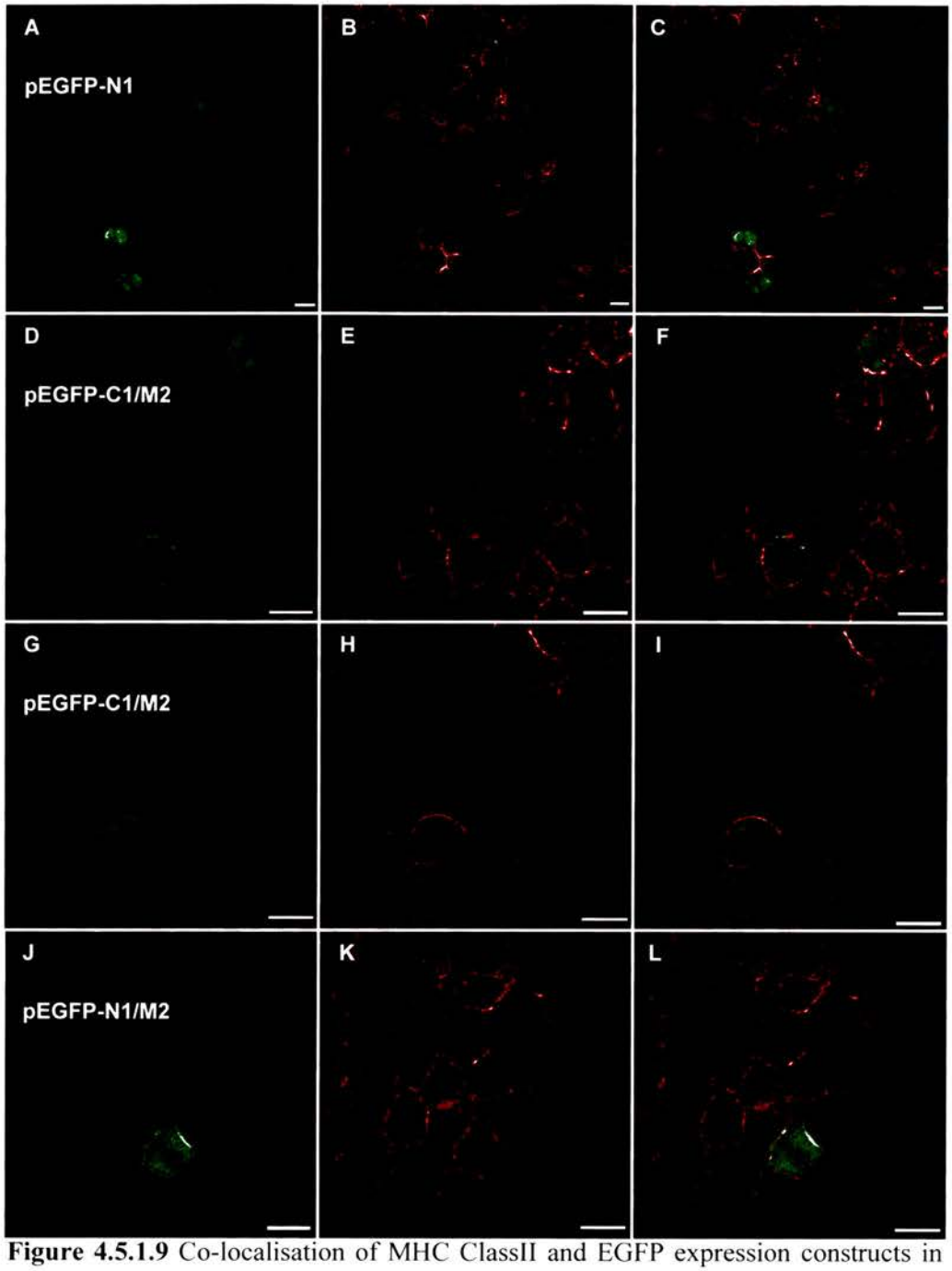

Figure 4.5.1.9 Co-localisation of MHC ClassII and EGFP expression constructs in A20 cells. Cells were transfected with 20μg of plasmid DNA, harvested 24 hours after transfection and stained with rat anti-MHC ClassII antibody, followed by anti-rat IgG TRITC conjugate. Panels A, D, G and J show EGFP localisation; panels B, E, H and K show MHC ClassII localisation; panels C, F, I and L show overlay images. Panels A, B and C show pEGFP-N1; panels D-I show pEGFP-C1/M2; panels J, K and L show pEGFP-N1/M2. All images are single confocal slices, with scale bar representing 10μm.

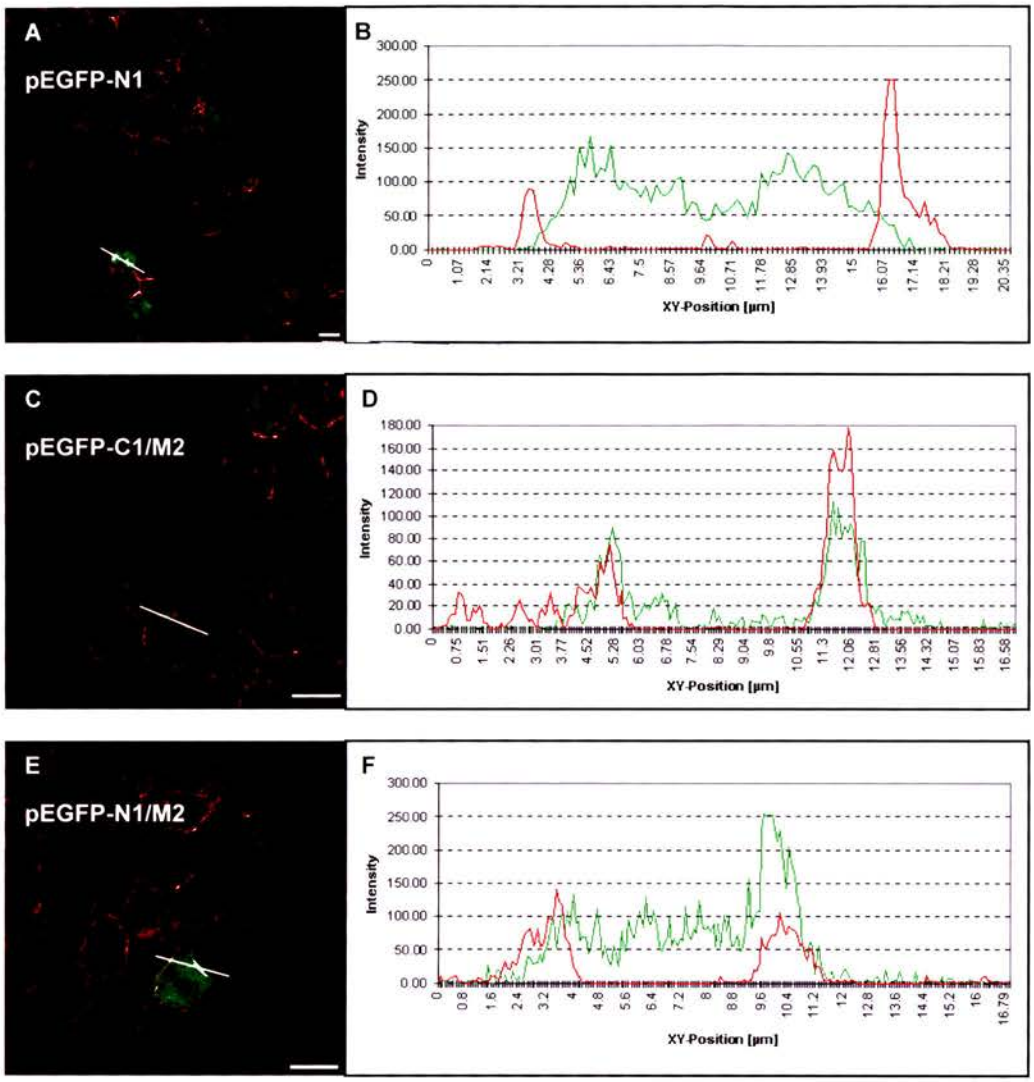

Figure 4.5.1.10 Analysis of confocal images of EGFP expression constructs transfected into A20 cells, and stained with anti-MHC ClassII antibody. The images in Figure 4.5.1.9 were analysed using Leica TCSNT confocal analysis software. Panels on the left show line of analysis (in white) superimposed on the overlay single slice image, and graph on the right shows the intensity of fluorescence of the image along the white line, plotted against XY position on the line. Panel A shows pEGFP-N1; panel B shows image analysis of pEGFP-N1; panel C shows pEGFP-C1/M2; panel D shows image analysis of pEGFP-C1/M2; panel E shows pEGFP-N1/M2; panel F shows image analysis of pEGFP-N1/M2. Scale bar represents 10µm.

glucopyranosyl present in the ER and has therefore been used previously to specifically stain the ER in a wide range of cell types (Virtanen *et al.*, 1980; Bergmann & Fusco, 1990; Cottin *et al.*, 1999). A20 cells were transfected with 20μg of plasmid DNA (pEGFP-C1, pEGFP-N1, pEGFP-C1/M2 and pEGFP-N1/M2) and harvested 24 hours after transfection. The cells were incubated for 5 minutes with 50μg/ml concanavalin A TRITC conjugate, then washed and fixed before analysis by confocal microscopy (see 2.7.5). Cells stained with concanavalin A TRITC conjugate exhibited two types of cellular staining; staining of the ER (shown in Figure 4.5.1.11B, E and H) or staining at the periphery of the cell (Figure 4.5.1.11B and E). This staining at the edge of the cell by concanavalin A was subsequently shown to be at the plasma membrane (Figure 4.5.1.13 and 4.5.1.14). There was no difference in the pattern of staining with concanavalin A exhibited between live cells or fixed cells (data not shown). Cells transfected with the control plasmid pEGFP-C1 showed typical localisation of EGFP throughout the cell, with no specific localisation with concanavalin A either at the periphery or ER (Figure 4.5.1.11A-C, Figure 4.5.1.12A and B). Cells transfected with pEGFP-C1/M2 showed no co-localisation of EGFP-M2 with concanavalin A at the ER, but did show co-localisation of EGFP-M2 with concanavalin A at the plasma membrane (Figure 4.5.1.11D-F). This is demonstrated by the analysis of the images using Leica TCSNT confocal analysis software in Figure 4.5.1.12C and D; the red (concanavalin A) and green (EGFP-M2) peaks on the graph show only slight co-localisation on the left edge of the graph at the ER (XY position 2.5-7μm) but strong co-localisation on the right edge of the graph at the plasma membrane (XY position 13-15μm). Cells transfected with pEGFP-N1/M2 showed a similar result, with no co-localisation observed between M2-EGFP and concanavalin A staining of the ER in A20 cells (Figure 4.5.1.11G-I, Figure 4.5.1.12E and F). Cells transfected with pEGFP-C1/M2 and pEGFP-N1/M2, stained with concanavalin A-TRITC and the DNA stained with TO-PRO-3 showed no co-localisation between either DNA and concanavalin A TRITC or DNA and EGFP-M2 (data not shown). This result showed that there was no co-localisation of EGFP-M2 and concanavalin A when

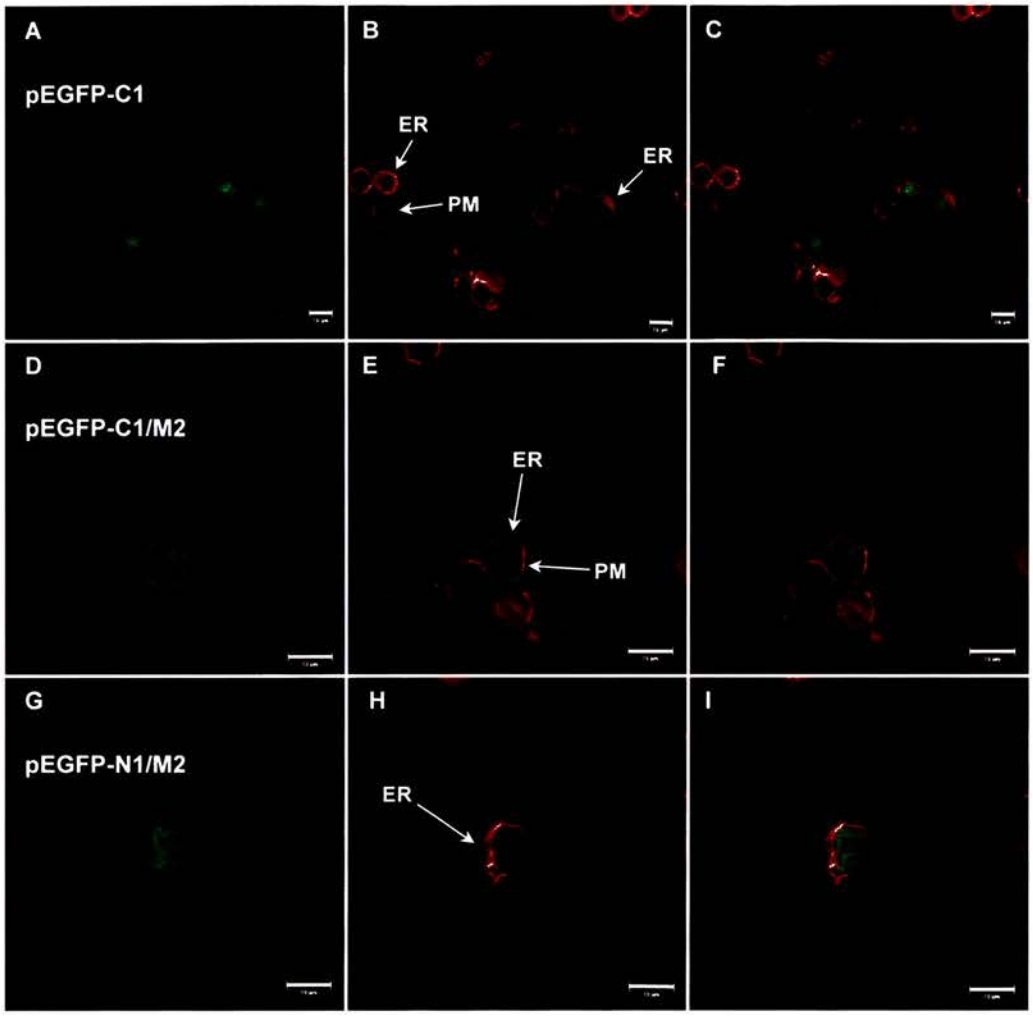

Figure 4.5.1.11 Co-localisation of the endoplasmic reticulum marker Concanavalin A and EGFP expression constructs in A20 cells. Cells were transfected with 20μg of plasmid DNA, harvested 24 hours after transfection and stained with 50μg/ml Concanavalin A TRITC conjugate. Panels A, D and G show EGFP localisation; panels B, E and H show Concanavalin A TRITC localisation; panels C, F and I show overlay images. Panels A, B and C show pEGFP-C1; panels D, E and F show pEGFP-C1/M2; panels G, H and I show pEGFP-N1/M2. Cells stained with Concanavalin A exhibited staining of the endoplasmic reticulum (**ER**) or plasma membrane (**PM**). All images are single confocal slices, with scale bar representing 10μm.

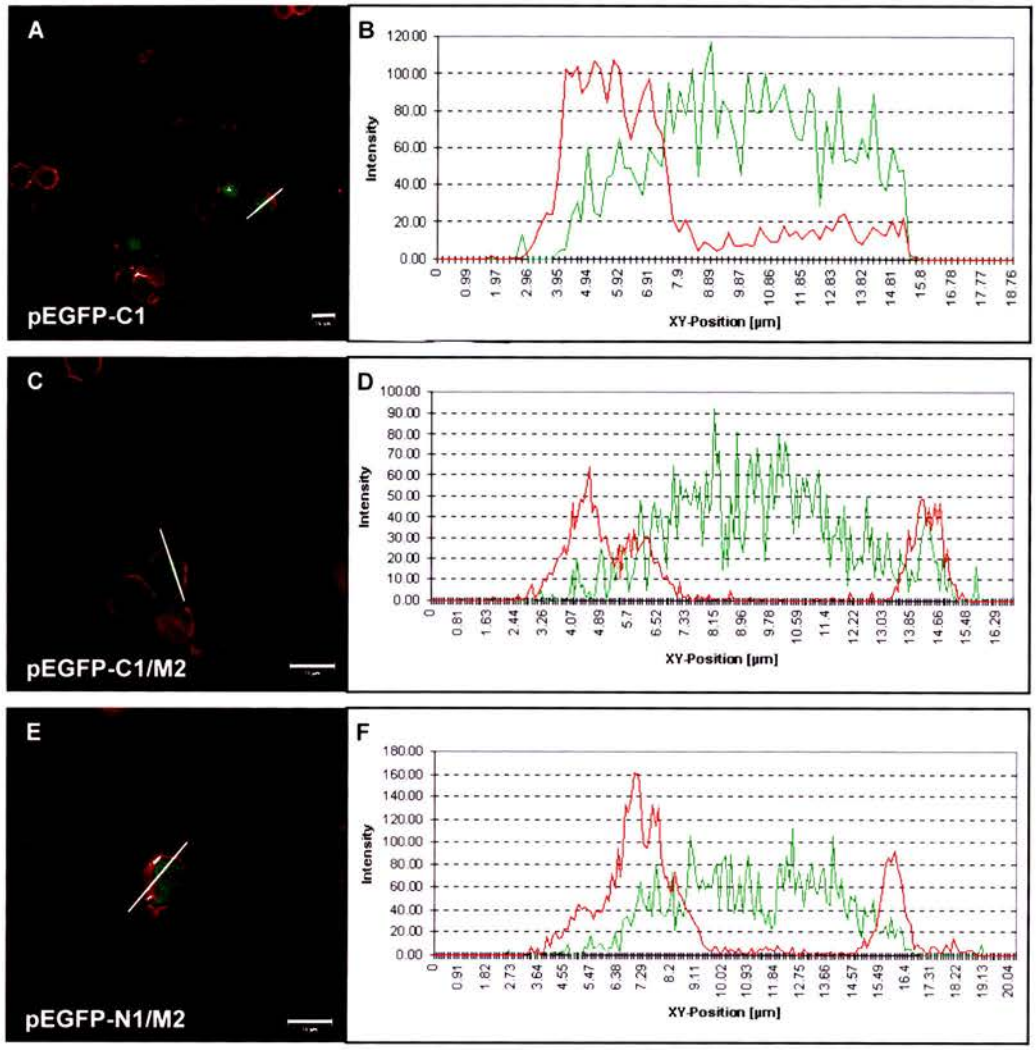

Figure 4.5.1.12 Analysis of confocal images of EGFP expression constructs transfected into A20 cells, and stained with concanavalin A TRITC conjugate. The images in Figure 4.5.1.11 were analysed using Leica TCSNT confocal analysis software. Panels on the left show line of analysis (in white) superimposed on the overlay single slice image, and graph on the right shows the intensity of fluorescence of the image along the white line, plotted against XY position on the line. Panel A shows pEGFP-C1; panel B shows image analysis of pEGFP-C1; panel C shows pEGFP-C1/M2; panel D shows image analysis of pEGFP-C1/M2; panel E shows pEGFP-N1/M2; panel F shows image analysis of pEGFP-N1/M2. Scale bar represents 10µm.

the concanavalin A stained the ER, but there was localisation of EGFP-M2 with concanavalin A at the edge of the cell.

Two distinct patterns of staining were observed with concanavalin A staining in A20 cells, with the expected staining of the ER and also staining at the periphery of the cell (Figure 4.5.1.11B, E and H). This staining at the periphery of the cell co-localised with M2-EGFP, and was assumed to be staining of the cell surface by concanavalin A. Concanavalin A has been shown to interact with immunoglobulin glycopeptides (Kornfeld & Ferris, 1975) and stimulate murine spleen lymphocytes (Ruscetti & Chervenick, 1975), properties that suggest that concanavalin A can bind to the cell surface of lymphocytes. Fluorescent concanavalin A conjugates have also been used to stain the cell surface in HeLa and 293 cells (Tarasova *et al.*, 1998; Kuwasako *et al.*, 2000). To show that this staining at the cell margin was staining of the plasma membrane, A20 cells were stained with rat anti-MHC Class II, followed by anti-rat Ig FITC and also concanavalin A TRITC as previously described. Control cells incubated with rat IgG or no primary antibody followed by anti-rat IgG FITC conjugate showed no FITC staining (data not shown). Figure 4.5.1.13 shows that MHC Class II molecules stained in green (Panels A and D) co-localise with the concanavalin A stained in red (Panels B and E). This co-localisation can be visualised as yellow staining on the overlay image (Panels C and F), and also a sharp peak of co-localisation between the green (MHC Class II) and red (concanavalin A) fluorescent images at the cell margin in the graphical analysis of the image (Figure 4.5.1.14A and B). Note that the analysis also shows concanavalin A staining of the ER, visualised as a peak of red fluorescence only (XY position 3-6μm). This result shows that the two patterns of concanavalin A staining visualised in A20 cells are the ER and the plasma membrane. Co-localisation was demonstrated between EGFP-M2 and the plasma membrane stained by concanavalin A, but not between EGFP-M2 and the ER stained by concanavalin A. There is therefore no evidence of localisation of EGFP-M2 and the ER.

The Golgi apparatus is the site of O-linked glycosylation of proteins, and modification of N-linked glycosylated proteins. It is also the major sorting centre of the cell, distributing proteins to lysosomes, secretory granules or the plasma

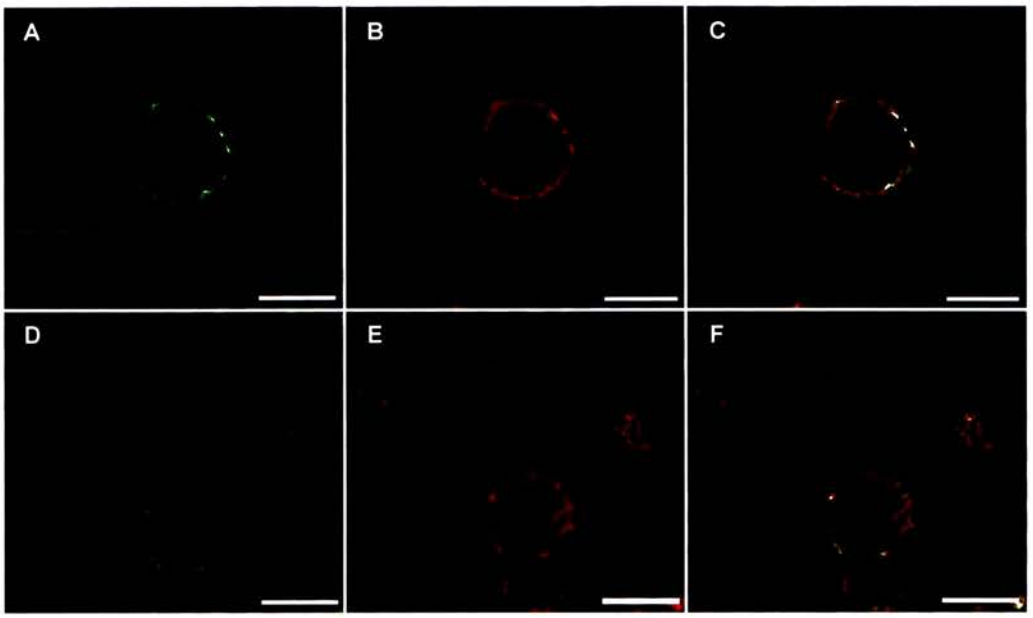

Figure 4.5.1.13 Co-localisation of Concanavalin A and MHC ClassII in A20 cells. A20 cells were stained with rat anti-MHC ClassII, followed by anti-rat Ig FITC. The cells were then stained with 50μg/ml Concanavalin A TRITC conjugate. Panels A and D show FITC localisation; panels B and E show Concanavalin A TRITC localisation; panels C and F show overlay images. All images are single confocal slices, with scale bar representing 10μm.

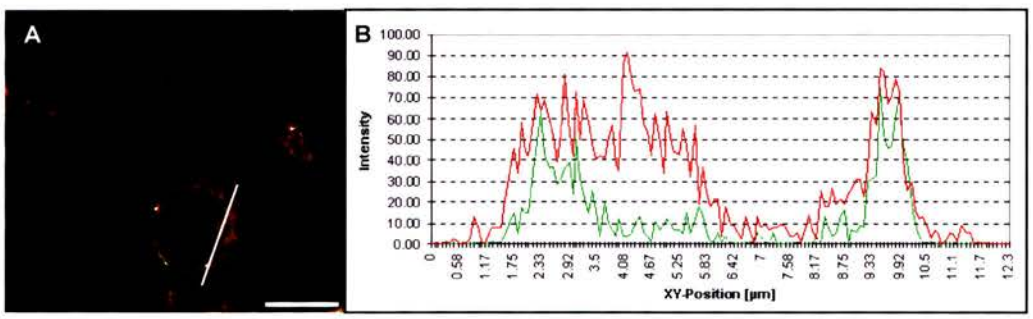

Figure 4.5.1.14 Analysis of confocal images of A20 cells stained with anti-MHC ClassII antibody and Concanavalin A TRITC. The images in Figure 4.5.1.13 were analysed using Leica TCSNT confocal analysis software. The panel on the left shows line of analysis (in white) superimposed on the overlay single slice image, and graph on the right shows the intensity of fluorescence of the image along the white line, plotted against XY position on the line. Panel A shows image in Figure 4.5.1.13 (panel F); panel B shows analysis of the image. Scale bar represents 10μm.

membrane. BODIPY TR ceramide is a fluorescent ceramide analogue, which has been shown to be a structural marker for the Golgi complex (Pagano *et al.*, 1991; McCabe & Berthiaume, 1999). A20 cells were transfected with 20μg of plasmid DNA (pEGFP-C1, pEGFP-N1, pEGFP-C1/M2 and pEGFP-N1/M2) and harvested 24 hours after transfection. The cells were incubated for 30 minutes with 50μM BODIPY TR ceramide complexed with BSA at 4°C, followed by incubation in fresh medium for 30 minutes at 37°C (see 2.7.7). The cells were washed and fixed before analysis by confocal microscopy. A20 cells showed strong red fluorescent staining of the Golgi complex, with a small amount of plasma membrane staining (Figure 4.5.1.15B, E and H). Cells transfected with pEGFP-C1 showed typical expression of EGFP throughout the cytoplasm and nucleus, with no specific co-localisation with the Golgi complex (Figure 4.5.1.15A-C, Figure 4.5.1.16A and B). Cells transfected with pEGFP-C1/M2 and pEGFP-N1/M2 showed typical EGFP-M2 localisation at the plasma membrane and diffusely throughout the cell. There was no evidence of any co-localisation of EGFP-M2 and the Golgi complex stained with BODIPY TR shown by lack of yellow fluorescence on the overlay images or simultaneous red and green peaks on the graph of analysis (Figure 4.5.1.15D-I, Figure 4.5.1.16C-F). There is therefore no evidence for localisation of EGFP-M2 to the Golgi complex.

Lysosomes contain hydrolytic enzymes in an acidic environment that degrade intracellular material. They are membrane-bound, and receive enzymes and membrane proteins from the Golgi via transport vesicles. LysoTracker Red DND-99 is a red fluorescent acidotropic probe used to label and track acidic organelles, such as lysosomes (Tarasova *et al.*, 1998; Bucci *et al.*, 2000). A20 cells were transfected with 20μg of plasmid DNA (pEGFP-C1, pEGFP-N1, pEGFP-C1/M2 and pEGFP-N1/M2) and harvested 24 hours after transfection. The cells were incubated for 2 hours at 37°C with 50nM LysoTracker Red DND-99 (see 2.7.6). The cells were washed and fixed before analysis by confocal microscopy. Examination of live cells prior to fixation revealed strong red fluorescent staining of lysosomes, as evidenced by the visualisation of red

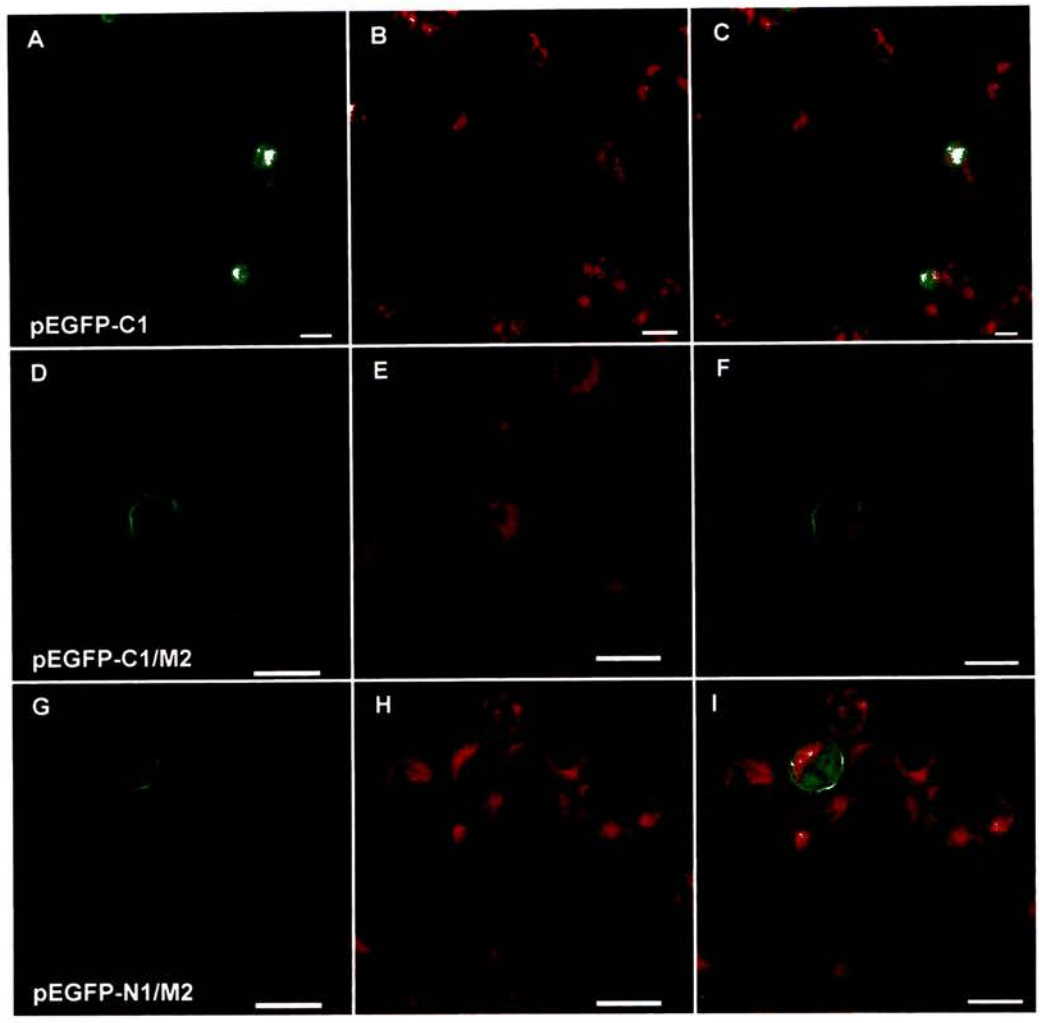

Figure 4.5.1.15 Co-localisation of the Golgi marker BODIPY TR and EGFP expression constructs in A20 cells. Cells were transfected with 20μg of plasmid DNA, harvested 24 hours after transfection and stained with 5μM BODIPY TR complexed with BSA. Panels A, D and G show EGFP localisation; panels B, E and H show BODIPY TR localisation; panels C, F and I show overlay images. Panels A, B and C show pEGFP-C1; panels D, E and F show pEGFP-C1/M2; panels G, H and I show pEGFP-N1/M2. All images are single confocal slices, with scale bar representing 10μm.

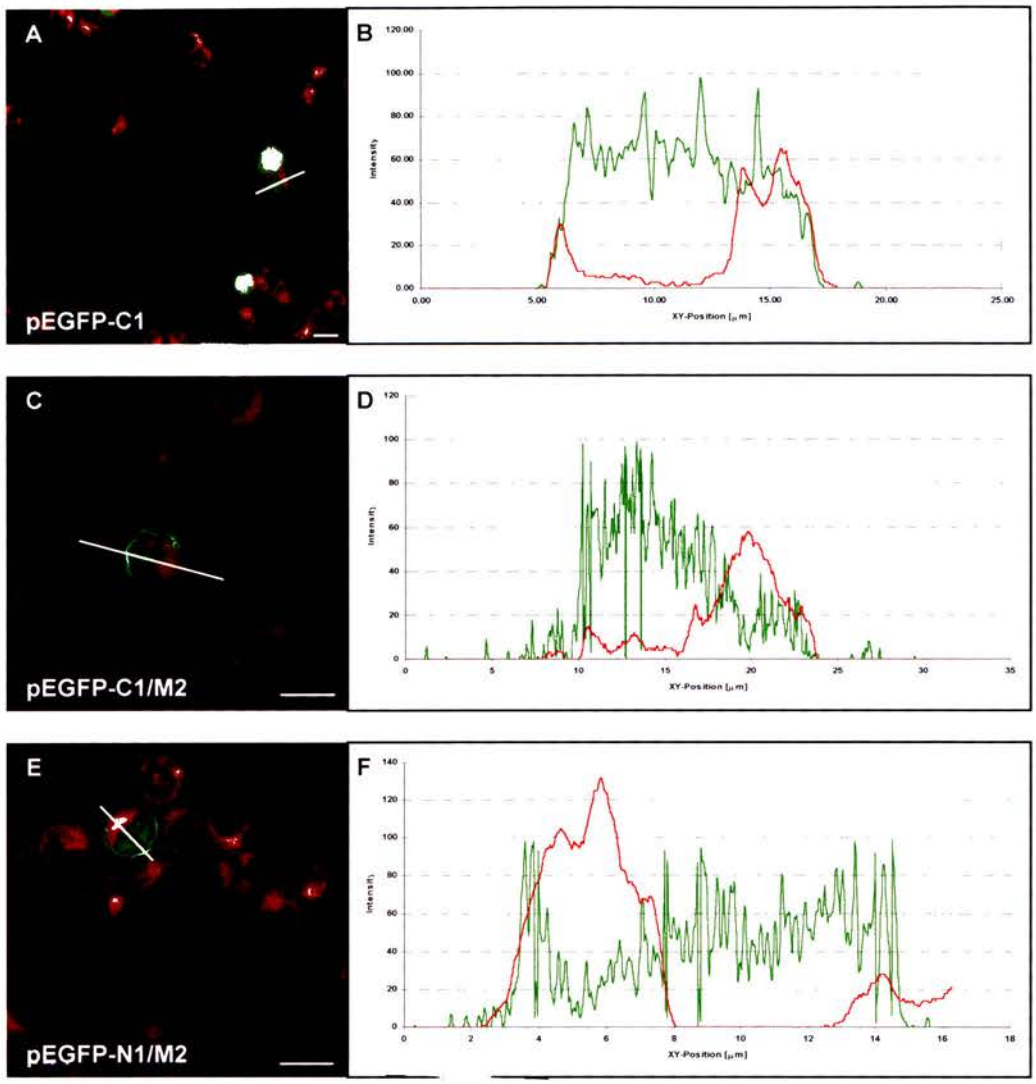

Figure 4.5.1.16 Analysis of confocal images of EGFP expression constructs transfected into A20 cells, and stained with BODIPY TR. The images in Figure 4.5.1.15 were analysed using Leica TCSNT confocal analysis software. Panels on the left show line of analysis (in white) superimposed on the overlay single slice image, and graph on the right shows the intensity of fluorescence of the image along the white line, plotted against XY position on the line. Panel A shows pEGFP-C1; panel B shows image analysis of pEGFP-C1; panel C shows pEGFP-C1/M2; panel D shows image analysis of pEGFP-C1/M2; panel E shows pEGFP-N1/M2; panel F shows image analysis of pEGFP-N1/M2. Scale bar represents 10μm.

spherical organelles in the cell cytoplasm. However, fixation led to a substantial decrease in the red fluorescence, even when the fixative was reduced to 2% w/v paraformaldehyde in PBS. Cells transfected with the control vector pEGFP-C1 showed typical expression of EGFP throughout the cytoplasm and nucleus, with no specific co-localisation with lysosomes (Figure 4.5.1.17A-C, Figure 4.5.1.18A and B). Cells transfected with pEGFP-C1/M2 and pEGFP-N1/M2 showed typical EGFP-M2 localisation at the plasma membrane and diffusely throughout the cell. There was no evidence of any co-localisation of EGFP-M2 and lysosomes stained with LysoTracker Red DND-99 shown by lack of yellow fluorescence on the overlay images or simultaneous red and green peaks on the graph of analysis (Figure 4.5.1.17D-I, Figure 4.5.1.18C-F). There is therefore no evidence for localisation of EGFP-M2 and lysosomes.

These experiments with the expression of M2 as a fusion protein with either the C or N terminus of EGFP showed that the EGFP-M2 fusion protein was expressed in 293, A20 and S11 cells, but that expression had a detrimental effect on 293 cells. There were no substantial differences in the localisation of M2 as a fusion protein with either the C or N terminus of EGFP, although expression of M2 as an N terminal EGFP fusion protein led to the production of free EGFP that localised diffusely throughout the cell. There did not appear to be any differences in the localisation of EGFP-M2 over longer periods of time. The EGFP-M2 protein was localised to the plasma membrane and diffusely throughout the cell. In 293 cells there was evidence of close association of EGFP-M2 with DNA as observed by yellow fluorescence in the overlay image, but artefacts produced in apoptotic 293 cells probably influenced this result. No specific association of M2 with DNA was observed in A20 cells. It was not localised to the ER, Golgi complex or lysosomes.

4.5.2. Expression of HA-tagged M2

The studies with the EGFP-M2 fusion proteins suggested that the M2 protein was localised to the plasma membrane, but concerns were expressed due to the large size of the EGFP tag (27kDa). This might affect the localisation and function of the M2-EGFP protein in cells and therefore might not be a true

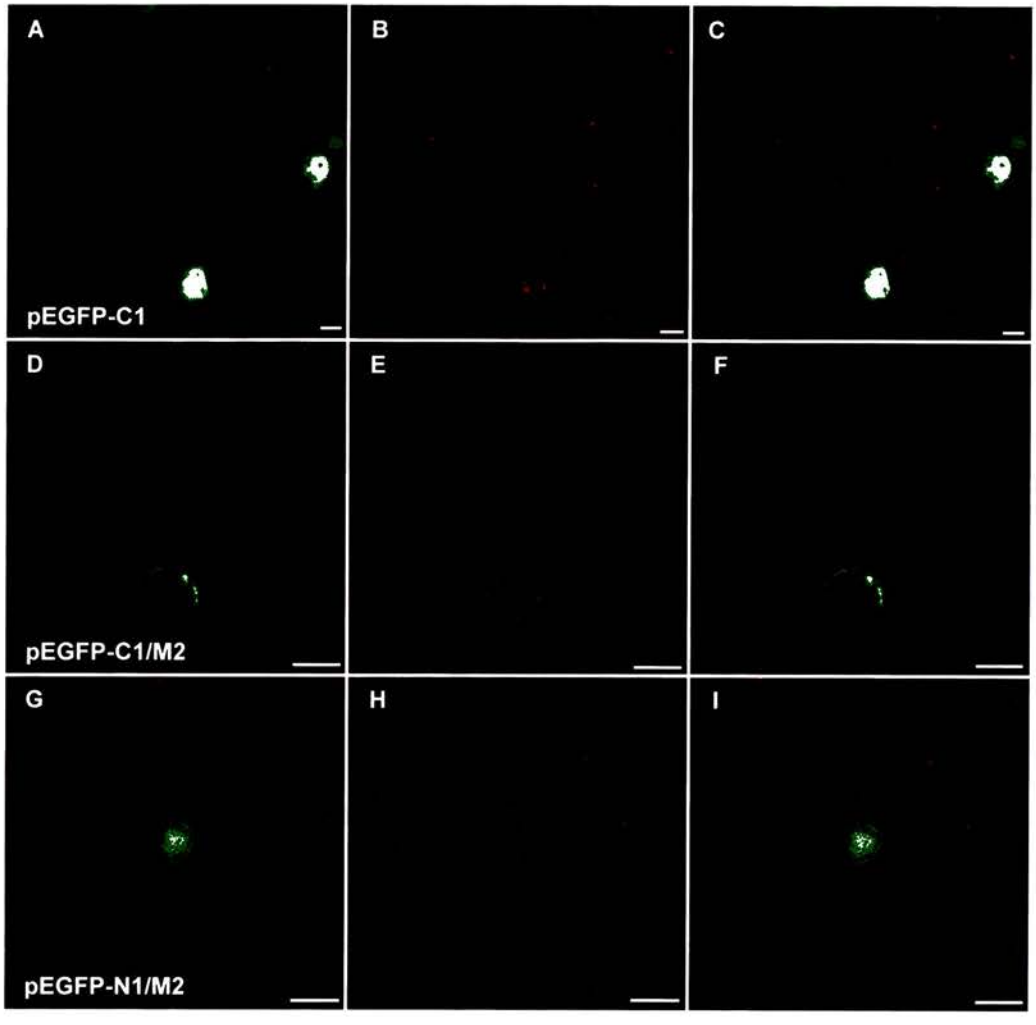

Figure 4.5.1.17 Co-localisation of the lysosome marker LysoTracker Red DND-99 and EGFP expression constructs in A20 cells. Cells were transfected with 20μg of plasmid DNA, harvested 24 hours after transfection and stained with 50nM LysoTracker Red DND-99. Panels A, D and G show EGFP localisation; panels B, E and H show LysoTracker Red DND-99 localisation; panels C, F and I show overlay images. Panels A, B and C show pEGFP-C1; panels D, E and F show pEGFP-C1/M2; panels G, H and I show pEGFP-N1/M2. All images are single confocal slices, with scale bar representing 10μm.

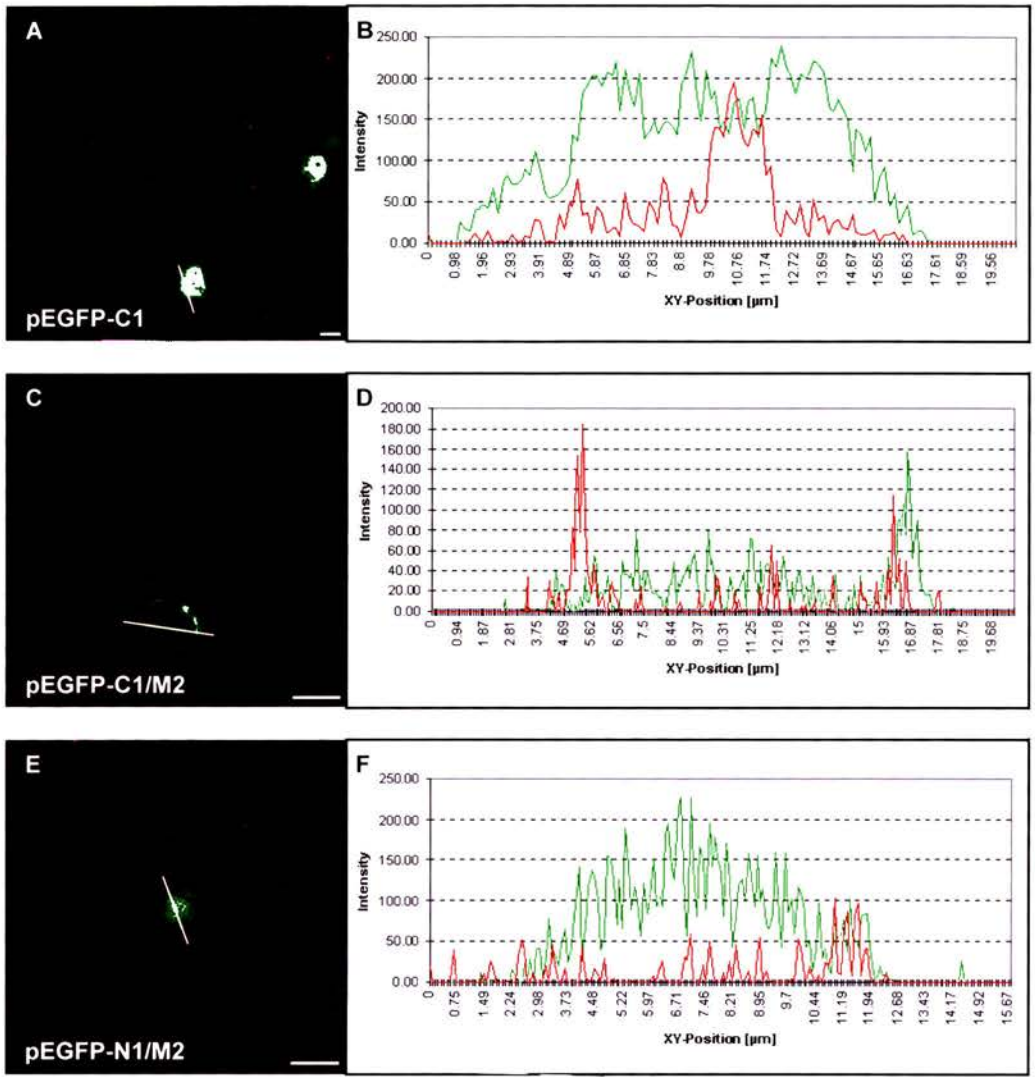

Figure 4.5.1.18 Analysis of confocal images of EGFP expression constructs transfected into A20 cells, and stained with LysoTracker Red DND-99. The images in Figure 4.5.1.17 were analysed using Leica TCSNT confocal analysis software. Panels on the left show line of analysis (in white) superimposed on the overlay single slice image, and graph on the right shows the intensity of fluorescence of the image along the white line, plotted against XY position on the line. Panel A shows pEGFP-C1; panel B shows image analysis of pEGFP-C1; panel C shows pEGFP-C1/M2; panel D shows image analysis of pEGFP-C1/M2; panel E shows pEGFP-N1/M2; panel F shows image analysis of pEGFP-N1/M2. Scale bar represents 10µm.

representation of the localisation of M2. It was therefore decided to use the HA-epitope tagged M2 to confirm the cellular localisation of M2 in mammalian cells. A20 cells were transfected with 20μg of plasmid DNA (pSG5/IRF7-HA, pSG5/M2-5'HA and pSG5/M2-3'HA) and harvested 24 hours after transfection. Negative control cells were transfected with no plasmid DNA (mock transfected). The cells were harvested 24 hours after transfection, fixed and permeabilised (see 2.7.1), and stained by indirect immunofluorescence using rat monoclonal anti-HA, followed by anti-rat Ig FITC conjugate (see 2.7.8). DNA was stained using propidium iodide, and the cells examined by confocal microscopy. A20 cells transfected with no plasmid DNA showed no evidence of FITC staining (Figure 4.5.2.1A-C). Control cells incubated with rat IgG or no primary antibody followed by anti-rat Ig FITC conjugate showed no FITC staining (data not shown). Cells transfected with pSG5/IRF7-HA showed characteristic cytoplasmic localisation of IRF7 (data not shown).

Cells transfected with pSG5/M2-5'HA express M2 with a triple HA-epitope tag at the N terminus of M2. As shown in Figure 4.5.2.1D-F, cells expressing M2-5'HA exhibited FITC staining predominantly at the periphery of the cell. This was confirmed by analysis of the confocal image (Figure 4.5.2.2A and B), which shows that peaks of FITC staining are present in the cell margins, with low levels of FITC present in the central region of the cell. Cells transfected with pSG5/M2-3'HA express M2 with a triple HA-epitope tag at the C terminus of M2. Figure 4.5.2.1G-I shows that cells expressing M2-3'HA showed an identical pattern of FITC staining to cells expressing M2-5'HA, and analysis of the confocal images confirmed this result (Figure 4.5.2.2C and D). These results show that in A20 cells expressing M2 with a triple HA-epitope tag, M2 is localised to the cell periphery with patchy low levels of M2 present in the central region of the cell. There was no difference in the localisation of M2 with a HA-epitope tag at the C or N terminus. Expression of M2 did not appear to have any deleterious effect on the cells, as evidenced by the normal nuclear morphology. The results of the indirect immunofluorescence are identical to the localisation studies using the EGFP-M2 fusion protein, and confirm the localisation of M2 at the cell margin.

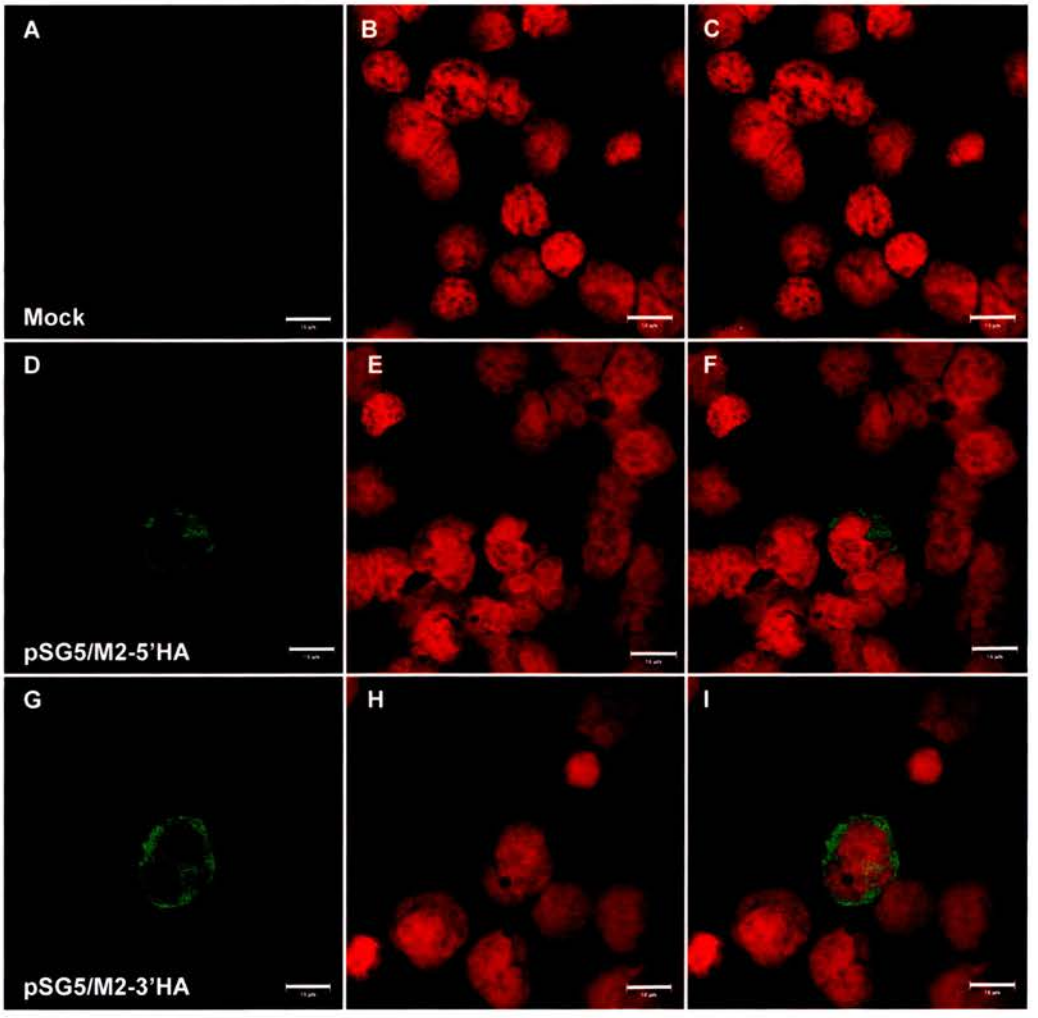

Figure 4.5.2.1 Indirect immunofluorescence of HA epitope-tagged expression constructs transfected into A20 cells. Cells were transfected with 20μg of plasmid DNA, harvested 24 hours after transfection and fixed with 4% paraformaldehyde in PBS. Cells were stained with rat anti-HA, followed by anti-rat Ig FITC conjugate. Panels A, D and G show FITC localisation; panels B, E and H show DNA stained with propidium iodide; panels C, F and I show overlay images. Panels A, B and C show mock transfected cells; panels D, E and F show pSG5/M2-5'HA; panels G, H and I show pSG5/M2-3'HA. All images are single confocal slices, with scale bar representing 10μm.

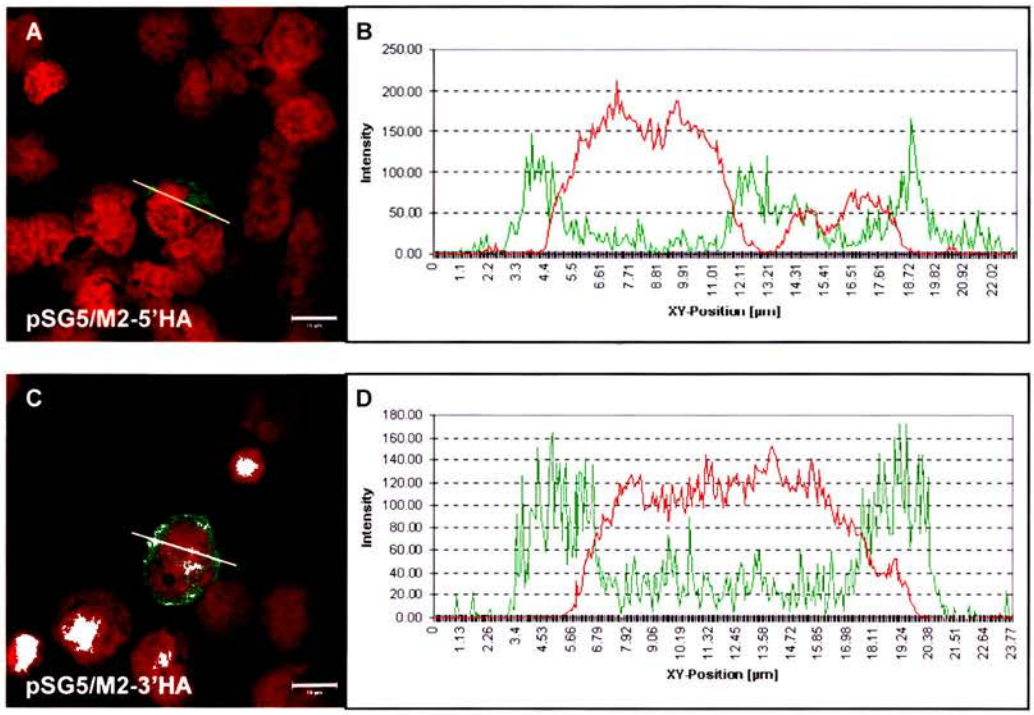

Figure 4.5.2.2 Analysis of confocal images of indirect immunofluorescence of HA epitope-tagged expression constructs transfected into A20 cells. The images in Figure 4.5.2.1 were analysed using Leica TCSNT confocal analysis software. Panels on the left show line of analysis (in white) superimposed on the overlay single slice image, and graph on the right shows the intensity of fluorescence of the image along the white line, plotted against XY position on the line. Panel A shows pSG5/M2-5'HA; panel B shows image analysis of pSG5/M2-5'HA; panel C shows pSG5/M2-3'HA; panel D shows image analysis of pSG5/M2-3'HA. Scale bar represents 10µm.

4.6. Post-translational modification of the M2 protein

4.6.1. N-linked glycosylation status of the M2 protein

N-linked glycosylation is a post-translational modification of proteins by the linkage of oligosaccharide residues to the amino acid asparagine. This modification has a wide variety of biological functions, including protein folding and the assistance of protein-protein interactions (Helenius & Aebi, 2001) and the targeting and recognition of cells (Rudd *et al.*, 2001). The M2 protein migrates at a higher relative molecular mass of 30kDa on SDS-PAGE analysis than the expected mass of 22.3kDa, and has one predicted N-linked glycosylation site at residue 58 (Figure 4.2.2). It was therefore decided to examine the M2 protein to see if this predicted N-linked glycosylation was occurring. A20 cells were transfected with 20μg of plasmid DNA (pSG5/M2-3'HA and pSG5/M2-5'HA). Negative control cells were transfected with no plasmid DNA (mock transfected). The cells were then placed immediately into medium containing 10μg/ml tunicamycin (tunicamycin positive) or untreated medium (tunicamycin negative; see 2.3.5). Tunicamycin is an antibiotic that inhibits the N-linked glycosylation of proteins by blocking the first step in the synthesis of the lipid-linked oligosaccharide precursor dolichol pyrophosphate N-acetylglucosamine (Elbein, 1987). The cells were harvested after 24 hours, and the cell lysates analysed on a 12.5% SDS-PAGE gel followed by immunoblot. The blot was incubated with rat anti-HA antibody, followed by biotinylated rabbit anti-rat Ig and then streptavidin-POD conjugate. Reactive proteins were visualised by ECL. Figure 4.6.1A shows that the M2 protein tagged with the HA epitope was expressed in A20 cells and visualised as a doublet with an apparent molecular weight of 30kDa, in agreement with previous results (see 4.4.2). This band was not visualised in the mock transfected A20 cells. There was no difference in the relative molecular mass of the M2 protein doublet band between A20 cells treated with tunicamycin or left untreated.

To ensure that the tunicamycin was effectively blocking N-linked glycosylation of proteins, the effect of tunicamycin on the glycosylation of MHV-

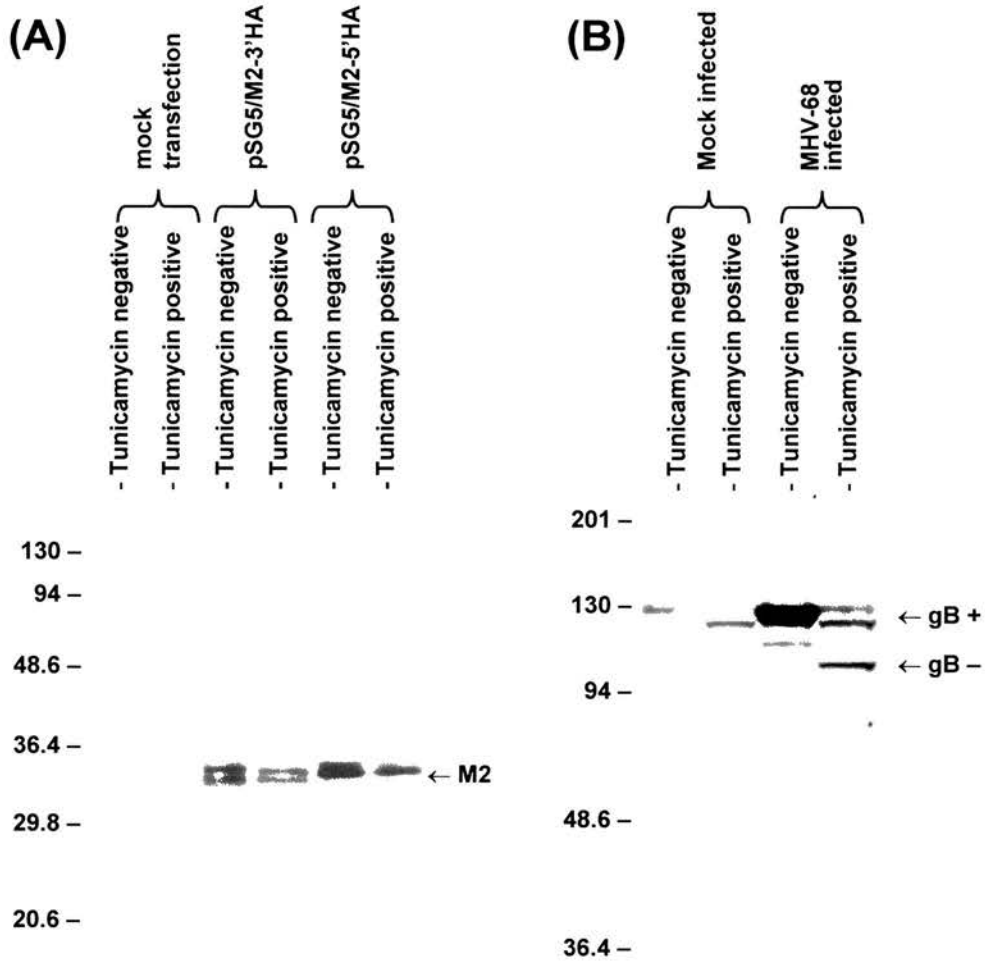

Figure 4.6.1 N-linked glycosylation status of the M2 protein. **(A)** A20 cells were transfected with 20μg of plasmid DNA, and immediately placed into medium containing 10 μg/ml tunicamycin (tunicamycin positive) or left untreated (tunicamycin negative). The cells were harvested 24 hours after transfection. Mock transfected A20 cells were used as a negative control. The cell lysates were analysed on a 12.5% SDS-PAGE gel, and transferred onto a membrane by Western blot. The blots were probed with rat monoclonal anti-HA, followed by biotinylated rabbit anti-rat Ig and then streptavidin-POD. The conjugates were visualised using ECL. **(B)** Positive control to ensure tunicamyicn efficacy. BHK-21 cells were mock infected (negative control) or infected with MHV-68 at an MOI of 5 for 1 hour. After infection, the inoculum was removed and replaced with medium containing 10 μg/ml tunicamycin (tunicamycin positive) or left untreated (tunicamycin negative). The cells were harvested after 24 hours, and the cell lysates were analysed on a 7.5% SDS-PAGE gel and transferred onto a membrane by Western blot. The blots were probed with rabbit polyclonal anti-gB, followed by donkey anti-rabbit Ig linked to peroxidase. The conjugates were visualised using ECL. Molecular weights are given in kilodaltons on the left side.

68 gB was examined. gB is a predominantly N-linked glycoprotein, with a mature relative molecular mass of 105kDa and a non-glycosylated core protein of approximately 92kDa (Stewart *et al.*, 1994). BHK-21 cells were infected with MHV-68 at an MOI of 5 for 1 hour. As a negative control, a duplicate mock infected experiment was performed with no viral inoculum. After infection, the viral inoculum was removed and replaced with medium containing 10μg/ml tunicamycin (tunicamycin positive) or untreated medium (tunicamycin negative). The cells were harvested after 24 hours, and the cell lysates analysed on a 7.5% SDS-PAGE gel followed by immunoblot. The blot was incubated with rabbit anti-gB antibody, followed by donkey anti-rabbit Ig linked to peroxidase. Reactive proteins were visualised by ECL. Figure 4.6.1B shows that MHV-68 infected cells produce gB with a relative molecular mass of approximately 110kDa. Treatment of MHV-68 infected cells with tunicamycin produced a novel band at approximately 95kDa, and completely abolished the gB band at 110kDa. Neither of these bands was present in the mock infected negative control samples. These results for gB are consistent with previous published work on gB (Stewart *et al.*, 1994), and indicate that tunicamycin is effective in blocking the N-glycosylation of viral proteins.

These results indicate that the M2 protein is not modified by N-linked glycosylation. The predicted site at position 58 is therefore not utilised, and the heavier than expected relative molecular mass is therefore not due to N-linked glycosylation of the M2 protein.

4.6.2. Phosphorylation status of the M2 protein

The M2 protein is predicted to contain 11 phosphorylated serine residues, 2 phosphorylated threonine residues and 2 phosphorylated tyrosine residues (Figure 4.2.2). These phosphorylated residues may be important for the function of M2, for example if the M2 protein has functional homology to the Gab2 proteins. The doublet observed for the HA epitope-tagged M2 protein on immunoblot analysis is characteristic of phosphorylated proteins. It was therefore decided to examine the phosphorylation status of M2.

A20 cells were transfected with 20μg of the HA epitope-tagged expression constructs pSG5/IRF7-HA, pSG5/Jκ-HA, pSG5/M2-5'HA and pSG5/M2-3'HA. Mock transfected cells were used as a negative control. The cells were harvested 24 hours after transfection, and the cell lysates were analysed on a 12.5% SDS-PAGE gel, and transferred onto a membrane by Western blot. The blot was incubated with mouse monoclonal anti-phosphotyrosine, anti-phosphothreonine or anti-phosphoserine antibody, followed by biotinylated rabbit anti-mouse Ig and then streptavidin-POD conjugate. The reactive proteins were visualised using ECL. The results of the immunoblot using anti-phosphotyrosine antibody are shown in Figure 4.6.2.1. No unique bands were observed at the expected relative molecular mass of M2 (approximately 30kDa) in the cells transfected with the HA epitope-tagged M2 expression vectors. No other unique bands were observed in the cells transfected with the HA epitope-tagged M2 expression vectors that might indicate the phosphorylation or activation of cellular proteins. However, high levels of background staining were observed in the immunoblot due to either non-specific binding or binding of antibody to a range of cellular phosphoproteins present in the crude cell lysates. This background was not reduced by altering the antibody concentrations, or by modifying the concentration and / or composition of the blocking agents (data not shown). Similar results were observed in immunoblots probed with anti-phosphothreonine and anti-phosphoserine (data not shown).

In order to try and reduce the levels of non-specific background staining and increase the amount and purity of the M2 protein present in the immunoblot analysis, the HA epitope-tagged proteins were immunoprecipitated. A20 cells were transfected with 20μg of the HA epitope-tagged expression constructs pSG5/IRF7-HA, pSG5/M2-5'HA and pSG5/M2-3'HA. Mock transfected cells were used as a negative control. The cells were harvested 24 hours after transfection, the cells lysed using RIPA buffer and the HA epitope-tagged proteins precipitated using either rat monoclonal anti-HA or rat IgG as a negative control (see 2.3.4). The proteins were precipitated using rabbit anti-rat Ig followed by protein A-sepharose beads, and after extensive washing of the beads with

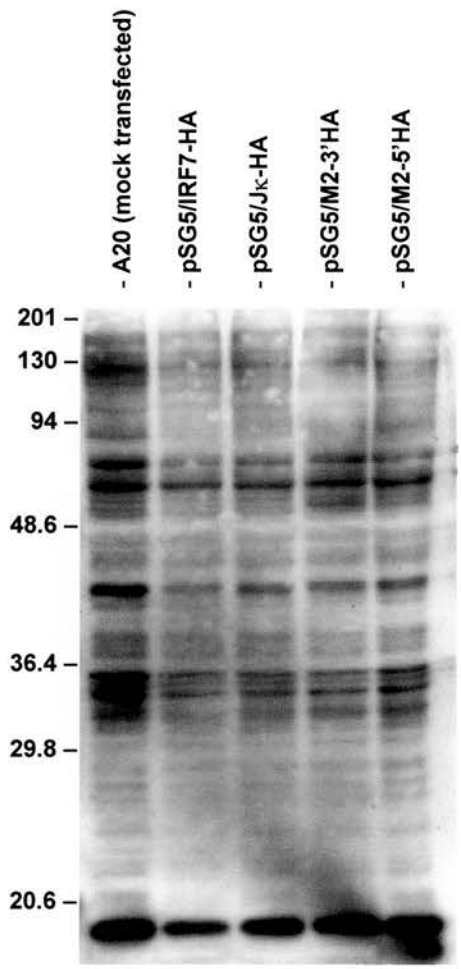

Figure 4.6.2.1 Immunoblot for the detection of phosphotyrosine residues. Cells were transfected with 20μg of plasmid DNA and harvested 24 hours after transfection. Mock transfected A20 cells were used as a negative control. The cell lysates were analysed on a 12.5% SDS-PAGE gel, and transferred onto a membrane by Western blot. The blots were probed with mouse monoclonal anti-phosphotyrosine, followed by biotinylated rabbit anti-mouse Ig and then streptavidin-POD. The conjugates were visualised using ECL. Molecular weights are given in kilodaltons on the left side.

RIPA buffer, the beads were resuspended in SDS-PAGE sample buffer. To check that HA epitope-tagged proteins were effectively immunoprecipitated, samples were analysed by immunoblot for the presence of HA epitope-tagged proteins. As shown in Figure 4.6.2.2, there was a high degree of background staining due to the cross-reactivity of the antibodies used in the immunoprecipitation (rat anti-HA followed by rabbit anti-rat Ig) and the antibodies used in the immunoblot analysis (rat anti-HA followed by biotinylated rabbit anti-rat Ig and then streptavidin-POD). The negative control samples also contained a high amount of background due to the rat IgG used as the negative control primary antibody in the immunoprecipitation. Immunoprecipitated HA epitope-tagged M2 (30kDa) was not visualised as it was obscured by the background levels caused by the immunoglobulin light chains at the same relative molecular mass (25-30kDa). However, a unique band was visualised for IRF-HA at the expected mass of 70kDa in the positive sample, which was not observed in the other samples. This result showed that the HA epitope-tagged IRF7 protein had been successfully immunoprecipitated, although this did not demonstrate that the M2-HA protein had been immunoprecipitated.

Samples of the immunoprecipitated proteins were analysed on a 12.5% SDS-PAGE gel, and transferred onto a membrane by Western blot. The blot was incubated with mouse monoclonal anti-phosphotyrosine, anti-phosphothreonine or anti-phosphoserine antibody, followed by biotinylated rabbit anti-mouse Ig and then streptavidin-POD conjugate. Further examination of the immunoblots for the presence of phosphotyrosine residues was performed using recombinant anti-phosphotyrosine directly conjugated to HRP. This recombinant conjugate contains only the high affinity binding site for phosphotyrosine residues, and the direct conjugation with HRP ensures low cross-reactivity with the antibodies used in the immunoprecipitation steps. The reactive proteins were visualised using ECL. Figure 4.6.2.3 shows that no unique bands were observed at the expected relative molecular mass of M2 (approximately 30kDa) in the samples that contained HA epitope-tagged M2 in immunoblots probed with recombinant anti-phosphotyrosine (Panel A) or anti-phosphothreonine (Panel B). An immunoblot probed with anti-phosphoserine gave similar results (data not shown). High non-

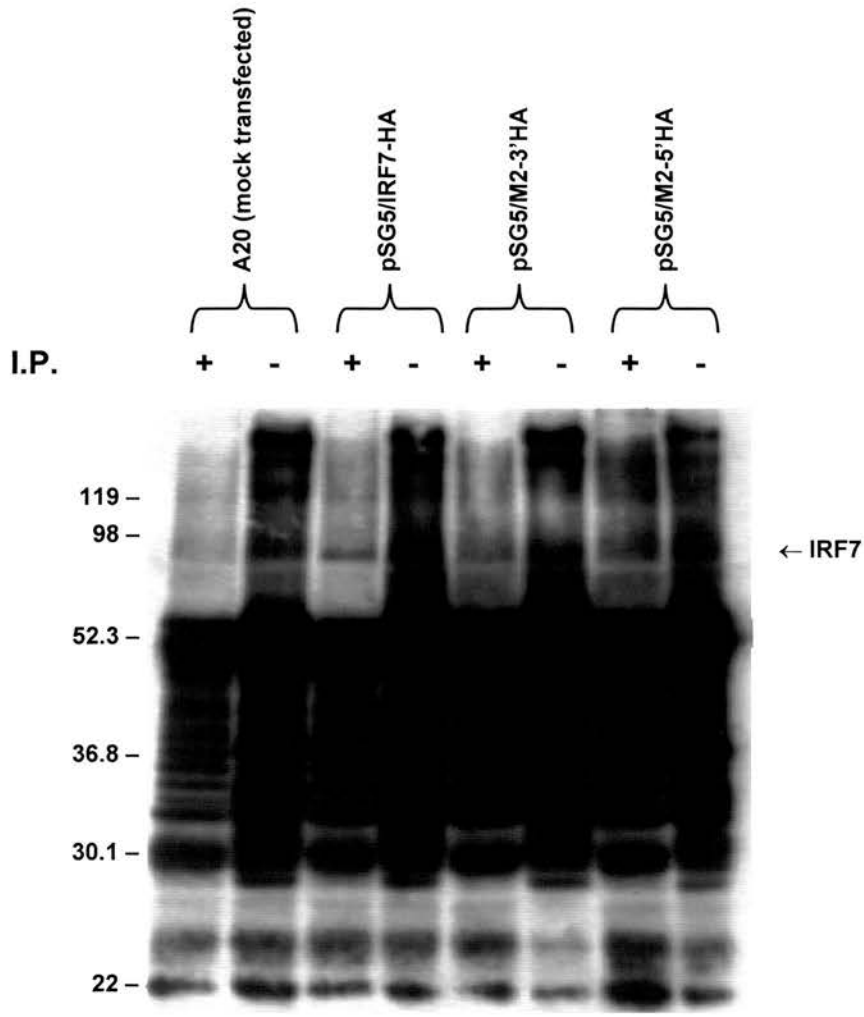

Figure 4.6.2.2 Immunoprecipitation of HA-epitope tagged proteins in A20 cells. Cells were transfected with 20μg of plasmid DNA and harvested 24 hours after transfection. Cells were lysed using RIPA buffer and pre-cleared. The HA-epitope tagged proteins were precipitated using rat anti-HA antibody (+) or rat IgG as negative control (-), followed by rabbit anti-rat Ig and then protein A-sepharose beads. The beads were extensively washed using RIPA buffer and then analysed on a 12.5% SDS-PAGE gel, and transferred onto a membrane by Western blot. The blots were probed with rat monoclonal anti-HA, followed by biotinylated rabbit anti-rat Ig and then streptavidin-POD. The conjugates were visualised using ECL. Molecular weights are given in kilodaltons on the left side.

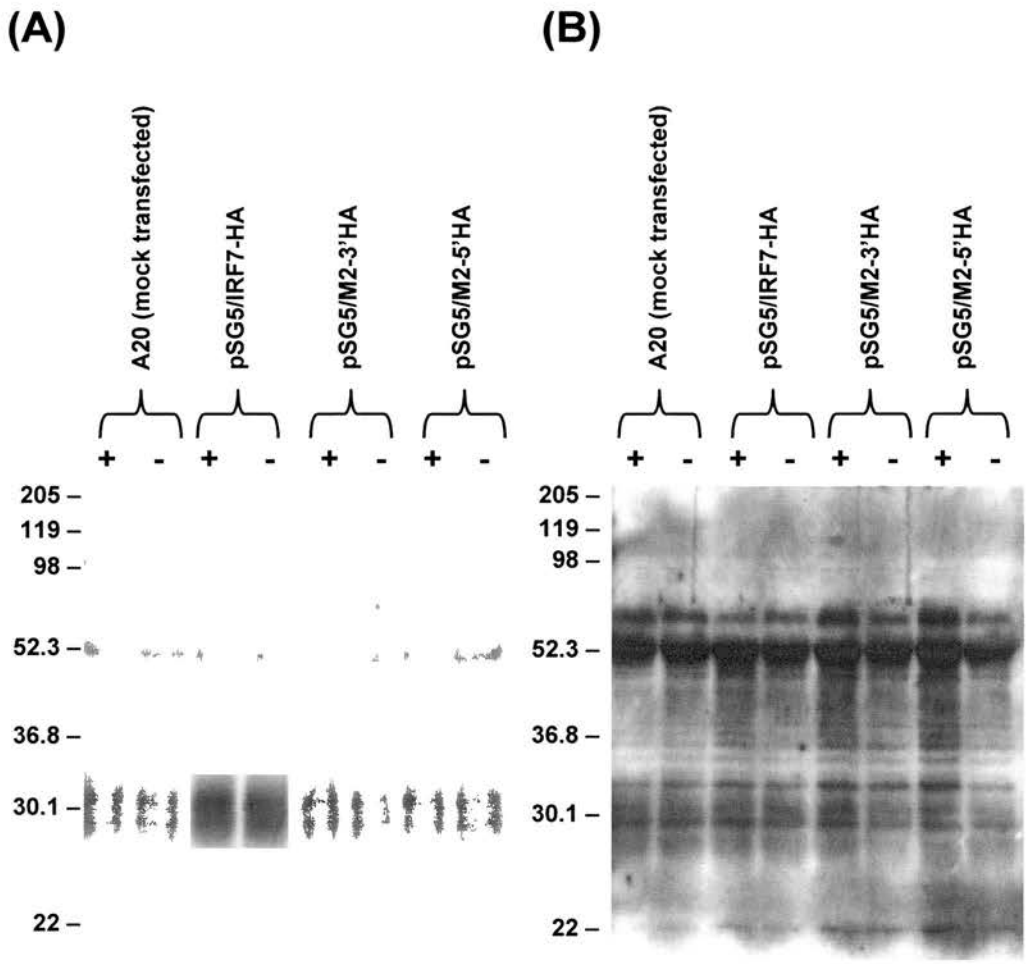

Figure 4.6.2.3 Purification of HA-epitope tagged proteins in A20 cells by immunoprecipitation, followed by immunoblot for the detection of phosphoprotein residues. Cells were transfected with 20μg of plasmid DNA and harvested 24 hours after transfection. Cells were lysed using RIPA buffer and pre-cleared. The HA-epitope tagged proteins were precipitated using rat anti-HA antibody (+) or rat IgG as negative control (-), followed by rabbit anti-rat Ig and then protein A-sepharose beads. The beads were extensively washed using RIPA buffer and then analysed on a 12.5% SDS-PAGE gel, and transferred onto a membrane by Western blot. **(A)** Immunoblot probed with recombinant anti-phosphotyrosine linked to peroxidase, visualised by ECL. **(B)** Immunoblot probed with mouse monoclonal anti-phosphothreonine, followed by biotinylated rabbit anti-mouse Ig and then streptavidin-POD. The conjugates were visualised using ECL. Molecular weights are given in kilodaltons on the left side.

specific background staining was also observed, with binding of the antibodies used in the immunoblot analysis to the light chains of the antibodies used in the immunoprecipitation masking the detection of possible phosphorylated residues in M2 (Figure 4.6.2.3A).

These results show that there is no evidence for the presence of phosphorylated residues in M2, using immunoblot analysis on cell lysates or immunoprecipitated proteins. However, problems encountered with high levels of non-specific background staining in the immunoblots and the lack of a suitable positive control to ensure good specificity and sensitivity of the technique mean that it has not been definitively proven that M2 does not contain phosphorylated residues.

4.6.3. Myristylation status of the M2 protein

The M2 protein contains three glycine residues that are predicted to be myristylated (Figure 4.2.2). The M2 protein migrates at a higher relative molecular mass of 30kDa on SDS-PAGE gel analysis than the expected mass of 22.3kDa, and myristylation may be one possible reason for this discrepancy. Myristylation of proteins has also been observed to play a role in the membrane association of proteins (Cross *et al.*, 1984; McCabe & Berthiaume, 1999). It was therefore decided to determine if this predicted myristylation of M2 was occurring. A20 cells were transfected with 20μg of the HA epitope-tagged expression constructs pSG5/IRF7-HA, pSG5/M2-5'HA and pSG5/M2-3'HA. Mock transfected cells were used as a negative control. After 24 hours, the cells were harvested and labelled for 4 hours at 37°C with 100μCi/ml [9,10(n)-^{3}H] myristic acid (see 2.3.6). The crude cell lysates or HA epitope-tagged immunoprecipitated proteins were then analysed by SDS-PAGE. The gel was impregnated with EN^{3}HANCE, dried and exposed to autoradiographic film for one month. No band specific for the M2 protein was observed (data not shown). However, there was no positive control to ensure correct labelling of the cells with [9,10(n)-^{3}H] myristic acid. These results show that there is no evidence for

myristylation of the M2 protein, but it has not been definitively proven that M2 is not myristylated.

4.7. Discussion

These results demonstrate the initial characterisation of the M2 protein of MHV-68, and illustrate a variety of possible functions. Methods including sequence analysis, expression in prokaryotic and eukaryotic cell types enabled the determination of the cellular localisation of M2 and the extent of any possible post-translational modifications.

Searches of the M2 amino acid sequence against protein databases has revealed low but significant homology to other proteins, which may help in the understanding of the function of M2. A search using the "BLAST" program revealed homology with the Gab2 protein. Gab2 belongs to a group of scaffolding proteins including the *Drosophila* Daughter of Sevenless (DOS) protein and insulin receptor substrate-1 (IRS-1). They contain an N-terminal pleckstrin homology domain (thought to be involved in the recruitment of proteins to plasma membranes and cytoplasmic signalling), a central proline-rich domain and multiple tyrosine residues that serve as targets for phosphorylation and docking sites for src homology 2 (SH2) domain-containing signalling molecules (Gu *et al.*, 1998; Nishida *et al.*, 1999). Gab2 is expressed in a wide range of tissues including haematopoietic cells, and functions as a scaffolding protein for the assembly of signalling proteins, leading to the transduction of intracellular signalling pathways involving cytokines (Gu *et al.*, 1998; Nishida *et al.*, 1999; Gadina *et al.*, 2000), the B-cell receptor (Gu *et al.*, 1998; Gold *et al.*, 2000) and macrophage activation and differentiation (Liu *et al.*, 2001). Gab2 has also been shown to be involved in the negative regulation of signal pathways (Zhao *et al.*, 1999), including T cell receptor signalling (Yamasaki *et al.*, 2001). The M2 protein is much smaller than Gab2 and the other proteins in the scaffolding protein family (which are over 600 amino acids in size), and contains no pleckstrin homology domain. However, these results show that the M2 protein is membrane-associated like Gab2.

It is also of interest that the homology between M2 and the Gab2 proteins is centred around two domains containing tyrosine residues (Figure 4.2.1A, 4.2.1C), which are predicted to be phosphorylated in Gab2 (human Gab2 residues 452 and 563), and the region of homology at human Gab2 residue 452 contains a binding motif for PI3 kinase. One of these conserved tyrosine residues is also predicted to be phosphorylated in M2, at residue 129 (Figure 4.2.3). Thus although M2 is much smaller than Gab2, it may contain some of the motifs necessary for interfering with signal transduction pathways. Previous studies using the adoptive transfer of $M2_{91-99}$ epitope-specific CD8+ T cells (Usherwood *et al.*, 2000) and DNA vaccination using M2 (Usherwood *et al.*, 2001) showed a reduction in the initial load of latently infected cells, and hypothesised that M2 may play a role in expanding the number of latently infected B cells during the establishment of latency. Disruption of the signalling pathways via Gab2 mimicry may be a mechanism for achieving this, and therefore allowing the establishment of latent virus in as many B-lymphocytes as possible to ensure virus survival in the host. Alternatively, disruption of Gab2 pathways may interfere with cytokine signalling and be a mechanism of immune evasion by MHV-68.

A search for conserved protein domains using the program "Block Searcher" revealed homology between $M2_{6-18}$ and a domain in the semaphorin family. Semaphorins are secreted, membrane glycosylphosphatidylinositol (GPI)-anchored or transmembrane molecules which contain a 500 amino acid protein element called the sema domain (Spriggs, 1999; Tamagnone & Comoglio, 2000). The region of homology to M2 is located in the middle of the sema domain. Some semaphorins also contain an immunoglobulin-like domain, signal sequences and transmembrane domains. They were initially discovered due to their involvement in the development of the nervous system and guidance of growth cone axons (Kolodkin *et al.*, 1993). Semaphorins bind to specific rceptors (plexins or neuropilins) and are involved in signal transduction pathways, possibly via tyrosine phosphorylation of the receptors (Tamagnone & Comoglio, 2000). The role of semaphorins in the immune response has only recently been uncovered (Spriggs, 1999). CD100 is a cell surface semaphorin that was first discovered as an activation molecule on T lymphocytes (Delaire *et al.*, 1998). It has been shown

to play a role in T-cell activation via CD45 (Delaire *et al.*, 1998), and the soluble isoform of CD100 has been shown to inhibit the migration of monocytes and B lymphocytes (Delaire *et al.*, 2001).

Further evidence for the involvement of semaphorins in the immune response comes from the discovery of two viral encoded semaphorins. The vaccinia virus A39R protein is the smallest known semaphorin at 441 amino acids, containing only a truncated sema domain (Kolodkin *et al.*, 1993). Interestingly, not all strains of vaccinia produce functional A39R, as a deletion and frameshift mutation in the Western Reserve strain leads to the production of a truncated, non-secreted protein (Gardner *et al.*, 2001). The secreted A39R glycoprotein binds to the plexin virus-encoded semaphorin protein receptor (VESPR) (Comeau *et al.*, 1998), and exerts pro-inflammatory effects via the activation of monocytes (Comeau *et al.*, 1998) and recruitment of inflammatory cells *in vivo* (Gardner *et al.*, 2001). The gammaherpesvirus AlHV-1 also contains a unique ORF A3 with significant homology to the semaphorin family (Ensser & Fleckenstein, 1995; Ensser *et al.*, 1997). The $M2_{6-18}$ region shows strong homology to the mouse semaphorin 3 domains, with less homology to the viral semaphorins of vaccinia virus and AlHV-1. Like semaphorins, the M2 protein is also associated with the plasma membrane. However, the M2 protein is much smaller than all known semaphorin family members (being less than 50% of the size of the smallest known member, A39R) and does not contain a recognisable sema domain, transmembrane or secreted signal sequence or immunoglobulin-like domains. It may however be possible that this conserved sequence is enough to interfere with signalling pathways and modify the immune response to the virus.

The expression of the entire M2 cDNA ORF in bacteria as a GST fusion protein using the pGEX system was achieved, but the low levels of expression of insoluble GST-M2 fusion protein meant that it was not possible to purify the fusion protein. This fusion protein was recognised by polyclonal anti-MHV-68 antibody, which was surprising as M2 is a latency-associated gene (Husain *et al.*, 1999; Virgin *et al.*, 1999), and the polyclonal antibody was raised against lytic cycle antigens (Sunil-Chandra *et al.*, 1992a). The polyclonal anti-MHV-68 antibody did not recognise the GST present in the control lane, signifying that the

antibody was not cross-reacting with the GST element of the fusion protein. This recognition of the M2 fusion protein suggests that there is anti-M2 reactivity in the polyclonal anti-MHV-68 antiserum, and concurs with recent data showing low level transcription of M2 during lytic replication *in vitro* (Rochford *et al.*, 2001; Bridgeman *et al.*, 2001). There are a number of possible reasons for the formation of insoluble proteins in *E. coli*, including the formation of inclusion bodies in the cytoplasm due to the high proline content of M2 (Wilkinson & Harrison, 1991). Possible factors in the poor expression of the GST-M2 fusion protein include the presence of infrequently used codons for arginine and proline in M2, protein degradation and toxicity (Makrides, 1996). M2 contains 38 proline residues, 86% of which are characterised as low-usage in *E. coli* (CCC, CCU, CCA); and 13 arginine residues, 7 of which are the rare codons AGA and AGG which have been shown to be a limiting factor in the expression of proteins in bacteria (Makrides, 1996). There was also evidence for the toxicity of the M2 protein in bacteria, as evidenced by the dramatic reduction in total bacterial protein yields following induction of GST-M2 protein expression. Although it is possible that this toxicity in bacteria might be due to the addition of the IPTG to induce fusion protein expression, varying the concentration of IPTG (0.5-1.5mM) did not have any significant effect on bacterial total protein yield (Figure 4.3.1.2). It is also possible that the induction of foreign protein expression in bacteria may have led to the disruption of normal bacterial protein synthesis, thus leading to the reduction in total bacterial protein yields observed.

These problems were partially overcome by the expression of a 75 amino acid fragment of M2 as a fusion protein with GST. Although this fragment of M2 contained the $M2_{91\text{-}99}$ CD8+ T cell epitope, it was not certain that this fragment would fold in an identical manner to the native M2 protein and thus present the same immunological epitopes. The GST-$M2_{74\text{-}148}$ fusion protein was also poorly expressed in bacteria, but the fact that it became soluble after the inclusion body preparation meant that it was possible to purify the fusion protein using glutathione-sepharose beads. The reason for this increase in solubility of the GST-$M2_{74\text{-}148}$ fusion protein after the inclusion body preparation (where the bacteria undergo gentle lysis using lysozyme and DNase I treatment) as compared to the

lack of solubility after sonication is unclear, but may be due to interaction of the GST-$M2_{74-148}$ fusion protein with other bacterial proteins and / or DNA which are removed during the inclusion body preparation. The GST-$M2_{74-148}$ fusion protein also underwent substantial degradation, as evidenced by the multiple forms of the fusion protein visualised by immunoblot analysis ranging from the entire GST-$M2_{74-148}$ fusion protein (40kDa) to GST alone (27.5kDa). Although attempts were made to reduce the activity of bacterial proteases by the use of inhibitors such as PMSF and Aprotinin and keeping all solutions at 4°C, it may be that the proteolytic pathways present in *E. coli* may have overwhelmed these barriers. The use of protease-deficient strains such as BL21 may have helped overcome this. Alternatively this degradation may have been due to an inherent property of the fusion protein, as instability or misfolding of the truncated M2 protein would lead to targeting of the protein for breakdown by bacteria (Makrides, 1996).

The GST-$M2_{74-148}$ fusion protein was purified and used as an antigen to raise antisera in sheep. The GST could have been removed from the GST-$M2_{74-148}$ fusion protein using the thrombin cleavage site, and the sheep immunised with only the M2 fragments. This might have reduced the non-specific background observed in the immunoblot analysis, but may have also reduced the antigenicity of the protein. Sheep were chosen to raise the antiserum due to their accessibility within the department, the availability of secondary antibodies and the ability to obtain large quantities of antiserum. The presence of the multiple forms of the fusion protein in the preparation due to the protein degradation may have either assisted in the generation of anti-M2 antisera by the presentation of multiple antigenic forms of the M2 polypeptide, or increased the amount of GST protein present in the preparation thus leading to a greater immune response against the GST moiety of the fusion protein. The majority of protein present in the GST-$M2_{74-148}$ fusion protein preparation was GST, or GST containing only a few amino acid residues of the M2 protein (Figure 4.3.3). The antisera was purified using caprylic acid and ammonium sulphate to give a relatively pure IgG antibody preparation. However, the IgG antibodies present would have had specificity for a wide range of antigens, as these purification steps did not select for antibodies specific for the GST-$M2_{74-148}$ fusion protein. The antibodies were tested against

Western blots containing the GST-$M2_{74-148}$ fusion protein, S11 cells which are known to express the M2 protein (Husain *et al.*, 1999) and cells transfected with pVR1255/M2-His. Antibodies from both sheep recognised the fragments of the GST-$M2_{74-148}$ fusion protein, which confirmed that an antibody response had been raised against the antigen. However, this could have been against either the M2 polypeptide or against the GST. No specific reactivity for M2 was observed using the antibodies raised for either of the sheep against proteins in the cell lysates from 293 cells transfected with pVR1255/M2-His. This agrees with other data showing a lack of detectable M2 expression using this vector (Figure 4.4.1.2), and the apparent toxicity of M2 expressed in 293 cells (Figure 4.5.1.1).

Antibodies raised by sheep 705D appeared to specifically react with a band of approximately 30-35kDa present in the S11 cell lysates. As this band was not present in the immunoblot probed with the pre-bleed antibody, this suggested that this sheep produced antibodies reactive to the M2 protein. This band was only observed in the S11 cell lysates and not in any of the different cell types transfected with M2 expression vectors. A probable explanation for this is that the majority of S11 cells express M2, whereas only a low number of transfected cells will express M2, and therefore the S11 cell lysate will contain a higher concentration of M2 protein. However, this reactivity of the sheep antibodies to a band close to the predicted size of M2 in S11 cells was obscured by the high background levels present on the immunoblot, due to non-specific binding of sheep antibodies to other proteins present on the blot. These high levels of background were also observed using indirect immunofluorescence analysis. Attempts to reduce this non-specific binding by using lower antibody dilutions or more sensitive detection techniques such as ECL were unsuccessful, and it was decided not to use immunoprecipitation as it was considered that the non-specific binding of the sheep antibodies would have precipitated other proteins as well as the M2 protein. This background could have been lowered by immunoaffinity purification of the antibodies, which would have yielded pure, M2 specific antibodies. This technique requires a source of pure antigen, which could have been obtained from the GST-$M2_{74-148}$ fusion protein by cleavage of the fusion

protein using the thrombin cleavage site, but needs specialist reagents and is expensive.

Due to the lack of a reliable anti-M2 antibody, it was decided to express M2 in mammalian cells using an epitope tag to enable detection of the M2 protein. Initially, an epitope tag containing six histidine residues was used, as this has been used to detect and purify recombinant proteins (Hochuli *et al.*, 1988; Bornhorst & Falke, 2000). A number of different expression vectors were used, which express inserted genes from either the powerful HCMV immediate-early promoter (pcDNA3.1 and pVR1255) or the Moloney murine leukaemia virus LTR (pBabe puro). A comparison of these promoter elements and the SV40 early promoter (contained within the plasmid pSG5) in expressing bovine growth hormone in murine cells found that the HCMV immediate-early promoter and SV40 early promoter were approximately two-fold more efficient that the Moloney murine leukaemia virus LTR in the expression of the inserted gene (Martin-Gallardo *et al.*, 1988). A similar study comparing the SV40 early promoter, HCMV immediate-early promoter and Rous sarcoma virus LTR found the HCMV immediate-early promoter to be most efficient at expressing luciferase in a range of human cell types (Xu *et al.*, 2001). Similarly, the intron A of HCMV (contained within the plasmid pVR1255) has been shown to increase the expression of heterologous genes *in vitro* and *in vivo* (Hartikka *et al.*, 1996; Xu *et al.*, 2001). However, no expression of M2 was detectable by either immunoblot or indirect immunofluorescence using expression vectors containing these elements (pcDNA3.1, pBabe puro or pVR1255) transiently transfected into a range of different cell types. However, expression of M2 by pcDNA3.1/M2-His and pBabe puro/M2-His was detectable using a *LacZ*-inducible T cell hybridoma specific for the $M2_{91-99}$ CD8+ T cell epitope. This is an extremely sensitive assay for the detection of M2, and suggested that M2 was being expressed by these vectors at levels that were below detection by immunoblot or indirect immunofluorescence. Further evidence for the expression of M2 by pcDNA3.1/M2-His is provided by data showing that DNA vaccination using pcDNA3.1/M2 induces a CD8+ T-cell response to the $M2_{91-99}$ CD8+ T cell epitope (Usherwood *et al.*, 2001). It is therefore probable that the inability to detect M2 expression by pcDNA3.1,

pVR1255 and pBabe puro was due to the detection methods used, and more sensitive techniques such as ECL and multiple epitope tags were necessary.

Another major problem encountered in the expression of M2 was toxicity of the M2 protein. The protein appeared to be toxic in bacteria as evidenced by the poor growth of the bacterial culture after induction of GST-M2 protein expression (Figure 4.3.1.2) and poor expression of the full-length M2 protein as a GST fusion protein. Detection of M2 expression in mammalian cells was only achieved using extremely sensitive techniques such as ECL and a *LacZ*-inducible T cell hybridoma specific for the $M2_{91-99}$ CD8+ T cell epitope. Further circumstantial evidence is provided by attempts to generate COS-7 cell lines stably transfected with M2 which resulted in the deletion of the M2 insert from the pcDNA3.1/M2-His vector (see 4.4.1), and attempts to generate a recombinant MHV-76 virus with the M2 ORF inserted ("knock-in" virus) when it was not possible to purify the virus due to spontaneous deletion of the M2 insert (see Chapter 5). The expression of M2 is extremely tightly regulated during the establishment of latency in the viral life cycle (Usherwood *et al.*, 2000), and this tight regulation is probably necessary to avoid problems associated with the toxicity of M2.

Expression of the M2 protein was detectable in A20 cells by transient transfection using the expression vector pSG5, and a triple HA epitope tag. This expression vector uses the SV40 early promoter and intron II of the rabbit β-globin gene to efficiently express inserted DNA sequences, neither of which would be expected to have a significant advantage in the efficiency of expression of heterologous DNA over the HCMV immediate-early promoter or intron A used in pcDNA3.1/M2-His or pVR1255/M2-His (Hartikka *et al.*, 1996; Xu *et al.*, 2001). Therefore, the reason for detection of M2 expression by this vector is probably due to the presence of three copies of the epitope (therefore amplifying the signal for detection) and the ECL technique used in detection. ECL is over ten times more sensitive than other methods used in the detection of proteins by immunoblot, with claims that the technique can detect as little as 1pg of protein antigen per sample (Amersham Pharmacia product literature), compared to 1ng protein antigen per sample using BCIP/NBT solution (Harlow & Lane, 1988).

Another factor was the cell type used, with A20 cells (a murine B-lymphocyte cell line) and 293 cells (a human epithelial cell line) used in the transient transfection assays. In contrast to the detection of M2 expression in A20 cells, no expression of M2 was detectable by transient transfection of pSG5/M2-3'HA and pSG5/M2-5'HA in 293 cells, despite the detection of expression of the positive control proteins IRF7-HA and Jκ-HA by the pSG5 vector. This correlates with the data showing that expression of EGFP-M2 fusion proteins in 293 cells leads to apoptosis of these cells (Figure 4.5.1.1). Although GFP and EGFP have been shown to be toxic and induce apoptosis in cells, these events occur at later timepoints (48 hours after transfection; Liu *et al.*, 1999a) or in stably expressing cell lines (Hanazono *et al.*, 1997) and would not be expected to occur in transiently transfected cells. Concurrent transfection of 293 cells with the control vectors pEGFP-C1 and pEGFP-N1 resulted in no evidence of apoptosis, suggesting that the M2 protein is the cause of the cell death. This lack of expression in 293 cells could therefore be due to either species or cell type specific factors. Species-specific factors are a possibility due to the restricted host range of the gammaherpesvirus family, although MHV-68 is an exception to this rule as it can infect a wide range of cell types from different species *in vitro* (Svobodova *et al.*, 1982a). However, cell type-specific factors might also be involved, which could explain the lack of expression detected from the His_6 epitope-tagged expression constructs, as all of the cells used in those studies were fibroblast or epithelial cell types. It is of note that another gammaherpesvirus, KSHV, also contains a latency-associated gene LANA2, that is only expressed in B lymphocytes, and is hypothesised to be involved in cell proliferation and / or immune evasion (Rivas *et al.*, 2001).

SDS-PAGE and immunoblot analysis of HA epitope-tagged M2 protein expressed in A20 cells showed that it migrated with a relative molecular mass of approximately 30kDa, which is substantially larger than the predicted mass of 22.3kDa. There were no differences in size with the HA epitope attached at either the N or C terminus of M2, suggesting that there is no post-translational cleavage of M2 occurring. A similar result was observed in A20 cells expressing EGFP-M2, with the fusion protein migrating with a relative molecular mass of

approximately 60kDa (consisting of the 27kDa EGFP with the 30kDa M2 protein). The migration of M2 at a larger than expected relative molecular mass may be due to a number of factors, including post-translational modification and high proline content of M2. Proline-rich proteins tend to migrate at a higher relative molecular mass than expected upon SDS-PAGE analysis (for example EBNA-1 of EBV; Frappier & O'Donnell, 1991; Kieff, 1996). Indirect evidence for the post-translational modification of M2 comes from the expression of M2 in prokaryotic and eukaryotic systems. M2 expressed as a GST fusion protein in prokaryotic cells migrated at a relative molecular mass of 50kDa (Figure 4.3.1.1), whereas M2 expressed as an EGFP fusion protein in eukaryotic cells migrated at a relative molecular mass of 60kDa (Figure 4.4.2.2). Both fusion protein partners are approximately the same mass (GST is 27.5kDa; EGFP is 27kDa), and the 10kDa difference in relative molecular masses could be due to the lack of post-translational modification of proteins in prokaryotic cells. There are a number of co-translational and post-translational modifications predicted to occur to the M2 protein, including N and O-linked glycosylation, myristylation and phosphorylation (Figure 4.2.3). Figure 4.6.1 showed that the M2 protein was not N-glycosylated, but it is possible that myristylation or O-linked glycosylation may occur.

The possible myristylation of M2 is of interest due to the membrane association of myristylated proteins (Cross *et al.*, 1984). Although the addition of myristic acid to a protein will increase its hydrophobicity and therefore increase its potential for membrane association, this is not thought to be sufficient to allow stable anchoring of the protein in a membrane (Resh, 1994; Bhatnagar & Gordon, 1997). Rather, this membrane affinity is thought to be due to electrostatic interactions or molecular "switches" that target myristylated proteins to the membrane compartments (Bhatnagar & Gordon, 1997), and localisation of myristylated proteins to the plasma membrane requires a second signal such as palmitylation (reversible post-translational linkage of palmitic acid to a cysteine residue) or a polybasic domain (Welker *et al.*, 1998; McCabe & Berthiaume, 1999). Thus although M2 is associated with the plasma membrane, there would need to be further signals other than myristylation to localise M2 to the plasma

membrane. Although there was no evidence for the attachment of ^{3}H-labelled myristic acid to M2, the lack of a suitable positive control to ensure adequate labelling prevents the definitive answer to the myristylation status of M2.

The presence of potential phosphorylated residues on the M2 protein is also significant, due to the role of phosphorylated proteins in the regulation of protein function and signalling pathways (Zhou *et al.*, 1997; Sylla *et al.*, 1998). The double band visible on the immunoblot analysis of HA epitope-tagged M2 is characteristic of phosphorylated proteins, but it was not possible to demonstrate the phosphorylation of M2 using antibodies specific for phosphoproteins. This was due to problems encountered with high backgrounds due to non-specific binding of these antibodies and binding to multiple phosphorylated proteins in crude cell lysates, which were not solved by the use of antibodies pre-absorbed to remove affinity for mouse proteins or recombinant antibodies. Attempts to purify and concentrate the M2 antigen by immunoprecipitation prior to immunoblot analysis were hindered by the fact that the M2 migrates at a similar relative molecular mass to the antibody light chain molecule, and non-specific binding to the light chain therefore masked the M2 protein. Another technique such as the labelling of cells expressing M2 with [^{32}P] orthophosphate might be required, although this will not show which residues (tyrosine, threonine or serine) are phosphorylated, and may not be as sensitive due to the low levels of M2 expression.

Studies using EGFP-M2 fusion proteins showed that M2 is present in diffuse patches throughout the cell, with a proportion of the protein localised to the plasma membrane. GFP and EGFP fusion proteins require no additional co-factors or substrates (Chalfie *et al.*, 1994), can be visualised in living cells and have therefore been used to characterise a wide range of cellular (Lorenzon *et al.*, 2001) and viral proteins (Welker *et al.*, 1998; Marechal *et al.*, 1999). Although GFP is a large protein of 27kDa, most GFP fusion proteins retain the biological activity and cellular localisation of the native protein. However, studies have shown that attachment of EGFP to the N terminus of a GPCR prevents the transport of the receptor to the cell membrane with consequent loss of function, in contrast to C terminal EGFP fusion proteins that retain the native protein function

(Tarasova *et al.*, 1997). It should also be noted that the placement of any foreign amino acid sequence could have a deleterious effect on protein function, as evidenced by the reduction in enzyme activity due to the presence of a His_6 residue (Araujo *et al.*, 2000). To control for these possibilities, it was decided to express M2 with EGFP fused to either the C terminus or the N terminus of M2 and also compare the results obtained with the EGFP-M2 fusion proteins with indirect immunofluorescence on cells expressing HA epitope-tagged M2 protein. These four different expression constructs (EGFP or a triple HA epitope fused to either the C terminus or the N terminus of M2) gave nearly identical results. The only slight difference observed was the more diffuse intracellular localisation of the M2-EGFP protein (expressed by pEGFP-N1/M2). This was probably due to the breakdown of the fusion protein observed in the immunoblot analysis (Figure 4.4.2.2), which led to the formation of native EGFP that would localise throughout the cell. The EGFP-M2 present in the central region of the cell did not closely associate with DNA in A20 cells as evidenced by the lack of yellow co-localisation, although transfections in S11 cells known to express M2 (Husain *et al.*, 1999) also showed central localisation of EGFP-M2. The significance of this result remains uncertain.

No difference in the localisation of EGFP-M2 was observed at later timepoints after transfection (Figure 4.5.1.6), which suggested that the intracellular EGFP-M2 fraction was not in the process of being transported to the plasma membrane and was therefore not an artefact due to the time of harvesting the cells. Three different cell surface markers were used to stain the plasma membrane (CD19, MHC Class II and Concanavalin A), all of which showed co-localisation with EGFP-M2 and thus demonstrate that M2 localises with the plasma membrane. However it is not possible to demonstrate whether or not M2 is located at the inner or outer aspect of the plasma membrane using confocal microscopy, and techniques such as immunogold electron microscopy would be required to identify the exact location of M2 on the plasma membrane. The hydropathicity plot reveals that M2 does not contain any membrane-associated domains and is largely hydrophilic, suggesting that M2 is probably associated at the inner plasma membrane, possibly associated with other proteins.

Circumstantial evidence for this hypothesis comes from the homology with the Gab2 family of proteins, and the presence of a semaphorin domain and predicted phosphorylated residues on M2 all of which point to the involvement of M2 in disruption of cellular signal transduction pathways. Cell signalling proteins also tend to be located on the inner plasma membrane.

These results therefore show the initial characterisation of the M2 protein of MHV-68. It has low level but significant homology to the Gab2 family of proteins and a domain in the semaphorin family. It migrates as a doublet with an apparent molecular mass of 30kDa on SDS-PAGE analysis. Studies using EGFP fused to either the N or C terminus of M2 show that M2 localises to the plasma membrane, but not to the Golgi apparatus, ER or lysosomes. These results were confirmed by indirect immunofluorescence studies using a different system, with a triple HA epitope fused to either the N or C terminus of M2. M2 is not post-translationally modified by N-linked glycosylation, but attempts to show the phosphorylation and myristylation of residues in M2 were not conclusive. These studies provide the basis for further research on the possible function of M2 during viral infection.

Chapter 5: The function of M2 during MHV-68 pathogenesis

5.1. Aims

The characterisation of MHV-76 (Chapter 3) has shown that the unique MHV-68 genes M1, M2, M3, M4 and the vtRNA genes play a major role in viral pathogenesis and the development of virus-mediated immunopathology. Previous studies have examined the contribution of the M1 and M3 ORFs in this region to viral pathogenesis using deletion analysis (Simas *et al.*, 1998; Clambey *et al.*, 2000; Bridgeman *et al.*, 2001), but little is known of the function of the M2 ORF. It is known to be a target for the CD8+ CTL response (Husain *et al.*, 1999), and expressed transiently during the establishment of latency (Usherwood *et al.*, 2000). Studies involving the modification of the immune response to the M2 protein by either the adoptive transfer of an M2-specific CD8+ T cell line or DNA vaccination with M2 prior to infection with MHV-68 led to a reduction in the number of latently infected cells during the establishment of latency (Usherwood *et al.*, 2000; Usherwood *et al.*, 2001), but no reduction in the long-term latent virus load. However, no studies have been undertaken using viruses solely defective in the M2 ORF to examine the function of M2 during MHV-68 pathogenesis.

The aim was therefore to utilise two different approaches to generate recombinant viruses for the study of M2 function, by either inserting the M2 ORF into MHV-76 ("knock-in" virus) or disrupting the M2 ORF in MHV-68 ("knock-out" virus). Production of these viruses would enable their characterisation *in vitro* and *in vivo*, and therefore help to determine the role of M2 in viral infection

5.2. Construction of recombinant viruses by insertion of genes into MHV-76 ("knock-in" virus)

A number of factors were taken into consideration when designing recombinant constructs for the insertion of genes into MHV-76. As transcription and translation of the M2 gene is under tight control during the establishment of latency (Usherwood *et al.*, 2000), it was decided to insert genes into MHV-76 under the control of their natural viral promoters. The transcriptional map of M2 has been revealed by cDNA sequencing (Husain *et al.*, 1999), and it was therefore

decided to include over 1kb of DNA upstream of the transcriptional start site in the M2 insertion construct (M2 insert; Figure 5.2.1). This upstream region was chosen to include all possible transcriptional regulatory regions as characterisation of other herpesvirus transcriptional control elements such as the HCMV major IE gene modulator, enhancer and promoter elements (Meier & Stinski, 1996), the KSHV LANA-1 promoter (Jeong *et al.*, 2001) and the ORF50 promoter of MHV-68 (Liu *et al.*, 2000) has shown that these are present up to approximately 1kb upstream of the transcriptional start site. This sequence includes M2 promoter and regulatory elements that have been previously characterised (M. Husain, J. Sample; unpublished data). This sequence at the 5' end of the M2 insert includes over 90% of the M3 ORF, but does not include the N-terminal 81 amino acids of M3 or any of the M3 promoter elements and would not therefore lead to the production of any M3 protein. Similarly, a 364bp sequence downstream of the M2 polyadenylation signal was included in the M2 insert to include any downstream regulatory elements for M2 expression. This sequence at the 3' end of the M2 insert includes some of the M1 ORF, but would not lead to the production of any full-length functional M1 protein.

The region of the MHV-68 genome to be included in the M2 insert also contains three of the vtRNA sequences (6,7 and 8). There was a possibility that any phenotype observed with the insertion of the M2 insert into MHV-76 might be due to the actions of these vtRNA sequences. It was therefore decided to make a control virus that contained vtRNA 7 and 8, which would enable the differentiation of any effects due to the vtRNAs from those due to M2. Promoter and regulatory elements for mammalian tRNAs are largely contained within the transcribed region (Paule & White, 2000). Mapping of the promoter elements necessary for the transcription of the EBERs of EBV (which are also transcribed by RNA polymerase III) showed that sequences up to 77bp upstream of the EBERs were required for efficient transcription (Howe & Shu, 1989), and it has been proposed that the vtRNAs of MHV-68 contain similar regulatory elements, with termination signals present approximately 140bp downstream of the vtRNA sequence (Bowden *et al.*, 1997). It was therefore decided to include

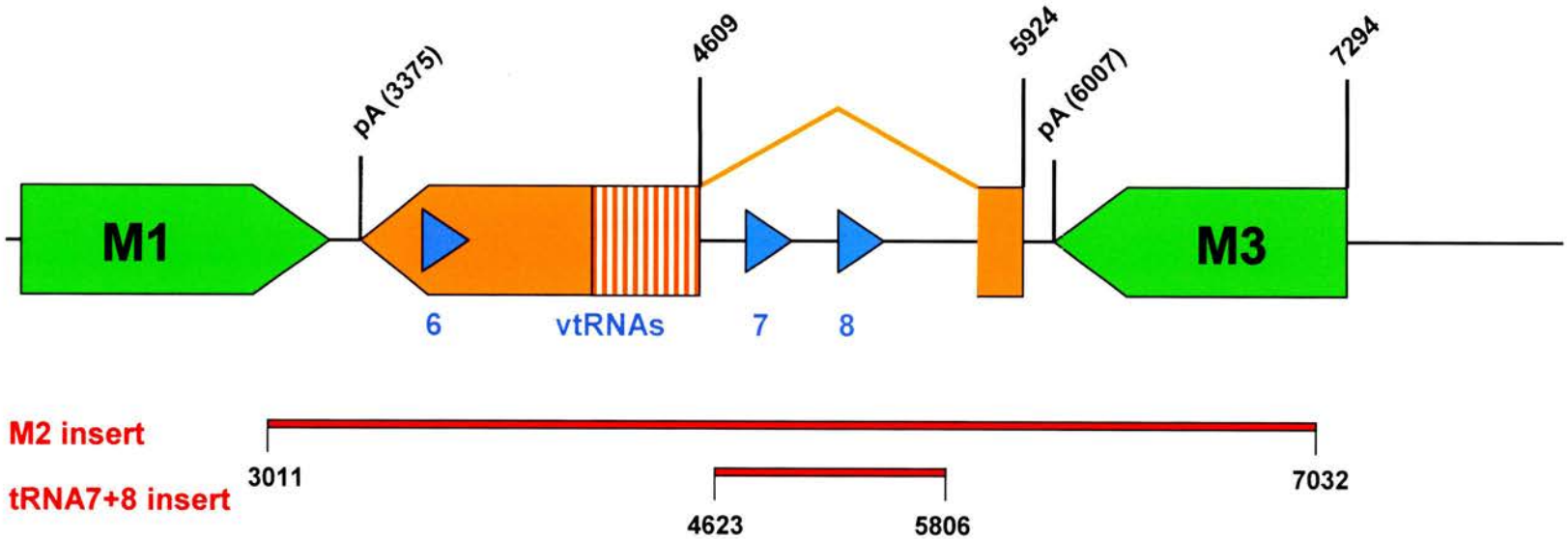

Figure 5.2.1 Schematic diagram (to scale) of the left end of the unique region of the MHV-68 genome (genomic co-ordinates 2 – 8kb), showing features relevant to the design of the recombination cassettes for the insertion of genes into MHV-76. The M1 and M3 transcripts are shown in green, and vtRNA 6,7 and 8 shown as blue triangles. The M2 transcript is shown in orange, with the translated M2 ORF shown in vertical orange bars. The red horizontal bars underneath show the regions amplified to construct the M2 insert (top bar) and tRNA7+8 insert (lower bar) for generation of the recombination cassettes. The genomic co-ordinates of relevant features such as transcriptional start sites, exon termini and polyadenylation signals (pA) are given according to Virgin *et al.*, 1997; Van Berkel *et al.*, 1999 and Husain *et al.*, 1999.

approximately 300bp of the sequence flanking vtRNA7 and 8 in the tRNA7+8 insertion construct (tRNA7+8 insert; Figure 5.2.1).

To obtain recombinant MHV-76 viruses with either M2 or tRNA7+8 inserted, it was decided to use a strategy of homologous recombination using a single crossover event to insert the relevant cassette into the junction of the left end of the unique region of the MHV-76 genome and the terminal repeats. This strategy was first developed for HVS, where it was found that insertion of DNA sequences at the junction of the terminal repeats and unique region occurred more efficiently in the correct locus if a single flanking sequence of unique genomic DNA is used with no terminal repeat units (Grassmann & Fleckenstein, 1989). This strategy has been used to successfully generate recombinant MHV-68 viruses (Simas *et al.*, 1998; Adler *et al.*, 2000). Recombinant viruses would then be selected for the presence of the desired insert. Standard techniques for the selection of recombinant herpesviruses include the insertion of marker genes, such as *lac*Z (Simas *et al.*, 1998; Bridgeman *et al.*, 2001) or GFP (Vieira *et al.*, 1998; Adler *et al.*, 2000), or genes encoding antibiotic resistance for the positive selection of recombinant viruses (Herrold *et al.*, 1996; Vieira *et al.*, 1998). However, there was concern that the insertion of foreign DNA into the left end of the virus and possible alterations in viral transcription due to the introduction of the HCMV IE promoter (used to express marker genes such as *lac*Z and GFP) might affect the expression of neighbouring genes. These effects have been observed with the introduction of foreign DNA into the left end of the MHV-68 genome (Clambey *et al.*, 2000; Adler *et al.*, 2001). It was therefore decided to reintroduce only MHV-68 viral sequences (with no marker genes), and utilise a PCR-based screening method to select recombinant viruses.

5.2.1. Design of recombination cassette for the insertion of M2 into MHV-76.

A region corresponding to the terminal 3kb of MHV-76 (nucleotide positions 9538-12563) was amplified using primer pair 76LHE1 and 76LHE2 (Chapter 2, Appendix 2) with *PfuTurbo*™ DNA polymerase, and inserted into the pKS(-) vector (pBluescriptII KS(-); Chapter 2, Appendix 3) using the *Bam*HI and

*Eco*RI restriction enzyme sites to give the vector pKS/76LHE. Sequence analysis of approximately 500bp of both termini of the 76LHE fragment in pKS(-) (see 2.2.24) confirmed that it was present in the correct orientation. The M2 insert (Figure 5.2.1; nucleotide positions 3011-7031) was amplified using primer pair M2-insert1 and M2-insert2 (Chapter 2, Appendix 2) with *PfuTurbo*™ DNA polymerase, and inserted into the pKS/76LHE vector using the *Bam*HI and *Not*I restriction enzyme sites to give the vector pKS/76LHE/M2insert (Figure 5.2.2A). Sequence analysis of approximately 500bp of the *Not*I termini of the M2insert in pKS/76LHE (see 2.2.24) confirmed that it was present in the correct orientation. A large scale preparation of pKS/76LHE/M2insert was made (see 2.2.15), and the 7kb recombination construct was excised from the pKS(-) plasmid by digestion with the restriction enzymes *Not*I and *Eco*RI prior to transfection to avoid any recombination events leading to the incorporation of the pKS(-) plasmid into the virus.

5.2.2. Design of recombination cassette for the insertion of vtRNA 7 and 8 into MHV-76.

The tRNA7+8 insert (Figure 5.2.1; nucleotide positions 4623-5806) was amplified using primer pair tRNA7+8-insert1 and tRNA7+8-insert2 (Chapter 2, Appendix 2) with *PfuTurbo*™ DNA polymerase, and inserted into the pKS/76LHE vector using the *Bam*HI and *Not*I restriction enzyme sites to give the vector pKS/76LHE/tRNA7+8insert (Figure 5.2.2B). Sequence analysis of approximately 500bp of the *Not*I termini of the tRNA7+8insert in pKS/76LHE (see 2.2.24) confirmed that it was present in the correct orientation. The sequence analysis also revealed the presence of a T residue at position 4945 (2bp upstream of vtRNA7) in the vtRNA7+8 insert compared with the published MHV-68 genome sequence (Virgin *et al.*, 1997), a difference that has been observed in MHV-68 strain g2.4 (Bowden *et al.*, 1997; Nash *et al.*, 2001). A large scale preparation of pKS/76LHE/tRNA7+8insert was made (see 2.2.15), and the 4.2kb recombination construct was excised from the pKS(-) plasmid by digestion with the restriction enzymes *Not*I and *Eco*RI prior to transfection to avoid any

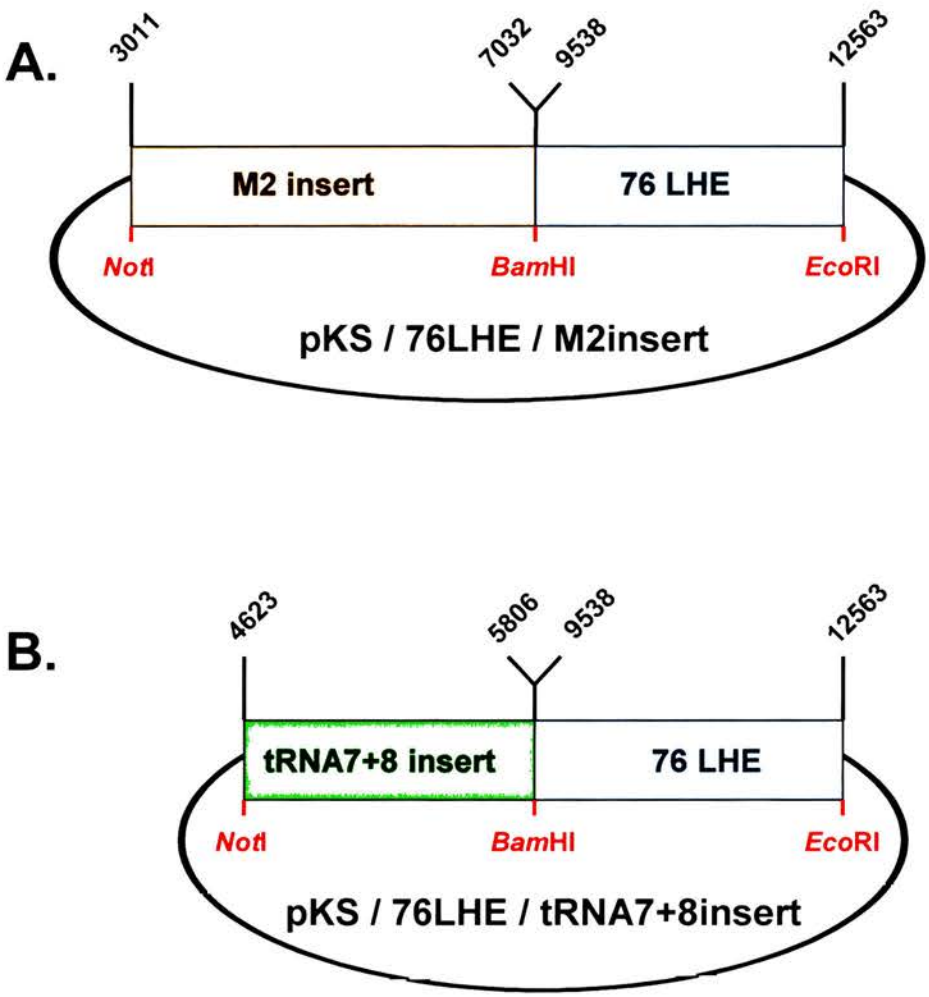

Figure 5.2.2 Schematic diagram (not to scale) of the recombination cassettes for the insertion of M2 (**A**) and vtRNA7 and 8 (**B**) into MHV-76. The 3kb region at the left end of MHV-76 was amplified by PCR and inserted into the vector pKS(-), to give the plasmid pKS/76LHE. The M2 insert region (4kb) was amplified by PCR and inserted into pKS/76LHE to give the plasmid pKS/76LHE/M2insert (**A**). The vtRNA7 and 8 region (1.1kb) was amplified by PCR and inserted into pKS/76LHE to give the plasmid pKS/76LHE/tRNA7+8insert (**B**). Unique restriction enzyme sites encoded by the primers to facilitate directional cloning are shown in red. MHV-68 genomic co-ordinates of the termini of the PCR fragments are shown according to Virgin *et al.*, 1997.

recombination events leading to the incorporation of the pKS(-) plasmid into the virus.

5.3. Construction of recombinant viruses with deletions in the M2 gene ("knock-out" virus)

Previous results showed that cosmid A8 (cA8) could be utilised to reintroduce the deleted 9.5kb sequence into MHV-76, and that this rescue virus [designated MHV-76(cA8+)4] was identical to MHV-68 in both genomic characterisation and *in vitro* and *in vivo* properties (Chapter 3). These results demonstrated that one method for the construction of recombinant viruses with deletions in the M2 gene was to generate mutations in the M2 ORF in cA8, and then use the mutated cosmid as the recombination cassette. Due to the extensive flanking sequences present in cA8, this represented a means of ensuring efficient homologous recombination to generate recombinant viruses, which would be almost genetically identical to MHV-68 except for mutations in the M2 ORF. A further advantage was that the lack of any M2 sequence in MHV-76 meant that contamination with wild-type virus (i.e. containing the M2 ORF) would not be a factor during purification of the recombinant virus, as would be the case during recombination with MHV-68.

As previously discussed (see 5.2), it was decided that the introduction of foreign DNA into the left end of the unique region of the virus (such as marker genes) might have deleterious effects on the expression of surrounding viral genes. It was therefore decided to introduce a series of deletions and frame-shift mutations into the M2 ORF to ensure disruption of the M2 protein, without the addition of marker genes. These small deletions would have minimal effect on surrounding genes. A PCR-based screening method would then be utilised to select for M2 positive recombinant viruses.

5.3.1. Deletion of internal sequences in the M2 ORF of cosmid A8.

Cosmid A8 (MHV-68 nucleotide positions 115,165 to 26,842 in modified SuperCosI vector; see Chapter 2, Appendix 3) contains a unique *Sal*I site at

nucleotide position 4335 (within the M2 ORF). *Sal*I digests DNA to leave 4bp 5'-protruding termini, and this was utilised to generate deletions in the M2 ORF. Cosmid A8 DNA was linearised with *Sal*I, and this was confirmed by agarose gel electrophoresis (data not shown). Deletions were produced by digesting the recessed 3'-termini with Exonuclease III (a 3' to 5' exonuclease), which resulted in the bi-directional deletion of sequences starting from the *Sal*I site at the rate of approximately 250bp of the M2 ORF per minute at 23°C (see 2.2.8). Aliquots were therefore removed at 20, 40, 60, 80 and 100-second intervals after the addition of Exonuclease III. The termini of the digested DNA were blunted using Mung Bean Nuclease, and ligated. In addition, one aliquot was removed before the addition of Exonuclease III and only digested with Mung Bean Nuclease to remove the 5'extensions at the *Sal*I site to leave blunt ends, which were then re-ligated. Digestions solely with Mung Bean Nuclease led to the deletion of 4bp in the *Sal*I site.

A sample of the ligated cosmid DNA from each of the reactions (labelled 0, 20, 40, 60, 80 and 100 seconds) was used to transform ElectroMAX DH10B bacteria by electroporation (see 2.2.12), and cosmid DNA from ampicillin resistant colonies was prepared by the mini-prep method (see 2.2.14). Four colonies that produced cosmid DNA of the expected size that was not linearised by digestion with *Sal*I (due to deletion of the *Sal*I site) were chosen for further analysis. Colonies 4 and 5 were solely digested with Mung Bean Nuclease (0 second aliquots), colony 21 was digested with Exonuclease III for 60 seconds and colony 32 was digested with Exonuclease III for 100 seconds.

5.3.2. Analysis of cosmid A8 mutants with deletions in the M2 ORF.

The M2 ORF was amplified using primer pair M2GEX1 and M2GEX2 (Chapter 2, Appendix 2) with *PfuTurbo*™ DNA polymerase using 1µl of mini-prep DNA from colonies 4, 5, 21 and 32 as template, and the products were analysed on a 0.8% TAE agarose gel. Figure 5.3.2.1 shows that the M2 ORF amplified from colonies 4 and 5 was the same size as the positive control (600bp). Digestion of the positive control M2 PCR fragment (amplified from MHV-68

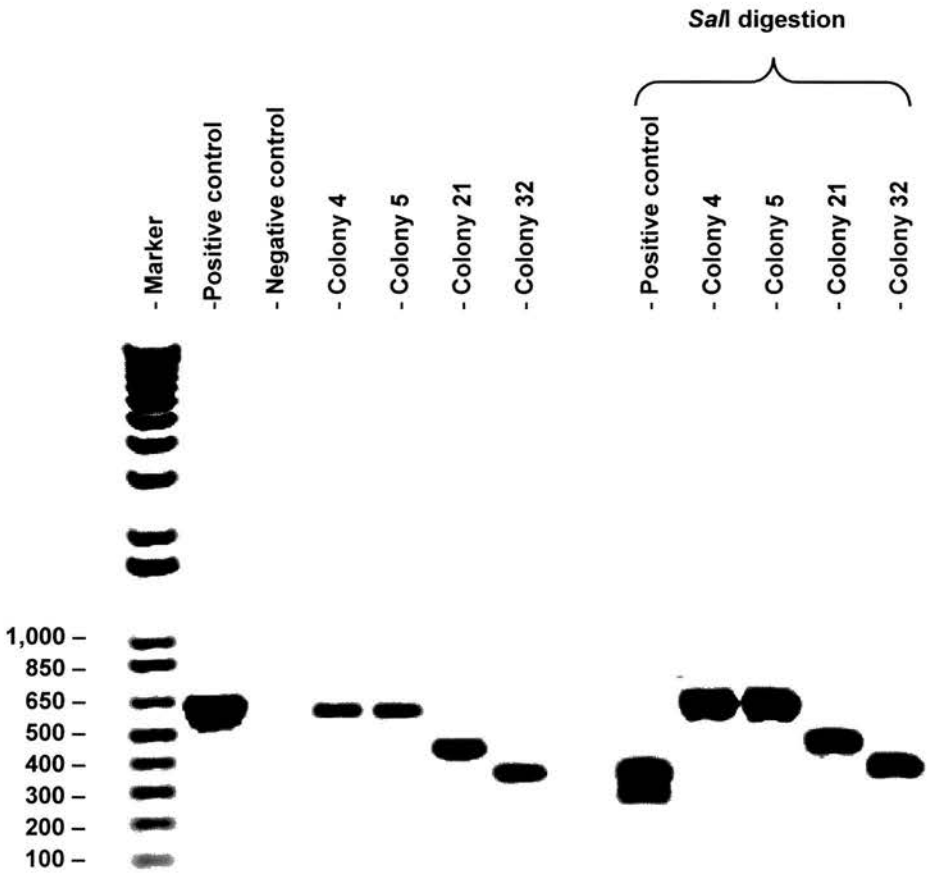

Figure 5.3.2.1. Analysis of cosmid A8 colonies with deletions of internal sequences in the M2 ORF. The M2 ORF was amplified by PCR using 1µl of mini-prep DNA from individual colonies 4, 5, 21 and 32 as template, and the products were analysed on a 0.8% TAE agarose gel. Positive control (MHV-68 genomic DNA template) and negative control (diH_20 template) reactions were also performed. To investigate the presence or absence of the *Sal*I restriction enzyme site in the amplified M2 ORF, a 5µl sample of each PCR reaction was also digested using the restriction endonuclease *Sal*I, and analysed on the same gel. Molecular weights are shown relative to the marker on the left side.

genomic DNA) with *Sal*I results in the production of 2 fragments (271bp and 335bp). However, the M2 fragments amplified from colonies 4, 5, 21 and 32 were resistant to cleavage by *Sal*I. The M2 fragment amplified from colony 21 was approximately 450bp, and the fragment amplified from colony 32 was approximately 350bp, indicating that they contained substantial deletions in the M2 ORF.

The M2 fragments amplified by PCR were inserted into the pKS(-) vector (Chapter 2, Appendix 3) using the *Bam*HI and *Eco*RI restriction enzyme sites, and the sequence was determined (see 2.2.24). Figure 5.3.2.2 shows the results of the sequence analysis of the deletions present in the M2 ORF of the cA8 mutants. Colonies 4 and 5 contained 4bp deletions in the *Sal*I site (deletion of nucleotides 4336-4339), and this also leads to a frame shift mutation. As such, the M2 ORF in these cosmids could potentially generate a 90 a.a. protein consisting of the N-terminal 89 residues of M2 fused to an arginine residue in an alternative reading frame before a stop codon arises. Significantly, this deletion also removes the last 3 residues of the $M2_{91\text{-}99}$ CD8+ T cell epitope. Colony 21 contains a 166bp deletion (nucleotides 4242-4407) that also leads to a frame shift mutation. This cosmid could therefore potentially generate a protein consisting of the N-terminal 66 residues of M2, with the deletion of the entire $M2_{91\text{-}99}$ CD8+ T cell epitope. Colony 32 contains a 256bp deletion in the M2 ORF (deletion of nucleotides 4239-4494). This M2 ORF could potentially generate a protein consisting of the N-terminal 37 amino acids of M2, with a frame shift present due to the deletion. This M2 ORF also does not contain any of the $M2_{91\text{-}99}$ CD8+ T cell epitope sequence.

It was therefore decided to utilise two cosmids to generate recombinant viruses; colony 4 (designated cA8-M2$\Delta_{4336\text{-}4339}$) containing the 4bp deletion and colony 32 (designated cA8-M2$\Delta_{4239\text{-}4494}$) containing the 256bp deletion. It was decided to use cA8-M2$\Delta_{4239\text{-}4494}$ in case the remaining N-terminal 89 residues of M2 present in cA8-M2$\Delta_{4336\text{-}4339}$ were able to encode a functional protein. The substantial deletion present in cA8-M2$\Delta_{4239\text{-}4494}$ was thought to be highly unlikely to encode any functional protein.

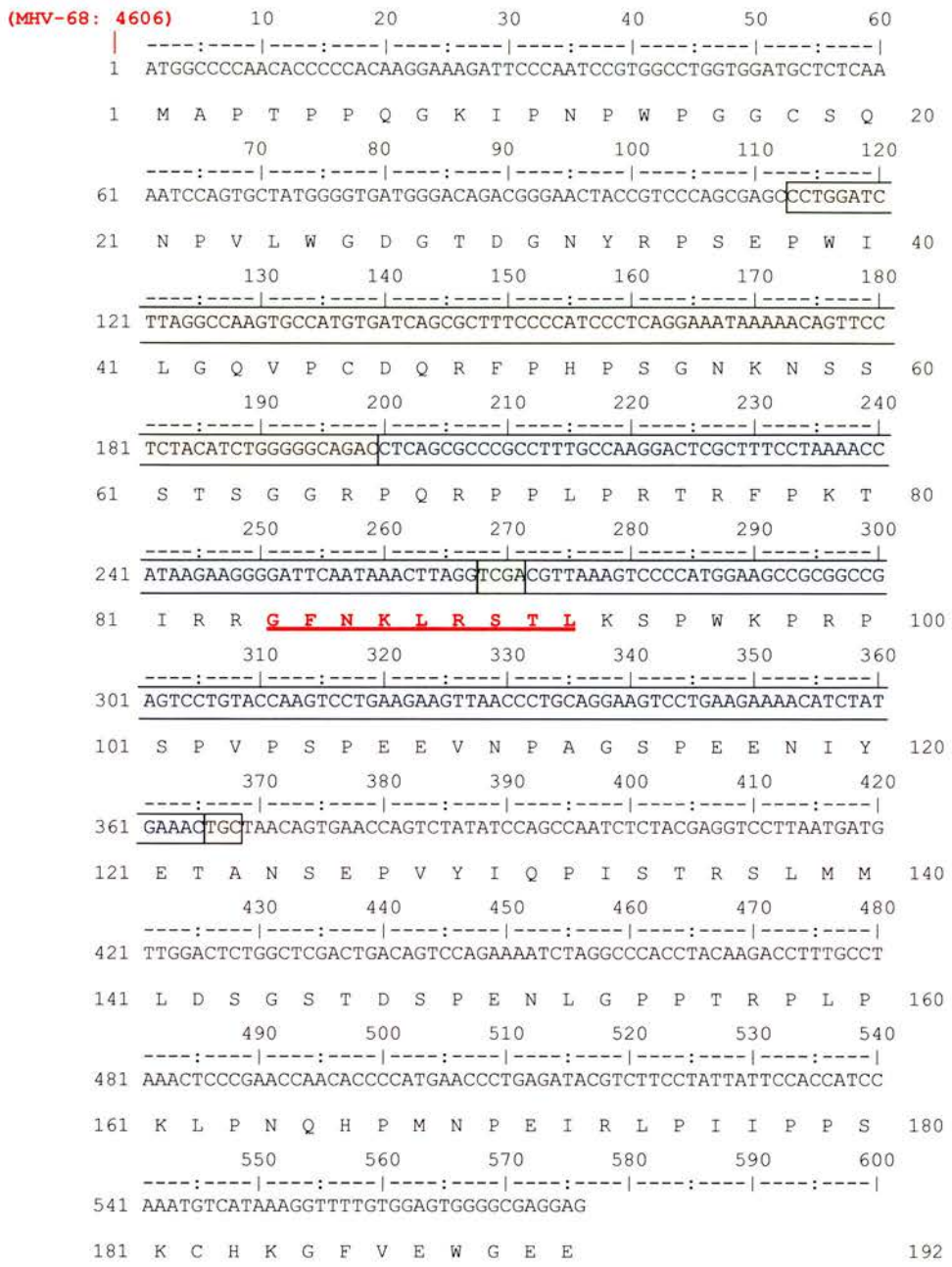

Figure 5.3.2.2 Analysis of cosmid A8 mutants with deletions in the M2 ORF. The M2 ORF was amplified by PCR from colonies 4,5,21 and 32. The PCR fragments were ligated into the plasmid pKS(-) and sequenced. The nucleotide sequence of the M2 ORF is shown, with nucleotide positions shown from 1 to 576 (MHV-68 genomic co-ordinates 4606 to 4031). The amino acid sequence of M2 is shown underneath the nucleotide sequence, with the $M2_{91\text{-}99}$ CD8+ T cell epitope shown in red underlined type. The extent of deletions in colonies 4 and 5 are shown highlighted in green ($M2\Delta_{4336\text{-}4339}$), the deletion in colony 21 is shown highlighted in green and blue ($M2\Delta_{4242\text{-}4407}$) and the deletion in colony 32 is shown highlighted in green, blue and orange ($M2\Delta_{4239\text{-}4494}$).

A large scale preparation of purified cosmid DNA was made of cA8-M2$\Delta_{4336\text{-}4339}$ and cA8-M2$\Delta_{4239\text{-}4494}$ (see 2.2.16). To ensure that there were no deletions or rearrangements within the cosmids, 1μg of cosmid DNA was digested with *Bam*HI, *Eco*RI or *Hin*dIII, analysed on a 0.8% TAE agarose gel and compared with restriction digests of the parent cA8. Figure 5.3.2.3 shows that restriction enzyme digests of cA8-M2$\Delta_{4336\text{-}4339}$ and cA8-M2$\Delta_{4239\text{-}4494}$ with three different enzymes were identical to the parent cA8. These digests also agree with published restriction enzyme maps of the MHV-68 genome (Efstathiou *et al.*, 1990b), with the presence of the 7.9kb SuperCosI vector. The one difference noted was the slight reduction in size of the *Hin*dIII E fragment in cA8-M2$\Delta_{4239\text{-}4494}$ due to the 256bp deletion within the M2 ORF. This result showed that the cosmids created were identical to parent cA8, except for deletions within the M2 ORF.

5.4. Production and purification of recombinant viruses

BHK-21 cells were transfected (see 2.1.4) with 5μg of MHV-76 viral DNA (see 2.2.18) and 10μg of plasmid (pKS/76LHE/M2insert and pKS/76LHE/tRNA7+8 insert, with the recombination cassette excised from pKS (-) prior to transfection) or cosmid (cA8-M2$\Delta_{4336\text{-}4339}$ and cA8-M2$\Delta_{4239\text{-}4494}$, undigested). The cells were overlaid with medium containing 1% w/v LGT agarose 24 hours after transfection (see 2.8.1) and viral plaques were harvested after 5-7 days (see 2.8.3).

As there were no marker genes present in any of the recombinant viruses, it was decided to use a PCR-based screening method to select for recombinant viruses. Viral plaques in the BHK-21 monolayer (from either 6 well plates or limiting dilution assay) were harvested, and divided into two 100μl aliquots. One aliquot was stored at -70°C and retained as the viral stock. The other aliquot was washed once with modified TE, and then resuspended in 50μl modified TE (see 2.8.3). After one freeze-thaw cycle, the sample was digested overnight with PCR Grade Proteinase K at 55°C. The sample was heated to 95°C for 10 min to inactivate the Proteinase K, and 10μl of the sample was used as template for PCR

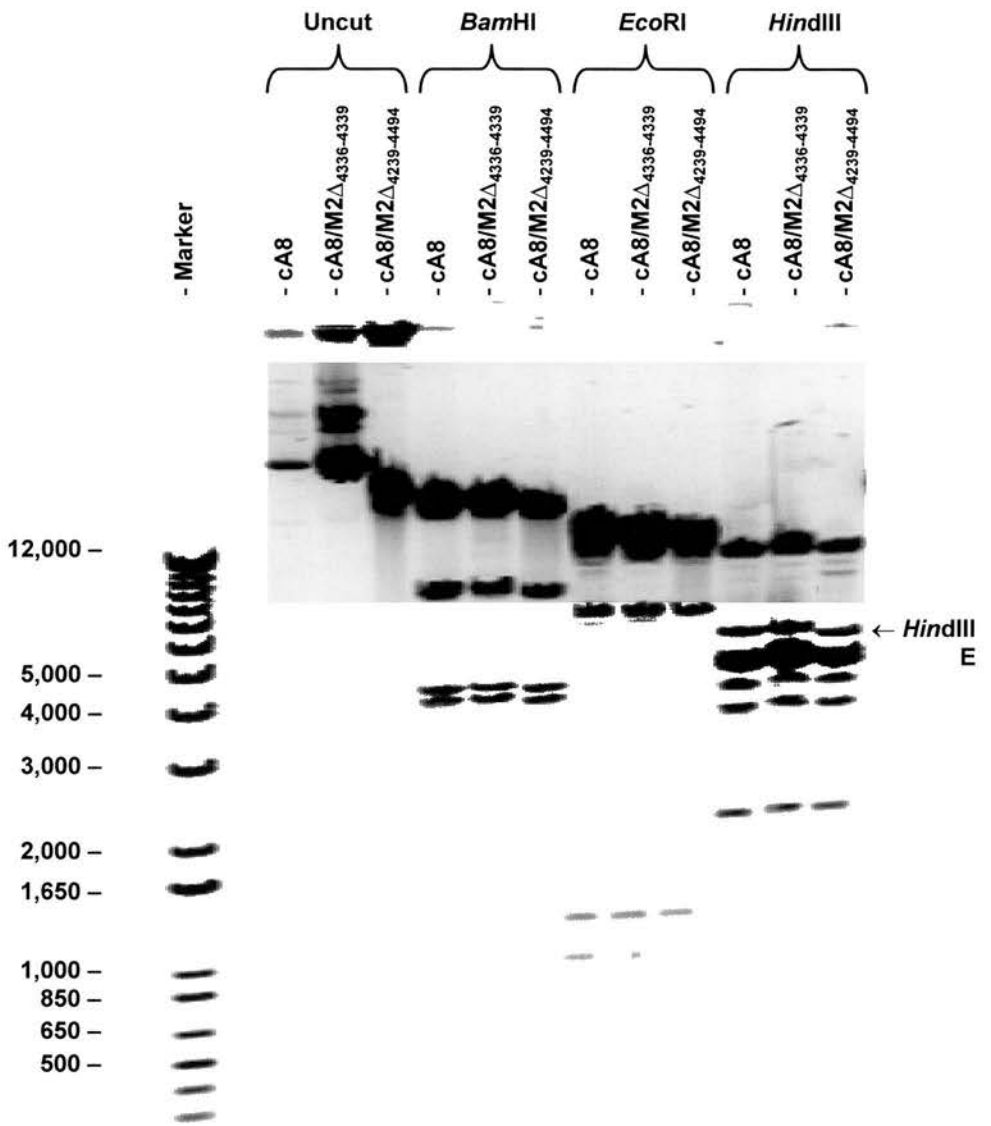

Figure 5.3.2.3 Restriction enzyme digestion of cA8 mutants with deletions in the M2 ORF. Large scale preparation of cosmid DNA (cA8, cA8/M2$\Delta_{4336\text{-}4339}$, cA8/M2$\Delta_{4239\text{-}4494}$) was performed using a QIAGEN Large-Construct Kit. A 1µg sample was digested with the restriction enzymes *Bam*HI, *Eco*RI and *Hin*dIII and analysed on 0.8% TAE agarose gel. A sample of uncut cosmid DNA (0.5µg) was also analysed on the same gel. Molecular weights are shown relative to the marker on the left side.

analysis. 40 cycles of PCR were performed using primers specific for the M2 ORF (M2GEX1 and M2GEX2; Chapter 2, Appendix 2) to select for recombinant viruses containing 76LHE/M2insert, cA8-M2$\Delta_{4336\text{-}4339}$ and cA8-M2$\Delta_{4239\text{-}4494}$. To select for recombinant viruses containing 76LHE/tRNA7+8insert, PCR analysis was performed using primers specific for the tRNA7+8insert (tRNA7+8insert1 and tRNA7+8insert2; Chapter 2, Appendix 2). As a control to check for the presence and suitability of viral DNA for PCR analysis, PCR analysis was also performed on all samples using primers specific for ORF74 (GCR-5' and GCR-3'; Chapter 2, Appendix 2). PCR products were then analysed on a 1% TAE agarose gel.

The sensitivity of this PCR-based screening method was assessed using the M2GEX1 and M2GEX2 primers to amplify the M2 ORF in samples of MHV-68 virus stock serially diluted tenfold in modified TE. Figure 5.4.1 shows that this technique was sensitive to the level of 1 PFU per sample. When the samples were only digested with Proteinase K for 20 minutes at 55°C (instead of overnight), the sensitivity of this method was 10 PFU (data not shown). These results showed that this technique was sensitive enough for the screening of recombinant virus samples.

Single plaques positive for the desired insert (the M2 ORF for recombinant viruses containing 76LHE/M2insert, cA8-M2$\Delta_{4336\text{-}4339}$ and cA8-M2$\Delta_{4239\text{-}4494}$, or the tRNA7+8insert for recombinant viruses containing 76LHE/tRNA7+8insert) were purified using a limiting dilution assay on BHK-21 cells (see 2.8.3). Single plaques per well of a 96 well plate were harvested after 6 days and analysed by PCR. If they contained the desired insert, the stock virus samples were used to infect the next limiting dilution assay. Recombinant viruses were purified until all virus samples analysed were positive for the desired insert for at least two rounds of purification. For viruses made by recombination with cA8-M2$\Delta_{4336\text{-}4339}$ and cA8-M2$\Delta_{4239\text{-}4494}$, purification was judged to be complete after 5 rounds of purification. Additionally, PCR analysis of cA8-M2$\Delta_{4239\text{-}4494}$ revealed the presence of the smaller M2 ORF (350bp), which showed that there was definitely no contamination with MHV-68 virus. A single purified viral plaque was used to

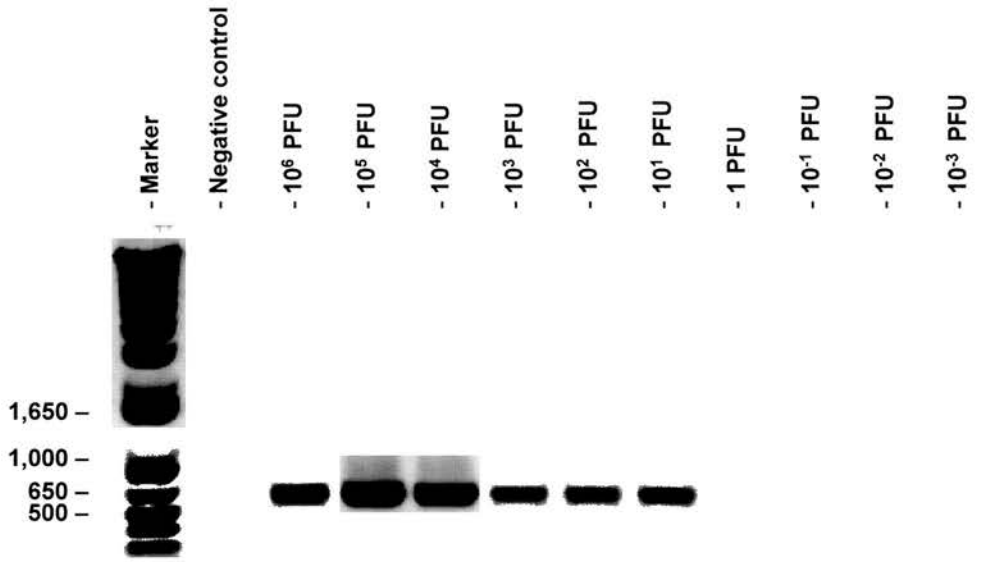

Figure 5.4.1 Sensitivity of a PCR-based screening method for the purification of recombinant viruses. MHV-68 virus stock of known titre was serially diluted tenfold in modified TE (pH8.0), freeze-thawed once and samples containing 10^6 to 10^{-3} PFU were digested overnight with PCR grade Proteinase K at 55°C. The samples were heated to 95 °C for 10 minutes to inactivate the Proteinase K, and 40 cycles of PCR amplification were performed using primers specific for the M2 ORF. The products were analysed on a 1% TAE agarose gel. Molecular weights are shown relative to the marker on the left side.

infect a TC 175cm^2 flask of BHK-21 cells, to prepare DNA for Southern analysis and PCR (see 2.2.19).

Problems were encountered with the purification of recombinant viruses made with 76LHE/M2insert and 76LHE/tRNA7+8insert. Selection of recombinant viruses positive for the 76LHE/M2insert by PCR analysis was initially successful, but was unable to purify recombinant viruses to the high degree of purity required, as the presence of single viral plaques negative for the M2 ORF was detectable during every round of purification. This occurred despite three separate attempts to purify MHV-76/M2insert viruses (each attempt consisting of 4-5 rounds of plaque purification). It was postulated that the recombinant MHV-76/M2insert viruses detectable in the initial rounds of plaque purification either had a selection disadvantage due to poor replication in tissue culture (possibly requiring the assistance of a "helper virus" to replicate *in vitro*) or spontaneously deleted the M2 insert during replication to revert back to MHV-76. It was decided to use a plaque from a stock of almost pure MHV-76/M2insert virus to infect a TC 175cm^2 flask of BHK-21 cells, to prepare DNA for Southern analysis and PCR (see 2.2.19).

Selection of recombinant viruses positive for the 76LHE/tRNA7+8insert by PCR analysis was problematic due to the PCR screening method used. Initially, primer pair tRNA7+8insert1 and tRNA7+8insert2 (Chapter 2, Appendix 2) was used but failed to reliably amplify DNA in samples known to be positive, despite adjustments to the PCR conditions. This was thought to be due to the large PCR product size (1.2kb) to be amplified in a high background of cellular DNA, with imperfect PCR conditions due to the presence of cellular ions. It was therefore decided to use primer pair tRNA7for and tRNA7rev (Chapter 2, Appendix 2) to amplify the tRNA7 gene. This amplified a very small product (68bp; B.Ebrahimi, unpublished data), which required the use of a 3% TAE agarose gel to differentiate the PCR products from the primer complexes. This primer pair also amplified other multiple larger bands non-specifically, which led to uncertainty in the interpretation of the PCR analysis. Recombinant MHV-76/tRNA7+8insert viruses were purified using primer pair tRNA7for and tRNA7rev to select for viruses containing tRNA7, and a single purified viral plaque was used to infect a

TC 175cm^2 flask of BHK-21 cells, to prepare DNA for Southern analysis and PCR (see 2.2.19).

5.5. Molecular characterisation of recombinant viruses

5.5.1. Southern analysis of recombinant viruses.

DNA was made from BHK-21 cells infected with MHV-76, MHV-68, MHV-76(cA8+)M2$\Delta_{4336\text{-}4339}$, MHV-76(cA8+)M2$\Delta_{4239\text{-}4494}$, MHV-76/M2insert and MHV-76/tRNA7+8insert (see 2.2.19) and Southern analysis was performed using diagnostic *Hin*dIII, *Hin*cII and *Bcl*I digestions (see 2.2.20). The *Hin*dIII digests were then probed with a ^{32}P-radiolabelled cA8 probe. The cA8 probe identifies the MHV-68 *Hin*dIII fragments B, C, E, G, I, J, N, S, T_2, U_2 and Z_2 (see Figure 3.7.2.2). Southern analysis showed that the recombinant viruses MHV-76(cA8+)M2$\Delta_{4336\text{-}4339}$ and MHV-76(cA8+)M2$\Delta_{4239\text{-}4494}$ yielded identical profiles to MHV-68, containing the *Hin*dIII fragments B, C, E, G, I, J and N (Figure 5.5.1.1A). The *Hin*dIII E fragment of recombinant virus MHV-76(cA8+)M2$\Delta_{4239\text{-}4494}$ appeared slightly smaller than in MHV-68 due to the 256bp deletion. The *Hin*dIII fragments S and Z_2 were too small to be visualised on the blot, and fragments containing the terminal repeats (U_2^+ and T_2^+) appear as high molecular weight products with laddering. In MHV-76, the *Hin*dIII E and U_2 fragments are deleted, and the truncated *Hin*dIII J fragment (JΔ) becomes bound to the terminal repeats and is visualised as a high molecular weight product (JΔ$^+$). The MHV-76/tRNA7+8insert virus contains a larger *Hin*dIII J fragment (2.7kb), which is bound to the terminal repeats and thus has an identical profile to MHV-76 (the Southern analysis of this virus is slightly obscured by smearing of the DNA). The MHV-76/M2insert virus contains a normal *Hin*dIII G fragment, a truncated *Hin*dIII J fragment (2.3kb) and 3.3kb *Hin*dIII E fragment bound to the terminal repeats (and thus observed as a high molecular weight product). The truncated 2.3kb *Hin*dIII J fragment was not observed on the blot, despite prolonged exposure (data not shown).

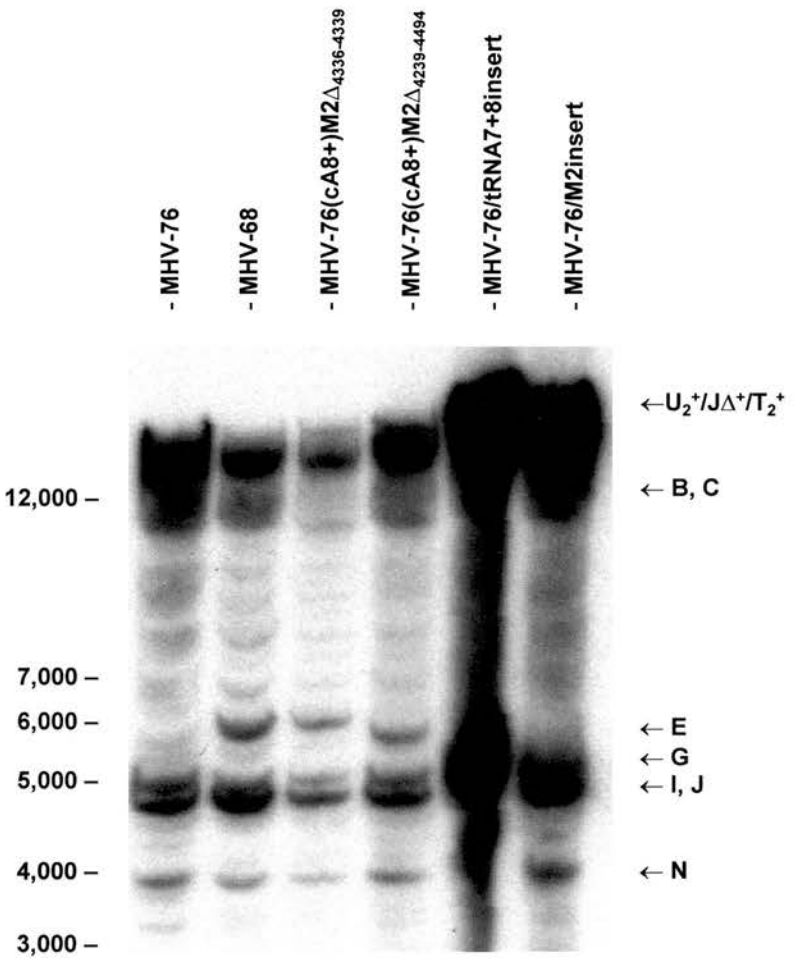

Figure 5.5.1.1A Southern analysis of recombinant viruses. DNA was isolated from BHK-21 cells infected with MHV-76, MHV-68, MHV-76(cA8+)M2$\Delta_{4336\text{-}4339}$, MHV-76(cA8+)M2$\Delta_{4239\text{-}4494}$, MHV-76/tRNA7+8insert and MHV-76/M2insert. The DNA was digested with *Hin*dIII and analysed by Southern blot on a 0.8% TAE agarose gel. The blot was hybridised with a ^{32}P-labelled probe of cosmid A8. The sizes of molecular weight markers in bp are shown on the left, and *Hin*dIII fragments on the right side of the autoradiograph.

To visualise the *Hin*dIII E and J fragments more easily, the *Hin*dIII digest was probed with a ^{32}P-radiolabelled M3 probe (nucleotides 6060-7277; see Figure 3.7.2.2). The results showed that the correct sized *Hin*dIII E and J fragments were present in MHV-68 and the recombinant viruses MHV-76(cA8+)M2$\Delta_{4336\text{-}4339}$ and MHV-76(cA8+)M2$\Delta_{4239\text{-}4494}$ (Figure 5.5.1.1B). The *Hin*dIII E fragment of recombinant virus MHV-76(cA8+)M2$\Delta_{4239\text{-}4494}$ appeared slightly smaller than in MHV-68 due to the 256bp deletion. As expected, the M3 probe did not hybridise with MHV-76 and MHV-76/tRNA7+8insert viral DNA. The M3 probe was expected to hybridise with the truncated *Hin*dIII J fragment (2.3kb) and 3.3kb *Hin*dIII E fragment bound to the terminal repeats present in MHV-76/M2insert. However, despite prolonged exposure, no evidence of this was seen.

To determine that the recombinant viruses had been satisfactorily purified so that no MHV-76 contamination was present, recombinant viral DNA was digested with *Hin*cII and *Bcl*I, and Southern analysis was performed using a ^{32}P-radiolabelled probe of 76LHE (nucleotides 9538-12563). Figure 5.5.1.2 shows that the 76LHE probe hybridised with the expected 1.4kb and 3.1kb *Hin*cII fragments and the 7.2kb *Bcl*I fragment in MHV-68 viral DNA. Figure 5.5.1.5 details the restriction map of the left end of MHV-68 for the enzymes *Hin*cII and *Bcl*I. In MHV-76, the 3.1kb *Hin*cII fragment is present but the 1.4kb *Hin*cII and 7.2kb *Bcl*I fragments become truncated and bound to the terminal repeats, and thus appear as a ladder of closely spaced high molecular weight bands. Recombinant virus MHV-76(cA8+)M2$\Delta_{4336\text{-}4339}$ yielded an identical profile to MHV-68, indicating that this virus was pure and free from MHV-76 contamination. However, recombinant virus MHV-76(cA8+)M2$\Delta_{4239\text{-}4494}$ exhibited a very similar profile to MHV-68, but also contained a ladder of closely spaced higher molecular weight bands indicating that this recombinant virus was contaminated with a small amount of MHV-76. MHV-76/tRNA7+8insert and MHV-76/M2insert displayed identical profiles to MHV-76, and did not show the expected novel fragments (3.6kb *Hin*cII and 4.7kb *Bcl*I fragments in MHV-76/M2insert; 2.4kb *Hin*cII and 3.5kb *Bcl*I fragments in MHV-76/tRNA7+8insert;

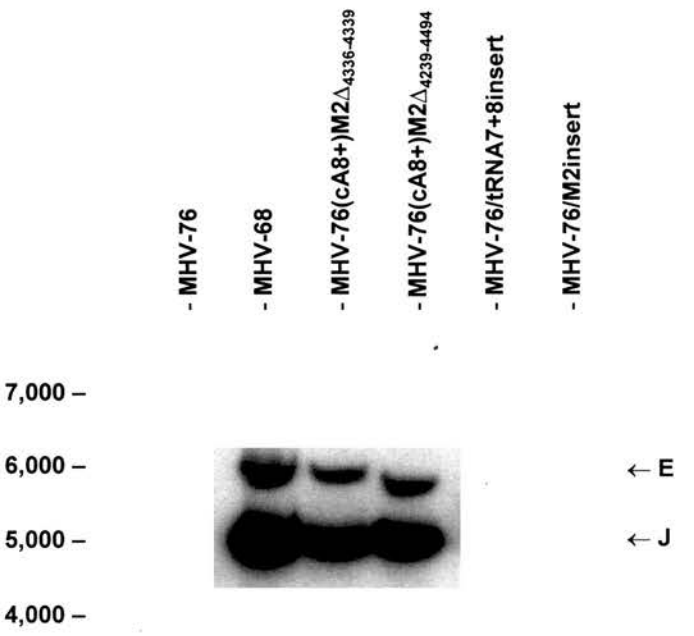

Figure 5.5.1.1B Southern analysis of recombinant viruses. DNA was isolated from BHK-21 cells infected with MHV-76, MHV-68, MHV-76(cA8+)M2$\Delta_{4336\text{-}4339}$, MHV-76(cA8+)M2$\Delta_{4239\text{-}4494}$, MHV-76/tRNA7+8insert and MHV-76/M2insert. The DNA was digested with *Hin*dIII and analysed by Southern blot on a 0.8% TAE agarose gel. The blot was hybridised with a ^{32}P-labelled probe of M3 (nucleotides 6060-7277). The sizes of molecular weight markers in bp are shown on the left, and *Hin*dIII fragments on the right side of the autoradiograph.

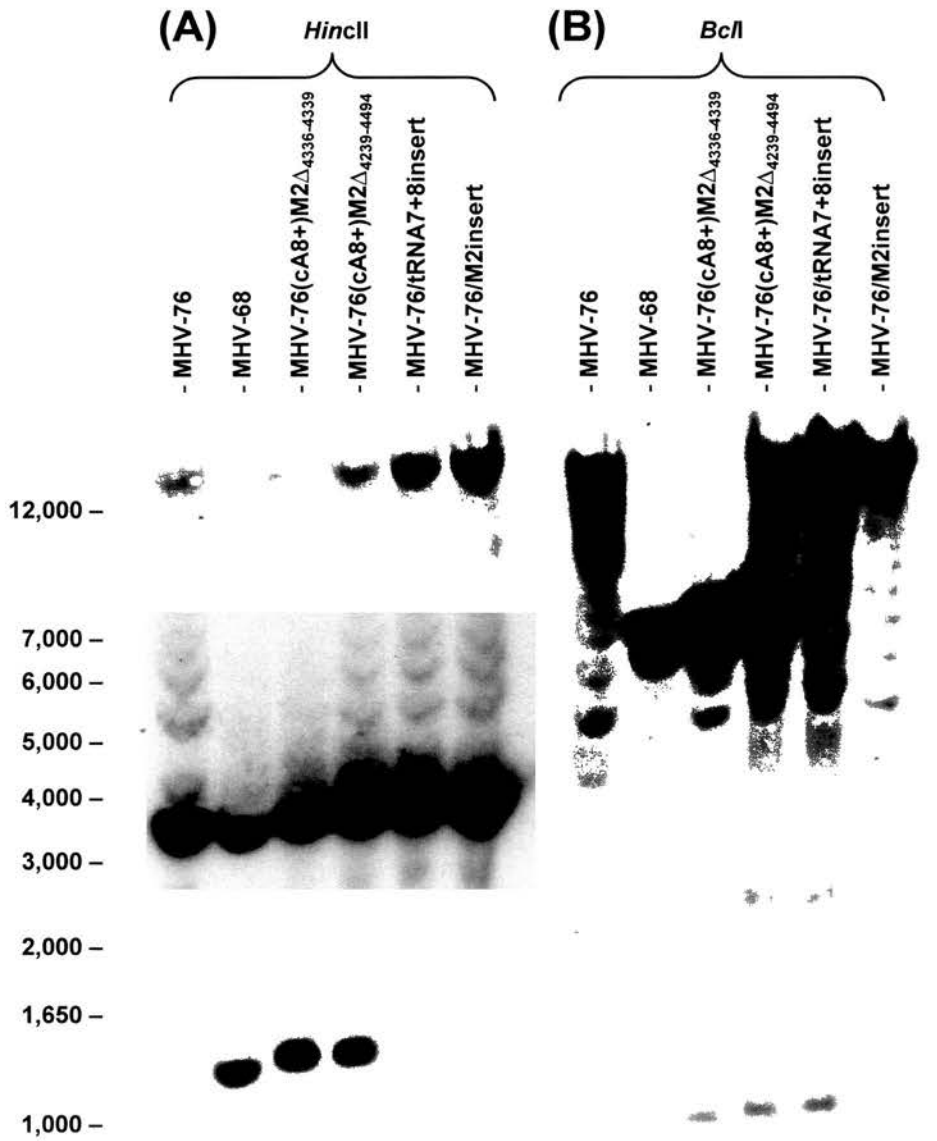

Figure 5.5.1.2 Southern analysis of recombinant viruses. DNA was isolated from BHK-21 cells infected with MHV-76, MHV-68, MHV-76(cA8+)M2$\Delta_{4336\text{-}4339}$, MHV-76(cA8+)M2$\Delta_{4239\text{-}4494}$, MHV-76/tRNA7+8insert and MHV-76/M2insert. The DNA was digested with *Hin*cII **(A)** and *Bcl*I **(B)** and analysed by Southern blot on a 0.8% TAE agarose gel. The blot was hybridised with a ^{32}P-labelled probe of 76LHE (nucleotides 9538-12563). The sizes of molecular weight markers in bp are shown on the left of the autoradiograph.

Figure 5.5.1.6). The recombinant viruses MHV-76/tRNA7+8insert and MHV-76/M2insert were thus predominantly composed of MHV-76 alone.

In order to characterise the recombinant viruses more completely, the *Hin*cII and *Bcl*I digests were probed with a ^{32}P-radiolabelled M2 probe (nucleotides 4000-4606). This probe identifies three MHV-68 fragments in the *Hin*cII digest (2.2kb, 354bp, 58bp) and two fragments in the *Bcl*I digest (1.2kb, and a 4.5kb fragment bound to the terminal repeats; Figure 5.5.1.5). Figure 5.5.1.3 shows that fragments of the expected size were visualised in MHV-68, with the exception of the 58bp *Hin*cII fragment that was too small to be visualised on the blot. This probe did not hybridise with any DNA in MHV-76 or MHV-76/tRNA7+8, consistent with the M2 ORF being absent in these viruses. In recombinant virus MHV-76(cA8+)M2$\Delta_{4336\text{-}4339}$, the deletion also leads to the loss of the *Hin*cII site at position 4337 and thus the 58bp and 354bp fragments become incorporated into a novel fragment of 408bp (Figure 5.5.1.5). In recombinant virus MHV-76(cA8+)M2$\Delta_{4239\text{-}4494}$, the substantial deletion in this virus leads to loss of the *Hin*cII sites at positions 4337 and 4279, and the *Bcl*I site at 4464 (Figure 5.5.1.5). Thus the *Hin*cII 58bp, 354bp and 2.2kb fragments become incorporated into one novel 2.3kb fragment, and the *Bcl*I 1.2kb fragment is lost and becomes incorporated into the fragment bound to the terminal repeats. The expected profiles were observed for both recombinant viruses MHV-76(cA8+)M2$\Delta_{4336\text{-}4339}$ and MHV-76(cA8+)M2$\Delta_{4239\text{-}4494}$ (Figure 5.5.1.3). The M2 probe was also expected to hybridise with three *Hin*cII fragments (58bp, 350bp and a 1.3kb fragment bound to the terminal repeats) and two *Bcl*I fragments (1.2kb and 1.5kb bound to the terminal repeats) in the recombinant virus MHV-76/M2insert (Figure 5.5.1.6). However, despite prolonged exposure, no evidence of this was seen (Figure 5.5.1.3).

The *Hin*cII and *Bcl*I digests were also probed with a ^{32}P-radiolabelled tRNA7+8 probe (nucleotides 4623-5806). This probe identifies two MHV-68 fragments in the *Hin*cII digest (2.5kb and 354bp) and two fragments in the *Bcl*I digest (1.2kb and 7.2kb; Figure 5.5.1.5). Figure 5.5.1.4 shows that fragments of the expected size were visualised in MHV-68, with weak hybridisation to the

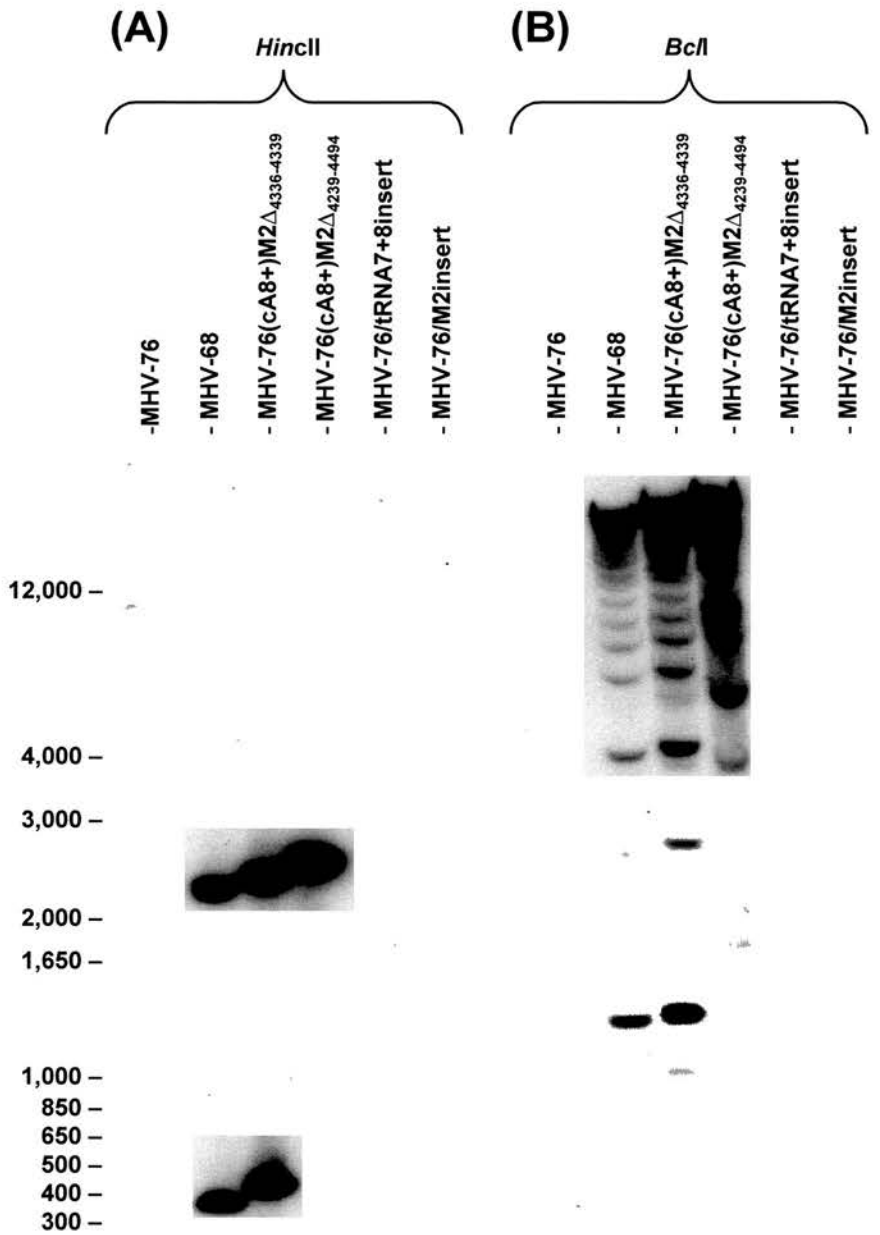

Figure 5.5.1.3 Southern analysis of recombinant viruses. DNA was isolated from BHK-21 cells infected with MHV-76, MHV-68, MHV-76(cA8+)M2$\Delta_{4336\text{-}4339}$, MHV-76(cA8+)M2$\Delta_{4239\text{-}4494}$, MHV-76/tRNA7+8insert and MHV-76/M2insert. The DNA was digested with *Hinc*II **(A)** and *Bcl*I **(B)** and analysed by Southern blot on a 0.8% TAE agarose gel. The blot was hybridised with a ^{32}P-labelled probe of M2 (nucleotides 4000-4606). The sizes of molecular weight markers in bp are shown on the left of the autoradiograph.

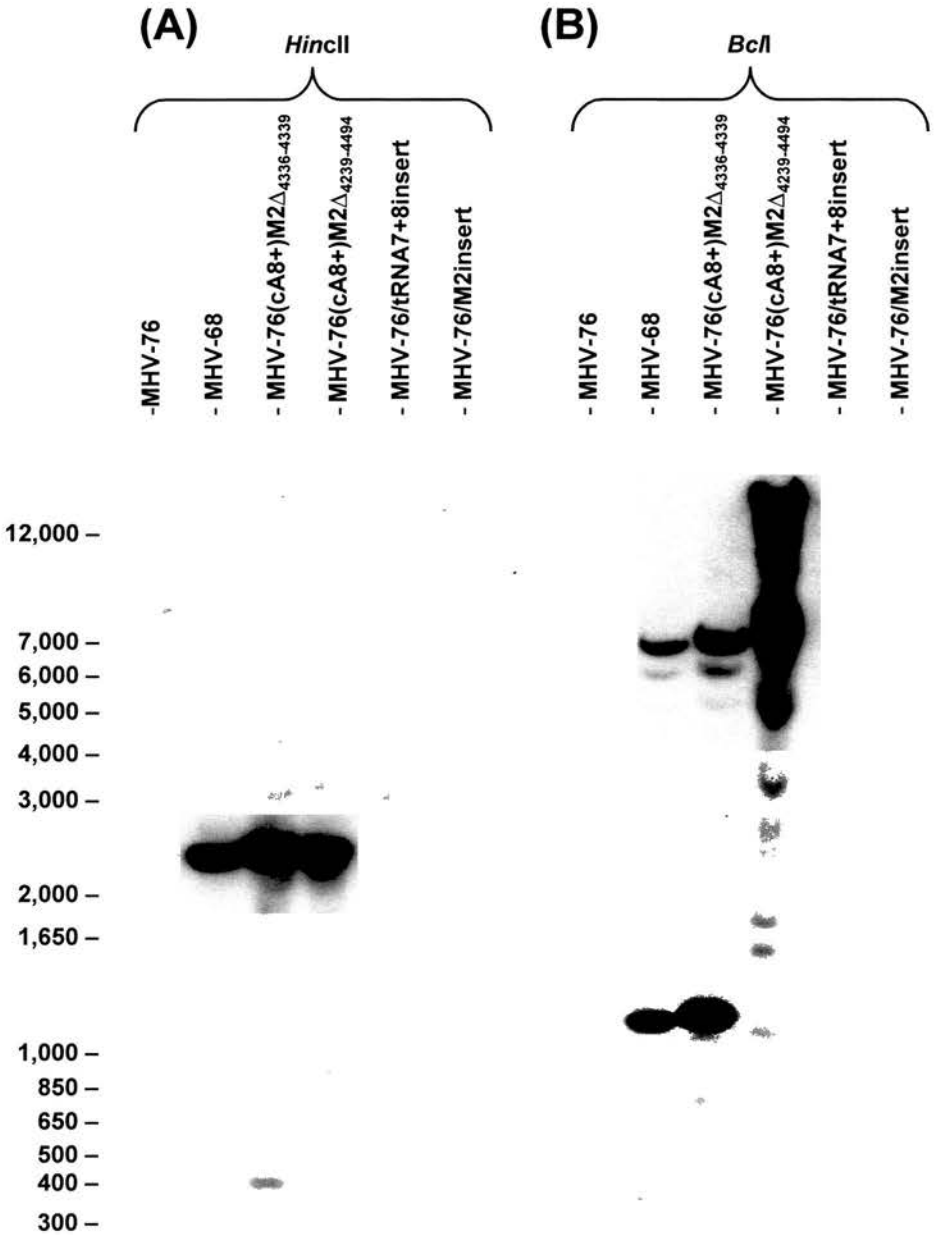

Figure 5.5.1.4 Southern analysis of recombinant viruses. DNA was isolated from BHK-21 cells infected with MHV-76, MHV-68, MHV-76(cA8+)M2$\Delta_{4336\text{-}4339}$, MHV-76(cA8+)M2$\Delta_{4239\text{-}4494}$, MHV-76/tRNA7+8insert and MHV-76/M2insert. The DNA was digested with *Hinc*II **(A)** and *Bcl*I **(B)** and analysed by Southern blot on a 0.8% TAE agarose gel. The blot was hybridised with a ^{32}P-labelled probe of tRNA7+8 insert (nucleotides 4623-5806). The sizes of molecular weight markers in bp are shown on the left of the autoradiograph.

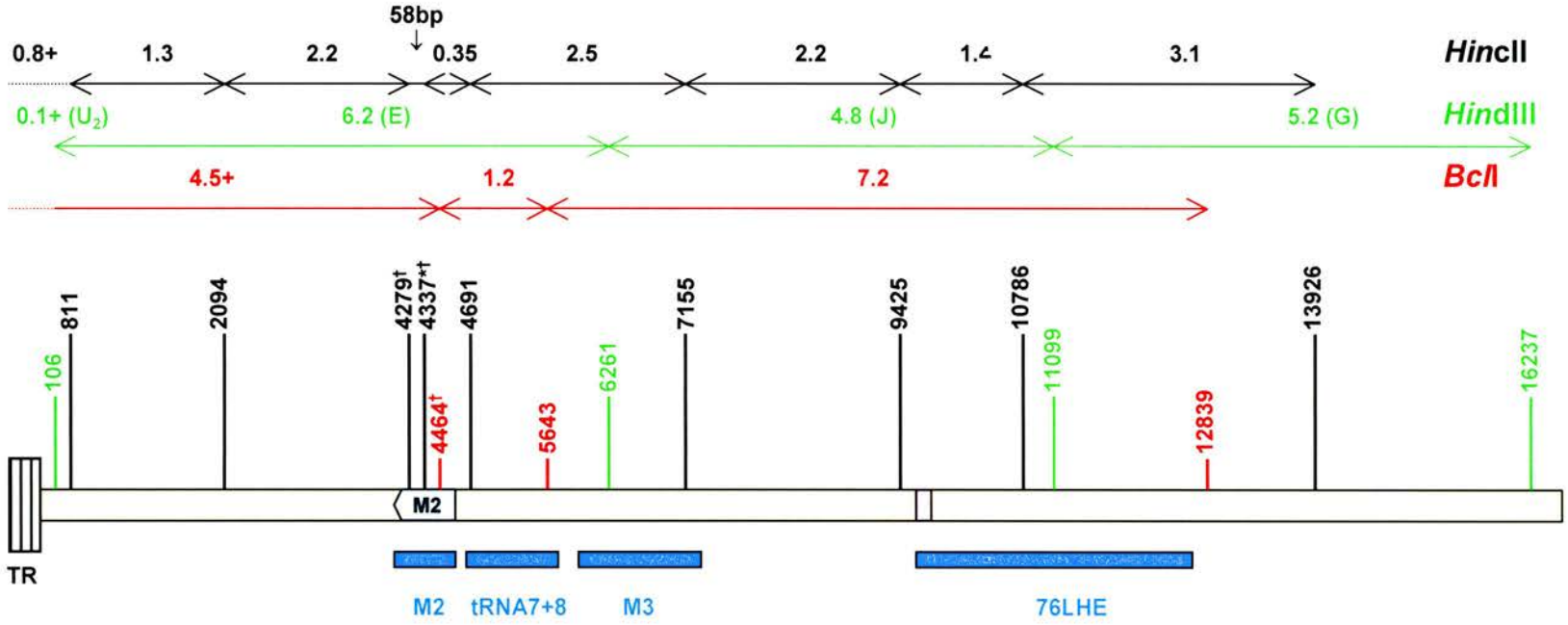

Figure 5.5.1.5 Interpretation of Southern analysis for recombinant viruses MHV-76(cA8+)M2$\Delta_{4336\text{-}4339}$ and MHV-76(cA8+)M2$\Delta_{4239\text{-}4494}$. 17kb at the left end of the unique region of the MHV-68 genome is shown, with the M2 ORF shown in blue, the terminal repeats (TR) in black vertical bars and the left end of the MHV-76 genome in purple (position 9538). Restriction enzyme sites for *Bcl*I (red), *Hin*dIII (green) and *Hin*cII (black) are shown, with the fragment sizes in kb above and *Hin*dIII fragment designation in brackets. + denotes fragments that are bound to the terminal repeats in MHV-68 and thus appear as a ladder of larger bands on Southern blot. * denotes the *Hin*cII restriction enzyme site deleted in MHV-76(cA8+)M2$\Delta_{4336\text{-}4339}$, and † denotes the restriction enzyme sites deleted in MHV-76(cA8+)M2$\Delta_{4239\text{-}4494}$.The location of probes used in Southern analysis is shown underneath by blue bars: M2 (4000-4606), tRNA7+8 (4623-5806), M3 (6060-7277) and 76LHE (9538-12563). Genomic co-ordinates are given according to Virgin *et al.*,1997.

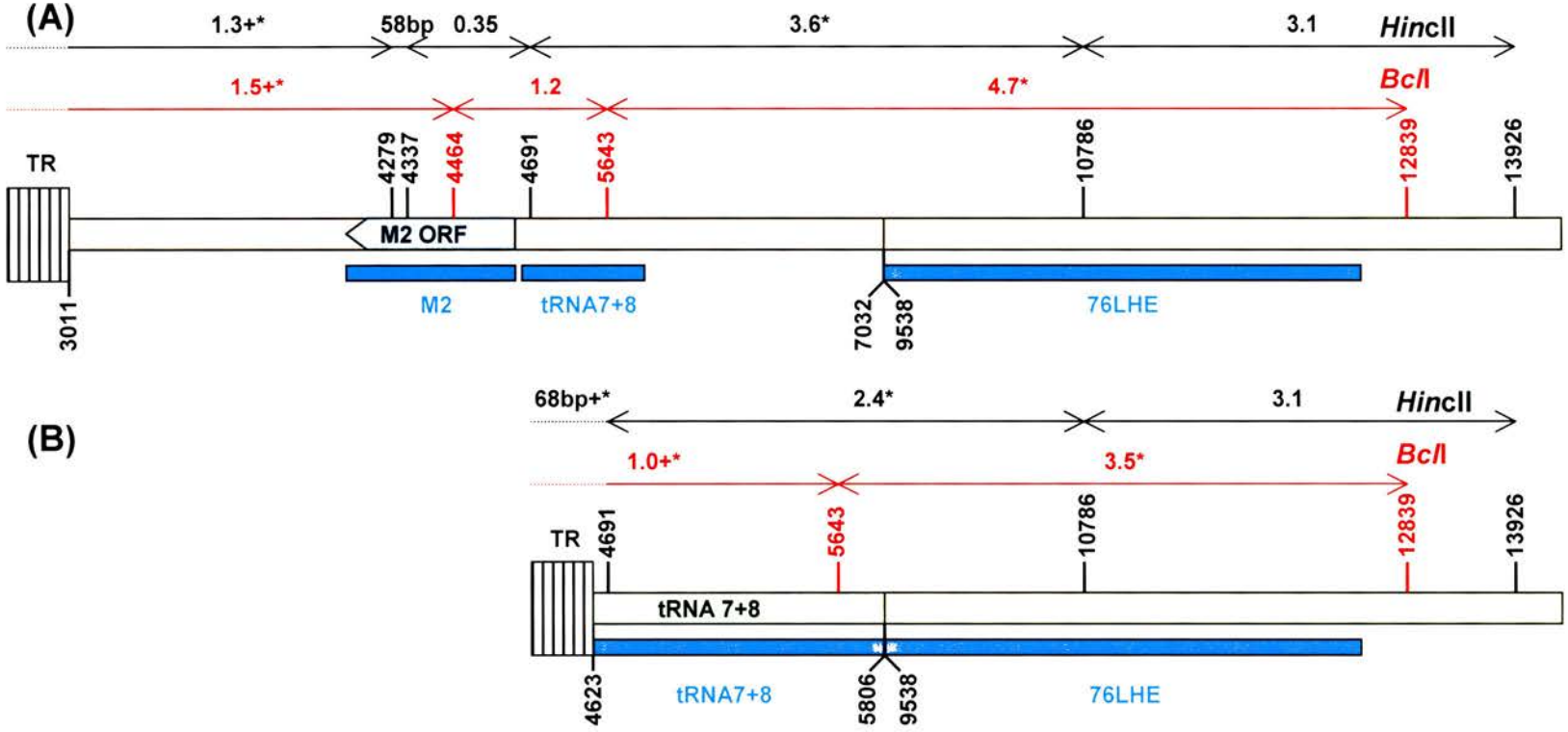

Figure 5.5.1.6 Predicted structure and restriction enzyme sites for recombinant viruses MHV-76/M2insert **(A)** and MHV-76/tRNA7+8 insert **(B)**. The left end of the MHV-76 genome is shown in yellow, with the M2 ORF in pale blue, the M2 insert (3011-7032) in orange, the tRNA7+8 insert (4623-5806) in green and the terminal repeats (TR) in black bars. Restriction enzyme sites for *Bcl*I (red) and *Hin*cII (black) are shown, with the fragment sizes above. + denotes fragments that are bound to the terminal repeats and thus appear as a ladder of larger bands on Southern blot. * denotes novel fragments that do not appear in the MHV-68 or MHV-76 restriction enzyme maps (see Figure 5.5.1.5). The location of probes used in the Southern analysis is shown underneath by blue bars; M2 (4000-4606), tRNA7+8 (4623-5806) and 76LHE (9538-12563). Genomic co-ordinates are given according to Virgin *et al.*, 1997.

354bp *Hin*cII fragment due to the small region (68bp) of cross-hybridisation. As expected, the tRNA7+8 probe did not hybridise with any DNA in MHV-76. In recombinant virus MHV-76(cA8+)M2$\Delta_{4336\text{-}4339}$, the loss of the *Hin*cII site at position 4337 led to the incorporation of the 354bp fragment into a novel fragment which was visualised at 408bp on the *Hin*cII digest (Figure 5.5.1.4). In recombinant virus MHV-76(cA8+)M2$\Delta_{4239\text{-}4494}$, the substantial deletion in this virus leads to loss of the *Hin*cII sites at positions 4337 and 4279, and the *Bcl*I site at 4464 (Figure 5.5.1.5). Thus the *Hin*cII 58bp, 354bp and 2.2kb fragments become incorporated into one novel 2.3kb fragment (appearing at the same region as the 2.5kb fragment). The *Bcl*I 1.2kb fragment is lost and becomes incorporated into the fragment bound to the terminal repeats. The expected profiles were observed for both recombinant viruses MHV-76(cA8+)M2$\Delta_{4336\text{-}4339}$ and MHV-76(cA8+)M2$\Delta_{4239\text{-}4494}$ (Figure 5.5.1.4), with minor bands present in the *Bcl*I digest due to partial digestion. The tRNA7+8 probe was also expected to hybridise with two *Hin*cII fragments (354bp and 3.6kb) and two *Bcl*I fragments (1.2kb and 4.7kb) in the MHV-76/M2insert virus, and two *Hin*cII fragments (2.4kb and 68bp bound to the terminal repeats) and two *Bcl*I fragments (3.5kb and 1.0kb bound to the terminal repeats) in the MHV-76/tRNA7+8insert virus (Figure 5.5.1.6). However, despite prolonged exposure, no evidence of this was seen (Figure 5.5.1.4).

The results of Southern analysis of the four recombinant viruses revealed that virus MHV-76(cA8+)M2$\Delta_{4336\text{-}4339}$ (containing a 4bp deletion in the M2 ORF) was a pure viral population containing the expected genomic composition. Recombinant virus MHV-76(cA8+)M2$\Delta_{4239\text{-}4494}$ (containing a 256bp deletion in the M2 ORF) also contained the expected genomic organisation, but was contaminated with a small amount of MHV-76 and was therefore not a pure viral population. Recombinant viruses MHV-76/M2insert and MHV-76/tRNA7+8insert appeared to be identical MHV-76, and contained no inserted sequences.

5.5.2. PCR analysis of recombinant viruses.

To fully characterise the recombinant viruses, recombinant virus DNA was analysed by PCR (see 2.2.1). Primers were used to amplify MHV-68 specific ORFs (see Chapter 2, Appendix 2) including M1 (M1for and M1rev primers), M2 (M2GEX1 and M2GEX2 primers), M3 (M3+ and M3- primers), M4 (M4A and M4B primers) and tRNA7 (tRNA7for and tRNA7rev primers). As a control to check for template DNA integrity and concentration, primers for ORF74 (GCR-5' and GCR-3' primers) were used to amplify the GPCR sequence present in all virus samples. Figure 5.5.2.1A shows that M1, M2, M3 and M4 were all present in the recombinant viruses MHV-76(cA8+)M2$\Delta_{4336\text{-}4339}$ and MHV-76(cA8+)M2$\Delta_{4239\text{-}4494}$, as well as the GPCR coding sequence. The M2 ORF is reduced in size in virus MHV-76(cA8+)M2$\Delta_{4239\text{-}4494}$, consistent with previous results (see Figure 5.3.2.1). Figure 5.5.2.1B shows that the GPCR region was amplified in recombinant viruses MHV-76/M2insert and MHV-76/tRNA7+8insert, indicating that viral DNA was present. The M2 ORF was also present in MHV-76/M2insert, but not present in MHV-76/tRNA7+8insert, and the M1, M3 and M4 genes were all absent in these viruses. The region amplified by the M3+ and M3- primers (nucleotides 6566-6946; Chapter 2, Appendix 2) is present within the M2insert sequence (nucleotides 3011-7032; see Figure 5.2.1) but was not amplified, showing that this region was not present in the MHV-76/M2insert virus.

Analysis of recombinant viruses by PCR for the vtRNA7 gene showed that this was present in MHV-68 as well as recombinant viruses MHV-76(cA8+)M2$\Delta_{4336\text{-}4339}$, MHV-76(cA8+)M2$\Delta_{4239\text{-}4494}$ and MHV-76/M2insert (Figure 5.5.2.2). The vtRNA7 gene was not present in MHV-76/tRNA7+8. In addition, the M2 ORF in recombinant viruses MHV-76(cA8+)M2$\Delta_{4336\text{-}4339}$ and MHV-76(cA8+)M2$\Delta_{4239\text{-}4494}$ was amplified using primer pair M2GEX1 and M2GEX2 (Chapter 2, Appendix 2) with *PfuTurbo*™ DNA polymerase, inserted into the pKS(-) vector (Chapter 2, Appendix 3) using the *Bam*HI and *Eco*RI restriction enzyme sites, and the sequence was determined (see 2.2.24). Sequence

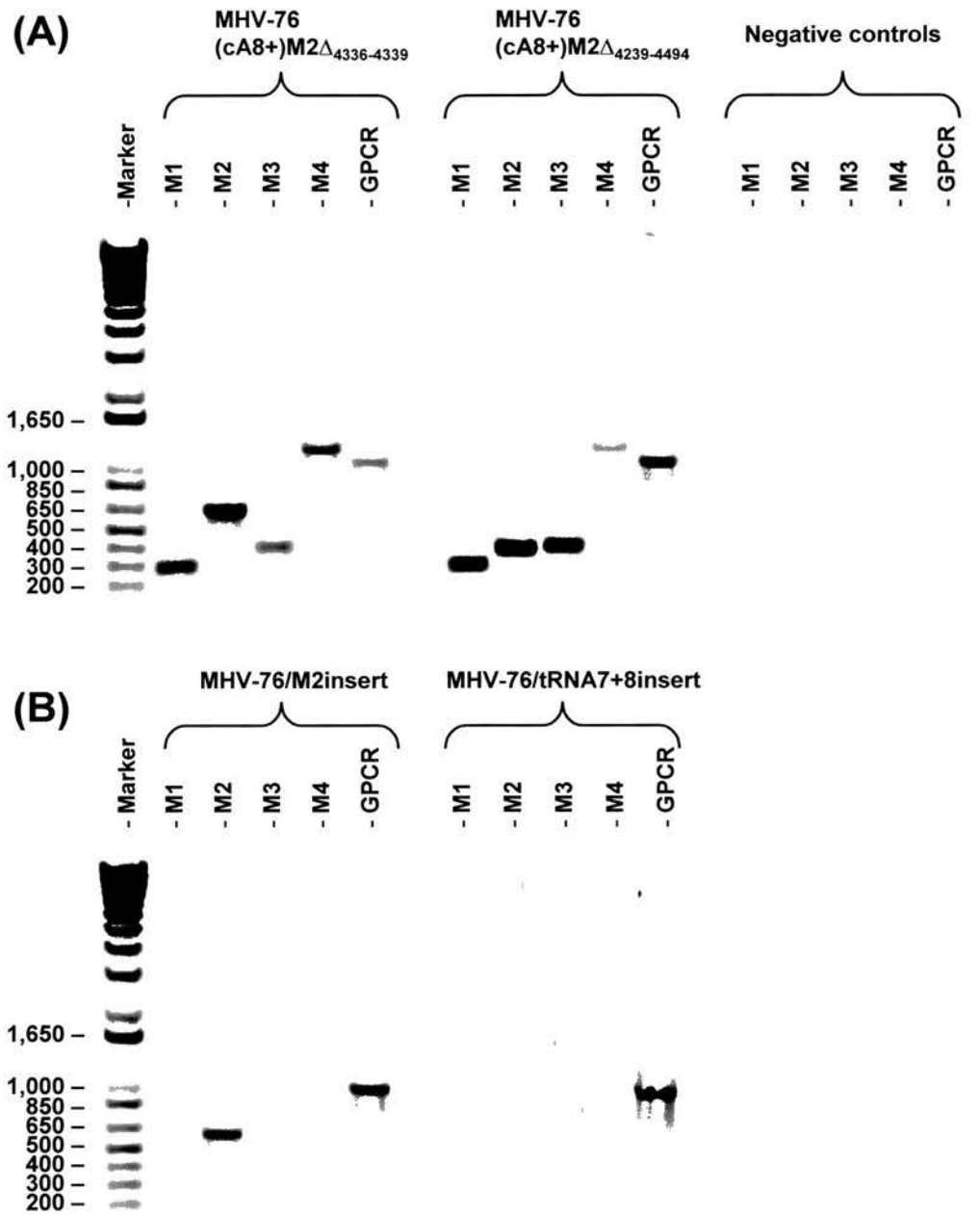

Figure 5.5.2.1 PCR analysis of viral DNA from recombinant viruses **(A)** MHV-76(cA8+)M2$\Delta_{4336\text{-}4339}$ and MHV-76(cA8+)M2$\Delta_{4239\text{-}4494}$ and **(B)** MHV-76/M2insert and MHV-76/tRNA7+8insert. 40 cycles of PCR analysis was performed using primers specific for the unique MHV-68 genes M1, M2, M3 and M4 and also ORF 74 (GPCR). Template consisted of either 500ng of DNA isolated from infected BHK-21 cells or diH_20 (negative control reactions). The products were analysed on a 1% TAE agarose gel. The sizes of molecular weight markers in bp are shown on the left.

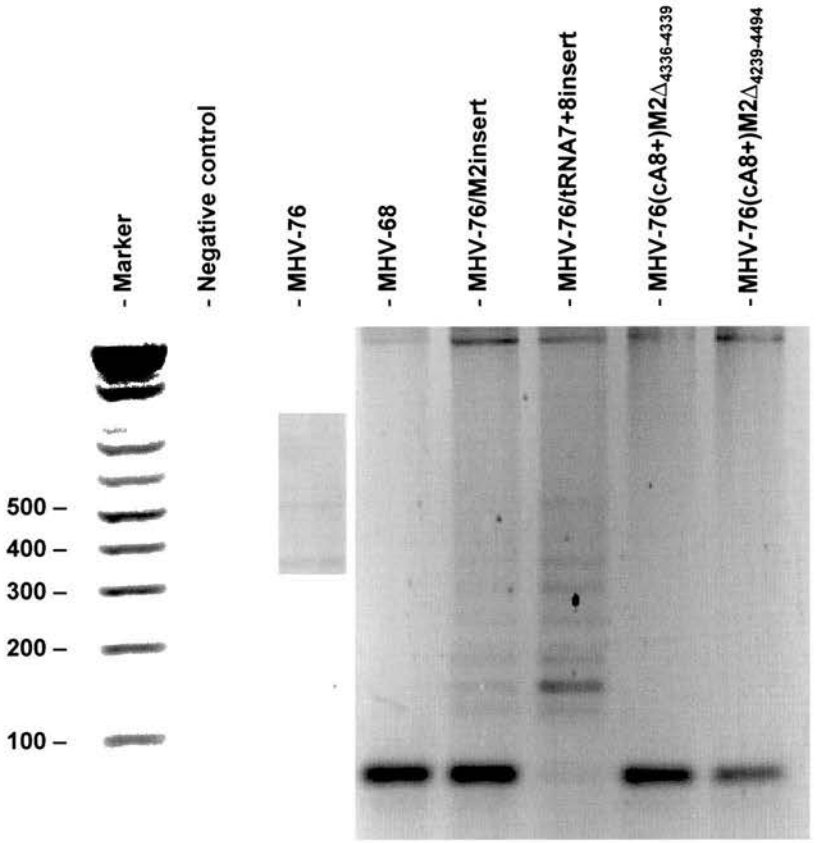

Figure 5.5.2.2 PCR analysis of viral DNA from MHV-76, MHV-68 and the recombinant viruses MHV-76(cA8+)M2$\Delta_{4336\text{-}4339}$, MHV-76(cA8+)M2$\Delta_{4239\text{-}4494}$, MHV-76/M2insert and MHV-76/tRNA7+8insert. 40 cycles of PCR analysis were performed using primers specific for vtRNA7. Template consisted of either 500ng of DNA isolated from infected BHK-21 cells or diH_20 (negative control reaction). The products were analysed on a 3% TAE agarose gel. The sizes of molecular weight markers in bp are shown on the left.

analysis showed that both viruses contained deletions in the M2 ORF identical to those observed in the parent cosmids (see Figure 5.3.2.2).

The results from Southern and PCR analysis of recombinant viral DNA revealed that viruses MHV-76(cA8+)M2$\Delta_{4336\text{-}4339}$ and MHV-76(cA8+)M2$\Delta_{4239\text{-}4494}$ were very similar to MHV-68, except for a 4bp and a 256bp deletion in the M2 ORF respectively. However, only virus MHV-76(cA8+)M2$\Delta_{4336\text{-}4339}$ had been successfully purified and was free from contamination with MHV-76. Recombinant virus MHV-76/M2insert contained the M2 ORF and the vtRNA7 gene, but only partial recombination had occurred as evidenced by the deletion of the region containing part of the M3 ORF. There was also contamination with MHV-76, such that none of the inserted sequences was detectable by Southern analysis. Recombinant virus MHV-76/tRNA7+8insert did not contain any of the desired insert, and was identical to MHV-76.

It was therefore decided to utilise recombinant virus MHV-76(cA8+)M2$\Delta_{4336\text{-}4339}$ (containing a 4bp deletion in M2) to assess the role of M2 in MHV-68 infection *in vitro* and *in vivo*. Comparison of this virus to MHV-76 (the parent virus) and MHV-76(cA8+)4 (the rescue virus generated in the same manner as the recombinant virus, and genetically and phenotypically identical to MHV-68; see Chapter 3) would enable assessment of the function of M2 in viral pathogenesis.

5.6. Preliminary results of the biological characterisation of recombinant viruses

5.6.1. Replication *in vitro*.

To investigate the effect of disruption of the M2 ORF on viral replication *in vitro*, the replication of MHV-76, MHV-76(cA8+)4 and MHV-76(cA8+)M2$\Delta_{4336\text{-}4339}$ was compared in BHK-21 cells. A single round of multiplication (one-step growth curve at a MOI of 5) showed that all viruses replicated at a similar rate *in vitro* (Figure 5.6.1.1). Studies using multiple rounds of growth (MOI of 0.01) also revealed that all viruses replicated with similar

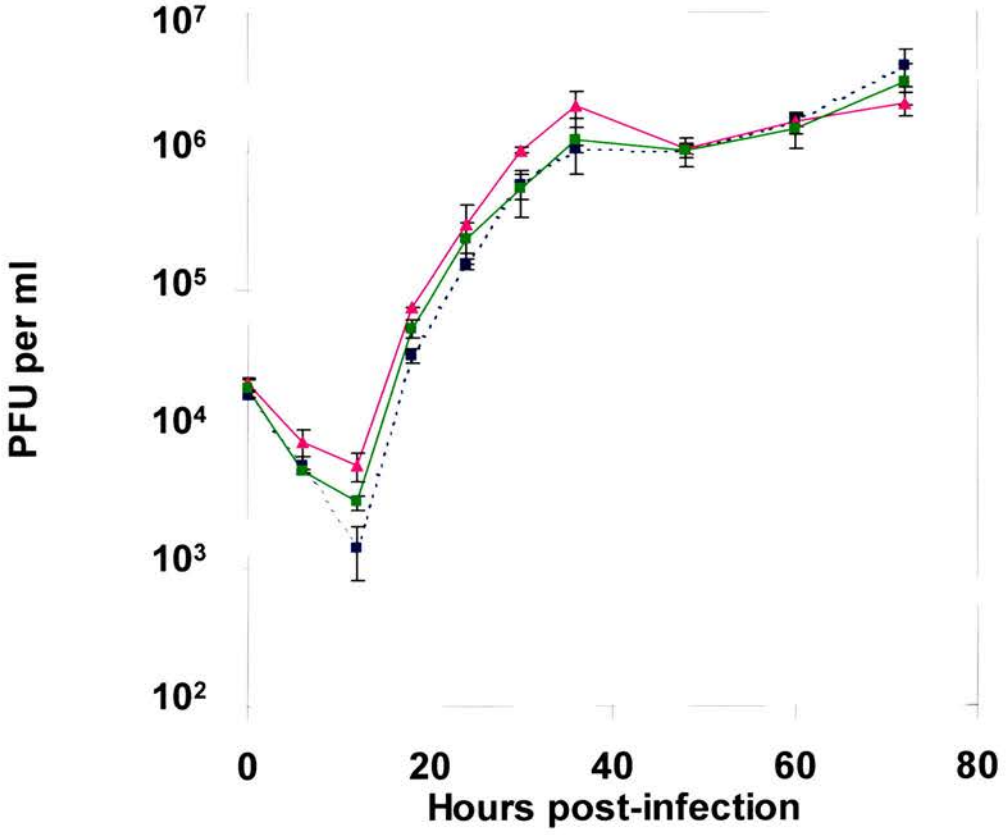

Figure 5.6.1.1 One step growth curve of MHV-76 (——▲——), MHV76(cA8+)4 (- - -■- - -) and MHV-76(cA8+)M2$\Delta_{4336\text{-}4339}$ (——■——) on BHK-21 cells at an MOI of 5. Data points are shown for virus titre $\log_{10}$ ± standard error.

kinetics and achieved comparable titres during replication in tissue culture (Figure 5.6.1.2). These results demonstrated that disruption of the M2 ORF has no effect on lytic replication in BHK-21 cells.

5.6.2. Replication in the lung.

BALB/c mice were infected with 2 x 10^5 PFU of MHV-76, MHV-76(cA8+)4 or MHV-76(cA8+)M2$\Delta_{4336\text{-}4339}$ intranasally, and the virus titre in the lungs was assessed at various timepoints post-infection by plaque assay (see 2.6.4). MHV-76(cA8+)M2$\Delta_{4336\text{-}4339}$ displayed peak viral titres in the lung at day 5 post-infection that were significantly higher than either MHV-76 or MHV-76(cA8+)4 (Figure 5.6.2)(Day 5 lung titre: MHV-76(cA8+)M2$\Delta_{4336\text{-}4339}$ vs. MHV-76(cA8+)4 or MHV-76; $P<0.001$). MHV-76 was cleared more rapidly from the lungs than MHV-76(cA8+)4 and MHV-76(cA8+)M2$\Delta_{4336\text{-}4339}$ at day 7 post-infection, in agreement with previous studies (see 3.8.2). This data therefore shows that disruption of the M2 ORF leads to significantly higher peak viral titres in the lung after intranasal infection, but has no effect on viral clearance from the lung when compared to a virus with an intact M2 ORF.

5.6.3. Virus-induced splenomegaly.

To determine the effect of disruption of the M2 ORF on splenomegaly during infection, BALB/c mice were infected with 2 x 10^5 PFU of MHV-76, MHV-76(cA8+)4 or MHV-76(cA8+)M2$\Delta_{4336\text{-}4339}$ intranasally. The extent of splenomegaly was determined using two independent measures, spleen weight (see 2.6.2) and determination of the total number of splenocytes (see 2.6.3). There was an increase in spleen weight (Figure 5.6.3.1) and total splenocyte numbers (Figure 5.6.3.2) after infection of mice with MHV-76(cA8+)M2$\Delta_{4336\text{-}4339}$ comparable with that observed following infection with MHV-76(cA8+)4, which peaked at day 14 post-infection. In agreement with previous studies (see 3.8.3), both MHV-76(cA8+)4 and MHV-76(cA8+)M2$\Delta_{4336\text{-}4339}$ demonstrated a much larger degree of splenomegaly compared to MHV-76. The spleen weights and total splenocyte numbers of mice infected with MHV-76(cA8+)M2$\Delta_{4336\text{-}4339}$

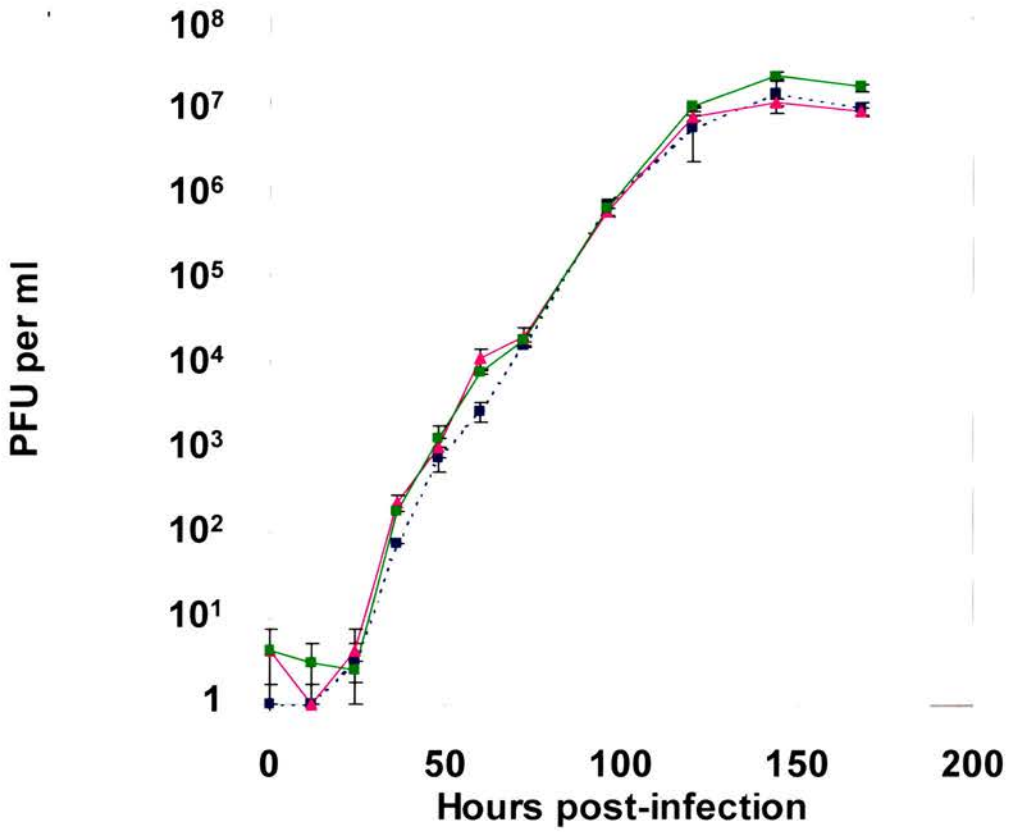

Figure 5.6.1.2 Multi step growth curve of MHV-76 (——▲——), MHV76(cA8+)4 (---■---) and MHV-76(cA8+)M2$\Delta_{4336\text{-}4339}$ (——■——) on BHK-21 cells at an MOI of 0.01. Data points are shown for virus titre $\log_{10} \pm$ standard error.

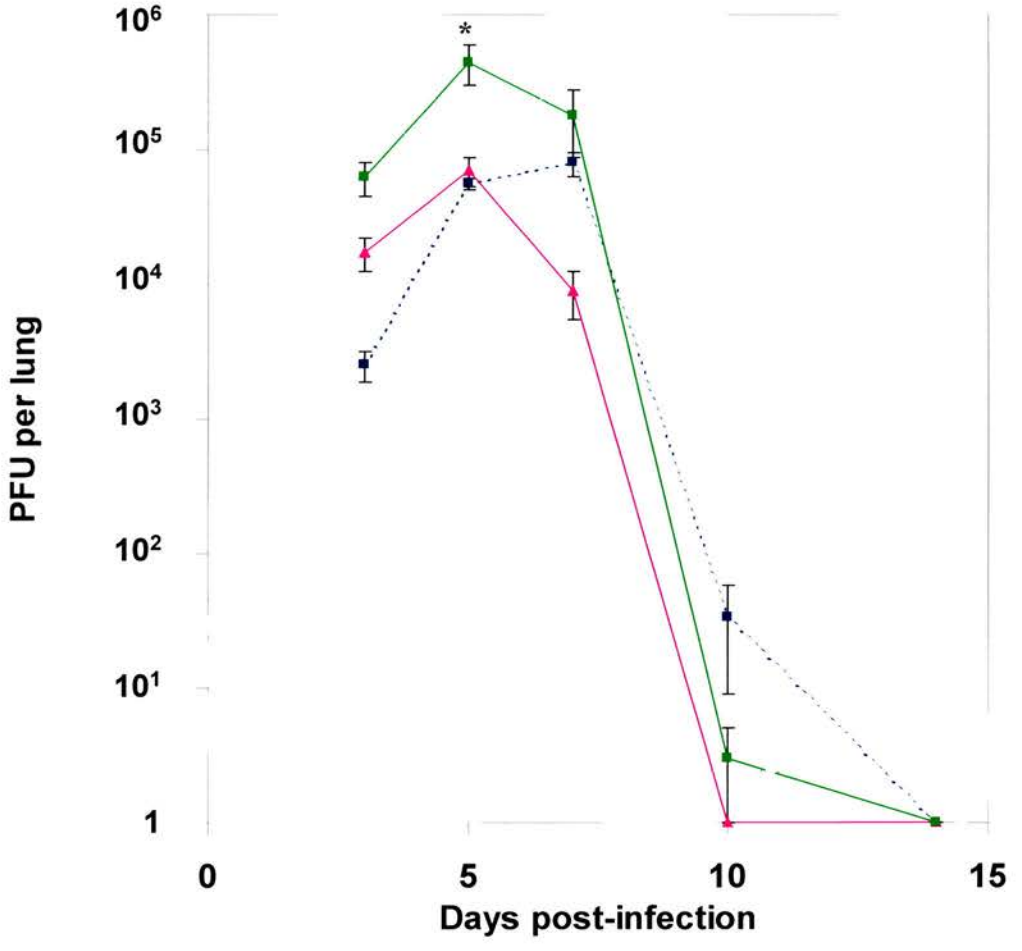

Figure 5.6.2 Viral titres in the lungs of BALB/c mice infected intranasally with 2 x 10^5 PFU of MHV-76 (——▲——), MHV76(cA8+)4 (--■--) and MHV-76(cA8+)M2$\Delta_{4336\text{-}4339}$ (——■——). Mean virus titre $\log_{10}$ per lung ± standard error for four mice per group is shown for each time point. * indicates statistically significant difference between peak viral titres at day 5 post-infection in mice infected with MHV-76(cA8+)M2$\Delta_{4336\text{-}4339}$ and mice infected with either MHV-76 or MHV76(cA8+)4 as determined by two-way ANOVA with Bonferroni post-tests.

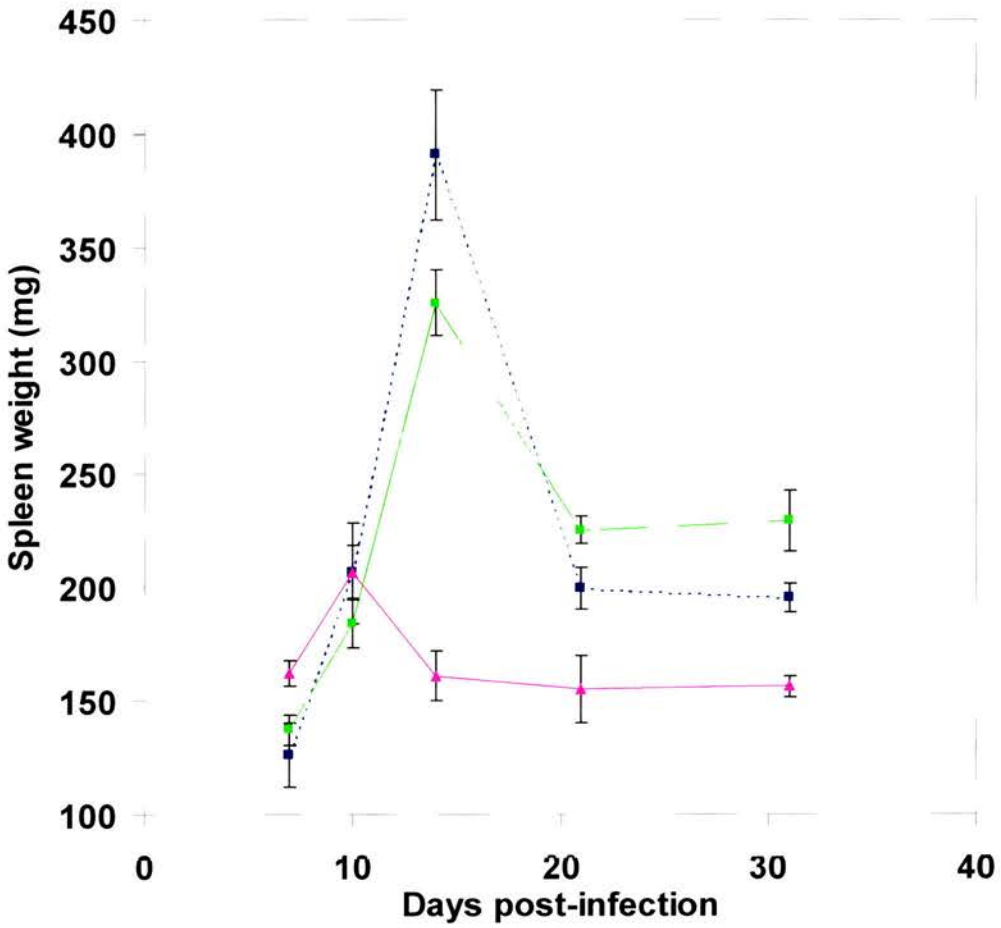

Figure 5.6.3.1 Spleen weights of BALB/c mice infected intranasally with 2 x 10^5 PFU of MHV-76 ( ), MHV76(cA8+)4 ( ) and MHV-76(cA8+)M2$\Delta_{4336\text{-}4339}$ ( ). Mean spleen weight (mg) ± standard error is shown for four mice per group for each time point.

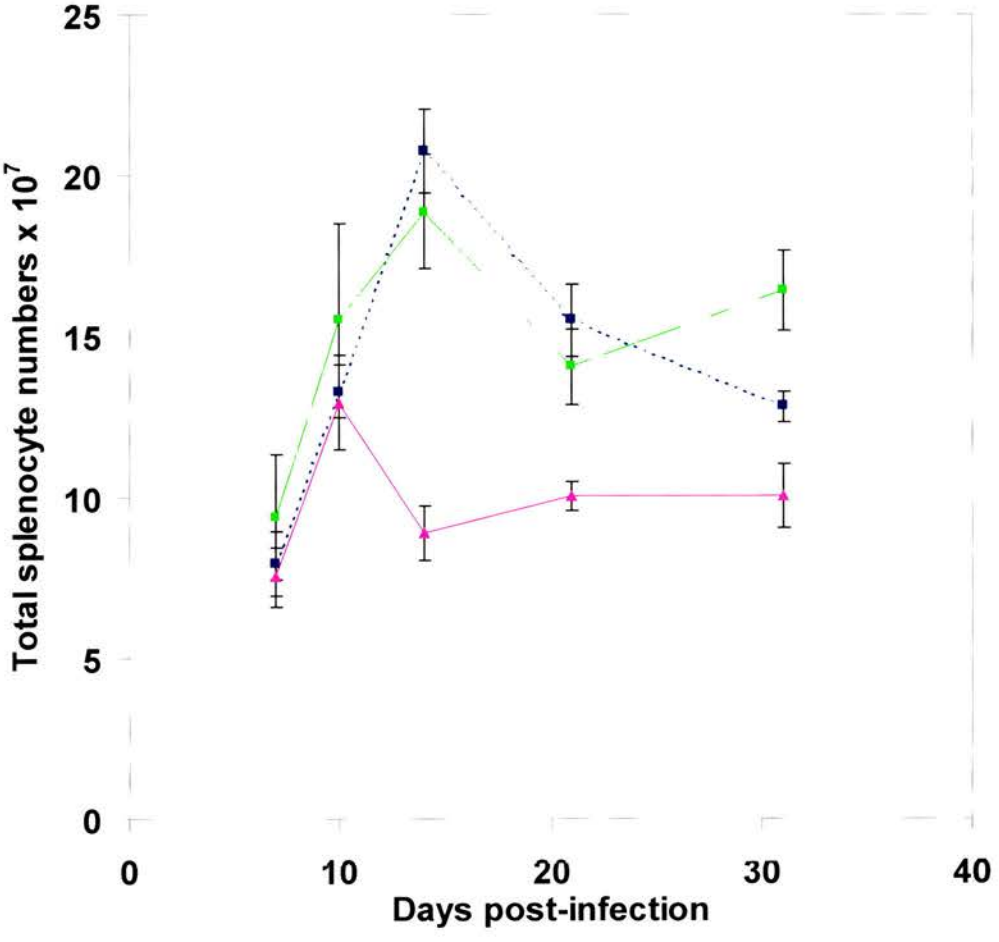

Figure 5.6.3.2 Total splenocyte numbers of BALB/c mice infected intranasally with 2 x 10^5 PFU of MHV-76 (—▲—), MHV76(cA8+)4 (- -■- -) and MHV-76(cA8+)M2$\Delta_{4336\text{-}4339}$ (—■—). Mean total number of splenocytes ± standard error is shown for four mice per group for each time point.

remained higher than those of mice infected with MHV-76(cA8+)4 at 31 days post-infection, although these results were not statistically significant. This data therefore shows that disruption of the M2 ORF does not lead to any impairment in the viral induction of splenomegaly when compared to a virus with an intact M2 ORF, although there may be possible evidence that the resolution of splenomegaly is more protracted.

5.6.4. Latent virus in the spleen.

BALB/c mice were infected with 2 x 10^5 PFU of MHV-76, MHV-76(cA8+)4 or MHV-76(cA8+)M2$\Delta_{4336\text{-}4339}$ intranasally, and the amount of latent virus in the spleen was quantitated at various timepoints post-infection by infective centre assay (see 2.6.3). Figure 5.6.4 shows that mice infected with MHV-76(cA8+)4 showed high levels of latent virus in the spleen, peaking at day 14 post-infection. Mice infected with MHV-76 showed much lower levels of latent virus in the spleen, but this latent virus was still detectable up to 31 days post-infection. These results are in agreement with previous studies (see 3.8.4). However, mice infected with MHV-76(cA8+)M2$\Delta_{4336\text{-}4339}$ showed low levels of latent virus in the spleen at day 10, and these levels then gradually rose during the time course of this experiment until the highest levels were observed at day 31 post-infection. There was no peak of latent virus detectable in the spleen during the height of splenomegaly observed at day 14 post-infection in mice infected with MHV-76(cA8+)M2$\Delta_{4336\text{-}4339}$. The difference in the amount of latent virus detectable in the spleens of mice infected with MHV-76(cA8+)4 or MHV-76(cA8+)M2$\Delta_{4336\text{-}4339}$ was statistically significant (MHV-76(cA8+)M2$\Delta_{4336\text{-}4339}$ vs. MHV-76(cA8+)4;Day 14, $P<0.001$; Day 31, $P<0.05$).

There was a possibility that the latent virus detectable in the spleens of mice infected with MHV-76(cA8+)M2$\Delta_{4336\text{-}4339}$ might be due to genetic recombination in these viruses leading to the production of virus more competent at establishing latency. This might occur by mutation at a second site in the M2 ORF, or by the insertion of a single nucleotide in the 4bp deletion to abolish the frame-shift mutation, and thus giving rise to pseudorevertant viruses. To examine

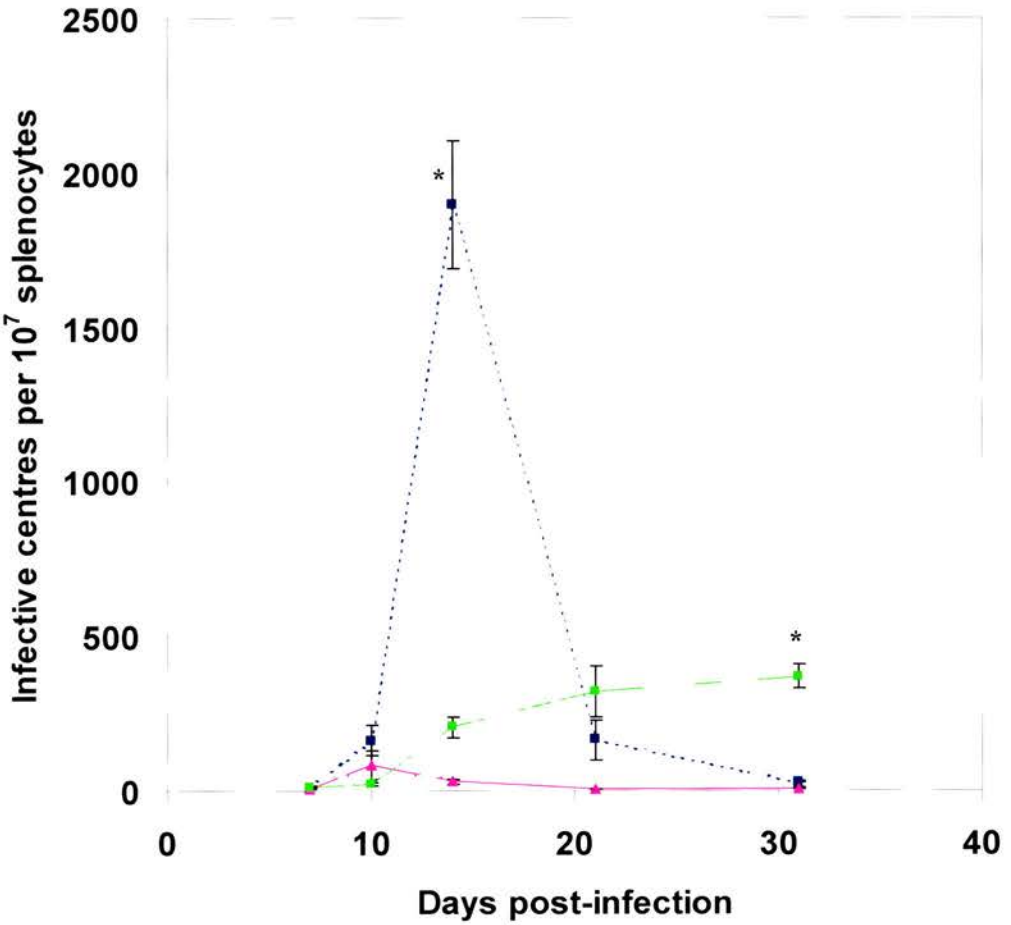

Figure 5.6.4. Latent virus in the spleens of BALB/c mice infected intranasally with 2 x 10^5 PFU of MHV-76 (——▲——), MHV76(cA8+)4 (---■---) and MHV-76(cA8+)M2$\Delta_{4336\text{-}4339}$ (——■——) as determined by infective centre assay. Infectious virus titres (less than 10 PFU per 10^7 splenocytes) were subtracted from the infective centre results. Mean infective centres per 10^7 splenocytes ± standard error is shown for four mice per group for each time point. * indicates statistically significant difference between the number of infective centres in mice infected with MHV76(cA8+)4 and MHV-76(cA8+)M2$\Delta_{4336\text{-}4339}$ as determined by two-way ANOVA with Bonferroni post-tests.

for this possibility, three separate viral plaques from three different mice that arose due to reactivation of latent MHV-76(cA8+)M2$\Delta_{4336\text{-}4339}$ in the infective centre assay at day 14 post-infection were harvested. The DNA was extracted (see 2.8.3), and the M2 ORF amplified using primer pair M2GEX1 and M2GEX2 (Chapter 2, Appendix 2) with *PfuTurbo*™ DNA polymerase. The fragment was inserted into the pKS(-) vector (Chapter 2, Appendix 3) using the *Bam*HI and *Eco*RI restriction enzyme sites, and the sequence was determined (see 2.2.24). Sequence analysis showed that all three independent reactivated viral plaques contained the 4bp deletion in the M2 ORF identical to that observed in the parent cosmid (see Figure 5.3.2.2). There was therefore no evidence for the formation of pseudorevertant viruses.

These results therefore show that disruption of the M2 ORF leads to a significant decrease in the amount of latent virus detectable during the establishment of latency in the spleen when compared to a virus with an intact M2 ORF. This may be due to either a decrease in the amount of latently infected splenocytes or a failure of the virus to reactivate from latency. However, at day 31 post-infection higher levels of latent virus were detectable in the virus with a disruption in the M2 ORF.

5.7. Discussion

These results describe a novel method for the generation of recombinant viruses for the study of individual gene function in MHV-68, using mutagenesis in cosmids to facilitate the creation of recombinant viruses. This method was used to create a virus with a 4bp internal deletion in the M2 ORF, and preliminary analysis of this virus showed that disruption of the M2 ORF had no effect on viral replication *in vitro*. However, this recombinant virus achieved higher peak viral titres in the lung but was significantly compromised in its ability to establish or reactivate from latency in the spleen early in the course of infection. This virus also appeared to be defective in the maintenance of latency at a later timepoint post-infection. Disruption of the M2 ORF had no effect on the genesis of

splenomegaly. These results show that M2 plays a significant role in MHV-68 pathogenesis.

The decision to construct recombinant viruses with no marker genes to enable the selection of recombinant viruses was made because previous studies have shown that the insertion of foreign DNA into the left end of the genome can have deleterious effects on viral phenotype (Clambey *et al.*, 2000; Adler *et al.*, 2001). This position-dependent effect does not occur in recombinant viruses that contain deletions rather than insertions of foreign DNA, and it may be that insertion of foreign DNA disrupts the expression of neighbouring genes. However, selectable markers provide an excellent method of enriching recombinant virus, and reducing the amount of wild-type virus that was a problem in the production of pure recombinant viruses in this study. Instead, a PCR-based screening method was employed, which meant that no selectable marker genes were required. This was a very sensitive technique, but had the disadvantage that it could not distinguish pure recombinant virus from wild-type MHV-76. A technique to detect the presence of MHV-76 is possible by using a PCR primer pair to amplify a region bridging the terminal repeats and the left end of MHV-76. However, this requires one primer to anneal in the region of the terminal repeats, which leads to non-specific annealing due to the repetitive nature and high GC content of the terminal repeats (Virgin *et al.*, 1997). This leads to amplification of a number of bands, and makes interpretation of these results problematical (B.Dutia, unpublished data). The experience of attempts to purify MHV-76/tRNA7+8insert demonstrates that a reliable and robust PCR product is required to enable proper selection of recombinant viruses.

The inability to purify recombinant virus MHV-76/M2insert despite three independent attempts was apparently due to loss of the recombinant insert during replication *in vitro*. Initially, most viral plaques were positive for the M2 ORF by PCR but attempts to purify single plaques always led to the appearance of plaques negative for the recombinant insert. One explanation for this is that the recombinant virus MHV-76/M2insert was severely attenuated during replication *in vitro*, and required the presence of wild-type MHV-76 to replicate ("helper" virus). However, this is unlikely as no differences were observed between viruses

containing an intact M2 ORF and a disrupted M2 ORF during viral replication in BHK-21 cells (see 5.6.1). Purification by the selection of single plaques in a 96 well plate, which have arisen from a single plaque-forming unit, should lead to purification or at least enrichment of the recombinant virus. However, it may be that co-infection of cells with MHV-76 and MHV-76/M2insert was required to propagate the recombinant virus. However, studies using MHV-76, MHV-76(cA8+)4 and MHV-76(cA8+)M2$\Delta_{4336\text{-}4339}$ have all shown that M2 is non-essential for viral replication *in vitro*, arguing against the need for a helper virus.

Previous work has shown that expression of M2 leads to toxicity in mammalian cells (Chapter 4), and this is supported by evidence showing that the expression of M2 is tightly regulated *in vivo* (Usherwood *et al.*, 2000). M2 is also transcribed at low levels *in vitro* (Bridgeman *et al.*, 2001; Rochford *et al.*, 2001), which are below the levels of sensitivity for detection by Northern blot analysis (Husain *et al.*, 1999; Virgin *et al.*, 1999). For this reason, it was decided to produce a recombinant virus that expressed M2 from the natural viral promoter rather than use an artificial promoter (such as the HCMV IE promoter) that may have over-expressed the M2 protein. Attempts to purify recombinant virus MHV-76/M2insert support the evidence for toxicity of the M2 protein, and suggest that the insertion of the M2 ORF into MHV-76 leads to a selective disadvantage for this virus, favouring deletion of this insert during replication. Attempts to purify this recombinant virus resulted in the deletion of a portion of the recombination cassette, as evidenced by the inability to amplify a section of the M3 ORF in the cassette but the M2 ORF and the vtRNA7 locus were still detectable. MHV-68 has already been shown to spontaneously delete regions at the left end of the virus during tissue culture passage (Chapter 3; Clambey *et al.*, 2000) and this may be assisted by the presence of deleterious sequences. The design of the recombinant cassette for the generation of the M2insert virus may also have not included long-range control elements further that 1kb upstream of the transcriptional start site, and it is also possible that the expression of M2 is tightly regulated or even repressed by other genes in this genomic locus (for example M1 or M3), and that it may not be feasible to insert the M2 ORF in isolation.

The inability to purify recombinant virus MHV-76/tRNA7+8insert was probably due to problems with the PCR-based screening method employed to select for recombinant virus. The initial primer pair used generated a product that was too large to be reliably amplified, and the second primer pair amplified a very small region that was prone to false positive results. This demonstrates that a reliable and robust PCR product is required to enable proper selection of recombinant viruses, especially as the PCR reaction must work in the background of cellular DNA and ions present in the sample (see 2.8.3). Two techniques could be employed to circumvent these problems; either the design and use of a more reliable primer pair to amplify a region of DNA in the insert sequence, or to produce high quality viral DNA for use as template in the PCR reaction, free from a background of cellular debris. Production of high quality DNA in sufficient quantity would require more time, and would lead to a reduction in the number of samples that it would be possible to screen for the presence of recombinant virus.

The manufacture of recombinant viruses by the construction of deletions in cA8 gave a number of advantages over the traditional method of making recombinant viruses by homologous recombination using plasmid constructs. The use of cosmids enables mutations to be introduced by recombination in bacteria, and by allowing homologous recombination with MHV-76, it facilitates the isolation of recombinant viruses in the absence of background virus containing the M2 ORF, making selection by a PCR-based screening method easier. The large areas of overlap between the cosmid and MHV-76 allow for efficient homologous recombination, and importantly viruses constructed in this manner have shown to have an identical phenotype to MHV-68 *in vitro* and *in vivo* (Chapter 3). As such, this technique should simplify the production of viruses with deletions in the unique ORFs at the left end of MHV-68.

It was decided to introduce small mutations in the M2 ORF in order to minimise the potential disruption to the surrounding genes. Effects on neighbouring genes are thought to be unlikely as the transcriptional control elements for the M1 and M3 ORFs are located upstream of their respective transcriptional start sites, away from the M2 ORF (see Figure 5.2.1), but this requires confirmation by analysis of these transcripts in the recombinant viruses

(for example, by RT-PCR or Northern analysis). There is also evidence of other transcripts at the left end of the MHV-68 genome (B.Dutia, unpublished data), which may be multiply-spliced transcripts crossing the terminal repeats in MHV-68 similar to the LMP2 transcripts in EBV. Therefore minimal mutations in this region are desirable to prevent effects on these transcripts. Disruption of the M2 ORF by the construction of a 4bp deletion at nucleotide positions 4336-4339 leads to the production of a 90 a.a. protein consisting of the N-terminal 89 residues of M2 fused to an arginine residue. This will lead to the deletion of the last three residues of the $M2_{91-99}$ CD8+ T cell epitope (Figure 5.3.2.2). This should be enough to prevent recognition of the truncated M2 protein by the CTL immune response, as the phenylalanine residue at position 2 and the leucine residue at position 9 of the CD8+ T cell epitope are considered to be the H-$2K^d$ allele critical anchor residues for binding (Rammensee *et al.*, 1995). However, it is still possible that the remaining 89 residues of M2 present in $M2\Delta_{4336-4339}$ retain some of the functions of M2. It is of note in this regard that a mutant of HSV-1 containing a 4bp deletion in UL14 generated using a similar method to that described in this chapter was predicted to generate a protein consisting of the N-terminal 96 a.a. of UL14. However, no UL14 protein was detectable by immunoprecipitation (Cunningham *et al.*, 2000). Studies using either independent recombinant viruses with larger deletions in the M2 ORF (such as MHV-76(cA8+)$M2\Delta_{4239-4494}$) or analysis of viral proteins using anti-M2 antibodies would be required to demonstrate that no functional M2 protein was produced.

The inability to purify recombinant virus MHV-76(cA8+)$M2\Delta_{4239-4494}$ was unexpected. This virus had been plaque purified five times on BHK-21 cells, and there had been no evidence of M2 ORF negative viral plaques during the last three rounds of purification. It is possible that the substantial deletion in the M2 ORF leads to a selective disadvantage *in vitro*, or it may be that spontaneous deletion of the region at the left end of the genome occurred during the process of producing viral stocks and viral DNA (similar to that which occurred to produce MHV-76). This serves to emphasise that although MHV-68 and MHV-76 grow well in tissue culture in a wide range of cell types, these viruses do not seem as

tractable as HSV-1 in the generation of viral mutants. Time constraints have meant that it was not possible to completely purify recombinant virus MHV-76(cA8+)M2$\Delta_{4239\text{-}4494}$, but initial attempts have been made by *in vivo* passage of the impure virus.

Preliminary results on the characterisation of the recombinant virus MHV-76(cA8+)M2$\Delta_{4336\text{-}4339}$ have shown that this virus replicates identically *in vitro* to the parent virus MHV-76 and a virus containing an intact M2 ORF, MHV-76(cA8+)4. However, during lytic replication in the lungs of BALB/c mice, MHV-76(cA8+)M2$\Delta_{4336\text{-}4339}$ exhibited peak lung viral titres that were approximately 10-fold higher than either MHV-76 or MHV-76(cA8+)4 (Figure 5.6.2). Although expression of M2 has been demonstrated at low levels in the lung during acute infection (Usherwood *et al.*, 2000; Rochford *et al.*, 2001), a role for M2 during lytic replication in the lung was thought unlikely due to the fact that M2 has been classified as a latency-associated gene (Husain *et al.*, 1999; Virgin *et al.*, 1999). This increase in peak lung viral titres is unlikely to be due to lytic viral replication alone, as the *in vitro* growth curves show that MHV-76(cA8+)M2$\Delta_{4336\text{-}4339}$ has no replication advantage over MHV-76 or MHV-76(cA8+)4. However, it would seem confusing why MHV-68 should possess the M2 gene, which appears to limit viral titres in the site of primary replication in the lung and therefore possibly reduce the seeding of virus to other organs and sites of latency, unless it confers a significant advantage to the establishment of latency.

Disruption of the M2 ORF had no effect on the viral induction of splenomegaly observed after infection with MHV-76(cA8+)M2$\Delta_{4336\text{-}4339}$. The induction of splenomegaly is dependent on the presence of B lymphocytes (Usherwood *et al.*, 1996c; Weck *et al.*, 1996), CD4+ T lymphocytes (Ehtisham *et al.*, 1993; Usherwood *et al.*, 1996a) and viral gene products present in the left end of the genome (Bridgeman *et al.*, 2001; see Chapter 3). It was hypothesised that the M2 gene may be involved in the genesis of splenomegaly, as M2 is transiently expressed in the spleen during the initiation of splenomegaly (Usherwood *et al.*, 2000). However, these results argue that the M2 ORF has no role in the generation of splenomegaly, with the important caveat that the N-terminal 98 a.a.

in M2 may still be functional in MHV-76(cA8+)M2$\Delta_{4336\text{-}4339}$. Studies using viruses such as MHV-76(cA8+)M2$\Delta_{4239\text{-}4494}$ with more substantial deletions in M2 would resolve this issue, and it is of note that subsequent steps to purify this recombinant virus by *in vivo* passage resulted in splenomegaly in BALB/c mice (data not shown).

In contrast to the generation of splenomegaly, disruption of the M2 ORF had a significant effect on the amount of latent MHV-76(cA8+)M2$\Delta_{4336\text{-}4339}$ detectable in the spleen, and this demonstrates a critical role for the M2 protein in the establishment or reactivation from latency. There was no peak of latently infected splenocytes at day 14 post-infection in mice infected with MHV-76(cA8+)M2$\Delta_{4336\text{-}4339}$, and this result is the first to dissociate splenomegaly and the peak of latently infected splenocytes. The latent infection of B lymphocytes leads to the activation and recruitment of CD4+ T lymphocytes, leading to a rapid increase in activated B and T lymphocyte populations (Usherwood *et al.*, 1996a; Stevenson & Doherty, 1999). This expansion is hypothesised to enable the virus to establish latency in as many splenocytes as possible, maximising the number of virus positive cells that escape CD8+ T lymphocyte-mediated control and thus establish life-long persistence and latency (Stewart *et al.*, 1998a; Nash *et al.*, 2001). These results suggest that the genesis of splenomegaly and the peak of latently infected splenocytes are not as intricately linked as previously thought. It is also thought that different MHV-68 viral genes are expressed in different stages of latency, analogous to the different EBV latency programs (Rochford *et al.*, 2001; Usherwood *et al.*, 2001). Infection of B cells by EBV *in vitro* leads to the expression of all the latent genes presumed to facilitate the transformation of B cells (termed Latency III; Rickinson & Kieff, 1996). Similarly, M2 may be expressed during a full latent gene expression program designed to expand the number of latently infected cells, and therefore disruption of M2 would prevent this peak in latently infected cells. The other possibility is that MHV-76(cA8+)M2$\Delta_{4336\text{-}4339}$ is efficiently establishing a latent infection in splenocytes, but that this virus has a greatly reduced efficiency of reactivation from latency in the infective centre assay. This hypothesis could be tested by using techniques

such as QF-PCR to quantitate the number of viral genome positive splenocytes compared to the number of splenocytes reactivating virus in the infective centre assay. However, the recombinant virus MHV-76(cA8+)M2$\Delta_{4336\text{-}4339}$ has no deficiencies in lytic cycle replication as evidenced by the *in vitro* growth curves, and the amount of virus reactivated in the infective centre assay increases over the timecourse of the experiment, suggesting that there is no defect in reactivation.

The kinetics of the amount of latent virus detectable in the spleens of mice infected with MHV-76(cA8+)M2$\Delta_{4336\text{-}4339}$ are also dramatically different from that of MHV-76(cA8+)4. There is a gradual increase in the amount of latently infected splenocytes detectable, such that the numbers are still increasing up to the end of this experiment (31 days post-infection). Sequence analysis of three independent reactivated viral plaques showed that this increase in the amount of reactivated virus was not due to the generation of pseudorevertant viruses. Due to time constraints, it was not possible to ascertain if the number of latently infected splenocytes would peak and then decline, or if the immune response was unable to control the latent infection and thus the numbers would continue to rise. The control and decline in the number of latently infected splenocytes is mediated by CD8+ T cells (Weck *et al.*, 1996; Stewart *et al.*, 1998a), and it is thought that the CTL response to the M2$_{91\text{-}99}$ CD8+ T cell epitope results in the control of the initial peak in latently infected cells during the first three weeks after infection (Usherwood *et al.*, 2000; Usherwood *et al.*, 2001). One possibility is that the lack of a functional M2$_{91\text{-}99}$ CD8+ T cell epitope leads to a failure of recognition of latently infected cells by the CD8+ T cell response, and thus a lack of control over the latent infection. This would suggest that the only method of immunological control over MHV-68 during the establishment of latency is via recognition of the M2 protein, and analysis of MHV-76 shows that this is not the case. During long-term MHV-68 latency, the expression of M2 is silenced (either by the CTL response or viral down-regulation) leading to a more restricted form of latency (Usherwood *et al.*, 2000). Along with the results showing that MHV-76 can maintain long-term latency (Chapter 3), this suggests that disruption in M2 will not prevent the virus MHV-76(cA8+)M2$\Delta_{4336\text{-}4339}$ maintaining long-term latency.

In conjunction with the results from the characterisation of MHV-76 (Chapter 3), the phenotype of a recombinant virus with a disruption in the M2 gene gives further insights into the role of this region in MHV-68 infection, and particularly the establishment and maintenance of latency. MHV-76 also lacks the $M2_{91-99}$ CD8+ T cell epitope and the entire M2 ORF, but the immune response still manages to quickly control the latent MHV-76 infection in the spleen, which suggests that other genes at the left end of the genome are involved with M2 in the subversion of the immune response. The most likely candidate is the M3 ORF, due to its demonstration as a soluble chemokine-binding protein (van Berkel *et al.*, 1999; Parry *et al.*, 2000; van Berkel *et al.*, 2000) and the fact that deletion of M3 severely reduces the ability of the virus to induce splenomegaly and establish latency (Bridgeman *et al.*, 2001). However, as shown by the studies with MHV-76, none of these genes are essential for the establishment and maintenance of latency suggesting that there is a degree of redundancy in the function of various viral proteins.

Future work is required to confirm these results on the preliminary characterisation of a recombinant virus disrupted in the M2 ORF. In particular, purification of recombinant virus MHV-76(cA8+)M2$\Delta_{4239-4494}$ will address the possibility that the remaining 98 N-terminal a.a. of M2 retain their function in recombinant virus MHV-76(cA8+)M2$\Delta_{4336-4339}$. The construction and analysis of revertant viruses will be necessary to show that there are no other deletions in the recombinant viruses, although the Southern blot and PCR analysis suggest that this is unlikely. It is also necessary to repeat these experiments over a longer timecourse to ascertain the kinetics of latent virus in the spleen following infection with MHV-76(cA8+)M2$\Delta_{4336-4339}$.

These results detail a novel method of producing recombinant viruses to study the function of genes at the left end of the MHV-68 genome. Analysis of a recombinant virus with a disruption in the M2 ORF reveals that this gene plays a crucial role in the establishment of a normal latent load in the spleen, and the control of latency after MHV-68 infection. Further studies using these viruses should help to discover the precise function of M2 during MHV-68 pathogenesis.

Chapter 6: Conclusions

The results presented in this thesis demonstrate that virus-specific gene products present at the left end of the unique region perform key roles in the pathogenesis of gammaherpesvirus infections, both in the evasion and exploitation of the immune system. The M1, M2, M3, M4 and eight vtRNA genes in this locus of the MHV-68 genome play a central role in viral pathogenesis, as deletion of these genes leads to a more rapid clearance of virus from the lungs accompanied by an enhanced inflammatory response, and a dramatic decrease in splenomegaly and the amount of latent virus during the establishment of latency in the spleen. However, they are not essential for viral replication or the maintenance of life-long latency. Herpesviruses only express an extremely restricted set of viral genes during latency that are thought to be crucial for viral persistence (see 1.1.3.2), and thus the classification of M2 and M3 as latency-associated genes that are non-essential for latency presents the query of their role during MHV-68 latency. In particular, M3 is expressed at late timepoints post-infection *in vivo* (Usherwood *et al.*, 2000) so whilst expression of M3 is not necessary for the virus to maintain latency, it is postulated to confer a significant advantage to the virus at this time as it is transcribed as part of an extremely restricted MHV-68 gene expression program (one of only 5 viral genes expressed at late latent timepoints; see 1.4.3). The tightly regulated expression of M2 during the establishment of latency is also of interest, as the downregulation of M2 transcription appears to coincide with the induction of the CTL response against the M2 protein (Usherwood *et al.*, 2000). The marked reduction in the amount of latent virus present during the establishment of latency shown by viruses which do not expresses M2 (Chapters 3 and 5) and M3 (Chapter 3; Bridgeman *et al.*, 2001) suggests that M2 and M3 play a key role in assisting MHV-68 establish an initial high latent viral load.

The spontaneous deletion of large sequences from the genome of herpesviruses is a widely recognised but poorly understood phenomenon. The deletion that resulted in the generation of MHV-76 most likely occurred during the *in vivo* and *in vitro* passage steps during viral isolation. Apart from the 9.5kb deletion, the remaining 20kb of sequence obtained from the MHV-76 genome showed a single nucleotide difference from the MHV-68 sequence. MHV-76 was

described as having been originally isolated from *Apodemus* species, which are very divergent in evolutionary terms from the *Clethrionomys* species from which MHV-68 was first isolated. Such a remarkably high degree of homology would therefore be extremely unlikely to occur if MHV-76 was a naturally occurring isolate, as the virus would be subject to variation due to mutations occurring during replication over thousands of years. The most likely explanation is that MHV-76 is not a true novel strain of murine herpesvirus but a deletion mutant of MHV-68 that has occurred after isolation *in vivo*. It remains to be seen if the other virus strains isolated at the same time are also closely related to MHV-68, but previous work and sequence analysis of MHV-72 suggests that it is very similar to MHV-68 (see 1.5). Conclusive results on the relationship of all the herpesvirus isolates will require partial sequence analysis of the viral genomes and a systematic evaluation of these viruses.

The precise mechanism whereby these deletions occur during replication is unknown, but one hypothesis is that during replication *in vitro* the virus is not under selective pressure from the immune system, and thus loss of these genes is not deleterious to the virus and may in fact be advantageous if these genes are toxic or impede lytic replication. However, these genes may be necessary for the virus to reactivate from latency and this may be one explanation for the apparent reduction in latent virus detectable by infective centre assay following MHV-76 infection. Future work to measure the amount of viral DNA present in the splenocytes will be necessary to determine this.

The precise function of the M2 gene of MHV-68 has still to be resolved, but the preliminary characterisation described in Chapter 4 gives some indication as to its possible role. The localised sequence homology to the Gab2 and semaphorin families is of interest due to their role in intracellular signal transduction. Many gammaherpesviruses target intracellular signalling pathways, such as the LMP-1 protein of EBV (Farrell, 1998), and it may be that the localised homology of M2 is sufficient to achieve this. The identification of a cellular counterpart for the M2 protein awaits future data from the mouse and human genome sequencing projects, but it may be that M2 has no cellular homologue and has evolved and adapted to its natural host. Other results also suggest that M2

may have a role in signal transduction such as the localisation of the M2 protein to the plasma membrane in the cell, the predicted phosphorylation and myristylation of M2 and circumstantial evidence for the phosphorylation of M2 as shown by the visualisation of M2 as a doublet band on Western analysis. It may be necessary to use other techniques to purify and analyse M2 for potential phosphorylation and myristylation, especially in view of the poor expression and toxicity problems encountered. Further circumstantial evidence for the role of M2 in signal transduction and in particular B lymphocyte activation pathways, is provided by data showing that the M2 promoter is B-lymphocyte specific (S.M. Husain, J.T. Sample, unpublished data), and that viruses containing a disruption in the M2 ORF are defective in the establishment of splenic latency (Chapter 5). These results suggest that M2 is expressed only in B cells during infection *in vivo*, and that the M2 protein may result in the activation of B cells thus enhancing the establishment of latency, particularly in the spleen. Future work to examine the effects of M2 on B lymphocytes, especially naïve cells, may help to resolve this issue.

The exact localisation of the M2 protein at the plasma membrane remains unknown, but due to the lack of a signal sequence suggestive of secretion and hydrophobic domains that would be necessary for the M2 protein to interact with the membrane, it is probable that the M2 protein is localised to the inner aspect of the plasma membrane. The expression of M2 in mammalian cells means that the use of techniques such as immunogold electron microscopy could be used to determine the exact localisation of M2 in the cell. This probable localisation on the inner aspect of the plasma membrane would enable M2 to interact with other proteins involved in signal transduction, or other scaffolding proteins such as Gab2. The role of the patchy nuclear and cytoplasmic expression of M2 observed in both the HA-epitope tagged M2 and the EGFP-M2 fusion proteins is unclear, as these patches did not co-localise with markers used to stain DNA, the endoplasmic reticulum, the Golgi apparatus or lysosomes. One explanation could be that these areas are artefacts caused by the high level of M2 expression promoted by the expression vectors, especially as M2 expression appears to be tightly regulated at low levels during viral infection. An alternative explanation is

that the M2 protein is in the process of being transported to the plasma membrane, but expression in cells harvested at later timepoints after transfection shows a similar pattern of expression (Figure 4.5.1.6) suggesting that this may not be the case. Studies with a reliable purified anti-M2 antibody would enable visualisation of M2 in S11 cells, and clarify whether or not the patchy cytoplasmic/nuclear expression occurred during endogenous M2 expression.

The manufacture of recombinant viruses using MHV-76 and a cosmid containing the left end of the unique portion of the viral genome enabled the rapid and reliable production of mutant viruses, with the advantage of allowing selection by a PCR-based screening method without wild-type virus background. However, ensuring complete purification of mutant virus from MHV-76 was a problem due to the lack of detection of MHV-76 and thus it may be advantageous to perform Southern analysis earlier during the purification process. Problems were encountered with the production of recombinant viruses with the M2 insert sequence due to the apparent toxicity of M2, and it therefore may be that expression of M2 is tightly regulated by other viral elements present in this region of the genome. The large flanking sequences present in the cosmid ensured efficient homologous recombination at the correct locus, and will enable the production of recombinant viruses with deletions at the left end of the unique portion of the genome to determine which genes are responsible for the altered phenotype of MHV-76.

The disruption of the M2 ORF using a 4bp deletion ensured that there was minimal disruption to surrounding genes, which had been postulated to occur previously during the insertion of foreign DNA into this region of the genome (Clambey *et al.*, 2000; Adler *et al.*, 2001). However, this disruption could have resulted in the formation of a protein containing the N-terminal 89 residues of M2 that retained some function. Although this was thought to be unlikely, studies using a mutant virus with a more substantial deletion in M2 (such as MHV-76(cA8+)M2$\Delta_{4239\text{-}4494}$) would help to resolve this issue. This disruption in the M2 ORF led to higher peak viral titres in the lung and a dramatic reduction in the amount and kinetics of latent virus in the spleen during the establishment and maintenance of latency. The suppressive effect of M2 during lytic replication in

the lung was unexpected, but may be explained by the observation that M2 is toxic during expression *in vitro* (Chapter 4) and thus deleterious to the virus during productive replication. Another explanation may be that the low levels of M2 expression in the lung (Rochford *et al.*, 2001) are sufficient to induce a CTL response that results in the suppression of lytic replication. Preliminary hypotheses that M2 was involved in the genesis of splenomegaly due to its possible involvement in signal transduction pathways leading to B cell proliferation also appear to be invalidated by these results showing that a disruption in the M2 ORF has no effect on splenomegaly. However further work is necessary to examine the expansion of particular splenocyte populations during infection with MHV-76(cA8+)M2$\Delta_{4336\text{-}4339}$, as it may be that B cell proliferation is impaired and this is concealed by the expansion in the T lymphocyte population.

However, the most significant finding is that following infection with a mutant virus with a disruption in the M2 ORF, the amount of latent virus increases gradually after infection with the highest levels observed at the last timepoint in the experiment (Figure 5.6.4). One possibility is that there is no immune recognition of the $M2_{91\text{-}99}$ CD8+ T cell epitope by BALB/c mice (H-2^d), and thus the CTL response cannot control the latent virus infection. However, the $M2_{91\text{-}99}$ CD8+ T cell epitope is not recognised in C57BL/6 mice (H-2^b) that can control latent MHV-68 infection, and this epitope is also absent in MHV-76, which has a much reduced latent virus load so it would appear that this is not the explanation. The other possibility is that there are compensatory mechanisms involved in establishment of latency by MHV-68 and thus when the virus is unable to establish latency efficiently during the period of splenomegaly, another process is utilised by the virus at a time when M2 expression is switched off during MHV-68 infection.

The results demonstrating that two viruses, MHV-76 and MHV-76(cA8+)M2$\Delta_{4336\text{-}4339}$, do not generate the peak of latently infected splenocytes normally observed at two weeks post-infection confirms previous findings that the amplification processes utilised by MHV-68 during lytic replication and latent

infection *in vivo* are separate. Thus a high titre of productive viral replication in the lung is not necessary for seeding of virus to the spleen and the establishment of normal levels of latent virus (Stevenson *et al.*, 1999b). These studies also suggest two other consequences during MHV-68 infection. Firstly, that splenomegaly and the peak of latently infected splenocytes observed during the establishment of latency can be dissociated, and also that the lymphoproliferative phase and expansion of latently infected cells is not necessary for the establishment and maintenance of latency. Previous results with EBV suggested that the Latency III gene expression programme is used during initial viral infection to result in cellular proliferation and thus amplify the number of B lymphocytes that can be latently infected, thus ensuring the establishment of latency. However, results presented here suggest that this is not necessary and that gammaherpesviruses can still establish and maintain latency at approximately normal levels without the generation of splenomegaly (in the case of MHV-76) or the initial peak of latently infected cells (in the case of MHV-76 and MHV-76(cA8+)M2$\Delta_{4336\text{-}4339}$). It therefore remains to be determined exactly why infection with MHV-68 results in an initial peak in the number of latently infected cells if this is unnecessary, and may even be detrimental to the virus as it results in an enhanced CD8+ T cell response via the M2 CTL epitope.

The amount of virus necessary to result in the establishment of lifelong latency during natural primary infection with herpesviruses is currently unknown, but thought to be low as the majority of the human population are infected with at least one herpesviruses (such as HSV, VZV, CMV and EBV) showing that natural infection is very efficient. However, most experimental techniques utilise relatively high doses of virus during primary infection, including experimental infection with MHV-68 using 2 x 10^5 PFU intranasally as described in this thesis. One explanation of the results observed following infection with MHV-76 and MHV-76(cA8+)M2$\Delta_{4336\text{-}4339}$ is that the high doses of infectious virus used resulted in high levels of replicating virus in the lung, and these levels overcame any defects that these viruses have during the establishment of latency. However, if low doses of infectious viruses were used, MHV-76 and MHV-

76(cA8+)M2$\Delta_{4336\text{-}4339}$ may have difficulty in establishing latency *in vivo*, with latent infection being reduced, delayed or prolonged. Thus infection with low doses of infectious viruses may reveal further defects in viral pathogenesis with MHV-76 and MHV-76(cA8+)M2$\Delta_{4336\text{-}4339}$.

These results reveal the importance of the genetic elements present in the left end of the unique region of the genome to MHV-68 pathogenicity, and also give new insights into the mechanisms by which gammaherpesviruses establish latency *in vivo*.

References

Abbot, S. D., Rowe, M., Cadwallader, K., Ricksten, A., Gordon, J., Wang, F., Rymo, L. & Rickinson, A. B. (1990). Epstein-Barr virus nuclear antigen 2 induces expression of the virus- encoded latent membrane protein. *Journal of Virology* **64**, 2126-34.

Adler, H., Messerle, M., Wagner, M. & Koszinowski, U. H. (2000). Cloning and mutagenesis of the murine gammaherpesvirus 68 genome as an infectious bacterial artificial chromosome. *Journal of Virology* **74**, 6964-74.

Adler, H., Messerle, M. & Koszinowski, U. H. (2001). Virus reconstituted from infectious bacterial artificial chromosome (BAC)-cloned murine gammaherpesvirus 68 acquires wild-type properties in vivo only after excision of BAC vector sequences. *Journal of Virology* **75**, 5692-6.

Albrecht, J. C., Nicholas, J., Biller, D., Cameron, K. R., Biesinger, B., Newman, C., Wittmann, S., Craxton, M. A., Coleman, H., Fleckenstein, B. & et al. (1992). Primary structure of the herpesvirus saimiri genome. *Journal of Virology* **66**, 5047-58.

Albrecht, J. C., Friedrich, U., Kardinal, C., Koehn, J., Fleckenstein, B., Feller, S. M. & Biesinger, B. (1999). Herpesvirus ateles gene product Tio interacts with nonreceptor protein tyrosine kinases. *Journal of Virology* **73**, 4631-9.

Albrecht, J. C. (2000). Primary structure of the Herpesvirus ateles genome. *Journal of Virology* **74**, 1033-7.

Alcami, A. & Smith, G. L. (1995). Cytokine receptors encoded by poxviruses: a lesson in cytokine biology. *Immunology Today* **16**, 474-8.

Alcami, A. & Koszinowski, U. H. (2000). Viral mechanisms of immune evasion. *Trends in Microbiology* **8**, 410-8.

Alexander, L., Denekamp, L., Knapp, A., Auerbach, M. R., Damania, B. & Desrosiers, R. C. (2000). The primary sequence of rhesus monkey rhadinovirus isolate 26-95: sequence similarities to Kaposi's sarcoma-associated herpesvirus and rhesus monkey rhadinovirus isolate 17577. *Journal of Virology* **74**, 3388-98.

Altschul, S. F., Madden, T. L., Schaffer, A. A., Zhang, J., Zhang, Z., Miller, W. & Lipman, D. J. (1997). Gapped BLAST and PSI-BLAST: a new generation of protein database search programs. *Nucleic Acids Research* **25**, 3389-402.

Anagnostopoulos, I., Hummel, M., Kreschel, C. & Stein, H. (1995). Morphology, immunophenotype, and distribution of latently and/or productively Epstein-Barr virus-infected cells in acute infectious mononucleosis: implications for the interindividual infection route of Epstein-Barr virus. *Blood* **85**, 744-50.

Aoki, Y., Jaffe, E. S., Chang, Y., Jones, K., Teruya-Feldstein, J., Moore, P. S. & Tosato, G. (1999). Angiogenesis and hematopoiesis induced by Kaposi's sarcoma-associated herpesvirus-encoded interleukin-6. *Blood* **93**, 4034-43.

Araujo, A. P., Oliva, G., Henrique-Silva, F., Garratt, R. C., Caceres, O. & Beltramini, L. M. (2000). Influence of the histidine tail on the structure and activity of recombinant chlorocatechol 1,2-dioxygenase. *Biochemical and Biophysical Research Communications* **272**, 480-4.

Armstrong, R. W., Imrey, P. B., Lye, M. S., Armstrong, M. J., Yu, M. C. & Sani, S. (1998). Nasopharyngeal carcinoma in Malaysian Chinese: salted fish and other dietary exposures. *International Journal of Cancer* **77**, 228-35.

Arzul, I., Renault, T., Lipart, C. & Davison, A. J. (2001). Evidence for interspecies transmission of oyster herpesvirus in marine bivalves. *Journal of General Virology* **82**, 865-70.

Baer, R., Bankier, A. T., Biggin, M. D., Deininger, P. L., Farrell, P. J., Gibson, T. J., Hatfull, G., Hudson, G. S., Satchwell, S. C., Seguin, C. & et al. (1984). DNA sequence and expression of the B95-8 Epstein-Barr virus genome. *Nature* **310**, 207-11.

Bais, C., Santomasso, B., Coso, O., Arvanitakis, L., Raaka, E. G., Gutkind, J. S., Asch, A. S., Cesarman, E., Gershengorn, M. C., Mesri, E. A. & Gerhengorn, M. C. (1998). G-protein-coupled receptor of Kaposi's sarcoma-associated herpesvirus is a viral oncogene and angiogenesis activator. *Nature* **391**, 86-9.

Ballestas, M. E., Chatis, P. A. & Kaye, K. M. (1999). Efficient persistence of extrachromosomal KSHV DNA mediated by latency- associated nuclear antigen. *Science* **284**, 641-4.

Barnes, A., Dyson, H., Sunil-Chandra, N. P., Collins, P. & Nash, A. A. (1999). 2'-Deoxy-5-ethyl-beta-4'-thiouridine inhibits replication of murine gammaherpesvirus and delays the onset of virus latency. *Antiviral Chemistry and Chemotherapy* **10**, 321-6.

Barry, M. & McFadden, G. (1998). Apoptosis regulators from DNA viruses. *Current Opinion in Immunology* **10**, 422-30.

Beaudoing, E., Freier, S., Wyatt, J. R., Claverie, J. M. & Gautheret, D. (2000). Patterns of variant polyadenylation signal usage in human genes. *Genome Research* **10**, 1001-10.

Bellamy, C. O., Malcomson, R. D., Harrison, D. J. & Wyllie, A. H. (1995). Cell death in health and disease: the biology and regulation of apoptosis. *Seminars in Cancer Biology* **6**, 3-16.

Beral, V., Peterman, T. A., Berkelman, R. L. & Jaffe, H. W. (1990). Kaposi's sarcoma among persons with AIDS: a sexually transmitted infection? *Lancet* **335**, 123-8.

Bergmann, J. E. & Fusco, P. J. (1990). The G protein of vesicular stomatitis virus has free access into and egress from the smooth endoplasmic reticulum of UT-1 cells. *Journal of Cell Biology* **110**, 625-35.

Bhatnagar, R. S. & Gordon, J. I. (1997). Understanding covalent modifications of proteins by lipids: where cell biology and biophysics mingle. *Trends in Cell Biology* **7**, 14-20.

Biesinger, B., Trimble, J. J., Desrosiers, R. C. & Fleckenstein, B. (1990). The divergence between two oncogenic Herpesvirus saimiri strains in a genomic region related to the transforming phenotype. *Virology* **176**, 505-14.

Biesinger, B., Muller-Fleckenstein, I., Simmer, B., Lang, G., Wittmann, S., Platzer, E., Desrosiers, R. C. & Fleckenstein, B. (1992). Stable growth transformation of human T lymphocytes by herpesvirus saimiri. *Proceedings of the National Academy of Sciences, USA* **89**, 3116-9.

Blaskovic, D., Stancekova, M., Svobodova, J. & Mistrikova, J. (1980). Isolation of five strains of herpesviruses from two species of free living small rodents. *Acta virologica* **24**, 468.

Blaskovic, D., Stanekova, D. & Rajcani, J. (1984). Experimental pathogenesis of murine herpesvirus in newborn mice. *Acta virologica* **28**, 225-31.

Blom, N., Gammeltoft, S. & Brunak, S. (1999). Sequence and structure-based prediction of eukaryotic protein phosphorylation sites. *Journal of Molecular Biology* **294**, 1351-62.

Bolovan-Fritts, C. A., Mocarski, E. S. & Wiedeman, J. A. (1999). Peripheral blood CD14(+) cells from healthy subjects carry a circular conformation of latent cytomegalovirus genome. *Blood* **93**, 394-8.

Bornhorst, J. A. & Falke, J. J. (2000). Purification of proteins using polyhistidine affinity tags. *Methods in Enzymology* **326**, 245-54.

Bornkamm, G. W., Delius, H., Zimber, U., Hudewentz, J. & Epstein, M. A. (1980). Comparison of Epstein-Barr virus strains of different origin by analysis of the viral DNAs. *Journal of Virology* **35**, 603-18.

Boshoff, C. & Weiss, R. A. (2001). Epidemiology and pathogenesis of Kaposi's sarcoma-associated herpesvirus. *Philosophical Transactions of The Royal Society (London) Series B. Biological Sciences* **356**, 517-34.

Bowden, R. J., Simas, J. P., Davis, A. J. & Efstathiou, S. (1997). Murine gammaherpesvirus 68 encodes tRNA-like sequences which are expressed during latency. *Journal of General Virology* **78**, 1675-87.

Bridgeman, A., Stevenson, P. G., Simas, J. P. & Efstathiou, S. (2001). A secreted chemokine binding protein encoded by murine gammaherpesvirus-68 is necessary for the establishment of a normal latent load. *Journal of Experimental Medicine* **194**, 301-12.

Bridgen, A. & Reid, H. W. (1991). Derivation of a DNA clone corresponding to the viral agent of sheep-associated malignant catarrhal fever. *Research in Veterinary Science* **50**, 38-44.

Brocksmith, D., Angel, C. A., Pringle, J. H. & Lauder, I. (1991). Epstein-Barr viral DNA in Hodgkin's disease: amplification and detection using the polymerase chain reaction. *Journal of Pathology* **165**, 11-5.

Brodsky, F. M., Lem, L., Solache, A. & Bennett, E. M. (1999). Human pathogen subversion of antigen presentation. *Immunological Reviews* **168**, 199-215.

Brooks, M. A., Ali, A. N., Turner, P. C. & Moyer, R. W. (1995). A rabbitpox virus serpin gene controls host range by inhibiting apoptosis in restrictive cells. *Journal of Virology* **69**, 7688-98.

Browne, H., Bell, S., Minson, T. & Wilson, D. W. (1996). An endoplasmic reticulum-retained herpes simplex virus glycoprotein H is absent from secreted virions: evidence for reenvelopment during egress. *Journal of Virology* **70**, 4311-6.

Bucci, C., Thomsen, P., Nicoziani, P., McCarthy, J. & van Deurs, B. (2000). Rab7: a key to lysosome biogenesis. *Molecular Biology of the Cell* **11**, 467-80.

Buckmaster, A. E., Scott, S. D., Sanderson, M. J., Boursnell, M. E., Ross, N. L. & Binns, M. M. (1988). Gene sequence and mapping data from Marek's disease virus and herpesvirus of turkeys: implications for herpesvirus classification. *Journal of General Virology* **69**, 2033-42.

Camarda, G., Spinetti, G., Bernardini, G., Mair, C., Davis-Poynter, N., Capogrossi, M. C. & Napolitano, M. (1999). The equine herpesvirus 2 E1 open reading frame encodes a functional chemokine receptor. *Journal of Virology* **73**, 9843-8.

Cardin, R. D., Brooks, J. W., Sarawar, S. R. & Doherty, P. C. (1996). Progressive loss of CD8+ T cell-mediated control of a gamma-herpesvirus in the absence of CD4+ T cells. *Journal of Experimental Medicine* **184**, 863-71.

Carel, J. C., Myones, B. L., Frazier, B. & Holers, V. M. (1990). Structural requirements for C3d/Epstein-Barr virus receptor (CR2/CD21) ligand binding, internalization, and viral infection. *Journal of Biological Chemistry* **265**, 12293-9.

Cesarman, E., Moore, P. S., Rao, P. H., Inghirami, G., Knowles, D. M. & Chang, Y. (1995). In vitro establishment and characterization of two acquired immunodeficiency syndrome-related lymphoma cell lines (BC-1 and BC-2) containing Kaposi's sarcoma-associated herpesvirus-like (KSHV) DNA sequences. *Blood* **86**, 2708-14.

Chalfie, M., Tu, Y., Euskirchen, G., Ward, W. W. & Prasher, D. C. (1994). Green fluorescent protein as a marker for gene expression. *Science* **263**, 802-5.

Chang, Y., Cesarman, E., Pessin, M. S., Lee, F., Culpepper, J., Knowles, D. M. & Moore, P. S. (1994). Identification of herpesvirus-like DNA sequences in AIDS-associated Kaposi's sarcoma. *Science* **266**, 1865-9.

Chen, S., Bacon, K. B., Li, L., Garcia, G. E., Xia, Y., Lo, D., Thompson, D. A., Siani, M. A., Yamamoto, T., Harrison, J. K. & Feng, L. (1998). In vivo inhibition of CC and CX3C chemokine-induced leukocyte infiltration and attenuation of glomerulonephritis in Wistar-Kyoto (WKY) rats by vMIP-II. *Journal of Experimental Medicine* **188**, 193-8.

Cho, M. S., Bornkamm, G. W. & zur Hausen, H. (1984). Structure of defective DNA molecules in Epstein-Barr virus preparations from P3HR-1 cells. *Journal of Virology* **51**, 199-207.

Cho, Y., Ramer, J., Rivailler, P., Quink, C., Garber, R. L., Beier, D. R. & Wang, F. (2001). An Epstein-Barr-related herpesvirus from marmoset lymphomas. *Proceedings of the National Academy of Sciences, USA* **98**, 1224-9.

Choi, J. K., Ishido, S. & Jung, J. U. (2000). The collagen repeat sequence is a determinant of the degree of herpesvirus saimiri STP transforming activity. *Journal of Virology* **74**, 8102-10.

Ciampor, F., Stancekova, M. & Blaskovic, D. (1981). Electron microscopy of rabbit embryo fibroblasts infected with herpesvirus isolates from Clethrionomys glareolus and Apodemus flavicollis. *Acta virologica* **25**, 101-7.

Clambey, E. T., Virgin, H. W. & Speck, S. H. (2000). Disruption of the murine gammaherpesvirus 68 M1 open reading frame leads to enhanced reactivation from latency. *Journal of Virology* **74**, 1973-84.

Cohen, G. B., Gandhi, R. T., Davis, D. M., Mandelboim, O., Chen, B. K., Strominger, J. L. & Baltimore, D. (1999). The selective downregulation of class I major histocompatibility complex proteins by HIV-1 protects HIV-infected cells from NK cells. *Immunity* **10**, 661-71.

Cohen, J. I., Wang, F., Mannick, J. & Kieff, E. (1989). Epstein-Barr virus nuclear protein 2 is a key determinant of lymphocyte transformation. *Proceedings of the National Academy of Sciences, USA* **86**, 9558-62.

Cohrs, R. J., Barbour, M. & Gilden, D. H. (1996). Varicella-zoster virus (VZV) transcription during latency in human ganglia: detection of transcripts mapping to genes 21, 29, 62, and 63 in a cDNA library enriched for VZV RNA. *Journal of Virology* **70**, 2789-96.

Comeau, M. R., Johnson, R., DuBose, R. F., Petersen, M., Gearing, P., VandenBos, T., Park, L., Farrah, T., Buller, R. M., Cohen, J. I., Strockbine, L. D., Rauch, C. & Spriggs, M. K. (1998). A poxvirus-encoded semaphorin induces cytokine production from monocytes and binds to a novel cellular semaphorin receptor, VESPR. *Immunity* **8**, 473-82.

Coppola, M. A., Flano, E., Nguyen, P., Hardy, C. L., Cardin, R. D., Shastri, N., Woodland, D. L. & Blackman, M. A. (1999). Apparent MHC-independent stimulation of CD8+ T cells in vivo during latent murine gammaherpesvirus infection. *Journal of Immunology* **163**, 1481-9.

Cottin, V., Van Linden, A. & Riches, D. W. (1999). Phosphorylation of tumor necrosis factor receptor CD120a (p55) by p42(mapk/erk2) induces changes in its subcellular localization. *Journal of Biological Chemistry* **274**, 32975-87.

Cross, F. R., Garber, E. A., Pellman, D. & Hanafusa, H. (1984). A short sequence in the p60src N terminus is required for p60src myristylation and membrane association and for cell transformation. *Molecular and Cellular Biology* **4**, 1834-42.

Cunningham, C. & Davison, A. J. (1993). A cosmid-based system for constructing mutants of herpes simplex virus type 1. *Virology* **197**, 116-24.

Cunningham, C., Davison, A. J., MacLean, A. R., Taus, N. S. & Baines, J. D. (2000). Herpes simplex virus type 1 gene UL14: phenotype of a null mutant and identification of the encoded protein. *Journal of Virology* **74**, 33-41.

Deiss, L. P., Chou, J. & Frenkel, N. (1986). Functional domains within the a sequence involved in the cleavage- packaging of herpes simplex virus DNA. *Journal of Virology* **59**, 605-18.

Delaire, S., Elhabazi, A., Bensussan, A. & Boumsell, L. (1998). CD100 is a leukocyte semaphorin. *Cellular and Molecular Life Sciences* **54**, 1265-76.

Delaire, S., Billard, C., Tordjman, R., Chedotal, A., Elhabazi, A., Bensussan, A. & Boumsell, L. (2001). Biological activity of soluble CD100. II. Soluble CD100, similarly to H- SemaIII, inhibits immune cell migration. *Journal of Immunology* **166**, 4348-54.

Desrosiers, R. C., Bakker, A., Kamine, J., Falk, L. A., Hunt, R. D. & King, N. W. (1985). A region of the Herpesvirus saimiri genome required for oncogenicity. *Science* **228**, 184-7.

Devereux, J., Haeberli, P. & Smithies, O. (1984). A comprehensive set of sequence analysis programs for the VAX. *Nucleic Acids Research* **12**, 387-95.

Djerbi, M., Screpanti, V., Catrina, A. I., Bogen, B., Biberfeld, P. & Grandien, A. (1999). The inhibitor of death receptor signaling, FLICE-inhibitory protein defines a new class of tumor progression factors. *Journal of Experimental Medicine* **190**, 1025-32.

Dobbelstein, M. & Shenk, T. (1996). Protection against apoptosis by the vaccinia virus SPI-2 (B13R) gene product. *Journal of Virology* **70**, 6479-85.

Duboise, S. M., Guo, J., Czajak, S., Desrosiers, R. C. & Jung, J. U. (1998). STP and Tip are essential for herpesvirus saimiri oncogenicity. *Journal of Virology* **72**, 1308-13.

Dunowska, M., Letchworth, G. J., Collins, J. K. & DeMartini, J. C. (2001). Ovine herpesvirus-2 glycoprotein B sequences from tissues of ruminant malignant catarrhal fever cases and healthy sheep are highly conserved. *Journal of General Virology* **82**, 2785-90.

Dupin, N., Fisher, C., Kellam, P., Ariad, S., Tulliez, M., Franck, N., van Marck, E., Salmon, D., Gorin, I., Escande, J. P., Weiss, R. A., Alitalo, K. & Boshoff, C. (1999). Distribution of human herpesvirus-8 latently infected cells in Kaposi's sarcoma, multicentric Castleman's disease, and primary effusion lymphoma. *Proceedings of the National Academy of Sciences, USA* **96**, 4546-51.

Dutia, B. M., Clarke, C. J., Allen, D. J. & Nash, A. A. (1997). Pathological changes in the spleens of gamma interferon receptor- deficient mice infected with murine gammaherpesvirus: a role for CD8 T cells. *Journal of Virology* **71**, 4278-83.

Dutia, B. M., Allen, D. J., Dyson, H. & Nash, A. A. (1999a). Type I interferons and IRF-1 play a critical role in the control of a gammaherpesvirus infection. *Virology* **261**, 173-9.

Dutia, B. M., Stewart, J. P., Clayton, R. A., Dyson, H. & Nash, A. A. (1999b). Kinetic and phenotypic changes in murine lymphocytes infected with murine gammaherpesvirus-68 in vitro. *Journal of General Virology* **80**, 2729-36.

Ebrahimi, B., Dutia, B. M., Brownstein, D. G. & Nash, A. A. (2001). Murine gammaherpesvirus-68 infection causes multi-organ fibrosis and alters leukocyte trafficking in interferon-gamma receptor knockout mice. *American Journal of Pathology* **158**, 2117-25.

Edelman, A. M., Blumenthal, D. K. & Krebs, E. G. (1987). Protein serine/threonine kinases. *Annual Reviews in Biochemistry* **56**, 567-613.

Efstathiou, S., Ho, Y. M., Hall, S., Styles, C. J., Scott, S. D. & Gompels, U. A. (1990a). Murine herpesvirus 68 is genetically related to the gammaherpesviruses Epstein-Barr virus and herpesvirus saimiri. *Journal of General Virology* **71**, 1365-72.

Efstathiou, S., Ho, Y. M. & Minson, A. C. (1990b). Cloning and molecular characterization of the murine herpesvirus 68 genome. *Journal of General Virology* **71**, 1355-64.

Ehtisham, S., Sunil-Chandra, N. P. & Nash, A. A. (1993). Pathogenesis of murine gammaherpesvirus infection in mice deficient in CD4 and CD8 T cells. *Journal of Virology* **67**, 5247-52.

Elbein, A. D. (1987). Inhibitors of the biosynthesis and processing of N-linked oligosaccharide chains. *Annual Reviews in Biochemistry* **56**, 497-534.

Emini, E. A., Luka, J., Armstrong, M. E., Banker, F. S., Provost, P. J. & Pearson, G. R. (1986). Establishment and characterization of a chronic infectious mononucleosis-like syndrome in common marmosets. *Journal of Medical Virology* **18**, 369-79.

Ensser, A. & Fleckenstein, B. (1995). Alcelaphine herpesvirus type 1 has a semaphorin-like gene. *Journal of General Virology* **76**, 1063-7.

Ensser, A., Pflanz, R. & Fleckenstein, B. (1997). Primary structure of the alcelaphine herpesvirus 1 genome. *Journal of Virology* **71**, 6517-25.

Epstein, M. A., Morgan, A. J., Finerty, S., Randle, B. J. & Kirkwood, J. K. (1985). Protection of cottontop tamarins against Epstein-Barr virus-induced malignant lymphoma by a prototype subunit vaccine. *Nature* **318**, 287-9.

Evan, G. & Littlewood, T. (1998). A matter of life and cell death. *Science* **281**, 1317-22.

Everett, H. & McFadden, G. (1999). Apoptosis: an innate immune response to virus infection. *Trends in Microbiology* **7**, 160-5.

Farrell, H. E., Vally, H., Lynch, D. M., Fleming, P., Shellam, G. R., Scalzo, A. A. & Davis-Poynter, N. J. (1997). Inhibition of natural killer cells by a cytomegalovirus MHC class I homologue in vivo. *Nature* **386**, 510-4.

Farrell, P. J. (1998). Signal transduction from the Epstein-Barr virus LMP-1 transforming protein. *Trends in Microbiology* **6**, 175-7; discussion 177-8.

Faulkner, G. C., Burrows, S. R., Khanna, R., Moss, D. J., Bird, A. G. & Crawford, D. H. (1999). X-Linked agammaglobulinemia patients are not infected with Epstein-Barr virus: implications for the biology of the virus. *Journal of Virology* **73**, 1555-64.

Faulkner, G. C., Krajewski, A. S. & Crawford, D. H. (2000). The ins and outs of EBV infection. *Trends in Microbiology* **8**, 185-9.

Fenner, F. J. (1993). Herpesviridae. In *Veterinary Virology*, Second edn., pp. 337 - 68. Edited by F. J. Fenner, Gibbs, E.P.J., Murphy, F.A., Rott, R., Studdert, M.J., White, D.O. San Diego: Academic Press.

Fickenscher, H. & Fleckenstein, B. (2001). Herpesvirus saimiri. *Philosophical Transactions of The Royal Society (London) Series B. Biological Sciences* **356**, 545-67.

Fingeroth, J. D., Weis, J. J., Tedder, T. F., Strominger, J. L., Biro, P. A. & Fearon, D. T. (1984). Epstein-Barr virus receptor of human B lymphocytes is the C3d receptor CR2. *Proceedings of the National Academy of Sciences, USA* **81**, 4510-4.

Flano, E., Woodland, D. L. & Blackman, M. A. (1999). Requirement for CD4+ T cells in Vβ4+ CD8+ T cell activation associated with latent murine gammaherpesvirus infection. *Journal of Immunology* **163**, 3403-8.

Flano, E., Husain, S. M., Sample, J. T., Woodland, D. L. & Blackman, M. A. (2000). Latent murine gamma-herpesvirus infection is established in activated B cells, dendritic cells, and macrophages. *Journal of Immunology* **165**, 1074-81.

Fleckenstein, B. & Desrosiers, R. C. (1982). Herpesvirus saimiri and Herpesvirus ateles. In *The Herpesviruses*, pp. 253-332. Edited by B. Roizman. New York: Plenum Press.

Flore, O., Rafii, S., Ely, S., O'Leary, J. J., Hyjek, E. M. & Cesarman, E. (1998). Transformation of primary human endothelial cells by Kaposi's sarcoma-associated herpesvirus. *Nature* **394**, 588-92.

Fodor, W. L., Rollins, S. A., Bianco-Caron, S., Rother, R. P., Guilmette, E. R., Burton, W. V., Albrecht, J. C., Fleckenstein, B. & Squinto, S. P. (1995). The complement control protein homolog of herpesvirus saimiri regulates serum complement by inhibiting C3 convertase activity. *Journal of Virology* **69**, 3889-92.

Foecking, M. K. & Hofstetter, H. (1986). Powerful and versatile enhancer-promoter unit for mammalian expression vectors. *Gene* **45**, 101-5.

Frank, A., Andiman, W. A. & Miller, G. (1976). Epstein-Barr virus and nonhuman primates: natural and experimental infection. *Advances in Cancer Research* **23**, 171-201.

Frappier, L. & O'Donnell, M. (1991). Overproduction, purification, and characterization of EBNA1, the origin binding protein of Epstein-Barr virus. *Journal of Biological Chemistry* **266**, 7819-26.

Friborg, J. Jr., Kong, W., Hottiger, M. O. & Nabel, G. J. (1999). p53 inhibition by the LANA protein of KSHV protects against cell death. *Nature* **402**, 889-94.

Gadina, M., Sudarshan, C., Visconti, R., Zhou, Y. J., Gu, H., Neel, B. G. & O'Shea, J. J. (2000). The docking molecule gab2 is induced by lymphocyte activation and is involved in signaling by interleukin-2 and interleukin-15 but not other common gamma chain-using cytokines. *Journal of Biological Chemistry* **275**, 26959-66.

Gardner, J. D., Tscharke, D. C., Reading, P. C. & Smith, G. L. (2001). Vaccinia virus semaphorin A39R is a 50-55 kDa secreted glycoprotein that affects the outcome of infection in a murine intradermal model. *Journal of General Virology* **82**, 2083-93.

Gluzman, Y. (1981). SV40-transformed simian cells support the replication of early SV40 mutants. *Cell* **23**, 175-82.

Gold, M. R., Ingham, R. J., McLeod, S. J., Christian, S. L., Scheid, M. P., Duronio, V., Santos, L. & Matsuuchi, L. (2000). Targets of B-cell antigen receptor signaling: the phosphatidylinositol 3-kinase/Akt/glycogen synthase kinase-3 signaling pathway and the Rap1 GTPase. *Immunological Reviews* **176**, 47-68.

Gompels, U. A., Nicholas, J., Lawrence, G., Jones, M., Thomson, B. J., Martin, M. E., Efstathiou, S., Craxton, M. & Macaulay, H. A. (1995). The DNA sequence of human herpesvirus-6: structure, coding content, and genome evolution. *Virology* **209**, 29-51.

Gong, M., Ooka, T., Matsuo, T. & Kieff, E. (1987). Epstein-Barr virus glycoprotein homologous to herpes simplex virus gB. *Journal of Virology* **61**, 499-508.

Gong, M. & Kieff, E. (1990). Intracellular trafficking of two major Epstein-Barr virus glycoproteins, gp350/220 and gp110. *Journal of Virology* **64**, 1507-16.

Goodbourn, S., Didcock, L. & Randall, R. E. (2000). Interferons: cell signalling, immune modulation, antiviral response and virus countermeasures. *Journal of General Virology* **81**, 2341-64.

Goodwin, D. J., Walters, M. S., Smith, P. G., Thurau, M., Fickenscher, H. & Whitehouse, A. (2001). Herpesvirus saimiri open reading frame 50 (Rta) protein reactivates the lytic replication cycle in a persistently infected A549 cell line. *Journal of Virology* **75**, 4008-13.

Graham, F. L., Smiley, J., Russell, W. C. & Nairn, R. (1977). Characteristics of a human cell line transformed by DNA from Human Adenovirus Type 5. *Journal of General Virology* **36**, 59-72.

Granzow, H., Klupp, B. G., Fuchs, W., Veits, J., Osterrieder, N. & Mettenleiter, T. C. (2001). Egress of alphaherpesviruses: comparative ultrastructural study. *Journal of Virology* **75**, 3675-84.

Grassmann, R. & Fleckenstein, B. (1989). Selectable recombinant herpesvirus saimiri is capable of persisting in a human T-cell line. *Journal of Virology* **63**, 1818-21.

Greenspan, J. S., Greenspan, D., Lennette, E. T., Abrams, D. I., Conant, M. A., Petersen, V. & Freese, U. K. (1985). Replication of Epstein-Barr virus within the epithelial cells of oral "hairy" leukoplakia, an AIDS-associated lesion. *The New England Journal of Medicine* **313**, 1564-71.

Grzimek, N. K., Dreis, D., Schmalz, S. & Reddehase, M. J. (2001). Random, asynchronous, and asymmetric transcriptional activity of enhancer-flanking major immediate-early genes ie1/3 and ie2 during murine cytomegalovirus latency in the lungs. *Journal of Virology* **75**, 2692-705.

Gu, H., Pratt, J. C., Burakoff, S. J. & Neel, B. G. (1998). Cloning of p97/Gab2, the major SHP2-binding protein in hematopoietic cells, reveals a novel pathway for cytokine-induced gene activation. *Molecular Cell* **2**, 729-40.

Haddad, R. S. & Hutt-Fletcher, L. M. (1989). Depletion of glycoprotein gp85 from virosomes made with Epstein-Barr virus proteins abolishes their ability to fuse with virus receptor- bearing cells. *Journal of Virology* **63**, 4998-5005.

Hahn, G., Jores, R. & Mocarski, E. S. (1998). Cytomegalovirus remains latent in a common precursor of dendritic and myeloid cells. *Proceedings of the National Academy of Sciences, USA* **95**, 3937-42.

Haig, D. M., McInnes, C. J., Thomson, J., Wood, A., Bunyan, K. & Mercer, A. (1998). The orf virus OV20.0L gene product is involved in interferon resistance and inhibits an interferon-inducible, double-stranded RNA-dependent kinase. *Immunology* **93**, 335-40.

Haig, D. M. (2001). Subversion and piracy: DNA viruses and immune evasion. *Research in Veterinary Science* **70**, 205-19.

Hall, K. T., Giles, M. S., Goodwin, D. J., Calderwood, M. A., Carr, I. M., Stevenson, A. J., Markham, A. F. & Whitehouse, A. (2000). Analysis of gene expression in a human cell line stably transduced with herpesvirus saimiri. *Journal of Virology* **74**, 7331-7.

Hamelin, C. & Lussier, G. (1992). Characterization of the DNA of rodent herpesviruses by restriction endonuclease analysis and hybridization. *Laboratory Animal Science* **42**, 142-5.

Hanazono, Y., Yu, J. M., Dunbar, C. E. & Emmons, R. V. (1997). Green fluorescent protein retroviral vectors: low titer and high recombination frequency suggest a selective disadvantage. *Human Gene Therapy* **8**, 1313-9.

Hansen, J. E., Lund, O., Tolstrup, N., Gooley, A. A., Williams, K. L. & Brunak, S. (1998). NetOglyc: prediction of mucin type O-glycosylation sites based on sequence context and surface accessibility. *Glycoconjugate Journal* **15**, 115-30.

Haque, T., Thomas, J. A., Falk, K. I., Parratt, R., Hunt, B. J., Yacoub, M. & Crawford, D. H. (1996). Transmission of donor Epstein-Barr virus (EBV) in transplanted organs causes lymphoproliferative disease in EBV-seronegative recipients. *Journal of General Virology* **77**, 1169-72.

Hardy, C. L., Silins, S. L., Woodland, D. L. & Blackman, M. A. (2000). Murine gamma-herpesvirus infection causes V(beta)4-specific CDR3- restricted clonal expansions within CD8(+) peripheral blood T lymphocytes. *International Immunology* **12**, 1193-204.

Harley, C. A., Dasgupta, A. & Wilson, D. W. (2001). Characterization of herpes simplex virus-containing organelles by subcellular fractionation: role for organelle acidification in assembly of infectious particles. *Journal of Virology* **75**, 1236-51.

Harlow, E. & Lane, D. (1988). Antibodies: A Laboratory Manual. New York: Cold Spring Harbor Laboratory Press.

Harris, A., Young, B. D. & Griffin, B. E. (1985). Random association of Epstein-Barr virus genomes with host cell metaphase chromosomes in Burkitt's lymphoma-derived cell lines. *Journal of Virology* **56**, 328-32.

Hartikka, J., Sawdey, M., Cornefert-Jensen, F., Margalith, M., Barnhart, K., Nolasco, M., Vahlsing, H. L., Meek, J., Marquet, M., Hobart, P., Norman, J. & Manthorpe, M. (1996). An improved plasmid DNA expression vector for direct injection into skeletal muscle. *Human Gene Therapy* **7**, 1205-17.

Hatfull, G., Bankier, A. T., Barrell, B. G. & Farrell, P. J. (1988). Sequence analysis of Raji Epstein-Barr virus DNA. *Virology* **164**, 334-40.

Hayashi, K. & Akagi, T. (2000). An animal model for Epstein-Barr virus (EBV)-associated lymphomagenesis in the human: malignant lymphoma induction of rabbits by EBV-related herpesvirus from cynomolgus. *Pathology International* **50**, 85-97.

Hayashi, K., Ohara, N., Teramoto, N., Onoda, S., Chen, H. L., Oka, T., Kondo, E., Yoshino, T., Takahashi, K., Yates, J. & Akagi, T. (2001). An animal model for human EBV-associated hemophagocytic syndrome: herpesvirus papio frequently induces fatal lymphoproliferative disorders with hemophagocytic syndrome in rabbits. *American Journal of Pathology* **158**, 1533-42.

Hayward, G. S. (1999). KSHV strains: the origins and global spread of the virus. *Seminars in Cancer Biology* **9**, 187-99.

Helenius, A. & Aebi, M. (2001). Intracellular functions of N-linked glycans. *Science* **291**, 2364-9.

Henikoff, S. & Henikoff, J. G. (1994). Protein family classification based on searching a database of blocks. *Genomics* **19**, 97-107.

Herrold, R. E., Marchini, A., Fruehling, S. & Longnecker, R. (1996). Glycoprotein 110, the Epstein-Barr virus homolog of herpes simplex virus glycoprotein B, is essential for Epstein-Barr virus replication in vivo. *Journal of Virology* **70**, 2049-54.

Hill, A., Jugovic, P., York, I., Russ, G., Bennink, J., Yewdell, J., Ploegh, H. & Johnson, D. (1995). Herpes simplex virus turns off the TAP to evade host immunity. *Nature* **375**, 411-5.

Hochuli, E., Bannwarth, W., Dobeli, H., Gentz, R. & Stuber, D. (1988). Genetic approach to facilitate purification of recombinant proteins with a novel chelate adsorbent. *Bio/Technology* **6**, 1321-1325.

Hofmann, K., Bucher, P., Falquet, L. & Bairoch, A. (1999). The PROSITE database, its status in 1999. *Nucleic Acids Research* **27**, 215-9.

Hoge, A. T., Hendrickson, S. B. & Burns, W. H. (2000). Murine gammaherpesvirus 68 cyclin D homologue is required for efficient reactivation from latency. *Journal of Virology* **74**, 7016-23.

Hopkins, J., Dutia, B. M. & McConnell, I. (1986). Monoclonal antibodies to sheep lymphocytes. I. Identification of MHC class II molecules on lymphoid tissue and changes in the level of class II expression on lymph-borne cells following antigen stimulation in vivo. *Immunology* **59**, 433-8.

Hopwood, P. & Crawford, D. H. (2000). The role of EBV in post-transplant malignancies: a review. *Journal of Clinical Pathology* **53**, 248-54.

Howe, J. G. & Shu, M. D. (1989). Epstein-Barr virus small RNA (EBER) genes: unique transcription units that combine RNA polymerase II and III promoter elements. *Cell* **57**, 825-34.

Howie, D., Sayos, J., Terhorst, C. & Morra, M. (2000). The gene defective in X-linked lymphoproliferative disease controls T cell dependent immune surveillance against Epstein-Barr virus. *Current Opinion in Immunology* **12**, 474-8.

Huang, C. A., Fuchimoto, Y., Gleit, Z. L., Ericsson, T., Griesemer, A., Scheier-Dolberg, R., Melendy, E., Kitamura, H., Fishman, J. A., Ferry, J. A., Harris, N. L., Patience, C. & Sachs, D. H. (2001). Post-transplantation lymphoproliferative disease in miniature swine after allogeneic hematopoietic cell transplantation: similarity to human PTLD and association with a porcine gammaherpesvirus. *Blood* **97**, 1467-73.

Husain, S. M., Usherwood, E. J., Dyson, H., Coleclough, C., Coppola, M. A., Woodland, D. L., Blackman, M. A., Stewart, J. P. & Sample, J. T. (1999). Murine gammaherpesvirus M2 gene is latency-associated and its protein a target for CD8(+) T lymphocytes. *Proceedings of the National Academy of Sciences, USA* **96**, 7508-13.

Imai, S., Nishikawa, J., Kuroda, M. & Takada, K. (2001). Epstein-Barr virus infection of human epithelial cells. *Current Topics in Microbiology and Immunology* **258**, 161-84.

Ishido, S., Choi, J. K., Lee, B. S., Wang, C., DeMaria, M., Johnson, R. P., Cohen, G. B. & Jung, J. U. (2000a). Inhibition of natural killer cell-mediated cytotoxicity by Kaposi's sarcoma-associated herpesvirus K5 protein. *Immunity* **13**, 365-74.

Ishido, S., Wang, C., Lee, B. S., Cohen, G. B. & Jung, J. U. (2000b). Downregulation of major histocompatibility complex class I molecules by Kaposi's sarcoma-associated herpesvirus K3 and K5 proteins. *Journal of Virology* **74**, 5300-9.

Jacob, R. J. & Roizman, B. (1977). Anatomy of herpes simplex virus DNA VIII. Properties of the replicating DNA. *Journal of Virology* **23**, 394-411.

Jacob, R. J., Morse, L. S. & Roizman, B. (1979). Anatomy of herpes simplex virus DNA. XII. Accumulation of head-to-tail concatemers in nuclei of infected cells and their role in the generation of the four isomeric arrangements of viral DNA. *Journal of Virology* **29**, 448-57.

Janeway, C. A., Travers, P., Walport, M. & Capra, J. D. (1999). Immunobiology: the immune system in health and disease, Fourth edn. London: Current Biology Ltd., Curchill Livingstone.

Janz, A., Oezel, M., Kurzeder, C., Mautner, J., Pich, D., Kost, M., Hammerschmidt, W. & Delecluse, H. J. (2000). Infectious Epstein-Barr virus lacking major glycoprotein BLLF1 (gp350/220) demonstrates the existence of additional viral ligands. *Journal of Virology* **74**, 10142-52.

Jenner, R. G., Alba, M. M., Boshoff, C. & Kellam, P. (2001). Kaposi's sarcoma-associated herpesvirus latent and lytic gene expression as revealed by DNA arrays. *Journal of Virology* **75**, 891-902.

Jeong, J., Papin, J. & Dittmer, D. (2001). Differential regulation of the overlapping Kaposi's sarcoma-associated herpesvirus vGCR (orf74) and LANA (orf73) promoters. *Journal of Virology* **75**, 1798-807.

Johannessen, I. & Crawford, D. H. (1999). In vivo models for Epstein-Barr virus (EBV)-associated B cell lymphoproliferative disease (BLPD). *Reviews in Medical Virology* **9**, 263-77.

Johnson, D. C., Frame, M. C., Ligas, M. W., Cross, A. M. & Stow, N. D. (1988). Herpes simplex virus immunoglobulin G Fc receptor activity depends on a complex of two viral glycoproteins, gE and gI. *Journal of Virology* **62**, 1347-54.

Jones, M. D., Foster, L., Sheedy, T. & Griffin, B. E. (1984). The EB virus genome in Daudi Burkitt's lymphoma cells has a deletion similar to that observed in a non-transforming strain (P3HR-1) of the virus. *The EMBO Journal* **3**, 813-21.

Jones, T. R., Wiertz, E. J., Sun, L., Fish, K. N., Nelson, J. A. & Ploegh, H. L. (1996). Human cytomegalovirus US3 impairs transport and maturation of major histocompatibility complex class I heavy chains. *Proceedings of the National Academy of Sciences, USA* **93**, 11327-33.

Judde, J. G., Lacoste, V., Briere, J., Kassa-Kelembho, E., Clyti, E., Couppie, P., Buchrieser, C., Tulliez, M., Morvan, J. & Gessain, A. (2000). Monoclonality or oligoclonality of human herpesvirus 8 terminal repeat sequences in Kaposi's sarcoma and other diseases. *Journal of the National Cancer Institute* **92**, 729-36.

Jung, J. U. & Desrosiers, R. C. (1991). Identification and characterization of the herpesvirus saimiri oncoprotein STP-C488. *Journal of Virology* **65**, 6953-60.

Jung, J. U., Trimble, J. J., King, N. W., Biesinger, B., Fleckenstein, B. W. & Desrosiers, R. C. (1991). Identification of transforming genes of subgroup A and C strains of Herpesvirus saimiri. *Proceedings of the National Academy of Sciences, USA* **88**, 7051-5.

Kanda, K., Decker, T., Aman, P., Wahlstrom, M., von Gabain, A. & Kallin, B. (1992). The EBNA2-related resistance towards alpha interferon (IFN-alpha) in Burkitt's lymphoma cells effects induction of IFN-induced genes but not the activation of transcription factor ISGF-3. *Molecular and Cellular Biology* **12**, 4930-6.

Kao, P. N., Chen, L., Brock, G., Ng, J., Kenny, J., Smith, A. J. & Corthesy, B. (1994). Cloning and expression of cyclosporin A- and FK506-sensitive nuclear factor of activated T-cells: NF45 and NF90. *Journal of Biological Chemistry* **269**, 20691-9.

Kapadia, S. B., Molina, H., van Berkel, V., Speck, S. H. & Virgin, H. W. (1999). Murine gammaherpesvirus 68 encodes a functional regulator of complement activation. *Journal of Virology* **73**, 7658-70.

Karttunen, J. & Shastri, N. (1991). Measurement of ligand-induced activation in single viable T cells using the lacZ reporter gene. *Proceedings of the National Academy of Sciences, USA* **88**, 3972-6.

Karttunen, J., Sanderson, S. & Shastri, N. (1992). Detection of rare antigen-presenting cells by the lacZ T-cell activation assay suggests an expression cloning strategy for T-cell antigens. *Proceedings of the National Academy of Sciences, USA* **89**, 6020-4.

Kaye, K. M., Izumi, K. M. & Kieff, E. (1993). Epstein-Barr virus latent membrane protein 1 is essential for B- lymphocyte growth transformation. *Proceedings of the National Academy of Sciences, USA* **90**, 9150-4.

Kennedy, P. G., Grinfeld, E. & Gow, J. W. (1999). Latent Varicella-zoster virus in human dorsal root ganglia. *Virology* **258**, 451-4.

Kerkau, T., Bacik, I., Bennink, J. R., Yewdell, J. W., Hunig, T., Schimpl, A. & Schubert, U. (1997). The human immunodeficiency virus type 1 (HIV-1) Vpu protein interferes with an early step in the biosynthesis of major histocompatibility complex (MHC) class I molecules. *Journal of Experimental Medicine* **185**, 1295-305.

Kieff, E. (1996). Epstein-Barr Virus and its replication. In *Fields Virology*, pp. 2343-96. Edited by B. N. Fields, D. M. Knipe & P. M. Howley. Philadelphia: Lippincott-Raven.

Kim, K. J., Kanellopoulos-Langevin, C., Merwin, R. M., Sachs, D. H. & Asofsky, R. (1979). Establishment and characterization of BALB/c lymphoma lines with B cell properties. *Journal of Immunology* **122**, 549-54.

Klein, G. & Klein, E. (1985). *Myc*/Ig juxtaposition by chromosomal translocations: some new insights, puzzles and paradoxes. *Immunology Today* **6**, 208-15.

Kolodkin, A. L., Matthes, D. J. & Goodman, C. S. (1993). The semaphorin genes encode a family of transmembrane and secreted growth cone guidance molecules. *Cell* **75**, 1389-99.

Komano, J., Maruo, S., Kurozumi, K., Oda, T. & Takada, K. (1999). Oncogenic role of Epstein-Barr virus-encoded RNAs in Burkitt's lymphoma cell line Akata. *Journal of Virology* **73**, 9827-31.

Kondo, K., Xu, J. & Mocarski, E. S. (1996). Human cytomegalovirus latent gene expression in granulocyte-macrophage progenitors in culture and in seropositive individuals. *Proceedings of the National Academy of Sciences, USA* **93**, 11137-42.

Koomey, J. M., Mulder, C., Burghoff, R. L., Fleckenstein, B. & Desrosiers, R. C. (1984). Deletion of DNA sequence in a nononcogenic variant of Herpesvirus saimiri. *Journal of Virology* **50**, 662-5.

Kornfeld, R. & Ferris, C. (1975). Interaction of immunoglobulin glycopeptides with concanavalin A. *Journal of Biological Chemistry* **250**, 2614-9.

Kotwal, G. J. (2000). Poxviral mimicry of complement and chemokine system components: what's the end game? *Immunology Today* **21**, 242-8.

Kulkarni, A. B., Holmes, K. L., Fredrickson, T. N., Hartley, J. W. & Morse, H. C., 3rd (1997). Characteristics of a murine gammaherpesvirus infection in immunocompromised mice. *In Vivo* **11**, 281-91.

Kuppers, R. & Rajewsky, K. (1998). The origin of Hodgkin and Reed/Sternberg cells in Hodgkin's disease. *Annual Reviews in Immunology* **16**, 471-93.

Kurz, S., Steffens, H. P., Mayer, A., Harris, J. R. & Reddehase, M. J. (1997). Latency versus persistence or intermittent recurrences: evidence for a latent state of murine cytomegalovirus in the lungs. *Journal of Virology* **71**, 2980-7.

Kurz, S. K., Rapp, M., Steffens, H. P., Grzimek, N. K., Schmalz, S. & Reddehase, M. J. (1999). Focal transcriptional activity of murine cytomegalovirus during latency in the lungs. *Journal of Virology* **73**, 482-94.

Kuwasako, K., Shimekake, Y., Masuda, M., Nakahara, K., Yoshida, T., Kitaura, M., Kitamura, K., Eto, T. & Sakata, T. (2000). Visualization of the calcitonin receptor-like receptor and its receptor activity-modifying proteins during internalization and recycling. *Journal of Biological Chemistry* **275**, 29602-9.

Kwong, A. D., Kruper, J. A. & Frenkel, N. (1988). Herpes simplex virus virion host shutoff function. *Journal of Virology* **62**, 912-21.

Kyte, J. & Doolittle, R. F. (1982). A simple method for displaying the hydropathic character of a protein. *Journal of Molecular Biology* **157**, 105-32.

Lackner, C. A. & Condit, R. C. (2000). Vaccinia virus gene A18R DNA helicase is a transcript release factor. *Journal of Biological Chemistry* **275**, 1485-94.

Laemmli, U. K. (1970). Cleavage of structural proteins during the assembly of the head of bacteriophage T4. *Nature* **227**, 680-5.

Lagunoff, M. & Roizman, B. (1994). Expression of a herpes simplex virus 1 open reading frame antisense to the gamma(1)34.5 gene and transcribed by an RNA 3' coterminal with the unspliced latency-associated transcript. *Journal of Virology* **68**, 6021-8.

Lagunoff, M., Majeti, R., Weiss, A. & Ganem, D. (1999). Deregulated signal transduction by the K1 gene product of Kaposi's sarcoma-associated herpesvirus. *Proceedings of the National Academy of Sciences, USA* **96**, 5704-9.

Lalani, A. S., Barrett, J. W. & McFadden, G. (2000). Modulating chemokines: more lessons from viruses. *Immunology Today* **21**, 100-6.

Lanier, L. L. (1997). Natural killer cells: from no receptors to too many. *Immunity* **6**, 371-8.

Lee, H., Guo, J., Li, M., Choi, J. K., DeMaria, M., Rosenzweig, M. & Jung, J. U. (1998a). Identification of an immunoreceptor tyrosine-based activation motif of K1 transforming protein of Kaposi's sarcoma-associated herpesvirus. *Molecular Cell Biology* **18**, 5219-28.

Lee, H., Veazey, R., Williams, K., Li, M., Guo, J., Neipel, F., Fleckenstein, B., Lackner, A., Desrosiers, R. C. & Jung, J. U. (1998b). Deregulation of cell growth by the K1 gene of Kaposi's sarcoma- associated herpesvirus. *Nature Medicine* **4**, 435-40.

Lee, L. F., Wu, P., Sui, D., Ren, D., Kamil, J., Kung, H. J. & Witter, R. L. (2000). The complete unique long sequence and the overall genomic organization of the GA strain of Marek's disease virus. *Proceedings of the National Academy of Sciences, USA* **97**, 6091-6.

Leib, D. A., Machalek, M. A., Williams, B. R., Silverman, R. H. & Virgin, H. W. (2000). Specific phenotypic restoration of an attenuated virus by knockout of a host resistance gene. *Proceedings of the National Academy of Sciences, USA* **97**, 6097-101.

Leonard, G. T. & Sen, G. C. (1996). Effects of adenovirus E1A protein on interferon-signaling. *Virology* **224**, 25-33.

Levitskaya, J., Coram, M., Levitsky, V., Imreh, S., Steigerwald-Mullen, P. M., Klein, G., Kurilla, M. G. & Masucci, M. G. (1995). Inhibition of antigen processing by the internal repeat region of the Epstein-Barr virus nuclear antigen-1. *Nature* **375**, 685-8.

Lin, S. F., Robinson, D. R., Miller, G. & Kung, H. J. (1999). Kaposi's sarcoma-associated herpesvirus encodes a bZIP protein with homology to BZLF1 of Epstein-Barr virus. *Journal of Virology* **73**, 1909-17.

Littman, D. R. (1998). Chemokine receptors: keys to AIDS pathogenesis? *Cell* **93**, 677-80.

Liu, H. S., Jan, M. S., Chou, C. K., Chen, P. H. & Ke, N. J. (1999a). Is green fluorescent protein toxic to the living cells? *Biochemical and Biophysical Research Communications* **260**, 712-7.

Liu, L., Flano, E., Usherwood, E. J., Surman, S., Blackman, M. A. & Woodland, D. L. (1999b). Lytic cycle T cell epitopes are expressed in two distinct phases during MHV-68 infection. *Journal of Immunology* **163**, 868-74.

Liu, L., Usherwood, E. J., Blackman, M. A. & Woodland, D. L. (1999c). T-cell vaccination alters the course of murine herpesvirus 68 infection and the establishment of viral latency in mice. *Journal of Virology* **73**, 9849-57.

Liu, S., Pavlova, I. V., Virgin, H. W. & Speck, S. H. (2000). Characterization of gammaherpesvirus 68 gene 50 transcription. *Journal of Virology* **74**, 2029-37.

Liu, Y., Jenkins, B., Shin, J. L. & Rohrschneider, L. R. (2001). Scaffolding protein Gab2 mediates differentiation signaling downstream of Fms receptor tyrosine kinase. *Molecular and Cellular Biology* **21**, 3047-56.

Lock, M., Miller, C. & Fraser, N. W. (2001). Analysis of protein expression from within the region encoding the 2.0- kilobase latency-associated transcript of herpes simplex virus type 1. *Journal of Virology* **75**, 3413-26.

Lomonte, P., Bublot, M., van Santen, V., Keil, G., Pastoret, P. P. & Thiry, E. (1996). Bovine herpesvirus 4: genomic organization and relationship with two other gammaherpesviruses, Epstein-Barr virus and herpesvirus saimiri. *Veterinary Microbiology* **53**, 79-89.

Lorenzon, N. M., Grabner, M., Suda, N. & Beam, K. G. (2001). Structure and targeting of RyR1: implications from fusion of green fluorescent protein at the amino-terminal. *Archives of Biochemistry and Biophysics* **388**, 13-7.

Lu, S. J., Day, N. E., Degos, L., Lepage, V., Wang, P. C., Chan, S. H., Simons, M., McKnight, B., Easton, D., Zeng, Y. & et al. (1990). Linkage of a nasopharyngeal carcinoma susceptibility locus to the HLA region. *Nature* **346**, 470-1.

Lungu, O., Panagiotidis, C. A., Annunziato, P. W., Gershon, A. A. & Silverstein, S. J. (1998). Aberrant intracellular localization of Varicella-Zoster virus regulatory proteins during latency. *Proceedings of the National Academy of Sciences, USA* **95**, 7080-5.

Luster, A. D. (1998). Chemokines--chemotactic cytokines that mediate inflammation. *The New England Journal of Medicine* **338**, 436-45.

Macpherson, I. & Stoker, M. (1962). Polyoma transformation of hamster cell clones - an investigation of genetic factors affecting cell competance. *Virology* **16**, 147-51.

Macrae, A. I., Dutia, B. M., Milligan, S., Brownstein, D. G., Allen, D. J., Mistrikova, J., Davison, A. J., Nash, A. A. & Stewart, J. P. (2001). Analysis of a novel strain of murine gammaherpesvirus reveals a genomic locus important for acute pathogenesis. *Journal of Virology* **75**, 5315-27.

Magrath, I. (1990). The pathogenesis of Burkitt's lymphoma. *Advances in Cancer Research* **55**, 133-270.

Mahr, J. A. & Gooding, L. R. (1999). Immune evasion by adenoviruses. *Immunological Reviews* **168**, 121-30.

Mair, T. (1999). Viral Respiratory Disease. In *Equine Medicine and Surgery*, Fifth edn., pp. 465 - 79. Edited by P. T. Colahan, Merritt, A.M., Moore, J.N., Mayhew, I.G. St. Louis: Mosby.

Makrides, S. C. (1996). Strategies for achieving high-level expression of genes in Escherichia coli. *Microbiological Reviews* **60**, 512-38.

Mansfield, K. G., Westmoreland, S. V., DeBakker, C. D., Czajak, S., Lackner, A. A. & Desrosiers, R. C. (1999). Experimental infection of rhesus and pig-tailed macaques with macaque rhadinoviruses. *Journal of Virology* **73**, 10320-8.

Marechal, V., Dehee, A., Chikhi-Brachet, R., Piolot, T., Coppey-Moisan, M. & Nicolas, J. C. (1999). Mapping EBNA-1 domains involved in binding to metaphase chromosomes. *Journal of Virology* **73**, 4385-92.

Martinand, C., Montavon, C., Salehzada, T., Silhol, M., Lebleu, B. & Bisbal, C. (1999). RNase L inhibitor is induced during human immunodeficiency virus type 1 infection and down regulates the 2-5A/RNase L pathway in human T cells. *Journal of Virology* **73**, 290-6.

Martin-Gallardo, A., Montoya-Zavala, M., Kelder, B., Taylor, J., Chen, H., Leung, F. C. & Kopchick, J. J. (1988). A comparison of bovine growth-hormone gene expression in mouse L cells directed by the Moloney murine-leukemia virus long terminal repeat, simian virus-40 early promoter or cytomegalovirus immediate-early promoter. *Gene* **70**, 51-6.

Maruo, S., Yang, L. & Takada, K. (2001). Roles of Epstein-Barr virus glycoproteins gp350 and gp25 in the infection of human epithelial cells. *Journal of General Virology* **82**, 2373-83.

McCabe, J. B. & Berthiaume, L. G. (1999). Functional roles for fatty acylated amino-terminal domains in subcellular localization. *Molecular Biology of the Cell* **10**, 3771-86.

McGeoch, D. J. (2001). Molecular evolution of the gamma-Herpesvirinae. *Philosophical Transactions of The Royal Society (London) Series B. Biological Sciences* **356**, 421-35.

Medveczky, P., Szomolanyi, E., Desrosiers, R. C. & Mulder, C. (1984). Classification of herpesvirus saimiri into three groups based on extreme variation in a DNA region required for oncogenicity. *Journal of Virology* **52**, 938-44.

Medveczky, M. M., Szomolanyi, E., Hesselton, R., DeGrand, D., Geck, P. & Medveczky, P. G. (1989). Herpesvirus saimiri strains from three DNA subgroups have different oncogenic potentials in New Zealand white rabbits. *Journal of Virology* **63**, 3601-11.

Meier, J. L. & Stinski, M. F. (1996). Regulation of human cytomegalovirus immediate-early gene expression. *Intervirology* **39**, 331-42.

Mesri, E. A. (1999). Inflammatory reactivation and angiogenicity of Kaposi's sarcoma- associated herpesvirus/HHV8: a missing link in the pathogenesis of acquired immunodeficiency syndrome-associated Kaposi's sarcoma. *Blood* **93**, 4031-3.

Messud-Petit, F., Gelfi, J., Delverdier, M., Amardeilh, M. F., Py, R., Sutter, G. & Bertagnoli, S. (1998). Serp2, an inhibitor of the interleukin-1beta-converting enzyme, is critical in the pathobiology of myxoma virus. *Journal of Virology* **72**, 7830-9.

Minson, A. C., Davison, A., Eberle, R., Desrosiers, R. C., Fleckenstein, B., McGeoch, D. J., Pellet, P. E., Roizman, B. & Studdert, D. M. J. (2000). Family *Herpesviridae*. In *Virus Taxonomy. Seventh Report of the International Committee on Taxonomy of Viruses*, pp. 203-25. Edited by M. H. V. van Regenmortel, C. M. Fauquet, D. H. L. Bishop, E. B. Carstens, M. K. Estes, S. M. Lemon, J. Maniloff, M. A. Mayo, D. J. McGeoch, C. R. Pringle & R. B. Wickner. San Diego: Academic Press.

Mistrikova, J., Remenova, A., Lesso, J. & Stancekova, M. (1994). Replication and persistence of murine herpesvirus 72 in lymphatic system and peripheral blood mononuclear cells of Balb/C mice. *Acta virologica* **38**, 151-6.

Mistrikova, J., Furdikova, D., Oravcova, I. & Rajcani, J. (1996a). Effect of immunosuppression on Balb/c mice infected with murine herpesvirus. *Acta virologica* **40**, 41-4.

Mistrikova, J., Rajcani, J., Mrmusova, M. & Oravcova, I. (1996b). Chronic infection of Balb/c mice with murine herpesvirus 72 is associated with neoplasm development. *Acta virologica* **40**, 297-301.

Mistrikova, J., Raslova, H., Mrmusova, M. & Kudelova, M. (2000). A murine gammaherpesvirus. *Acta virologica* **44**, 211-26.

Moghaddam, A., Rosenzweig, M., Lee-Parritz, D., Annis, B., Johnson, R. P. & Wang, F. (1997). An animal model for acute and persistent Epstein-Barr virus infection. *Science* **276**, 2030-3.

Moghaddam, A., Koch, J., Annis, B. & Wang, F. (1998). Infection of human B lymphocytes with lymphocryptoviruses related to Epstein-Barr virus. *Journal of Virology* **72**, 3205-12.

Moore, P. S., Gao, S. J., Dominguez, G., Cesarman, E., Lungu, O., Knowles, D. M., Garber, R., Pellett, P. E., McGeoch, D. J. & Chang, Y. (1996). Primary characterization of a herpesvirus agent associated with Kaposi's sarcoma [published erratum appears in Journal of Virology (1996) Dec;70(12):9083]. *Journal of Virology* **70**, 549-58.

Morgenstern, J. P. & Land, H. (1990). Advanced mammalian gene transfer: high titre retroviral vectors with multiple drug selection markers and a complementary helper-free packaging cell line. *Nucleic Acids Research* **18**, 3587-96.

Murphy, P. M. (2001). Viral exploitation and subversion of the immune system through chemokine mimicry. *Nature Immunology* **2**, 116-22.

Murthy, S. C., Trimble, J. J. & Desrosiers, R. C. (1989). Deletion mutants of herpesvirus saimiri define an open reading frame necessary for transformation. *Journal of Virology* **63**, 3307-14.

Nash, A. A., Dutia, B. M., Stewart, J. P. & Davison, A. J. (2001). Natural history of murine gamma-herpesvirus infection. *Philosophical Transactions of The Royal Society (London) Series B. Biological Sciences* **356**, 569-79.

Neipel, F., Albrecht, J. C. & Fleckenstein, B. (1997). Cell-homologous genes in the Kaposi's sarcoma-associated rhadinovirus human herpesvirus 8: determinants of its pathogenicity? *Journal of Virology* **71**, 4187-92.

Nemerow, G. R. & Cooper, N. R. (1984). Early events in the infection of human B lymphocytes by Epstein-Barr virus: the internalization process. *Virology* **132**, 186-98.

Nemerow, G. R., Wolfert, R., McNaughton, M. E. & Cooper, N. R. (1985). Identification and characterization of the Epstein-Barr virus receptor on human B lymphocytes and its relationship to the C3d complement receptor (CR2). *Journal of Virology* **55**, 347-51.

Niedobitek, G., Hansmann, M. L., Herbst, H., Young, L. S., Dienemann, D., Hartmann, C. A., Finn, T., Pitteroff, S., Welt, A., Anagnostopoulos, I. & et al. (1991a). Epstein-Barr virus and carcinomas: undifferentiated carcinomas but not squamous cell carcinomas of the nasopharynx are regularly associated with the virus. *Journal of Pathology* **165**, 17-24.

Niedobitek, G., Young, L. S., Lau, R., Brooks, L., Greenspan, D., Greenspan, J. S. & Rickinson, A. B. (1991b). Epstein-Barr virus infection in oral hairy leukoplakia: virus replication in the absence of a detectable latent phase. *Journal of General Virology* **72**, 3035-46.

Nishida, K., Yoshida, Y., Itoh, M., Fukada, T., Ohtani, T., Shirogane, T., Atsumi, T., Takahashi-Tezuka, M., Ishihara, K., Hibi, M. & Hirano, T. (1999). Gab-family adapter proteins act downstream of cytokine and growth factor receptors and T- and B-cell antigen receptors. *Blood* **93**, 1809-16.

Oda, T., Imai, S., Chiba, S. & Takada, K. (2000). Epstein-Barr virus lacking glycoprotein gp85 cannot infect B cells and epithelial cells. *Virology* **276**, 52-8.

Ott, G., Ott, M. M., Feller, A. C., Seidl, S. & Muller-Hermelink, H. K. (1992). Prevalence of Epstein-Barr virus DNA in different T-cell lymphoma entities in a European population. *International Journal of Cancer* **51**, 562-7.

Pagano, R. E., Martin, O. C., Kang, H. C. & Haugland, R. P. (1991). A novel fluorescent ceramide analogue for studying membrane traffic in animal cells: accumulation at the Golgi apparatus results in altered spectral properties of the sphingolipid precursor. *Journal of Cell Biology* **113**, 1267-79.

Parker, B. D., Bankier, A., Satchwell, S., Barrell, B. & Farrell, P. J. (1990). Sequence and transcription of Raji Epstein-Barr virus DNA spanning the B95-8 deletion region. *Virology* **179**, 339-46.

Parry, C. M., Simas, J. P., Smith, V. P., Stewart, C. A., Minson, A. C., Efstathiou, S. & Alcami, A. (2000). A broad spectrum secreted chemokine binding protein encoded by a herpesvirus. *Journal of Experimental Medicine* **191**, 573-8.

Paule, M. R. & White, R. J. (2000). Survey and summary: transcription by RNA polymerases I and III. *Nucleic Acids Research* **28**, 1283-98.

Peacock, J. W. & Bost, K. L. (2000). Infection of intestinal epithelial cells and development of systemic disease following gastric instillation of murine gammaherpesvirus-68. *Journal of General Virology* **81 Pt 2**, 421-9.

Peacock, J. W. & Bost, K. L. (2001). Murine gammaherpesvirus-68-induced interleukin-10 increases viral burden, but limits virus-induced splenomegaly and leukocytosis. *Immunology* **104**, 109-17.

Piguet, V., Schwartz, O., Le Gall, S. & Trono, D. (1999). The downregulation of CD4 and MHC-I by primate lentiviruses: a paradigm for the modulation of cell surface receptors. *Immunological Reviews* **168**, 51-63.

Piolot, T., Tramier, M., Coppey, M., Nicolas, J. C. & Marechal, V. (2001). Close but distinct regions of human herpesvirus 8 latency-associated nuclear antigen 1 are responsible for nuclear targeting and binding to human mitotic chromosomes. *Journal of Virology* **75**, 3948-59.

Pluymers, W., Cherepanov, P., Schols, D., De Clercq, E. & Debyser, Z. (1999). Nuclear localization of human immunodeficiency virus type 1 integrase expressed as a fusion protein with green fluorescent protein. *Virology* **258**, 327-32.

Pollock, J. L. & Virgin, H. W. (1995). Latency, without persistence, of murine cytomegalovirus in the spleen and kidney. *Journal of Virology* **69**, 1762-8.

Raab-Traub, N., Flynn, K., Pearson, G., Huang, A., Levine, P., Lanier, A. & Pagano, J. (1987). The differentiated form of nasopharyngeal carcinoma contains Epstein- Barr virus DNA. *International Journal of Cancer* **39**, 25-9.

Rabkin, C. S., Janz, S., Lash, A., Coleman, A. E., Musaba, E., Liotta, L., Biggar, R. J. & Zhuang, Z. (1997). Monoclonal origin of multicentric Kaposi's sarcoma lesions. *The New England Journal of Medicine* **336**, 988-93.

Rajcani, J., Blaskovic, D., Svobodova, J., Ciampor, F., Huckova, D. & Stanekova, D. (1985). Pathogenesis of acute and persistent murine herpesvirus infection in mice. *Acta virologica* **29**, 51-60.

Rammensee, H. G., Friede, T. & Stevanoviic, S. (1995). MHC ligands and peptide motifs: first listing. *Immunogenetics* **41**, 178-228.

Raslova, H., Matis, J., Rezuchova, I., Macakova, K., Berebbi, M. & Kudelova, M. (2000). The bystander effect mediated by the new murine gammaherpesvirus 72--thymidine kinase/5'-fluoro-2'-deoxyuridine (MHV72-TK/5-FUdR) system in vitro. *Antiviral Chemistry and Chemotherapy* **11**, 273-82.

Raslova, H., Berebbi, M., Rajcani, J., Sarasin, A., Matis, J. & Kudelova, M. (2001). Susceptibility of mouse mammary glands to murine gammaherpesvirus 72 (MHV-72) infection: evidence of MHV-72 transmission via breast milk. *Microbial Pathogenesis* **31**, 47-58.

Ravanel, K., Castelle, C., Defrance, T., Wild, T. F., Charron, D., Lotteau, V. & Rabourdin-Combe, C. (1997). Measles virus nucleocapsid protein binds to FcgammaRII and inhibits human B cell antibody production. *Journal of Experimental Medicine* **186**, 269-78.

Reichel, M., Matis, J., Lesso, J. & Stancekova, M. (1991). Polypeptides synthesized in rabbit cells infected with murine herpesvirus (MHV): a comparison of proteins specified by various MHV strains. *Acta virologica* **35**, 268-75.

Reid, H. W., Buxton, D., Berrie, E., Pow, I. & Finlayson, J. (1984). Malignant catarrhal fever. *The Veterinary Record* **114**, 581-3.

Resh, M. D. (1994). Myristylation and palmitylation of Src family members: the fats of the matter. *Cell* **76**, 411-3.

Reyburn, H. T., Mandelboim, O., Vales-Gomez, M., Davis, D. M., Pazmany, L. & Strominger, J. L. (1997). The class I MHC homologue of human cytomegalovirus inhibits attack by natural killer cells. *Nature* **386**, 514-7.

Rickinson, A. B., Young, L. S. & Rowe, M. (1987). Influence of the Epstein-Barr virus nuclear antigen EBNA 2 on the growth phenotype of virus-transformed B cells. *Journal of Virology* **61**, 1310-7.

Rickinson, A. B. & Kieff, E. (1996). Epstein-Barr Virus. In *Fields Virology*, pp. 2396-446. Edited by B. N. Fields, D. M. Knipe & P. M. Howley. Philadelphia: Lippincott-Raven.

Rivailler, P., Jiang, H., Cho Yg, Y., Quink, C. & Wang, F. (2002). Complete Nucleotide Sequence of the Rhesus Lymphocryptovirus: Genetic Validation for an Epstein-Barr Virus Animal Model. *Journal of Virology* **76**, 421-426.

Rivas, C., Thlick, A. E., Parravicini, C., Moore, P. S. & Chang, Y. (2001). Kaposi's sarcoma-associated herpesvirus LANA2 is a B-cell-specific latent viral protein that inhibits p53. *Journal of Virology* **75**, 429-38.

Rochford, R., Lutzke, M. L., Alfinito, R. S., Clavo, A. & Cardin, R. D. (2001). Kinetics of murine gammaherpesvirus 68 gene expression following infection of murine cells in culture and in mice. *Journal of Virology* **75**, 4955-63.

Roizman, B., Carmichael, L. E., Deinhardt, F., de-The, G., Nahmias, A. J., Plowright, W., Rapp, F., Sheldrick, P., Takahashi, M. & Wolf, K. (1981). Herpesviridae. Definition, provisional nomenclature, and taxonomy. The Herpesvirus Study Group, the International Committee on Taxonomy of Viruses. *Intervirology* **16**, 201-17.

Roizman, B., Desrosiers, R. C., Fleckenstein, B., Lopez, C., Minson, A. C. & Studdert, M. J. (1992). The family Herpesviridae: an update. The Herpesvirus Study Group of the International Committee on Taxonomy of Viruses. *Archives of Virology* **123**, 425-49.

Roizman, B. (1996). Herpesviridae. In *Fields Virology*, Third edn, pp. 2221-30. Edited by B. N. Fields, D. M. Knipe & P. M. Howley. Philadelphia: Lippincott-Raven.

Roizman, B. & Sears, A. E. (1996). Herpes Simplex Viruses and their replication. In *Fields Virology*, pp. 2231-95. Edited by B. N. Fields, D. M. Knipe & P. M. Howley. Philadelphia: Lippincott-Raven.

Rother, R. P., Rollins, S. A., Fodor, W. L., Albrecht, J. C., Setter, E., Fleckenstein, B. & Squinto, S. P. (1994). Inhibition of complement-mediated cytolysis by the terminal complement inhibitor of herpesvirus saimiri. *Journal of Virology* **68**, 730-7.

Rowe, M., Young, L. S., Crocker, J., Stokes, H., Henderson, S. & Rickinson, A. B. (1991). Epstein-Barr virus (EBV)-associated lymphoproliferative disease in the SCID mouse model: implications for the pathogenesis of EBV-positive lymphomas in man. *Journal of Experimental Medicine* **173**, 147-58.

Roy, D. J., Ebrahimi, B. C., Dutia, B. M., Nash, A. A. & Stewart, J. P. (2000). Murine gammaherpesvirus M11 gene product inhibits apoptosis and is expressed during virus persistence. *Archives of Virology* **145**, 2411-20.

Rudd, P. M., Elliott, T., Cresswell, P., Wilson, I. A. & Dwek, R. A. (2001). Glycosylation and the immune system. *Science* **291**, 2370-6.

Ruf, I. K., Rhyne, P. W., Yang, H., Borza, C. M., Hutt-Fletcher, L. M., Cleveland, J. L. & Sample, J. T. (1999). Epstein-barr virus regulates c-MYC, apoptosis, and tumorigenicity in Burkitt lymphoma. *Molecular Cell Biology* **19**, 1651-60.

Ruf, I. K., Rhyne, P. W., Yang, C., Cleveland, J. L. & Sample, J. T. (2000). Epstein-Barr virus small RNAs potentiate tumorigenicity of Burkitt lymphoma cells independently of an effect on apoptosis. *Journal of Virology* **74**, 10223-8.

Ruscetti, F. W. & Chervenick, P. A. (1975). Regulation of the release of colony-stimulating activity from mitogen - stimulated lymphocytes. *Journal of Immunology* **114**, 1513-7.

Russo, J. J., Bohenzky, R. A., Chien, M. C., Chen, J., Yan, M., Maddalena, D., Parry, J. P., Peruzzi, D., Edelman, I. S., Chang, Y. & Moore, P. S. (1996). Nucleotide sequence of the Kaposi sarcoma-associated herpesvirus (HHV8). *Proceedings of the National Academy of Sciences, USA* **93**, 14862-7.

Sambrook, J., Fritsch, E. F. & Maniatis, T. (1989). Molecular Cloning: A Laboratory Manual, Second edn. New York: Cold Spring Harbor Laboratory Press.

Sample, J., Young, L., Martin, B., Chatman, T., Kieff, E. & Rickinson, A. (1990). Epstein-Barr virus types 1 and 2 differ in their EBNA-3A, EBNA-3B, and EBNA-3C genes. *Journal of Virology* **64**, 4084-92.

Sarawar, S. R., Cardin, R. D., Brooks, J. W., Mehrpooya, M., Tripp, R. A. & Doherty, P. C. (1996). Cytokine production in the immune response to murine gammaherpesvirus 68. *Journal of Virology* **70**, 3264-8.

Sarawar, S. R., Cardin, R. D., Brooks, J. W., Mehrpooya, M., Hamilton-Easton, A. M., Mo, X. Y. & Doherty, P. C. (1997). Gamma interferon is not essential for recovery from acute infection with murine gammaherpesvirus 68. *Journal of Virology* **71**, 3916-21.

Sarawar, S. R., Brooks, J. W., Cardin, R. D., Mehrpooya, M. & Doherty, P. C. (1998). Pathogenesis of murine gammaherpesvirus-68 infection in interleukin- 6-deficient mice. *Virology* **249**, 359-366.

Sarid, R., Flore, O., Bohenzky, R. A., Chang, Y. & Moore, P. S. (1998). Transcription mapping of the Kaposi's sarcoma-associated herpesvirus (human herpesvirus 8) genome in a body cavity-based lymphoma cell line (BC-1). *Journal of Virology* **72**, 1005-12.

Schalling, M., Ekman, M., Kaaya, E. E., Linde, A. & Biberfeld, P. (1995). A role for a new herpes virus (KSHV) in different forms of Kaposi's sarcoma. *Nature Medicine* **1**, 707-8.

Scherer, W. F., Syverton, J. T. & Gey, G. O. (1953). Studies on the propagation in vitro of poliomyelitis viruses. *Journal of Experimental Medicine* **97**, 695-709.

Scherer, M. T., Ignatowicz, L., Winslow, G. M., Kappler, J. W. & Marrack, P. (1993). Superantigens: bacterial and viral proteins that manipulate the immune system. *Annual Reviews in Cell Biology* **9**, 101-28.

Schulz, T. F. (2000). Kaposi's sarcoma-associated herpesvirus (human herpesvirus 8): epidemiology and pathogenesis. *Journal of Antimicrobial Chemotherapy* **45 Suppl T3**, 15-27.

Schust, D. J., Tortorella, D., Seebach, J., Phan, C. & Ploegh, H. L. (1998). Trophoblast class I major histocompatibility complex (MHC) products are resistant to rapid degradation imposed by the human cytomegalovirus (HCMV) gene products US2 and US11. *Journal of Experimental Medicine* **188**, 497-503.

Searles, R. P., Bergquam, E. P., Axthelm, M. K. & Wong, S. W. (1999). Sequence and genomic analysis of a Rhesus macaque rhadinovirus with similarity to Kaposi's sarcoma-associated herpesvirus/human herpesvirus 8. *Journal of Virology* **73**, 3040-53.

Sharp, T. V., Schwemmle, M., Jeffrey, I., Laing, K., Mellor, H., Proud, C. G., Hilse, K. & Clemens, M. J. (1993). Comparative analysis of the regulation of the interferon-inducible protein kinase PKR by Epstein-Barr virus RNAs EBER-1 and EBER-2 and adenovirus VAI RNA. *Nucleic Acids Research* **21**, 4483-90.

Sharp, T. V., Moonan, F., Romashko, A., Joshi, B., Barber, G. N. & Jagus, R. (1998). The vaccinia virus E3L gene product interacts with both the regulatory and the substrate binding regions of PKR: implications for PKR autoregulation. *Virology* **250**, 302-15.

Sharp, T. V., Raine, D. A., Gewert, D. R., Joshi, B., Jagus, R. & Clemens, M. J. (1999). Activation of the interferon-inducible (2'-5') oligoadenylate synthetase by the Epstein-Barr virus RNA, EBER-1. *Virology* **257**, 303-13.

Sheets, M. D., Ogg, S. C. & Wickens, M. P. (1990). Point mutations in AAUAAA and the poly (A) addition site: effects on the accuracy and efficiency of cleavage and polyadenylation in vitro. *Nucleic Acids Research* **18**, 5799-805.

Shope, T., Dechairo, D. & Miller, G. (1973). Malignant lymphoma in cottontop marmosets after inoculation with Epstein-Barr virus. *Proceedings of the National Academy of Sciences, USA* **70**, 2487-91.

Simas, J. P., Bowden, R. J., Paige, V. & Efstathiou, S. (1998). Four tRNA-like sequences and a serpin homologue encoded by murine gammaherpesvirus 68 are dispensable for lytic replication in vitro and latency in vivo. *Journal of General Virology* **79**, 149-53.

Simas, J.P. & Efstathiou, S. (1998). Murine gammaherpesvirus 68: a model for the study of gammaherpesvirus pathogenesis. *Trends in Microbiology* **6**, 276-82.

Simas, J. P., Swann, D., Bowden, R. & Efstathiou, S. (1999). Analysis of murine gammaherpesvirus-68 transcription during lytic and latent infection. *Journal of General Virology* **80**, 75-82.

Sixbey, J. W., Vesterinen, E. H., Nedrud, J. G., Raab-Traub, N., Walton, L. A. & Pagano, J. S. (1983). Replication of Epstein-Barr virus in human epithelial cells infected in vitro. *Nature* **306**, 480-3.

Skepper, J. N., Whiteley, A., Browne, H. & Minson, A. (2001). Herpes simplex virus nucleocapsids mature to progeny virions by an envelopment --> deenvelopment --> reenvelopment pathway. *Journal of Virology* **75**, 5697-702.

Smith, V. P., Bryant, N. A. & Alcami, A. (2000). Ectromelia, vaccinia and cowpox viruses encode secreted interleukin-18- binding proteins. *Journal of General Virology* **81 Pt 5**, 1223-30.

Soderberg-Naucler, C. & Nelson, J. Y. (1999). Human cytomegalovirus latency and reactivation - a delicate balance between the virus and its host's immune system. *Intervirology* **42**, 314-21.

Soulier, J., Grollet, L., Oksenhendler, E., Cacoub, P., Cazals-Hatem, D., Babinet, P., d'Agay, M. F., Clauvel, J. P., Raphael, M., Degos, L. & et al. (1995). Kaposi's sarcoma-associated herpesvirus-like DNA sequences in multicentric Castleman's disease. *Blood* **86**, 1276-80.

Spriggs, M. K. (1999). Shared resources between the neural and immune systems: semaphorins join the ranks. *Current Opinion in Immunology* **11**, 387-91.

Stauber, R. H. & Pavlakis, G. N. (1998). Intracellular trafficking and interactions of the HIV-1 Tat protein. *Virology* **252**, 126-36.

Stevenson, P. G. & Doherty, P. C. (1998). Kinetic analysis of the specific host response to a murine gammaherpesvirus. *Journal of Virology* **72**, 943-9.

Stevenson, P. G., Belz, G. T., Altman, J. D. & Doherty, P. C. (1998). Virus-specific CD8(+) T cell numbers are maintained during gamma- herpesvirus reactivation in CD4-deficient mice. *Proceedings of the National Academy of Sciences, USA* **95**, 15565-70.

Stevenson, P. G., Belz, G. T., Altman, J. D. & Doherty, P. C. (1999a). Changing patterns of dominance in the CD8+ T cell response during acute and persistent murine gamma-herpesvirus infection. *European Journal of Immunology* **29**, 1059-67.

Stevenson, P. G., Belz, G. T., Castrucci, M. R., Altman, J. D. & Doherty, P. C. (1999b). A gamma-herpesvirus sneaks through a CD8(+) T cell response primed to a lytic-phase epitope. *Proceedings of the National Academy of Sciences, USA* **96**, 9281-9286.

Stevenson, P. G., Cardin, R. D., Christensen, J. P. & Doherty, P. C. (1999c). Immunological control of a murine gammaherpesvirus independent of CD8+ T cells. *Journal of General Virology* **80**, 477-83.

Stevenson, P. G. & Doherty, P. C. (1999). Non-antigen-specific B-cell activation following murine gammaherpesvirus infection is CD4 independent in vitro but CD4 dependent in vivo. *Journal of Virology* **73**, 1075-1079.

Stevenson, A. J., Frolova-Jones, E., Hall, K. T., Kinsey, S. E., Markham, A. F., Whitehouse, A. & Meredith, D. M. (2000a). A herpesvirus saimiri-based gene therapy vector with potential for use in cancer immunotherapy. *Cancer Gene Therapy* **7**, 1077-85.

Stevenson, P. G., Efstathiou, S., Doherty, P. C. & Lehner, P. J. (2000b). Inhibition of MHC class I-restricted antigen presentation by gamma 2-herpesviruses. *Proceedings of the National Academy of Sciences, USA* **97**, 8455-60.

Stewart, J. P., Janjua, N. J., Sunil-Chandra, N. P., Nash, A. A. & Arrand, J. R. (1994). Characterization of murine gammaherpesvirus 68 glycoprotein B (gB) homolog: similarity to Epstein-Barr virus gB (gp110). *Journal of Virology* **68**, 6496-504.

Stewart, J. P., Usherwood, E. J., Dutia, B. & Nash, A. A. (1998a). Immunobiology of Murine Gamma Herpesvirus-68. In *Herpesviruses and Immunity*, pp. 149 - 163. Edited by Medveczky et al. New York: Plenum Press.

Stewart, J. P., Usherwood, E. J., Ross, A., Dyson, H. & Nash, T. (1998b). Lung epithelial cells are a major site of murine gammaherpesvirus persistence. *Journal of Experimental Medicine* **187**, 1941-51.

Stewart, J. P., Micali, N., Usherwood, E. J., Bonina, L. & Nash, A. A. (1999). Murine gamma-herpesvirus 68 glycoprotein 150 protects against virus- induced mononucleosis: A model system for gamma-herpesvirus vaccination. *Vaccine* **17**, 152-157.

Stine, J. T., Wood, C., Hill, M., Epp, A., Raport, C. J., Schweickart, V. L., Endo, Y., Sasaki, T., Simmons, G., Boshoff, C., Clapham, P., Chang, Y., Moore, P., Gray, P. W. & Chantry, D. (2000). KSHV-encoded CC chemokine vMIP-III is a CCR4 agonist, stimulates angiogenesis, and selectively chemoattracts TH2 cells. *Blood* **95**, 1151-7.

Straight, S. W., Hinkle, P. M., Jewers, R. J. & McCance, D. J. (1993). The E5 oncoprotein of human papillomavirus type 16 transforms fibroblasts and effects the downregulation of the epidermal growth factor receptor in keratinocytes. *Journal of Virology* **67**, 4521-32.

Sugden, B., Phelps, M. & Domoradzki, J. (1979). Epstein-Barr virus DNA is amplified in transformed lymphocytes. *Journal of Virology* **31**, 590-5.

Sun, R., Lin, S. F., Gradoville, L., Yuan, Y., Zhu, F. & Miller, G. (1998). A viral gene that activates lytic cycle expression of Kaposi's sarcoma- associated herpesvirus. *Proceedings of the National Academy of Sciences, USA* **95**, 10866-71.

Sun, R., Lin, S. F., Staskus, K., Gradoville, L., Grogan, E., Haase, A. & Miller, G. (1999). Kinetics of Kaposi's sarcoma-associated herpesvirus gene expression. *Journal of Virology* **73**, 2232-42.

Sunil-Chandra, N. P., Efstathiou, S., Arno, J. & Nash, A. A. (1992a). Virological and pathological features of mice infected with murine gamma-herpesvirus 68. *Journal of General Virology* **73**, 2347-56.

Sunil-Chandra, N. P., Efstathiou, S. & Nash, A. A. (1992b). Murine gammaherpesvirus 68 establishes a latent infection in mouse B lymphocytes in vivo. *Journal of General Virology* **73**, 3275-9.

Sunil-Chandra, N. P., Arno, J., Fazakerley, J. & Nash, A. A. (1994). Lymphoproliferative disease in mice infected with murine gammaherpesvirus 68. *American Journal of Pathology* **145**, 818-26.

Svobodova, J., Blaskovic, D. & Mistrikova, J. (1982a). Growth characteristics of herpesviruses isolated from free living small rodents. *Acta virologica* **26**, 256-63.

Svobodova, J., Stancekova, M., Blaskovic, D., Mistrikova, J., Lesso, J., Russ, G. & Masarova, P. (1982b). Antigenic relatedness of alphaherpesviruses isolated from free-living rodents. *Acta virologica* **26**, 438-43.

Swaminathan, S., Tomkinson, B. & Kieff, E. (1991). Recombinant Epstein-Barr virus with small RNA (EBER) genes deleted transforms lymphocytes and replicates in vitro. *Proceedings of the National Academy of Sciences, USA* **88**, 1546-50.

Swaminathan, S., Huneycutt, B. S., Reiss, C. S. & Kieff, E. (1992). Epstein-Barr virus-encoded small RNAs (EBERs) do not modulate interferon effects in infected lymphocytes. *Journal of Virology* **66**, 5133-6.

Sylla, B. S., Hung, S. C., Davidson, D. M., Hatzivassiliou, E., Malinin, N. L., Wallach, D., Gilmore, T. D., Kieff, E. & Mosialos, G. (1998). Epstein-Barr virus-transforming protein latent infection membrane protein 1 activates transcription factor NF-kappaB through a pathway that includes the NF-kappaB-inducing kinase and the IkappaB kinases IKKalpha and IKKbeta. *Proceedings of the National Academy of Sciences, USA* **95**, 10106-11.

Takada, K. (2001). Role of Epstein-Barr virus in Burkitt's lymphoma. *Current Topics in Microbiology and Immunology* **258**, 141-51.

Takada, K. & Nanbo, A. (2001). The role of EBERs in oncogenesis. *Seminars in Cancer Biology* **11**, 461-7.

Talbot, S. J., Weiss, R. A., Kellam, P. & Boshoff, C. (1999). Transcriptional analysis of human herpesvirus-8 open reading frames 71, 72, 73, K14, and 74 in a primary effusion lymphoma cell line. *Virology* **257**, 84-94.

Tamagnone, L. & Comoglio, P. M. (2000). Signalling by semaphorin receptors: cell guidance and beyond. *Trends in Cell Biology* **10**, 377-83.

Taniguchi, T., Ogasawara, K., Takaoka, A. & Tanaka, N. (2001). IRF family of transcription factors as regulators of host defense. *Annual Reviews in Immunology* **19**, 623-55.

Tarasova, N. I., Stauber, R. H., Choi, J. K., Hudson, E. A., Czerwinski, G., Miller, J. L., Pavlakis, G. N., Michejda, C. J. & Wank, S. A. (1997). Visualization of G protein-coupled receptor trafficking with the aid of the green fluorescent protein. Endocytosis and recycling of cholecystokinin receptor type A. *Journal of Biological Chemistry* **272**, 14817-24.

Tarasova, N. I., Stauber, R. H. & Michejda, C. J. (1998). Spontaneous and ligand-induced trafficking of CXC-chemokine receptor 4. *Journal of Biological Chemistry* **273**, 15883-6.

Telford, E. A., Studdert, M. J., Agius, C. T., Watson, M. S., Aird, H. C. & Davison, A. J. (1993). Equine herpesviruses 2 and 5 are gamma-herpesviruses. *Virology* **195**, 492-9.

Telford, E. A., Watson, M. S., Aird, H. C., Perry, J. & Davison, A. J. (1995). The DNA sequence of equine herpesvirus 2. *Journal of Molecular Biology* **249**, 520-8.

Thale, R., Lucin, P., Schneider, K., Eggers, M. & Koszinowski, U. H. (1994). Identification and expression of a murine cytomegalovirus early gene coding for an Fc receptor. *Journal of Virology* **68**, 7757-65.

Thomas, J. A., Hotchin, N. A., Allday, M. J., Amlot, P., Rose, M., Yacoub, M. & Crawford, D. H. (1990). Immunohistology of Epstein-Barr virus-associated antigens in B cell disorders from immunocompromised individuals. *Transplantation* **49**, 944-53.

Thome, M., Schneider, P., Hofmann, K., Fickenscher, H., Meinl, E., Neipel, F., Mattmann, C., Burns, K., Bodmer, J. L., Schroter, M., Scaffidi, C., Krammer, P. H., Peter, M. E. & Tschopp, J. (1997). Viral FLICE-inhibitory proteins (FLIPs) prevent apoptosis induced by death receptors. *Nature* **386**, 517-21.

Thompson, J. D., Higgins, D. G. & Gibson, T. J. (1994). CLUSTAL W: improving the sensitivity of progressive multiple sequence alignment through sequence weighting, position-specific gap penalties and weight matrix choice. *Nucleic Acids Research* **22**, 4673-80.

Thorley-Lawson, D. A. & Babcock, G. J. (1999). A model for persistent infection with Epstein-Barr virus: the stealth virus of human B cells. *Life Sciences* **65**, 1433-53.

Tokunaga, M., Land, C. E., Uemura, Y., Tokudome, T., Tanaka, S. & Sato, E. (1993). Epstein-Barr virus in gastric carcinoma. *American Journal of Pathology* **143**, 1250-4.

Tomasec, P., Braud, V. M., Rickards, C., Powell, M. B., McSharry, B. P., Gadola, S., Cerundolo, V., Borysiewicz, L. K., McMichael, A. J. & Wilkinson, G. W. (2000). Surface expression of HLA-E, an inhibitor of natural killer cells, enhanced by human cytomegalovirus gpUL40. *Science* **287**, 1031.

Tomazin, R., Boname, J., Hegde, N. R., Lewinsohn, D. M., Altschuler, Y., Jones, T. R., Cresswell, P., Nelson, J. A., Riddell, S. R. & Johnson, D. C. (1999). Cytomegalovirus US2 destroys two components of the MHC class II pathway, preventing recognition by CD4+ T cells. *Nature Medicine* **5**, 1039-43.

Tomkinson, B., Robertson, E. & Kieff, E. (1993). Epstein-Barr virus nuclear proteins EBNA-3A and EBNA-3C are essential for B-lymphocyte growth transformation. *Journal of Virology* **67**, 2014-25.

Tortorella, D., Gewurz, B. E., Furman, M. H., Schust, D. J. & Ploegh, H. L. (2000). Viral subversion of the immune system. *Annual Reviews in Immunology* **18**, 861-926.

Tripp, R. A., Hamilton-Easton, A. M., Cardin, R. D., Nguyen, P., Behm, F. G., Woodland, D. L., Doherty, P. C. & Blackman, M. A. (1997). Pathogenesis of an infectious mononucleosis-like disease induced by a murine gamma-herpesvirus: role for a viral superantigen? *Journal of Experimental Medicine* **185**, 1641-50.

Usherwood, E. J., Ross, A. J., Allen, D. J. & Nash, A. A. (1996a). Murine gammaherpesvirus-induced splenomegaly: a critical role for CD4 T cells. *Journal of General Virology* **77**, 627-30.

Usherwood, E. J., Stewart, J. P. & Nash, A. A. (1996b). Characterization of tumor cell lines derived from murine gammaherpesvirus-68-infected mice. *Journal of Virology* **70**, 6516-8.

Usherwood, E. J., Stewart, J. P., Robertson, K., Allen, D. J. & Nash, A. A. (1996c). Absence of splenic latency in murine gammaherpesvirus 68-infected B cell-deficient mice. *Journal of General Virology* **77**, 2819-25.

Usherwood, E. J., Hogg, T. L. & Woodland, D. L. (1999). Enumeration of antigen-presenting cells in mice infected with Sendai virus. *Journal of Immunology* **162**, 3350-5.

Usherwood, E. J., Roy, D. J., Ward, K., Surman, S. L., Dutia, B. M., Blackman, M. A., Stewart, J. P. & Woodland, D. L. (2000). Control of gammaherpesvirus latency by latent antigen-specific CD8(+) T cells. *Journal of Experimental Medicine* **192**, 943-52.

Usherwood, E. J., Ward, K. A., Blackman, M. A., Stewart, J. P. & Woodland, D. L. (2001). Latent antigen vaccination in a model gammaherpesvirus infection. *Journal of Virology* **75**, 8283-8.

van Berkel, V., Preiter, K., Virgin, H. W. & Speck, S. H. (1999). Identification and initial characterization of the murine gammaherpesvirus 68 gene M3, encoding an abundantly secreted protein. *Journal of Virology* **73**, 4524-9.

van Berkel, V., Barrett, J., Tiffany, H. L., Fremont, D. H., Murphy, P. M., McFadden, G., Speck, S. H. & Virgin, H. W. (2000). Identification of a gammaherpesvirus selective chemokine binding protein that inhibits chemokine action. *Journal of Virology* **74**, 6741-7.

van Dyk, L. F., Hess, J. L., Katz, J. D., Jacoby, M., Speck, S. H. & Virgin, H. W. (1999). The murine gammaherpesvirus 68 v-cyclin gene is an oncogene that promotes cell cycle progression in primary lymphocytes. *Journal of Virology* **73**, 5110-22.

van Dyk, L. F., Virgin, H. W. & Speck, S. H. (2000). The murine gammaherpesvirus 68 v-cyclin is a critical regulator of reactivation from latency. *Journal of Virology* **74**, 7451-61.

Vieira, J., Schall, T. J., Corey, L. & Geballe, A. P. (1998). Functional analysis of the human cytomegalovirus US28 gene by insertion mutagenesis with the green fluorescent protein gene. *Journal of Virology* **72**, 8158-65.

Virgin, H. W., Latreille, P., Wamsley, P., Hallsworth, K., Weck, K. E., Dal Canto, A. J. & Speck, S. H. (1997). Complete sequence and genomic analysis of murine gammaherpesvirus 68. *Journal of Virology* **71**, 5894-904.

Virgin, H. W., Presti, R. M., Li, X. Y., Liu, C. & Speck, S. H. (1999). Three distinct regions of the murine gammaherpesvirus 68 genome are transcriptionally active in latently infected mice. *Journal of Virology* **73**, 2321-32.

Virtanen, I., Ekblom, P. & Laurila, P. (1980). Subcellular compartmentalization of saccharide moieties in cultured normal and malignant cells. *Journal of Cell Biology* **85**, 429-34.

Wakeling, M. N., Roy, D. J., Nash, A. A. & Stewart, J. P. (2001). Characterization of the murine gammaherpesvirus 68 ORF74 product: a novel oncogenic G protein-coupled receptor. *Journal of General Virology* **82**, 1187-97.

Wan, F. (2002) Characterisation of the murine gammaherpesvirus-68 M4 gene. PhD Thesis, University of Edinburgh.

Wang, G. H., Garvey, T. L. & Cohen, J. I. (1999). The murine gammaherpesvirus-68 M11 protein inhibits Fas- and TNF- induced apoptosis. *Journal of General Virology* **80**, 2737-40.

Wang, X., Kenyon, W. J., Li, Q., Mullberg, J. & Hutt-Fletcher, L. M. (1998). Epstein-Barr virus uses different complexes of glycoproteins gH and gL to infect B lymphocytes and epithelial cells. *Journal of Virology* **72**, 5552-8.

Weck, K. E., Barkon, M. L., Yoo, L. I., Speck, S. H. & Virgin, H. W. (1996). Mature B cells are required for acute splenic infection, but not for establishment of latency, by murine gammaherpesvirus 68. *Journal of Virology* **70**, 6775-80.

Weck, K. E., Dal Canto, A. J., Gould, J. D., Oguin, A. K., Roth, K. A., Saffitz, J. E., Speck, S. H. & Virgin, H. W. (1997). Murine gamma-herpesvirus 68 causes severe large-vessel arteritis in mice lacking interferon-gamma responsiveness: A new model for virus- induced vascular disease. *Nature Medicine* **3**, 1346-1353.

Weck, K. E., Kim, S. S., Virgin, H. W. & Speck, S. H. (1999a). B cells regulate murine gammaherpesvirus 68 latency. *Journal of Virology* **73**, 4651-61.

Weck, K. E., Kim, S. S., Virgin, H. W. & Speck, S. H. (1999b). Macrophages are the major reservoir of latent murine gammaherpesvirus 68 in peritoneal cells. *Journal of Virology* **73**, 3273-83.

Wedderburn, N., Edwards, J. M., Desgranges, C., Fontaine, C., Cohen, B. & de The, G. (1984). Infectious mononucleosis-like response in common marmosets infected with Epstein-Barr virus. *Journal of Infectious Diseases* **150**, 878-82.

Weiss, L. M., Strickler, J. G., Warnke, R. A., Purtilo, D. T. & Sklar, J. (1987). Epstein-Barr viral DNA in tissues of Hodgkin's disease. *American Journal of Pathology* **129**, 86-91.

Welker, R., Harris, M., Cardel, B. & Krausslich, H. G. (1998). Virion incorporation of human immunodeficiency virus type 1 Nef is mediated by a bipartite membrane-targeting signal: analysis of its role in enhancement of viral infectivity. *Journal of Virology* **72**, 8833-40.

Whitby, D., Howard, M. R., Tenant-Flowers, M., Brink, N. S., Copas, A., Boshoff, C., Hatzioannou, T., Suggett, F. E., Aldam, D. M., Denton, A. S. & et al. (1995). Detection of Kaposi sarcoma associated herpesvirus in peripheral blood of HIV-infected individuals and progression to Kaposi's sarcoma. *Lancet* **346**, 799-802.

White, K. L., Slobedman, B. & Mocarski, E. S. (2000). Human cytomegalovirus latency-associated protein pORF94 is dispensable for productive and latent infection. *Journal of Virology* **74**, 9333-7.

Whiteley, A., Bruun, B., Minson, T. & Browne, H. (1999). Effects of targeting herpes simplex virus type 1 gD to the endoplasmic reticulum and trans-Golgi network. *Journal of Virology* **73**, 9515-20.

Wilkinson, D. L. & Harrison, R. G. (1991). Predicting the solubility of recombinant proteins in Escherichia coli. *Biotechnology* **9**, 443-8.

Woisetschlaeger, M., Yandava, C. N., Furmanski, L. A., Strominger, J. L. & Speck, S. H. (1990). Promoter switching in Epstein-Barr virus during the initial stages of infection of B lymphocytes. *Proceedings of the National Academy of Sciences, USA* **87**, 1725-9.

Woisetschlaeger, M., Jin, X. W., Yandava, C. N., Furmanski, L. A., Strominger, J. L. & Speck, S. H. (1991). Role for the Epstein-Barr virus nuclear antigen 2 in viral promoter switching during initial stages of infection. *Proceedings of the National Academy of Sciences, USA* **88**, 3942-6.

Wu, T. T., Usherwood, E. J., Stewart, J. P., Nash, A. A. & Sun, R. (2000). Rta of murine gammaherpesvirus 68 reactivates the complete lytic cycle from latency. *Journal of Virology* **74**, 3659-67.

Xu, Z. L., Mizuguchi, H., Ishii-Watabe, A., Uchida, E., Mayumi, T. & Hayakawa, T. (2001). Optimization of transcriptional regulatory elements for constructing plasmid vectors. *Gene* **272**, 149-56.

Yamasaki, S., Nishida, K., Hibi, M., Sakuma, M., Shiina, R., Takeuchi, A., Ohnishi, H., Iiirano, T. & Saito, T. (2001). Docking protein Gab2 is phosphorylated by ZAP-70 and negatively regulates T cell receptor signaling by recruitment of inhibitory molecules. *Journal of Biological Chemistry* **276**, 45175-83.

Yates, J. L., Warren, N. & Sugden, B. (1985). Stable replication of plasmids derived from Epstein-Barr virus in various mammalian cells. *Nature* **313**, 812-5.

Yokoyama, A., Tanaka, M., Matsuda, G., Kato, K., Kanamori, M., Kawasaki, H., Hirano, H., Kitabayashi, I., Ohki, M., Hirai, K. & Kawaguchi, Y. (2001). Identification of major phosphorylation sites of Epstein-Barr virus nuclear antigen leader protein (EBNA-LP): ability of EBNA-LP to induce latent membrane protein 1 cooperatively with EBNA-2 is regulated by phosphorylation. *Journal of Virology* **75**, 5119-28.

Yoshiyama, H., Imai, S., Shimizu, N. & Takada, K. (1997). Epstein-Barr virus infection of human gastric carcinoma cells: implication of the existence of a new virus receptor different from CD21. *Journal of Virology* **71**, 5688-91.

Young, L. S., Finerty, S., Brooks, L., Scullion, F., Rickinson, A. B. & Morgan, A. J. (1989). Epstein-Barr virus gene expression in malignant lymphomas induced by experimental virus infection of cottontop tamarins. *Journal of Virology* **63**, 1967-74.

Yuhasz, S. A., Dissette, V. B., Cook, M. L. & Stevens, J. G. (1994). Murine cytomegalovirus is present in both chronic active and latent states in persistently infected mice. *Virology* **202**, 272-80.

Zhang, L. & Pagano, J. S. (1997). IRF-7, a new interferon regulatory factor associated with Epstein-Barr virus latency. *Molecular and Cellular Biology* **17**, 5748-57.

Zhao, B., Marshall, D. R. & Sample, C. E. (1996). A conserved domain of the Epstein-Barr virus nuclear antigens 3A and 3C binds to a discrete domain of Jkappa. *Journal of Virology* **70**, 4228-36.

Zhao, C., Yu, D. H., Shen, R. & Feng, G. S. (1999). Gab2, a new pleckstrin homology domain-containing adapter protein, acts to uncouple signaling from ERK kinase to Elk-1. *Journal of Biological Chemistry* **274**, 19649-54.

Zhou, Y. J., Hanson, E. P., Chen, Y. Q., Magnuson, K., Chen, M., Swann, P. G., Wange, R. L., Changelian, P. S. & O'Shea, J. J. (1997). Distinct tyrosine phosphorylation sites in JAK3 kinase domain positively and negatively regulate its enzymatic activity. *Proceedings of the National Academy of Sciences, USA* **94**, 13850-5.

Zong, J. C., Ciufo, D. M., Alcendor, D. J., Wan, X., Nicholas, J., Browning, P. J., Rady, P. L., Tyring, S. K., Orenstein, J. M., Rabkin, C. S., Su, I. J., Powell, K. F., Croxson, M., Foreman, K. E., Nickoloff, B. J., Alkan, S. & Hayward, G. S. (1999). High-level variability in the ORF-K1 membrane protein gene at the left end of the Kaposi's sarcoma-associated herpesvirus genome defines four major virus subtypes and multiple variants or clades in different human populations. *Journal of Virology* **73**, 4156-70.

Appendix

Publications

Macrae, A.I., Dutia, B.M., Milligan, S., Brownstein, D.G., Allen, D.J., Mistrikova, J., Davison, A.J., Nash, A.A. & Stewart, J.P. (2001). Analysis of a novel strain of murine gammaherpesvirus reveals a genomic locus important for acute pathogenesis. *Journal of Virology* **75**, 5315-27

JOURNAL OF VIROLOGY, June 2001, p. 5315–5327 Vol. 75, No. 11
0022-538X/01/$04.00+0 DOI: 10.1128/JVI.75.11.5315–5327.2001

Analysis of a Novel Strain of Murine Gammaherpesvirus Reveals a Genomic Locus Important for Acute Pathogenesis

ALASTAIR I. MACRAE,[1] BERNADETTE M. DUTIA,[1] STEVEN MILLIGAN,[2] DAVID G. BROWNSTEIN,[1] DEBORAH J. ALLEN,[1] JELA MISTRIKOVA,[3] ANDREW J. DAVISON,[2] ANTHONY A. NASH,[1] AND JAMES P. STEWART[1]*

Laboratory for Clinical and Molecular Virology, The University of Edinburgh, Edinburgh EH9 1QH,[1] and MRC Virology Unit, Institute of Virology, Glasgow G11 5JR,[2] United Kingdom, and Department of Microbiology and Virology, Faculty of Natural Sciences, Comenius University, 842 15 Bratislava, Slovak Republic[3]

Received 22 December 2000/Accepted 1 March 2001

Infection of mice by murine gammaherpesvirus 68 (MHV-68) is an excellent small-animal model of gammaherpesvirus pathogenesis in a natural host. We have carried out comparative studies of another herpesvirus, murine herpesvirus 76 (MHV-76), which was isolated at the same time as MHV-68 but from a different murid host, the yellow-necked mouse (*Apodemus flavicollis*). Molecular analyses revealed that the MHV-76 genome is essentially identical to that of MHV-68, except for deletion of 9,538 bp at the left end of the unique region. MHV-76 is therefore a deletion mutant that lacks four genes unique to MHV-68 (*M1*, *M2*, *M3*, and *M4*) as well as the eight viral tRNA-like genes. Replication of MHV-76 in cell culture was identical to that of MHV-68. However, following infection of mice, MHV-76 was cleared more rapidly from the lungs. In line with this, there was an increased inflammatory response in lungs with MHV-76. Splenomegaly was also significantly reduced following MHV-76 infection, and much less latent MHV-76 was detected in the spleen. Nevertheless, MHV-76 maintained long-term latency in the lungs and spleen. We utilized a cosmid containing the left end of the MHV-68 genome to reinsert the deleted sequence into MHV-76 by recombination in infected cells, and we isolated a rescuant virus designated MHV-76(cA8+)4 which was ostensibly genetically identical to MHV-68. The growth properties of the rescuant in infected mice were identical to those of MHV-68. These results demonstrate that genetic elements at the left end of the unique region of the MHV-68 genome play vital roles in host evasion and are critical to the development of splenic pathology.

Infection of laboratory mice by murine gammaherpesvirus 68 (MHV-68) (formally designated murid herpesvirus 4) is an excellent model system for the study of gammaherpesvirus pathogenesis and for the development of therapeutic strategies against these viruses (31). Following intranasal inoculation of mice with MHV-68, productive infection initially occurs in the lung (34). The acute, productive infection is cleared from the lung by day 10 postinfection (p.i.) by $CD8^+$ T cells (12), but the virus then persists in a latent form in epithelial cells at this site (32). MHV-68 spreads to the spleen during the subsequent viremia, where it becomes latent in B lymphocytes, macrophages, and dendritic cells (13, 35, 39, 44). Establishment of latency in the spleen is associated with a marked splenomegaly and a mononucleosis that resembles that caused by primary infection of humans by Epstein-Barr virus (36). Splenomegaly is driven by $CD4^+$ T cells (12, 37) and is dependent on the presence of MHV-68-infected B cells in the spleen (39, 43). The resolution of splenomegaly is achieved by $CD8^+$ T cells (12, 43), which are also important in the long-term control of persistent infection (5, 32, 43).

The MHV-68 genome consists of a unique region of 118,237 bp flanked on each side by multiple copies of a 1,213-bp terminal repeat (11, 42). The left end of the unique region has attracted considerable interest owing to the presence of four protein-coding genes (*M1*, *M2*, *M3*, and *M4*) and eight viral tRNA-like (vtRNA) genes, all of which lack counterparts in other gammaherpesviruses (4, 42). Of these, only the function of *M3* has been elucidated. This gene encodes a secreted chemokine binding protein that is expressed during acute infection and persistence in mice (25, 38, 40, 41). *M1* has been shown to be nonessential for lytic replication in vitro and in vivo for the maintenance and establishment of latency (6, 28). *M2* is expressed during latency in vitro and in vivo (14, 41) and contains a $CD8^+$ T-cell epitope, which is a target for the host immune response (14, 38). The vtRNA genes are abundantly expressed during lytic and latent infection (4), but their functional significance is not known.

Field studies in Slovakia aimed at identifying a small-animal vector for flaviviruses resulted in the isolation of five herpesviruses from two species of murid rodents (3). MHV-60, -68, and -72 were isolated from the bank vole (*Clethrionomys glareolus*), and MHV-76 and -78 were isolated from the yellow-necked wood mouse (*Apodemus flavicollis*). Further molecular studies of MHV-68 and sequencing of the genome showed that it belongs to the genus *Rhadinovirus* (often referred to as gamma-2 herpesviruses), which includes Kaposi's sarcoma-associated herpesvirus and herpesvirus saimiri (HVS) (10, 24, 42).

Of the other herpesvirus strains isolated alongside MHV-68 (3), only MHV-72 has been studied. This virus, which was isolated from the same host as MHV-68, appears to have similar biological properties in that it infects B lymphocytes

* Corresponding author. Mailing address: Laboratory for Clinical and Molecular Virology, The University of Edinburgh, Summerhall, Edinburgh EH9 1QH, United Kingdom. Phone: 44 131 650 7939. Fax: 44 131 650 6511. E-mail: james.stewart@ed.ac.uk.

(22, 26) and long-term infection is associated with tumorigenesis (21). In contrast, MHV-76 was isolated from a different murid species (3). Therefore, we hypothesized that it may have different biological characteristics and thus yield additional insights into gammaherpesvirus pathogenesis. In this paper, we describe the characterization of MHV-76. We demonstrate that the MHV-76 genome is essentially identical to that of MHV-68 except that it lacks *M1*, *M2*, *M3*, *M4*, and all of the vtRNA genes. We show that MHV-76 shares many biological features with MHV-68, including identical growth in vitro, productive infection in the lung, and the establishment and maintenance of latency in B lymphocytes. However, it is much less pathogenic in vivo than MHV-68, and reduced pathogenicity is associated with an increased inflammatory response. A rescuant virus was constructed by insertion of the left end of the MHV-68 genome into that of MHV-76. The MHV-76-derived rescuant regained the in vivo properties of MHV-68. We conclude that this region of the MHV-68 genome plays an important role in pathogenesis.

MATERIALS AND METHODS

Cell line and virus. Viruses were grown and titrated using BHK-21 cells as described previously (34). MHV-68 was originally isolated during field studies from the bank vole, *C. glareolus* (3), and was subsequently plaque purified on BHK-21 cells to obtain clone g2.4 as described by Efstathiou et al. (11). MHV-76 was isolated from the yellow-necked mouse, *A. flavicollis*, during the same field study and was plaque purified thrice on BHK-21 cells to obtain a pure stock

Purification of viral DNA. MHV-76 or MHV-68 DNA was prepared from purified virions as described previously (11). The DNAs migrated as a single band of high molecular weight by agarose gel electrophoresis and resulted in the production of infectious virus when transfected into BHK-21 cells (not shown). For some experiments, high-molecular-weight DNA was also prepared from infected cells.

Analyses of MHV-76 DNA. Restriction endonuclease digestion and Southern blot hybridization were carried out using standard procedures. Cosmid clones of MHV-68 and MHV-76 DNAs were prepared as described previously (7) using infected-cell DNA and were identified by standard colony hybridization protocols. Pertinent cosmids were an MHV-68 cosmid (cA8) containing nucleotides 115165 to 26842 and an MHV-76 cosmid (cM1) containing the region equivalent to nucleotides 115587 to 26842. Both cosmids originated from circular or concatemeric forms and thus contain both ends of the genome. Nucleotide coordinates are given according to the genome sequence published by Virgin et al. (42).

The DNA sequence of cosmid M1 was determined by standard procedures of sonication, end repair, and cloning into bacteriophage M13mp19. Inserts were sequenced using an ABI Prism 377 DNA sequencer, and the data were assembled into the finished sequence using the Sequence Assembly Program (30).

Determination of viral DNA in tissue samples. Viral DNA was extracted from blood and tissues using QIAmp DNA minikits (Qiagen) according to the manufacturer's instructions. DNA quantification was performed using a DNA fluorimeter (DyNA Quant 200; Pharmacia). PCR amplification was performed on 1 μg of high-molecular-weight DNA using primers specific for the *gp150* or *M3* gene as described below. PCR products (15 μl) were electrophoresed through 1.5% agarose gels and analyzed by Southern blot hybridization to confirm the specificity of the products. DNA was blotted onto Hybond N^+ membranes (Amersham) and hybridized to ^{32}P-labeled probes specific for *gp150* or *M3*.

PCR analysis of viral genomes. PCR amplification was performed using 1 μg of viral DNA as the template for 40 cycles under conditions described previously (38). In addition, negative control reactions for all primer sets were performed using water instead of template DNA (not shown). Primer sequences were as follows: for *M1*, 5′-GTT ACC TAG GAC ATA CAG TGG-3′ and 5′-CAG AAC CTT ACC AGT CAT GTG-3′ (product size, 279 bp); for *M2*, 5′-GCG GGA TCC ATG GCC CCA ACA CCC CCA C-3′ and 5′-GCG GAA TTC GTT ATG TTC TGC GTT AGC ACC-3′ (product size, 654 bp); for *M3*, 5′-TGG CAC TCA AAC TTG GTT GTG G-3′ and 5′-TAA CAG GCA GAT TGC CAT TCC C-3′ (product size, 381 bp); for *M4*, 5′-GCG CGG ATC CGA CAC CTG GAG AAG ATG ATG ATA TTC C-3′ and 5′-CGC GGA ATT CGG TTC TAG AAA GTC ATA AAT CTC AAT ACC-3′ (product size, 1,452 bp); for *gp150*, 5′-GCG CAA GCT TCG CCG CCA CCA TGT GTG GCG TTA AAT-3′ and 5′-CGC GCT CGA GTT ATT CAT GTA AAC ACA CAC AG-3′ (product size, 1,533 bp); and for *ORF 74*, 5′-GCC ACG ATG CTT GTC CTG CG-3′ and 5′-TTA GGA GCT TAG TCT ACA AAC TG-3′ (product size, 1,010 bp).

A modification was used to analyze viral plaques or viral stocks. The virus sample (10 μl; approximately 10 PFU) was added to PCR mix without *Taq* DNA polymerase. Proteinase K (Roche) was then added to 0.2 μg/μl. After incubation at 65°C for 15 min and then at 95°C for 10 min, 1 U of *Taq* DNA polymerase (Gibco/BRL) was added and 40 cycles of amplification were performed.

Construction of rescuant viruses. MHV-76 genomic DNA and cosmid A8 were cotransfected into BHK-21 cells by electroporation. After 6 days, the monolayer was harvested and the supernatant was used to infect BALB/c mice. After 14 days, the spleens were harvested and analyzed by infective-center assay. Individual plaques containing rescued virus were identified by PCR amplification of the *M2* and *ORF 74* open reading frames (ORFs). Viruses were plaque purified by limiting-dilution assay on BHK-21 cells until they were homogeneous by PCR screening.

Southern analysis. High-molecular-weight DNA was isolated from infected BHK-21 cells and cut with restriction enzymes according to the instructions of the manufacturer (Gibco/BRL). Southern analysis was then performed by established procedures (27), and probes were labeled with ^{32}P using a random-primed DNA labeling kit (Roche).

In vitro infections. Single-step growth curves were obtained by infecting subconfluent BHK-21 cells at a multiplicity of infection (MOI) of 5. After adsorption for 1 h, the wells were washed with medium to remove unbound virus and fresh medium was added. At various times p.i., the wells were harvested and infectious virus was quantified by plaque assay as described below. All experiments were carried out in duplicate.

Infection of mice and analysis of tissues. BALB/c mice were purchased from Bantin and Kingman and infected when 4 to 6 weeks old. Mice were anesthetized with halothane and inoculated intranasally with 2×10^5 PFU of virus in 40 μl of sterile phosphate-buffered saline. At various times p.i., mice were euthanized by cervical dislocation and tissues were harvested for analysis. Plaque assays were performed using BHK-21 cells to detect infectious virus as described previously (34). The limit of detection of the plaque assay was 10 PFU per organ. An infective-center assay was used to detect latent virus as described previously (34). The data were analyzed statistically using the two-sample *t* test. *P* values are indicated in Results.

Histopathology. After euthanasia by CO_2 asphyxiation, the lungs were perfused in situ via the trachea using 10% neutral buffered Formol saline. Portions of spleen were also fixed in 10% buffered Formol saline, and the tissues were processed routinely into paraffin wax-embedded sections. These were stained with hematoxylin and eosin and examined by light microscopy.

Nucleotide sequence accession number. The sequence of the MHV-76 insert in cosmid M1 was deposited with the GenBank data library under accession number AF324455.

RESULTS

The MHV-76 genome is essentially identical to that of MHV-68, except for a 9,538-bp deletion at the left end of the unique region. To assess the genetic differences between MHV-68 and MHV-76, we compared the restriction fragment banding patterns of the two strains. Figure 1A shows the products of MHV-68 and MHV-76 DNAs digested with eight restriction endonucleases cleaving at a total of 185 unique sites. Each enzyme produced several fragments of identical mobility from both DNAs, indicating that the genomes are closely related. However, differences in the restriction profiles were apparent. Using maps predicted from the MHV-68 genome sequence, three regions of difference were identified. These are summarized in Fig. 1B.

Two regions correspond to noncoding tandem repeats containing variable copy numbers of 40- or 100-bp elements, at approximately kbp 27 and 100 in the genome, respectively. The former region was 0.4 kbp smaller in MHV-76 (approximately 10 copies fewer of the 40 bp element), and the latter region was 1.2 kbp larger (approximately 12 copies more of the 100-bp element). As examples, relevant bands are indicated for the

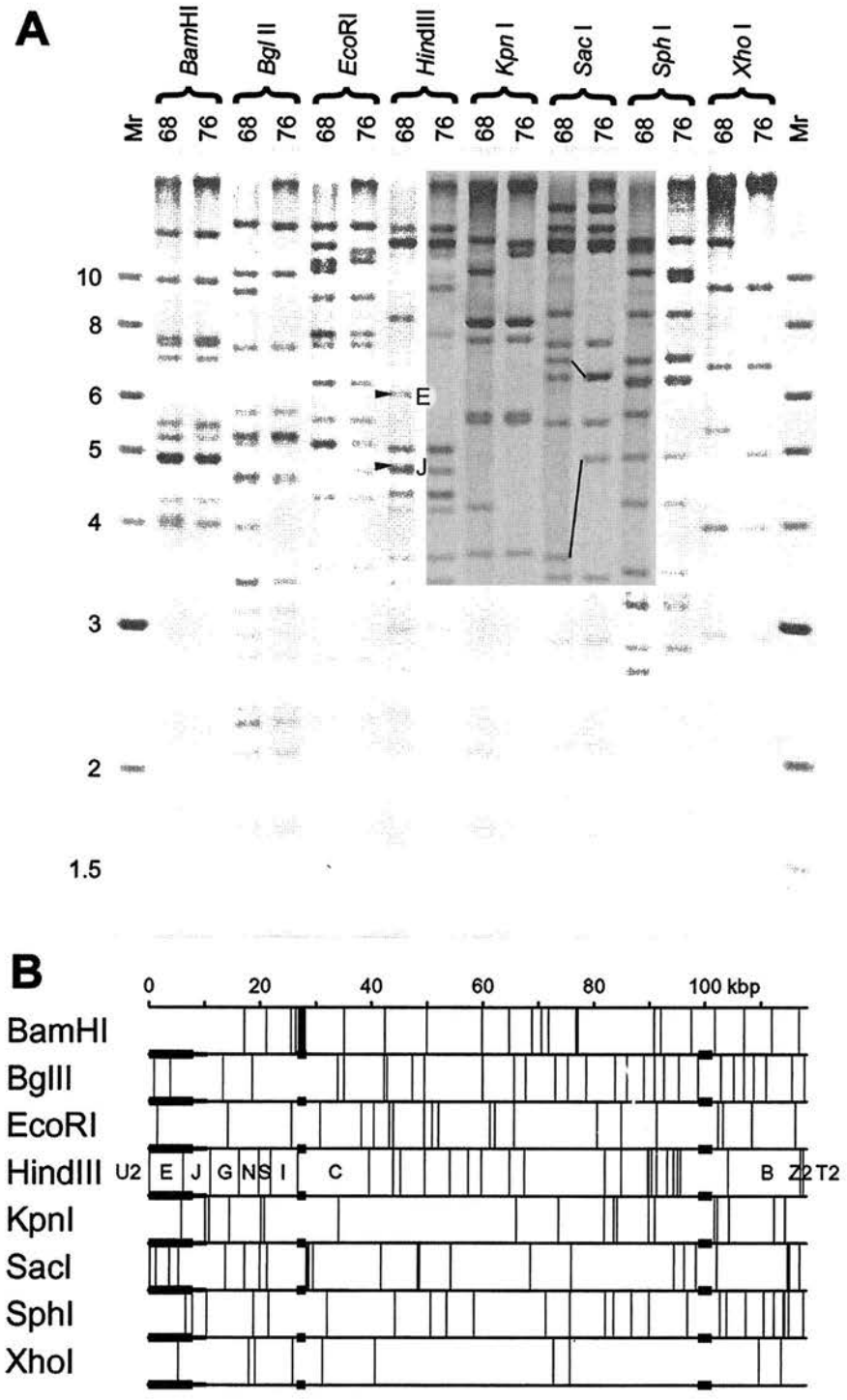

FIG. 1. Structure of the MHV-76 genome. (A) Restriction endonuclease profiles of MHV-68 and MHV-76 virion DNAs. Samples were analyzed on a 0.8% agarose gel. Fragments E and J are indicated in the *Hin*dIII profile of MHV-68. These are absent from the *Hin*dIII profile of MHV-76. Fragments containing the 40-bp repeat (upper pair) and the 100-bp repeat (lower pair) are connected by lines in the *Sac*I profiles of MHV-68 and MHV-76. Molecular size markers and their sizes in kilobase pairs are indicated to the left. (B) Restriction endonuclease maps of the unique region of the MHV-68 genome, highlighting the three regions that differ in MHV-76. Variable copy numbers of the terminal repeat (not shown) flank the unique region, resulting in heterogeneous populations of fragments from the genome termini differing by increments of 1.2 kbp. None of the restriction endonucleases for which maps are shown cleave the terminal repeat. Three regions in which MHV-76 and MHV-68 differ are denoted by thicker horizontal lines. Two correspond to variations in the copy number of reiterations in the 40-bp repeat (at kbp 27) and 100-bp repeat (at kbp 100). The third represents a deletion at the left end. Minimal and maximal extents of the deletion as deduced from panel A are indicated by thicker and thinner lines, respectively. The location of the insert in MHV-68 cosmid A8 is indicated at the bottom, with terminal repeat sequences dashed, and the corresponding fragment nomenclature is included in the *Hin*dIII map.

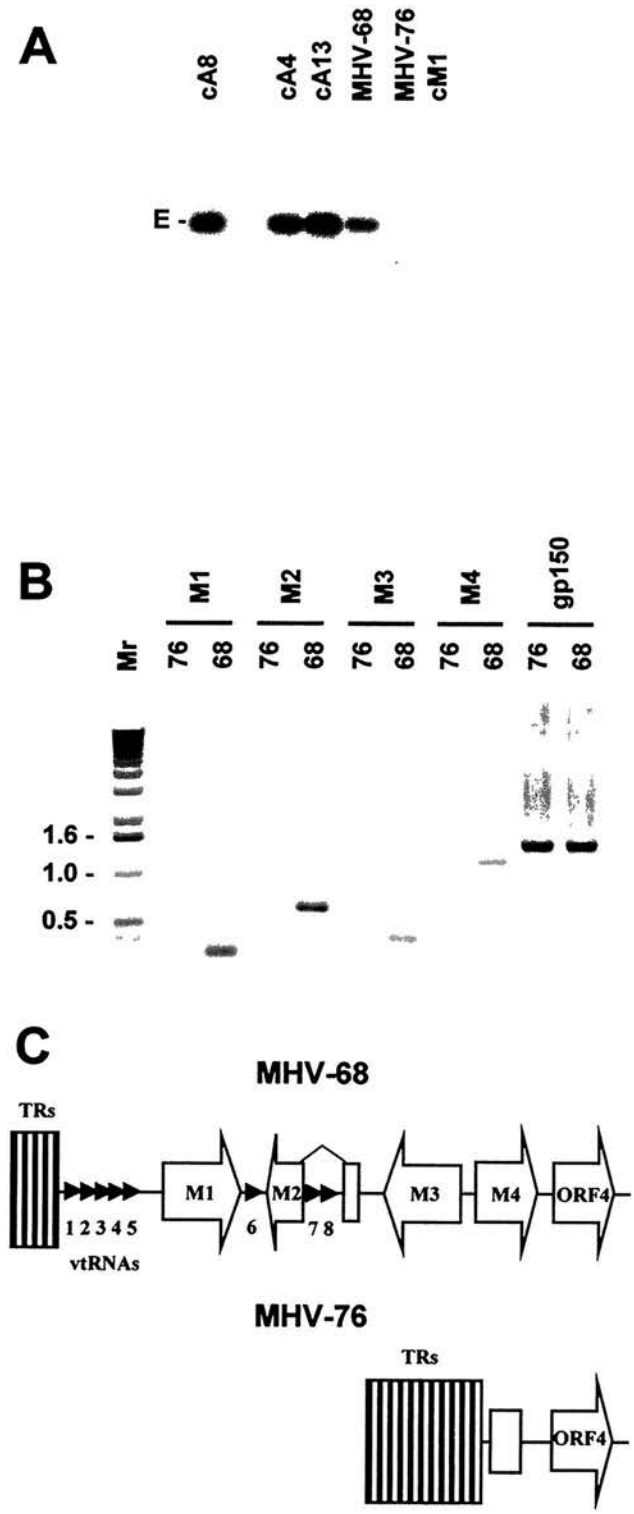

FIG. 2. (A) Autoradiograph of a Southern blot of a 0.8% agarose gel showing the results of hybridizing radiolabeled *Hin*dIII E (isolated from a plasmid [11]) to the *Hin*dIII products of MHV-68 and MHV-76 DNAs and three MHV-68 cosmids (cA8, cA4, and cA13) and one MHV-76 cosmid (cM1) containing the left end of the genome. The *Hin*dIII E fragment (6,155 bp) is indicated. (B) PCR analysis of the MHV-68 and MHV-76 genomes. PCR amplification was performed on viral DNA templates using primers specific for *M1*, *M2*, *M3*, *M4*, and *gp150* as indicated. Reaction products were analyzed on a 1% agarose gel. Molecular size markers and their sizes in kilobase pairs are indicated to the left. (C) Schematic diagram (not to scale) showing the structures of the left ends of the MHV-68 and MHV-76 genomes. The open arrows indicate protein-coding regions, and the small arrowheads indicate the vtRNA genes. The open rectangle in MHV-76 indicates residual *M4* sequence. TRs, terminal repeats.

*Sac*I profile in Fig. 1A. Copy number variation in repeats has long been known to occur in herpesvirus genomes (for example, see reference 8).

The third region corresponds to the left end of the unique region. The profiles were consistent with the absence from the MHV-76 genome of a sequence which extends in the MHV-68 genome from a position between nucleotides 1 and 111 to a position between nucleotides 7962 and 10526. As examples, relevant bands (E and J) are indicated for the *Hin*dIII profile in Fig. 1A. The absence of sequences in *Hin*dIII E from MHV-76 and cosmid M1 (derived from MHV-76 DNA) was confirmed by Southern blot hybridization (Fig. 2A). The only other difference detected between the two genomes was the presence of an additional *Sph*I site in the MHV-76 *Sph*I fragment at nucleotides 32139 to 44301. This could in principle be the result of a single nucleotide difference.

To characterize the sequence absent from MHV-76 accurately, the sequence of cosmid M1 was determined. In comparison with MHV-68, a 9,538-bp region corresponding to the last nucleotide of the terminal repeat and the first 9,537 bp of the unique region in MHV-68 was absent from the cosmid. The absence of this sequence is fully consistent with the genomic restriction profiles described above. Two minor differences were also observed between the 21,168-bp sequence of the cosmid insert and the relevant part of the MHV-68 sequence. One is trivial, mapping in a GC tract in the terminal repeat known to be variable in length (24). The other consists of a G residue at nucleotide 12280 in the coding region for MHV-68 ORF 6, which is present as an A residue in MHV-76, resulting in substitution of a serine for a glycine residue. This difference was confirmed by PCR and sequencing of the appropriate regions of the MHV-68 and MHV-76 DNAs (not shown).

We conclude that MHV-76 and MHV-68 are essentially identical, except for the absence from MHV-76 of 9,538 bp at the left end of the unique region. MHV-76 therefore represents a deletion mutant of MHV-68 or another highly related virus rather than a distinct viral species.

MHV-76 lacks MHV-68 genes *M1*, *M2*, *M3*, and *M4* and vtRNAs. To check that none of the sequences from the 9,538-bp deletion are present elsewhere in the genome, MHV-76 DNA was analyzed by PCR. MHV-76 and MHV-68 genomic DNAs were tested using primers specific for the *M1*, *M2*, *M3*, *M4*, and *gp150* genes. The results are shown in Fig. 2B. All of the sequences assayed were amplified from MHV-68 DNA, but only the *gp150* sequence was amplified from MHV-76 DNA.

These results are consistent with the findings described above. MHV-76 is thus a deletion mutant of MHV-68 that lacks *M1*, *M2*, *M3*, most of the 5′ portion of *M4*, and all eight vtRNA genes. This is depicted schematically in Fig. 2C.

MHV-76 growth in vitro is similar to that of MHV-68. Figure 3A shows single-step growth curves determined for MHV-76 and MHV-68 in BHK-21 cells infected at an MOI of

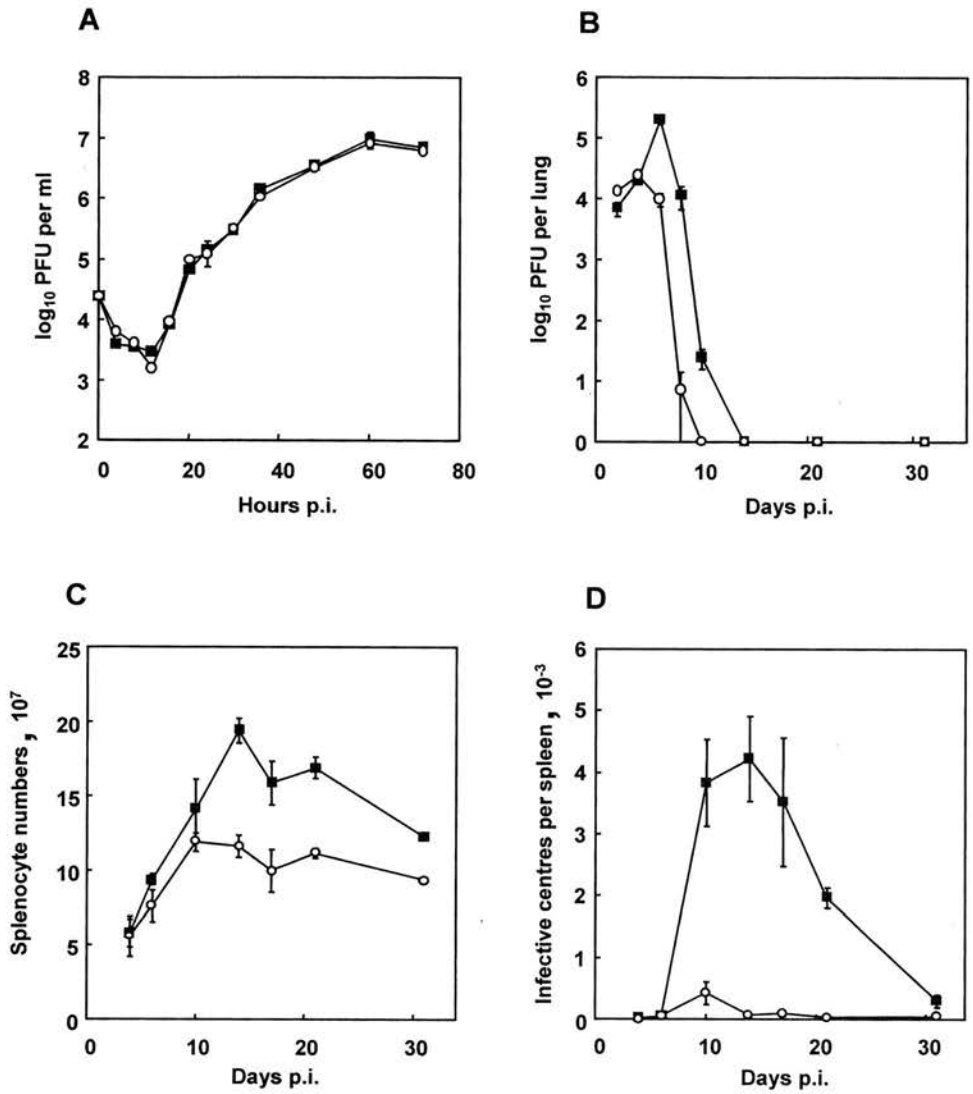

FIG. 3. Biological characterization of MHV-76. (A) Single-step growth curves of MHV-68 (■) and MHV-76 (○) on BHK-21 cells at an MOI of 5. Data are shown as mean $\log_{10}$ virus titer ± standard error and are representative of two separate experiments, each carried out in duplicate. (B) Viral replication in the lungs of BALB/c mice infected intranasally with 2×10^5 PFU of MHV-68 (■) or MHV-76 (○). The mean $\log_{10}$ virus titer ± standard error for four mice per group is shown for each time point. (C) Numbers of spleen cells during intranasal infection of BALB/c mice with 2×10^5 PFU of MHV-68 (■) or MHV-76 (○). The mean total number of splenocytes ± standard error for four mice per group is shown for each time point. (D) Latent virus in the spleens of BALB/c mice infected with 2×10^5 PFU of MHV-68 (■) or MHV-76 (○) as determined by infective-center assay. Infectious virus titers (less than 50 PFU per spleen) were subtracted from the infective-center results. The mean number of infective centers per spleen ± standard error for four mice per group is shown for each time point.

5. As reported previously (33), MHV-68 replicated efficiently, attaining maximal titers at around 60 h p.i. MHV-76 replicated with the same kinetics and attained titers similar to those of MHV-68. Thus, there was no significant difference between MHV-68 and MHV-76 in their ability to replicate in vitro.

MHV-76 is cleared more rapidly than MHV-68 from the lung. The ability of MHV-76 to replicate productively in vivo was assessed. Mice were infected with MHV-76 or MHV-68, and the virus titer in the lungs was assessed at various times p.i. by plaque assay. Figure 3B shows that the titers of infectious MHV-68 peaked at day 6 p.i. and remained detectable through day 12 p.i. In contrast, MHV-76 titers peaked at day 4 p.i. and were undetectable at day 10 p.i. There was also a significant quantitative difference between the maximal titers achieved by each virus (MHV-68, 1.9×10^5 PFU/lung; MHV-76, 2.4×10^4 PFU/lung [$P = 0.001$]). These results indicate that MHV-76 replicates productively in vivo but is cleared more rapidly than MHV-68 from the site of primary viral replication.

MHV-76-induced splenomegaly is less marked than that induced by MHV-68. To determine the extent of splenomegaly after MHV-76 infection, the total number of splenocytes in mice infected with MHV-76 or MHV-68 was determined. As seen in Fig. 3C, MHV-68 induced a characteristic increase in splenocyte number that peaked at 14 days p.i. MHV-76 infection also caused an increase in cellularity in the spleen, but the peak was significantly lower than that detected after MHV-68 infection ($P = 0.01$). In addition, maximal cell numbers were achieved slightly earlier, at between 10 and 14 days p.i.

MHV-76 establishes latency in the spleen but at much lower levels than MHV-68. To investigate the ability of MHV-76 to establish latency in vivo, mice were infected and latent virus in the spleen was measured using an infective-center assay. The results are shown in Fig. 3D. MHV-68 infective centers were detected at around day 7 p.i. and peaked at day 14 p.i. In contrast, latent MHV-76 in the spleen peaked at day 10 p.i., and the amount of latent virus was very much less (day 10, $P = 0.003$; day 21, $P < 0.001$). MHV-76 infective centers were still detectable at 31 days p.i., at levels of approximately 5 per 10^7 splenocytes. This indicates that MHV-76 can establish latency in the spleen cell population but at much-reduced levels compared to MHV-68.

To check that MHV-76 did not have an altered cellular tropism in the spleen, we harvested spleens at 14 days p.i. and fractionated cells into $CD19^+$ cells (B lymphocytes) and $CD19^-$ cells (non-B cells) using magnetic cell sorting as described previously (9). The purity of the separated fractions was tested by fluorescence-activated cell sorter analysis and found to be >95%. The two cell fractions as well as the total cell population were analyzed for the presence of latent virus using the infective-center assay. Greater than 90% of the infective centers present in the splenocytes were present within the $CD19^+$-B-cell subpopulation (not shown). A small amount (<5%) of latent virus was also detected in the $CD19^-$ fractions. Thus, the distribution of the MHV-76 within different cell types in the spleen during splenomegaly appears to be similar to that of MHV-68 (35), in that the majority of infective centers were associated with B lymphocytes.

MHV-76 maintains long-term persistence in the spleen and lung. The results of the infective-center assays described above demonstrated that MHV-76 was able to establish latency during the first 30 days of infection, albeit at a lower level than MHV-68. To ascertain whether MHV-76 is subsequently cleared or is able to persist, mice were infected with MHV-76 and MHV-68. After 5 months, organs from these mice were analyzed for the presence of virus. Three of the four mice were positive for MHV-76 infective centers in the spleen, at levels of approximately 1 to 2 latently infected cells per 10^7 splenocytes. No infectious virus was detected in this organ by plaque assay.

To analyze the presence of persisting virus in other organs, DNA was extracted from the livers, lungs, kidneys, spleens, and white blood cells of four MHV-76-infected mice at 5 months p.i. Organs from one mouse infected with MHV-68 were also harvested at 5 months p.i as a positive control, and those from two uninfected mice were harvested as negative controls. Extracted DNA was analyzed for the presence of the viral genome by PCR amplification using primers specific for MHV-68 *gp150*, followed by Southern blot hybridization with a *gp150*-specific probe to confirm the identity of the products. For each set of PCRs, samples containing purified viral DNA or no DNA were included as positive and negative controls, respectively. Using known amounts of cloned template, it was determined that this process was sensitive to 1 to 10 copies of the viral genome in 1 μg of high-molecular-weight DNA (not shown).

As shown in Fig. 4A, viral DNA was not detected in either of the uninfected mice. In agreement with our previous findings (32), viral genomes were detected in the spleens and lungs of the MHV-68-infected mouse but not in the blood or other organs. Viral DNA was found in spleens of all four mice infected with MHV-76 but in the lungs of only one of these mice. To address the possibility that MHV-76-infected mice may have been contaminated with MHV-68, we tested the same DNA samples by PCR using primers specific for the MHV-68 *M3* gene, which is absent from MHV-76. Figure 4B shows that the *M3* sequence was detected only in the MHV-68-infected mouse and not in any of the MHV-76-infected or uninfected mice. The inability to detect the *M3* sequence confirmed that the MHV-76 viral stocks were free of MHV-68 and that the persisting virus in MHV-76-infected mice was definitely MHV-76.

These results show that MHV-76 is able to persist as efficiently as MHV-68 in the spleen but that it was not as efficient at persisting in lungs.

The inflammatory response is greater in the lung during MHV-76 infection than during MHV-68 infection. The results described above show that there were clear differences between MHV-76 and MHV-68 in their ability to replicate productively in the lung and cause splenomegaly. This was probably due to differences in the host response to the virus, as there was no intrinsic difference in the ability of the viruses to replicate in vitro. As a preliminary response to this hypothesis, we undertook a histopathological study of organs after infection, examining the lungs and spleens of infected mice at various times p.i. Representative results are shown in Fig. 5.

At 4 days p.i. with MHV-76, there was a marked inflammatory response in the lungs, consisting of perivascular lymphoid infiltrates and edema. Subpleural lymphoid accumulations were also seen at this time p.i. (not shown). In contrast, no inflammatory response was observed at day 4 p.i. in the lungs of MHV-68-infected mice. By day 6 p.i., the inflammatory changes seen during MHV-76 infection were more severe and extensive than those on day 4, consisting of perivascular and interstitial lymphoid infiltration, thickened alveolar walls, and vasculitis. In contrast, the inflammatory changes were less pronounced in MHV-68 infection at day 6 p.i., consisting mostly of perivascular and interstitial lymphoid aggregations. At later times (days 8 and 10 p.i.), the inflammatory responses following MHV-76 and MHV-68 infections were similar (not shown).

These results demonstrate that the inflammatory changes seen in the infected lung occur earlier and are more substantial with MHV-76 than with MHV-68.

In the spleens of both MHV-68- and MHV-76-infected mice at day 10 p.i., there was evidence of follicular hyperplasia as revealed by germinal center formation and an increase in the marginal zone of the white pulp. However, the differences between the two groups, if any, were marginal and hard to quantify by histopathology alone (not shown).

Construction of rescuant viruses. To determine definitively whether the differences observed between MHV-76 and -68 were due to deletion of genes at the left end of the genome or to unidentified mutations elsewhere in the genome, we constructed rescuants by cotransfecting MHV-76 genomic DNA with MHV-68 cosmid A8 into BHK-21 cells. Since rescuants in which the deletion was restored were likely to be less attenuated in vivo, the progeny were passaged in mice. Spleens were harvested, and virus was reactivated using an infective-center assay. Plaques were screened for the presence or absence of the *M2* gene by PCR and assessed as representing pure viral

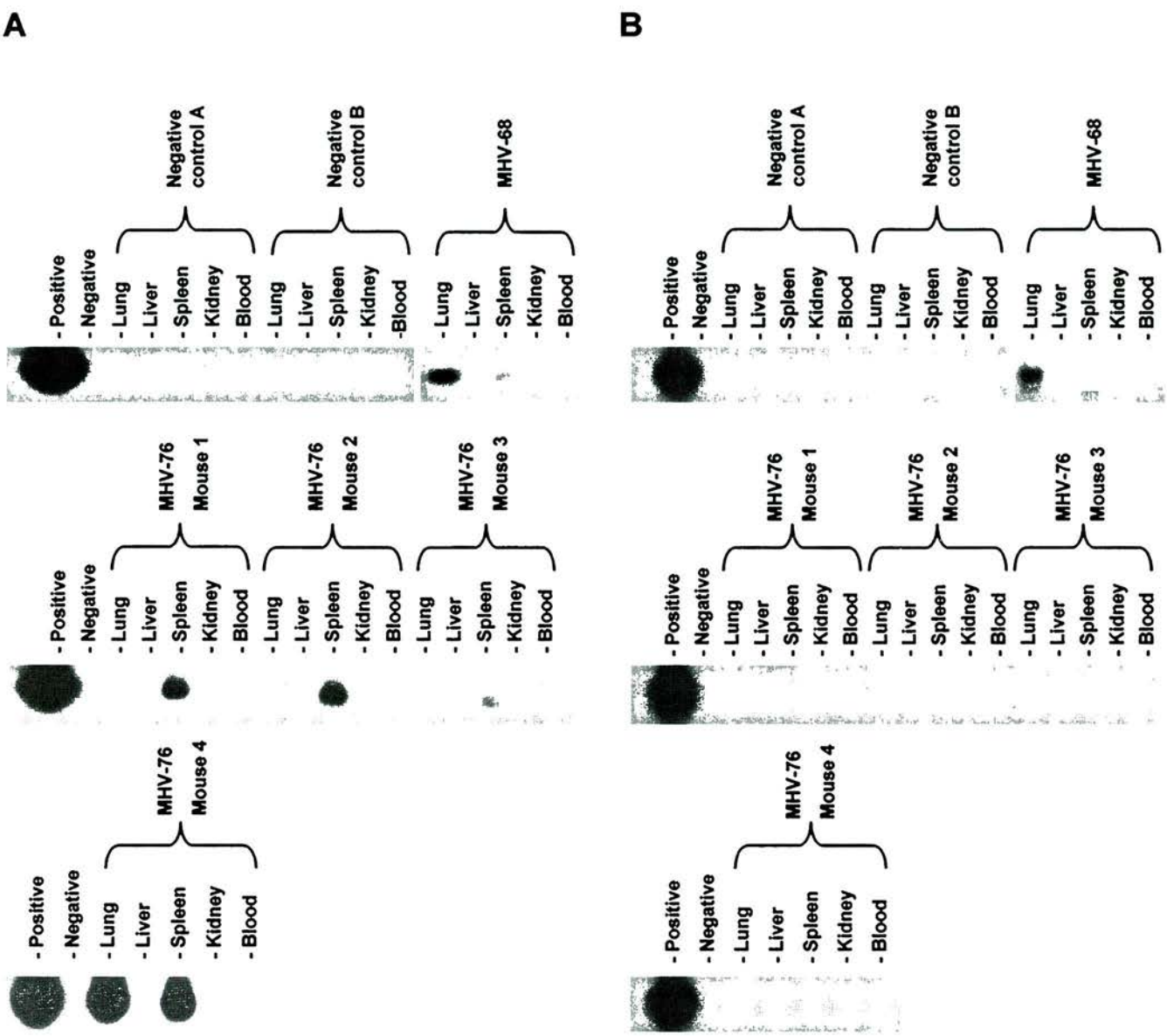

FIG. 4. Detection of MHV-76 DNA in the tissues of mice at 5 months p.i. Four BALB/c mice were infected with 2×10^5 PFU of MHV-76, and the lungs, livers, spleens, kidneys, and blood were harvested at 5 months p.i. Two uninfected mice were also harvested as negative controls, and one mouse infected 5 months previously with MHV-68 was harvested as a positive control. Viral DNA was extracted, and PCR amplification was performed on 1 μg of high-molecular-weight DNA. Samples containing MHV-68 viral DNA as a template (first lanes) or lacking DNA (second lanes) were used as positive and negative controls, respectively. (A) PCR amplification using primers specific for *gp150*. PCR products were analyzed by Southern blot hybridization with a ^{32}P-labeled *gp150* probe to confirm specificity. (B) PCR amplification using primers specific for *M3* (a gene absent from MHV-76). PCR products were analyzed by Southern blot hybridization with a ^{32}P-labeled *M3* probe to confirm specificity.

clones on the basis of the presence or absence of *M2* from all subsequent plaques.

Three progeny clones were selected for further characterization. MHV-76(cA8+)3 and MHV-76(cA8+)4 were both positive for *M2* and thus represented rescuants in which the deleted region had been restored. MHV-76(cA8-)5 was negative for *M2* and thus represented unrestored MHV-76, which had been subjected to in vivo passage in precisely the same way as the rescuants. To check the genome structures, *Hin*dIII and *Eco*RI digests were analyzed by Southern blot hybridization using MHV-68 cosmid A8 as a probe. The results are shown in Fig. 6A. Cosmid A8 contains sequences from MHV-68 *Hin*dIII B, C, E, G, I, J, N, S, T_2, U_2, and Z_2 (Fig. 1B). *Hin*dIII E, J, and U_2 are absent from MHV-76, and the remaining part of *Hin*dIII J is present in a novel fragment containing the terminal repeats. This fragment (JΔ) and T_2 should thus appear as a faint ladder of bands increasing to substantial sizes in increments of 1.2 kbp. As expected, rescuant viruses MHV-76(cA8+)3 and MHV-76(cA8+)4 yielded profiles identical to that of MHV-68, and *Hin*dIII E was absent from MHV-76 and MHV-76(cA8-)5. *Hin*dIII S and Z_2 were too small to be present on the blot. Hybridization to fragments containing the

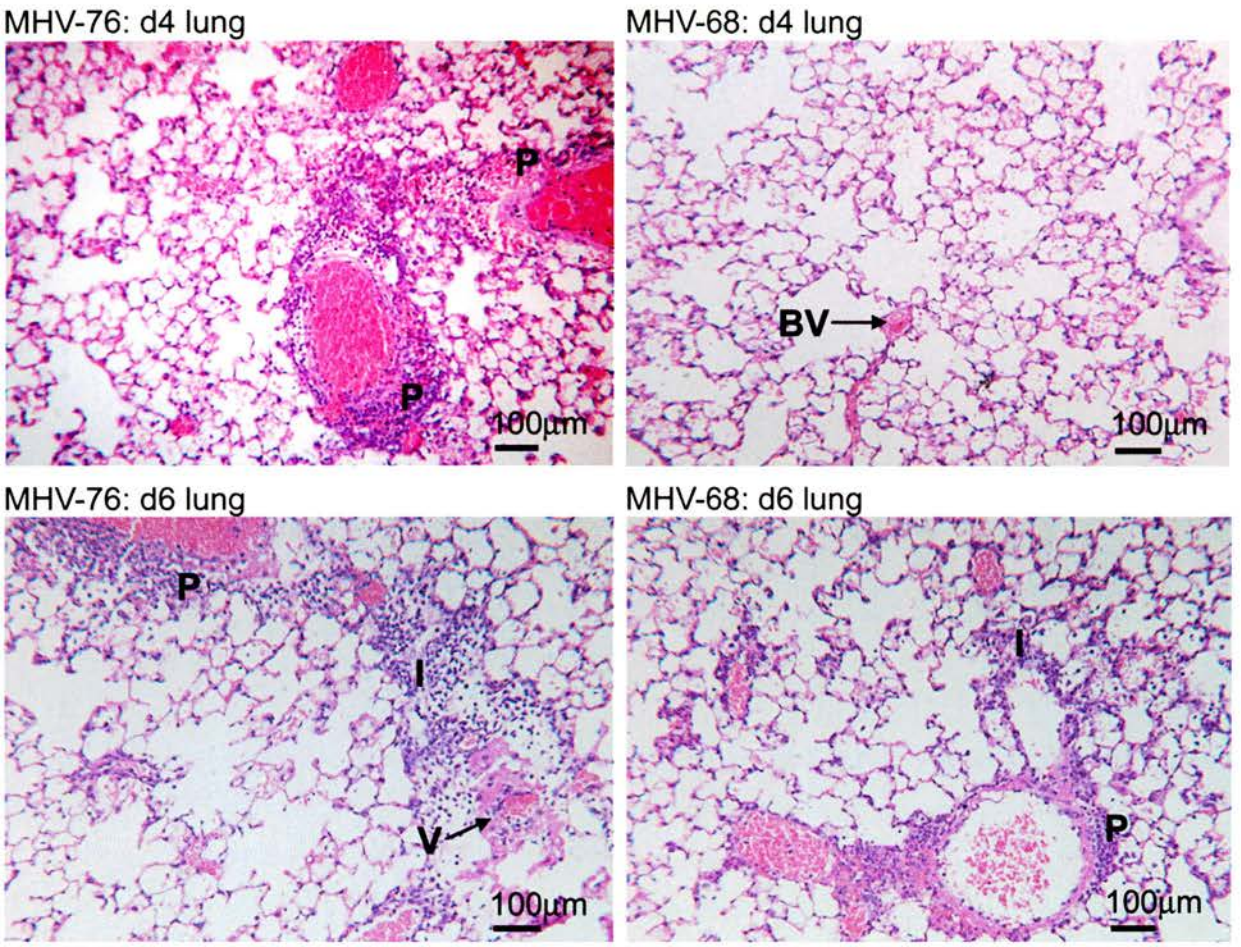

FIG. 5. Histopathological changes in the lungs of mice infected with MHV-76 or MHV-68. Representative sections of lung and spleen stained with hematoxylin and eosin are shown for mice infected for the times indicated. Salient pathological features are highlighted as follows: P, perivascular infiltration; BV, blood vessel; I, interstitial infiltration; V, vasculitis.

terminal repeats (U_2^+, T_2^+, and $J\Delta^+$) appeared as high-molecular-weight products, and the laddering normally associated with such fragments was too weak to be detected. The same blot was reprobed with a fragment containing full-length *M3* which crosses the boundary between *Hin*dIII E and J. Figure 6B shows that both fragments are present in MHV-68 and the two rescuants but absent from MHV-76 or MHV-76(cA8-)5. These data indicate that the sequence absent from MHV-76 was restored in MHV-76(cA8+)3 and MHV-76(cA8+)4.

Sequence analysis of the region containing nucleotide 12280, which is a G residue in MHV-68 but an A residue in MHV-76, showed that the rescuants contain a G residue and MHV-76(cA8-)5 contains an A residue. This is consistent with rescue not only of the deleted sequences in MHV-76 by cosmid A8 but also of adjacent sequences.

We also analyzed viral DNA by PCR using primers specific for *M1*, *M2*, *M3*, and *M4*. The results are shown in Fig. 6C. *ORF 74* primers amplified fragments of the anticipated size from all three viral DNA samples. Primers specific for *M1*, *M2*, *M3*, and *M4* generated appropriately sized products from the rescuants but not from MHV-76(cA8-)5. PCR of the viral stocks produced the same results (not shown). This confirms that *M1*, *M2*, *M3*, and *M4* were restored in the rescuants but not in MHV-76(cA8-)5.

Evidence that the rescuants were derived from MHV-76. Variation in the copy number of reiterated sequences has been shown to occur in MHV-68 (1). Therefore, we utilized the copy number of the 100-bp repeat to assess the origin of the rescuants. Viral DNA was digested with *Hin*cII and analyzed by Southern blot hybridization using a radiolabeled *Bam*M probe, which is predicted to hybridize to a fragment containing the 100-bp repeat and to an adjacent fragment of 5,032 bp. The results are shown in Fig. 6D. The MHV-68 fragment containing the 100-bp repeat was approximately 2.4 kbp in size, whereas that derived from MHV-76 was 4 kbp. A fragment of approximately 4 kbp was identified in both rescuants and MHV-76(cA8-)5, except that MHV-76(cA8+)3 also produced a fragment of 3.4 kbp. These results show that the copy number in MHV-68 DNA is approximately 22, as described previously (42). However, MHV-76 and three derived viruses contained a larger number (approximately 37 copies), and a subpopulation of MHV-76(cA8+)3 also contained an intermediate number (approximately 30). These results are consistent with derivation of the rescuants from rescued MHV-76 rather than from

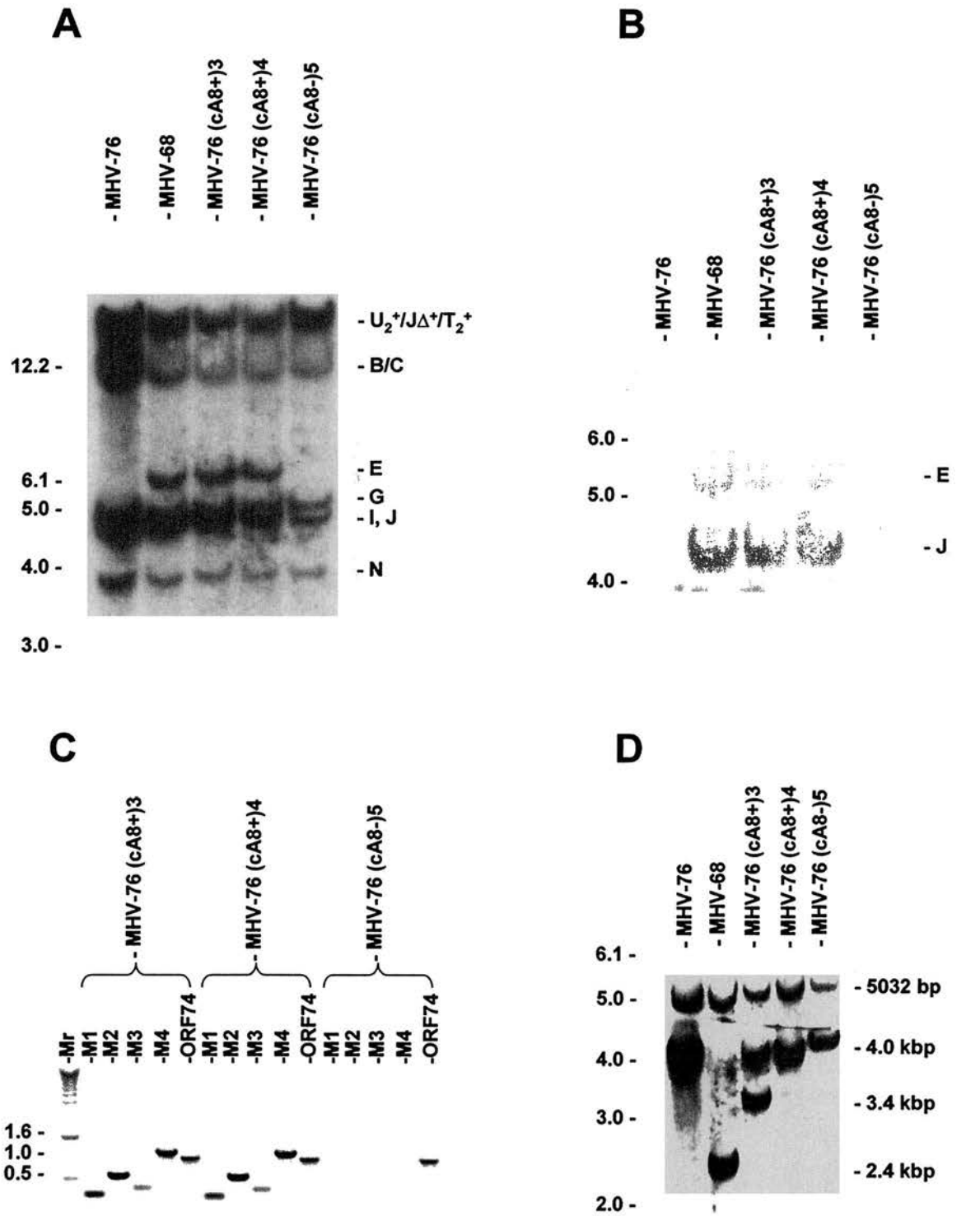

FIG. 6. Molecular characterization of rescuant viruses. (A) Autoradiograph of a Southern blot of a 0.8% agarose gel showing the results of hybridizing radiolabeled MHV-68 cosmid A8 to the *Hin*dIII products of DNAs isolated from BHK-21 cells infected with MHV-76, MHV-68, MHV-76(cA8+)3, MHV-76(cA8+)4, and MHV-76(cA8-)5. The sizes of molecular size markers (in kilobase pairs) are shown on the left, and *Hin*dIII fragments are shown on the right (see Fig. 1B for a map). (B) Autoradiograph of a Southern blot of a 0.8% agarose gel showing the results of hybridizing radiolabeled *M3* probe (nucleotides 6060 to 7277 in the MHV-68 genome) to the *Hin*dIII products of DNA isolated from BHK-21 cells infected with MHV-76, MHV-68, MHV-76(cA8+)3, MHV-76(cA8+)4, or MHV-76(cA8-)5. The sizes of molecular size markers (in kilobase pairs) are shown on the left, and *Hin*dIII fragments are shown on the right (see Fig. 1B for a map). (C) PCR analysis of viral DNA from MHV-76(cA8+)3, MHV-76(cA8+)4, or MHV-76(cA8-)5 using primers specific for the MHV-68 *M1*, *M2*, *M3*, and *M4* genes and *ORF 74*. Reaction products were analyzed on a 1% agarose gel. Molecular size markers and their sizes are shown to the left, with sizes in kilobase pairs. (D) Autoradiograph of a Southern blot of a 0.8% agarose gel showing the results of hybridizing a radiolabeled *Bam*HI M probe (which contains the 100-bp repeat) to the *Hin*cII products of DNA isolated from BHK-21 cells infected with MHV-76, MHV-68, MHV-76(cA8+)3, MHV-76(cA8+)4, or MHV-76(cA8-)5. The sizes of molecular size markers (in kilobase pairs) are shown on the left. Fragments containing the 100-bp repeat, with approximate sizes, are indicated on the right, along with the adjacent 5,032-bp fragment present in each genome.

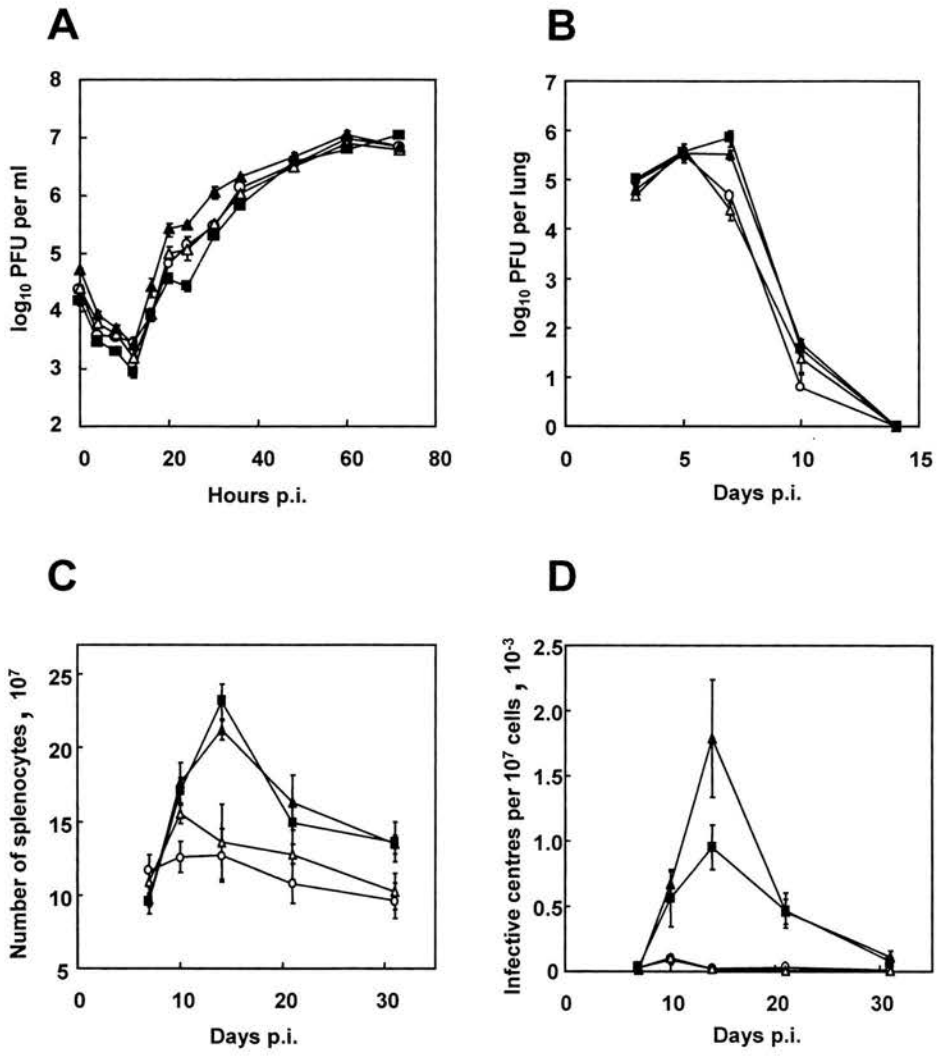

FIG. 7. Biological characterization of MHV-68, MHV-76, and the rescuant viruses. Data points (mean value ± standard error) are shown in each graph for MHV-68 (■), MHV-76 (○), MHV-76(cA8+)4 (▲), and MHV-76(cA8-)5 (△). (A) Single-step growth curves comparing growth of viruses on BHK-21 cells at an MOI of 5. The data are representative of two separate experiments, and each experiment was done in duplicate. (B) Viral replication in the lungs of BALB/c mice infected intranasally with 2×10^5 PFU of virus. Data for four mice per group are shown at each time point. (C) Numbers of spleen cells during intranasal infection of BALB/c mice with 2×10^5 PFU of virus. Data for four mice per group are shown at each time point. (D) Latent virus in the spleens of BALB/c mice infected with 2×10^5 PFU of virus as determined by infective-center assay. Infectious virus titers (less than 50 PFU per spleen in every case) have been subtracted from the infective-center results. Data for four mice per group are shown at each time point.

contaminating MHV-68. Since MHV-76(cA8+)3 contained variable numbers of this repeat domain, we did not include this rescuant in any further biological analyses.

The viruses are indistinguishable in vitro. To investigate the effect of the deletion on viral replication in vitro, single-step growth curves of MHV-68, MHV-76, MHV-76(cA8+)4, and MHV-76(cA8-)5 were compared (Fig. 7A). All four viruses replicated with the same kinetics and attained similar maximal titers at around 60 h p.i. There was no indication that the deleted sequence had any effect on lytic replication in BHK-21 cells.

A lack of *M1*, *M2*, *M3*, *M4*, and the vtRNA genes leads to attenuation in the lung. Mice were infected with MHV-68, MHV-76, MHV-76(cA8+)4, or MHV-76(cA8-)5, and the virus titer in the lungs was assessed at various times p.i. by plaque assay. As shown in Fig. 7B, MHV-68 and MHV-76(cA8+)4 achieved peak titers at around 7 days p.i. and were cleared by 14 days p.i. MHV-76 and MHV-76(cA8-)5 achieved similar maximum titers, but the decrease in titer from this peak occurred earlier and was more rapid [MHV-68 versus MHV-76 at day 7 p.i., $P = 0.037$; MHV-76(cA8+)4 versus MHV-76 at day 7 p.i., $P = 0.010$]. These data show that the deletion leads to a significant attenuation of infection in the lungs.

Deletion of *M1*, *M2*, *M3*, *M4*, and the vtRNA genes severely attenuates virus pathogenicity in the spleen. Mice were infected with MHV-68, MHV-76, MHV-76(cA8+)4, or MHV-76(cA8-)5, and the extent of ensuing splenomegaly was determined by counting the total number of splenocytes and the

increase in latently infected cells as monitored by infective-center assay. The results are shown in Fig. 7C and D. After infection with MHV-68 or MHV-76(cA8+)4, there was a sharp increase in splenocyte number, peaking at around 14 days p.i. However, after infection with MHV-76 or MHV-76(cA8-)5, there was only a modest rise in splenocyte number, peaking earlier at around day 10 p.i. [MHV-68 versus MHV-76, $P = 0.003$; MHV-76(cA8+)4 versus MHV-76, $P = 0.005$].

In mice infected with MHV-68 and MHV-76(cA8+)4, infective centers rose sharply from day 7 p.i. to a peak at day 14 p.i. Infective centers from mice infected with MHV-76 and MHV-76(cA8-)5 were detectable in the spleen, but the peak occurred earlier (day 10 p.i.) and was significantly less [MHV-68 versus MHV-76, $P = 0.002$; MHV-76(cA8+)4 versus MHV-76, $P = 0.008$]. However, latently infected cells were detected in mice infected with MHV-76(cA8-)5 or MHV-76 even at the latest time point tested (32 days p.i.). These data show that the deleted sequence contributes significantly to splenomegaly and the acute rise in latently infected cells in the spleen but is not essential for the establishment of latency and persistence.

DISCUSSION

This work describes a primary analysis of a novel murine gammaherpesvirus, MHV-76. The genome of this virus was found to be essentially identical to that of MHV-68, with the single major difference being the absence of 9,538 bp at the left end of the unique region of the genome. MHV-76 replicated similarly in cell culture and had similar biological properties as MHV-68, but it appeared to be significantly less pathogenic in vivo in the context of a much more rapid and intense inflammatory response in the lungs. Recombinant viruses that had the deletion in MHV-76 rescued had biological properties similar to those of MHV-68.

MHV-68 was reported as having been isolated from the bank vole, *C. glareolus* (3), whereas MHV-76 was described as an independent isolate derived in the same study from the yellow-necked wood mouse, *A. flavicollis*. Our data strongly suggest that MHV-76 is a deletion mutant derived from MHV-68 or an extremely similar virus during passage. It is formally possible that this could have occurred in nature, since *Clethrionomys* and *Apodemus* species share similar habitats. This question is an important one and is currently being addressed by the investigation of free-living rodent samples from the United Kingdom.

MHV-76 lacks 9,538 bp containing the *M1*, *M2*, *M3*, *M4,* and vtRNA genes. We have shown that MHV-76 and MHV-68 differ dramatically in their pathogenic potential in mice. This could be due to the deletion or to unidentified mutations elsewhere in the genome. Consequently, we utilized rescuants in which the deleted region in MHV-76 had been restored by recombination with MHV-68 sequences. Replacement of the deleted sequence changed the phenotype of MHV-76 to one that was not significantly different from that of MHV-68. This shows definitively that the left end of the MHV-68 genome is nonessential for viral productive replication but plays a key role in pathogenesis. It is overwhelmingly likely that the key determinants are located in the deleted sequence. However, our results have not formally ruled out the possibility that the single nucleotide substitution at nucleotide 12280, resulting in replacement of a glycine by a serine residue in the ORF 6 protein, may play a role. We consider this unlikely, since a deleterious point mutation (unlike a deletion) can readily revert and is unlikely to survive under selection in mice. We are also encouraged to view this residue as noncritical, since it is not conserved in an independently isolated murine herpesvirus in which the ORF 6 protein is 91.3% identical to that of MHV-68 (it is an asparagine [S. Milligan, C. Chastel, S. Efstathiou, and A. J. Davison, unpublished data]).

The left end of the MHV-68 genome appears to have a propensity for undergoing recombination events in vitro (28). This could be due to the proximity of multiple terminal repeats or to the presence of highly transcribed vtRNA genes or a putative origin of replication (4). Naturally occurring deletions have been described for other gammaherpesvirus genomes. The strains of Epstein-Barr virus in the Raji, Daudi, and P3HR-1 cell lines all carry deletions of various sizes (15). For HVS, spontaneous deletions at the left end of the genome have been described (16). Indeed, the heterogeneity of the left end of the HVS genome has been held responsible for the oncogenic potential of the virus (19, 20). It is also of note that the left end of the HVS genome encodes seven small viral RNAs (2).

Unique genes at the left end of the genome have attracted considerable attention in other gammaherpesviruses as well as in MHV-68. In Kaposi's sarcoma-associated herpesvirus, this region contains the K1 gene, which shows unusual levels of divergence in different virus isolates (45) and has been associated with cellular transformation (17). In HVS, this region contains the *STP* gene, which is required for cellular immortalization and oncogenesis (16, 23), as well as the HVS small viral RNAs (2). In Epstein-Barr virus, this region encodes LMP-1, a classic oncoprotein that is essential for B-cell immortalization (15). For MHV-68, however, less is known about the function of the genes in this region and their contribution to viral pathogenesis. Indeed, only the function of M3 has been identified, as a soluble chemokine binding protein (25, 40) potentially subverting the inflammatory response. Deletion of *M1* had no phenotypic effect on viral replication in vitro or in vivo (6, 28), although one study implicated this region of the genome in the regulation of latency (6). Also, deletion of vtRNA genes 1 to 4 had no effect on viral pathogenesis (28). Our studies confirm and extend these findings in demonstrating that genes *M1*, *M2*, *M3,* and *M4* and all eight vtRNA genes are nonessential for lytic virus replication in vitro and in vivo and for the establishment and maintenance of latency in vivo.

Functions encoded at the left end of the MHV-68 genome are nevertheless involved in virus pathogenicity. The more rapid clearance from the lungs characteristic of MHV-76, combined with an enhanced inflammatory response, indicates a key role for this region in the avoidance of restrictions placed on viral productive replication, for example, via interferons or the immune response. The *M1*, *M3*, *M4,* and vtRNA genes are transcribed during lytic infection (29, 41) and thus potentially play roles in infection of the lung. Previous studies have analyzed MHV-68 mutants lacking *M1* (6, 28) but did not assess viral replication in the lung after intranasal infection.

The dramatically smaller extent of splenomegaly and lower number of infective centers observed during MHV-76 infection constitute the first evidence that genes at the left end of

the MHV-68 genome are specifically involved in splenomegaly and generation of latently infected B cells. It is not clear, however, precisely which of the known genes is responsible. *M2* and the vtRNA genes are candidates, since they are transcribed during latent infection of splenocytes (14, 29). *M2* is also expressed predominantly in B cells during splenomegaly (38). *M1*, *M3,* and *M4* have not been shown definitively to be associated with latency (14, 41) but may still have a role in splenomegaly, since low levels of productive viral replication occur in the spleen during the establishment of latency. Chemokines play an important role in directing the migration of leukocytes to sites of inflammation (18). Thus, the chemokine-binding actions of M3 may play an important role in splenomegaly. One report has implicated *M1* in the suppression of viral reactivation (6). However, the effect was observed only at later time points in peritoneal exudate cells after intraperitoneal infection. In addition, that study employed recombinant viruses containing the human cytomegalovirus immediate-early promoter, which may in itself affect MHV-68 replication. A suppressive effect of *M1* was not observed in our experiments.

Both MHV-76 and MHV-68 persisted in the spleens of infected mice for at least 5 months p.i. Thus, the genetic elements necessary for this process are clearly not present in the left unique portion of the genome. However, the persistence of MHV-76 in the lungs was much less consistent, occurring in only one of four mice. Long-term persistence of virus in the lung is a consistent feature of MHV-68 infection (32). Thus, although the numbers are low, our data suggest that sequences missing in MHV-76 are important for long-term persistence in the lung. The more rapid and intense inflammatory response seen in the lung during MHV-76 infection may indicate that the virus is more effectively cleared from this site by the host response. In addition, there may be subtle variations in genome copy number in the spleen that are influenced by the locus absent in MHV-76. These questions await the results of quantitative experiments on DNA load over an extended time course.

In summary, we have demonstrated that a region of the genome containing *M1*, *M2*, *M3*, *M4,* and the vtRNA genes plays a key role in infection in mice by MHV-68, probably though evasion of the host innate defense mechanisms and immune response. Ongoing studies in this laboratory are expected to reveal the contributions of individual genes. MHV-76 is anticipated to be a useful virus from which to construct appropriate mutants.

ACKNOWLEDGMENTS

This work was funded by the Wellcome Trust, The Royal Society, and the MRC (United Kingdom). A.I.M. holds a Wellcome Trust Veterinary Clinical Scholarship. J.P.S. is a Royal Society University Research Fellow.

REFERENCES

1. **Adler, H., M. Messerle, M. Wagner, and U. H. Koszinowski.** 2000. Cloning and mutagenesis of the murine gammaherpesvirus 68 genome as an infectious bacterial artificial chromosome. J. Virol. **74:**6964–6974.
2. **Albrecht, J. C., J. Nicholas, D. Biller, K. R. Cameron, B. Biesinger, C. Newman, S. Wittmann, M. A. Craxton, H. Coleman, B. Fleckenstein, et al.** 1992. Primary structure of the herpesvirus saimiri genome. J. Virol. **66:**5047–5058.
3. **Blaskovic, D., M. Stancekova, J. Svobodova, and J. Mistrikova.** 1980. Isolation of five strains of herpesviruses from two species of free living small rodents. Acta Virol. **24:**468.
4. **Bowden, R. J., J. P. Simas, A. J. Davis, and S. Efstathiou.** 1997. Murine gammaherpesvirus 68 encodes tRNA-like sequences which are expressed during latency. J. Gen. Virol. **78:**1675–1687.
5. **Cardin, R. D., J. W. Brooks, S. R. Sarawar, and P. C. Doherty.** 1996. Progressive loss of $CD8^+$ T cell-mediated control of a gamma-herpesvirus in the absence of $CD4^+$ T cells. J. Exp. Med. **184:**863–871.
6. **Clambey, E. T., H. W. Virgin, and S. H. Speck.** 2000. Disruption of the murine gammaherpesvirus 68 M1 open reading frame leads to enhanced reactivation from latency. J. Virol. **74:**1973–1984.
7. **Cunningham, C., and A. J. Davison.** 1993. A cosmid-based system for constructing mutants of herpes simplex virus type 1. Virology **197:**116–124.
8. **Davison, A. J., and N. M. Wilkie.** 1981. Nucleotide sequences of the joint between the L and S segments of herpes simplex virus types 1 and 2. J. Gen. Virol. **55:**315–331.
9. **Dutia, B. M., J. P. Stewart, R. A. Clayton, H. Dyson, and A. A. Nash.** 1999. Kinetic and phenotypic changes in murine lymphocytes infected with murine gammaherpesvirus-68 in vitro. J. Gen. Virol. **80:**2729–2736.
10. **Efstathiou, S., Y. M. Ho, S. Hall, C. J. Styles, S. D. Scott, and U. A. Gompels.** 1990. Murine herpesvirus 68 is genetically related to the gammaherpesviruses Epstein-Barr virus and herpesvirus saimiri. J. Gen. Virol. **71:**1365–1372.
11. **Efstathiou, S., Y. M. Ho, and A. C. Minson.** 1990. Cloning and molecular characterization of the murine herpesvirus 68 genome. J. Gen. Virol. **71:**1355–1364.
12. **Ehtisham, S., N. P. Sunil-Chandra, and A. A. Nash.** 1993. Pathogenesis of murine gammaherpesvirus infection in mice deficient in CD4 and CD8 T cells. J. Virol. **67:**5247–5252.
13. **Flano, E., S. M. Husain, J. T. Sample, D. L. Woodland, and M. A. Blackman.** 2000. Latent murine gamma-herpesvirus infection is established in activated B cells, dendritic cells, and macrophages. J. Immunol. **165:**1074–1081.
14. **Husain, S. M., E. J. Usherwood, H. Dyson, C. Coleclough, M. A. Coppola, D. L. Woodland, M. A. Blackman, J. P. Stewart, and J. T. Sample.** 1999. Murine gammaherpesvirus M2 gene is latency-associated and its protein a target for CD8(+) T lymphocytes. Proc. Natl. Acad. Sci. USA **96:**7508–7513.
15. **Kieff, E.** 1996. Epstein-Barr virus and its replication, p. 2343–2396. *In* B. N. Fields, D. M. Knipe, and P. M. Howley (ed.), Fields virology, vol. 2. Lippincott-Raven, Philadelphia, Pa.
16. **Koomey, J. M., C. Mulder, R. L. Burghoff, B. Fleckenstein, and R. C. Desrosiers.** 1984. Deletion of DNA sequence in a nononcogenic variant of herpesvirus saimiri. J. Virol. **50:**662–665.
17. **Lee, H., R. Veazey, K. Williams, M. Li, J. Guo, F. Neipel, B. Fleckenstein, A. Lackner, R. C. Desrosiers, and J. U. Jung.** 1998. Deregulation of cell growth by the K1 gene of Kaposi's sarcoma-associated herpesvirus. Nat. Med. **4:**435–440.
18. **Luster, A. D.** 1998. Chemokines—chemotactic cytokines that mediate inflammation. N. Engl. J. Med. **338:**436–445.
19. **Medveczky, M. M., E. Szomolanyi, R. Hesselton, D. DeGrand, P. Geck, and P. G. Medveczky.** 1989. Herpesvirus saimiri strains from three DNA subgroups have different oncogenic potentials in New Zealand White rabbits. J. Virol. **63:**3601–3611.
20. **Medveczky, P., E. Szomolanyi, R. C. Desrosiers, and C. Mulder.** 1984. Classification of herpesvirus saimiri into three groups based on extreme variation in a DNA region required for oncogenicity. J. Virol. **52:**938–944.
21. **Mistrikova, J., J. Rajcani, M. Mrmusova, and I. Oravcova.** 1996. Chronic infection of Balb/c mice with murine herpesvirus 72 is associated with neoplasm development. Acta Virol. **40:**297–301.
22. **Mistrikova, J., A. Remenova, J. Lesso, and M. Stancekova.** 1994. Replication and persistence of murine herpesvirus 72 in lymphatic system and peripheral blood mononuclear cells of Balb/C mice. Acta Virol. **38:**151–156.
23. **Murthy, S. C., J. J. Trimble, and R. C. Desrosiers.** 1989. Deletion mutants of herpesvirus saimiri define an open reading frame necessary for transformation. J. Virol. **63:**3307–3314.
24. **Nash, A. A., B. M. Dutia, J. P. Stewart, and A. J. Davison.** Natural history of murine gammaherpesvirus infection. Philos. Trans. R. Soc. Lond. B, in press.
25. **Parry, C. M., J. P. Simas, V. P. Smith, C. A. Stewart, A. C. Minson, S. Efstathiou, and A. Alcami.** 2000. A broad spectrum secreted chemokine binding protein encoded by a herpesvirus. J. Exp. Med. **191:**573–578.
26. **Raslova, H., J. Mistrikova, M. Kudelova, Z. Mishal, A. Sarasin, D. Blangy, and M. Berebbi.** 2000. Immunophenotypic study of atypical lymphocytes generated in peripheral blood and spleen of nude mice after MHV-72 infection. Viral Immunol. **13:**313–327.
27. **Sambrook, J., E. F. Fritsch, and T. Maniatis.** 1989. Molecular cloning: a laboratory manual, 2nd ed. Cold Spring Harbor Laboratory Press, Cold Spring Harbor, N.Y.
28. **Simas, J. P., R. J. Bowden, V. Paige, and S. Efstathiou.** 1998. Four tRNA-like sequences and a serpin homologue encoded by murine gammaherpesvirus 68 are dispensable for lytic replication *in vitro* and latency *in vivo*. J. Gen. Virol. **79:**149–153.
29. **Simas, J. P., D. Swann, R. Bowden, and S. Efstathiou.** 1999. Analysis of murine gammaherpesvirus-68 transcription during lytic and latent infection. J. Gen. Virol. **80:**75–82.
30. **Staden, R.** 1987. Computer handling of DNA sequencing projects, p. 173–

217. *In* M. J. Bishop and C. J. Rawlings (ed.), Nucleic acid and protein sequence analysis: a practical approach. IRL Press, Oxford, United Kingdom.
31. **Stewart, J. P.** 1999. Of mice and men: murine gammaherpesvirus 68 as a model. EBV Rep. **6:**31–35.
32. **Stewart, J. P., E. J. Usherwood, A. Ross, H. Dyson, and T. Nash.** 1998. Lung epithelial cells are a major site of murine gammaherpesvirus persistence. J. Exp. Med. **187:**1941–1951.
33. **Sunil-Chandra, N. P.** 1991. Studies on the pathogenesis of a murine gammaherpesvirus (MHV-68). Ph.D. thesis. University of Cambridge, Cambridge, United Kingdom.
34. **Sunil-Chandra, N. P., S. Efstathiou, J. Arno, and A. A. Nash.** 1992. Virological and pathological features of mice infected with murine gamma-herpesvirus 68. J. Gen. Virol. **73:**2347–2356.
35. **Sunil-Chandra, N. P., S. Efstathiou, and A. A. Nash.** 1992. Murine gammaherpesvirus 68 establishes a latent infection in mouse B lymphocytes in vivo. J. Gen. Virol. **73:**3275–3279.
36. **Tripp, R. A., A. M. Hamilton-Easton, R. D. Cardin, P. Nguyen, F. G. Behm, D. L. Woodland, P. C. Doherty, and M. A. Blackman.** 1997. Pathogenesis of an infectious mononucleosis-like disease induced by a murine gamma-herpesvirus: role for a viral superantigen? J. Exp. Med. **185:**1641–1650.
37. **Usherwood, E. J., A. J. Ross, D. J. Allen, and A. A. Nash.** 1996. Murine gammaherpesvirus-induced splenomegaly: a critical role for CD4 T cells. J. Gen. Virol. **77:**627–630.
38. **Usherwood, E. J., D. J. Roy, K. Ward, S. L. Surman, B. M. Dutia, M. A. Blackman, J. P. Stewart, and D. L. Woodland.** 2000. Control of gammaherpesvirus latency by latent antigen-specific CD8(+) T cells. J. Exp. Med. **192:**943–952.
39. **Usherwood, E. J., J. P. Stewart, K. Robertson, D. J. Allen, and A. A. Nash.** 1996. Absence of splenic latency in murine gammaherpesvirus 68-infected B cell-deficient mice. J. Gen. Virol. **77:**2819–2825.
40. **van Berkel, V., J. Barrett, H. L. Tiffany, D. H. Fremont, P. M. Murphy, G. McFadden, S. H. Speck, and H. W. Virgin IV.** 2000. Identification of a gammaherpesvirus selective chemokine binding protein that inhibits chemokine action. J. Virol. **74:**6741–6747.
41. **Virgin, H. W., R. M. Presti, X. Y. Li, C. Liu, and S. H. Speck.** 1999. Three distinct regions of the murine gammaherpesvirus 68 genome are transcriptionally active in latently infected mice. J. Virol. **73:**2321–2332.
42. **Virgin, H. W., P. Latreille, P. Wamsley, K. Hallsworth, K. E. Weck, A. J. Dal Canto, and S. H. Speck.** 1997. Complete sequence and genomic analysis of murine gammaherpesvirus 68. J. Virol. **71:**5894–5904.
43. **Weck, K. E., M. L. Barkon, L. I. Yoo, S. H. Speck, and H. W. Virgin.** 1996. Mature B cells are required for acute splenic infection, but not for establishment of latency, by murine gammaherpesvirus 68. J. Virol. **70:**6775–6780.
44. **Weck, K. E., S. S. Kim, H. W. Virgin IV, and S. H. Speck.** 1999. Macrophages are the major reservoir of latent murine gammaherpesvirus 68 in peritoneal cells. J. Virol. **73:**3273–3283.
45. **Zong, J. C., D. M. Ciufo, D. J. Alcendor, X. Wan, J. Nicholas, P. J. Browning, P. L. Rady, S. K. Tyring, J. M. Orenstein, C. S. Rabkin, I. J. Su, K. F. Powell, M. Croxson, K. E. Foreman, B. J. Nickoloff, S. Alkan, and G. S. Hayward.** 1999. High-level variability in the ORF-K1 membrane protein gene at the left end of the Kaposi's sarcoma-associated herpesvirus genome defines four major virus subtypes and multiple variants or clades in different human populations. J. Virol. **73:**4156–4170.